

1988

The effect of oil on heat transfer and pressure drop during evaporation and condensation of refrigerant inside augmented tubes

Lynn Michael Schlager
Iowa State University

Follow this and additional works at: <https://lib.dr.iastate.edu/rtd>

 Part of the [Mechanical Engineering Commons](#)

Recommended Citation

Schlager, Lynn Michael, "The effect of oil on heat transfer and pressure drop during evaporation and condensation of refrigerant inside augmented tubes " (1988). *Retrospective Theses and Dissertations*. 8889.
<https://lib.dr.iastate.edu/rtd/8889>

This Dissertation is brought to you for free and open access by the Iowa State University Capstones, Theses and Dissertations at Iowa State University Digital Repository. It has been accepted for inclusion in Retrospective Theses and Dissertations by an authorized administrator of Iowa State University Digital Repository. For more information, please contact digirep@iastate.edu.

INFORMATION TO USERS

The most advanced technology has been used to photograph and reproduce this manuscript from the microfilm master. UMI films the text directly from the original or copy submitted. Thus, some thesis and dissertation copies are in typewriter face, while others may be from any type of computer printer.

The quality of this reproduction is dependent upon the quality of the copy submitted. Broken or indistinct print, colored or poor quality illustrations and photographs, print bleedthrough, substandard margins, and improper alignment can adversely affect reproduction.

In the unlikely event that the author did not send UMI a complete manuscript and there are missing pages, these will be noted. Also, if unauthorized copyright material had to be removed, a note will indicate the deletion.

Oversize materials (e.g., maps, drawings, charts) are reproduced by sectioning the original, beginning at the upper left-hand corner and continuing from left to right in equal sections with small overlaps. Each original is also photographed in one exposure and is included in reduced form at the back of the book. These are also available as one exposure on a standard 35mm slide or as a 17" x 23" black and white photographic print for an additional charge.

Photographs included in the original manuscript have been reproduced xerographically in this copy. Higher quality 6" x 9" black and white photographic prints are available for any photographs or illustrations appearing in this copy for an additional charge. Contact UMI directly to order.

U·M·I

University Microfilms International
A Bell & Howell Information Company
300 North Zeeb Road, Ann Arbor, MI 48106-1346 USA
313/761-4700 800/521-0600



Order Number 8909191

**The effect of oil on heat transfer and pressure drop during
evaporation and condensation of refrigerant inside augmented
tubes**

Schlager, Lynn Michael, Ph.D.

Iowa State University, 1988

U·M·I

**300 N. Zeeb Rd.
Ann Arbor, MI 48106**



**The effect of oil on heat transfer and pressure drop
during evaporation and condensation
of refrigerant inside augmented tubes**

by

Lynn Michael Schlager

**A Dissertation Submitted to the
Graduate Faculty in Partial Fulfillment of the
Requirements for the Degree of
DOCTOR OF PHILOSOPHY
Major: Mechanical Engineering**

Approved:

Signature was redacted for privacy.

In Charge of Major Work

Signature was redacted for privacy.

For the Major Department

Signature was redacted for privacy.

For the Graduate College

**Iowa State University
Ames, Iowa**

1988

TABLE OF CONTENTS

	Page
NOMENCLATURE	xvi
ACKNOWLEDGMENTS	xxi
CHAPTER 1 INTRODUCTION	1
Background	1
Description of the Research	1
CHAPTER 2 THE EFFECT OF OIL ON MIXTURE PROPERTIES	6
Thermal and Transport Properties	6
Thermodynamic Properties	9
Other Effects of Oil	12
CHAPTER 3 LITERATURE REVIEW OF TWO-PHASE REFRIGERANT HEAT TRANSFER AND PRESSURE DROP EMPHASIZING OIL EFFECTS AND IN-TUBE AUGMENTATION	14
Previous Literature Surveys	14
The Effect of Oil on Refrigerant Heat Transfer and Pressure Drop	15
In-Tube Augmentation of Two-Phase Refrigerant Heat Transfer	23
Summary	32
CHAPTER 4 TEST FACILITY	37
Flow Loop Components	37
Instrumentation	43
Data Acquisition System	45
CHAPTER 5 DATA ANALYSIS	47
Assumptions	47
Data Presentation	48
Limitations on Data	50
Data Reduction Equations	53
Experimental Uncertainties	57

CHAPTER 6	RESULTS WITH THE SMOOTH TUBE	59
	Pure Refrigerant Heat Transfer	59
	Heat Transfer with Refrigerant-Oil Mixtures	61
	Pressure Drop	70
	Oil Hold-Up	81
	Summary	84
CHAPTER 7	RESULTS WITH THE MICRO-FIN TUBE	87
	Pure Refrigerant Heat Transfer	87
	Heat Transfer with Refrigerant-Oil Mixtures	92
	Pressure Drop	102
	Oil Hold-Up	112
	Summary	115
CHAPTER 8	RESULTS WITH THE LOW-FIN TUBE	118
	Pure Refrigerant Heat Transfer	118
	Heat Transfer with Refrigerant-Oil Mixtures	122
	Pressure Drop	132
	Summary	141
CHAPTER 9	COMPARISON AND PERFORMANCE EVALUATION OF THE THREE TUBES	144
	Previous Performance Evaluation Criteria	144
	Performance Evaluation of the Tubes Tested	148
	Summary	165
CHAPTER 10	CORRELATIONS FOR DESIGN WITH REFRIGERANT-OIL MIXTURES	167
	Review of Correlations from the Literature	167
	Correlation of Experimental Heat Transfer Results	184
	Correlation of Experimental Pressure Drop Results	208
	Summary	227

CHAPTER 11 CONCLUSIONS AND RECOMMENDATIONS	229
Conclusions	229
Recommendations for Further Research	233
REFERENCES	235
APPENDIX A EQUIPMENT AND MATERIAL SPECIFICATIONS	251
Flow Loops	251
Instrumentation	252
Expendable Materials	253
APPENDIX B EXPERIMENTAL PROCEDURES	254
Heat Transfer and Pressure Drop Testing	254
Oil Injection and Sampling	255
Oil Hold-up	258
APPENDIX C DATA ACQUISITION AND ANALYSIS PROGRAM	260
APPENDIX D ERROR ANALYSIS	289
Uncertainty of the Inside Convective Coefficient	290
Uncertainty of the Mass Flux	297
Uncertainty of the Vapor Quality	299
Uncertainty of the Oil Concentration	302
Uncertainty of the Pressure Drop	302
Uncertainty of the Regression Lines	302
Uncertainty of the Enhancement Factors, ϵ and Ψ	307
Uncertainty of the Performance Enhancement Ratio, θ	308
APPENDIX E TABULATED DATA	309

LIST OF FIGURES

		Page
Figure 2.1.	Saturation temperature of refrigerant-oil mixtures as a function of vapor quality	10
Figure 2.2.	Pressure-enthalpy diagram for mixtures of R-12 and oil	11
Figure 3.1.	Examples of passive enhancement techniques	24
Figure 4.1.	Schematic diagram of the test facility	38
Figure 4.2.	Assembly detail of the annulus	41
Figure 4.3.	Oil injection and sampling device	43
Figure 6.1.	Comparison of experimental Nusselt number with predictions	60
Figure 6.2.	Comparison of experimental heat transfer coefficients with predicted values for evaporation and condensation	62
Figure 6.3.	Heat transfer coefficient versus mass flux for evaporation and condensation with pure R-22 in a smooth tube	63
Figure 6.4.	Heat transfer coefficient versus mass flux for evaporation and condensation with mixtures of R-22 plus 150-SUS oil	64
Figure 6.5.	Heat transfer coefficient versus mass flux for evaporation and condensation with mixtures of R-22 plus 300-SUS oil	66
Figure 6.6.	Evaporation heat transfer enhancement factor ($\epsilon_{s'/s}$) versus oil concentration for 150- and 300-SUS oil at two mass fluxes	67
Figure 6.7.	Condensation heat transfer enhancement factor ($\epsilon_{s'/s}$) versus oil concentration for 150- and 300-SUS oil at two mass fluxes	69
Figure 6.8.	Evaporation and condensation pressure drop versus mass flux with pure R-22	71
Figure 6.9.	Comparison of experimental evaporation pressure drop with predicted values	72
Figure 6.10.	Comparison of experimental condensation pressure drop with predicted values	74

Figure 6.11.	Evaporation pressure drop versus mass flux with 150- and 300-SUS oil	75
Figure 6.12.	Evaporation pressure drop enhancement factor ($\Psi_{s/s}$) versus mass flux with 150- and 300-SUS oil	76
Figure 6.13.	Condensation pressure drop versus mass flux with 150- and 300-SUS oil	78
Figure 6.14.	Condensation pressure drop enhancement factor ($\Psi_{s/s}$) versus mass flux with 150- and 300-SUS oil	79
Figure 6.15.	Baker flow regime map with typical condensation test conditions	80
Figure 6.16.	Quantity of oil in the smooth tube with 150-SUS oil	82
Figure 6.17.	Quantity of oil in the smooth tube with 300-SUS oil	83
Figure 7.1.	Drawing of the micro-fin tube	88
Figure 7.2.	Heat transfer coefficient versus mass flux for pure refrigerant evaporation in a micro-fin tube and a smooth tube	90
Figure 7.3.	Heat transfer enhancement factor ($\epsilon_{a/s}$) for evaporation and condensation of R-22 in a micro-fin tube	90
Figure 7.4.	Heat transfer coefficient versus mass flux for pure refrigerant condensation in a micro-fin tube and a smooth tube	91
Figure 7.5.	Heat transfer coefficient versus mass flux for evaporation with mixtures of R-22 and 150-SUS oil in a micro-fin tube	92
Figure 7.6.	Heat transfer coefficient versus mass flux for evaporation with mixtures of R-22 and 300-SUS oil in a micro-fin tube	93
Figure 7.7.	Evaporation enhancement factor ($\epsilon_{a/a}$) versus oil concentration in a micro-fin tube	94
Figure 7.8.	Evaporation enhancement factors for smooth and micro-fin tubes ($\epsilon_{s/s}$ and $\epsilon_{a/a}$) as a function of oil concentration	95
Figure 7.9.	Evaporation enhancement factor showing the combined effects of oil and augmentation ($\epsilon_{a/s}$) in a micro-fin tube	96

Figure 7.10.	Heat transfer coefficient versus mass flux for condensation with mixtures of R-22 and 150-SUS oil in a micro-fin tube	97
Figure 7.11.	Heat transfer coefficient versus mass flux for condensation with mixtures of R-22 and 300-SUS oil in a micro-fin tube	98
Figure 7.12.	Condensation enhancement factor ($\epsilon_{a/a}$) versus oil concentration in a micro-fin tube	99
Figure 7.13.	Condensation enhancement factors for smooth and micro-fin tubes ($\epsilon_{s/s}$ and $\epsilon_{a/a}$) as a function of oil concentration	100
Figure 7.14.	Condensation enhancement factor showing the combined effects of oil and augmentation ($\epsilon_{a/s'}$) in a micro-fin tube	101
Figure 7.15.	Evaporation and condensation pressure drop with pure R-22 in smooth and micro-fin tubes	102
Figure 7.16.	Pressure drop enhancement factor ($\psi_{a/s}$) for evaporation and condensation in a micro-fin tube	103
Figure 7.17.	Evaporation pressure drop in a micro-fin tube with mixtures of R-22 and oil	105
Figure 7.18.	Pressure drop enhancement factor ($\psi_{a/a}$) for evaporation in a micro-fin tube	106
Figure 7.19.	Pressure drop enhancement factor ($\psi_{a/s}$ or $\psi_{a/s'}$) for evaporation in a micro-fin tube	107
Figure 7.20.	Condensation pressure drop in a micro-fin tube with mixtures of R-22 and oil	109
Figure 7.21.	Pressure drop enhancement factor ($\psi_{a/a}$) for condensation in a micro-fin tube	110
Figure 7.22.	Pressure drop enhancement factor ($\psi_{a/s}$ or $\psi_{a/s'}$) for condensation in a micro-fin tube	111
Figure 7.23.	Quantity of oil in a micro-fin tube with 150-SUS oil	113
Figure 7.24.	Quantity of oil in a micro-fin tube with 300-SUS oil	114
Figure 8.1.	Drawing of the low-fin tube	119

Figure 8.2.	Heat transfer coefficient versus mass flux for pure refrigerant evaporation in a smooth tube and a low-fin tube	120
Figure 8.3.	Heat transfer enhancement factor ($\epsilon_{a/s}$) for evaporation and condensation of R-22 in a low-fin tube	121
Figure 8.4.	Heat transfer coefficient versus mass flux for pure refrigerant condensation in a smooth tube and a low-fin tube	122
Figure 8.5.	Heat transfer enhancement factor ($\epsilon_{a/s}$) for evaporation and condensation of R-22 in a micro-fin tube and a low-fin tube	123
Figure 8.6.	Heat transfer coefficient versus mass flux for evaporation with mixtures of R-22 and 150-SUS oil in a low-fin tube	123
Figure 8.7.	Evaporation enhancement factor due to the effects of oil ($\epsilon_{a/a}$) in a low-fin tube	125
Figure 8.8.	Evaporation enhancement factors for smooth, micro-fin, and low-fin tubes ($\epsilon_{s/s}$ and $\epsilon_{a/a}$) as a function of oil concentration	126
Figure 8.9.	Evaporation enhancement factor showing the combined effects of oil and augmentation ($\epsilon_{a/s'}$) in a micro-fin tube and a low-fin tube	127
Figure 8.10.	Heat transfer coefficient versus mass flux for condensation with mixtures of R-22 and 150-SUS oil in a low-fin tube	128
Figure 8.11.	Condensation enhancement factor due to the effects of oil ($\epsilon_{a/a}$) in a low-fin tube	129
Figure 8.12.	Condensation enhancement factors for smooth, micro-fin, and low-fin tubes ($\epsilon_{s/s}$ and $\epsilon_{a/a}$) as a function of oil concentration	130
Figure 8.13.	Evaporation enhancement factor showing the combined effects of oil and augmentation ($\epsilon_{a/s'}$) in a micro-fin tube and a low-fin tube	131
Figure 8.14.	Evaporation and condensation pressure drop with pure R-22 in smooth and low-fin tubes	133
Figure 8.15.	Pressure drop enhancement factor ($\Psi_{a/s}$) for evaporation and condensation in a micro-fin tube and a low-fin tube	133

Figure 8.16.	Evaporation pressure drop in a low-fin tube with mixtures of R-22 and oil	135
Figure 8.17.	Pressure drop enhancement factor due to the effects of oil ($\Psi_{a/a}$) for evaporation in a low-fin tube	136
Figure 8.18.	Pressure drop enhancement factor showing the combined effects of oil and augmentation ($\Psi_{a/s}$) for evaporation in a micro-fin tube and a low-fin tube	137
Figure 8.19.	Condensation pressure drop in a low-fin tube with mixtures of R-22 and oil	138
Figure 8.20.	Pressure drop enhancement factor due to the effects of oil ($\Psi_{a/a}$) for condensation in a low-fin tube	139
Figure 8.21.	Pressure drop enhancement factor showing the combined effects of oil and augmentation ($\Psi_{a/s}$) for condensation in a micro-fin tube and a low-fin tube	140
Figure 9.1.	Enhancement performance ratio ($\theta_{a/s}$) for evaporation and condensation of pure R-22 in micro-fin and low-fin tubes	149
Figure 9.2.	Evaporation enhancement performance ratio showing the effects of oil alone ($\theta_{s/s}$) in a smooth tube	151
Figure 9.3.	Condensation enhancement performance ratio showing the effects of oil alone ($\theta_{s/s}$) in a smooth tube	153
Figure 9.4.	Evaporation enhancement performance ratio showing the effects of oil alone ($\theta_{a/a}$) in a micro-fin tube	154
Figure 9.5.	Condensation enhancement performance ratio showing the effects of oil alone ($\theta_{a/a}$) in a micro-fin tube	156
Figure 9.6.	Evaporation enhancement performance ratio showing the effects of oil alone ($\theta_{a/a}$) in a low-fin tube	157
Figure 9.7.	Condensation enhancement performance ratio showing the effects of oil alone ($\theta_{a/a}$) in a low-fin tube	158
Figure 9.8.	Evaporation enhancement performance ratio showing the combined effects of oil and augmentation ($\theta_{a/s}$) in a	160

	micro-fin tube	
Figure 9.9.	Condensation enhancement performance ratio showing the combined effects of oil and augmentation ($\theta_{a/s}$) in a micro-fin tube	161
Figure 9.10.	Evaporation enhancement performance ratio showing the combined effects of oil and augmentation ($\theta_{a/s}$) in a micro-fin tube and a low-fin tube	163
Figure 9.11.	Condensation enhancement performance ratio showing the combined effects of oil and augmentation ($\theta_{a/s}$) in a micro-fin tube and a low-fin tube	164
Figure 10.1.	Comparison of refrigerant-oil mixture evaporation heat transfer predictions with experimental data	188
Figure 10.2.	Examples of oil concentration profiles used with correlations	189
Figure 10.3.	Results using refrigerant-oil mixture properties in pure refrigerant evaporation heat transfer correlations	190
Figure 10.4.	Example showing the residual enhancement factor, ϵ^* , relative to enhancement factors from experiments and from a correlation	193
Figure 10.5.	Comparison of experimental evaporation heat transfer enhancement factors with predicted values ($\epsilon_{s/s}$ and $\epsilon_{a/a}$) using correlation-based equations	194
Figure 10.6.	Comparison of experimental evaporation heat transfer enhancement factors with predicted values ($\epsilon_{s/s}$ and $\epsilon_{a/a}$) using statistical equations	196
Figure 10.7.	Heat transfer enhancement factor ($\epsilon_{a/s}$) versus mass flux, normalized to values at $300 \text{ kg/m}^2\cdot\text{s}$	199
Figure 10.8.	Comparison of a refrigerant-oil mixture condensation heat transfer correlation with experimental data	201
Figure 10.9.	Results using refrigerant-oil mixture properties in pure refrigerant condensation heat transfer correlations	202

Figure 10.10. Comparison of experimental condensation heat transfer enhancement factors ($\epsilon_{s'/s}$) with predictions using statistical and correlation-based equations	203
Figure 10.11. Comparison of experimental condensation heat transfer enhancement factors ($\epsilon_{a'/a}$) with predictions using correlation-based equations	205
Figure 10.12. Comparison of experimental condensation heat transfer enhancement factors ($\epsilon_{a'/a}$) with predictions using statistical equations	206
Figure 10.13. Condensation heat transfer enhancement factor ($\epsilon_{a/s}$) versus mass flux, normalized to values at 300 kg/m ² ·s	208
Figure 10.14. Results using refrigerant-oil mixture properties in pure refrigerant condensation pressure drop correlations	211
Figure 10.15. Comparison of experimental evaporation pressure drop enhancement factors ($\Psi_{s'/s}$) with predictions using correlations and correlation-based equations	213
Figure 10.16. Comparison of experimental evaporation pressure drop enhancement factors ($\Psi_{s'/s}$) with predictions using statistical equations	215
Figure 10.17. Comparison of experimental evaporation pressure drop enhancement factors ($\Psi_{a'/a}$) with predictions using correlations and correlation-based equations	217
Figure 10.18. Comparison of experimental evaporation pressure drop enhancement factors ($\Psi_{a'/a}$) with predictions using statistical equations	218
Figure 10.19. Comparison of experimental condensation pressure drop enhancement factors ($\Psi_{s'/s}$) with predictions using statistical equations	223
Figure 10.20. Comparison of experimental condensation pressure drop enhancement factors ($\Psi_{a'/a}$) with predictions using correlations and correlation-based equations	224

Figure 10.21.	Comparison of experimental condensation pressure drop enhancement factors ($\Psi_{a/a}$) with predictions using statistical equations	226
Figure D.1.	Regression lines and confidence intervals (95%) for typical evaporation and condensation heat transfer cases	305
Figure D.2.	Regression lines and confidence intervals (95%) for typical evaporation and condensation pressure drop cases	306

LIST OF TABLES

	Page
Table 3.1. Studies of refrigerant-oil mixture evaporation inside smooth, horizontal tubes	17
Table 3.2. Studies of the in-tube augmentation of refrigerant evaporation	33
Table 3.3. Studies of the in-tube augmentation of refrigerant condensation	34
Table 3.4. Evaporation of chlorofluorocarbon refrigerants in micro-fin and low-fin tubes	35
Table 3.5. Condensation of chlorofluorocarbon refrigerants in micro-fin and low-fin tubes	36
Table 6.1. Smooth tube dimensions	59
Table 6.2. Summary of two-phase test conditions	61
Table 7.1. Micro-fin tube dimensions	89
Table 8.1. Low-fin tube dimensions	118
Table 9.1. Enhancement performance ratios of each tube with refrigerant-oil mixtures compared to the same tube with pure refrigerant ($\theta_{s'/s}$ and $\theta_{a'/a}$) at 300 kg/m ² ·s	166
Table 9.2. Enhancement performance ratios of the augmented tubes compared to the smooth tube with pure refrigerant ($\theta_{a/s}$) and refrigerant-oil mixtures ($\theta_{a'/s'}$) at 300 kg/m ² ·s	166
Table 10.1. Constants for void fraction correlation equations	182
Table 10.2. Convective and nucleate boiling predictions for pure refrigerant and refrigerant-oil mixtures	191
Table 10.3. Summary of predictive equations to account for the effects of oil and augmentation with R-22	228
Table A.1. Components in the flow rig	251
Table A.2. Data acquisition and instrumentation components	252
Table D.1. Conditions from condensation test run COX300	289
Table D.2. Average standard deviations of the pressure drop measurements	303

Table D.3.	Summary of pressure drop standard deviations	303
Table D.4.	Calculated confidence intervals for heat transfer coefficient regression equations at 95% confidence level	304
Table D.5.	Calculated confidence intervals for pressure drop regression equations at 95% confidence level	305
Table D.6.	Estimated uncertainty of enhancement factors ($\epsilon_{a/s}$ and $\psi_{a/s}$) as a percentage of the calculated values	307
Table D.7.	Uncertainty estimate for the enhancement performance ratio (θ) as a percentage of calculated values	308
Table E.1.	Smooth tube evaporation with pure refrigerant	309
Table E.2.	Smooth tube evaporation with refrigerant plus 150-SUS oil	309
Table E.3.	Smooth tube evaporation with refrigerant plus 300-SUS oil	310
Table E.4.	Smooth tube condensation with pure refrigerant	311
Table E.5.	Smooth tube condensation with refrigerant plus 150-SUS oil	312
Table E.6.	Smooth tube condensation with refrigerant plus 300-SUS oil	312
Table E.7.	Micro-fin tube evaporation with pure refrigerant	314
Table E.8.	Micro-fin tube evaporation with refrigerant plus 150-SUS oil	314
Table E.9.	Micro-fin tube evaporation with refrigerant plus 300-SUS oil	315
Table E.10.	Micro-fin tube condensation with pure refrigerant	317
Table E.11.	Micro-fin tube condensation with refrigerant plus 150-SUS oil	317
Table E.12.	Micro-fin tube condensation with refrigerant plus 300-SUS oil	318
Table E.13.	Low-fin tube evaporation with pure refrigerant	319
Table E.14.	Low-fin tube evaporation with refrigerant plus 150-SUS oil	320
Table E.15.	Low-fin tube condensation with pure refrigerant	321
Table E.16.	Low-fin tube condensation with refrigerant plus 150-SUS oil	321
Table E.17.	Smooth tube evaporative pressure drop with pure refrigerant	322

Table E.18. Smooth tube evaporative pressure drop with refrigerant plus 150-SUS oil	323
Table E.19. Smooth tube condensing pressure drop with pure refrigerant	324
Table E.20. Smooth tube condensing pressure drop with refrigerant plus 150-SUS oil	324
Table E.21. Smooth tube evaporation oil hold-up with 150-SUS oil	325
Table E.22. Smooth tube condensation oil hold-up with 150-SUS oil	325
Table E.23. Micro-fin tube evaporation oil hold-up with 150-SUS oil	326
Table E.24. Micro-fin tube condensation oil hold-up with 150-SUS oil	326
Table E.25. Smooth tube oil hold-up with 300-SUS oil	326
Table E.26. Micro-fin tube oil hold-up with 300-SUS oil	326

NOMENCLATURE

A	area (m^2)
A*	area increase ratio (A_a/A_s)
C	constant
C1–C5	constants
C_p	constant pressure specific heat (J/kg)
CI	confidence interval about a regression curve
d	diameter (m)
E	experimental constant
E	enhancement multiplier
e	2.71828...
f	fin height (m)
f	friction factor
F1,F2	factors in Traviss et al. correlation
F₁–F₄	geometric correction factors for finned tubes
F_{fl}	fluid-specific term in Kandlikar correlation
G	mass flux ($\text{kg/m}^2\cdot\text{s}$) (based on actual flow area)
G*	superficial mass flux ($\text{kg/m}^2\cdot\text{s}$) ($G^*_l = G \cdot (1-X)$; $G^*_v = G \cdot X$)
G'	normalized mass flux, relative to $300 \text{ kg/m}^2\cdot\text{s} = G/300$
g	acceleration of gravity (9.81 m/s^2)
h	convective heat transfer coefficient ($\text{W/m}^2\cdot\text{C}$)
I	electrical current (A)
i_{fg}	enthalpy of vaporization (J/kg)
k	thermal conductivity ($\text{W/m}\cdot\text{C}$)
k₁,k₂	factors in Tichy et al. correlation
l	length (m)
LMTD	logarithmic mean temperature difference ($^{\circ}\text{C}$)
M	mass (kg , g)
M	molecular weight ($\text{kg/kg}\cdot\text{mol}$)
m	mass flow rate (kg/s)
n	number of fins
n	number of data points or independent samples
P	pressure (Pa)

P	power (W)
P*	reduced pressure (P / P_{crit})
p	pitch of fins (m)
Q	heat flow (W)
q	heat flux (W/m^2)
R_h	size reduction index
R_{ΔP}	pressure drop index
r	radius (m)
S	suppression multiplier
s²	variance (units vary)
T	temperature (°C)
U	overall heat transfer coefficient ($W/m^2 \cdot ^\circ C$)
V	electrical potential (V)
v	specific volume (m^3/kg)
W	weight fraction of refrigerant
W	precision index (units vary)
W1	weight of empty sampling cylinder plus tube and filter attachments (kg)
W2	weight of full sampling cylinder plus tube and filter attachments (kg)
W3	weight of oil and sampling cylinder plus tube and filter attachments (kg)
w	groove width (m)
X	vapor quality
y	mole fraction
z	axial position (m)

Greek Symbols

α	void fraction
β	spiral angle (degrees)
γ	statistical confidence level (%)
Δ	change in value
δ	factor in Dukler correlation
ε	enhancement factor (heat transfer)
ε*	residual enhancement factor ($\epsilon_{s'/s_{exp}} - \epsilon_{s'/s_{corr}}$)
η	factor in Dukler correlation

θ	enhancement performance ratio (ϵ/Ψ)
Λ	factor from Baker's flow pattern map $\left(\left\{ \left[\frac{\rho_v}{\rho_A} \right] \left[\frac{\rho_l}{\rho_w} \right] \right\}^{0.5} \right)$
λ	$-\ln(1-\alpha)$, Dukler correlation
μ	dynamic viscosity (Pa·s)
μ	mean (units vary)
ν	degrees of freedom
π	3.14159...
ρ	density (kg/m^3)
σ	surface tension (N/m)
σ	standard deviation (units vary)
δ	standard error of the estimate (units vary)
Φ	severity ($f^2/p \cdot d_i$)
ϕ	two-phase pressure drop multiplier
χ_{tt}	Lockhart-Martinelli parameter $\left(\left[\frac{1-X}{X} \right]^{0.9} \left[\frac{\rho_v}{\rho_l} \right]^{0.5} \left[\frac{\mu_l}{\mu_v} \right]^{0.1} \right)$
Ψ	two-phase heat transfer multiplier (h_{TP}/h_l)
Ψ	enhancement factor (pressure drop)
Ω	factor from Baker's flow pattern map $\left(\left[\frac{\sigma_w}{\sigma} \right] \left\{ \left[\frac{\mu_l}{\mu_w} \right] \left[\frac{\rho_w}{\rho_l} \right]^2 \right\}^{1/3} \right)$
ω_o	mass fraction of oil on a sample basis

Subscripts

A	air
a	augmented tube with pure refrigerant
a'	augmented tube with refrigerant-oil mixture
atm	atmospheric
avg	average
boil	boiler (first heater—constant heat flux)
bs	bubble suppression regime
cb	convective boiling

cond	condensation
corr	based on correlation
crit	critical
e	equivalent
evap	evaporation
exp	experimental
f	friction
H	hydraulic
h	heaters (boiler and superheater combined)
h	homogeneous
i	inside
i	index
in	inlet
l	liquid or based on liquid properties
l-f	low-fin tube
lo	total flow considered as a liquid
lat	latent
m	mixture
m	momentum
m-f	micro-fin tube
max	maximum
nb	nucleate boiling
o	oil
o	outside
out	outlet
pred	predicted
r	refrigerant
s	smooth tube with pure refrigerant
s'	smooth tube with refrigerant-oil mixture
s-h	superheater (second heater—wrapped resistance heating element)
sat	saturation conditions
sens	sensible
SP	single-phase

t	test section
TP	two-phase
v	vapor or based on vapor properties
W	water
w	wall
x	cross-sectional
1,2,3	index numbers indicating different conditions, etc.

Superscripts

e	empirical exponent
m,n	empirical exponent
-	average value

Dimensionless Groups

Bo	boiling number $(q / G \cdot i_{fg})$
Co	convection number $\left(\left[\frac{1-X}{X} \right]^{0.8} \cdot \left[\frac{\rho_v}{\rho_l} \right]^{0.5} \right)$
Fr	Froude number $(G^2 / \rho_l \cdot g \cdot d_i)$
Ja	Jakob number $(C_p \cdot \Delta T / i_{fg})$
Nu	Nusselt number $(h \cdot d / k)$
Pr	Prandtl number $(C_p \cdot \mu / k)$
K	Pierre boiling number $(\Delta X \cdot i_{fg} / l \cdot g)$
Re	Reynolds number $(G \cdot d / \mu)$

ACKNOWLEDGMENTS

This work was sponsored by the American Society of Heating, Refrigerating and Air Conditioning Engineers (ASHRAE) as research project 469-RP. The monetary and technical support of ASHRAE is gratefully acknowledged. Particular appreciation is given to technical committee TC1.3, Heat Transfer and Fluid Flow, and to the Research Monitoring Subcommittee of TC1.3, whose members provided guidance and advice throughout the course of the work. The members of the subcommittee were: Dr. N. Z. Azer, Dr. Floyd Hayes, Dr. Jerry Robertson, and Dr. Keith Starner.

Although several alterations and improvements were made to test facility during the course of this work, much is owed my predecessor, Dr. Jatin Khanpara, for the initial building and debugging of the rig, as well as for providing training in its use. For help with instrumentation and the installation of a new data acquisition system, I am indebted to Mr. Hap Steed of the Department of Mechanical Engineering. Mr. Doug Westra, a fellow graduate student, was also of great assistance in the conversion to a new computer system. Mr. Wayne Stensland of the Research Equipment Assistance Program helped in the acquisition of numerous parts in both routine and emergency situations.

Many individuals deserve thanks, even though not formally associated with my work. Colleagues in the Heat Transfer Laboratory and the Building Energy Utilization Laboratory gave both tangible and intangible support throughout my time at Iowa State. With them I could consult, discuss technical (or non-technical) matters, and at times commiserate; without them, my work would have been considerably less enjoyable. Of this group, I would particularly like to thank Dr. James Baustian and Mr. Chris Gersey, with whom I spent many hours in the Heat Transfer Lab, and who cheerfully tolerated the constant noise associated with my rig. One final colleague whom I should acknowledge is Dr. Bill Copenhaver, who entered the Ph.D. program concurrently, and was of great help during the intensive course work my first year.

I would like to acknowledge the firm Wieland-Werke AG, Ulm, W. Germany, for supplemental financial support and for providing the opportunity to present a paper at a meeting of the Deutsche Kälte- und Klimatechnische Verein in Cologne. In particular, I

appreciate the efforts of Mr. Klaus Menze of Wieland who watched for and forwarded German publications relevant to my research; for the most part these references would have gone unnoticed using routine literature-search resources. Appreciation is also given to the Amoco Oil Company for providing fellowship support during my first year at Iowa State.

The members of my doctoral committee provided assistance and guidance both before and during the experimental portion of my work, and made the dreaded experience of preliminary exams a positive (if not completely enjoyable) experience. I am grateful to Professors W. J. Cook of Mechanical Engineering, B. R. Munson of Engineering Science and Mechanics, and D. L. Ulrichson of Chemical Engineering for their time and interest in my work. A special thanks is also given to Professor B. C. Gerstein of the Department of Chemistry, who substituted for Professor Ulrichson at the final oral examination.

The feelings with which one leaves a graduate program are in great part determined by one's major professor(s). I feel very fortunate to have had the guidance and encouragement of Professors Arthur E. Bergles and Michael B. Pate. In large measure, the quality of work produced during these past three years, as represented by this document, is due to the supervision and scrutiny of these two gentlemen. The extensive experience and knowledge of Professor Bergles is without parallel in the field and I have benefitted greatly from an association with him, not only in this research program, but also in the classroom. Professor Pate's day-to-day oversight of the project, his positive outlook on difficulties, and his patience with all-too-frequent problems was always appreciated. He was there with encouragement and suggestions, and at times showed more confidence in me than was perhaps merited. It is therefore with deep gratitude that I thank Professors Bergles and Pate for their careful guidance of my work.

Lastly, I would like to express my appreciation to my family. To my parents, who instilled in me the desire and, more importantly, the discipline and organization to succeed, and who never hesitated to sacrifice for my benefit, I owe a debt that can never be adequately repaid. A sacrifice was also made by Susan's parents, who watched their daughter and grandchildren move 2000 miles away. I would like to acknowledge my father-in-law in particular, whose example of pursuing an advanced degree at an "advanced"

age was a factor in my decision to return to graduate school. And to my wife, Susan, and children, Anna, Sarah, and William, I give my deepest appreciation. Susan has stood by me and supported me throughout graduate school, has sacrificed many comforts, and has generally tolerated the sometimes not-so-friendly confines of student housing with patience and good humor. The children, too, have been wonderful, sharing one tiny bedroom for three years and losing daddy to the lab more than a few evenings and weekends during that time. Whenever things were rough, I could count on their bright smiles and big hugs for a much needed morale boost.

CHAPTER 1

INTRODUCTION

The growing use of internally augmented tubes in refrigeration systems has led to an increased interest in the combined effects of oil and augmentation on refrigerant evaporation and condensation. This document reports on an experimental program that investigated two-phase heat transfer and pressure drop of refrigerant-oil mixtures inside augmented tubes. This first chapter contains background information, discusses the need for such research, and gives a brief description of the research program.

Background

Vapor compression refrigeration systems always have some amount of oil circulating along with the refrigerant. The primary purpose of the oil is to lubricate the compressor, but oil also serves as a seal between the suction and discharge sides of the compressor and may help to cool the compressor. Although some systems include oil separators to minimize the quantity of circulating oil, many smaller refrigeration units make no provision for oil separation. Relatively little research has been conducted on the effects of this oil on the heat transfer and pressure drop in refrigerant evaporators and condensers.

During the past decade, an emphasis on energy conservation and more compact heat exchangers has led to an increased interest in internally augmented tubes for use in refrigeration evaporators and condensers. A search of the literature revealed numerous augmented tube studies, but only pure refrigerants or refrigerants with unspecified small quantities of oil (less than 0.5%) were used in these studies.

The refrigeration system design process is based on models that require good experimental data to accurately predict component performance. Prior to the inception of this study, there had been no published data for the designer on the heat transfer and pressure drop of refrigerant-oil mixtures inside augmented tubes [1].

Description of the Research

This research, accomplished under the sponsorship of the American Society of Heating, Refrigerating and Air Conditioning Engineers (ASHRAE), was initiated to study the effects of oil on two-phase refrigerant heat transfer and pressure drop in augmented

tubes. The study was divided into three phases: a literature review, an experimental investigation, and an analysis of the experimental data. A brief description of the research is presented in the following paragraphs.

Phase I — Literature Review

The literature review consisted of two major categories: (1) oil effects on heat transfer and pressure drop inside smooth tubes and (2) in-tube augmentation studies using pure refrigerants. There were no previous papers reporting on the combined effects of oil and augmentation. In addition to the two major categories listed above, some areas of peripheral interest were also reviewed. These areas were (1) thermo-physical properties of refrigerant-oil mixtures, (2) effects of oil on pool boiling and vapor space condensation (using both plain and augmented surfaces), and (3) adiabatic transport and pressure drop of refrigerant-oil mixtures. Chapter 2 discusses the properties of refrigerant-oil mixtures and Chapter 3 reviews the literature on heat transfer and pressure drop.

Phase II — Experimental Investigation

The experimental investigation, which comprised the bulk of the effort for the project, consisted of a series of tests in which several parameters were systematically varied. Since this was the first research using refrigerant-oil mixtures inside augmented tubes, an effort was made to cover a wide range of conditions within practical constraints. A description of the data reduction program is given in Chapter 5 and results from the testing are reported in Chapters 6, 7, and 8.

When possible, results are compared with results from earlier investigations, but the addition of oil to the test matrix makes it even more difficult than with pure refrigerants to find other investigations at similar conditions. There have been few previous studies of refrigerant-oil mixtures inside tubes, particularly during condensation, and many of these were at conditions which varied greatly from those reported here. Because of the limited quantity of data available from other sources, the conclusions drawn from this work are, of necessity, based on a rather small set of data.

The following paragraphs describe the range of conditions, tube geometries, refrigerants, etc., that were used in the test program. The original test plan was modified

slightly by the results of the literature review in Phase I and the recommendations of an ASHRAE committee, which included engineers active in the refrigeration industry.

Refrigerant Since it is currently one of the most popular refrigerants, R-22 was used for all of the tests. The current concern with ozone depletion caused by chloro-fluorocarbons (CFC's) indicates that R-22, due to its relatively benign effects, will probably gain in popularity. On the other hand, another currently popular refrigerant, R-12, is much more harmful to the ozone and may be phased out of new systems. For this reason, no tests with R-12 were attempted. Refrigerant 502 was also eliminated because the naphthenic mineral oils used in the project are not fully miscible in R-502 at the desired test conditions.

Oil type Due to its popularity and its compatibility with R-22, a naphthenic base mineral oil was chosen for the test program. The majority of testing was done with 150-SUS oil, but tests were also run with an oil having a viscosity of 300 SUS.

Oil concentrations In most cases, knowledge of the exact amount of oil circulating in refrigeration systems is limited, but it is generally less than 5% in many systems [2]. For this test program, oil concentration was limited to a maximum of 5%, with additional tests carried out at intermediate nominal concentrations of 0.6%, 1.25%, and 2.5%. These concentrations are all within the fully miscible region of R-22, but at evaporation temperatures ($\approx 0^{\circ}\text{C}$) and high vapor qualities, it is possible that the region of partial miscibility may have been entered. In this document, oil concentrations are stated in terms of weight percent on a total sample basis.

Test rig A pre-existing test rig was modified for oil and used for these tests. A description of the test facility is presented in Chapter 4. The tests were conducted using fluid heating and cooling of the test section. This allowed both evaporation and condensation testing, as well as faster changes of test tubes, but heat transfer coefficients were limited to average, rather than local values. There was no provision to inject and remove oil on a continuous basis, so oil was injected in a batch process, proceeding from pure refrigerant to progressively higher oil concentrations.

Test conditions Test conditions were established to approximate the conditions in actual refrigeration systems while remaining within the capabilities of the test rig. Mass

fluxes were varied from 125 to 400 kg/m²·s. Evaporation conditions were 0.5 to 0.6 MPa (0 to 6°C) and condensation was carried out at 1.5 to 1.6 MPa (39 to 42°C).

Refrigerant remained within the two-phase region in the test section, avoiding the superheated and subcooled regions. The subcooled region consists of a homogeneous mixture and can be handled by existing single-phase correlations. The high quality and superheated regions are more complex and require more instrumentation capabilities than were available. Due to the effects of oil, the saturation temperature becomes a variable at higher qualities and two-phase flow persists into what would generally be regarded as the superheated region (refrigerant vapor plus liquid mixture of oil with dissolved refrigerant). The upper quality limit was fixed at 85% and the lower limit was set at 10% to 15%.

Tube geometries The rig was designed for tubes with an outside diameter of 9.52 mm, a size typical of air-conditioning units. Although many types of internal augmentation have been reported in the literature, testing was limited to two types which are of current interest in the industry. The bulk of the testing was carried out with a so-called spiral micro-fin tube, a tube having 60 very small (0.2-mm) fins with a spiral, or rifling, of 18°. One test series was done with a tube, referred to as a low-fin tube, having 21 somewhat higher fins (0.4 mm) and a spiral angle of 30°. Both of these tubes have found application in the refrigeration industry, but the greater popularity of the micro-fin tube led to its use in most of the tests.

Phase III — Analytical Evaluation

One part of the evaluation phase was an analysis of the overall performance of the tubes, made by comparing the increase in heat transfer to the increase in pressure drop. This is important since the designer wishes to maximize heat transfer while minimizing pressure drop. Several performance parameters, such as ratios of augmented tube performance to smooth tube performance, were used to evaluate the effects of oil. Results of the performance evaluation are presented in Chapter 9.

In the second part of the evaluation phase, an attempt was made to generalize the experimental results from Phase II in the form of correlations. Due to the limited number of data points and limited range of test conditions, no generally applicable correlations based

only on physical properties and dimensions were developed. The predictive equations presented are (1) based on previously developed correlations from the literature, corrected for the presence of oil and/or the augmented surface or (2) determined by pure statistical curve fitting techniques. Correlations are discussed in Chapter 10.

CHAPTER 2

THE EFFECT OF OIL ON MIXTURE PROPERTIES

Oil can have a significant effect on transport and thermodynamic properties of refrigerant-oil mixtures, especially at higher oil concentrations. These property changes can, in turn, affect heat transfer and pressure drop performance of an evaporator or condenser. This chapter describes some of these properties, how much they may be altered by the presence of oil, and the possible impact on heat exchanger performance.

Since oil is essentially a non-volatile component when mixed with refrigerants, only liquid properties are varied by the addition of oil. The vapor phase remains almost pure refrigerant, although minute quantities of oil may diffuse into the vapor and liquid droplets of oil or refrigerant-oil mixture may be present in the vapor stream.

Thermal and Transport Properties

Various methods are used to estimate the properties of a mixture based on the properties of the pure components. These methods range from simple, ideal solution approximations to highly empirical and system-specific equations for determining the properties. Recent publications by Baustian et al. [3] and Baustian [4] have reviewed the literature and recommended suitable equations to determine the properties of refrigerant-oil mixtures. These recommended equations are included in the sections that follow. Properties of R-22 are from the ASHRAE Handbook [5,6].

Density

Oils are generally 20% to 50% less dense than CFC refrigerants. Density is used in several parameters of interest in heat transfer analysis, such as Reynolds number (Re), Lockhart-Martinelli parameter (χ_{lt}), Froude number (Fr), and convection number (Co). The equation used to estimate mixture density was [7]

$$\rho_m = \frac{\rho_r}{1 - (1 - W) \cdot \left(1 - \frac{\rho_r}{\rho_o}\right)} \quad (2.1)$$

With 5% oil in R-22, Equation 2.1 predicts a density change of only about 1%.

This equation assumes that mass and volume are both additive, although this is not strictly true of refrigerant-oil mixtures. A multiplicative factor [7] can be applied to this equation to correct for non-ideal mixing, however the correction is less than 1% for all conditions in the current study, so no such factor was included.

Viscosity

Refrigeration oils are typically two or more orders of magnitude more viscous than pure halocarbon refrigerants. The viscosity difference is greater as the temperature is lowered. The equation used to determine the viscosity of refrigerant-oil mixtures was that of Kendall and Monroe [8]:

$$\mu_m^{1/3} = y_r \cdot \mu_r^{1/3} + y_o \cdot \mu_o^{1/3} \quad (2.2)$$

With 150-SUS naphthenic mineral oil in R-22, this equation indicates that the viscosity of a mixture at 38°C with 5% oil would be about 21% higher than the viscosity of pure refrigerant. At 0°C, the viscosity of the mixture would be almost 70% higher.

Higher viscosities generally lead to an increase in pressure drop and can alter heat transfer by changing the wall velocity profile and the liquid-phase turbulence. In single-phase flow, a higher viscosity leads to a reduction of heat transfer, but in two-phase flow, the flow regime may also be affected by viscosity changes and this effect can be positive or negative, depending on which flow regime transition is caused by the viscosity change. Based on one nucleate boiling correlation [9], increased viscosity could be expected to degrade heat transfer in that region, but there is experimental evidence to the contrary [10]. Of the forced convection correlations reviewed in Chapter 10, those that have viscosity-dependent terms predict decreasing heat transfer with increasing viscosity.

Thermal Conductivity

The thermal conductivity of oils is typically 50% to 100% higher than that of halocarbon refrigerants. The equation used to predict thermal conductivity of the mixture was [11]:

$$k_m = k_r \cdot W + k_o(1-W) - 0.72(k_o - k_r)(1-W)W \quad (2.3)$$

This equation shows only a modest increase in mixture conductivity with increasing oil concentration. At 5% oil in R-22, the conductivity of the mixture is only about 1% higher than that of pure refrigerant.

In general, higher thermal conductivity tends to enhance heat transfer performance by producing higher temperature gradients at the wall, where velocity is zero. This trend is reflected in many single-phase correlations as well as several of the two-phase correlations mentioned in Chapter 10, in which $h \propto k^e$, where e is a positive fraction.

Surface Tension

The surface tension of oil is two to three times as large as that of refrigerants. Mixture surface tension was predicted by [11]:

$$\sigma_m = \sigma_r + (\sigma_o - \sigma_r)\sqrt{1 - W} \quad (2.4)$$

For R-22 and naphthenic mineral oil, mixture surface tension increases by about 45% with the addition of 5% oil.

Surface tension can affect heat transfer, particularly in the nucleate boiling region. Using one nucleate boiling correlation [9], increased surface tension reduces heat transfer at a given wall superheat. Nucleate boiling, however, is most important at low qualities and it is estimated that this contribution to overall performance is only 15% to 25% of the total for the tests reported here. At higher qualities, surface tension affects the degree to which the liquid occurs as droplets in the vapor stream or as a film on the tube walls. Increased surface tension can help delay dryout by drawing liquid upward to wet the upper part of the tube, thereby increasing heat transfer. Surface tension is also a key parameter in flow regime transitions, which in turn affect convective heat transfer. None of the forced convection vaporization correlations in Chapter 10 include surface tension as a variable.

Specific Heat

The specific heat of naphthenic oils is generally higher than most halocarbon refrigerants, approximately one third higher than R-22. The equation used to predict the specific heat of mixtures was [11]:

$$C_{pm} = C_{pr} \cdot W + C_{po}(1 - W) \quad (2.5)$$

The specific heat of a 5% mixture of oil in R-22 is less than 2% higher than that of pure refrigerant based on this equation.

Through the Prandtl number influence, many two-phase, as well as single-phase, heat transfer correlations predict higher heat transfer with increasing specific heat capacity.

Thermodynamic Properties

Little has appeared in the literature dealing with the thermodynamic properties of refrigerant-oil mixtures. McMullan et al. [12] wrote a set of computer routines to calculate the thermodynamic properties of R-12 and oil mixtures; Hughes et al. [13] published pressure-enthalpy diagrams for R-12 and paraffinic mineral oil mixtures. No publications were found dealing with general thermodynamic properties for R-22 and oil mixtures.

Vapor Pressure

The vapor pressure of oil is so much higher than that of refrigerants that oil can be considered a non-volatile component. Therefore, the vapor in two-phase regions is pure refrigerant. Conservation of mass then dictates that the remaining liquid must have a higher oil concentration than the overall average oil concentration. As vapor quality increases, the oil concentration in the remaining liquid also increases. At high qualities, the oil concentration can reach very high levels (>90%), even though the average oil concentration in the system is 5% or less.

No explicit equation was located to estimate the vapor pressure of refrigerant-oil mixtures, but some plots of vapor pressure versus weight percent of oil are available in the literature [7,14]. These plots show that the increase in liquid oil concentration at high quality markedly increases the local vapor pressure. Since pressure is approximately constant in a heat exchanger, the effect of this increase in vapor pressure is actually to increase the saturation temperature of the liquid mixture at the local pressure. In high quality regions of an evaporator, oil curtails heat transfer by reducing the temperature difference. In addition, small quantities of residual refrigerant remain in a liquid solution with the oil, reducing the capacity of heat exchangers.

Zimmermann [15,16] presented equations to convert vapor pressure versus oil concentration data into saturation temperature rise versus local vapor quality coordinates.

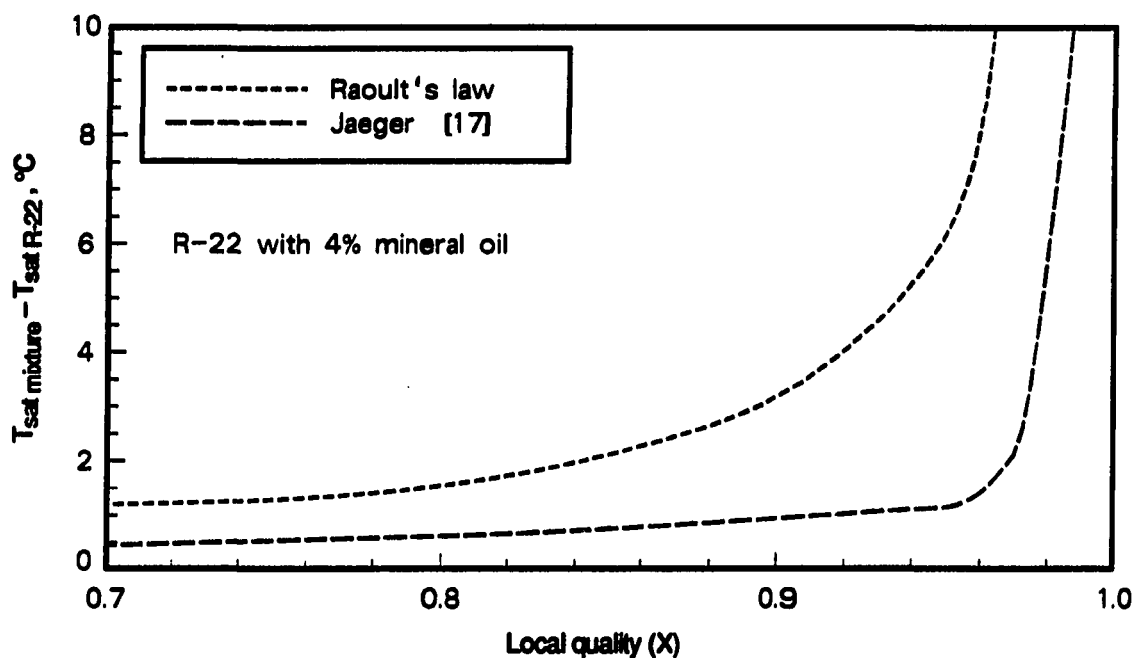


Figure 2.1. Saturation temperature of refrigerant-oil mixtures as a function of vapor quality [15,16]

Using a theoretical model and experimental data [17], Figure 2.1 shows how the saturation temperature of a refrigerant-oil mixture increases with increasing local quality, becoming very large as 100% quality is approached. According to these equations, 100% quality, in the usual sense, cannot be reached, but only approached asymptotically. Zimmermann assumed that the local oil concentration in the liquid increased solely according to the amount of refrigerant vaporized, with no additional increase caused by viscous effects, etc.

Because instrumentation was not available to measure local mixture temperatures inside the test section, an estimate of temperature based on pressure had to be made in the data analysis. The quality in the test section was limited to about 85% maximum to ensure that this estimate was sufficiently close to the actual temperature. The cutoff at 85% quality is before the rapid rise in mixture saturation temperature shown in Figure 2.1.

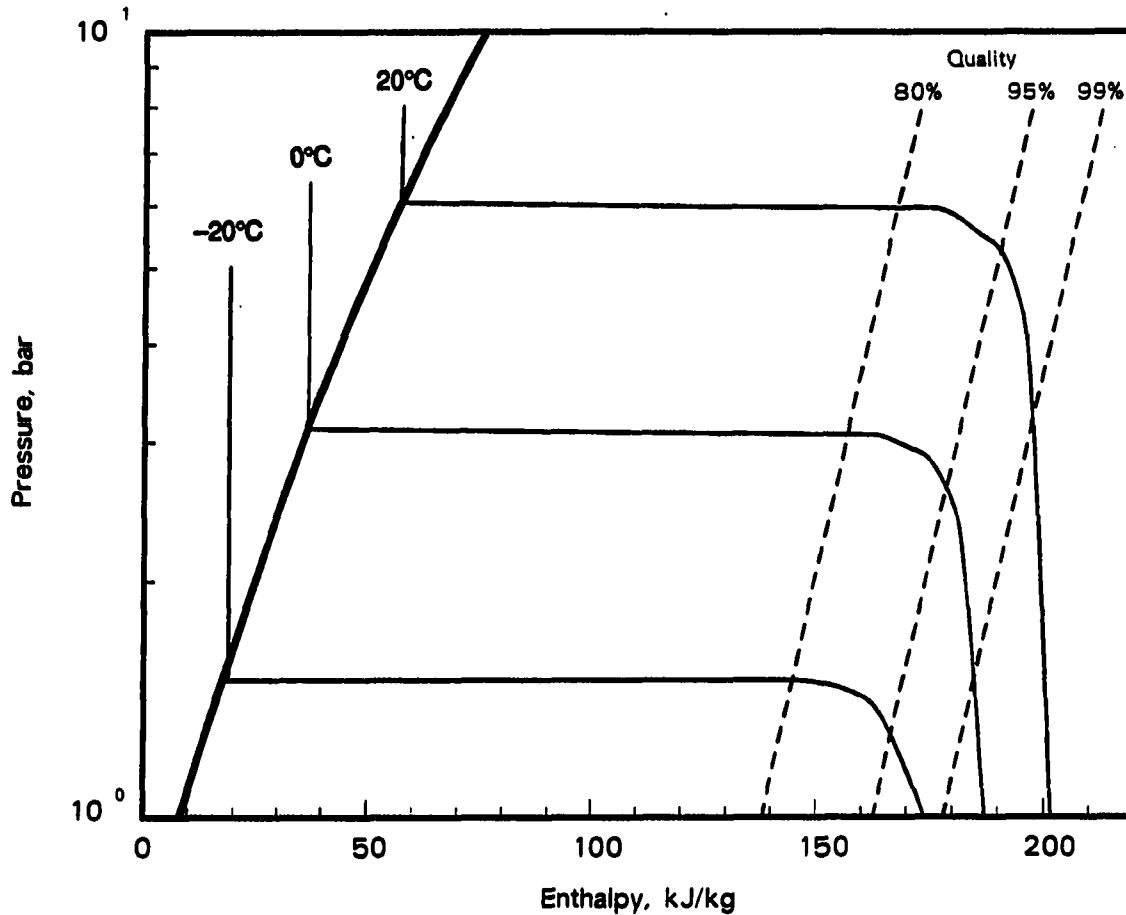


Figure 2.2. Pressure-enthalpy diagram for mixtures of R-12 and oil [13]

Enthalpy of Vaporization

The enthalpy of vaporization of refrigerant-oil mixtures is important in determining the vapor quality. If enthalpy of vaporization were to increase with the addition of oil, then the actual vapor quality would be somewhat lower than that calculated using an assumption of pure refrigerant.

No experimental data were located, but pressure-enthalpy curves for R-12 and oil from Hughes et al. [13] give an indication of expected trends. Figure 2.2 is a representation of one of these diagrams. It can immediately be seen that a vapor dome no longer exists, as is the case with pure substances. The right side of the dome becomes indistinct, i.e., there is no single 100% quality line. This supports the observation noted in the previous section

regarding an asymptotic approach to 100% quality. In physical terms, this means that even with temperatures far above pure refrigerant saturation temperatures, there is still some small quantity of refrigerant held in solution with the oil.

Although this figure illustrates once more the phenomenon discussed in the previous section, it does not show the local enthalpy of vaporization. The figure represents a batch process, that is, the evaporation of a quantity of refrigerant-oil mixture to a particular quality. It does not indicate the energy required to vaporize an infinitesimal amount of refrigerant when the liquid is at a particular oil concentration. This, however, is the information needed to accurately determine vapor quality in tests such as were run in this investigation.

Without data on enthalpy of vaporization as a function of oil concentration, and lacking the ability to determine the local oil concentration, it was assumed in this study that changes in the enthalpy of vaporization were negligible as oil was added to refrigerant.

Other Effects of Oil

In addition to the effects of oil on the properties discussed above, other properties of the oil can also affect the heat transfer and pressure drop. Examples of factors which may have an effect on heat transfer and pressure drop are additives in the oil and the age of the oil in the system. Additives include viscosity improvers, rust inhibitors, antifoam agents, dispersants, thermal stability enhancers, etc.

One additive that could reasonably be expected to affect heat transfer is an antifoam agent. These agents are added to inhibit foaming in the compressor. Because it has been hypothesized that some of the positive effects of oil on evaporation heat transfer can be attributed to foaming in the liquid mixture, these additives could have an impact on heat transfer results. Although additives may be important to fully describe the effects of oil, additives are different for each brand of oil and are often proprietary, making information difficult to obtain. This study did not attempt to include oil additives as a variable in the test matrix.

Some testing has indicated that the heat transfer performance of the refrigerant-oil mixture may depend on the age of the oil in the system [18]. In a smooth tube, there was

not a significant difference in the heat transfer performance, but in augmented tubes (a micro-fin tube and a tube with a star-shaped insert) the performance with a new oil was as much as 12% lower than the performance with an old oil. This performance difference was observed even though chemical analysis revealed no difference between the old and new oils.

CHAPTER 3
LITERATURE REVIEW OF TWO-PHASE REFRIGERANT
HEAT TRANSFER AND PRESSURE DROP EMPHASIZING
OIL EFFECTS AND IN-TUBE AUGMENTATION

No previous work was found on the combined effects of oil and augmentation inside tubes, so the literature review has been divided into two major categories: (1) effect of oil on evaporation and condensation inside smooth tubes and (2) evaporation and condensation of pure refrigerant inside augmented tubes. For completeness, pool boiling, vapor space condensation, and adiabatic pressure drop with refrigerant-oil mixtures were also reviewed. In general, this review has been limited to chlorofluorocarbon refrigerants (CFC's), although some references with ammonia have also been included.

Previous Literature Surveys

Green [2] published a brief review of refrigerant-oil mixture evaporation, dealing with flow inside tubes and pool boiling. Chaddock [19] surveyed the effects of oil on refrigerant evaporator performance in a paper dealing with mixture properties and two-phase flow patterns, as well as pool boiling and in-tube evaporation of refrigerant-oil mixtures. No similar surveys were found on the effect of oil in condensers, although Shah [20] briefly considers oil in a condensation review paper. Shah found no papers dealing with oil in CFC's, but he cited several studies with oil in ammonia.

Due to the lack of previous research on refrigerant-oil mixtures in augmented tubes, there have been no surveys on this topic. However, several surveys dealing with pure refrigerant evaporation and condensation in augmented tubes were found. Bergles [21] surveyed two-phase heat transfer enhancement, emphasizing refrigerants as the working fluid. Active and passive enhancement techniques were discussed as applied to pool boiling, vapor space condensation, flow boiling and in-tube condensation. Lazarek [22] reviewed in-tube heat transfer augmentation and pressure drop of two-phase refrigerant flows, limiting the discussion to passive enhancement techniques. His paper also reviewed several correlations.

Bergles et al. [23] published a comprehensive bibliography on augmentation of convective heat transfer, including studies of two-phase heat transfer with refrigerants.

Yoshida and Fujita [24] reviewed the literature for boiling heat transfer to CFC refrigerants. Included in this review were heat transfer augmentation and the influence of oil. Turaga and Guy [25] published a survey of estimation methods for refrigerant heat transfer and pressure drop. A section dealing with the effects of oil on refrigerant evaporation was included, but citations were quite limited.

The Effect of Oil on Refrigerant Heat Transfer and Pressure Drop In-Tube Evaporation

No studies were located dealing with refrigerant-oil mixtures in augmented tubes; hence, the discussion is limited to smooth tube evaporation.

Heat transfer For 40 years attempts have been made to determine the effects of oil on heat transfer processes in refrigeration systems. The main concern in the past has been with the evaporator. Published studies (limited to horizontal tubes) are summarized in Table 3.1.

Witzig et al. [26] added only 1% oil to the system and found heat transfer rates slightly lower than for pure refrigerants. Seigel et al. [27] reported no noticeable change in heat transfer for "small" amounts of oil. Oil concentration was qualitatively inferred from the color of the liquid as viewed through sight glasses. Yoder and Dodge [28] evaporated R-12 with 5.1% oil in a vertical tube, but had no pure refrigerant data for comparison.

Pierre [29] conducted several tests with oil concentration varying from 0% to 13% by volume. He found no influence of oil on the average heat transfer coefficients. It is possible, however, that the effect of the oil was lost in the scatter of the data.

The first comprehensive experiment with refrigerant-oil mixtures was that of Worsøe-Schmidt [30], who obtained local heat transfer coefficients. In all cases, an augmentation of heat transfer was observed at low qualities while heat transfer degradation occurred at high qualities. For 1.9% oil, a 50% increase in heat transfer coefficient was observed over most of the tube length. The average heat transfer coefficient decreased as oil concentration was increased further. The enhancement observed at low qualities decreased as the evaporating temperature was reduced.

Green and Furse [31] varied the average quality in a short test section by changing inlet quality. Trends were difficult to determine from the data presentation. It was implied that the average heat transfer coefficient for an evaporator was a maximum at 4% oil. Their cross-plot of the Worsøe-Schmidt [30] results suggested a maximum at 3% oil.

Deane [32] reported a decrease in average heat transfer coefficient of about 25% with 4% oil. These results contradict those of Worsøe-Schmidt [30] and Green and Furse [31] even though all three investigations used completely miscible refrigerant-oil mixtures.

Several comprehensive investigations since 1976 have further clarified the effects of miscible and immiscible mixtures of refrigerant and oil. Mathur [33] and Chaddock and Mathur [34] obtained results consistent with those of Worsøe-Schmidt [30]. A 1% oil concentration in R-22 resulted in a 20% to 30% increase in the heat transfer coefficient over most of the tube length. The maximum average heat transfer coefficient was found at an oil concentration between 1% and 2.9%.

Using the data from Chaddock and Mathur [34], Tichy et al. [35] developed a model for the evaporation and condensation of refrigerant-oil mixtures. Their model predicted trends correctly; magnitudes, however, were not predicted well.

Malek [36] found the heat transfer coefficient for R-12 and oil mixtures to be strongly dependent on heat flux. The heat transfer coefficient was increased by a maximum of 15% with 2% oil at a heat flux of 5 kW/m². However, decreases in the coefficient were observed for heat fluxes from 10 to 20 kW/m².

Hughes et al. [37] found mixture and oil-free heat transfer coefficients to be different, but the data are contradictory and difficult to interpret. Zimmermann [15,16] found that the average heat transfer coefficient for R-22 was increased by a maximum of about 10% at an oil concentration of 2%. His results were similar to those of Chaddock and Mathur [34].

Chaddock and Buzzard [38-40] investigated oil in both R-502 and ammonia (R-717). The R-502 experiments with 1% oil were in the completely miscible region and indicated no significant change in the heat transfer coefficients from those with pure refrigerant. For 2% and higher oil concentrations, the oil was only partially miscible and the heat transfer coefficients were 30% to 50% below those of oil-free refrigerant.

Table 3.1. Studies of refrigerant-oil mixture evaporation inside smooth, horizontal tubes

Researchers	Apparatus	Tube od (mm)	Refrigerant	Oil	Effect of oil on h
Witzig et al. [26]	Heat coil wrap Local h	9.52	R-12	0% - 1%	Slight decrease
Seigel et al. [27]	Average h	16.0	R-12	"small amount"	None observable
Pierre [29]	Average h	12.7, 19.0	R-12	0% - 13%	None
Worsøe-Schmidt [30]	Heat coil wrap Local h	16.0	R-12	Mineral 0% - 10%	Decrease at high X Increase at low X
Green and Furse [31]	Condensing vapor Avg. h for short test section	9.52	R-12	Mineral 0% - 7.8%	Max h at 4% oil
Deane [32]	Shell-and-tube Average h	?	R-11	Mineral 0% - 2.6%	Decrease
Chaddock and Mathur [19,33,34]	Direct elec heat Local h	9.52	R-22	Mineral 0% - 5.7%	Decrease at high X Increase at low X Max h at 1% - 2.9%
Chaddock and Buzzard [38,40]	Heat tape wrap Local h	9.52	R-502	Naphthenic 0% - 10% Part miscible	Decrease
Malek [36]	Water heating Average h	?	R-12	Mineral, 2 type 0% - 10%	Function of oil % and heat flux
Hughes et al. [37]	Water heating Sectional avg. h	16.0	R-12	Mineral 0% - 15%	Function of flow regime
Zimmermann [15,16]	Average h	16.0	R-22	Half synthetic 0% - 4%	Max h at 2% oil
Tichy et al. [41]	Water heating Local h	12.7	R-12	Naphthenic 0% - 5%	Increase at low X

Ammonia and mineral oil are immiscible and the heat transfer coefficients of ammonia and oil mixtures were 50% to 90% below those of oil-free ammonia.

The work of Tichy et al. [41] suggested a small increase in heat transfer with oil at low qualities. For most of the conditions reported, however, the heat transfer coefficient was decreased. A complicated correlation was also developed with different constants for each of the three oil concentrations investigated.

Pressure drop The addition of oil generally increases evaporator pressure drop, especially with immiscible refrigerant-oil mixtures. Shah [42] attributed the high pressure drop in immiscible mixtures to a reduction in flow area caused by a thick oil film held up in the evaporator.

For a mixture of R-22 and half synthetic oil, Chawla and Gauler [43] observed modest increases in pressure drop for 1% and 2% oil. Pierre [44] reported substantial increases in evaporator pressure drop with oil and developed friction factor correlations. Hughes et al. [37] reported a nearly linear relation of evaporator pressure drop to oil concentration with a pressure drop increase of about 50% as oil concentration approached 10%.

Hatada et al. [45] reported extensive measurements of pressure drop with R-22 and oil. The pressure drop increased with increasing oil concentration up to a maximum of about 40% at a concentration of 20%. Zimmermann [15,16] found that evaporation pressure drop with a 2% oil concentration increased as the heat flux increased, whereas pressure drop remained constant with increasing heat flux for pure refrigerant. Tichy et al. [46] reported increases in the frictional pressure gradient of over 80% with 5% oil in R-12. It was suggested that the effect was due to changes in the flow pattern, especially a promotion of annular rather than stratified annular flow.

In-Tube Condensation

As with evaporation, discussion is limited to the case of smooth tubes due to the lack of published research dealing with oil effects inside augmented tubes.

Heat transfer Compared to the research on evaporation, relatively little work has been done to assess the influence of oil on condenser performance. As mentioned earlier,

Tichy et al. [35] developed a model for condensing, as well as evaporating, refrigerant-oil mixtures. They relied on data from other investigators, so no original data were presented.

Tichy et al. [47] studied a single, water-cooled condenser tube with 2% or 5% oil added to R-12 immediately upstream of the condenser entrance. Relative to oil-free performance, 2% oil reduced the heat transfer coefficient by 10% while 5% oil reduced the coefficient by 23%. These effects were generally independent of local quality. It was suggested that the increased viscosity of the mixture dampens the molecular and turbulent transport in the condensate film. It appears that in-tube condensation heat transfer, unlike evaporation, is always degraded by the presence of oil in the refrigerant.

Pressure drop Tichy et al. [46] later reported on condensation pressure drop in their R-12 system. It was found that 2% oil increased the frictional pressure gradient by about 2% and 5% oil increased the gradient by only about 6%.

Pool Boiling

Plain surfaces Stephan and Mitrovic [48] reviewed the literature up till 1981 and found that published experimental results were partly contradictory. According to numerous studies conducted with miscible mixtures, the nucleate boiling heat transfer generally decreased with increasing oil concentration [11,49–52].

For certain conditions of pressure and heat flux, the heat transfer coefficient was found to increase at low oil concentrations. This was first reported by Stephan [50], who attributed the phenomenon to foaming. Burkhardt and Hahne [53] found a maximum heat transfer coefficient 10% to 15% above the oil-free value at a 4% oil concentration.

Sauer et al. [8] tested oils of three different viscosities in R-12. They found general enhancement of heat transfer for concentrations below 5% to 7% and also found that higher viscosity oil yielded a higher heat transfer coefficient at a given temperature difference. Chongrungreong and Sauer [54] developed correlations for refrigerant-oil mixture pool boiling on single, plain tubes. They found that heat transfer decreased with increasing oil concentration, but that the effects were less severe at higher pressures.

Hahne and Noworyta [55] also developed pool boiling correlations for refrigerant-oil mixtures. Their correlation required three adjustable constants which varied with the

particular refrigerant-oil combination used. Anikin et al. [56] developed a correlation for boiling of refrigerant-oil mixtures on tubes, based on the data of other investigators. They used the change in mixture oil concentration and saturation temperature in the diffusion layer as defining characteristics for the heat transfer. Their semi-empirical formula correlated the experimental data within $\pm 20\%$.

Jensen [57] found that oil in refrigerant increased the peak nucleate boiling heat flux. The maximum increase was 90% with 18% oil in R-113, however the increased peak heat flux was accompanied by a large increase in wall superheat.

An experimental program with mixtures of oil and R-113 was carried out by Yamazaki and Sakaguchi [58]. Their results showed that oil degraded heat transfer at all concentrations and that the degradation became more severe at higher heat fluxes. Wall superheat was also found to increase with increasing oil concentrations.

Monde and Hahne [59] boiled mixtures of oil with R-11 and R-115 from a fine wire. With R-115, in which oil has limited solubility, they found that above a critical heat flux, the heat transfer coefficient decreased with increasing heat flux. With R-11, the effect of oil depended on the system pressure. At a pressure of 2 bar, oil enhanced heat transfer for concentrations below 3%, but degraded heat transfer for all concentrations at pressures of 1 or 5 bar. Oil type influenced the intensity of the oil's effect on the boiling heat transfer.

In a paper dealing with the effect of an electric field on boiling heat transfer of R-11, Kawahira et al. [60] also did tests with 2% oil, as well as pure refrigerant. They found that the application of an electric field caused refrigerant-oil mixture performance to generally be equal to that of pure R-11. A positive DC voltage was found to enhance the heat transfer of the refrigerant-oil mixture relative to pure refrigerant.

Bell et al. [61] tested smooth and finned tubes with mixture concentrations of up to 10% oil in R-113. With smooth tubes, oil was found to always degrade heat transfer, but the degradation was relatively small for concentrations under 5%. In general, the degradation was higher at higher heat fluxes. With 5% oil, the heat transfer coefficient decreased by as much as 25% while with 10% oil, it decreased by up to 50%.

Augmented surfaces Sauer et al. [62] tested finned tubing with several types of oil in R-11. Heat transfer increased marginally at low oil concentrations and degraded at higher concentrations. Heat transfer degradation became larger as the oil concentration increased to 10%. Plain tubes showed a similar heat transfer degradation, so finned tubes still outperformed plain tubes.

Stephan and Mitrovic [49,63] reported on tests with a bundle of seven tubes with T-shaped fins, three of which were heated and instrumented. The behavior was similar to pool boiling from a single, plain tube. The heat transfer coefficient peaked at an oil concentration between 2% and 5% and degraded with higher oil concentrations. Arai et al. [64] tested bent-over profiled-fin (tunnel and pore) tubes in a flooded evaporator. Up to 3.4% oil was dissolved in R-12 and the performance generally increased at low heat flux. This was attributed to intense foaming. At high heat fluxes, normal pool boiling dominated. Although clogging of the tunnels was expected, there was no evidence of such behavior.

Czikk et al. [65] found no effect with 2% oil in R-11 on a porous surface of sintered metal powder, but speculated that such surfaces might not be suitable with immiscible mixtures. Reilly [66] and Wanniarachchi et al. [67] boiled a mixture of oil and R-114 from a porous coated tube. The presence of 3% oil reduced the heat transfer coefficient by 35% at all heat fluxes. With 6% or more oil, the coefficient was reduced sharply as heat flux increased to higher levels. This behavior was attributed to the creation of an oil-rich mixture within the porous structure.

Bell et al. [61], mentioned earlier, used a 22.2-mm root diameter finned tube with 3.2-mm fins in mixtures of oil and R-113. The effect of oil on the heat transfer coefficient with the finned tube was found to be quite complex and depended on the temperature difference. At some temperature differences, the heat transfer coefficient increased with increasing oil concentration, while at other temperature differences, the coefficient decreased.

All of the augmented tubes discussed above showed heat transfer coefficients significantly better than those of plain tubes under similar conditions. There is a consensus that augmented tubes can be successfully used in flooded evaporators with refrigerant-oil mixtures and that advanced structured surfaces are more effective than simple, finned tubes.

Vapor Space Condensation

Plain surfaces Several studies have investigated the effects of oil carry-over from the compressor into the condenser, usually by spraying a refrigerant-oil mixture onto the condenser surface. Williams and Sauer [68] reported oil concentrations below 7% had no significant effect, whereas Wang et al. [69,70], reporting on R-12 and R-22 with up to 8% oil, found a reduction in the condensing coefficient at all oil concentrations. The reduction was reported to be 2% to 3% for each 2% increase in the oil concentration.

Abdulmanov and Mirmov [71] found that an unspecified amount of oil in ammonia increased the condensing coefficient by about 40%. No explanation was provided for this surprising behavior.

Augmented surfaces For Sauer and Williams [72], heat transfer performance did not significantly degrade when an atomized oil mist was sprayed on a finned-tube R-11 condenser. They noted that the fins forced the oil droplets into the valleys where they mixed with refrigerant, leaving the tips free of excessive oil.

Adiabatic Transport and Pressure Drop

Riedle et al. [73] carried out an extensive program to determine the transport and pressure drop characteristics of refrigerant-oil mixtures in compressor suction and discharge lines. In both cases, a two-phase flow was present, with pure refrigerant in the vapor phase and oil with dissolved refrigerant in the liquid phase. Pressure drop increased relative to pure vapor flow. Information on oil accumulation in component piping was also obtained.

Scheideman and Macken [74] found that the Lockhart and Martinelli [75] relation correlated pressure drop data for R-12 and a naphthenic oil flowing in horizontal tubes. Scheideman et al. [76] included R-22 and developed more refined correlations, as well as extending the previous R-12 work to include vertical flow. Macken et al. [77] presented design tables for pressure drop and liquid transport based on the earlier correlations.

Yanagisawa and Shimizu [78] investigated the flow characteristics of refrigerant-oil mixtures in a 62 μm -diameter channel. They found that the pressure drop in the channel became larger as the flow progressed due to disassociation of refrigerant vapor from the oil.

System Performance

Downing [79] published an estimate of the overall system performance degradation with an unspecified oil in a system using R-12. He estimated that total performance would fall by slightly less than 1% for each 1% increase in oil concentration.

McMullan [80] and Hughes et al. [81] reported system performance studies for heat pumps. They determined that heat transfer degradation, increased pressure drop, elevation of the boiling point, and reduction of the latent heat capacity can combine to degrade system performance by as much as 30%. McMullan et al. [82,83] reported on the construction and initial results of a new facility to investigate the effects of oil on R-12 system performance. The maximum coefficient of performance (COP) for the system fell by about 15% as oil concentration increased to 6.4%. The maximum COP tended to occur at higher superheat with the addition of oil. Evaporator pressure drop was found to double with the addition of about 2% oil and triple when the oil concentration reached about 8%. This work suggested the possibility of both evaporator and condenser acting as a heat rejector in the extreme case of very high (~25%) oil concentration and very low (~3°C) superheat.

Reporting on actual field experience with oil separators in ammonia refrigeration plants, Koster [84] reported an overall increase in the COP of about 6%. It was noted that the negative effects of oil on the performance of an ammonia plant could be as much as 30%, but the total improvement achieved with the oil separator was less than this due to increased pressure losses in the separator.

In-Tube Augmentation of Two-Phase Refrigerant Heat Transfer

Passive augmentation techniques can be classified as treated surfaces, rough surfaces, extended surfaces, displaced enhancement devices, and swirl flow devices [23]. Figure 3.1 shows examples in each of these categories; Tables 3.2 and 3.3 at the end of the chapter summarize in-tube augmentation studies with refrigerants. Emphasis is placed on work with the types of tubes used in this project (micro-fin and low-fin tubes) but other types are discussed. Tables 3.4 and 3.5 at the end of the chapter are more detailed summaries of previous research using micro-fin or low-fin tubes for refrigerant evaporation or condensation. Papers are discussed in approximately chronological order. Unless noted

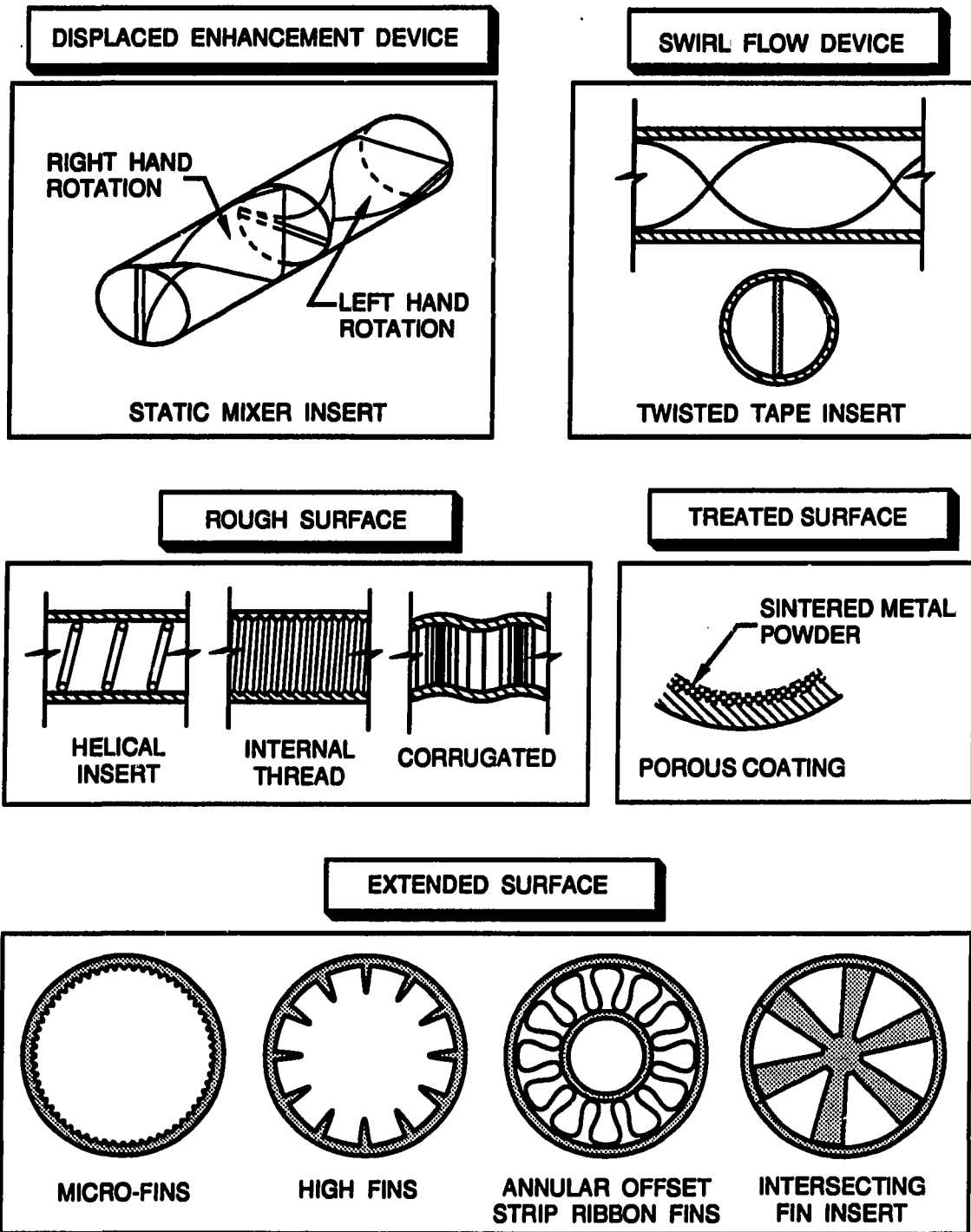


Figure 3.1. Examples of passive enhancement techniques

otherwise, the enhancement reported in the following sections is relative to a plain tube with an inside diameter equal to the characteristic diameter of the augmented tube (the maximum inside diameter for finned tubes). Mass flux, quality range, and pressure are held constant. Tubes are generally classified and sized by the outside diameter and are so listed.

Refrigerant-Oil Mixtures

No systematic studies of the effects of oil on in-tube augmentation of refrigerant heat transfer were found. Reisbig [85] used oil separators to minimize oil content while condensing R-12 in internally finned tubes and made no measurements of oil concentration. Kubanek and Miletti [86,87] also used an oil separator and measured an oil concentration of 0.1% during their R-22 evaporation tests inside finned tubes. They concluded that such low concentrations of oil had no measurable effect on heat transfer and pressure drop. Numerous other studies have used compressors with oil separators [88-90], but no oil concentration measurements have been reported. Tests using oil separators are classified as pure refrigerant tests for purposes of this discussion.

Evaporation

Treated surfaces Ikeuchi et al. [91] reported on the evaporation of R-22 in two tubes with internal porous coatings. One of the tubes had the inside tube wall coated with copper powder and the other tube had a smooth inner surface, but with a porous-coated, thin plate inserted. The coated tube had a heat transfer coefficient approximately 7.5 times as large as that of a smooth tube for incomplete evaporation and 2.6 times as large for complete evaporation. For the tube with a porous fin, the heat transfer coefficient increased by factors of 1.7 and 1.3 for incomplete and complete evaporation, respectively.

Rough surfaces Early work in evaporative augmentation utilized helical spring inserts in smooth tubes. Larson et al. [92] were the first to publish results of augmented refrigerant evaporation inside tubes. They used R-12 and found a doubling of heat transfer and an "appreciable" increase in pressure drop. Bryan and Quaint [93] found no enhancement in their R-11 tests, probably due to an unfortunate choice of spring dimensions. Bryan and Seigel [94], also using R-11, parametrically varied spring dimensions and found that heat transfer increased by a factor of two at optimum spring

parameters. Flow visualization in this study indicated that the upper surface of the tube remained wetted for flow conditions that would normally have led to stratified flow in smooth tubes.

Withers and Habdas [95] found that the heat transfer coefficient of R-12 boiling in corrugated tubes increased by up to 100% when compared to a plain tube. They also reported a two- to fourfold increase in the friction factor. Kawai and Machiyama [96] tested R-12 and Kawai and Yamada [97] tested both R-12 and R-22 in corrugated tubes. They concluded that these tubes were superior to an inner-fin tube used for comparison. Heat transfer was enhanced by a factor of two.

With R-113 in a vertical, annular duct, Danilova et al. [98] used wire and fiberglass on a heated central tube to create roughness. They reported heat transfer enhancement factors of 1.2 to 2. Dembi et al. [99] placed wire mesh flush on the inside diameter of an R-22 evaporator. Mesh size and flow conditions affected the enhancement factor, which was as high as 1.8 in some cases.

In an investigation of flow instabilities, Menten et al. [100,101] used R-12 in threaded tubes, in a tube with a helical wire insert, and in tubes with porous coatings. Pressures, temperatures, and photographic observations of the flow patterns were reported.

Extended surfaces Extended surfaces, which include fins of all types, have long been used to enhance heat transfer. Historically, the trend has generally been toward lower fins, with the popularity of the micro-fin tube currently high. Due to the number of publications reporting on micro-fin tubes, these papers are reported in a separate section after other extended surface publications are discussed.

Boling et al. [88] reported on evaporation of R-12 in annuli with offset strip ribbon fins. A threefold increase in boiling heat transfer coefficient based on internal area was achieved. Pressure drop was reported but not compared to a comparable smooth tube. Using the same type of tube, Ditzler [102] investigated evaporation of R-12 and R-22. He emphasized correlation expressions, so no comparison with smooth tubes was presented.

Lavin and Young [103] tested tubes with internal threads, axial fins, spiral fins, and cruciform fins with R-12 and R-22. Their study was primarily concerned with flow

regimes, but they reported that the cruciform tube had a Nusselt number over twice that of a plain tube.

Schlünder and Chawla [104] used various axial fin inserts with R-11. Heat transfer was enhanced for all finned tubes, ranging from only nominal to approximately fourfold. D'Yachkov [105] investigated tubes with similar inserts using R-22. He made no comparisons with smooth tubes, but reported flow pattern observations.

Using R-22, Kubanek and Miletti [86,87] investigated evaporation performance inside a variety of finned tubes. Increases in the heat transfer coefficient ranged from a factor of 1.3 to 7.6, while pressure drop increased by a factor 1.1 to over a factor of 20. Kikkawa et al. [106] studied evaporation and condensation of R-12 and R-22 in tubes with circumferential ribs but reported no comparisons with smooth tubes.

Malek and Colin [107] reported on results using horizontal tubes with star-shaped inserts and also tubes with a flattened profile. At low heat fluxes, heat transfer was enhanced by about 400% and the enhancement decreased as the heat flux increased. No pressure drop data were presented.

Sivakumar [108] and Azer and Sivakumar [109] boiled R-113 in vertically oriented, straight and spirally finned tubes. Heat transfer coefficient enhancement as high as 146% was obtained, while pressure drop increased by about a factor of 2.0.

Using a fluted tube formed by welding a bias-wrapped, grooved strip of aluminum, Panchal et al. [110] found heat transfer enhancement of more than a factor of 2.0 in addition to an area enhancement of 1.6. This results in an enhancement factor based on a smooth tube area of over 3.0. The refrigerants were R-11 and R-114 and flowed vertically upward in the tube. No pressure drop data were reported.

Reid et al. [111] reported on the evaporation of R-113 inside four inner-fin tubes having straight and spiral fins, as well as in two other types of augmented tubes. The higher finned tubes had heat transfer enhancement factors varying from about 1.3 to 2.5 and pressure drop factors ranging from about 1.5 to nearly 3.0.

Micro-fin tubes Since 1977, so-called micro-fin tubes have been emphasized in research and, more recently, they have been introduced in commercial equipment. Micro-

fin tubes are defined as tubes having a large number (usually more than 50) of very small fins. The fin height is less than 2.5% of the inside diameter.

Ito et al. [112] used R-22 and varied spiral pitch and fin height. The optimum pitch angle was found to be 10° and the pressure drop increase remained minimal if fins were lower than 0.2 mm. Heat transfer was increased by as much as a factor of 2.0. Ito and Kimura [113] refined the earlier work and found an optimum spiral angle of 7° . Extending the work to R-12, Kimura and Ito [114] found an optimum spiral angle of 15° . In the annular flow region, heat transfer was enhanced by a factor of 2.0, but in the stratified flow regime, augmentation was almost an order of magnitude. Pressure drop was not reported.

In a general summary paper based on previously acquired data, Tatsumi et al. [115] reported on the performance of a particular 7° -spiral micro-fin tube used in Japan. Their R-22 data showed augmentation by up to a factor of 2.0. A pressure drop penalty was not discernable from plots presented.

Tojo et al. [90], who investigated both evaporation and condensation, reported evaporation results with spiral micro-fin tubes very similar to those of earlier investigators. For R-22, they found up to twice the heat transfer of plain tubes and a pressure drop penalty factor ranging from 1.1 to 1.3.

Shinohara and Tobe [116], also reporting on both evaporation and condensation, used tubes of three different diameters. Heat transfer enhancement factors of 1.7 to 2.5 were reported with R-22. The pressure drop factor was about 1.05. Uekusa et al. [117] found heat transfer coefficients to be a function of mean liquid velocity and local heat transfer coefficients were not a function of local quality from 20% to 80% quality.

Using an unspecified refrigerant, Aoki et al. [118] compared a production micro-fin tube to prototype tubes having fewer fins and a wider groove bottom. One prototype had heat transfer almost twice that of the baseline micro-fin tube, but no performance data for the baseline tube was given. Pressure drop was about 8% higher than the baseline tube.

Khanpara [119] and Khanpara et al. [120-122] published results from an extensive investigation attempting to optimize micro-fin geometry. Evaporation was investigated with R-113 and R-22 in both electrically and fluid heated tubes. With R-113, heat transfer enhancement factors of 1.2 to 2.7 were found, with heat transfer coefficients relatively

independent of local quality. The lowest pressure drop factors were generally between 1.1 and 1.5, although some penalty factors of over 3.0 were reported. The optimum tube from R-113 testing was also tested with R-22. Again, heat transfer was relatively independent of local quality but the heat transfer enhancement factors with R-22 were somewhat lower, from 1.1 to 1.9 for direct electrical heating and 1.1 to 1.3 for fluid heating. Pressure drop penalties with R-22 were not discussed.

Micro-fin tube results from the previously mentioned paper of Reid et al. [111] showed heat transfer enhanced by a factor of about 1.6, with a corresponding pressure drop factor of about 1.5. The refrigerant used was R-113.

Displaced enhancement devices Fan et al. [123] found heat transfer increased by nearly an order of magnitude using in-line static mixers and R-113. Pressure drop also increased substantially, but not as much as pressure drop. Additionally, the mixers had a stabilizing influence on the flow in the sense that they helped prevent the transition from the homogeneous regime to the annular regime. Lin [124] and Azer et al. [125] reported further work with static mixers. Their tests varied the arrangement of the mixers and extended the conditions to subcooled nucleate boiling.

Swirl flow devices Consisting of a thin metal strip twisted into a spiral, twisted-tape inserts to enhance evaporative heat transfer have been investigated for over 20 years. Blatt and Adt [89] evaporated water and R-11 in tubes with twisted tapes. The performance varied with fluid, heat flux, and temperature. For R-11, higher heat transfer was obtained with swirl, accompanied by higher pressure drops. Heat transfer was enhanced by up to a factor of 2.0 at a given temperature difference.

Agrawal et al. [126–130] investigated boiling R-12 in swirl flow. They found heat transfer to be strongly dependent on heat flux and twist ratio. Enhancement was not compared to a plain tube. Heat transfer and pressure drop were found to increase with a "tighter" spiral.

In related papers, Bensler [131], Jensen et al. [132], and Jensen and Bensler [133] investigated saturated boiling of R-113 using twisted-tape inserts. Heat transfer was found to approximately double at some conditions with pressure drops from 1.2 to 3.5 times the plain tube pressure drop.

Reid et al. [111] reported evaporation results for a smooth tube with a twisted-tape insert. Heat transfer was enhanced by approximately a factor of 1.5 for a broad range of qualities. Pressure drop, on the other hand, was over twice as high with the twisted tape than in a plain tube.

Condensation

Rough surfaces Bergles, [21], Luu [134], and Luu and Bergles [135,136] reported on condensation of R-113 in spirally fluted tubes and tubes with repeated-rib roughness. Spirally fluted tubes increased both heat transfer and pressure drop by about a factor of 1.5, while repeated-rib roughness increased heat transfer by up to a factor of 1.8 with only a moderate pressure drop increase.

Extended surfaces Reisbig [85] investigated R-12 condensation inside splined (axially finned) tubes. When superheated vapor entered the condenser, he found only a small change in the heat transfer coefficient based on smooth tube area. For wet vapor, however, the heat transfer coefficient increased by up to an order of magnitude, especially at higher temperature differences.

Vrable [137] and Vrable et al. [138] found only a small increase in heat transfer coefficient based on actual area for internally finned tubes, but overall performance was greater due to the increased area of the finned tubes. They combined experimental with analytical work and also investigated flow regime models.

Investigating the inclination of internally finned condenser tubes, Kröger [139] reported performance improvements of 15% for a prototype R-12 condenser when compared to a commercial, air-cooled condenser.

Luu and Bergles [135,140,141] and Luu [134] found that the best internally finned tubes in their study increased heat transfer coefficients by over a factor of 2.0 with only a modest increase in pressure drop. They used R-113 as the working fluid.

Azer and Said [142,143] and Said [144] used four different geometries of internally finned tubes and found heat transfer enhancement factors as high as 1.5 with only a small increase in pressure drop. The test fluid was R-113. Venkatesh [145] and Venkatesh and Azer [146] condensed R-11 in tubes of varying diameter with straight or spiral fins.

Augmentation of the heat transfer coefficient by a factor of 1.55 was obtained while total pressure drop approximately doubled. Azer and Kaushik [147] investigated heat transfer in doubly augmented tubes. Inside heat transfer was augmented by a factor of 1.55 with spiral fins, while pressure drop increased by about a factor of 3.0.

Micro-fin tubes Mori and Nakayama [148] looked at several different spiral micro-fin tubes in R-113 condenser applications. For the best geometry tested, the heat transfer coefficient increased by a factor of 2.0 with only a minor pressure drop increase.

In papers already mentioned in the evaporation discussion [90,115,116], condensation results for spiral micro-fin tubes were also reported. Tatsumi et al. reported enhancement of R-22 condensation by a factor of 1.6 to 2, similar to their evaporation results. Tojo et al., also using R-22, reported a condensation coefficient 1.6 times higher than smooth tubes with only a slight increase in pressure drop. For Shinohara and Tobe, the condensation heat transfer enhancement factor lay between 1.2 and 2.4 with a pressure drop factor of 1.05.

Condensation heat transfer coefficients in prototype micro-fin tubes test by Aoki et al. [118] were found to be up to 2.3 times of the coefficient in a production micro-fin tube. Pressure drop increased by a factor of 1.08 when compared to the same production tube. The refrigerant was not specified.

Khanpara [119] and Khanpara et al. [149] tested the condensing performance of several micro-fin tubes with both R-22 and R-113. With R-113, heat transfer was enhanced by as much as 3.8 times for some conditions, but the enhancement factor was more typically in the range of 2.0 to 2.2 for the better tubes. The pressure drop factor was generally in the range of 1.2 to 1.5 and was, in most cases, less than the corresponding heat transfer enhancement factor. Some pressure drop factors as high as 3.2 were reported. With R-22, only the optimal tube from the R-113 study was tested. Heat transfer enhancement factors were 1.6 to 1.8 and no pressure drop data were reported.

Displaced enhancement devices In a series of publications, all reporting on results with R-113 in the same test facility, Lin [124], Azer et al. [150], and Lin et al. [151] gave results for condensation with static mixer inserts. The mixers always increased heat transfer coefficients, but the increase was strongly dependent on Reynolds number. The maximum

heat transfer enhancement of 85% was accompanied by a significant increase in pressure drop.

Swirl flow devices A study of R-113 condensation using twisted-tape augmentation was reported by Luu and Bergles [140,141] and Luu [134]. Heat transfer coefficients increased by a factor of 1.3 compared to plain tubes, while pressure drop increased by a much larger factor of 3.5. Flow pattern observations and correlations were also reported.

Azer and Said [142,143,152], Said and Azer [153], and Said [144] also used R-113 in tubes with twisted tapes. Twisted tapes enhanced the heat transfer coefficient by as much as 23% relative to smooth tube results and pressure drop increased significantly. An correlation was developed that predicted heat transfer coefficients within $\pm 30\%$ of experimental values.

Summary

The literature reveals that oil does affect the physical properties of refrigerants and that these property changes can in turn affect the heat transfer and pressure drop performance in smooth tubes. There is a considerable body of literature reporting on results with refrigerants inside augmented tubes of various types, but none of these studies have included oil in the test matrix. The current research is the first attempt to systematically investigate the effects of oil on refrigerant heat transfer and pressure drop inside augmented tubes.

Table 3.2. Studies of the in-tube augmentation of refrigerant evaporation

Technique	Researchers	Description	Refrigerant
Treated surface	Mentes et al. [100,101]	Porous coating	R-11
	Ikeuchi et al. [91]	Porous coating	R-22
Rough surface	Larson et al. [92]	Helical wire insert	R-12
	Bryan et al. [93,94]	Helical wire insert	R-11
	Withers and Habdas [95]	Corrugated tube	R-12
	Kawai and Machiyama [96]	Corrugated tube	R-12
	Kawai and Yamada [97]	Corrugated tube	R-12,R-22
	Danilova et al. [98]	Wire and fiberglass	R-113
	Dembi et al. [99]	Wire screen	R-22
Mentes et al. [100,101]	Internal thread	R-11	
Extended surface	Boling et al. [88]	Ribbon annular fin	R-12
	Ditzler [102]	Ribbon annular fin	R-12,R-22
	Lavin and Young [103]	Axial/spiral fins	R-12,R-22
	Schlünder and Chawla [104]	Intersecting fins	R-11
	Kikkawa et al. [106]	Circum. fins	R-12,R-22
	Kubanek and Miletti [86,87]	Internal fins	R-22
	Ito, Kimura & Senshu [112-114]	Spiral micro-fin	R-22
	D'Yachkov [105]	Intersecting fins	R-22
	Tatsumi et al. [115]	Spiral micro-fin	R-22
	Azer and Sivakumar [108,109]	Straight/spiral fins	R-113
	Malek and Colin [107]	Intersecting fins	R-12
	Tojo et al. [90]	Spiral micro-fin	R-22
	Shinohara and Tobe [116]	Spiral micro-fin	R-22
	Uekusa et al. [117]	Spiral micro-fin	R-22
	Aoki et al. [118]	Spiral micro-fin	?
	Khanpara et al. [119-122]	Spiral micro-fin	R-22,R-113
Panchal et al. [110]	Spirally fluted	R-11,R-114	
Reid et al. [111]	Micro-fin and low-fin	R-113	
Displaced enhance. device	Azer, Lin, and Fan [123-125]	Static mixer insert	R-113
	Mentes et al. [100,101]	Helical wire insert	R-11
Swirl flow device	Blatt and Adt [89]	Twisted tape	R-11
	Agrawal et al. [126-130]	Twisted tape	R-12
	Jensen et al. [131-133]	Twisted tape	R-113
	Reid et al. [111]	Twisted tape	R-113

Table 3.3. Studies of the in-tube augmentation of refrigerant condensation

Technique	Researchers	Description	Refrigerant
Rough surface	Kawai and Machiyama [96]	Corrugated tube	R-12
	Luu and Bergles [134-136]	Repeated-rib roughness and spirally fluted	R-113
	Bergles [21]	Spirally fluted	R-113
Extended surface	Reisbig [85]	Splined tube	R-12
	Vrable et al. [137,138]	Axial fins	R-12
	Kikkawa et al. [106]	Circum. ribs	R-12, R-22
	Kröger [139]	Internal fins	R-12
	Luu and Bergles [134,135,140,141]	Internal fins	R-113
	Azer and Said [142-144]	Internal fins	R-113
	Tatsumi et al. [115]	Spiral micro-fin	R-22
	Mori and Nakayama [148]	Spiral micro-fin	R-113
	Tojo et al. [90]	Spiral micro-fin	R-22
	Venkatesh and Azer [145,146]	Spiral fins	R-11
	Shinohara and Tobe [116]	Spiral micro-fin	R-22
	Aoki et al. [118]	Spiral micro-fin	?
Khanpara et al. [119,149]	Spiral micro-fin	R-22,R-113	
Azer and Kaushik [147]	Spiral fins	R-113	
Displaced enhance. device	Azer, Lin, and Fan [124,150,151]	Static mixer insert	R-113
Swirl flow device	Luu and Bergles [134,135,140,141]	Twisted tape	R-113
	Azer and Said [144,152,153]	Twisted tape	R-113

Table 3.4. Evaporation of chlorofluorocarbon refrigerants in micro-fin and low-fin tubes

MICRO-FIN TUBES							
Researchers	Tube d_o (mm)	Refrigerant	h	Quality (%)	f/ d_i (%)	ϵ_{max}^a	Parameters varied b
Ito et al. [112]	12.7	R-22	avg.	?	0.4-3.5	2.0	β , f, G
Ito and Kimura [113]	12.7	R-22	local	25-90	0.4-3.5	2.0	p, β , f, G, q
Kimura and Ito [114]	6.35	R-12	local	55	2.0	2.0	β , G, q
Tatsumi et al. [115]	9.52	R-22	avg.	25-95	1.4-1.8	2.1	n, β , f, G
Tojo et al. [90]	9.52	R-22	avg.	?	2.0-2.6	2.0	n, β , f, G
Shinohara and Tobe [116]	9.52	R-22	avg.	$\bar{X}=60$	1.3-2.7	2.5	n, β , s, f, G
Aoki et al. [118]	9.52	?	avg.	$\bar{X}=50$?	>2.0	n, p, s, f
Khanpara et al. [120]	9.52	R-113	local	15-85	1.1-2.5	2.0	n, p, β , s, f, G
Khanpara et al. [121]	9.52	R-113	avg./local	10-90	1.1-2.5	2.7	n, p, β , s, f, G, q
Khanpara et al. [122]	9.52	R-22, R-113	local	5-75	1.1-2.5	2.2	G, q

LOW-FIN TUBES							
Researchers	Tube d_o (mm)	Refrigerant	h	Quality (%)	f/ d_i (%)	ϵ_{max}^a	Parameters varied b
Lavin and Young [103]	19.0	R-12, R-22	local	17-100	15.	≈ 1.8	β
Kubanek and Miletti [86,87]	12.7, 15.9	R-22	avg.	20-90	4.0	≈ 7	n, p, β , f, G, q
Azer and Sivakumar [108,109]	15.9, 22.2	R-113	avg.	0-80	4.7-9.7	1.5	n, p, β , f, G, q
Reid et al. [111]	9.52	R-113	local	0-70	4.0-5.0	1.9	n, β , f, G, q

a Maximum reported heat transfer enhancement factor, $\epsilon_{a/s}$.

b_n = number of fins

β = spiral angle

f = fin height

q = heat flux

p = pitch of fins

s = fin shape

G = mass flux

Table 3.5. Condensation of chlorofluorocarbon refrigerants in micro-fin and low-fin tubes

MICRO-FIN TUBES							
Researchers	Tube d_o (mm)	Refrigerant	h	Quality ^a (%)	f/d_i (%)	ϵ_{max} ^b	Parameters varied ^c
Tatsumi et al. [115]	9.52	R-22	avg.	75-10	1.4-1.8	1.8	n, β, f, G
Mori and Nakayama [148]	25.4	R-113	avg./local	80-20	1.0-2.0	2.0	p, s, f, G
Tojo et al. [90]	9.52	R-22	avg.	?	2.0-2.6	1.6	n, β, f, G
Shinohara and Tobe [116]	9.52	R-22	avg.	100+ - ?	1.3-2.7	2.4	n, β, s, f, G
Aoki et al. [118]	9.52	?	avg.	$\bar{X}=50$?	>2.3	n, p, s, f
Khanpara et al. [149]	9.52	R-113	local	80-20	1.1-2.5	2.2	n, p, β, s, f, G

LOW-FIN TUBES							
Researchers	Tube d_o (mm)	Refrigerant	h	Quality ^a (%)	f/d_i (%)	ϵ_{max} ^b	Parameters varied ^c
Luu and Bergles [134,135,140,141]	32.5, 40.4	R-113	avg.	100+ - <0	4.0-15.	2.2	n, f, G, q
Azer and Said [142-144]	40.4, 67.6	R-113	avg.	100+ - <0	8.0-11.	1.5	n, p, β, f, G
Venkatesh and Azer [145,146]	40.4	R-11	avg.	100+ - <0	8.0-11.	1.6	n, p, β, f, G
Azer and Kaushik [147]	15.7-19.1	R-113	avg.	100+ - <0	3.0-5.0	1.6	n, p, f, G

^a100+ indicates superheated inlet; <0 indicates subcooled outlet.

^bMaximum reported heat transfer enhancement factor, $\epsilon_{a/s}$.

^c n = number of fins

β = spiral angle

f = fin height

q = heat flux

p = pitch of fins

s = fin shape

G = mass flux

CHAPTER 4 TEST FACILITY

The flow loop was designed specifically for measuring in-tube heat transfer coefficients. The original rig was constructed by Khanpara for use with pure R-22 [119]. Although several modifications were made to accommodate oil injection, sample removal, and an investigation of hold-up in the test section, the major components in the test apparatus remained unchanged.

Flow Loop Components

The test rig consisted of three major flow loops: (1) a refrigerant flow loop containing the test section, (2) a loop circulating water with which the refrigerant in the test section was heated or cooled, and (3) a water and glycol loop, cooled by a commercial refrigeration unit, which condensed and subcooled the refrigerant leaving the test section. A schematic diagram of the test rig is shown in Figure 4.1. The schematic shows not only the components in the flow rig, but also the location of the instrumentation. Flow loop components are described in the following paragraphs, while instrumentation is presented in a later section. Table A.1 of Appendix A gives the manufacturer and model number for each major component and Appendix B discusses procedures for the operation of the test facility.

Refrigerant Loop

The flow loop was primarily constructed of 12.7-mm outside diameter copper tubing and insulated with flexible foam to minimize heat loss or gain. The test section had an outside diameter of 9.52 mm. Sight glasses were installed at various locations in order to visually monitor the flow conditions, but the inside diameter of the sight glasses was larger than that of the test section (approximately 12 mm versus 8 mm), so flow regime observations were not made. The loop was designed with no reservoirs or obstructions that might cause local oil hold-up.

Pump The refrigerant was circulated by a positive displacement diaphragm pump. By using this type of pump, no oil was introduced into the flow, as would occur with a compressor. The pump was run at constant speed; flow was varied by means of throttle

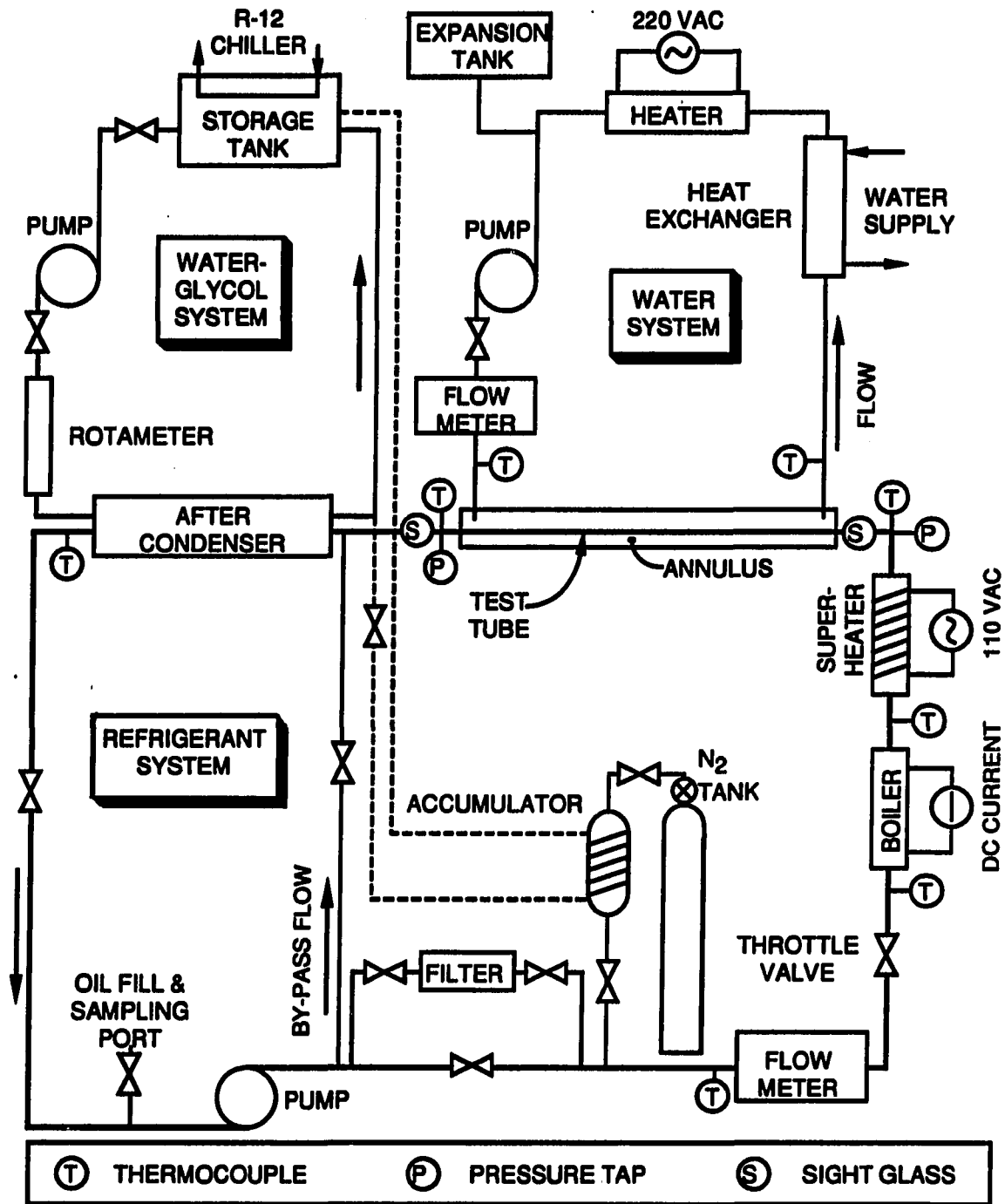


Figure 4.1. Schematic diagram of the test facility

valves and a by-pass line from the pump discharge to the inlet. The pump was connected to the rest of the flow loop with high-pressure, flexible hoses.

Filter dryer A filter dryer was installed in the flow line between the pump discharge and the flow meter to protect the flowmeter from particle contamination, as well as to remove moisture from the refrigerant.

Heaters Two back-to-back, flow-through heaters were installed just prior to the test section to control the vapor quality at the inlet of the test section. Both were electrically isolated from the rest of the rig by short lengths of high-pressure rubber hose.

The first heater, referred to as the boiler, was constructed of a 2.6-m long section of stainless steel tubing through which direct electrical current passed. The boiler had an outside diameter of 12.7 mm and a wall thickness of 1.4 mm. A high current rectifier supplied power to this heater through water cooled cables. Since this heater was a constant heat flux device, care had to be taken to avoid the dryout region. For this reason, vapor quality at the exit of the boiler was limited. To help avoid dryout, a twisted tape was installed to maintain wetting of the tube wall. As a safety measure, temperature limit switches were installed at the downstream end of the heater.

The second heater, referred to as the superheater, consisted of a resistance heating element with a rating of 1500 W wrapped around a 12.7-mm outside diameter, 1.9-m long copper tube. The heater was covered by ceramic beads for electrical isolation. The AC power input was controlled with a variable autotransformer. Because this type of heater is easily controlled and is not dependent on wetting of the tube wall to prevent overheating, it is suitable for dryout and superheated regions. The facility was capable of superheated conditions at the test section inlet, but quality was limited to about 85% maximum.

Test section Immediately following the superheater was the test section. The tubes tested were 9.52 mm in outside diameter with inside diameters ranging from 8.00 to 8.72 mm. The active length of the test section was 3.67 m. To allow for connection to the rest of the system, total test tube length was approximately 4.0 m. The test tubes were installed by sliding them through the annulus section and connecting them to the flow loop with compression fittings. To remove the test tube, the swaged ferrule on one end of the tube was cut off, allowing the tube to slide out. Even though the tube was shortened about

10 mm with each removal, a flexible section in the rig allowed the tube to be installed several times before it became too short.

After-condenser Located at the exit of the test section was a shell-and-tube heat exchanger with refrigerant flowing on the tube side and a chilled water and glycol mixture on the shell side. All of the vapor at the exit of the test section was condensed and then subcooled to assure a liquid flow through the pump and flow meter and at the boiler entrance. For low temperature evaporation tests, refrigerant leaving the after-condenser was -20°C or colder.

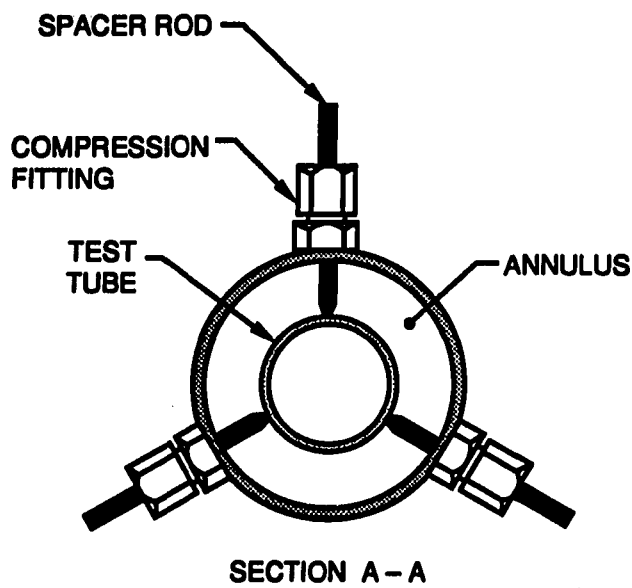
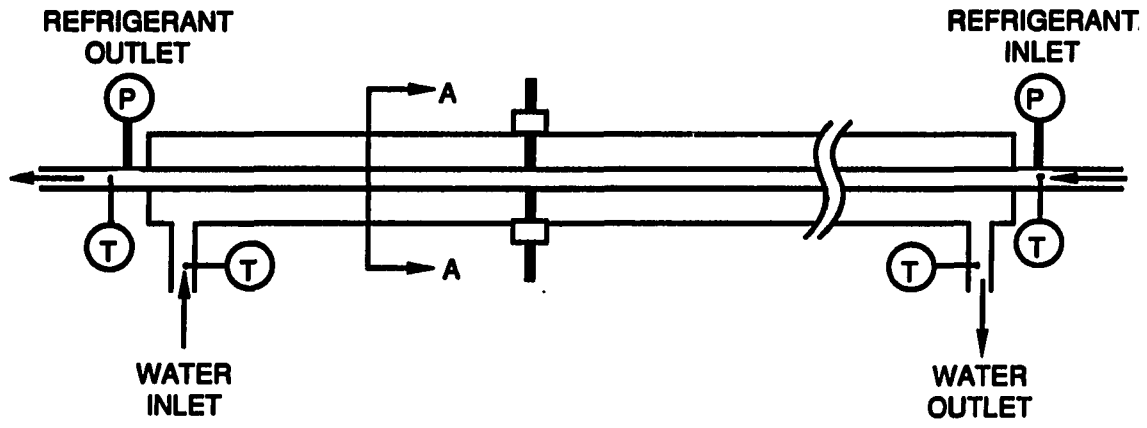
Bladder accumulator An accumulator with an elastomeric bladder was installed at the pump discharge. A nitrogen tank was used to pressurize the accumulator and set system pressure. The accumulator also served as a dampener for oscillations caused by the positive displacement pump and as an expansion tank. During evaporation testing, the accumulator was cooled with the water and glycol mixture to achieve lower system pressures.

Water Loop

Pump Water was circulated with a magnetically-coupled, centrifugal pump. The flow rate was controlled by a throttling valve at the pump discharge. Water flow rates up to 0.4 kg/s were obtainable.

Annulus of the test section The annulus was the shell side of a single-pass, counterflow, shell-and-tube heat exchanger with refrigerant flowing on the tube side. The annulus assembly is illustrated in Figure 4.2. The inside diameter of the annulus was 17.9 mm, giving a hydraulic diameter of 8.4 mm. Spacers were installed at three locations to center the test tube in the annulus.

Heat exchangers To maintain the water at a constant temperature, energy had to be added or removed. To accomplish this, an electric heater and a water-to-water heat exchanger were installed in the water flow loop. The immersion-type heater consisted of two, 2000-W elements using AC power. These heaters were inserted into a large diameter pipe through which water flowed. Power to each heater was controlled by a variable autotransformer.



- Ⓣ THERMOCOUPLE
- Ⓟ PRESSURE TAP

SPACERS AT 3
AXIAL LOCATIONS,
EVENLY SPACED

Figure 4.2. Assembly detail of the annulus (not to scale)

The heat exchanger was a shell-and-tube type with flow loop water on the tube side. On the shell side, water from one of the building supplies was circulated: (1) city water supply, which varied in temperature throughout the year, (2) hot water with a temperature of approximately 50°C, and (3) a chilled water supply with a temperature of approximately 10°C. Hot and cold water could be mixed to achieve desired conditions.

Water and Glycol Loop

Pump A centrifugal pump, similar to the one used in the water flow loop, circulated the chilled water and glycol mixture. The mixture was pumped from the storage tank through the after-condenser and back to the tank. For evaporation tests, some of the flow was diverted to cool the bladder accumulator so that lower system pressures could be obtained.

Tank A 210-L insulated tank served as the heat sink for the test rig. The tank was filled with a 50/50 mixture of water and glycol and cooled to approximately -25°C prior to beginning test runs. In the tank was the evaporator coil of a 17.5-kW (5-ton) commercial refrigeration unit. Part of the evaporator coil had an externally finned surface to enhance heat transfer. A stirrer was used to further promote heat transfer. Even so, for the low temperatures and larger heat loads needed for evaporation, the temperature of the water and glycol mixture rose gradually during testing, limiting the time available during a given test run.

Oil Injection and Sampling

Oil was injected into the refrigerant loop with a modified double-acting air cylinder as shown in Figure 4.3. Air pressure was used to inject the oil in much the same manner as a hypodermic syringe operates. The device was connected to a toggle valve on the rig with a short length of tubing and compression fittings. The same device was used to withdraw samples from the flow loop by bleeding high-pressure air slowly from the air side. Since oil was injected as a batch process with no accommodation for continuous oil removal, the sequence of testing always proceeded from pure refrigerant to progressively higher concentrations of oil. The procedures for oil injection and sample removal are described in more detail in Appendix B.

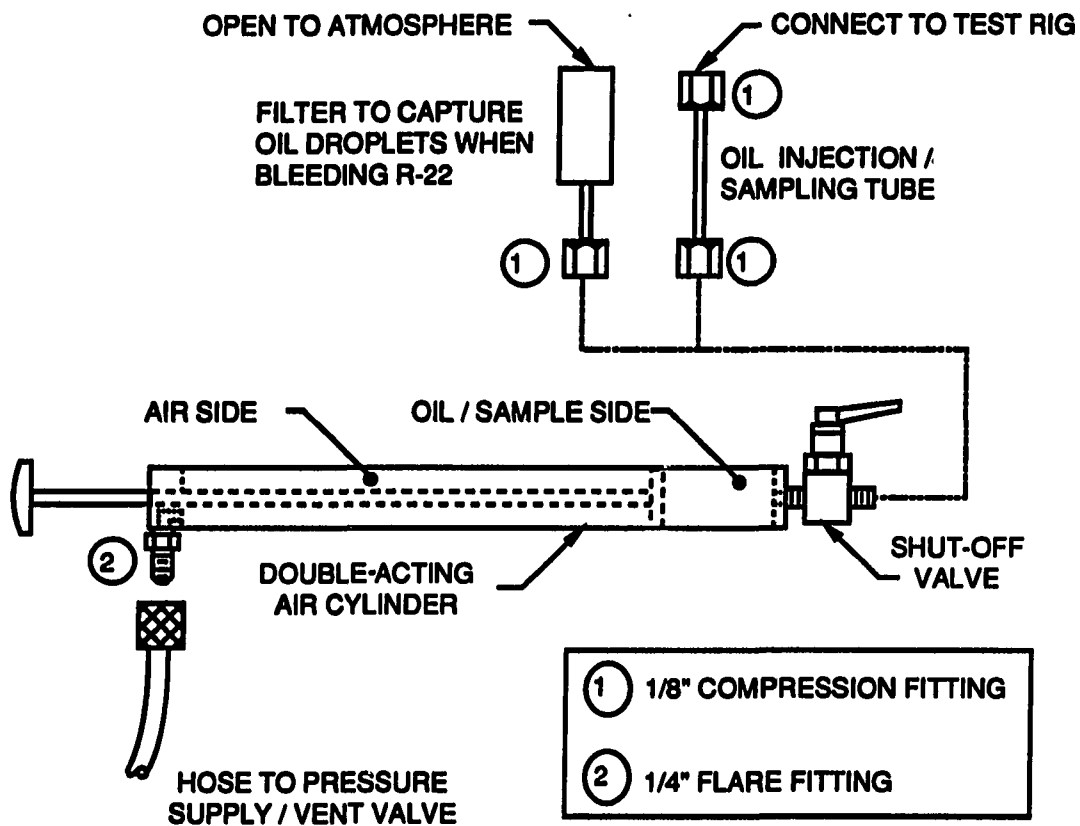


Figure 4.3. Oil injection and sampling device

Instrumentation

Like the flow loop hardware, the instrumentation was similar to that used earlier [119]. The data acquisition computer and software, however, were new. The following paragraphs give a description of the instrumentation; the manufacturer and model of each item are specified in Table A.2 of Appendix A.

Temperature

Twenty copper-constantan (Type-T) thermocouples were used to measure temperatures throughout the rig. Thermocouples inserted into flow streams were encased in 1.6-mm diameter stainless steel sheaths and inserted through compression fittings. All external thermocouples were bare junctions of 30 gage wire. An electronic cold junction

reference was used in lieu of an ice bath. Voltage to temperature conversions were done with a library subroutine supplied with the computer system data acquisition software.

Redundant thermocouples were inserted at the entrance and exit of both the test tube and the annulus to ensure proper temperature readings. Because the fluid temperature difference through the annulus was a particularly critical measurement, these thermocouples were calibrated to within $\pm 0.01^\circ\text{C}$ in a constant temperature bath prior to insertion in the rig.

One thermocouple was enclosed in a small box, along with the bulb of a calibrated mercury-in-glass thermometer. The thermometer reading was manually fed into the computer for each test run so the software could correct for any systematic temperature offset through the electronics.

Pressure

The refrigerant pressure at the entrance to the test section was measured with a strain-gage-type pressure transducer having an accuracy of 0.25%. A 10-VDC power supply provided voltage to the bridge circuit. Because the transducer measured gage pressure, atmospheric pressure was read from a mercury barometer and input manually, allowing the software to compute the absolute pressure. Several test gages were installed in the rig to allow visual monitoring of pressure during operation.

Pressure drop across the test section was measured with a variable-reluctance-type differential pressure transducer with an accuracy of $\pm 0.25\%$. The electronics supplied with the transducer served as a power supply and converted the output signal to a DC voltage.

The calibration of each transducer was periodically checked with a dead weight tester. It was discovered that the differential pressure transducer experienced some drift in the zero point during testing. To solve this problem, valves were installed in the pressure lines so the transducer could be isolated with equal pressure at both ports. The zero point was then checked and adjusted before and after each test run. The pressure drop lines had needle valves installed to dampen pressure fluctuations. Even so, at low mass fluxes where the pressure drop was small, the standard deviation of the pressure drop was sometimes as large as the measurement itself. (Refer to Table D.2 for pressure drop standard deviations.)

Flow

Refrigerant flow was measured with a piston-type positive displacement flowmeter having an accuracy of better than 1% of the instantaneous rate. The flow meter required no external power and produced a DC voltage for the output signal. This voltage was read not only by the data acquisition system, but was also fed to a digital panel meter so that the refrigerant flow rate could be visually monitored on a continuous basis.

Water flow in the annulus was measured with a magnetic-type flowmeter having an accuracy of $\pm 2\%$. This flowmeter required an external 110-VAC power source and produced an output signal of 4 to 20 mA. The flow of the water and glycol mixture was monitored with a rotameter, but the rate was not recorded because it was not required in the data analysis.

Heater Power

The voltage across the boiler was measured directly by the multimeter. The current was measured indirectly by measuring the voltage across a shunt resistor. A calibration constant was then used to calculate the current based on the shunt resistor voltage. The AC voltage to the superheater was within the range of the multimeter and was read directly. A current transducer having an accuracy of $\pm 0.25\%$ was used to convert AC current into a DC voltage, which was then measured with the multimeter.

Data Acquisition System

The data acquisition system consisted of a small, stand-alone digital computer, a scanner with a maximum capacity of 50 channels, and a digital multimeter. These components communicated via an IEEE-488 interface bus. A library of subroutines for IEEE-488 communications was included in the computer's system software. This small computer was connected directly to the university's computer system, so data could be sent electronically for further analysis or plotting. System components are listed in Table A.2 of Appendix A.

Computer software was written in FORTRAN and included a routine to initialize the bus, a routine to check operating parameters prior to initiating the data acquisition, and a

routine to scan the data channels and pass this data to the analysis routines. A complete listing of data acquisition and analysis routines is included in Appendix C. Data analysis was done on the same computer and will be described in Chapter 5.

All data channels were scanned a total of five times, with the exception of pressure drop, which was scanned a total of 35 times due to the small magnitude of the measurement and relatively high fluctuations present in two-phase flow. The pressure drop fluctuations were particularly serious at low mass flows, where pressure drop magnitude was small, but fluctuations tended to stay the same as those when total pressure drop was an order of magnitude higher. Because conditions were approximately steady state, fast data sampling was not required. The entire data acquisition cycle took approximately two minutes for each test run.

Three items of data were not acquired automatically, but rather were entered manually at the outset of the acquisition cycle. These were (1) atmospheric pressure, which was read from a mercury barometer, (2) ambient temperature, which was obtained from a calibrated mercury-in-glass thermometer, and (3) oil concentration, which was obtained through a separate sampling procedure. (See Appendix B for a description of oil sampling.)

CHAPTER 5 DATA ANALYSIS

Convective heat transfer coefficients were calculated from the raw data using a FORTRAN code on the same computer used for data acquisition. Results were saved on a disk and printed. Final results are based on the average value of five scans during a single test run. This chapter looks at some of the assumptions behind the data analysis, limitations of the analysis, equations used in the data reduction code, and experimental uncertainties. A listing of the data acquisition and reduction code is included in Appendix C.

Assumptions

All engineering calculations are based on a set of simplifying assumptions, allowing a problem to be modelled. The goal is to reach a compromise between a model that is overly simplified, and one that is so complex that the acquisition of sufficient input data becomes difficult or impossible. A recognition of the assumptions underlying an investigation is important and this section lays out the key assumptions used in the reduction of data for this project.

Properties

Refrigerant and water properties were calculated from curve fits of tabulated data [6]. Properties of the refrigerant-oil mixture were calculated from equations which were presented in Chapter 2. Vapor was assumed to be pure refrigerant.

Test Section Conditions

The enthalpy of vaporization and the temperature-pressure relationship at saturation for refrigerant-oil mixtures were assumed equal to those of pure refrigerant. Since this assumption becomes poorer as the vapor quality increases, the maximum vapor quality for all tests was kept below 85%. It was impossible to know precise values for local oil concentration or temperature, because no local measurement techniques were available.

The temperature in the test section was determined based on the saturation temperature of the refrigerant at the average pressure in the test section. As mentioned above, it was assumed that the saturation temperature for the refrigerant-oil mixture

corresponded to that for pure refrigerant. The average test section pressure was determined by subtracting one-half the pressure drop measurement from the system pressure at the test section inlet. The calculated saturation temperature was assumed constant throughout the length of the test tube. Because pressure drop occurs in an evaporator or condenser, the temperature through the test section is actually changing, not constant. An analysis of the temperature change based on pressure drop, however, revealed that the error in the LMTD by using the constant temperature assumption was typically less than 1.5% for evaporation and less than 0.5% for condensation. Typical errors in the inside convective coefficient, h_i , caused by this assumption were 3% and 1% for evaporation and condensation, respectively. In the worst case, the error in h_i due to basing temperature on average pressure was less than one half its total uncertainty from a propagation-of-error analysis (see Appendix D). Because of the small errors caused by this assumption, and the inability to precisely determine the local temperature based on pressure with refrigerant-oil mixtures (see Chapter 2), the simplified assumption of constant refrigerant temperature through the test section was used.

Data Presentation

Heat Transfer and Pressure Drop

Heat transfer coefficients and pressure drops are plotted as a function of mass flux on Cartesian coordinates. Least squares curve fits are used to draw lines through the data points. For heat transfer, the shape of the curve chosen is determined by the fit. Condensation heat transfer results are well described by linear curves, whereas evaporation heat transfer results require quadratic curves to describe the data with a similar accuracy. Pressure drop results are fitted with quadratic curves because frictional pressure drop is proportional to the square of the mass flux.

To reduce clutter, individual data points are not included on most of the figures in this document, but all data are tabulated in Appendix E. To give a visual indication of typical data scatter, some of the early figures in Chapters 6, 7, and 8 include data points as well as best-fit curves, but later figures in these chapters show only the curves.

Nondimensional Ratios

Ratios, often called by descriptive names such as enhancement factors, penalty factors, performance ratios, etc., have often been used to make comparisons easier, especially performance comparisons of different tube geometries. These factors can also be used to compare the effects of other variables, such as oil. A performance factor is the ratio of some performance parameter at one condition (tube geometry, oil concentration, etc.) to that same performance parameter (or a related one) at a different condition. Except for the particular parameter(s) of interest, all other variables, such as tube diameter, mass flux, quality, pressure, etc., are kept as constant as possible. The sections that follow give descriptions and definitions of the performance ratios used in this document.

Heat transfer and pressure drop enhancement factors It is desirable to have heat transfer enhancement factors greater than one, since higher heat transfer is the goal. However, because pressure drop should be minimized, an enhancement factor greater than one for pressure drop might be referred to as a penalty factor. Discussions in subsequent chapters refer to both factors as enhancement factors. Heat transfer enhancement factors are noted by ϵ (epsilon) and similar factors for pressure drop are noted by Ψ (psi). Four distinct enhancement factors are defined below. These factors are defined at constant mass flux, constant inlet and outlet quality, constant pressure, and constant characteristic dimension. In this research, the log mean temperature difference and the annulus side Nusselt number were allowed to vary in order to maintain a constant quality change through the test section. All of the enhancement factors reported are based on a comparison of least-squares curve fits of the data and not on a comparison of individual data points.

1. Smooth tube oil-enhancement factor ($\epsilon_{s'/s}$ or $\Psi_{s'/s}$) — This is the ratio of the smooth tube heat transfer coefficient (or pressure drop) with a refrigerant-oil mixture to the coefficient (or pressure drop) of the smooth tube with pure refrigerant.
2. Augmented tube oil-enhancement factor ($\epsilon_{a'/a}$ or $\Psi_{a'/a}$) — This is the ratio of the heat transfer (or pressure drop) of the augmented tube with a refrigerant-oil mixture to the heat transfer (or pressure drop) of the same tube with pure refrigerant.

3. Augmented tube enhancement factor for pure refrigerant ($\epsilon_{a/s}$ or $\Psi_{a/s}$) — This is the ratio of the heat transfer (or pressure drop) of the augmented tube to the heat transfer (or pressure drop) of a similar smooth tube using pure refrigerant for both. Earlier work dealing with in-tube augmentation has often reported this factor.
4. Augmented tube enhancement factor for refrigerant-oil mixtures ($\epsilon_{a'/s'}$ or $\Psi_{a'/s'}$) — This is the ratio of the heat transfer coefficient (or pressure drop) of the augmented tube with a particular oil concentration to the coefficient (or pressure drop) of a smooth tube with the same oil concentration

The a in the subscripts above represents an augmented tube while s represents a comparable smooth tube. A prime ' indicates the presence of oil, whereas no prime shows that pure refrigerant values are used. The solidus / is indicative of a ratio.

Unlike curves describing heat transfer and pressure drop data, which are determined statistically, the curves of enhancement factors versus oil concentration are simply splines. These curves are meant to aid the reader in visually associating related data points and are not intended to be used to interpolate or extrapolate results.

Enhancement performance ratio The enhancement performance ratio combines heat transfer and pressure drop results to give an indication of the overall performance of a tube relative to a baseline. Definition of this factor is delayed until Chapter 9, which also discusses various performance parameters used by earlier researchers.

Area ratio The area ratio, denoted A^* , is defined as the ratio of the inside surface area of the augmented tube to the inside surface area of a hypothetical smooth tube having an inside diameter equal to the maximum inside diameter of the augmented tube. Note that this factor is strictly geometric, so it is constant for a given tube.

Limitations on Data

Due to the design of the test apparatus and the instrumentation available, there are certain limitations to the final results. These limitations are described below.

Test Conditions

Because the test rig was controlled manually without automatic feedback, it required constant operator attention to maintain desired equilibrium conditions. Due to the large

number of parameters that had to be simultaneously controlled (flow rates, pressures, etc.), it was difficult to exactly reproduce test conditions from one run to the next. An additional difficulty was limited time for evaporation tests—the rig warmed up gradually and after about an hour, a shut-down was required to recool the water and glycol mixture. For these reasons, conditions varied somewhat from one test to the next, but were generally maintained within a narrow range: system pressure, ± 0.05 MPa; mass flux, ± 15 kg/m²·s; inlet and outlet qualities, ± 0.08 . Conditions for each test run are listed in Appendix E.

Due to limited availability of tubes, the inside diameters of the three tubes used were not identical. The diameters varied by less than 10%, ranging from a maximum inside diameter of 8.7 mm for the micro-fin tube to an inside diameter of 8.0 mm for the smooth tube. The low-fin tube had a maximum inside diameter of 8.5 mm.

Heat and Mass Flux

Because a constant quality change was maintained through the test section for all tests and there was only one test section length, mass flux and heat flux could not both be independent variables. That is, as mass flux increased, heat flux also had to increase to maintain the same quality change. For this reason, it is impossible to separate the effects of heat flux from those of mass flux in this investigation. Because mass flux was used as the independent variable during testing, discussions and conclusions are generally relative to mass flux, even though some of the apparent effects of mass flux may actually be due to heat flux. Heat flux, however, has only a minor effect on condensation heat transfer. During evaporation, there may be a larger effect, but it is generally limited to lower qualities (<40%), where nucleate boiling is the more dominant heat transfer mechanism.

Heat Transfer Coefficient

Heat transfer coefficients calculated during this investigation are average, rather than local. To be able to run both condensation and evaporation tests with the same test rig, an annular test section with fluid heating and cooling was chosen. Direct electrical heating would have limited testing to evaporation, and, additionally, fluid heating or cooling more closely models actual boundary conditions in a refrigerant evaporator or condenser. A requirement that tubes be changed relatively quickly and easily limited the instrumentation

that could be placed in the annulus, such as surface thermocouples or additional pressure taps. For these reasons, only data to calculate average heat transfer coefficients were obtained.

Pressure Drop

Because of the annulus design, it was impossible to sample pressures at intermediate points in the test tube. For this reason, only total pressure drop measurements over the entire length of the test tube were measured.

Another limitation to pressure drop results is large experimental uncertainty. Two-phase flow is inherently fluctuating, leading to pressure fluctuations. Additionally, the pulsations caused by the positive displacement pump were not completely damped out. During liquid flow, pump pulses were visible on the small test gage used to monitor test section pressure. Upon the initiation of two-phase flow, the pulses were attenuated, but needle motion on the test gage was still detectable, indicating that the pulses were approximately ± 0.02 MPa or smaller. This magnitude of pressure variation had little effect on system pressure or heat transfer, as evidenced by the agreement with established correlations. However, it was sometimes significant compared with the magnitude of the pressure drop. As mentioned earlier, a small part of the variation from one test to another may have been due to varying quality change through the test section.

Enhancement Factors

Enhancement factors are determined from least-squares curve fits of heat transfer or pressure drop data. Curves depicting pressure drop enhancement factors, in particular during condensation and at low mass fluxes, often have large variations which may not have a physical basis. One reason for this is the large uncertainty relative to the magnitude of the measurement. Another reason is that pressure drop curves should theoretically pass through zero, with a slope near zero, when mass flux is zero, but there was no such constraint applied to the curve fitting. At low or high mass fluxes, the curves may cross each other, causing swings in the value of enhancement factors. At the extreme mass fluxes, absolute uncertainty is at a maximum, although relative uncertainty may not be a maximum (see Figure D.1, for example). Slightly different degrees of curvature can also

affect Ψ , causing relative minima or maxima that would not be present, for example, with linear curve fits. In the data presented here, medium to high mass flux values are generally better for comparison purposes, with the minimum uncertainty generally occurring in the vicinity of $300 \text{ kg/m}^2\cdot\text{s}$.

For these reasons, care should be taken when drawing specific conclusions regarding trends in enhancement factors as a function of other variables. Conclusions regarding general, overall trends, such as performance of one tube relative to another, are not so sensitive to the choice of curve fit and are, therefore, reliable. Local trends, however, such as the effect of incremental oil concentration changes at a particular mass flux, should not be estimated without also considering adjacent data points and taking into account trends over a wider range of conditions. As a rule, discussions in this document are limited to conclusions drawn from more general trends.

As discussed earlier in the section on data presentation, curves connecting individual enhancement factor data points are splines, intended to help the reader to visually associate related points. These curves may skew the actual location and magnitude of minima and maxima compared to a statistical, best-fit curve. Care should be used when interpolating or extrapolating with these curves, especially in regions with relative minima or maxima.

Oil Concentration

All oil concentrations are reported as a weight percent on a total sample basis (see Appendix B) and are based on the average concentration of oil and refrigerant in the system. As mentioned in the previous section, no local oil concentrations in two-phase flow regions are reported.

Data Reduction Equations

Heat Transfer Coefficient

The heat transferred in the test section is calculated from an energy balance in the annulus. Defining heat transfer to the refrigerant as positive, an energy balance in the annulus yields

$$Q_{W_r} = \dot{m}_W \cdot c_{pW} (T_{W_{out}} - T_{W_{in}}) \quad (5.1)$$

For single-phase tests, a similar calculation can be made on the refrigerant side:

$$Q_{tr} = \dot{m}_r \cdot c_{pr} (T_{rout} - T_{rin}) \quad (5.2)$$

The overall heat transfer coefficient based on the outside area of the tube is

$$U_o = \frac{Q_t}{(A_o \cdot \text{LMTD})} \quad (5.3)$$

where

$$\text{LMTD} = \frac{\Delta T_1 - \Delta T_2}{\ln(\Delta T_1 / \Delta T_2)} \quad (5.4)$$

$$\Delta T_1 = T_{rout} - T_{Win} \quad (5.5)$$

$$\Delta T_2 = T_{rin} - T_{Wout} \quad (5.6)$$

For single-phase tests, Q_t in Equation 5.3 is the average of Q_{tw} and Q_{tr} from Equations 5.1 and 5.2. For two-phase tests, Q_t is equivalent to Q_{tw} and the definitions of ΔT_1 and ΔT_2 are modified as follows:

$$\Delta T_1 = T_{rsat} - T_{Win} \quad (5.7)$$

$$\Delta T_2 = T_{rsat} - T_{Wout} \quad (5.8)$$

where T_{rsat} is the saturation temperature of pure R-22 at the average tube pressure.

In terms of thermal resistances, another expression for U_o is given by

$$\frac{1}{U_o} = \frac{A_o}{A_i} \frac{1}{h_i} + \frac{A_o \cdot \ln(d_o/d_i)}{2 \cdot k_w \cdot l} + \frac{1}{h_o} \quad (5.9)$$

The middle term in Equation 5.9 represents the wall resistance which can be considered negligible in this case. Equation 5.9 can be rearranged and solved for h_i , the average heat transfer coefficient:

$$h_i = \frac{1}{\left[\frac{1}{U_o} - \frac{1}{h_o} \right] \frac{A_i}{A_o}} \quad (5.10)$$

For finned tubes, A_i is the inside area of a smooth tube having an inside diameter equal to the maximum inside diameter of the finned tube. Because U_o is known from Equation 5.3,

the only unknown in Equation 5.10 is h_o , the convective heat transfer coefficient on the annulus (water) side of the test section. This coefficient is calculated from an experimentally derived calibration expression obtained by using a modified Wilson plot technique [154]. The calibration of the annulus was performed by Khanpara [119] and his expression for h_o is

$$h_o = E \cdot Re^e \cdot Pr^{0.33} \cdot k_w / d_H \quad (5.11)$$

where E and e are constants obtained from the calibration tests. Water properties are calculated at the average temperature in the annulus. Test conditions for the investigation reported here were somewhat different than those of Khanpara, requiring somewhat lower water flow rates. For this reason, additional calibration runs, using the same procedure, were made at low water flow rates and adjustments were made to the Reynolds number exponent for Reynolds numbers below 10,000. The values of E and e are

$$\begin{aligned} E &= 0.027 && \text{for } Re > 2000 \\ e &= 0.806 && \text{for } Re > 12,000 \\ e &= 0.752 + (7.98 \times 10^{-6}) \cdot Re - (2.92 \times 10^{-10}) \cdot Re^2 && \text{for } 2000 < Re \leq 12,000 \end{aligned}$$

Vapor Quality

For two-phase tests, the test section inlet and outlet qualities must be established. The inlet quality is determined by an energy balance on the heaters immediately before the test section, assuming that oil has no effect on the heat of vaporization. The total energy transferred from the heaters to the refrigerant is

$$Q_{hcond} = 0.98 \cdot ((V \cdot I)_{boil} + (V \cdot I)_{s-h}) \quad (5.12)$$

$$Q_{hevap} = ((V \cdot I)_{boil} + (V \cdot I)_{s-h}) + 80 \quad (5.13)$$

For condensation, the heat loss is estimated as 2% [119]; hence, the factor of 0.98 in Equation 5.12. The energy gain during evaporation testing was estimated by measuring single-phase temperature rise through the heaters with no power. It was found that heat gain is not a strong function of mass flow rate and at evaporation temperatures, the gain is

about 80 W after steady state is reached. This estimate is used for all tests and is reflected in Equation 5.13.

The refrigerant entered the boiler as a subcooled liquid which had to first be raised to the saturation temperature and then evaporated to the desired inlet quality. Accordingly, the total heat added to the refrigerant can be divided into sensible and latent heat

$$Q_h = Q_{sens} + Q_{lat} \quad (5.14)$$

where

$$Q_{sens} = \dot{m}_r \cdot c_{p_r} (T_{sat} - T_{h in}) \quad (5.15)$$

$$Q_{lat} = \dot{m}_r \cdot i_{fg} \cdot X_{h out} \quad (5.16)$$

As stated earlier, the saturation temperature and enthalpy of vaporization are assumed to be those of pure refrigerant at the average pressure of the test section.

The quality change through the test section is calculated from an energy balance in the annulus. Neglecting any losses in the heavily insulated annulus, the quality change is

$$\Delta X = \frac{Q_t}{\dot{m}_r \cdot i_{fg}} \quad (5.17)$$

Pressure

Pressure and pressure drop are calculated from calibration equations for the particular transducer used. Both calibration curves are second-order polynomials. The system pressure is

$$P_{tin} = (-2.65 + 16.6 \cdot V - 0.00258 \cdot V^2) \cdot 6894.4 + P_{atm} \quad (5.18)$$

where V is measured in millivolts. The pressure drop is

$$\Delta P_t = (0.102 + 1.02 \cdot V - 0.00534 \cdot V^2) \cdot 6894.4 \quad (5.19)$$

where V is measured in volts. The average tube pressure is

$$P_{tavg} = P_{tin} - 0.5(\Delta P)_t \quad (5.20)$$

Experimental Uncertainties

This section summarizes the uncertainty analysis. For a more detailed discussion of uncertainties, along with sample calculations, the reader is referred to Appendix D.

The uncertainty of the heat transfer coefficient from a single test run, based on a propagation-of-error analysis, ranges from $\pm 7\%$ to $\pm 13\%$, with a typical value of about 10%. For pressure drop, uncertainty of ± 3.0 to ± 4.8 kPa is typical for evaporation in a single test run and ± 2.0 to ± 4.2 kPa for condensation. These values are determined statistically and represent two standard deviations, or a 95% confidence level. Table D.2 is a tabulation of the standard deviations of the pressure drop measurements.

The curves of h_i and ΔP versus G , determined from a regression analysis, generally have correlation coefficients greater than 0.95. The minimum correlation coefficient for any of the curves is about 0.8. The construction of confidence intervals about the regression curves gives an estimate of the uncertainty of these equations. Tables D.4 and D.5 present these values at a 95% confidence level. As a percentage of predicted value, the uncertainty of h_i varies from about 2% to 10%. For pressure drop, the uncertainty ranges from 2% to 62%, with uncertainties greater than 20% for both evaporation and condensation at the lowest mass flux. In general, the percentage uncertainty for condensation pressure drop is about twice that for evaporation.

The high uncertainty for pressure drop, especially during condensation and at low mass fluxes, is due to the proximity of the curves to zero. Figure D.2 in Appendix D plots pressure drop regression curves along with confidence intervals. It shows that the absolute uncertainty does not increase dramatically at low mass fluxes, but the small absolute values of ΔP cause the relative uncertainty to be quite high.

Enhancement factors for heat transfer (ϵ) have an uncertainty of $\pm 3\%$ to $\pm 12\%$, based on 95% confidence levels. Pressure drop enhancement factors (Ψ) have higher uncertainties, ranging from $\pm 4\%$ to over $\pm 60\%$. At medium to high mass fluxes, however, the uncertainty is generally below $\pm 15\%$. Uncertainties for typical conditions are presented in Table D.6. The enhancement performance ratio, defined in Chapter 9, has uncertainties

similar to pressure drop enhancement factors, but slightly higher. These are shown in Table D.7.

The oil concentration uncertainty is about ± 0.1 weight percent, as determined using ASHRAE Standard 41.4-1984 [155]. Inlet vapor quality and quality change through the test section each have an estimated uncertainty of $\pm 4\%$ quality. Mass flux has an uncertainty of slightly more than $\pm 1\%$ of the measured value.

CHAPTER 6

RESULTS WITH THE SMOOTH TUBE

Smooth tube results are important because they provide a baseline against which results with augmented tubes can be compared. Additionally, through comparisons with established heat transfer correlations, pure refrigerant tests serve to verify the performance of the test facility and the data acquisition and analysis system. Both single-phase and two-phase tests were carried out. All data shown in graphical form in this document are tabulated in Appendix E. Table 6.1 gives the dimensions of the smooth tube.

Table 6.1. Smooth tube dimensions

Outside diameter, mm	9.52
Wall thickness, mm	0.76
Inside diameter, mm	8.00
Cross section area, mm ²	50.3

Pure Refrigerant Heat Transfer

Single-Phase

Single-phase testing was carried out at Reynolds numbers from 12,000 to 40,000. Two established correlations are used for comparison with experimental Nusselt numbers. The first is the classical Dittus-Boelter/McAdams expression [154]:

$$Nu = 0.023 Re^{0.8} Pr^n \quad (6.1)$$

where $n = 0.4$ for heating and $n = 0.3$ for cooling.

The other correlation is a more recent one of Petukhov-Popov [156]. The form is somewhat more complex, but agreement with experimental data is generally better. The correlation is

$$Nu = \frac{(f/8) \cdot (Re \cdot Pr)}{1.07 + 12.7 \cdot (f/8)^{0.5} \cdot (Pr - 1)^{0.67}} \quad (6.2)$$

where

$$f = [1.82 \cdot \log_{10} Re - 1.64]^{-2} \quad (6.3)$$

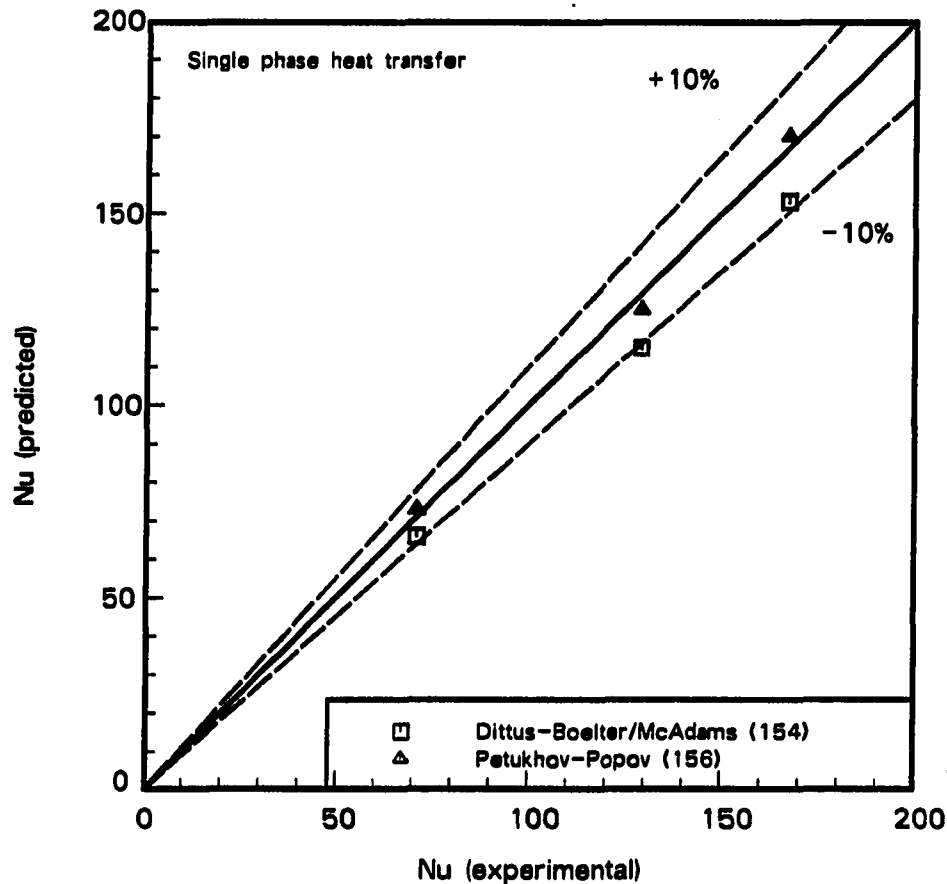


Figure 6.1. Comparison of experimental Nusselt numbers with predictions

Figure 6.1 compares the experimental and predicted Nusselt numbers for the single-phase tests. In general, agreement with the correlations is within $\pm 10\%$, but the Petukhov-Popov expression gives somewhat better results.

During single-phase tests, an energy balance was performed to compare heat transfer calculated from the tube side (refrigerant) with that calculated from the annulus side (water). Agreement between the two values was within $\pm 5\%$ in all cases and generally within $\pm 3\%$.

Two-Phase

Evaporation and condensation testing with pure refrigerant was carried out at the same conditions that were later used with augmented tubes. These conditions are summarized in Table 6.2.

Table 6.2. Summary of two-phase test conditions

	Evaporation	Condensation
G, kg/m ² ·s	125–400	125–400
P, MPa	0.5–0.6	1.5–1.6
T _{sat} , °C	0–6	39–42
Inlet quality, %	10–20	80–88
Outlet quality, %	80–88	5–15

In addition to establishing a performance baseline against which results with oil and with augmented tubes are compared, smooth tube evaporation and condensation results are compared to several correlations from the literature. These correlations are chosen because of the broad base of refrigerant data used in their formulations and their success in correlating refrigerant heat transfer. For evaporation, the correlations of Gungor and Winterton [157], Kandlikar [158], and Shah [159] are used for comparison. Condensation results are compared with the correlations of Shah [160], Traviss et al. [161], and Cavallini and Zecchin [162]. These correlation are described in more detail in Chapter 10. To obtain average heat transfer coefficients from local correlations, a numerical integration is performed over the quality range of interest.

Figure 6.2 shows a comparison of experimental evaporation and condensation results with predictions from the correlations. Results generally agree within $\pm 20\%$ except for two cases: all condensation correlations at low mass flux and Shah's evaporation correlation. (Tichy et al. [47] also noted that the condensation correlation of Shah underpredicted heat transfer at low mass fluxes.) Figure 6.3 is a plot of the heat transfer coefficient versus mass flux for both evaporation and condensation. Curves are least-squares fits of the individual data points and show that the heat transfer coefficient increases with increasing mass flux for both evaporation and condensation.

Heat Transfer with Refrigerant-Oil Mixtures

Tests were run at several oil concentrations up to a maximum of 5%. For 150-SUS oil, nominal oil concentrations of 1.25%, 2.5%, and 5.0% were used. With 300-SUS oil, an additional condition of 0.6% oil was also included. Figures are presented showing heat

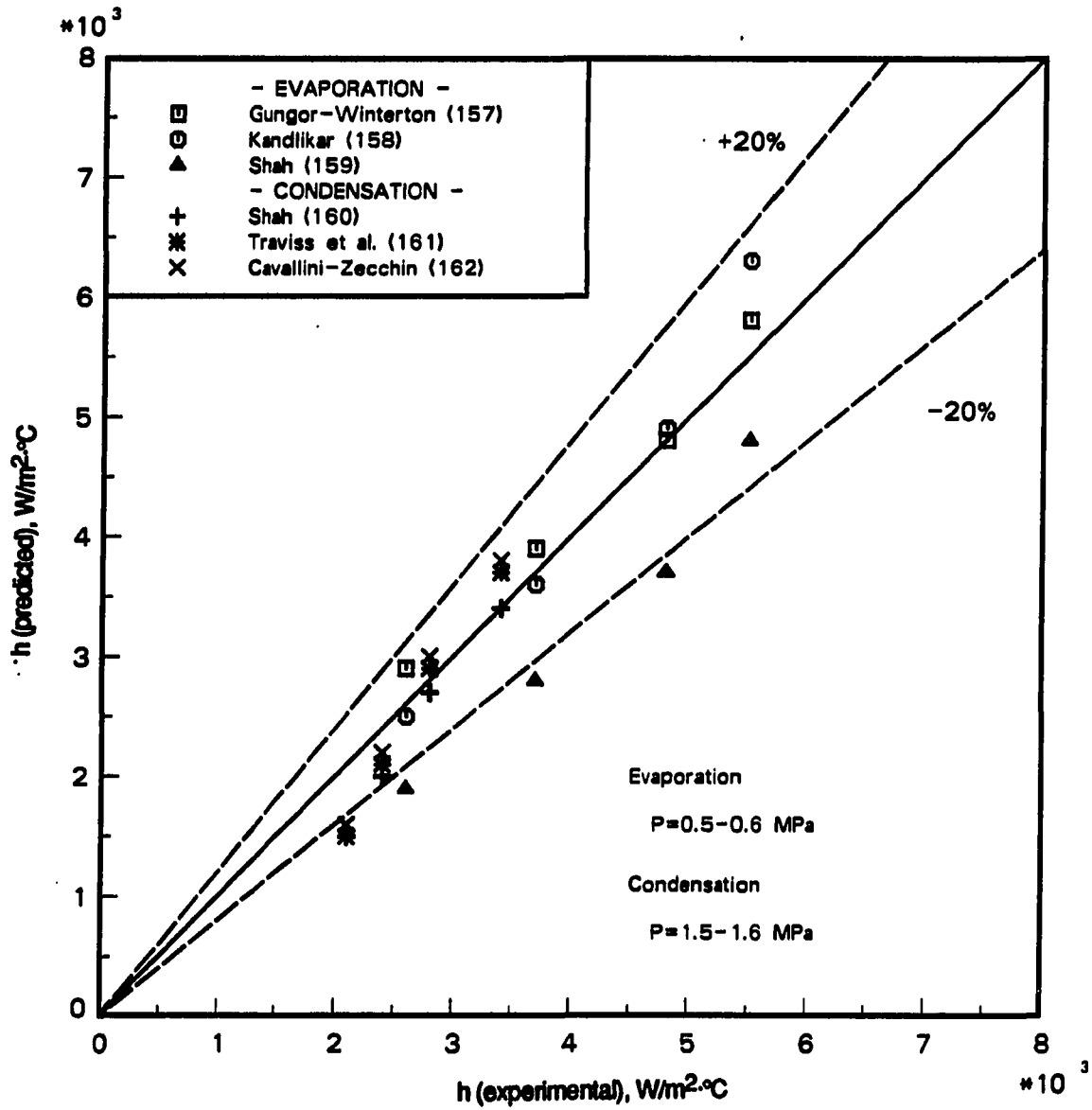


Figure 6.2. Comparison of experimental heat transfer coefficients with predicted values for evaporation and condensation

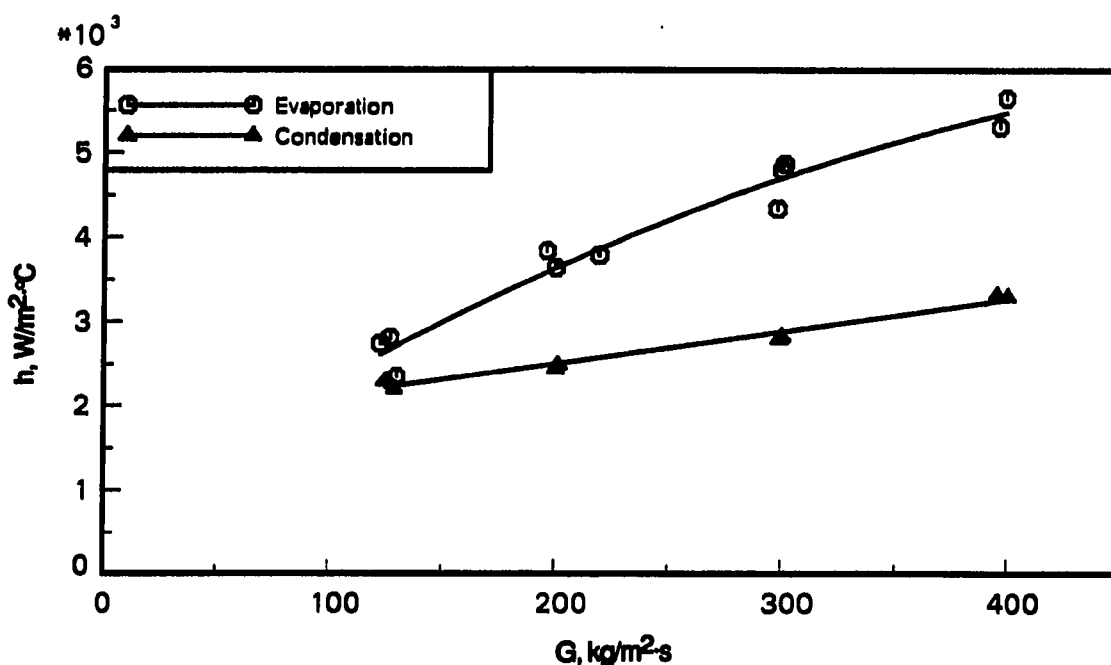


Figure 6.3. Heat transfer coefficient versus mass flux for evaporation and condensation with pure R-22 in a smooth tube

transfer coefficient versus mass flux for evaporation and condensation of refrigerant-oil mixtures with 150- and 300-SUS oil. For comparison purposes, the figures also include the pure refrigerant data shown earlier.

Evaporation

150-SUS oil From Figure 6.4, it is seen that the heat transfer coefficient is enhanced for all three oil concentrations. The enhancement peaks at about 2.5% oil and then diminishes as the concentration is further increased. At 200 kg/m²·s, the heat transfer coefficient increases by about 35% with 2.5% oil; at 1.25% and 5% oil, coefficients are about 15% higher than with pure refrigerant.

Evaporation enhancement with the addition of small amounts of oil, as well as the occurrence of a maximum at approximately 1% to 3% oil concentration, has previously been reported by several investigators [15,16,19,31,33,34]. Results from papers reporting on R-22 testing [15,16,19,33,34] are compared with results from the current investigation.

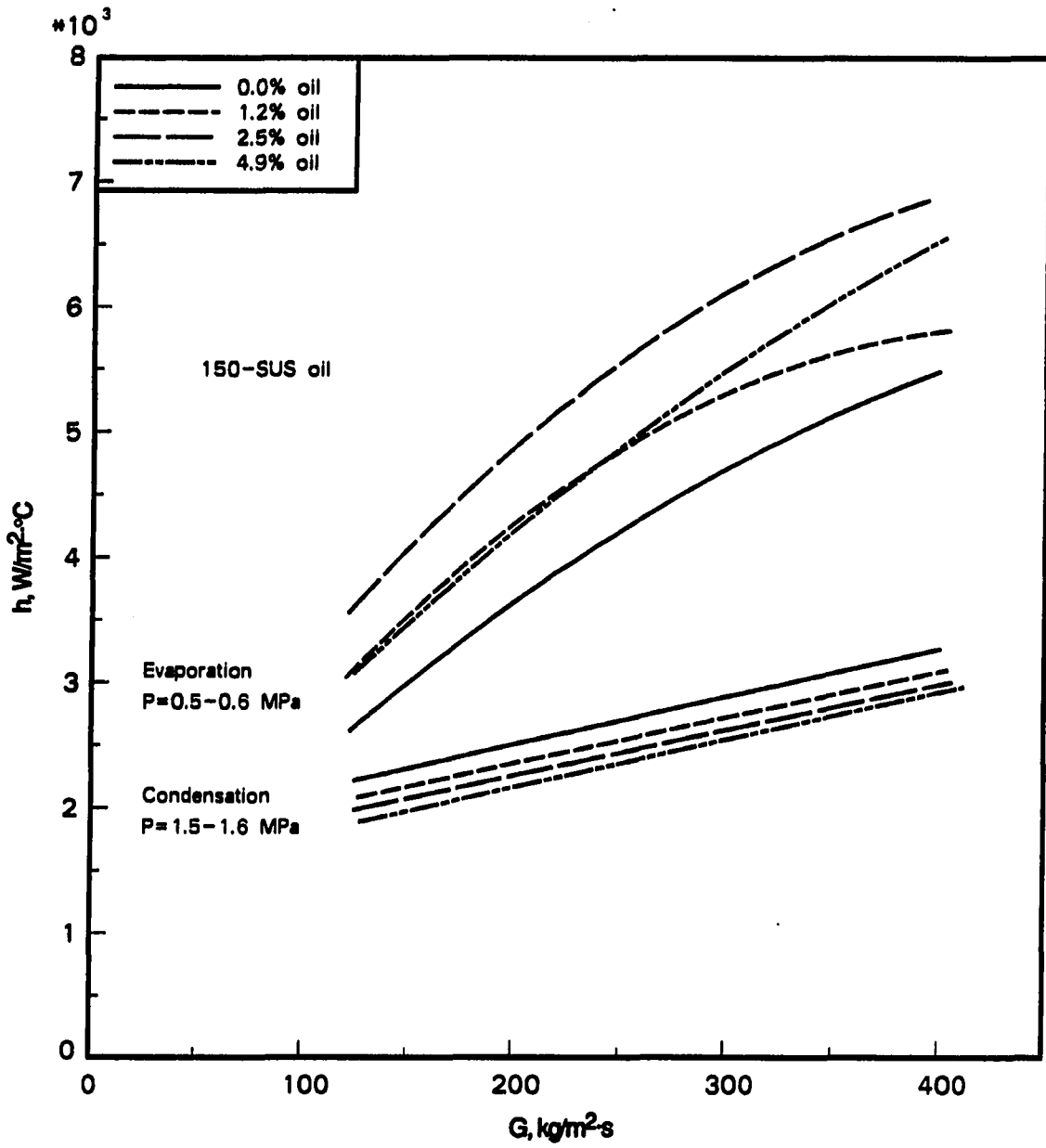


Figure 6.4. Heat transfer coefficient versus mass flux for evaporation and condensation with mixtures of R-22 plus 150-SUS oil

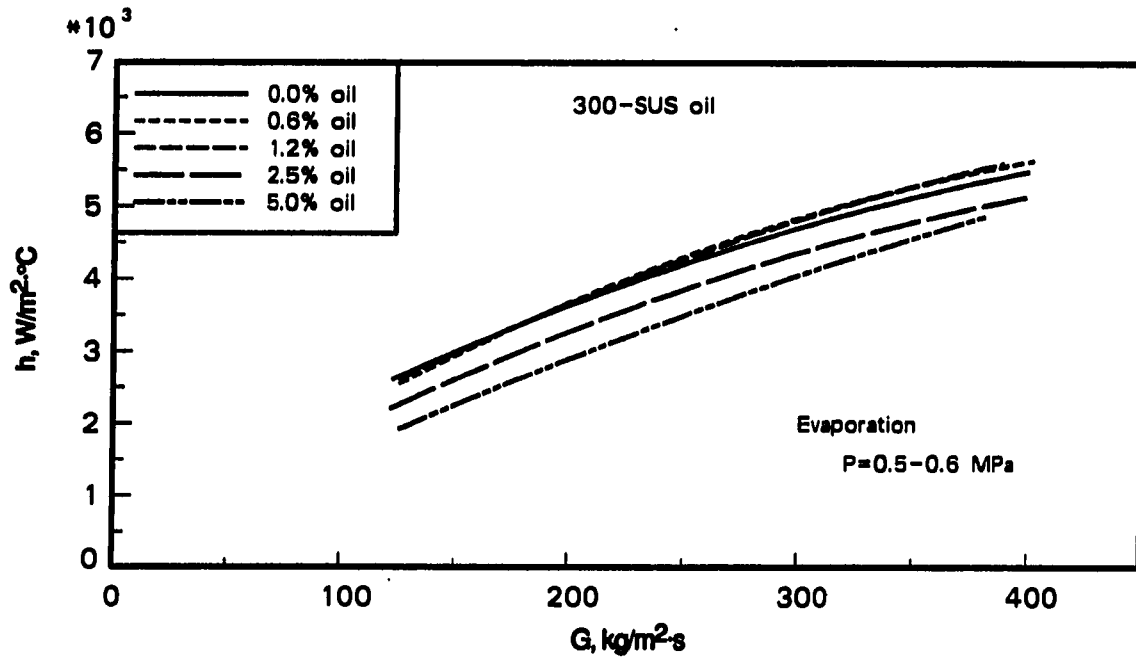
Zimmermann [15,16], using average heat transfer coefficients, found a maximum enhancement factor due to oil of about 1.12 at an oil concentration of 2%. At a mass flux similar to Zimmermann's ($400 \text{ kg/m}^2\text{-s}$), data from the current investigation show $\epsilon_{s'/s}$ of around 1.23 at the same oil concentration. Comparison with Zimmermann's work is complicated by his use of a more viscous, half-synthetic, rather than naphthenic, oil.

Chaddock [19], Mathur [33], and Chaddock and Mathur [34] reported only local heat transfer coefficients using an oil similar to that used in the current study. Graphical integration of their data between 15% and 85% quality is used for comparison. Neither oil concentrations nor mass fluxes correspond exactly to those of this study, but both are relatively close. Integrated average heat transfer coefficients calculated from Chaddock's data agree with those from the current study within $\pm 20\%$ at all oil concentrations except 2.5%, which shows a discrepancy of about 30%. Chaddock's data show a slight dip in $\epsilon_{s'/s}$ at 2.9% oil concentration, whereas Zimmermann and the current investigation indicate a maximum enhancement at about 2.5% oil.

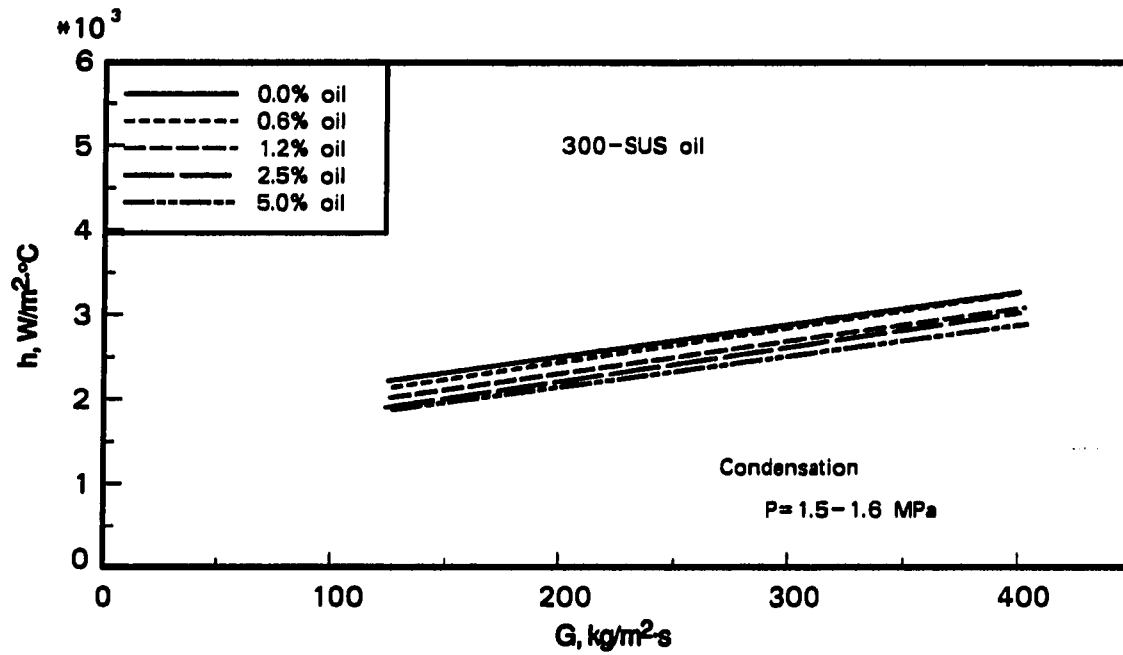
300-SUS oil Results with 300-SUS oil are shown in Figure 6.5. Below 1.3% oil, there is very little effect on the heat transfer coefficient when compared to the performance with pure refrigerant. There appears to be a slight enhancement of heat transfer at these low concentrations, but the curves for pure refrigerant, 0.6% oil, and 1.3% oil are all quite close. At higher concentrations, there is a degradation of heat transfer by as much as 20%.

No previous publications have reported results with mixtures of refrigerant and 300-SUS oil during in-tube evaporation, so comparisons are not possible.

Comparison of 150- and 300-SUS oil For comparison, heat transfer coefficient data discussed above have been recast in terms of heat transfer enhancement factors (ϵ), as defined in Chapter 5. Figure 6.6 shows $\epsilon_{s'/s}$ for each oil as a function of oil concentration at two mass fluxes. It is evident that results with 150-SUS oil are significantly above those with 300-SUS oil. At the lower mass flux, an enhancement of over 30% is seen with 150-SUS oil, while there is a general degradation with 300-SUS oil. The 300-SUS oil does, however, show a slight enhancement for low concentrations below 1.3%.

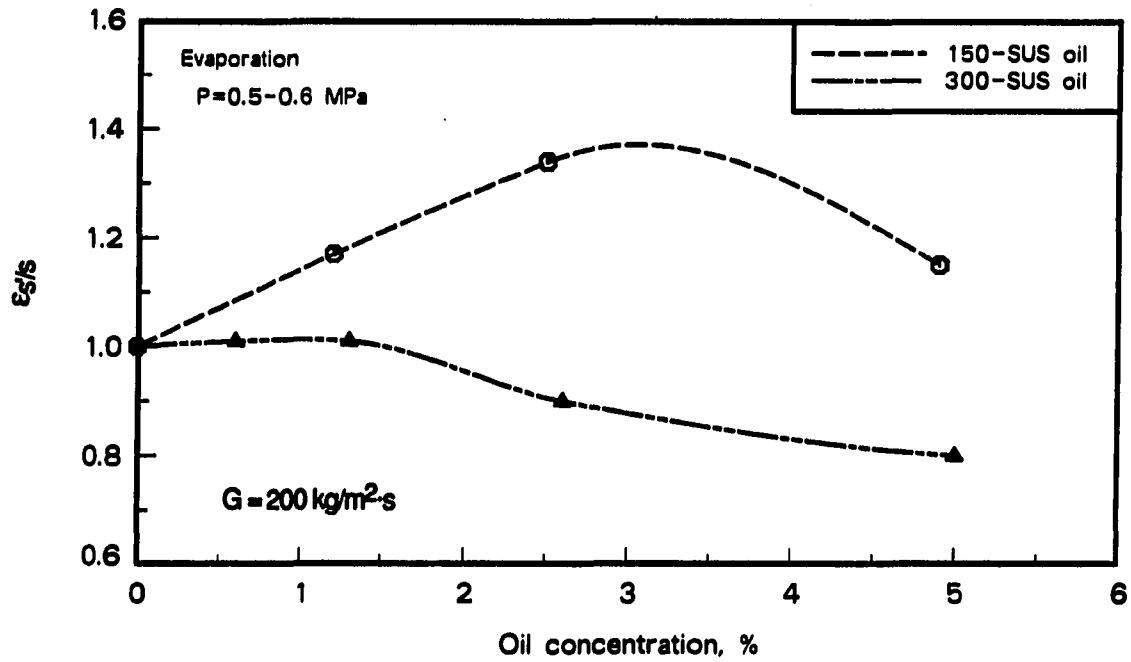


(a)

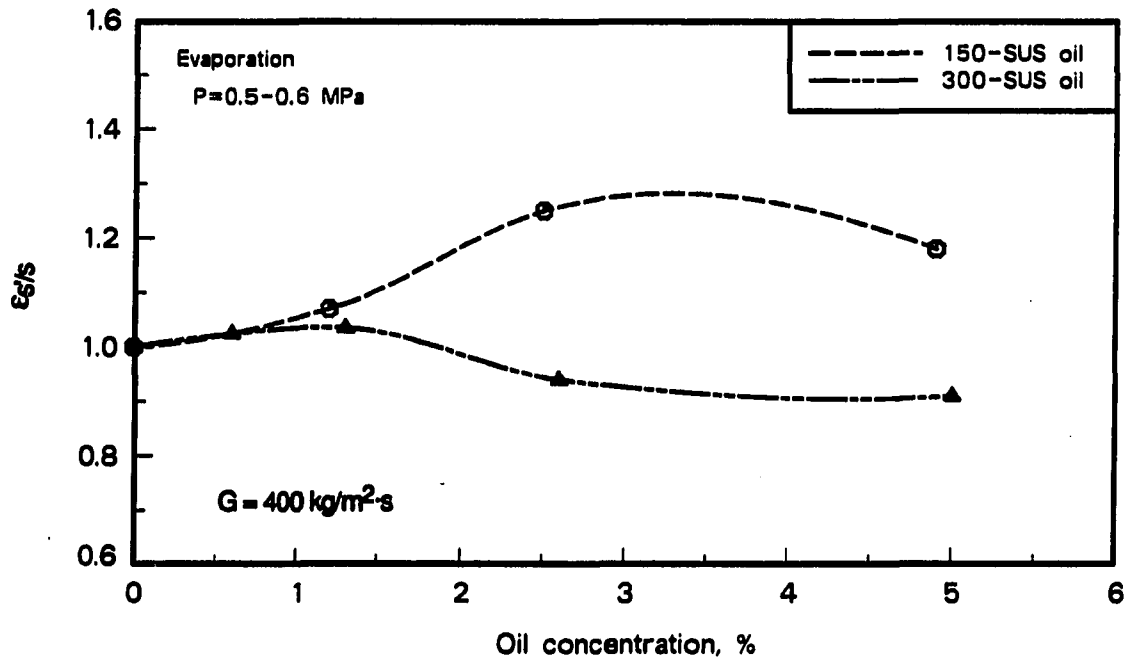


(b)

Figure 6.5. Heat transfer coefficient versus mass flux for evaporation and condensation with mixtures of R-22 plus 300-SUS oil



(a)



(b)

Figure 6.6. Evaporation heat transfer enhancement factor (ϵ_s/s) versus oil concentration for 150- and 300-SUS oil at two mass fluxes

The enhancement with 150-SUS oil decreases at the higher mass flux, but the maximum enhancement is still more than 20%, while the degradation with 300-SUS oil is somewhat less than is observed at the lower mass flux. The performance difference between mixtures of the two oils narrows as the mass flux increases.

Condensation

150-SUS oil Figure 6.4, shown earlier, shows condensation heat transfer data with 150-SUS oil. In general, heat transfer is degraded by the presence of oil, with larger oil concentrations yielding lower heat transfer coefficients. This trend is in agreement with the literature [47]. Compared with evaporation, oil appears to have a less dramatic and more orderly effect on condensation heat transfer. The heat transfer coefficient decreases by about 8% and 15% for mixtures of 2.5% and 4.9% oil, respectively.

Relatively little has been published on in-tube condensation of refrigerant-oil mixtures. No studies were found that used either R-22 or 150-SUS mineral oil. Therefore, comparisons with earlier results are presented in the next section, where Tichy's [47] work with mixtures of R-12 and 300-SUS oil is discussed.

300-SUS oil Condensation results with 300-SUS oil are shown in Figure 6.5, which was introduced earlier. There is no observed enhancement of heat transfer with the addition of oil, but rather a steadily decreasing heat transfer coefficient as the oil concentration rises. The heat transfer coefficient decreases by about 13% and 8% at oil concentrations of 5.0% and 2.5%, respectively.

The publication of Tichy et al. [47] was the only literature that reported on in-tube condensation experiments with refrigerant-oil mixtures. Using R-12 rather than R-22, the addition of 5% 300-SUS oil caused condensation heat transfer to degrade by 23%, almost twice that of the current investigation. With 2% oil, they found a degradation of 10%, while the current results show a degradation of about 8%.

Comparison of 150- and 300-SUS oil As before, an enhancement factor is used as a basis for comparing the performance of the two oils. Figure 6.7 plots $\epsilon_{s'/s}$ for both oils versus oil concentration at two mass fluxes. At both mass fluxes, heat transfer performance is similar with mixtures of both oils. There is an apparent tendency for heat transfer

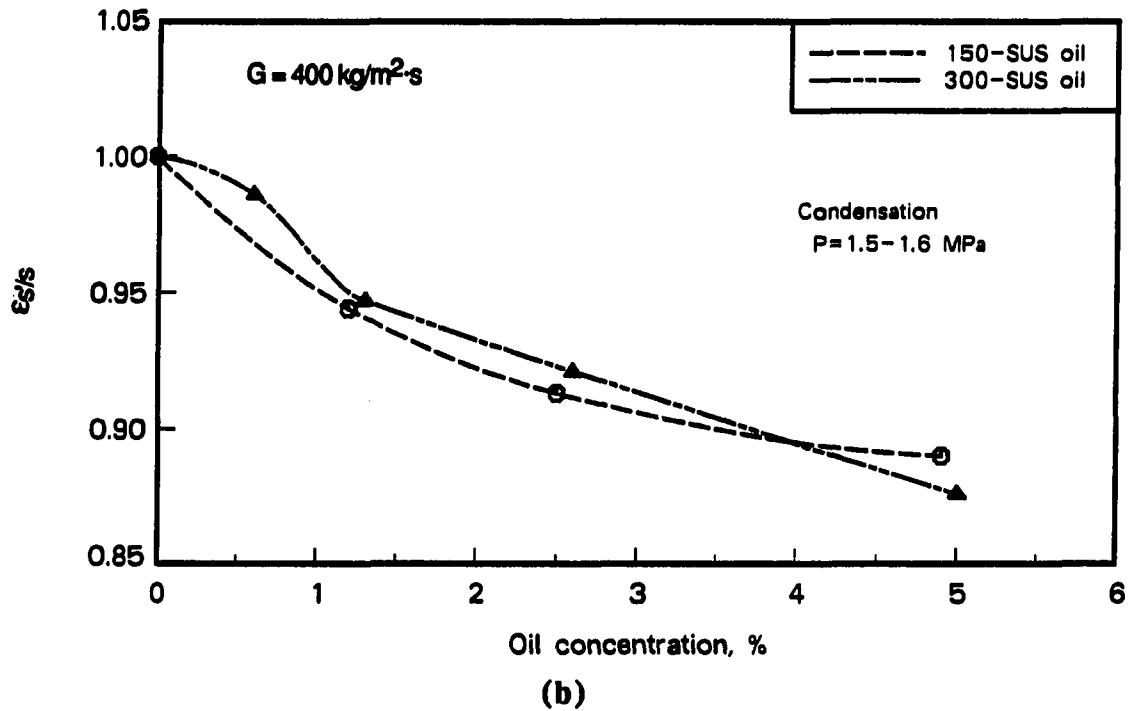
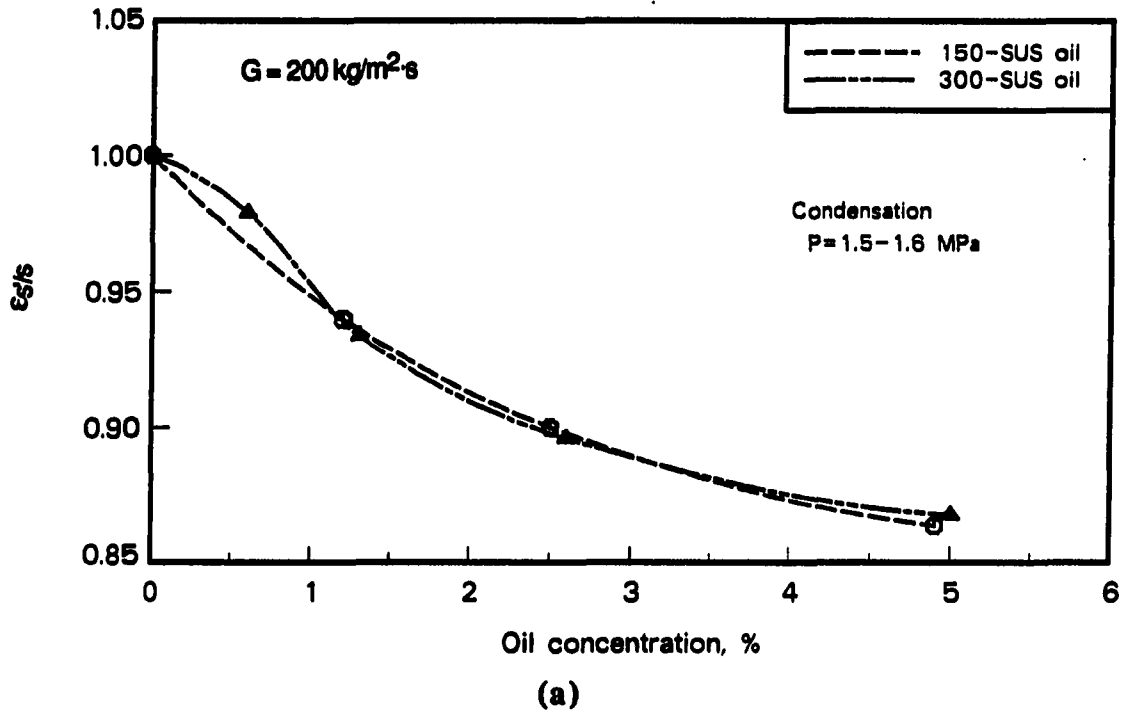


Figure 6.7. Condensation heat transfer enhancement factor ($\epsilon_{s/s}$) versus oil concentration for 150- and 300-SUS oil at two mass fluxes

degradation to attenuate (that is, for ϵ_s/s to increase) with increasing mass flux; however, all data lie within a range narrower than the uncertainty of ϵ_s/s .

Initially, it seems somewhat surprising how similar condensation performance is with such different oil viscosities. Equation 2.2, however, indicates that at condensation conditions and 5% oil concentration, mixture viscosities with the two oils differ by less than 4%. Oil hold-up tests, which are reported in the last section of this chapter, show that the actual oil concentration in the test section is higher than the flowing average. Again using Equation 2.2, but with 10% oil concentration as a hypothetical example, the viscosity difference between mixtures with the two oils is still only about 7%. In light of these relatively small changes in mixture viscosity, the results are not unreasonable.

Pressure Drop

As with heat transfer, curves are fitted to pressure drop data and these are used to determine the pressure drop enhancement factor, ψ . The data are especially uncertain at low mass fluxes, where the magnitude of the measurement itself is small (see Appendix D). As discussed in Chapter 4, pressure drop was sampled 35 times during each test run, due to the fluctuations. To illustrate the magnitude of the uncertainty, at a 95% confidence level ($\pm 2\sigma$), the uncertainty for a single condensation test run ranges from about ± 1 kPa to more than ± 3 kPa, while the magnitude of the pressure drop itself is less than 4 kPa for mass fluxes of $200 \text{ kg/m}^2\text{-s}$ or less. Uncertainties for pressure drop, both for single samples and for values from regression equations, are tabulated in Appendix D.

In addition to the effects of friction, pressure drop during evaporation or condensation is also a function of quality change because of the momentum contribution to pressure drop. Since only total pressure drop across the test section was measured in this investigation, similar inlet and outlet qualities for each pressure drop test was the goal; but test conditions, including quality, could not be held perfectly constant from one test to another. Inlet and outlet qualities are generally within ± 0.08 of the target value. Momentum pressure drop, however, is less than 15% of frictional pressure drop for the conditions of this investigation. Some of the observed scatter may be due to quality

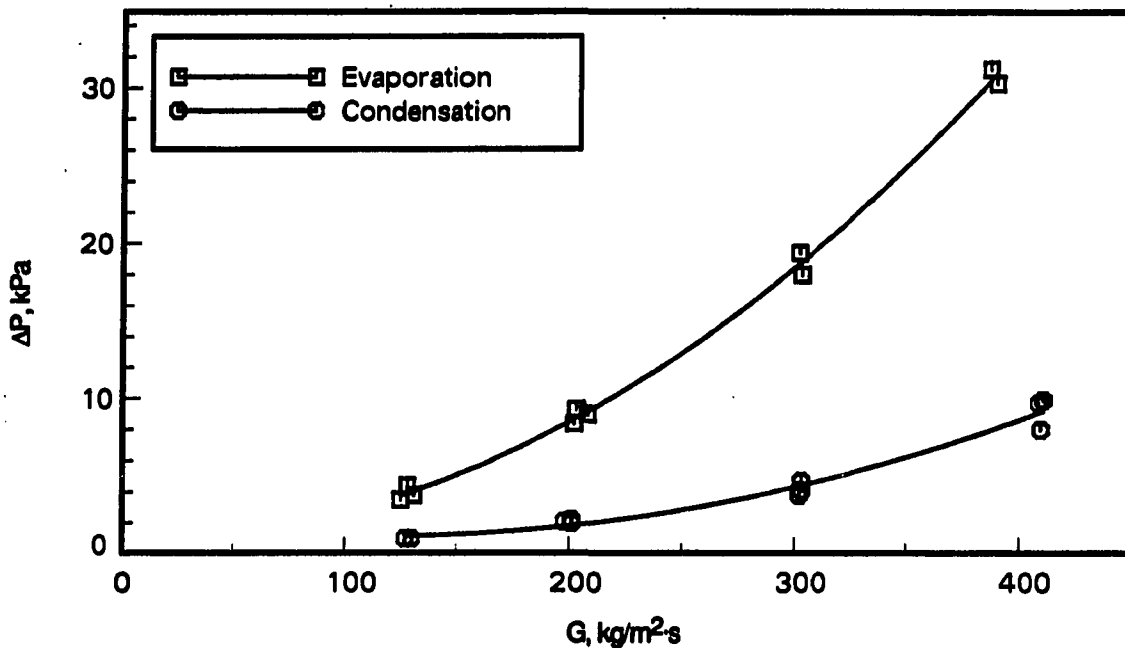


Figure 6.8. Evaporation and condensation pressure drop versus mass flux with pure R-22

variations, but the primary reason for scatter is the fluctuating nature of the two-phase flow, as indicated by the large standard deviations from the pressure drop measurements.

Pure Refrigerant

Pure refrigerant total pressure drop during evaporation and condensation is shown in Figure 6.8 as a function of mass flux. The evaporation pressure drop is approximately three times higher than that of condensation. The major reason for this is the difference between evaporation and condensation conditions.

Evaporation Pressure drop is compared with the correlations of Pierre [44], Lockhart and Martinelli [75], Baroczy [163], Chisholm [164], and Reddy et al. [165], as well as with the homogeneous model. Chapter 10 gives a description of these correlations. Momentum pressure drop is estimated using the homogeneous model because the separated flow model yields almost identical results and the momentum term accounts for less than 15% of the total pressure drop. Figure 6.9 compares experimental pressure drop with that predicted by the correlations. The homogeneous, Lockhart-Martinelli, Baroczy, and Pierre

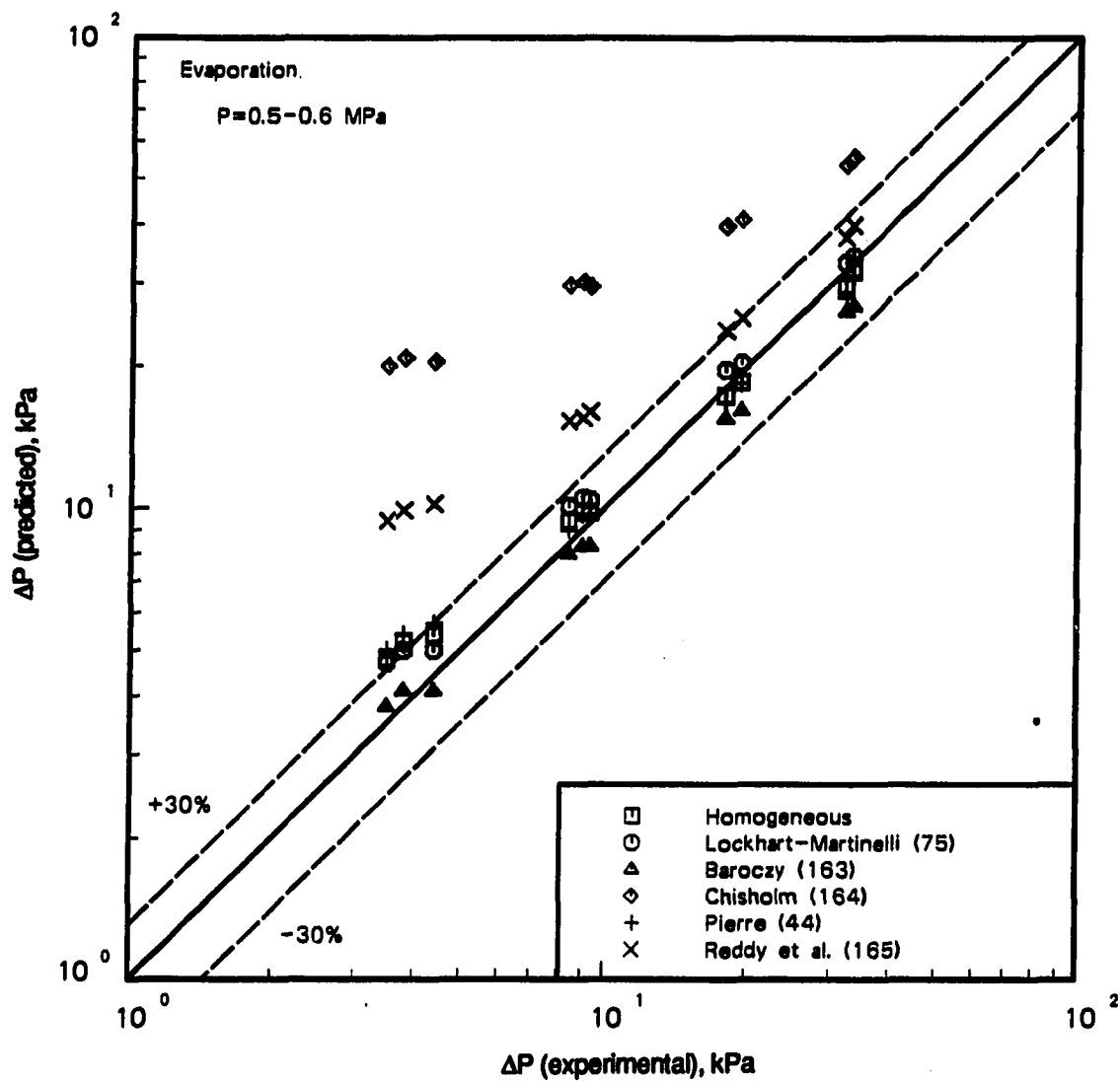


Figure 6.9. Comparison of experimental evaporation pressure drop with predicted values

correlations all predict pressure drop within $\pm 30\%$ of measured values for most conditions. The Pierre correlation was derived exclusively from refrigerant data (R-12 and R-22) in horizontal tubes, so it might be expected to predict results well. The other correlations are more general and are primarily based on steam-water flow; however, Baroczy includes a procedure to correct for fluids other than water.

Chisholm and Reddy are both significantly high in their predictions, probably because of the low mass flux range used in this study. Both of these correlations improve as the mass flux increases. At a hypothetical mass flux of about $800 \text{ kg/m}^2\text{-s}$, these correlations agree more closely with the others, but these higher mass fluxes were beyond the range of the current test program.

Condensation Condensation pressure drop with pure refrigerant is compared to the same correlations as used for evaporation. With the exception of the Lockhart-Martinelli correlation, which does not predict condensation results well, the same correlations that successfully predicted evaporation performance also predict condensation performance. A comparison of predicted and measured pressure drop results is shown in Figure 6.10. The Pierre correlation, although developed solely from evaporation data, is also a good predictor of condensation pressure drop. The homogeneous, Baroczy, and Pierre correlations generally predict pressure drop within $\pm 30\%$ of experimental values. As with evaporation, the poorer predictors tend to improve at higher mass fluxes, and the total predicted pressure drop is insensitive to the choice of void fraction model.

Refrigerant-Oil Mixtures

Evaporation Figure 6.11(a) shows a general increase in evaporation pressure drop as 150-SUS oil is added, but given the uncertainty, the increase cannot be considered definitive at all conditions. The lines of pressure drop cross at some conditions, but this is probably due to scatter and the process of curve fitting. Figure 6.11(b) shows similar results with the addition of 300-SUS oil. Trends are similar to those with 150-SUS oil and the magnitude of the pressure drop increase is not significantly higher with the more viscous oil. At a 5% oil concentration, the pressure drop increase with 150-SUS oil is about 25% to 35% while the increase with 300-SUS oil is around 30% to 45%.

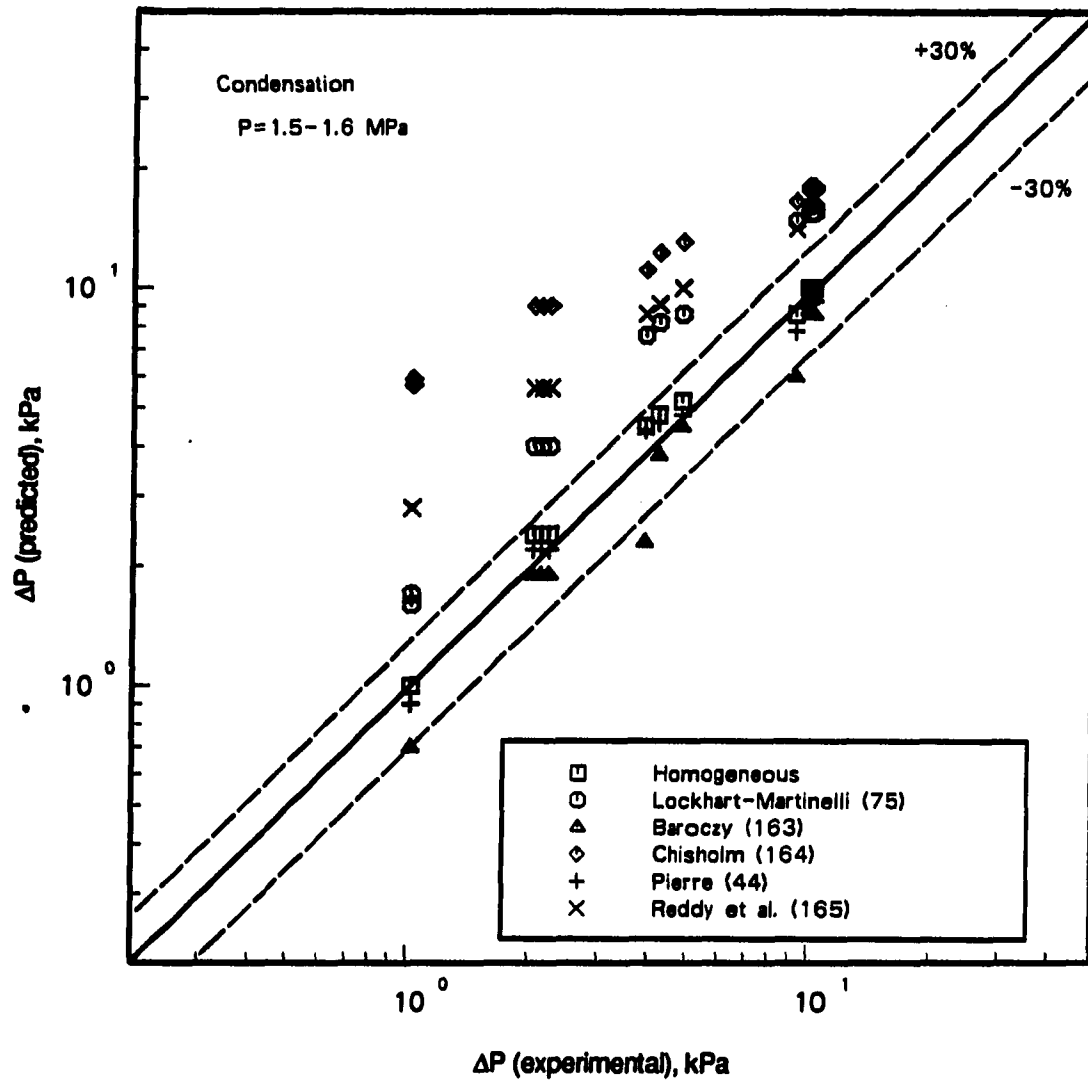
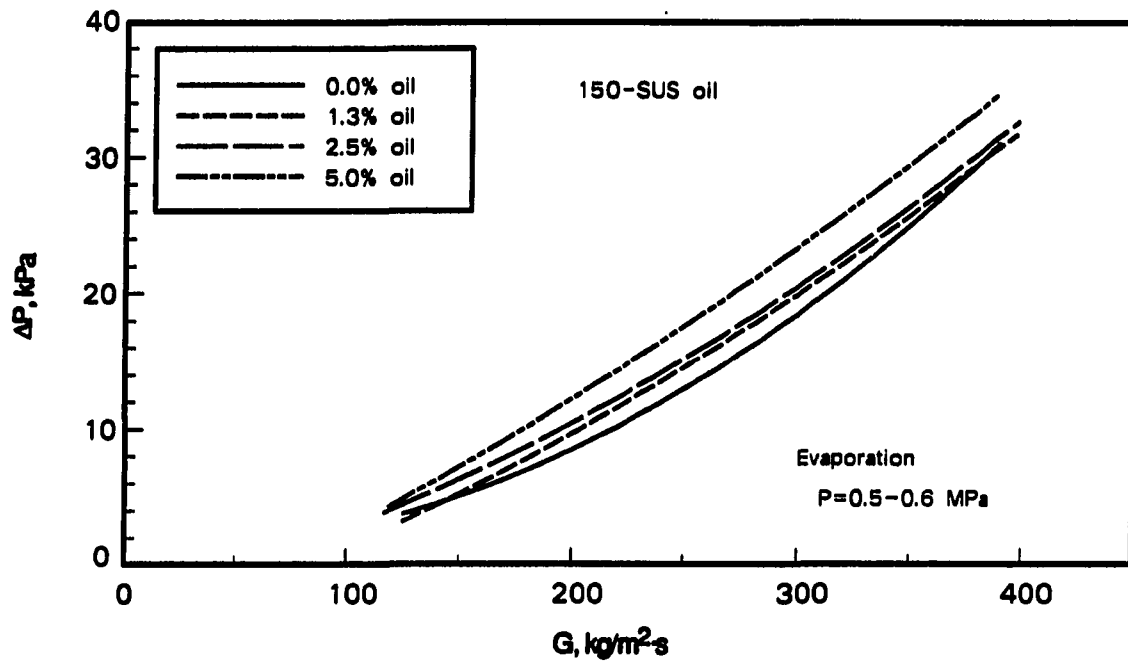
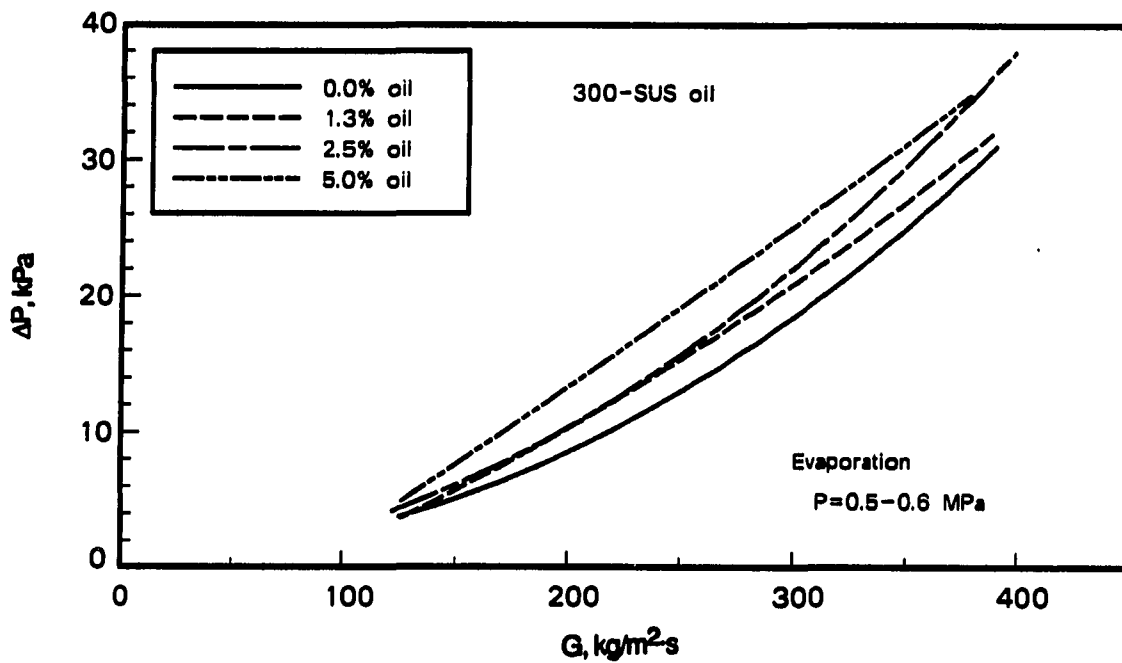


Figure 6.10. Comparison of experimental condensation pressure drop with predicted values



(a)



(b)

Figure 6.11. Evaporation pressure drop versus mass flux with 150- and 300-SUS oil

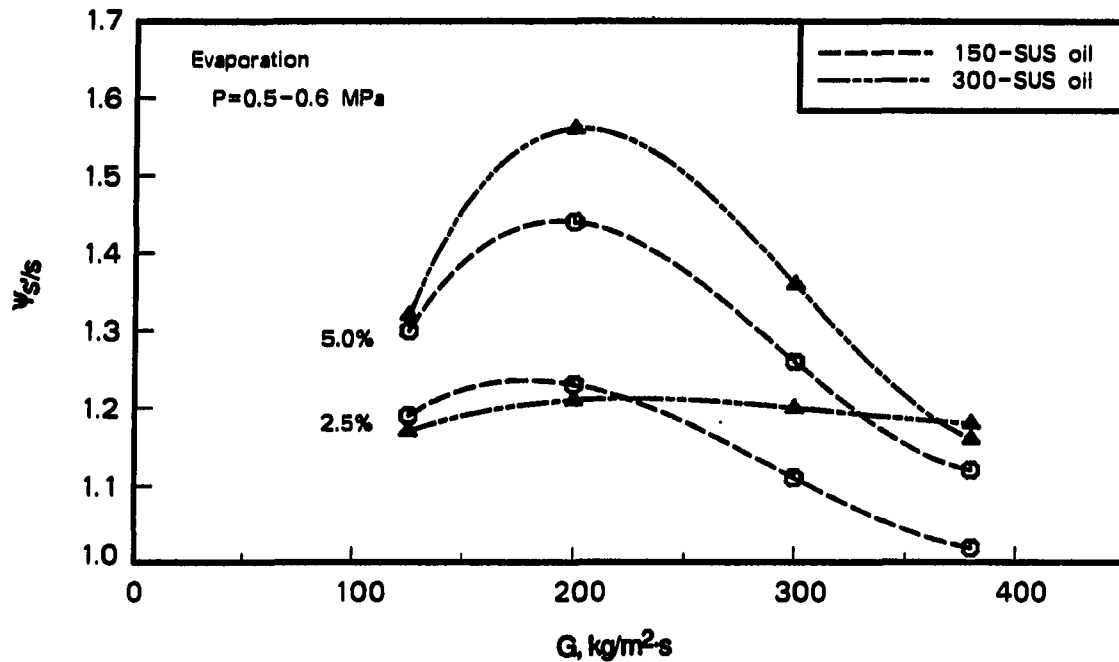


Figure 6.12. Evaporation pressure drop enhancement factor ($\Psi_{s'/s}$) versus mass flux with 150- and 300-SUS oil

The pressure drop enhancement factor, $\Psi_{s'/s}$, is shown in Figure 6.12 for both oils as a function of mass flux at concentrations of 2.5% and 5.0%. In general, mixtures with 300-SUS oil have a higher pressure drop than those with 150-SUS oil, although this appears to reverse at low mass flux (where uncertainty is highest). Over most of the mass flux range, $\Psi_{s'/s}$ with 5.0% oil is substantially higher than it is with an oil concentration of 2.5%. At higher mass fluxes, however, the pressure drop penalty at both concentrations becomes similar. The curves of $\Psi_{s'/s}$ versus mass flux tend to group themselves according to oil concentration, with both oils showing similar trends at a given oil concentration.

Pierre [44] did not test with oil in R-22 but rather with oil in R-12. With oil concentrations in the range of 6% to 12% by volume, he found that the friction factor approximately doubled. Tichy et al. [46] also reported a substantial pressure drop increase of about 80% with the addition of 300-SUS oil to R-12. Other investigators have not found as great an increase with oil. Hatada et al. [45] had a pressure drop increase of about 25%

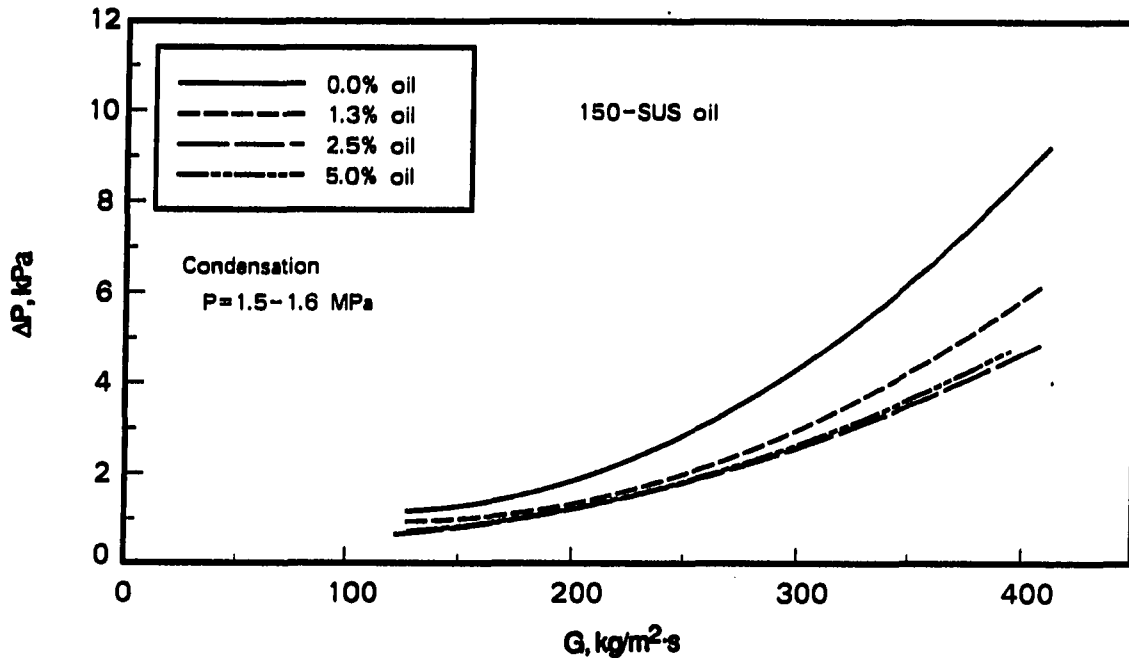
with 6% oil in R-22 and an increase of about 40% with 20% oil. Hughes et al. [37] found the total evaporator pressure drop to increase by about 34% with 5% oil.

There is a rather large spread in the results of earlier investigators, probably due to a combination of several factors, such as types of refrigerant and oil used, evaporation temperature, flow regime, etc. This illustrates again the difficulty when comparing results from different investigations. Results from the current investigation generally fall at the lower end of the earlier results mentioned above.

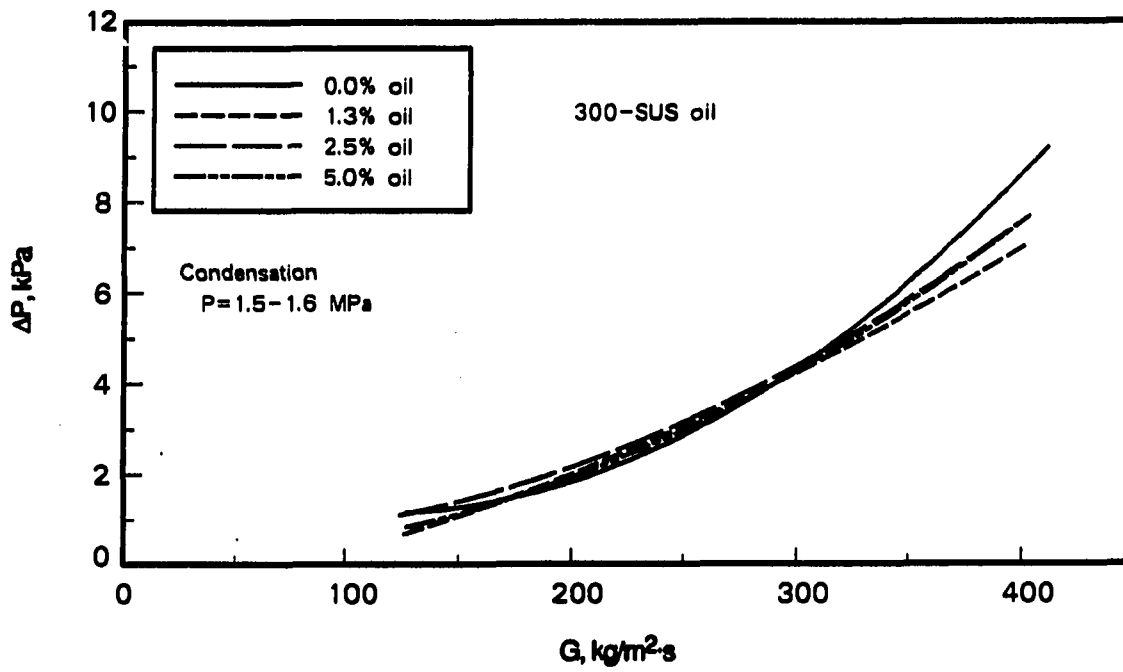
Condensation Figure 6.13 presents condensation pressure drop results for 150- and 300-SUS oil. It is surprising in Figure 6.13(a) that the pressure drop decreases substantially with the addition of 150-SUS oil. With 300-SUS oil, there is no clear trend of increasing or decreasing pressure drop, except perhaps at high mass flux, where there appears to be a slight decrease with the addition of oil. With 150-SUS oil, the decrease in pressure drop is as much as 45% with concentrations of 2.5% and 5.0% oil.

Figure 6.14 shows $\Psi_{s'/s}$ for both types of oil at concentrations of 2.5% and 5.0%. Pressure drop with mixtures of 150-SUS oil is about 60% of that with pure refrigerant and remains relatively constant with changes in mass flux and oil concentration. Mixtures of 300-SUS oil show more variation of $\Psi_{s'/s}$ with mass flux, but the value of $\Psi_{s'/s}$ is around 1.0 on average. With evaporation (see Figure 6.12), curves of like oil concentration tend to fall together for both oils, whereas with condensation, curves of the same oil type tend to be grouped at varying concentrations. For 300-SUS oil, this is perhaps explained by the relatively narrow range in which all data lie. Much of the fluctuation of $\Psi_{s'/s}$ is probably due to the curve fitting, rather than to a physical phenomenon. With 150-SUS oil, this particular grouping of curves might be attributed to passing through a relative minimum somewhere between 2.5% and 5.0%. The data on Figure 6.13(a) show a trend of decreasing $\Psi_{s'/s}$ with the addition of 1.25% oil, a further decrease with 2.5%, and a slight increase with 5.0%.

The unusual behavior of decreasing pressure drop with increasing viscosity can perhaps be attributed to changes of flow pattern in the tube with the addition of oil. Typical condensation conditions are plotted on the flow pattern map of Baker [166] in Figure 6.15. It is seen that tests do cross one of Baker's boundaries as quality changes and that the



(a)



(b)

Figure 6.13. Condensation pressure drop versus mass flux with 150- and 300-SUS oil

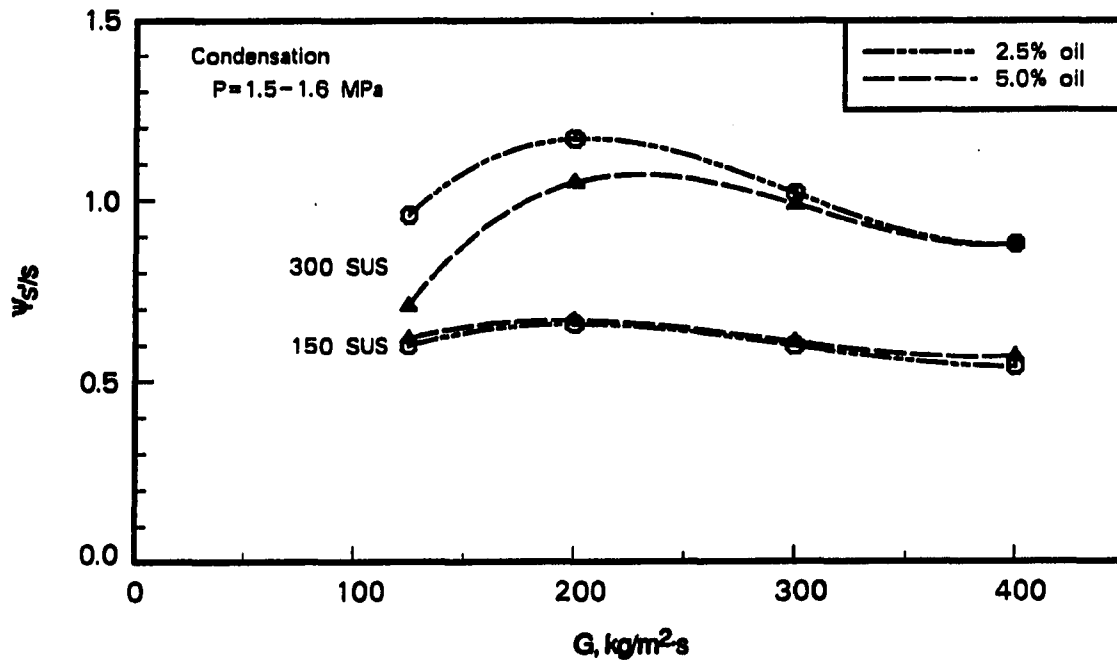
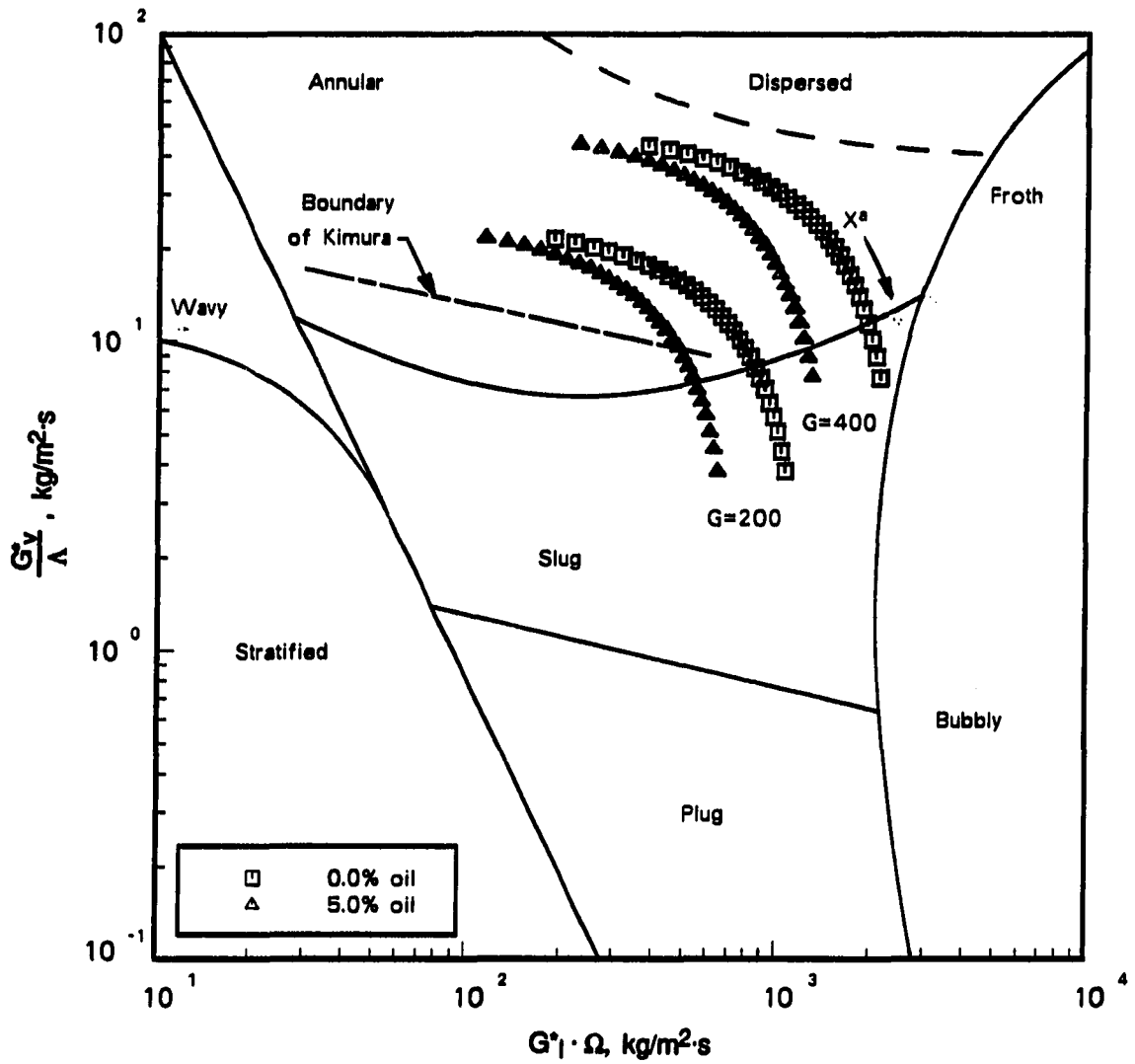


Figure 6.14. Condensation pressure drop enhancement factor (Ψ_s/s) versus mass flux with 150- and 300-SUS oil

addition of oil changes the trajectory somewhat. The annular regime boundary of Kimura (Kimura and Ito [114]), which was developed using R-22, is also added for reference. None of the boundaries on the flow regime map can be used to definitively explain the observed pressure drop behavior, but the location of the data—straddling a flow regime boundary—lends support to the theory that the anomalous behavior may be caused by changes in the flow regime.

Only Tichy et al. [46] have reported condensation pressure drop results with refrigerant-oil mixtures. They found only minor pressure drop increases with increasing concentrations of 300-SUS oil in R-12. At a concentration of 2% oil, the pressure drop increased by only about 2%, while with a 5% oil concentration, pressure drop increased by about 6%.



^aArrow shows direction of decreasing vapor quality.

Figure 6.15. Baker flow regime map with typical condensation test conditions [166]

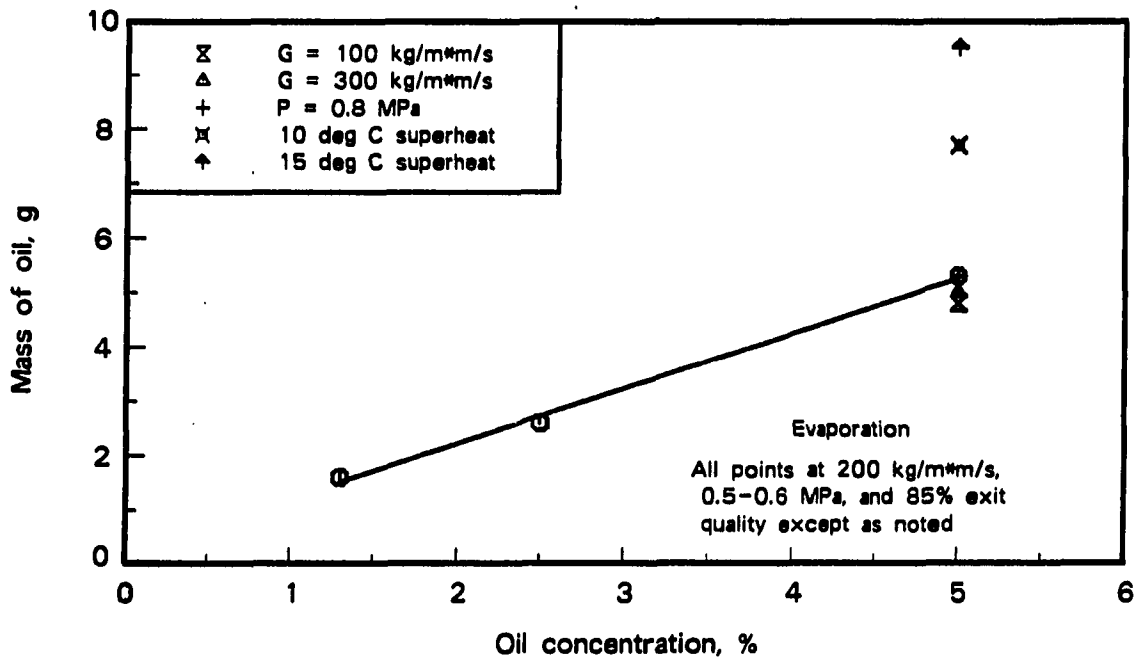
Oil Hold-Up

In order to gain insight into the observed heat transfer and pressure drop behavior, several hold-up tests were performed. In this document, hold-up generally refers to the quantity of oil in the test section. The discussion also attempts to relate this quantity to the average concentration flowing through the entire system to see if viscous effects lead to significantly higher oil concentrations in two-phase flow regions. For the most part, these tests determined only the mass of oil present at varying conditions. For four cases, the mass of refrigerant, as well as that of oil, was measured to give the mass fraction of oil in the test section. Parameters whose effect on hold-up was investigated are mass flux (100 to 300 kg/m²·s), oil concentration (1.2% to 5.0%), viscosity (150 and 300 SUS), evaporation exit conditions (80% to 85% quality and 10 to 15°C superheat), and evaporation pressure (0.5 and 0.8 MPa).

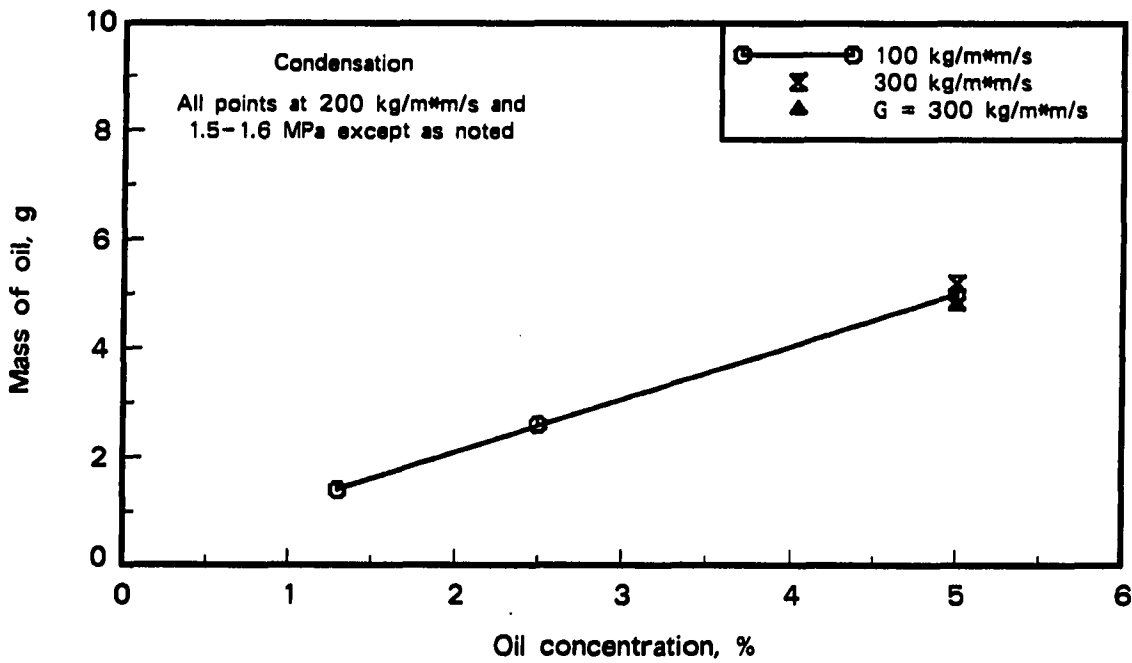
Additional conditions, such as inlet superheating, were not attempted during condensation. The inlet to the test section was much different in geometry, flow path, etc., than the entrance to a refrigerant condenser. Additionally, an actual condenser might have a large amount of atomized oil coming from the compressor which could not be simulated in the test rig. Since these differences were so apparent, the extra test conditions for condensation were not attempted.

Figure 6.16 shows the amount of oil in the smooth tube with 150-SUS oil and Figure 6.17 shows the amount with 300-SUS oil. Tabular data are included in Appendix E. Several conclusions appear to be valid for both evaporation and condensation: (1) the amount of oil in the test section is proportional to the average flowing oil concentration, (2) mass flux has little effect on the oil in the test section, and (3) the viscosity of the oil, at least in the range of 150 to 300 SUS, does not have a dramatic effect on the hold-up, although the higher viscosity oil does have about 25% more oil in the test section.

The additional conditions tested during evaporation show that pressure has very little effect on the hold-up, but introducing an exit superheat increases the quantity of oil rather significantly. The mass of oil in the test section almost doubles with 15°C exit superheat. This result might be expected, since for a significant portion of the evaporator, the flowing liquid mixture would be primarily oil and, therefore, quite viscous.



(a)



(b)

Figure 6.16. Quantity of oil in the smooth tube with 150-SUS oil

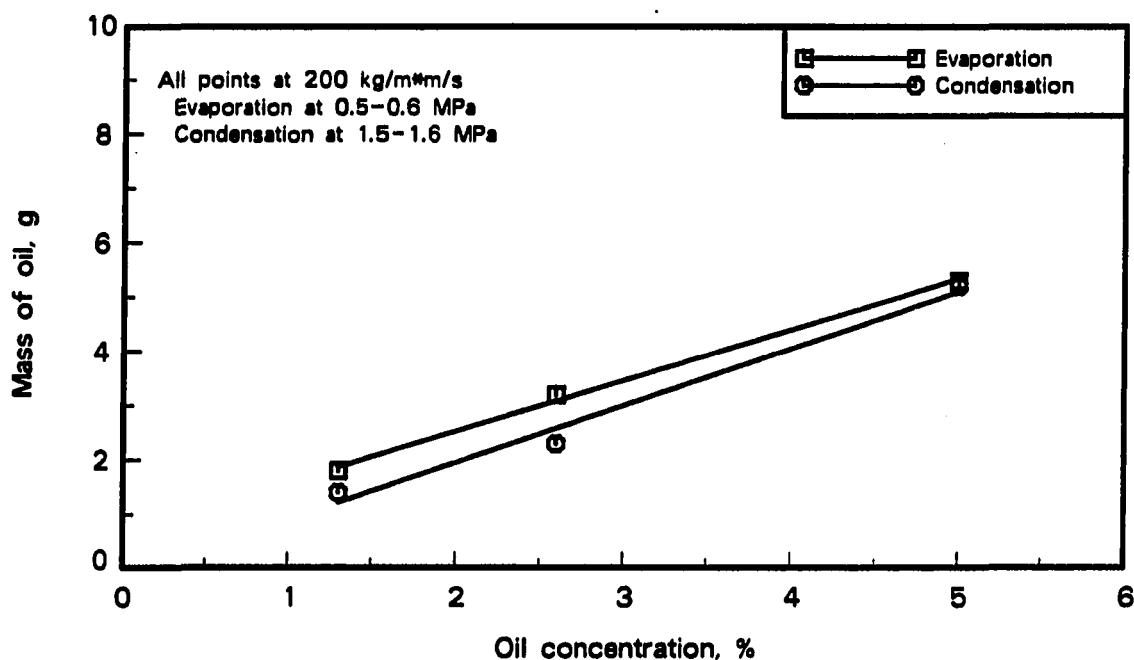


Figure 6.17. Quantity of oil in the smooth tube with 300-SUS oil

Tests to determine the actual mass fraction of oil in the test section were carried out at 200 kg/m²-s and 5.0% oil with 150-SUS oil only. The evaporation case was over a quality range of 15% to 90% and at a pressure of 0.49 MPa, while the condensation case was over a quality range of 80% to 5% with a pressure of 1.49 MPa. There were 28 g of refrigerant (5.3 g oil) in the evaporator and 58 g of refrigerant in the condenser (5.0 g oil), which yield oil concentrations of 16% and 8%, respectively, based on total mass in the test section. These concentrations are about triple and double, respectively, the average flowing concentration in the system, which was nominally 5.0%. Even though the mass of oil in the test section during evaporation and condensation is similar, the amount of refrigerant in the two cases is quite different, leading to different oil concentrations.

Because the viscosity of the oil is much higher relative to the refrigerant at evaporation conditions, the higher oil concentration during evaporation is not unexpected. The larger refrigerant mass in the test section during condensation could be due to several factors. One possibility is a difference in average quality during evaporation and condensation. Average quality was about 10% higher for evaporation, which would lead to

a higher void fraction and, hence, a lower mass. Another possibility is that the entrance region of the test section might produce different effects for evaporation and condensation.

Summary

This section summarizes results from the testing of a smooth tube using pure refrigerant and refrigerant-oil mixtures. The major conclusions drawn from the experimental work are given below.

The results for pure refrigerant heat transfer are in good agreement with established correlations. For single-phase flow, the correlation of Petukhov-Popov [156] provides the best agreement with experimental data. For evaporation, the correlations of Kandlikar [158] and Gungor and Winterton [157] predict results well and for condensation, the correlations of Traviss et al. [161], Shah [160], and Cavallini and Zecchin [162] are all within $\pm 20\%$ of experiment, except at the lowest mass flux. Experiments with refrigerant-oil mixtures yielded data similar to those observed by earlier researchers, but the magnitude of the effect is different in some cases.

Evaporation pressure drop is predicted within $\pm 30\%$ by the homogeneous model and the correlations of Lockhart and Martinelli [75], Baroczy [163], and Pierre [44]. The Baroczy correlation agrees best with experimental data. For condensation, the homogeneous model and the correlations of Baroczy and Pierre generally predict results with $\pm 30\%$. The homogeneous model and Pierre correlation are the best predictors of condensation pressure drop. Results for pressure drop are subject to higher relative uncertainties than those for heat transfer, especially at low mass fluxes and for condensation.

The addition of oil to the test matrix makes it very difficult to find previous work that approximates the conditions of the current research and, consequently, comparison with earlier work is difficult. Following is a listing of the main conclusions based on smooth tube testing. Numerical examples, unless stated otherwise, are at a representative mass flux of $300 \text{ kg/m}^2\cdot\text{s}$.

Evaporation

1. Small quantities of oil can enhance heat transfer in the quality range of 15% to 85%. The enhancement is very minor for 300-SUS oil, with $\epsilon_{s'/s}$ never more than 1.05; but the maximum enhancement factor for 150-SUS oil is about 1.3. The enhancement factor remains greater than 1.0 at all concentrations with 150-SUS oil but falls under 1.0 for 2.5% or higher concentrations of 300-SUS oil, indicating heat transfer degradation. The peak enhancement occurs at about 2.5% oil with 150-SUS oil and at about 1.3% with 300-SUS oil.
2. The heat transfer coefficient increases with increasing mass flux for both pure refrigerant and refrigerant-oil mixtures. Enhancement factors due to oil ($\epsilon_{s'/s}$) generally decrease as mass flux increases, but the trend is more pronounced with 150-SUS oil. With a 2.5% concentration of 150-SUS oil, $\epsilon_{s'/s}$ falls from 1.36 to 1.25 as mass flux increases from 200 to 400 kg/m²·s. With the same concentration of 300-SUS oil at the corresponding mass fluxes, $\epsilon_{s'/s}$ falls from 0.94 to 0.90.
3. Pressure drop increases with increasing mass flux, with higher oil concentrations, and with increasing oil viscosity. For a 2.5% concentration of 150-SUS oil, the pressure drop enhancement factor ($\Psi_{s'/s}$) is about 1.1; for 5%, $\Psi_{s'/s}$ is over 1.25. With 300-SUS oil at the same concentrations, the values of $\Psi_{s'/s}$ increase to 1.2 and 1.35, respectively.
4. Average oil concentration in the test section is approximately three times the system average. The amount of oil hold-up increases significantly with superheated exit conditions, but shows little influence of mass flux or evaporation pressure.

Condensation

1. Oil consistently diminishes heat transfer performance during condensation. The value of $\epsilon_{s'/s}$ for 2.5%, 150-SUS oil is slightly under 0.95 and it falls to around 0.85 as the oil concentration increases to 5%. Oil viscosity has only minor influence on the condensation heat transfer.

2. The heat transfer coefficient increases with increasing mass flux, regardless of the oil concentration. For the enhancement factor, however, it is not possible to identify a mass flux dependence within the constraints of experimental uncertainties.
3. Condensation pressure drop increases with increasing mass flux, but the addition of 150-SUS oil causes a decrease in pressure drop by as much as 40%. On the other hand, the effects of 300-SUS oil appear to be minor, with values of $\Psi_{s/s}$ remaining near 1.0.
4. Oil concentration in the test section is about 1.6 times the system average.

CHAPTER 7

RESULTS WITH THE MICRO-FIN TUBE

As noted earlier, micro-fin tubes are defined as tubes having a large number of very small fins. For example, a typical 9.5-mm diameter tube has 50 or more fins with a fin height less than 2.5% of the inside diameter. There is generally a rifling of the fins at an angle ranging from 7° to 30°. The particular tube used in this study was state-of-the-art at the time of testing, with 60 fins, a fin height of 0.2 mm, and a spiral angle of 18°. The fins were triangular in shape with a rounded peak and a flat valley. More recent work [118] has found that a tube with fewer fins and a wider valley width improved performance, but the fin shape was quite similar to that of the tube used in this study.

The heat transfer enhancement with micro-fin tubes is due to a combination of several factors [119]. The inside heat transfer area is increased by the addition of fins, leading to higher heat flows, even if the convective coefficient is unchanged. For tubes having spiral fins, there may be an increase in the effective length of the tube since fluid in the valleys travels a longer path. Also, with spiral angles, the possibility exists for flow separation, secondary flows, and increased mixing downstream of fin tips. For annular flow, fins act to disturb the liquid film, which is a significant, if not the dominant, thermal resistance. Finally, for condensation, fins tend to thin the condensate film by surface tension forces.

Figure 7.1 is a drawing of the tube and Table 7.1 gives the tube's dimensions. It may be noted that the inside diameter of the micro-fin tube is slightly larger than that of the smooth tube, but correlations indicate that this diameter difference affects heat transfer coefficients by less than 2%. Test conditions were the same as those of the smooth tube (see Table 6.2). Tabulated data for all of the test runs can be found in Appendix E.

Pure Refrigerant Heat Transfer

As with the smooth tube, pure refrigerant tests form a baseline with which to measure the effect of oil on the performance of the micro-fin tube. These results also establish the heat transfer enhancement of the micro-fin tube relative to the smooth tube with pure refrigerant, $\epsilon_{a/s}$. This is the enhancement reported in past augmentation studies.

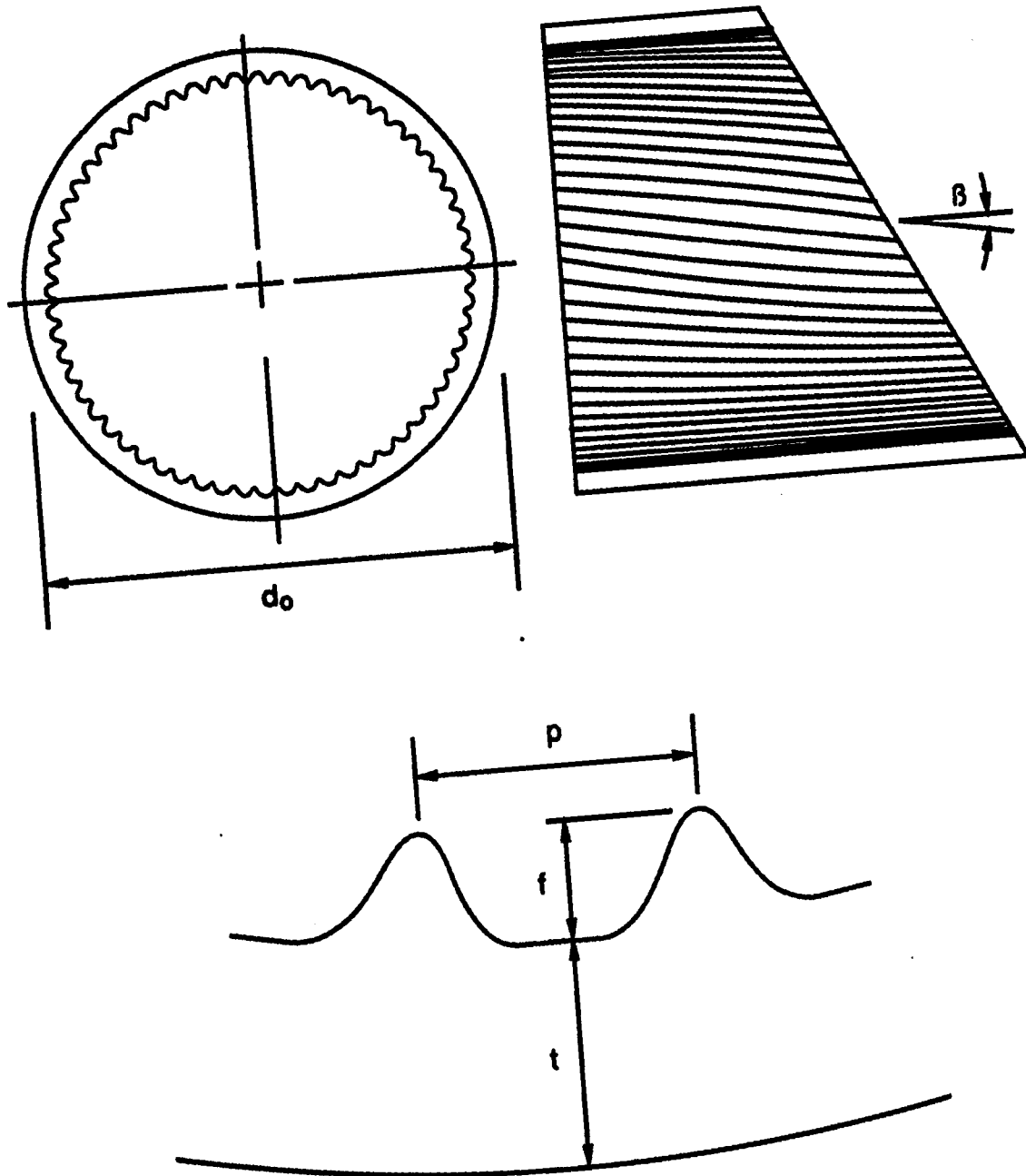


Figure 7.1. Drawing of the micro-fin tube

Table 7.1. Micro-fin tube dimensions

Outside diameter, mm	9.52
Minimum wall thickness, mm	0.4
Maximum inside diameter, mm ^a	8.72
Cross section area, mm ²	57.0
Fin height, mm	0.2
Spiral angle, degrees	18
Number of fins	60
Area ratio ^b	1.5

^aCharacteristic diameter to calculate heat transfer coefficient.

^bRatio of micro-fin tube inside surface area to inside surface area of a smooth tube having an inside diameter equal to the maximum inside diameter of the micro-fin tube.

Evaporation

Heat transfer performance of the micro-fin tube as a function of mass flux is shown in Figure 7.2. For comparison, results for the smooth tube with pure refrigerant are also included. It is evident that heat transfer is significantly enhanced by the micro-fin tube. Heat transfer with the micro-fin tube is greater than that of the smooth tube by as much as a factor of 2.7 at low mass flux and about 1.8 at the highest mass flux.

Enhancement factors versus mass flux are shown in Figure 7.3. Although the heat transfer coefficient for both tubes increases with increasing mass flux, the enhancement factor decreases with increasing mass flux. Enhancement factors are higher than the area ratio over the entire range of mass fluxes. At 200 kg/m²-s, the enhancement factor $\epsilon_{a/s}$ is 2.4. Shinohara and Tobe [116], using R-22 in a tube with a similar internal configuration, reported an enhancement factor of 2.5 at the same mass flux. Numerous other studies, using tubes with varying geometries, have reported enhancement factors ranging from around 1.5 to 2.7. Table 3.4 in Chapter 3 summarizes earlier studies with micro-fin tubes.

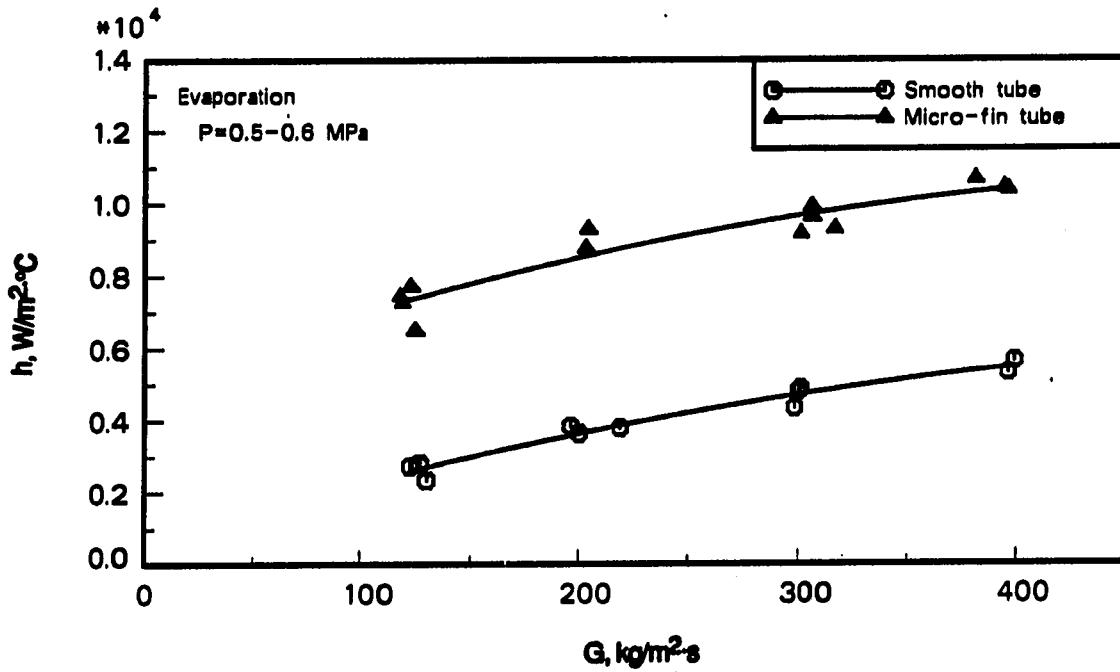


Figure 7.2. Heat transfer coefficient versus mass flux for pure refrigerant evaporation in a micro-fin tube and a smooth tube

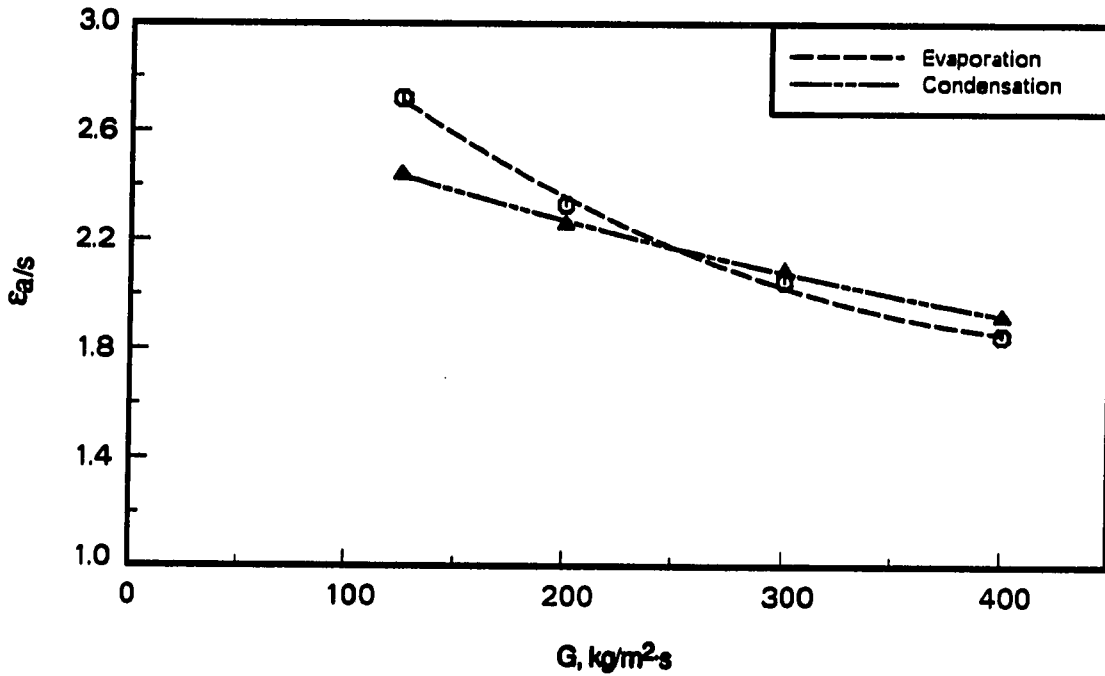


Figure 7.3. Heat transfer enhancement factor ($\epsilon_{a/s}$) for evaporation and condensation of R-22 in a micro-fin tube

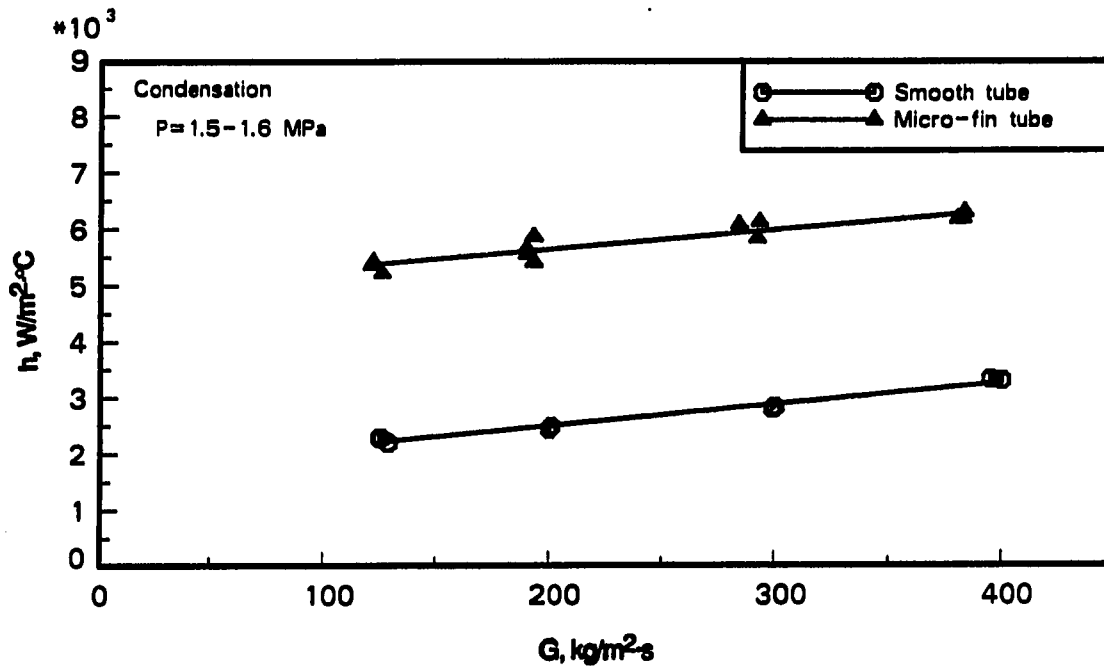


Figure 7.4. Heat transfer coefficient versus mass flux for pure refrigerant condensation in a micro-fin tube and a smooth tube

Condensation

Figure 7.4 presents condensation results for the micro-fin tube and repeats smooth tube results. Again, heat transfer in the micro-fin tube is significantly increased. The greatest relative increase occurs at low mass fluxes and, therefore, the enhancement factor becomes smaller as mass flux increases. For example, the maximum value of $\epsilon_{a/s}$ shown in Figure 7.3 is 2.4 at the lowest mass flux, falling to about 1.9 at the highest mass flux.

Comparing with the results of Shinohara and Tobe [116], their enhancement factor of 2.4 at 200 kg/m²·s is in good agreement with the enhancement factor of 2.3 obtained from the current data. Shinohara and Tobe, however, included superheated inlet conditions in their study, while the current test program was limited to inlet qualities no higher than 90%. Condensation enhancement factors for other micro-fin tubes, as summarized earlier in Table 3.5, range from about 1.4 to 2.4.

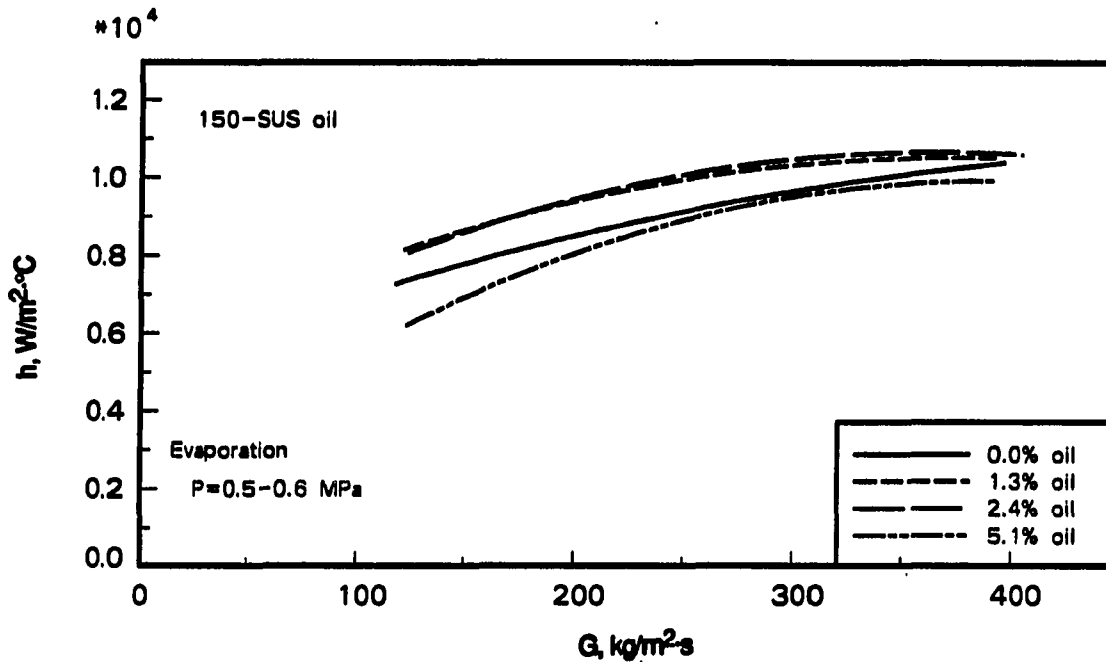


Figure 7.5. Heat transfer coefficient versus mass flux for evaporation with mixtures of R-22 and 150-SUS oil in a micro-fin tube

Heat Transfer with Refrigerant-Oil Mixtures

As with the smooth tube, both 150- and 300-SUS oil were used with R-22 for micro-fin tube tests. Nominal concentrations also matched the smooth tube tests: 1.25%, 2.5%, and 5.0% with 150-SUS oil; 0.6%, 1.25%, 2.5%, and 5.0% with 300-SUS oil.

Evaporation

150-SUS oil As shown in Figure 7.5, heat transfer is enhanced for oil concentrations of 1.25% and 2.5% but it is degraded slightly with 5.0% oil. The maximum enhancement factor, $\epsilon_{a/a}$, at 200 kg/m²·s is about 1.1, occurring at an oil concentration between 1% and 2%. At the same mass flux with 5.0% oil, $\epsilon_{a/a}$ falls to about 0.93. At a higher mass flux (400 kg/m²·s), the maximum enhancement factor is less than 1.05. At 5.0% oil and 400 kg/m²·s, the degradation is less severe than at 200 kg/m²·s, with a value just slightly under 1.0.

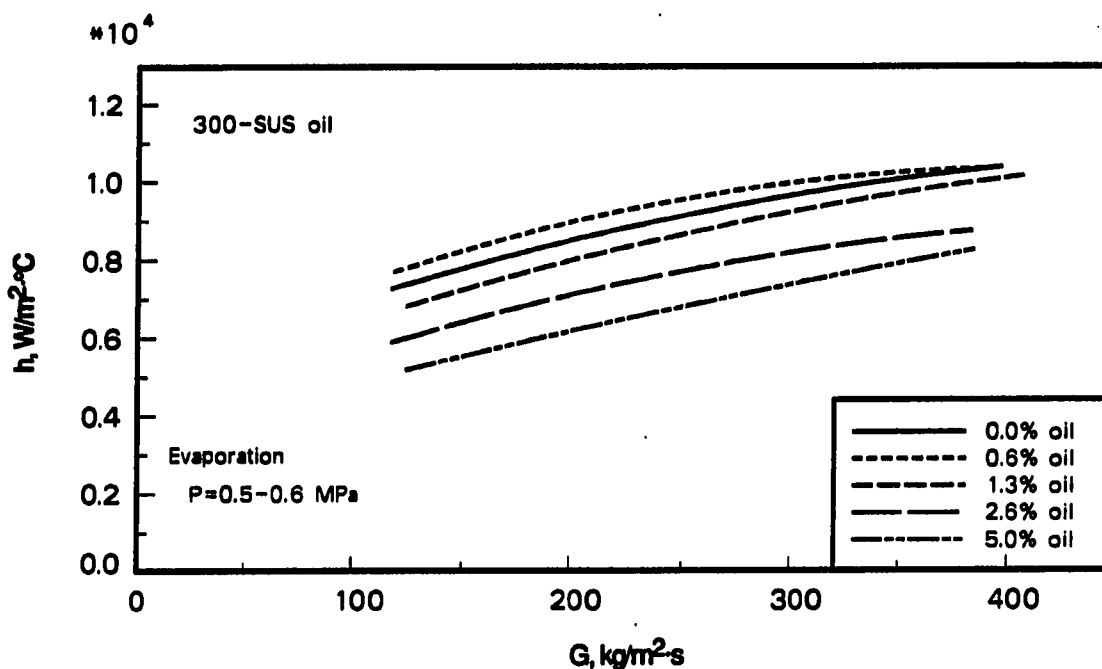


Figure 7.6. Heat transfer coefficient versus mass flux for evaporation with mixtures of R-22 and 300-SUS oil in a micro-fin tube

300-SUS oil Figure 7.6 shows heat transfer results for the micro-fin tube using 300-SUS oil mixed with refrigerant. There is very little enhancement of heat transfer with 300-SUS oil. For only the lowest concentration (0.6% oil) is there evidence of any enhancement, and the magnitude is quite small. For all higher concentrations, there is a decrease of performance in the micro-fin tube. At $200 \text{ kg/m}^2\text{-s}$, $\epsilon_{a/a}$ is around 1.01 with 0.6% oil. At a higher mass flux ($400 \text{ kg/m}^2\text{-s}$), enhancement at the lowest oil concentration is similar, with a value of around 1.02. At higher oil concentrations, the effect of the oil is generally negative, but the negative effects tend to be less severe at higher mass fluxes. At a high mass flux, $\epsilon_{a/a}$ is about 0.8 with 5.0% oil, somewhat higher than the value of 0.7 at a lower mass flux.

Comparison of 150- and 300-SUS oil A comparison of the two oil viscosities is made by looking at enhancement factors due to oil, $\epsilon_{a/a}$. Such a plot is shown in Figure 7.7 at two different mass fluxes. The enhancement with 150-SUS oil at low mass flux stands

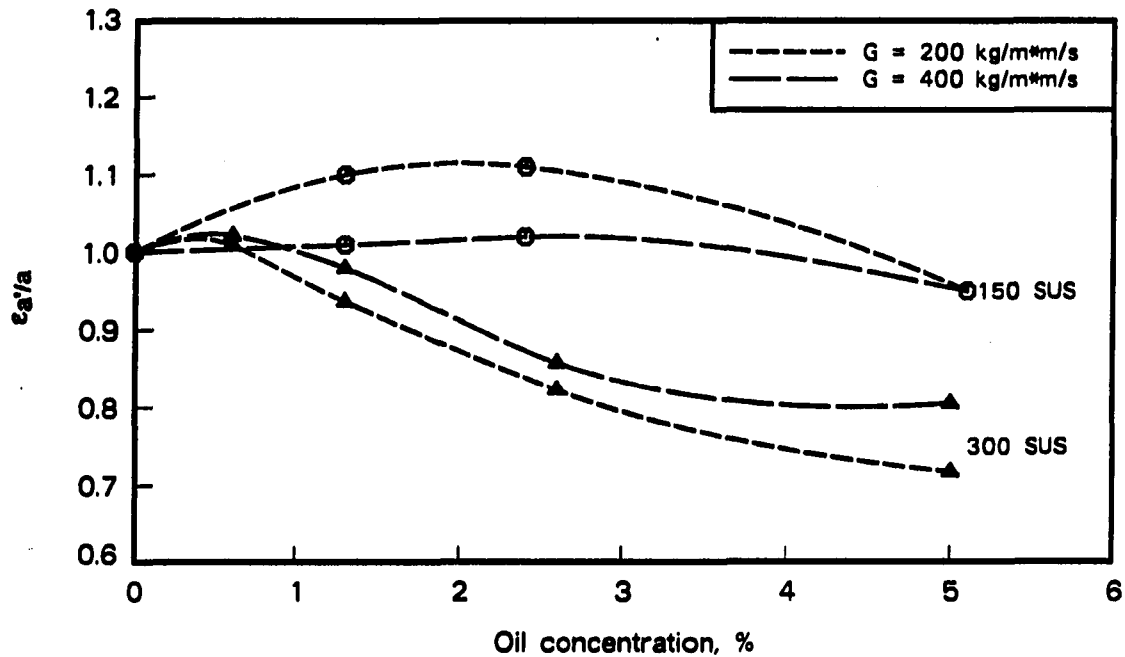
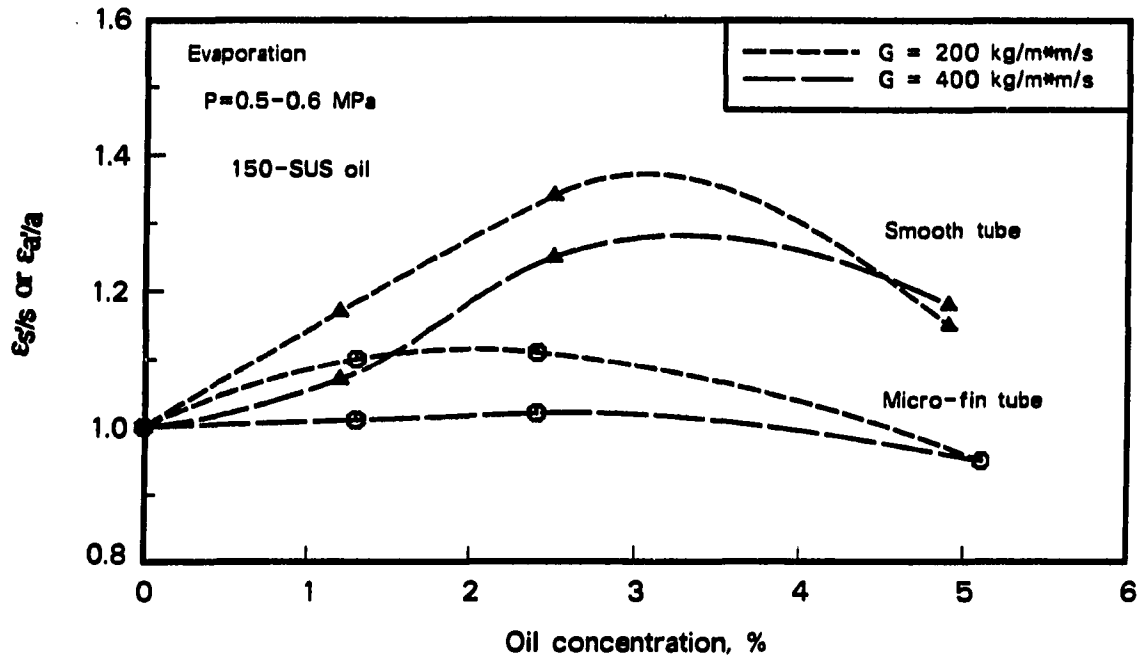


Figure 7.7. Evaporation enhancement factor (ϵ_a/a) versus oil concentration in a micro-fin tube

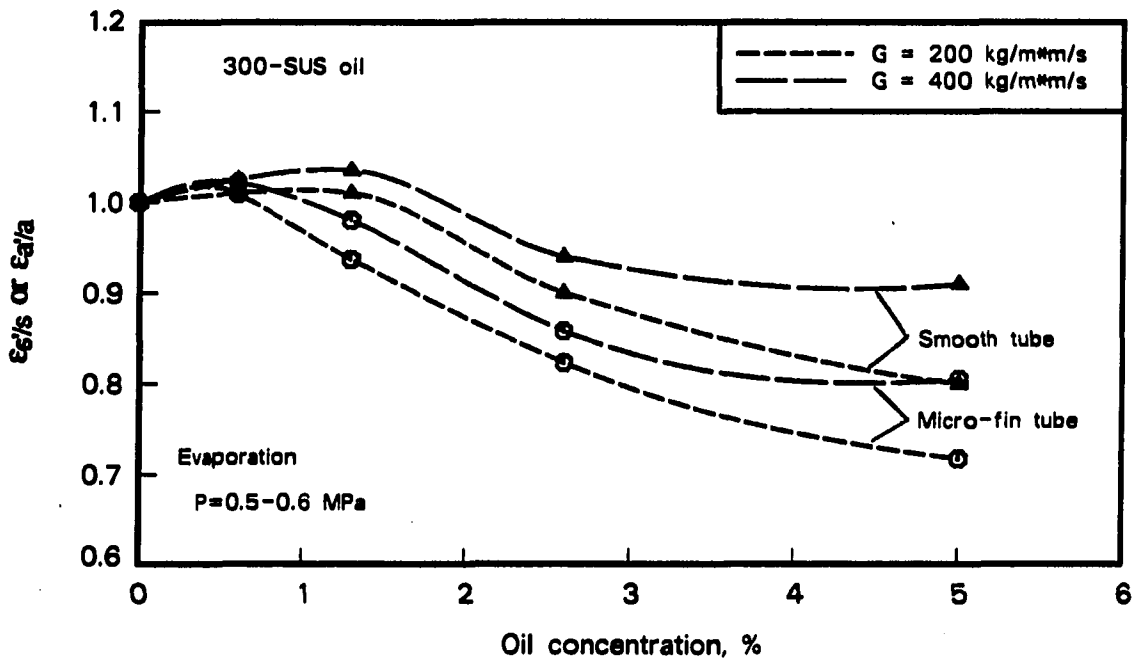
out in contrast to the general flat or decreasing performance at higher mass fluxes and with 300-SUS oil. Higher mass flux appears to have a moderating influence on the performance with oil; enhancement factors, whether greater than one or less than one, move closer to a value of 1.0 as mass flux increases.

Comparison with smooth tube Figure 7.8 compares the effect of oil on the micro-fin tube and on the smooth tube by plotting ϵ_a/a and ϵ_s/s versus oil concentration for both 150- and 300-SUS oil. Figure 7.9 combines the effects of oil and augmentation by presenting ϵ_a/s' as a function of oil concentration for both oils tested.

Parts (a) and (b) of Figure 7.8 show results with 150- and 300-SUS oil, respectively. The moderation of oil effects at higher mass fluxes, which was noted for the micro-fin tube, also appears to hold for the smooth tube. Figure 7.8 also shows that for evaporation, the effect of oil is more positive in the smooth tube than in the micro-fin tube—for the same oil type, smooth tube performance is higher than micro-fin tube performance.



(a)



(b)

Figure 7.8. Evaporation enhancement factors for smooth and micro-fin tubes ($\epsilon_{s/s}$ and $\epsilon_{a/a}$) as a function of oil concentration

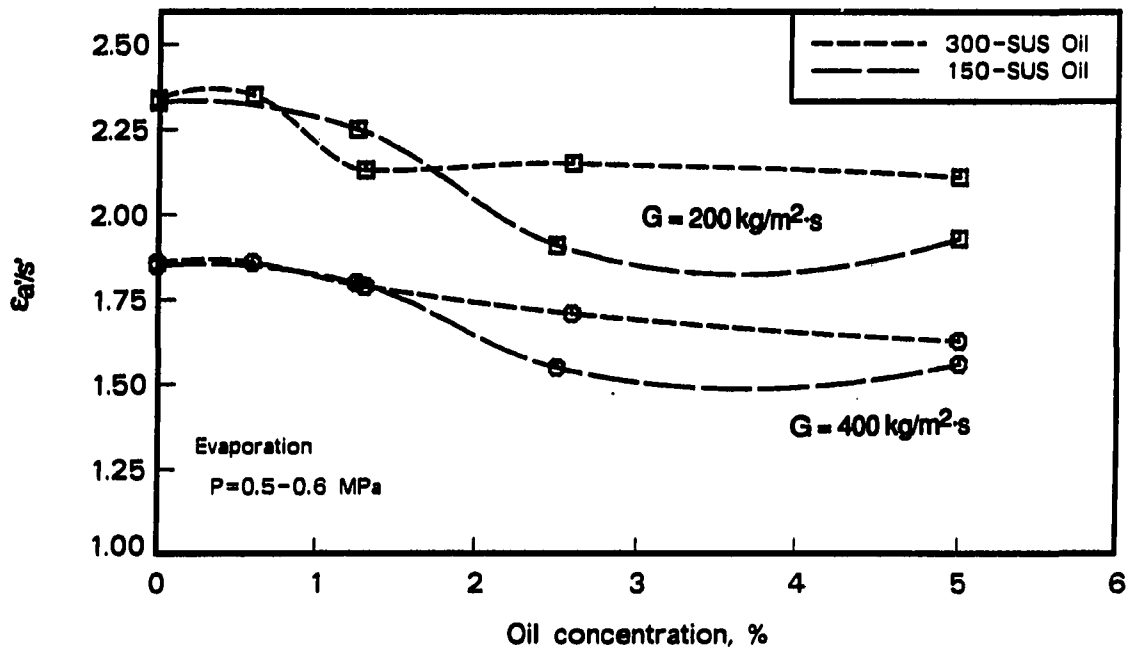


Figure 7.9. Evaporation enhancement factor showing the combined effects of oil and augmentation ($\epsilon_{a/s'}$) in a micro-fin tube

The overall performance of the micro-fin tube relative to a smooth tube is shown in Figure 7.9, which plots $\epsilon_{a/s'}$ versus oil concentration for both oils. This factor represents the increase in heat transfer performance of the micro-fin tube relative to a smooth tube at an arbitrary oil concentration. At oil concentrations below about 1.5%, there is no significant difference in the relative performance of the micro-fin tube with either oil. At higher oil concentrations, curves for 300-SUS oil are flatter and lie above those for 150-SUS oil.

With 300-SUS oil, $\epsilon_{a/s'}$ is higher than with 150-SUS oil, even though the absolute performance with 300-SUS oil is lower. This is caused by the large enhancement of smooth tube heat transfer with 150-SUS oil, a phenomenon not seen in either tube with 300-SUS oil or in the micro-fin tube with 150-SUS oil.

As indicated above, $\epsilon_{a/s'}$ varies with the two oils, but the difference is less than 15% over the concentration range tested, indicating that the performance of the micro-fin tube relative to the smooth tube is not strongly influenced by the oil's viscosity. Heat transfer

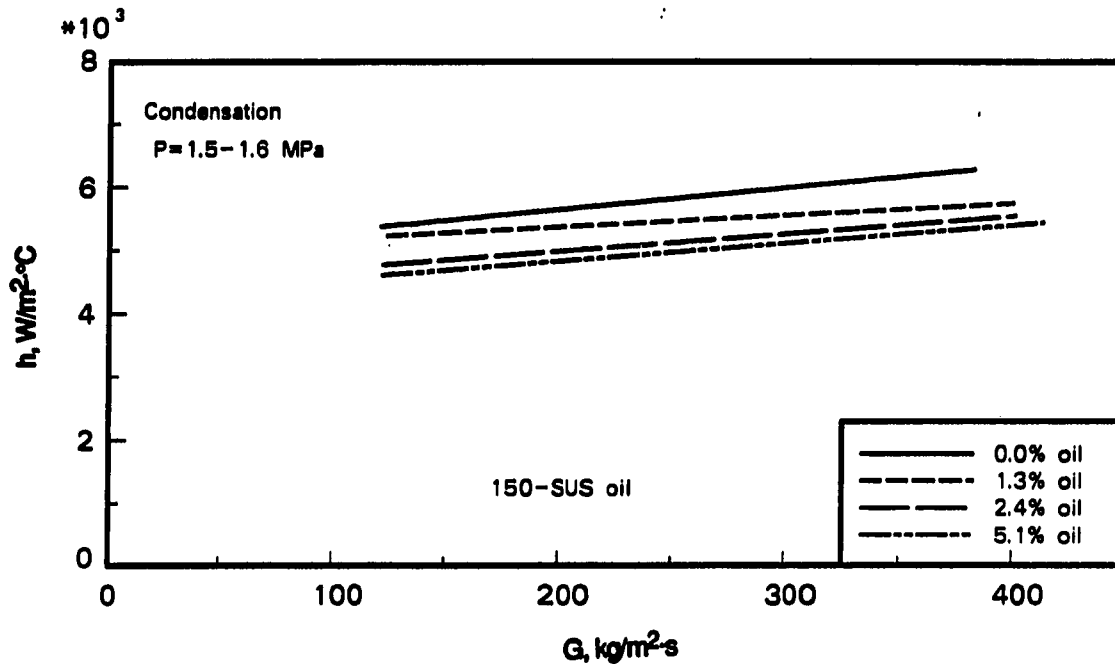


Figure 7.10. Heat transfer coefficient versus mass flux for condensation with mixtures of R-22 and 150-SUS oil in a micro-fin tube

enhancement with the micro-fin tube remains significant, even in the presence of oil. The lowest observed value of $\epsilon_{a'/s}$ is just under 1.6, greater than the area ratio ($A^* = 1.5$).

Condensation

150-SUS oil Figure 7.10 shows condensation heat transfer results for mixtures with 150-SUS oil. All cases show a degradation of heat transfer ($\epsilon_{a'/a} < 1$) with the addition of oil and the magnitude of the degradation increases with increasing oil concentration. The effect of oil does not appear to be a strong function of mass flux as the decrease in the heat transfer coefficient appears fairly uniform and orderly over the entire range of mass fluxes. The lowest observed enhancement factor, $\epsilon_{a'/a}$, is about 0.85 at 5.0% oil concentration.

300-SUS oil Results for mixtures of refrigerant and 300-SUS oil are shown in Figure 7.11. For all oil concentrations, $\epsilon_{a'/a}$ is less than one, with the degradation in heat transfer becoming greater as the oil concentration increases. Again, the degradation appears

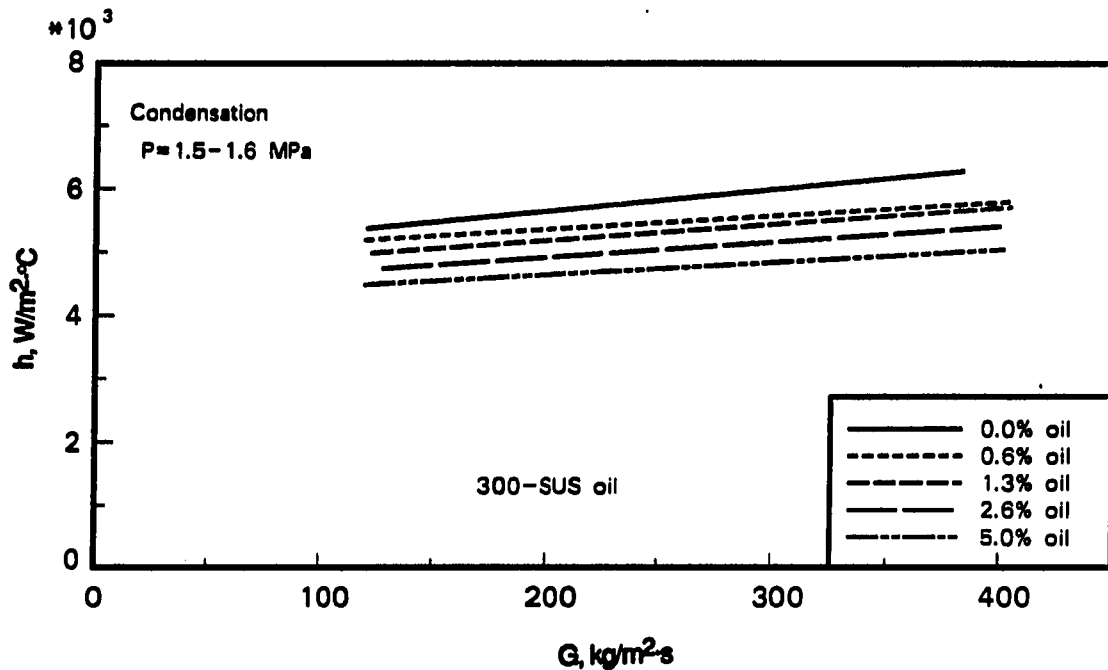


Figure 7.11. Heat transfer coefficient versus mass flux for condensation with mixtures of R-22 and 300-SUS oil in a micro-fin tube

orderly without a strong mass flux influence. The lowest observed enhancement factor, ϵ_a/a , is just under 0.8 at an oil concentration of 5.0%.

Comparison of 150- and 300-SUS oil Figure 7.12 plots ϵ_a/a for both oils as a function of oil concentration at two different mass fluxes. At both mass fluxes, the performance with 150-SUS oil is slightly higher than with 300-SUS oil. The difference in enhancement factors is less than 6% over the entire range of oil concentrations, indicating that oil viscosity is not a strong influence on condensation performance. However, as discussed with smooth tubes, mixture viscosity changes at most by about 7% with changing oil viscosity; over most of the tube length, the change would be somewhat less.

Unlike evaporation, higher mass flux does not appear to moderate the effects of the oil, but rather appears to slightly amplify the magnitude of the effects. The mass flux effect, however, is less than 5% at its greatest and can be considered negligible.

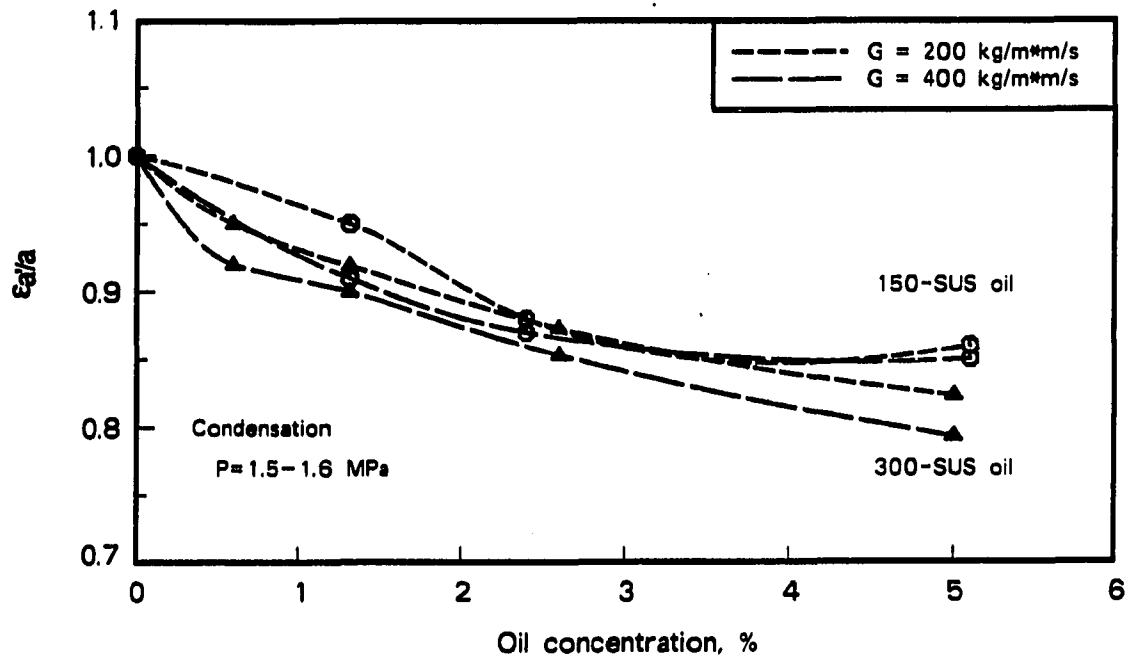
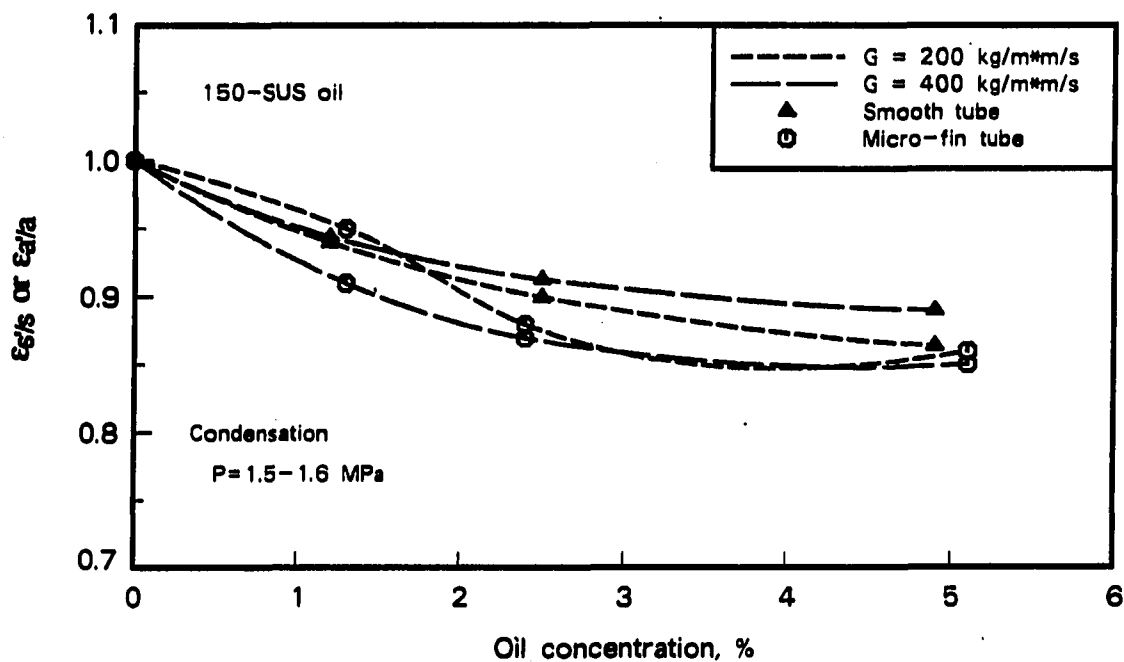
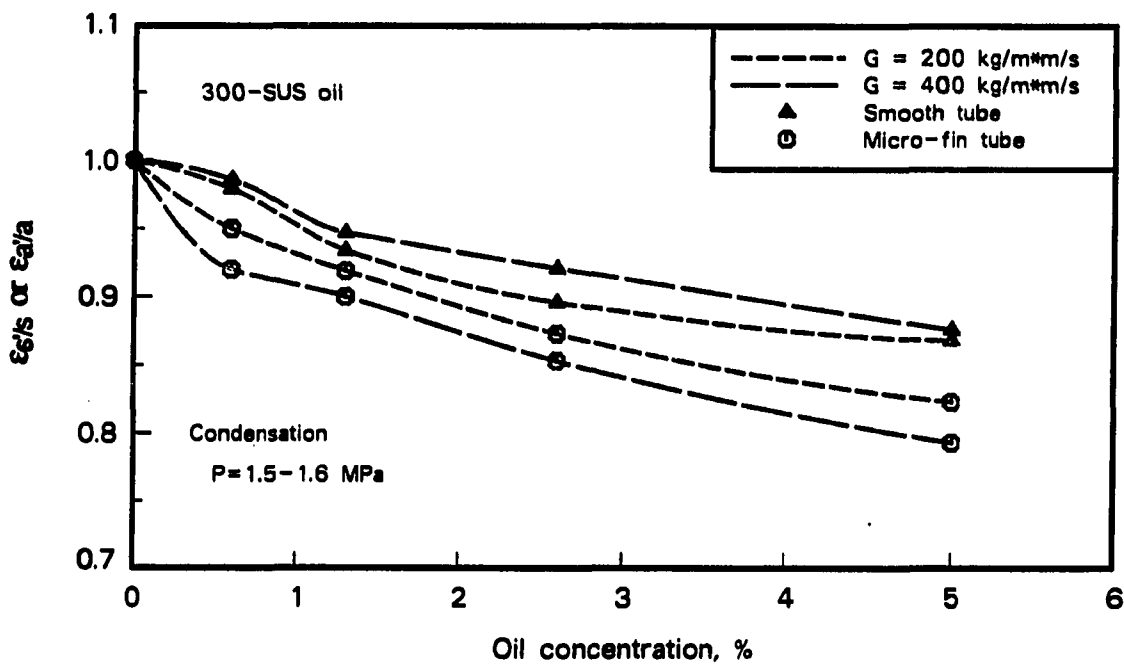


Figure 7.12. Condensation enhancement factor (ϵ_a/a) versus oil concentration in a micro-fin tube

Comparison with smooth tube Figure 7.13 is divided into two parts, with part (a) showing results with 150-SUS oil and part (b) showing results with 300-SUS oil. Trends are less pronounced in Figure 7.13 than are seen with evaporation in Figure 7.8. For most conditions, the performance of the smooth tube degrades slightly less with the addition of oil than that of the micro-fin tube. Comparing the lower mass flux ($200 \text{ kg/m}^2\cdot\text{s}$) with the higher mass flux ($400 \text{ kg/m}^2\cdot\text{s}$), the effect appears to be opposite in the two tubes; with the smooth tube, performance at the higher mass flux is slightly better, while the situation reverses with the micro-fin tube. It is probable that these observations are due to experimental uncertainty, rather than to physical phenomena, since all data shown lie within a relatively narrow band. Note that the scale used for condensation (as compared to the scale for evaporation in Figure 7.8) gives the impression of a greater spread than actually exists due to the smaller range of values on the ordinate.



(a)



(b)

Figure 7.13. Condensation enhancement factors for smooth and micro-fin tubes (ϵ_s/s and ϵ_a/a) as a function of oil concentration

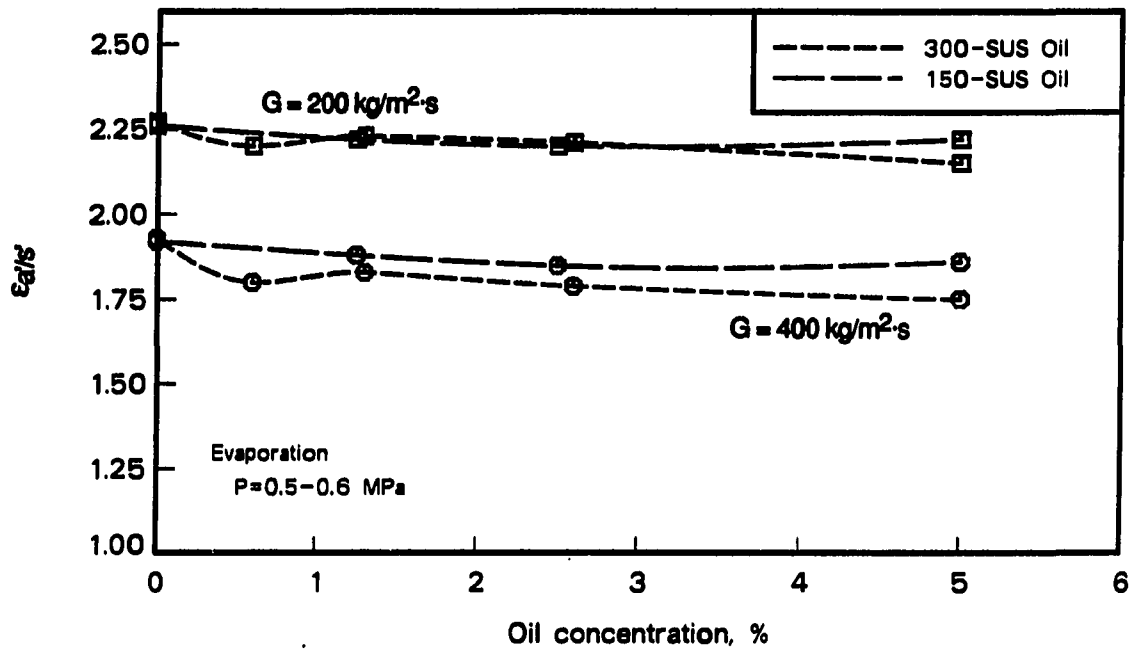


Figure 7.14. Condensation enhancement factor showing the combined effects of oil and augmentation ($\epsilon_{a'/s'}$) in a micro-fin tube

Figure 7.14 presents the overall condensation performance of the micro-fin tube relative to a smooth tube as a function of oil concentration. The plot shows $\epsilon_{a'/s'}$ for both oils at two different mass fluxes. The earlier observation of a rather uniform and orderly degradation of heat transfer with the addition of oil is repeated, as evidenced by the flatness of the curves and the small scatter in the figure. This indicates that the effect of the oil is similar in both tubes for both types of oil. The curves for both oils lie within $\pm 5\%$ at both mass fluxes, and the difference between $\epsilon_{a'/s'}$ with 5.0% oil and $\epsilon_{a/s}$ with pure refrigerant is less than 10% for the conditions shown in Figure 7.14.

As with evaporation, the performance of the micro-fin tube relative to a smooth tube is not significantly different with small concentrations of oil and the viscosity of the oil is of little influence. The enhancement of heat transfer with the micro-fin tube is significant over the entire range of oil concentrations tested and it is greater than A^* at all conditions.

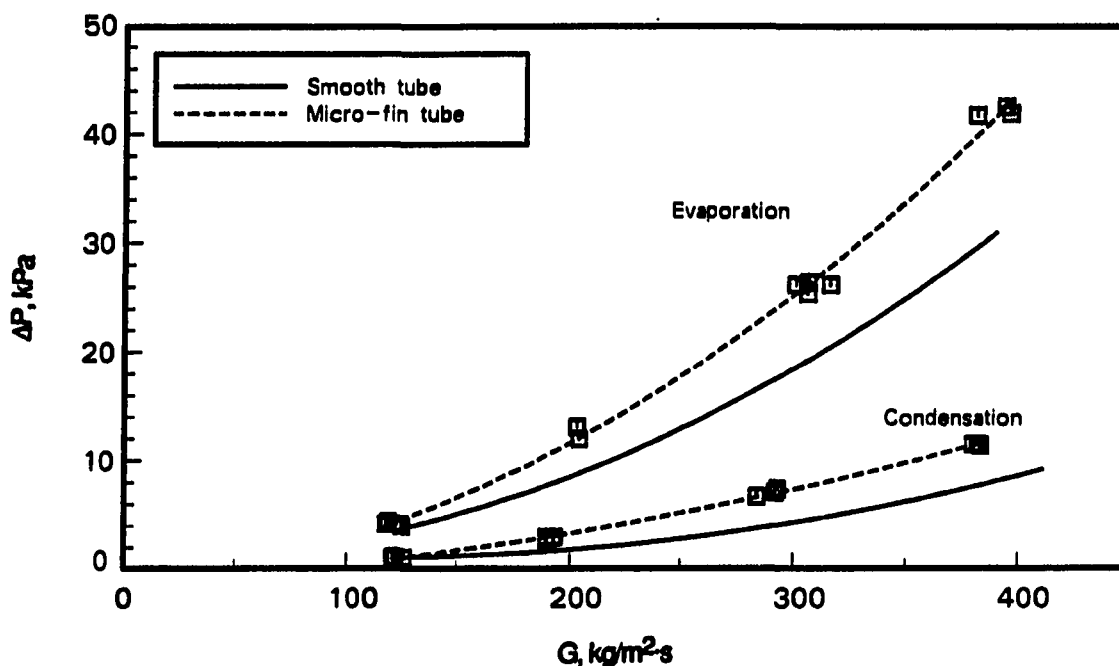


Figure 7.15. Evaporation and condensation pressure drop with pure R-22 in smooth and micro-fin tubes

Pressure Drop

As with the smooth tube, pressure drop data are fitted with curves and enhancement factors (ψ) are then calculated from these curves. Comments regarding uncertainties and data scatter with the smooth tube, as discussed in Chapter 6, hold equally for the micro-fin tube. Pressure drop uncertainties are shown in Appendix D.

Pure Refrigerant

Figure 7.15 shows pressure drop results for the micro-fin tube as a function of mass flux. Previously shown results for smooth tube pressure drop are also included for reference. For both evaporation and condensation, the pressure drop in the micro-fin tube is noticeably higher than that in the smooth tube. The same data, transformed into enhancement factors, are shown in Figure 7.16. For evaporation, $\psi_{a/s}$ rises from about 1.2 at low mass flux and levels off between 1.3 and 1.4 at higher mass fluxes. The condensation plot shows much more variance than the one for evaporation. At low mass

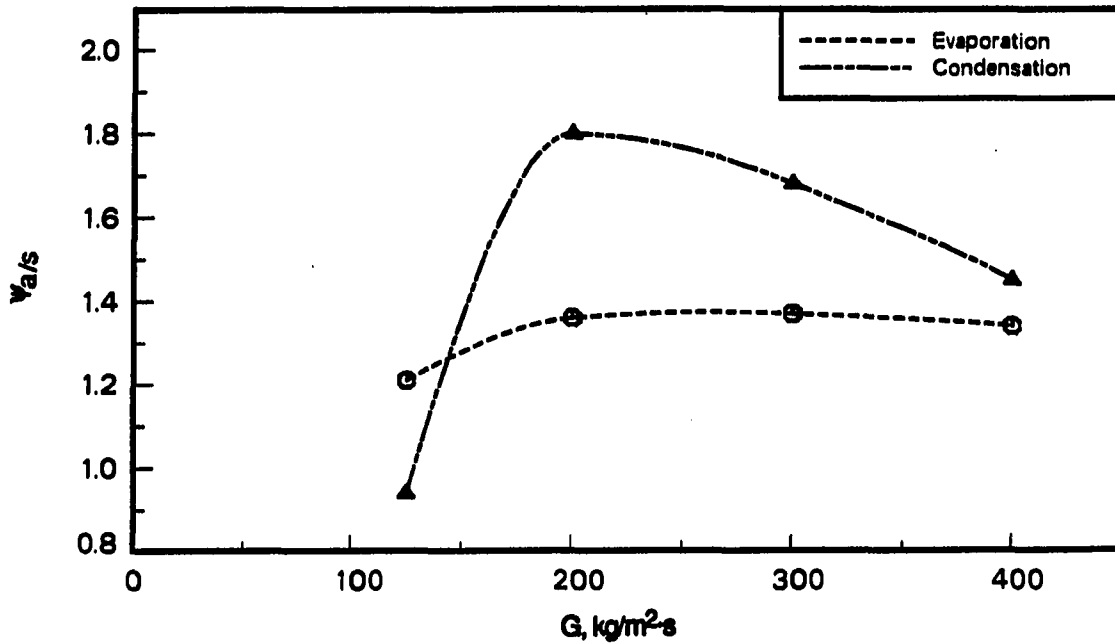


Figure 7.16. Pressure drop enhancement factor ($\Psi_{a/s}$) for evaporation and condensation in a micro-fin tube

flux, $\Psi_{a/s}$ is less than 1.0 and rises sharply to peak of about 1.8, then falls to less than 1.5 at high mass flux.

The large range in $\Psi_{a/s}$ for condensation is due to a combination of experimental uncertainties and curve fitting. Both of these factors have more impact on condensation results because of the small magnitude of the measurements. Problems with determining enhancement factors from curve fits were discussed in Chapter 5; uncertainty and data scatter were discussed in Chapter 6.

In spite of the large relative pressure drop increase indicated for condensation, comparison with Figure 7.3 shows that heat transfer enhancement, $\epsilon_{a/s}$, is larger than pressure drop enhancement, $\Psi_{a/s}$, for both condensation and evaporation at all mass fluxes. The maximum value of $\Psi_{a/s}$ is around 1.8, while the minimum value of $\epsilon_{a/s}$ is about 1.9.

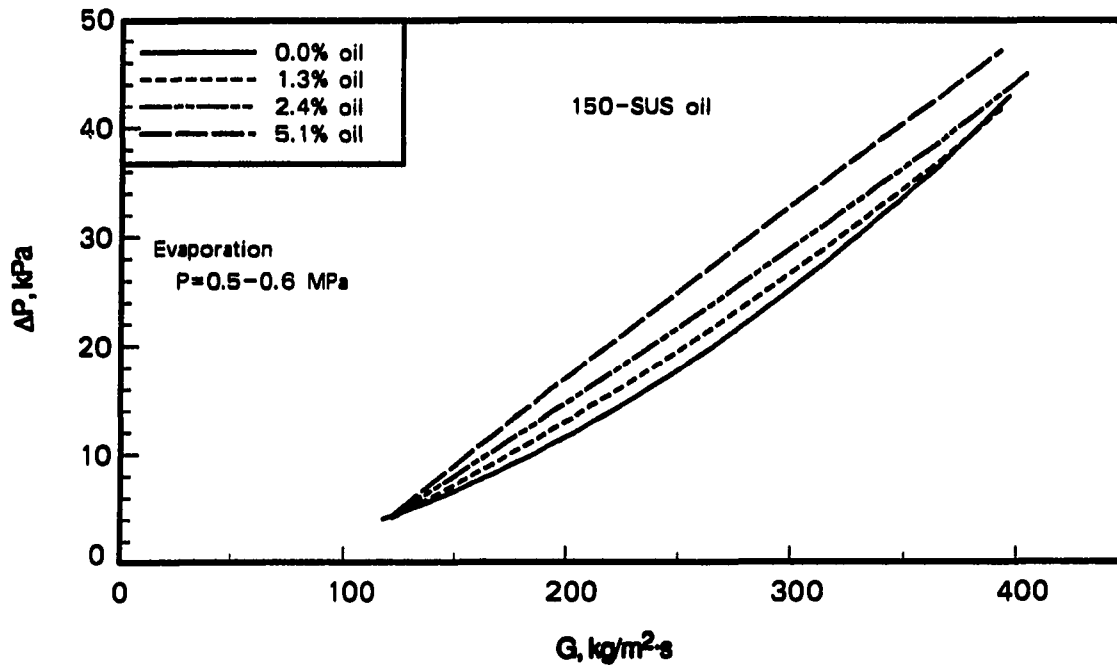
Refrigerant-Oil Mixtures

Evaporation Figure 7.17(a) shows evaporation pressure drop in the micro-fin tube as 150-SUS oil concentration increases. Oil causes an increase in pressure drop at most conditions, with pressure drop generally increasing with higher oil concentrations. Results with 300-SUS oil, shown in Figure 7.17(b), are similar both qualitatively and quantitatively to those with 150-SUS oil. Both plots have some intersecting curves, especially at high and low mass fluxes.

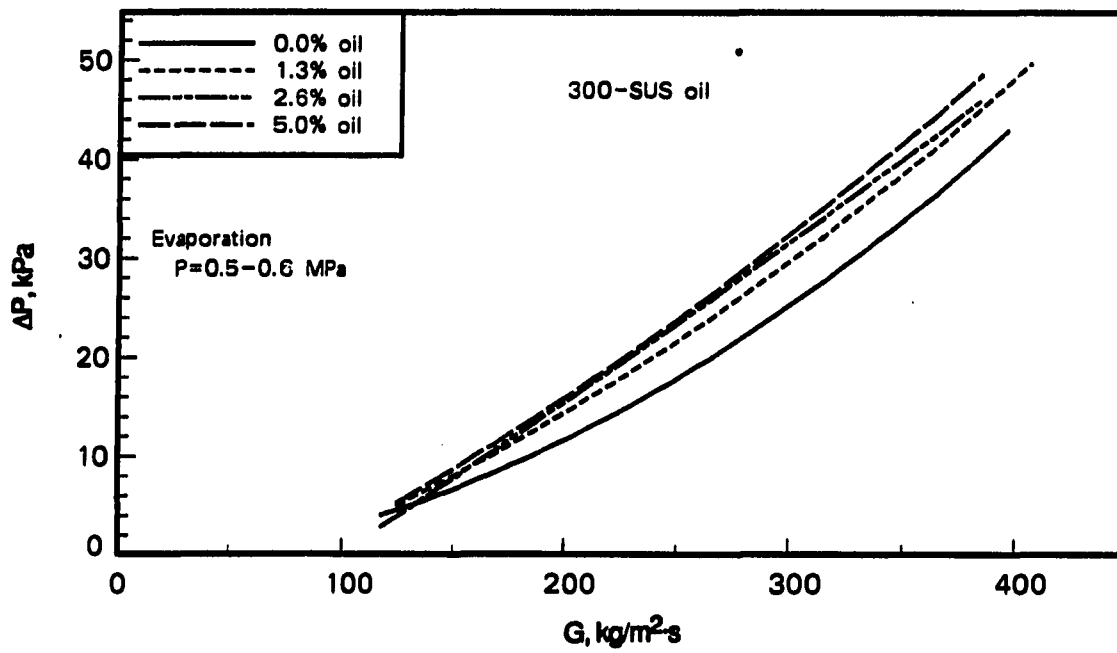
Figure 7.18 shows the same pressure drop data in the form of enhancement factors. A plot of $\Psi_{a/a}$ versus mass flux is presented in Figure 7.18(a) while Figure 7.18(b) plots $\Psi_{a/a}$ as a function of oil concentration. The range in Ψ is from less than 1.0 to about 1.5, but at medium mass flux, it is between 1.2 and 1.4. Part (a) shows a shape similar to that seen earlier for both oil effects and augmentation: a sharp increase in Ψ at low mass flux, a peak, and then a decrease as mass flux increases further (see Figures 6.12 and 7.16).

As shown in Figure 7.18(b), a general increase in $\Psi_{a/a}$ with increasing oil concentration and decreasing mass flux is observed with both oils. Note, however, that a plot for the lowest mass flux ($125 \text{ kg/m}^2\cdot\text{s}$) is not shown and would show a contradictory trend with mass flux. It is not included because medium and high mass fluxes are more representative of actual trends and have smaller uncertainties. At higher mass fluxes, 300-SUS oil has a somewhat higher enhancement factor, but the trend becomes mixed at $200 \text{ kg/m}^2\cdot\text{s}$. In no case is the difference in enhancement factor with the two oils greater than about 10%, indicating that viscosity has a relatively weak effect at the test conditions.

Figure 7.19 shows the combined effects of oil and augmented surface on the pressure drop by plotting $\Psi_{a/s'}$ versus mass flux in part (a) and versus oil concentration in part (b). Results without oil ($\Psi_{a/s}$) are also included. In part (a), there is initially an abrupt rise in $\Psi_{a/s'}$ at low mass flux, peaking at about 1.5 with 2.5% oil. At mass fluxes greater than $200 \text{ kg/m}^2\cdot\text{s}$, the enhancement factors for both oil concentrations and for pure R-22 tend to level off and converge to a value between 1.3 and 1.4. All values of $\Psi_{a/s'}$ are within $\pm 15\%$ of $\Psi_{a/s}$ over the range of mass fluxes and at both oil concentrations shown.

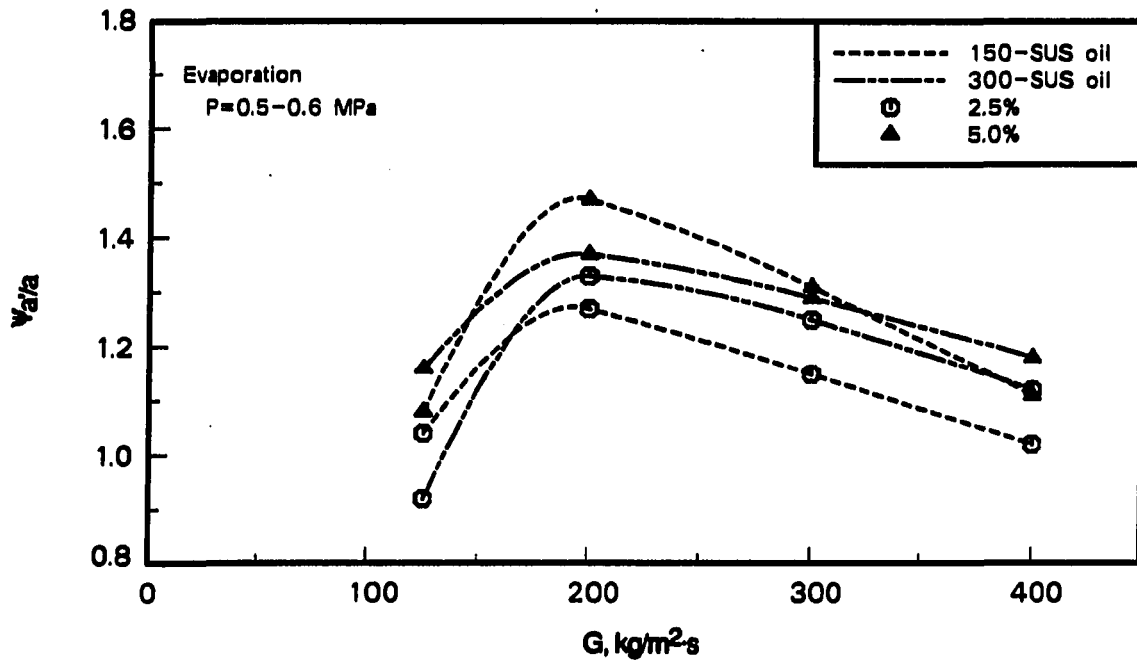


(a)

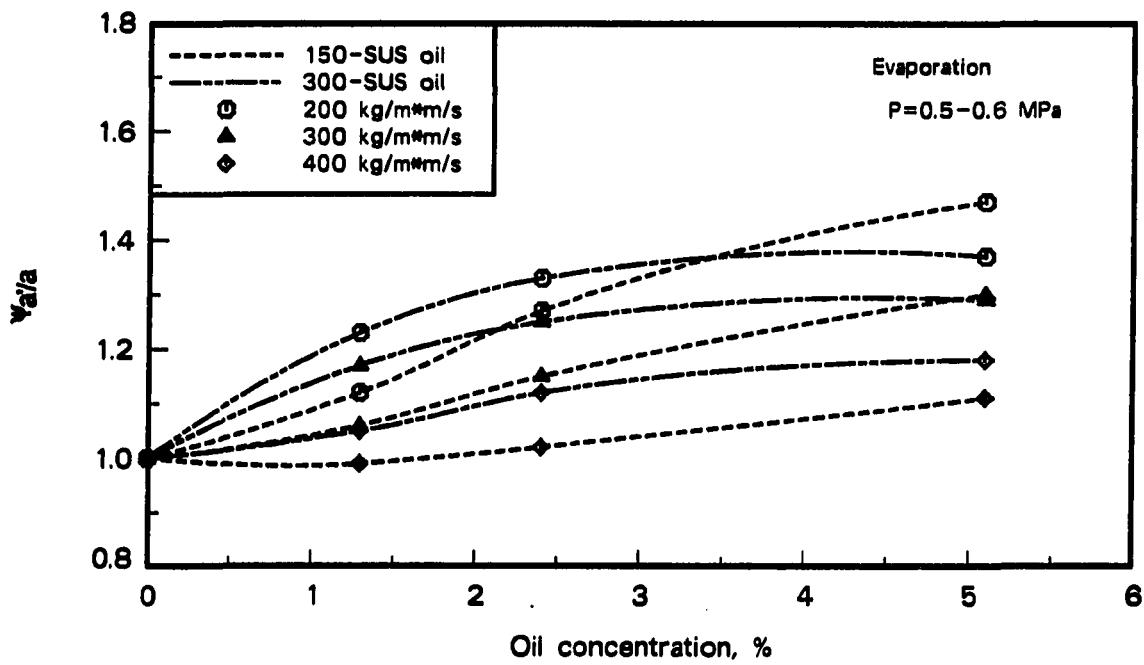


(b)

Figure 7.17. Evaporation pressure drop in a micro-fin tube with mixtures of R-22 and oil

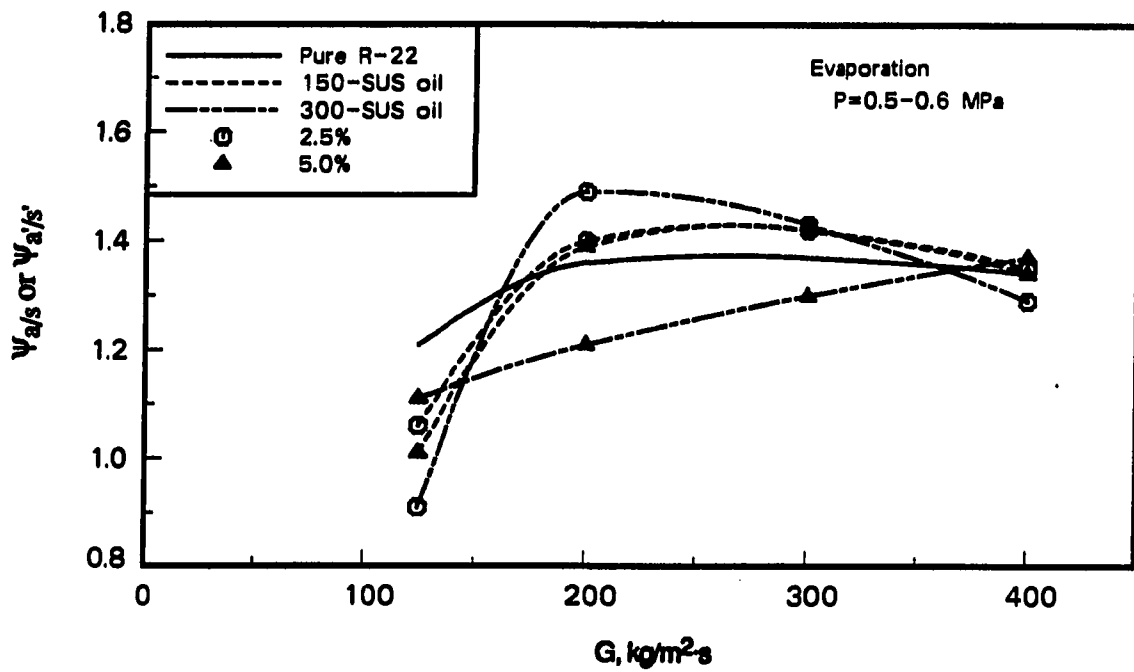


(a)

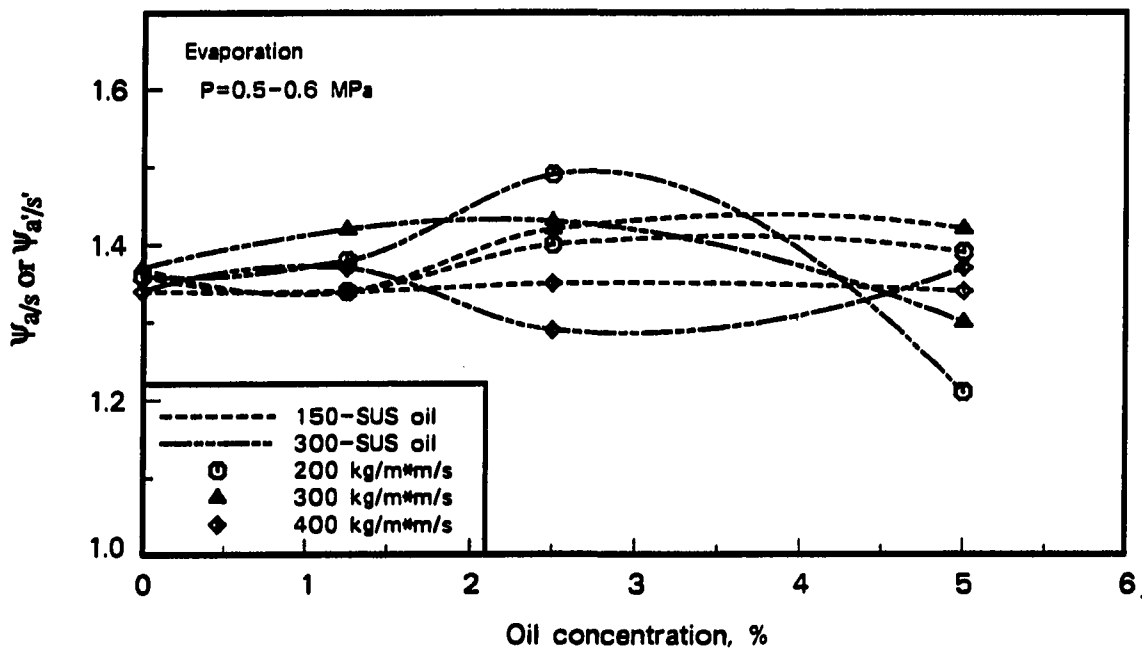


(b)

Figure 7.18. Pressure drop enhancement factor ($\Psi_{a/a}$) for evaporation in a micro-fin tube



(a)



(b)

Figure 7.19. Pressure drop enhancement factor ($\Psi_{a/s}$ or $\Psi_{a'/s'}$) for evaporation in a micro-fin tube

There is no noticeable trend with oil concentration—results with 300-SUS oil are at the high and low extremes, while results with 150-SUS oil and with pure R-22 lie in the middle.

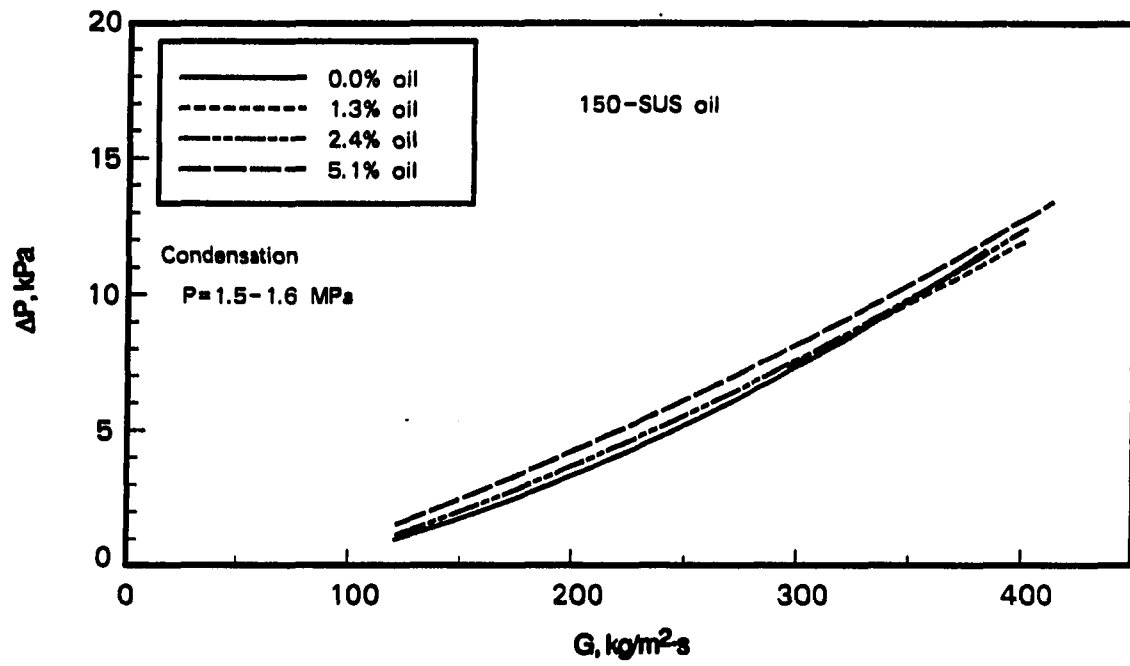
Figure 7.19(b) reinforces the observation that $\Psi_{a'/s}$ shows no consistent trend with varying oil concentration. All of the curves are relatively flat and are grouped between 1.2 and 1.5. The maximum variance of $\Psi_{a'/s}$ from the pure refrigerant value ($\Psi_{a/s}$) is about 15%. This indicates that the effect of oil on the smooth tube pressure drop is quite similar to its effect on pressure drop in the micro-fin tube.

Condensation Condensation pressure drop results are depicted in Figure 7.20. Part (a) shows the effect of 150-SUS oil, while part (b) shows 300-SUS oil. Tests with both oils show a general increase in pressure drop with the addition of oil, with the more viscous oil causing a slightly greater pressure drop increase. As noted before, varying curvature causes the curves to intersect at low and high mass fluxes.

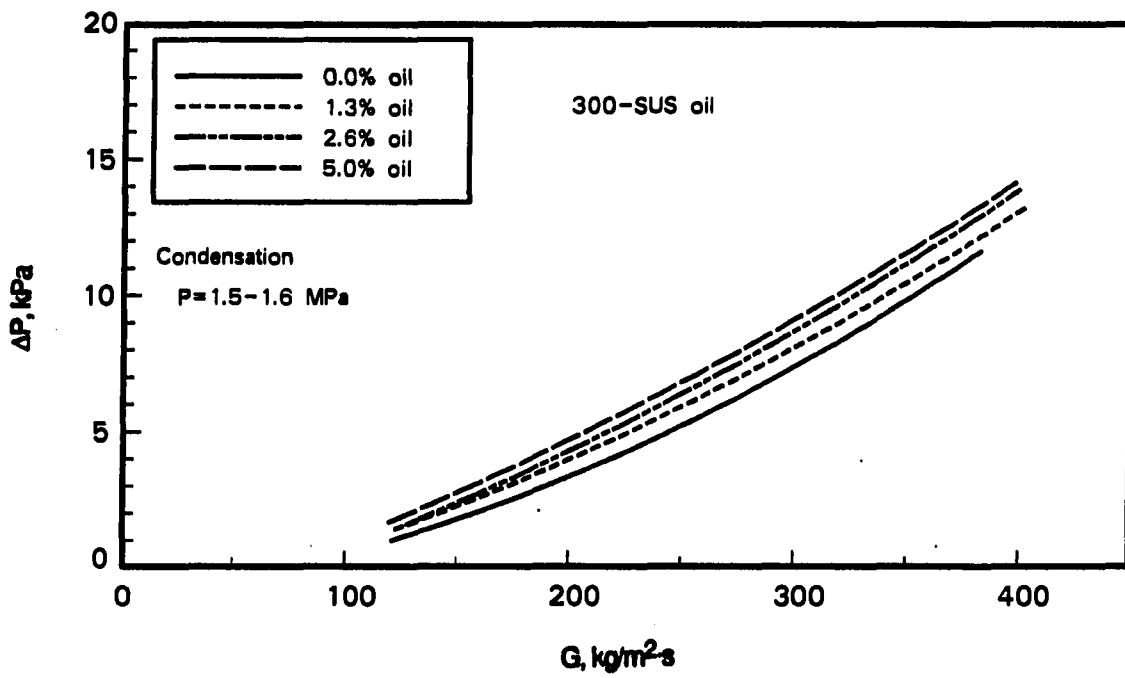
Pressure drop enhancement factors due to the effect of oil alone, $\Psi_{a'/a}$, are presented in Figure 7.21. Unlike previous plots of Ψ versus mass flux, Figure 7.21(a) does not show a sharp increase at low mass flux, but rather a steady decline with increasing mass flux from an initially high value. The trend in this figure, however, matches that of earlier figures for mass fluxes greater than $200 \text{ kg/m}^2\text{-s}$. Values of $\Psi_{a'/a}$ are as high as 1.7 at low mass flux with a 5.0% concentration of 300-SUS oil, but fall to the range of 1.0 to 1.2 for both oils and both concentrations at higher mass fluxes. The more viscous 300-SUS oil causes a greater pressure drop increase than the corresponding concentration of 150-SUS oil over the entire range of mass fluxes.

Figure 7.21(b) shows $\Psi_{a'/a}$ as a function of oil concentration. There is a steady, but not dramatic, increase in $\Psi_{a'/a}$ as oil concentration increases. At the highest oil concentration, the value of $\Psi_{a'/a}$ ranges from near 1.0 to about 1.4, with higher values occurring at lower mass fluxes. As in part (a), curves for 300-SUS oil consistently lie above those of the corresponding concentration of 150-SUS oil.

The combined effects of oil and augmentation are shown in Figure 7.22. Part (a) is plotted as a function of mass flux and once again shows a sharp increase at low mass flux. The values of $\Psi_{a'/s}$ are quite high, reaching a maximum of 3.4, and all the curves with oil lie above the pure refrigerant pressure drop enhancement factor, $\Psi_{a/s}$ (shown for reference).

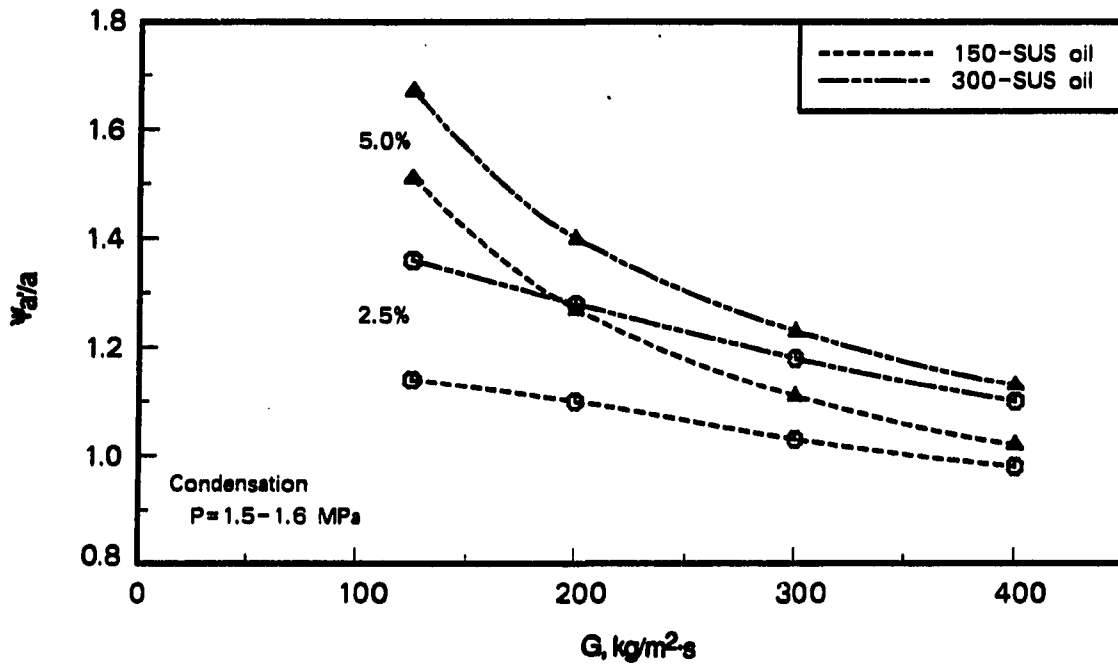


(a)

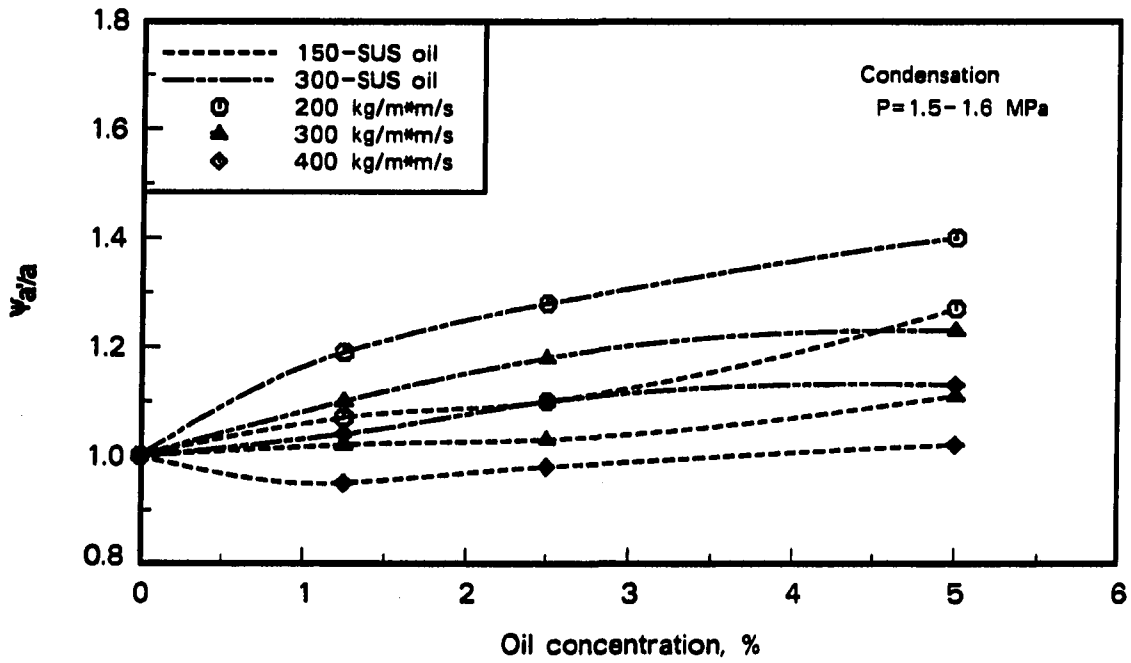


(b)

Figure 7.20. Condensation pressure drop in a micro-fin tube with mixtures of R-22 and oil

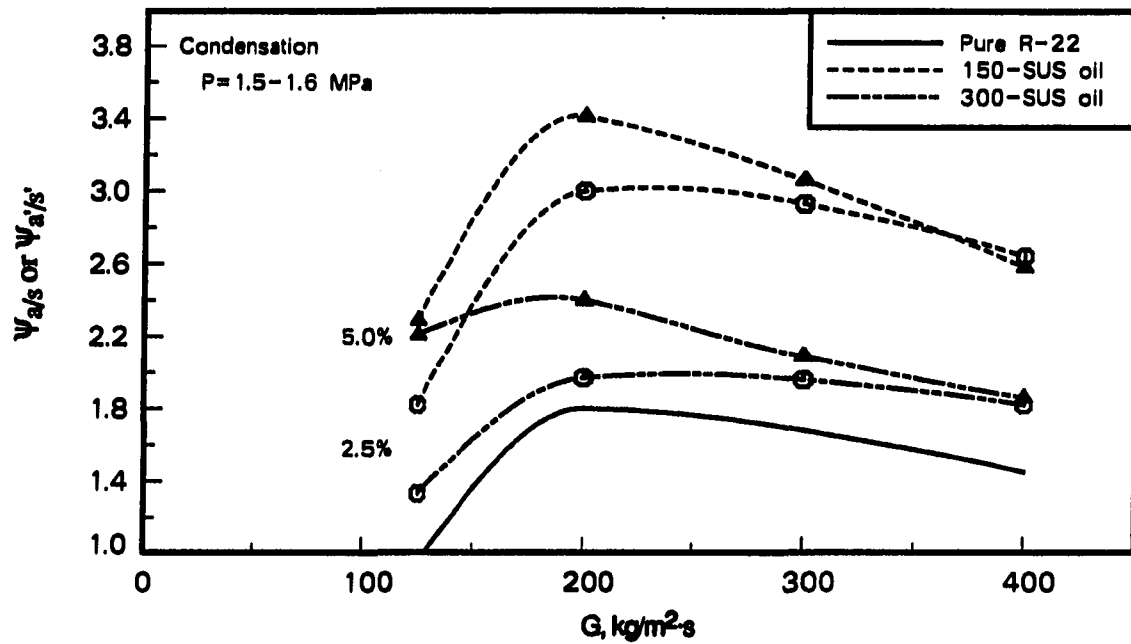


(a)

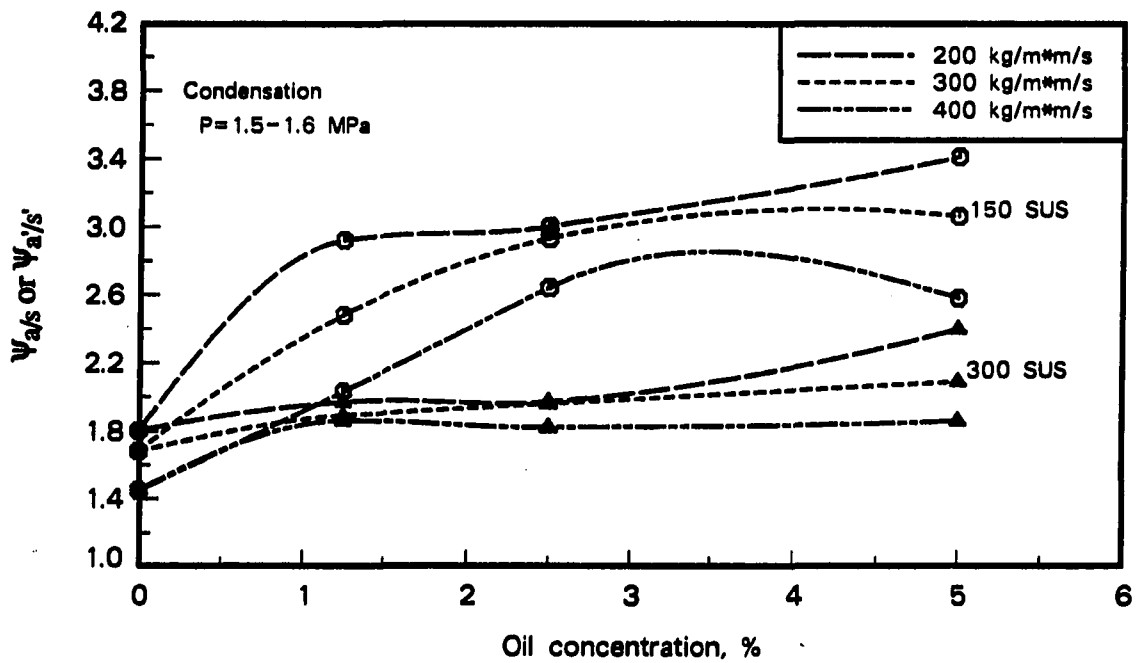


(b)

Figure 7.21. Pressure drop enhancement factor ($\Psi_{a/a}$) for condensation in a micro-fin tube



(a)



(b)

Figure 7.22. Pressure drop enhancement factor ($\Psi_{a/s}$ or $\Psi_{a'/s'}$) for condensation in a micro-fin tube

The high values for $\Psi_{a/s'}$ are due to the measured decrease in condensation pressure drop with the addition of oil in the smooth tube. Since $\Psi_{a/s'}$ is relative to the smooth tube, the performance of the micro-fin tube tends to worsen in comparison to the smooth tube as oil is added.

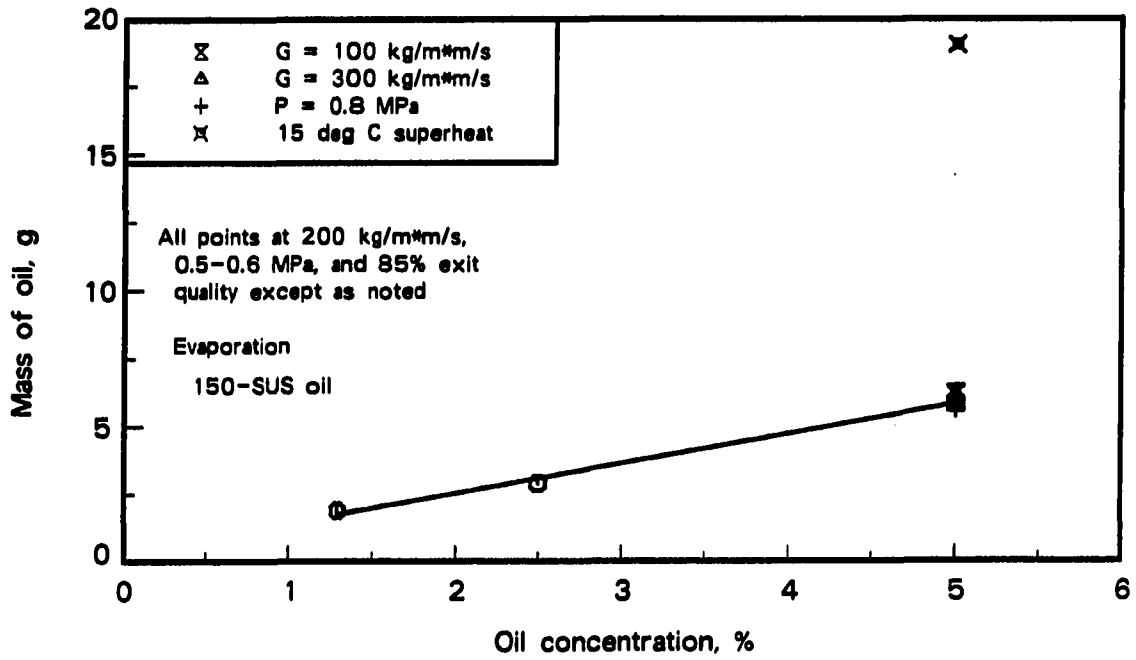
Figure 7.22(b) plots $\Psi_{a/s'}$ versus oil concentration. An upward trend is indicated for both oils with increasing concentration, but the trend is much more pronounced with 150-SUS oil. With 300-SUS oil, $\Psi_{a/s'}$ rises 20% or less from pure refrigerant values ($\Psi_{a/s}$), whereas with 150-SUS oil, it rises by nearly a factor of two in the worst case.

Although the factor $\Psi_{a/s'}$ is quite poor for the micro-fin tube, this is due to the previously discussed decrease in pressure drop with the addition of oil to smooth tube tests. It is unknown whether this observed decrease in the smooth tube is a coincidence caused by rig-specific flow pattern changes, or it would generally be observed in real condensers at similar oil concentrations. In any case, condensation pressure drop is significantly less than that of evaporation, so a large percentage increase in condenser pressure drop is not as detrimental to total system pressure drop as the same percentage increase in the evaporator would be.

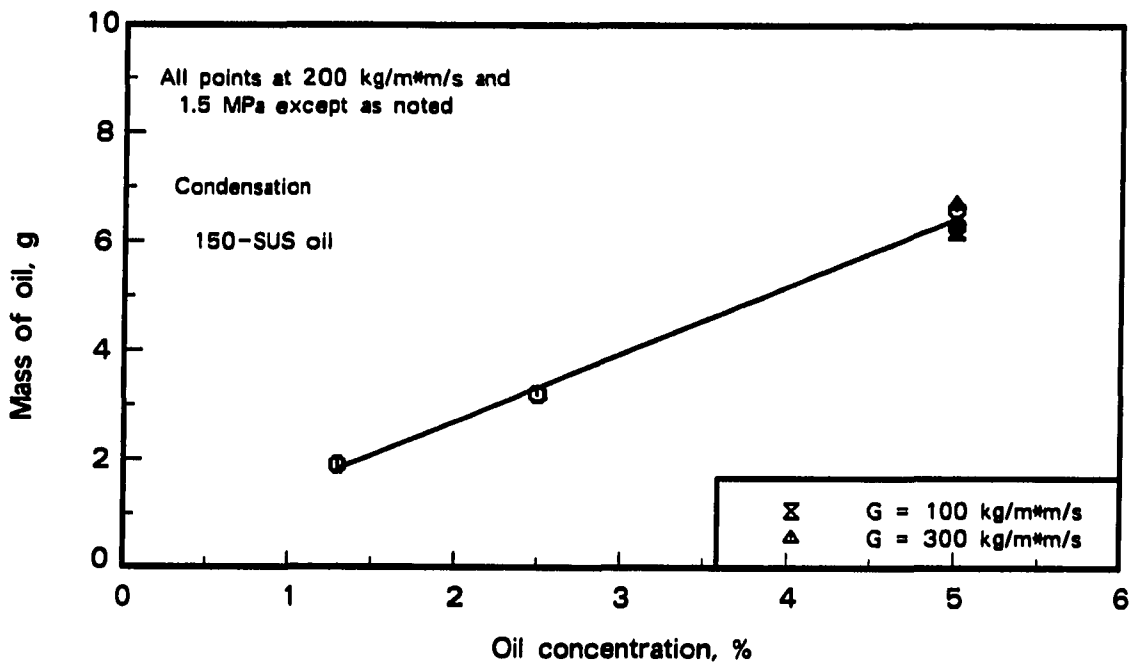
Oil Hold-Up

Tests were run to determine the amount of oil in the micro-fin tube at conditions similar to those previously discussed for smooth tube tests. Results with 150-SUS oil are shown in Figure 7.23 and 300-SUS oil results in Figure 7.24. For the most part, general conclusions drawn from micro-fin tube tests mirror those drawn earlier from smooth tube results: oil mass in the test section is proportional to average oil concentration and mass flux does not influence the hold-up. The effect of viscosity on hold-up in micro-fin tubes is even less significant than in smooth tubes.

As with the smooth tube, most tests measured only the mass of oil in the test section. Two tests, however, also obtained the refrigerant mass in order to determine the oil concentration in the test section. For these tests, the average flowing concentration of 150-SUS oil was 5%. During evaporation, 33 g of refrigerant and 5.8 g of oil were present, while during condensation, the test section held 67 g of refrigerant and 6.3 g of oil.



(a)



(b)

Figure 7.23. Quantity of oil in a micro-fin tube with 150-SUS oil

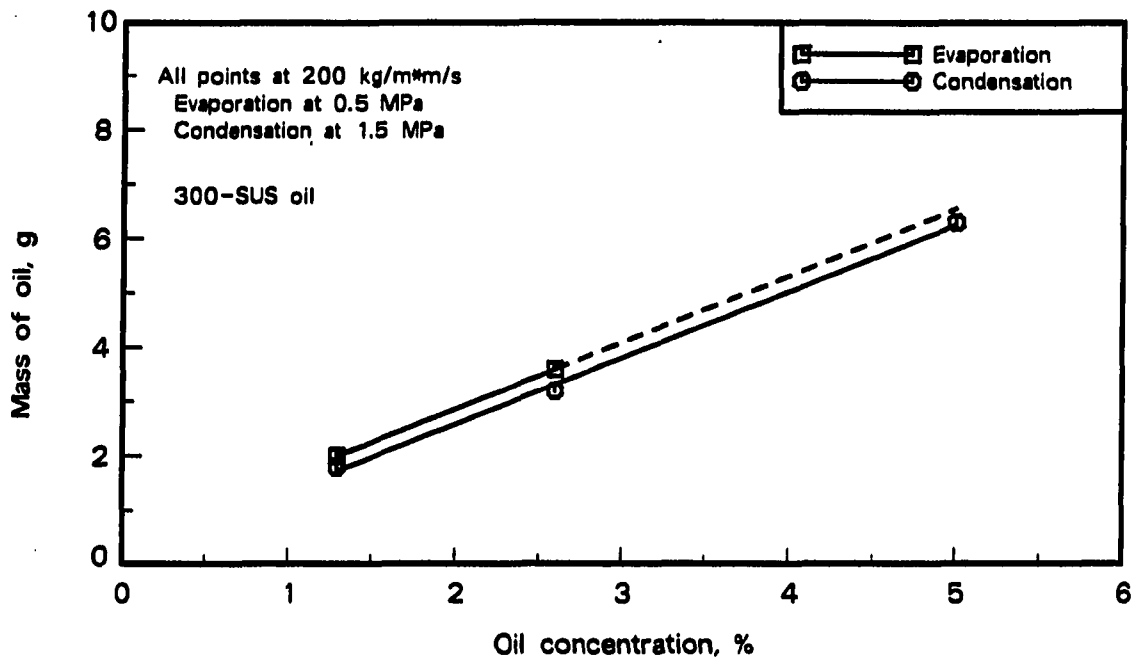


Figure 7.24. Quantity of oil in a micro-fin tube with 300-SUS oil

Oil concentrations based on total mass are 15% and 9% for evaporation and condensation, respectively. These are quite similar to the smooth tube results of 16% and 8%.

At the higher evaporation pressure, no change in hold-up is detected, but with 15°C exit superheat, the increase in hold-up with the micro-fin tube is greater than with the smooth tube. The amount of oil in the micro-fin test section triples when exit conditions change from about 80% quality to 15°C superheat, while in the smooth tube, the amount of oil in the test section doubles.

When comparing results in the micro-fin tube with those in the smooth tube at similar conditions, it is observed that the micro-fin tube generally has somewhat more oil in the test section for both evaporation and condensation and for both types of oil. The increase in mass ranges from being negligible to about 30%, with a typical value of 20%. The volume of the micro-fin tube, however, was about 18% greater due to a larger inside diameter, so the increase in mass in the micro-fin tube is probably due to a volume increase rather than to effects of the fins. This conclusion is further supported by similar values for

the actual oil concentration in the two tubes. It appears that as long as the flow remains in the two-phase region, the hold-up with smooth and micro-fin tubes is not significantly different. The fins in the micro-fin tube increase the oil hold-up only as the liquid mixture viscosity becomes quite large, as in the case of superheated exit conditions.

Summary

In this chapter, results from micro-fin tube testing were presented for pure refrigerants, as well as for refrigerant-oil mixtures. No previous work using refrigerant-oil mixtures in micro-fin tubes is available in the literature. Major conclusions are summarized below with numerical examples at a representative mass flux of $300 \text{ kg/m}^2\cdot\text{s}$ unless stated otherwise.

Evaporation

1. Pure refrigerant results compare well to results from similar tubes. The heat transfer enhancement factor, $\epsilon_{a/s}$, shows a tendency to decrease with increasing mass flux. It has a value of around 2.3 at $200 \text{ kg/m}^2\cdot\text{s}$ and falls to slightly less than 1.9 at $400 \text{ kg/m}^2\cdot\text{s}$.
2. Oil with a viscosity of 150 SUS causes a minor enhancement of heat transfer except at the highest oil concentration (5%), where $\epsilon_{a/a}$ falls just below 1.0. The enhancement factor peaks at about 1.3% oil concentration with a value of about 1.1. This compares to an enhancement factor ($\epsilon_{s'/s}$) in the smooth tube of 1.3 at similar conditions. With mixtures of 300-SUS oil, there is very minimal enhancement and it is only at the lowest oil concentration. At higher concentrations, there is a degradation of heat transfer, with $\epsilon_{a/a}$ falling to about 0.8 with 5% oil. This is similar to trends in the smooth tube, but the enhancement factor due to oil is generally somewhat lower in the micro-fin tube ($\epsilon_{a/a} < \epsilon_{s'/s}$).
3. The heat transfer performance of the micro-fin tube relative to the smooth tube falls somewhat when the effects of 150-SUS oil are considered. The enhancement factor, however, remains greater than the increase in internal surface area for all conditions. With pure refrigerant, $\epsilon_{a/s}$ is just over 2.0, while with 5% oil, $\epsilon_{a/s'}$ is about 1.75.

With 300-SUS oil, the performance of the micro-fin tube relative to the smooth tube remains virtually unchanged from the pure refrigerant case.

4. With pure refrigerant, the pressure drop enhancement factor, $\Psi_{a/s}$, is around 1.4, lower than the corresponding heat transfer enhancement factor.
5. Pressure drop in the micro-fin tube increases with the addition of oil, but the effect of the oil diminishes as mass flux increases. Considering uncertainties, results with both oils are approximately the same. With 5% oil, the pressure drop enhancement factor due to oil, $\Psi_{a/a}$, is about 1.3. The effect of oil on pressure drop in the micro-fin tube is quite similar to that in the smooth tube.
6. Average oil concentration in the test section is about three times the system average, just as in the smooth tube. Exit superheating causes added oil hold-up.

Condensation

1. Heat transfer results with pure refrigerant agree well with published results. There is a tendency for $\epsilon_{a/s}$ to fall with increasing mass flux. At 200 kg/m²·s, $\epsilon_{a/s}$ is about 2.25, falling to 1.9 at 400 kg/m²·s.
2. Oil diminishes the heat transfer coefficient in the micro-fin tube. The coefficient decreases with each incremental increase in oil concentration. Neither oil viscosity nor mass flux has a strong influence on the heat transfer enhancement factor due to oil, $\epsilon_{a/a}$. With 5% oil, $\epsilon_{a/a}$ is between 0.85 and 0.90.
3. The effect of oil on heat transfer in the micro-fin tube is much the same as that in the smooth tube. Therefore, the enhancement factor for refrigerant-oil mixtures, $\epsilon_{a/s'}$, remains virtually constant with the addition of oil.
4. The pure refrigerant pressure drop enhancement factor, $\Psi_{a/s}$, is about 1.7, lower than the corresponding heat transfer enhancement factor.
5. Condensation pressure drop increases with the addition of oil to the refrigerant. In general, 300-SUS oil increases the pressure drop slightly more than 150-SUS oil and the pressure drop becomes higher with increasing oil concentrations. With 5% oil, $\Psi_{a/a}$ is around 1.2 with 300-SUS oil and 1.1 with 150-SUS oil.

6. Pressure drop results in the micro-fin tube differ from those in the smooth tube, particularly with 150-SUS oil. Because of this, the value of the enhancement factor for refrigerant-oil mixtures, $\Psi_{a/s'}$, is considerably different than the pure refrigerant value, $\Psi_{a/s}$. The value of $\Psi_{a/s'}$ reaches about 3.0 with 150-SUS oil and 2.0 with 300-SUS oil, compared with a pure refrigerant value ($\Psi_{a/s}$) of 1.7.
7. Oil concentration in the test section is about 1.7 times the system average. This result is similar to that in the smooth tube.

CHAPTER 8

RESULTS WITH THE LOW-FIN TUBE

Low-fin tubes are defined here as tubes having a fin height greater than 2.5% and less than 15% of the maximum inside diameter. Compared to micro-fin tubes, these tubes generally have fewer fins, but, like micro-fin tubes, spiraling of the fins is common. The tube used in this study, which has been used commercially in refrigeration applications, had 21 fins, a fin height of 0.38 mm, and a spiral angle of 30°. The fins were approximately rectangular in shape with a flat peak and a flat valley. Table 8.1 gives the tube dimensions and Figure 8.1 is a drawing of the tube. Test conditions matched those of the other two tubes and were given in Table 6.2. Appendix E contains tabular data for all test runs.

Table 8.1. Low-fin tube dimensions

Outside diameter, mm	9.52
Minimum wall thickness, mm	0.51
Maximum inside diameter, mm ^a	8.51
Cross section area, mm ²	53.3
Fin height, mm	0.38
Spiral angle, degrees	30
Number of fins	21
Area ratio ^b	1.8

^aCharacteristic diameter to calculate heat transfer coefficient.

^bRatio of low-fin tube inside surface area to inside surface area of a smooth tube having an inside diameter equal to the maximum inside diameter of the low-fin tube.

Pure Refrigerant Heat Transfer

As with smooth and micro-fin tubes, pure refrigerant tests form the basis of comparison for tests with oil and are used to determine the pure refrigerant enhancement factor, $\epsilon_{a/s}$.

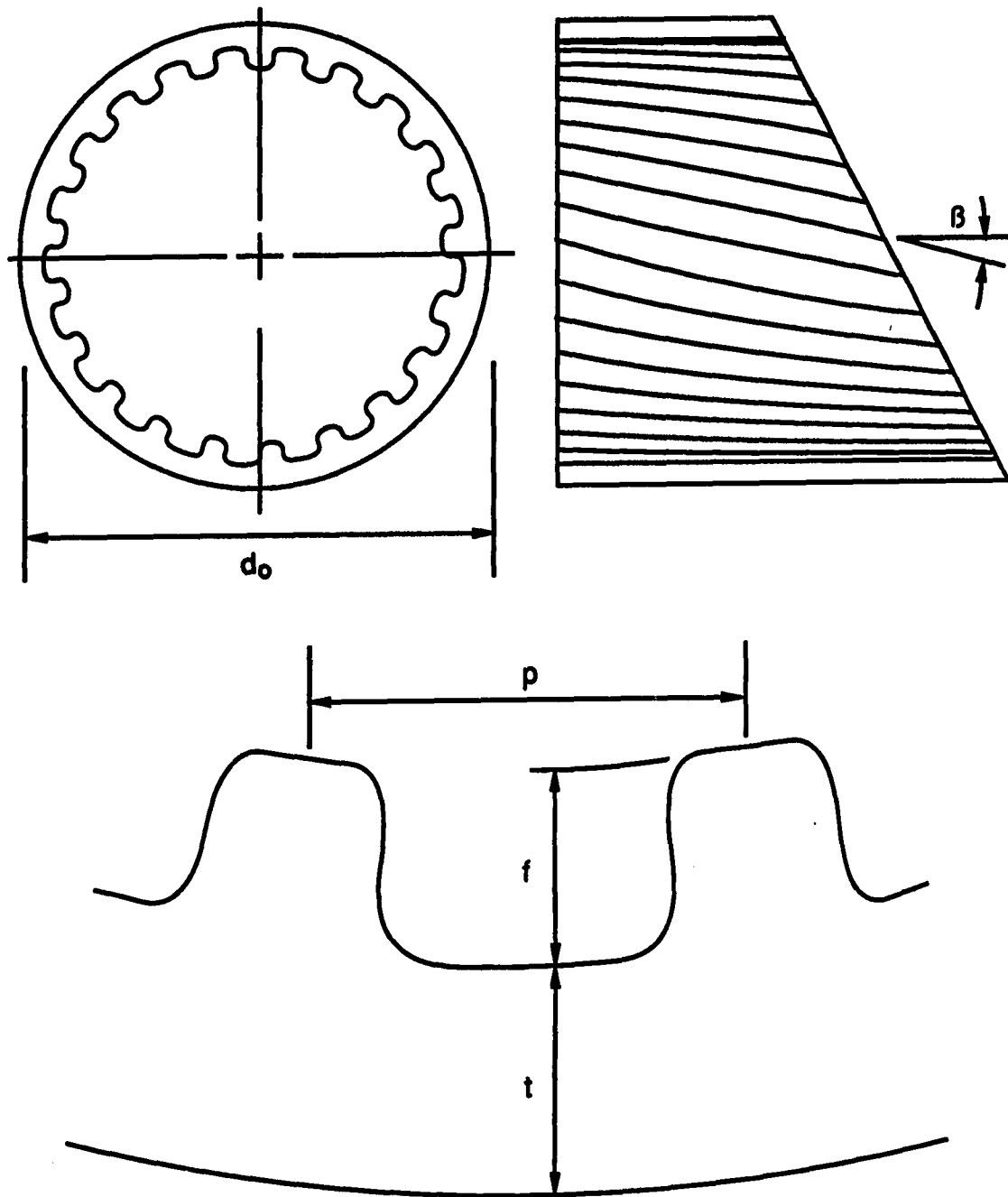


Figure 8.1. Drawing of the low-fin tube

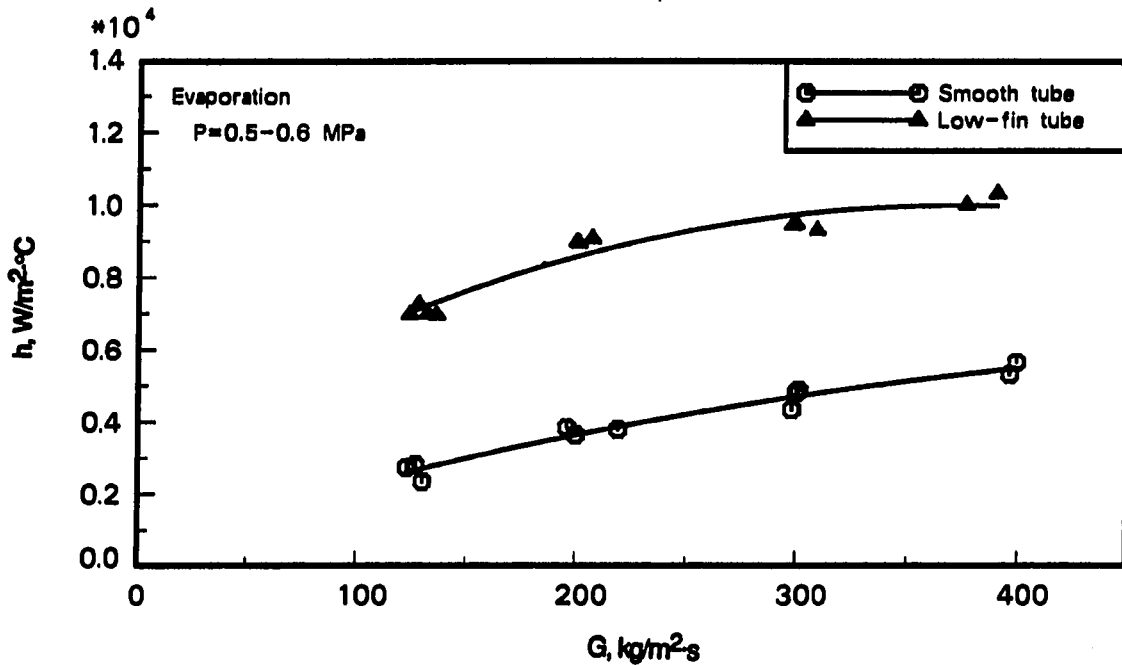


Figure 8.2. Heat transfer coefficient versus mass flux for pure refrigerant evaporation in a smooth tube and a low-fin tube

Evaporation

Pure refrigerant evaporation results for the low-fin tube and the smooth tube are shown in Figure 8.2. The heat transfer coefficient of the low-fin tube is significantly higher than that of the smooth tube. Heat transfer in both tubes increases with increasing mass flux, but the enhancement of the low-fin tube relative to the smooth tube decreases with increasing mass flux. At $125 \text{ kg/m}^2\text{-s}$, $\epsilon_{a/s}$ is as high as 2.6, but falls to about 1.8 at the highest mass flux, as shown in Figure 8.3. The increase in the internal surface area of the finned tube is about 80% ($A^*=1.8$), so the heat transfer enhancement is greater than or equal to the area increase over the range of test conditions.

Results with a very similar tube were reported by Reid et al. [111], however R-113 was the test fluid and direct electrical heating, rather than fluid heating, was used. A heat transfer enhancement factor of around 1.5 was reported at a mass flux of $395 \text{ kg/m}^2\text{-s}$, about 15% lower than the value of 1.8 reported here. Other workers, using low-fin tubes of

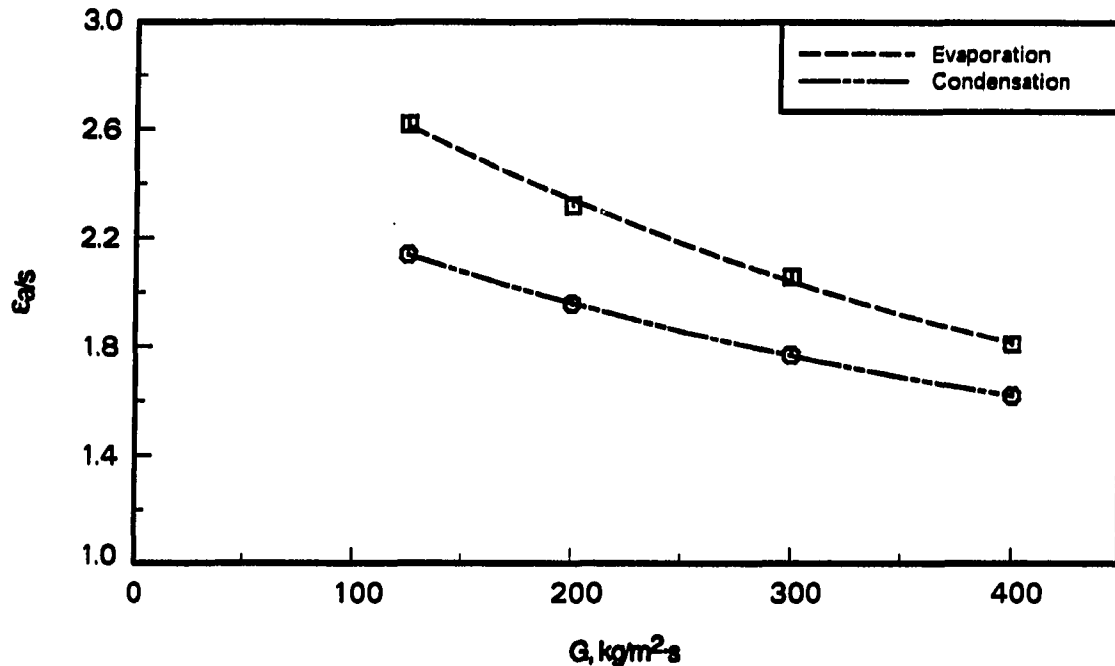


Figure 8.3. Heat transfer enhancement factor ($\epsilon_{a/s}$) for evaporation and condensation of R-22 in a low-fin tube

different sizes, have reported enhancement factors ranging from less than 2.0 to almost 7.0. The high values (> 3.0) were generally from tests having a small quality change ($\Delta X \approx 0.2$) through the test section. Table 3.4 in Chapter 3 summarizes these earlier studies.

Condensation

Figure 8.4 shows low-fin tube and smooth tube results during condensation with pure R-22. As with evaporation, there is a substantial increase in heat transfer due to the augmented surface, but the increase is less than in the case of evaporation. The heat transfer enhancement factor, $\epsilon_{a/s}$, varies from 2.1 at the lowest mass flux to 1.6 at the highest mass flux and is depicted in Figure 8.3. At higher mass fluxes, heat transfer enhancement is no longer greater than the increase in internal surface area, A^* .

All of the earlier condensation work with low-fin tubes was done with tubes at least three times as large as those used in the current study and none was carried out with R-22 as the working fluid. Enhancement factors as high as 2.2 were reported in these earlier papers, which are summarized in Table 3.5.

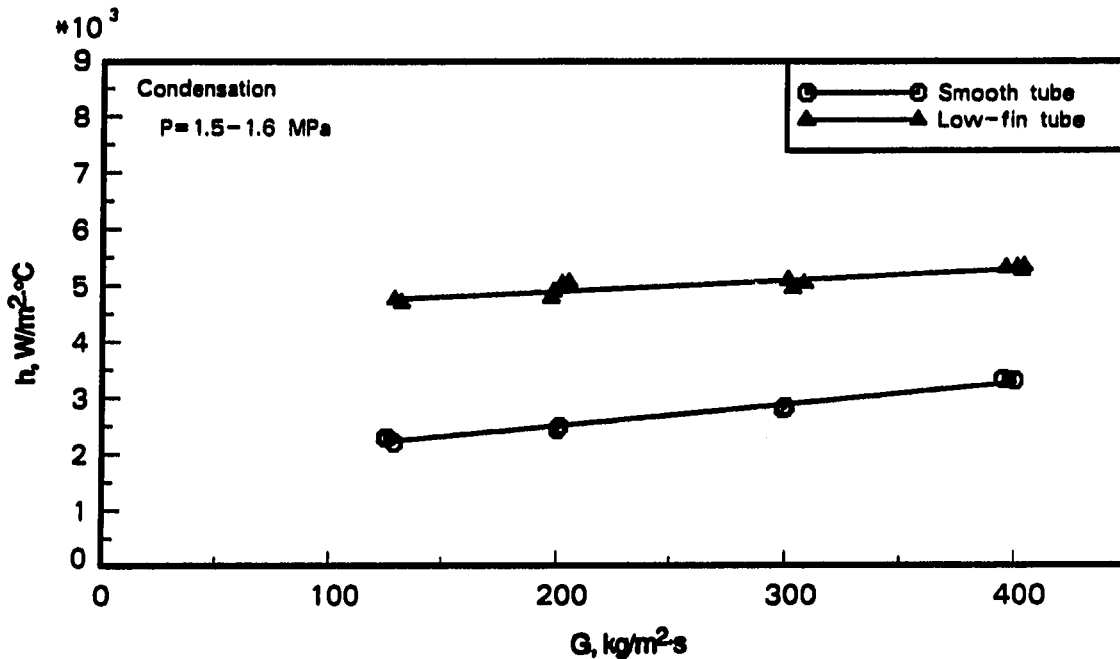


Figure 8.4. Heat transfer coefficient versus mass flux for pure refrigerant condensation in a smooth tube and a low-fin tube

Comparison with Micro-Fin Tube

The pure refrigerant enhancement factors of the low-fin tube are compared with those of the micro-fin tube in Figure 8.5. With both tubes, the enhancement factor tends to decrease with increasing mass flux and the decrease is slightly more severe for evaporation. The evaporation performance of both tubes is virtually identical, with each curve lying within $\pm 3\%$ of the other. During condensation, the micro-fin tube outperforms the low-fin tube by 10% to 15% over the entire range of mass fluxes.

Heat Transfer with Refrigerant-Oil Mixtures

Only 150-SUS oil was tested with the low-fin tube. Nominal oil concentrations of 1.25%, 2.5%, and 5% were used for these tests.

Evaporation

Evaporation results for the low fin tube with refrigerant-oil mixtures, as well as pure refrigerant, are presented in Figure 8.6. With 1.3% oil, the heat transfer performance is

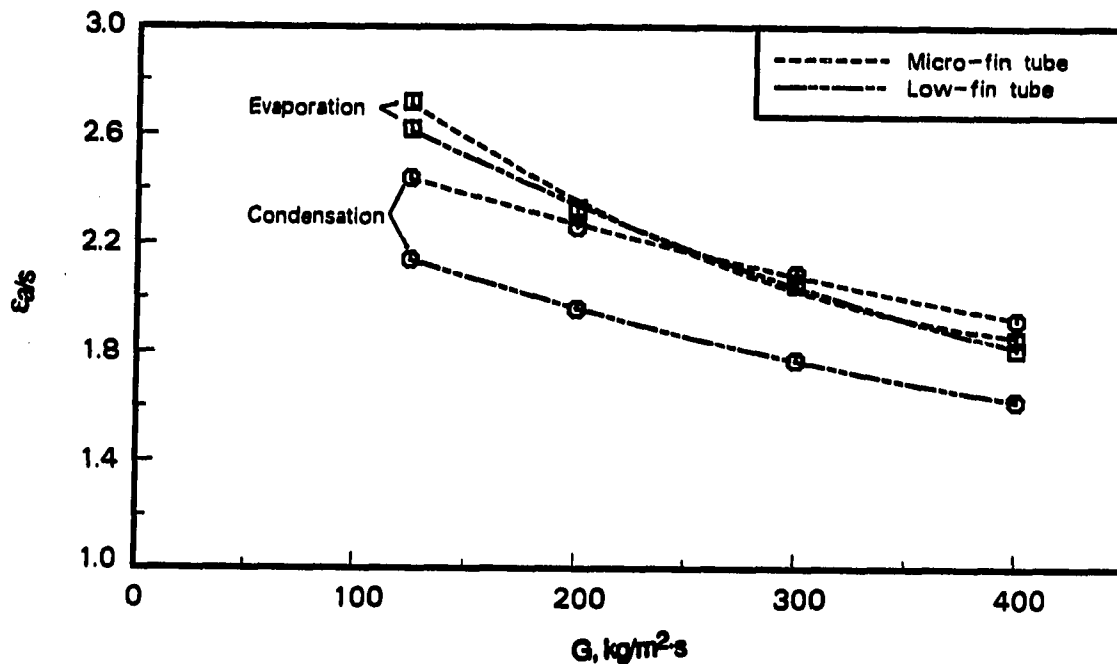


Figure 8.5. Heat transfer enhancement factor ($\epsilon_{a/s}$) for evaporation and condensation of R-22 in a micro-fin tube and a low-fin tube

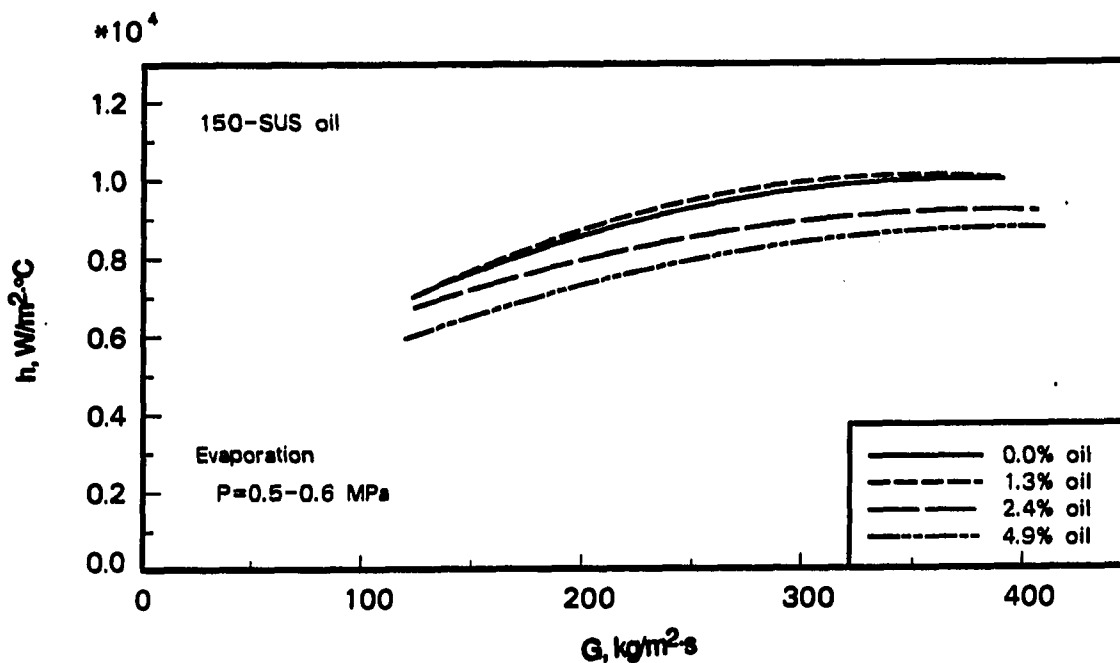


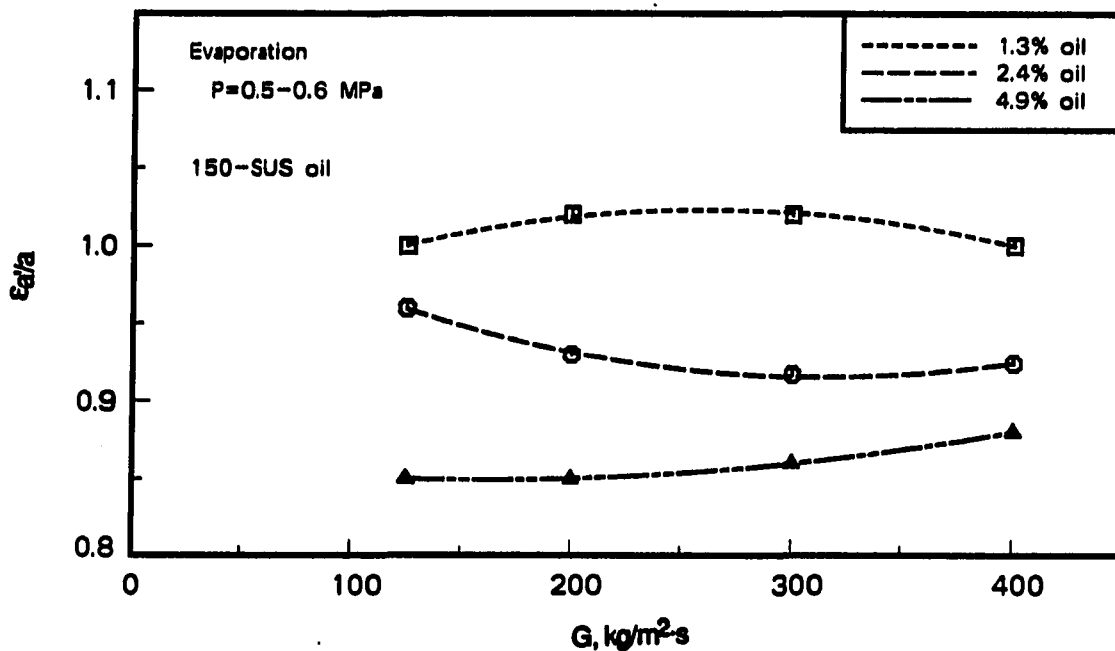
Figure 8.6. Heat transfer coefficient versus mass flux for evaporation with mixtures of R-22 and 150-SUS oil in a low-fin tube

very close to that with pure refrigerant, but with a slight tendency toward enhancement. For higher oil concentrations, the performance decreases. With 5.0% oil concentration, heat transfer decreases by about 15% when compared to the pure refrigerant case.

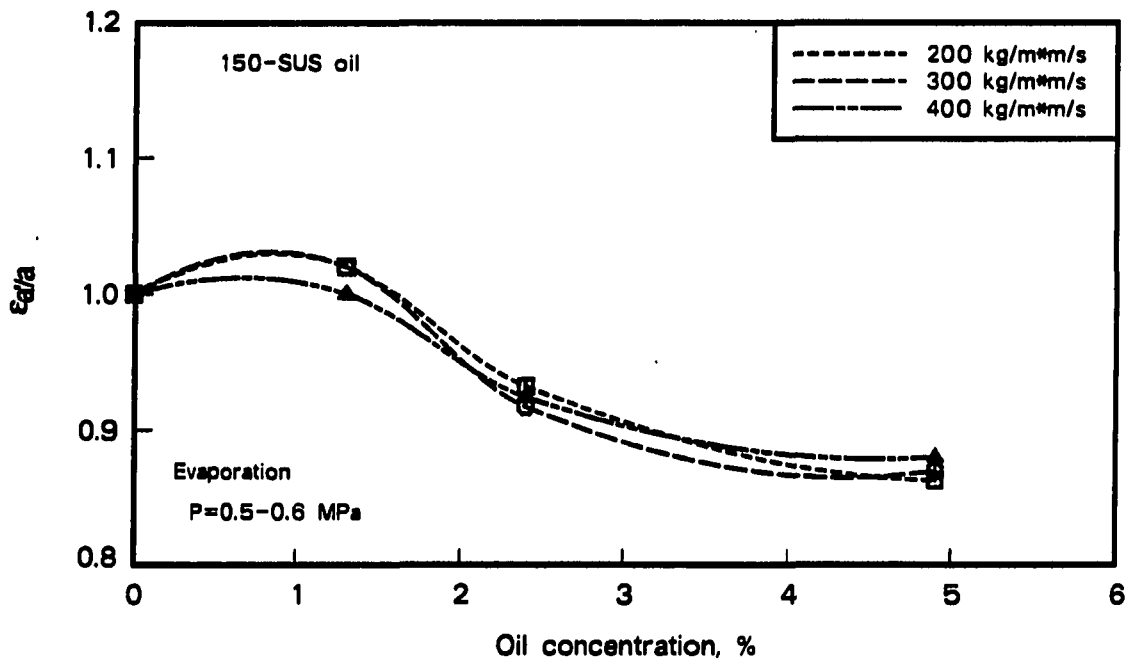
Figure 8.7(a) shows the enhancement factor for the low fin tube, $\epsilon_{a/a}$, as a function of mass flux and part (b) shows it as a function of oil concentration. Mass flux does not have a strong influence on $\epsilon_{a/a}$ and, except for slight enhancement with 1.3% oil, performance is degraded with each incremental increase in oil concentration.

Comparison with other tubes A comparison of the effects of oil in smooth, low-fin, and micro-fin tubes is shown in Figure 8.8, where $\epsilon_{s/s}$ and $\epsilon_{a/a}$ are plotted versus oil concentration. For the low-fin tube, the maximum value of $\epsilon_{a/a}$ is only about 1.02 with 1% oil, and $\epsilon_{a/a}$ is less than unity for oil concentrations greater than 1.5%, falling to under 0.9 as the oil concentration approaches 5.0%. This behavior is in contrast to the smooth tube, which exhibits a pronounced heat transfer enhancement over the entire range of oil concentrations. The effect of oil on micro-fin tube performance is between these extremes. Also from Figure 8.8, it is seen that the effect of oil on heat transfer performance in the low-fin tube is less dependent on oil concentration and mass flux than in the smooth tube. Curves showing low-fin tube performance are flatter and lie closer to one another than the smooth tube curves.

Figure 8.9 shows the combined effects of oil and augmented surface, $\epsilon_{a/s'}$. Part (a) shows only low-fin tube results over the entire range of mass fluxes and oil concentrations, while part (b) shows only two mass fluxes, but also includes micro-fin results for comparison. Figure 8.9(a) shows a general trend of decreasing enhancement factor with increasing oil concentration, but $\epsilon_{a/s'}$ recovers slightly as 5.0% oil concentration is approached. The values of $\epsilon_{a/s'}$ with 5.0% oil are 5% to 15% higher than those with 2.5% oil. This does not mean that the performance of the low fin tube is increasing at the higher oil concentrations, but rather that the degradation of heat transfer in this concentration range is slower in the low-fin tube than in the smooth tube. Both tubes show a lower performance in absolute terms with 5.0% oil than with 2.5% oil. Another trend is the reduction of $\epsilon_{a/s}$ and $\epsilon_{a/s'}$ by about 30% from lowest to highest mass flux with both pure refrigerant and refrigerant-oil mixtures. Because the shapes of all the curves are similar, the effect of oil



(a)



(b)

Figure 8.7. Evaporation enhancement factor due to the effects of oil ($\epsilon_{a/a}$) in a low-fin tube

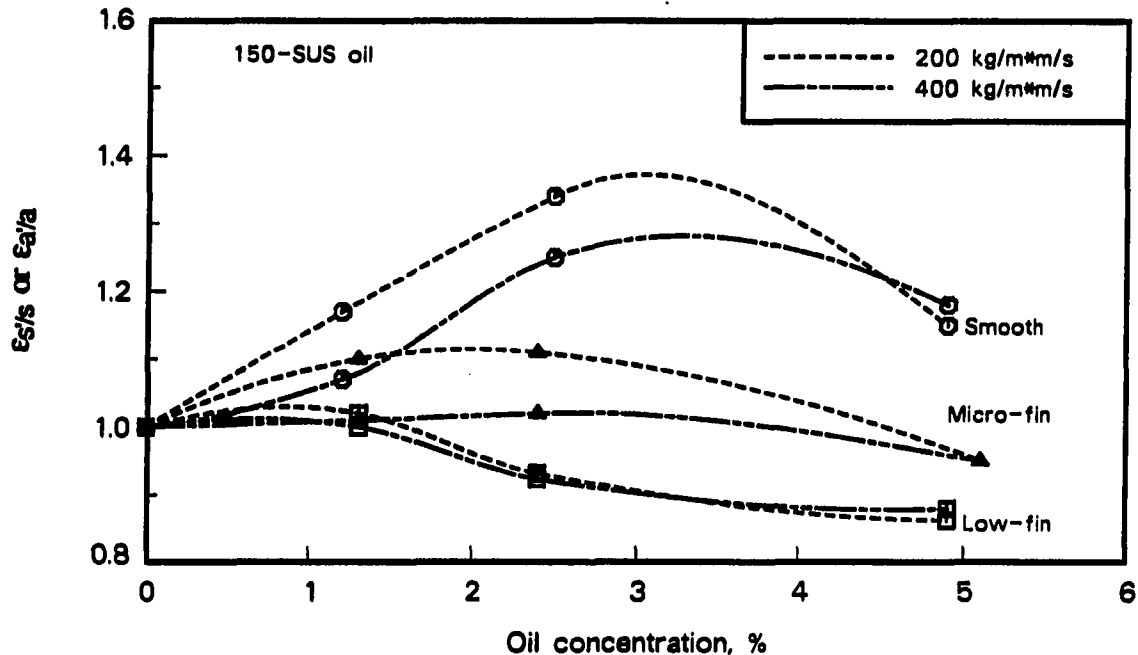


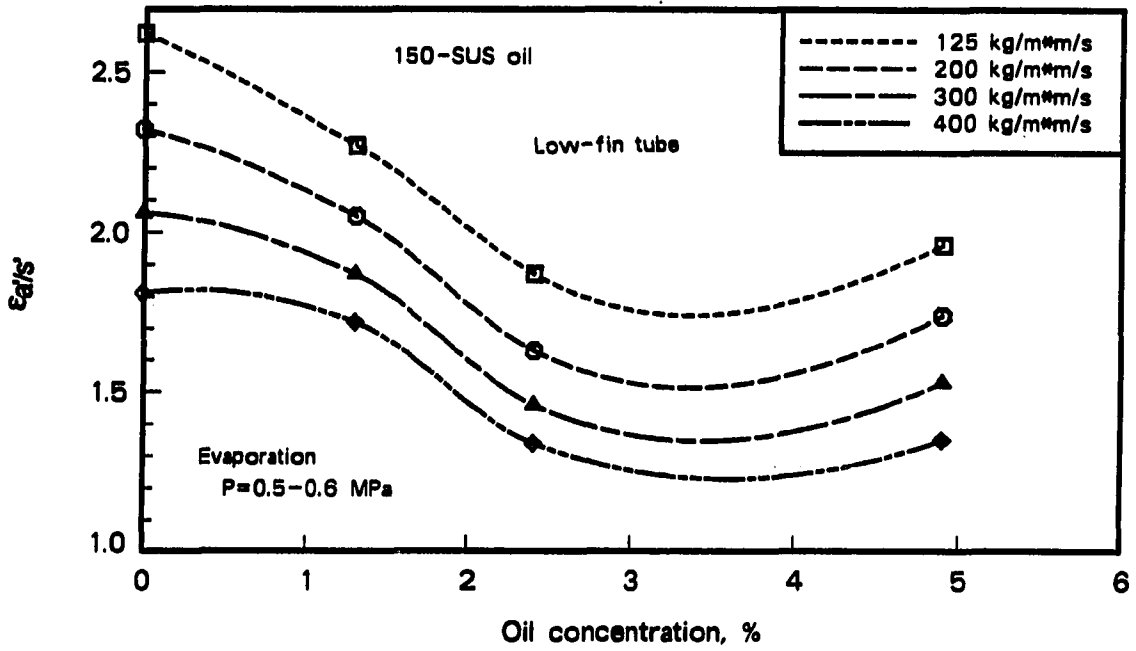
Figure 8.8. Evaporation enhancement factors for smooth, micro-fin, and low-fin tubes ($\epsilon_{s/s}$ and $\epsilon_{a/a}$) as a function of oil concentration

on $\epsilon_{a/s}$ is similar at all mass fluxes. The minimum observed value of $\epsilon_{a/s}$ is between 1.3 and 1.4, so the low fin tube maintains an advantage over the smooth tube at all conditions tested, but the enhancement is often less than the internal area increase, A^* .

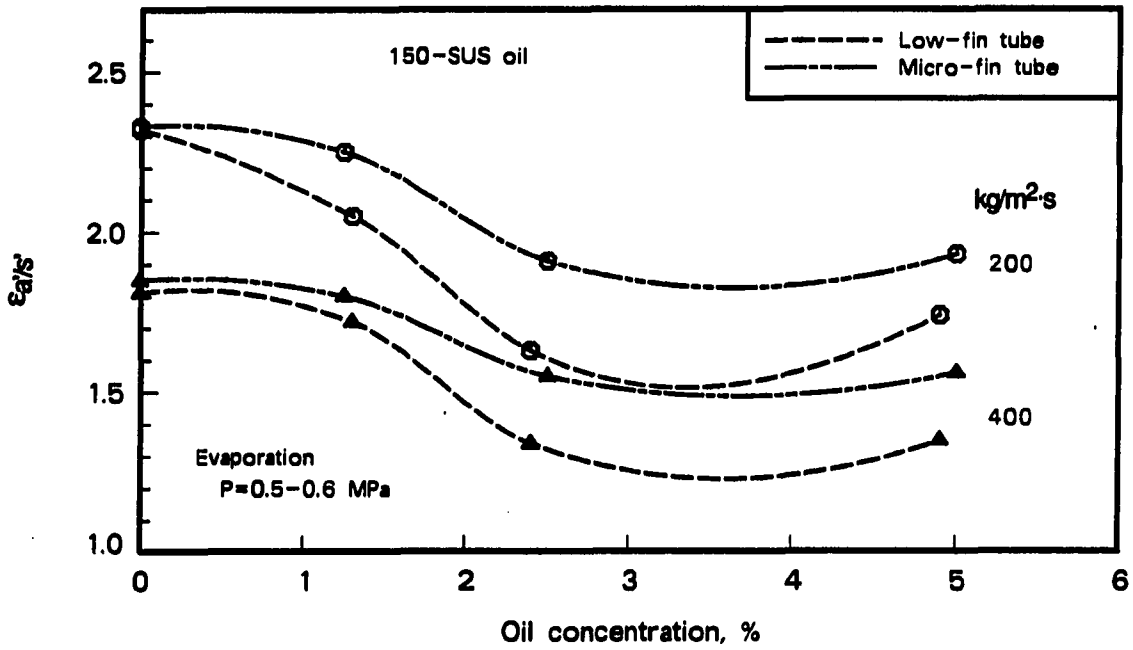
Figure 8.9(b) allows a comparison of the low-fin tube with the micro-fin tube. The curves for both tubes are similar in shape and show approximately the same trends with increasing oil concentration. With pure R-22, $\epsilon_{a/s}$ values for both tubes are quite similar. As oil is added, the performance of the micro-fin tube relative to the low-fin tube improves, although both tubes show decreasing performance relative to the smooth tube. At 2.5% oil concentration and 200 kg/m²·s, $\epsilon_{a/s}$ of the micro-fin tube is about 40% higher than that of the low-fin tube. As the concentration increases further and approaches 5.0%, the curves for the finned tubes start to converge. With 5.0% oil and at 200 kg/m²·s, $\epsilon_{a/s}$ of the micro-fin tube is only about 15% higher than that of the low-fin tube.

Condensation

Results for condensation of refrigerant-oil mixtures in the low-fin tube are given in Figure 8.10. All cases show a degradation of heat transfer with the addition of oil, and



(a)



(b)

Figure 8.9. Evaporation enhancement factor showing the combined effects of oil and augmentation ($\epsilon_{a/s'}$) in a micro-fin tube and a low-fin tube

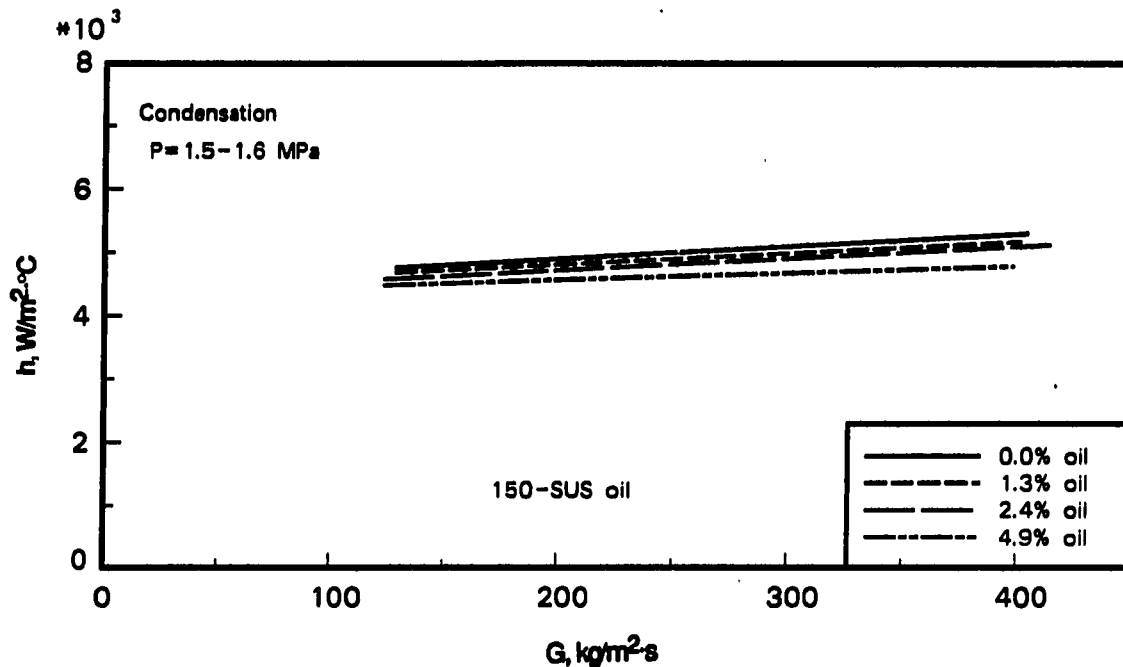
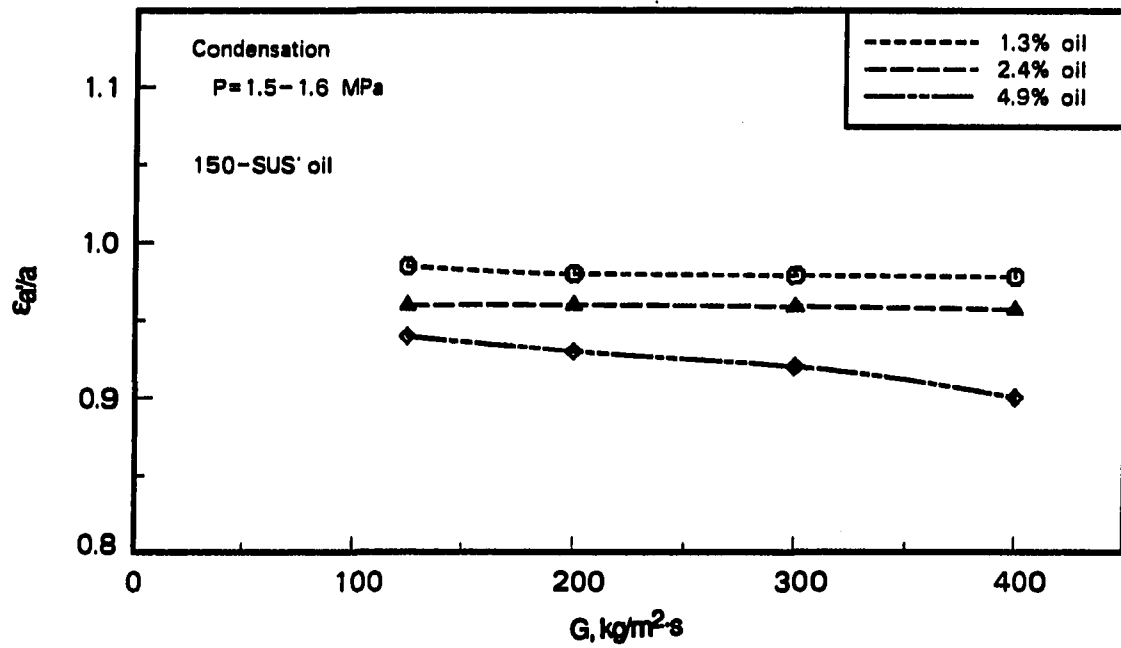


Figure 8.10. Heat transfer coefficient versus mass flux for condensation with mixtures of R-22 and 150-SUS oil in a low-fin tube

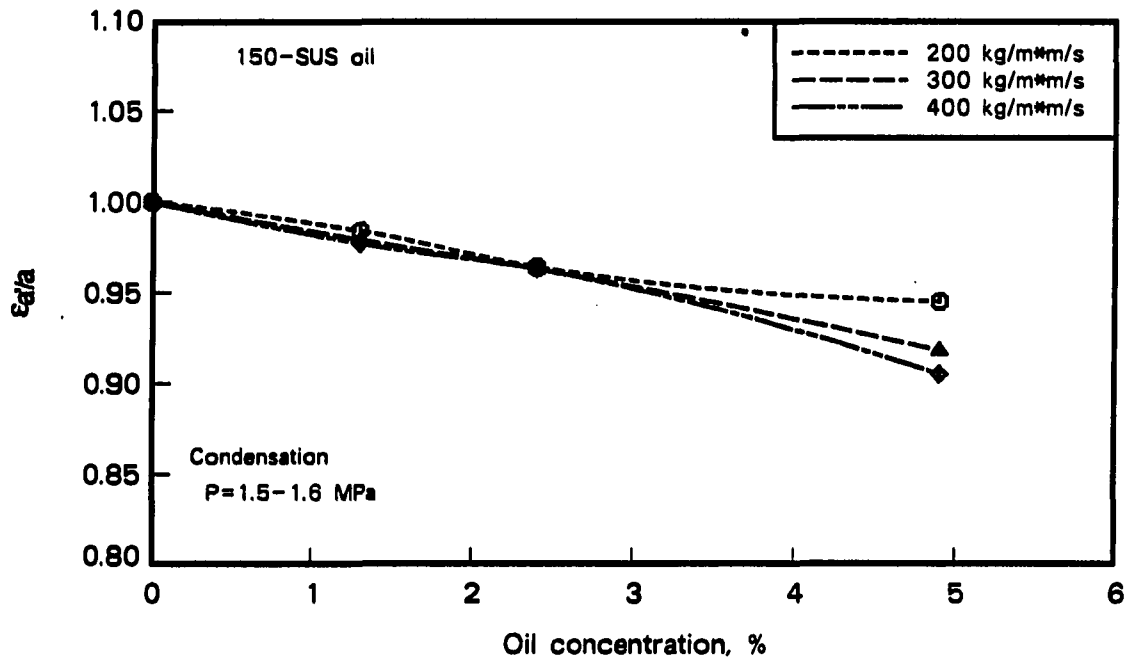
the magnitude of the degradation increases with increasing oil concentration. With an oil concentration of 5.0%, the heat transfer coefficient is 5% to 10% lower than with pure refrigerant.

The effect of oil on heat transfer performance is shown in Figure 8.11, with a plot of $\epsilon_{a/a}$ versus mass flux in part (a) and versus oil concentration in part (b). Mass flux does not have a large influence on oil effects as shown by the flat curves in part (a). With increasing oil concentration, the enhancement factor decreases steadily and the decrease is approximately proportional to the concentration.

Comparison with other tubes Low-fin tube condensation trends are similar to those of the smooth tube and micro-fin tube. All tubes show a steady, though not dramatic, reduction in heat transfer as the oil concentration increases. The oil effects alone for all three tubes are depicted in Figure 8.12 with $\epsilon_{a/a}$ and $\epsilon_{s/s}$ plotted against oil concentration. The steady decline in performance with increasing oil concentration can be clearly seen, but the rate of decrease is lower for the low-fin tube than for the other two tubes. Data for the



(a)



(b)

Figure 8.11. Condensation enhancement factor due to the effects of oil (ϵ_a/a) in a low-fin tube

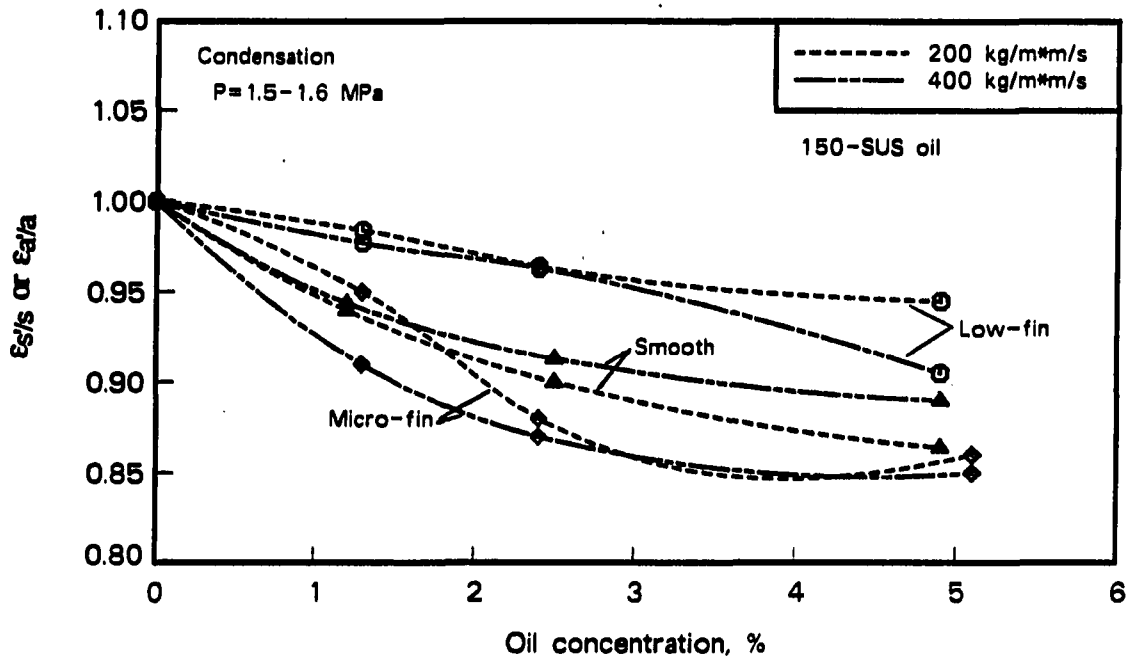
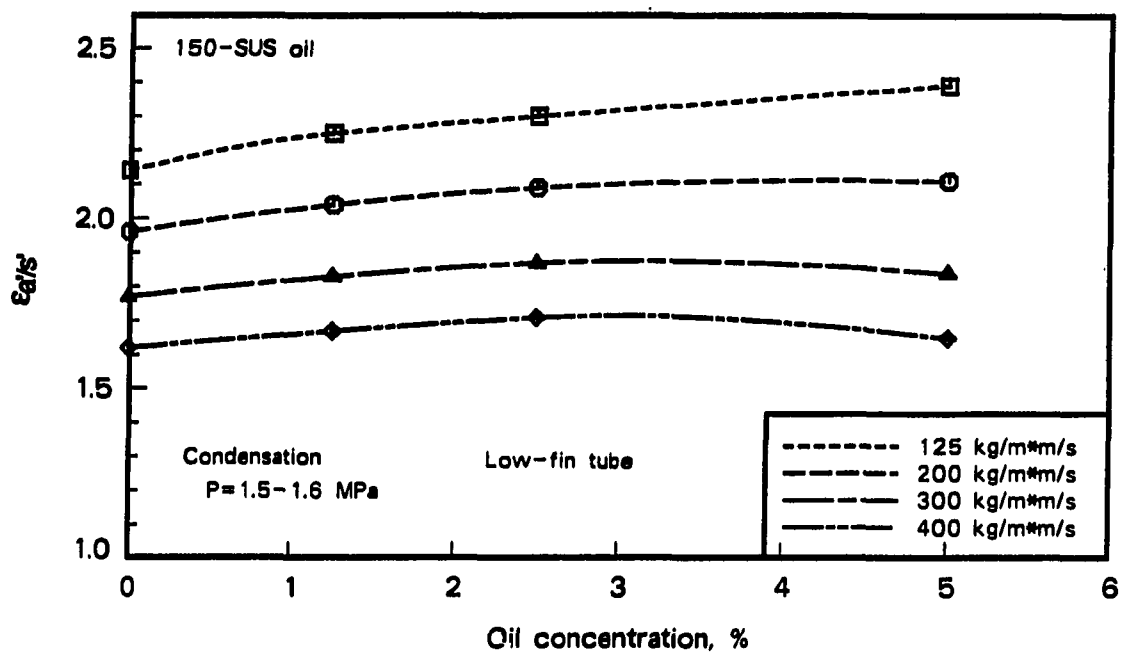


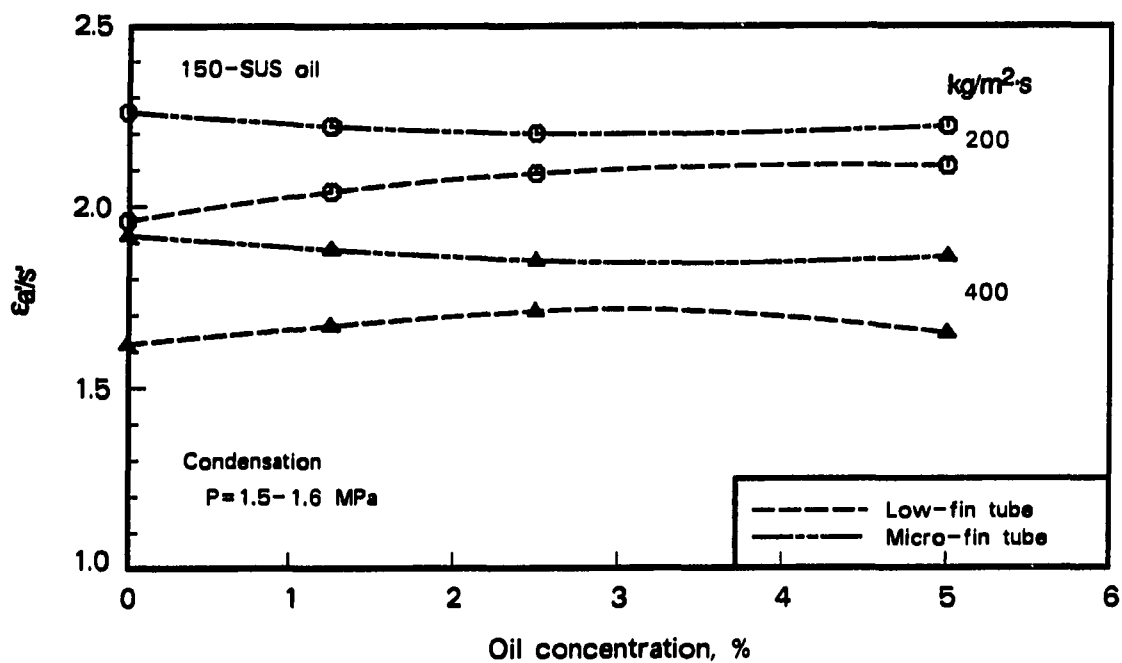
Figure 8.12. Condensation enhancement factors for smooth, micro-fin, and low-fin tubes ($\epsilon_{s/s}$ and $\epsilon_{a/a}$) as a function of oil concentration

smooth tube and micro-fin tube lie in a narrow band, with values of $\epsilon_{a/a}$ in the low-fin tube somewhat higher. At 200 kg/m²·s, heat transfer in the low-fin tube falls by about 1% and 5% for oil concentrations of 2.5% and 5.0%, respectively. For the same conditions and oil concentrations, heat transfer in the smooth tube falls by 10% and 13%, and in the micro-fin tube by 12% and 13%. The results show little variation with mass flux for any tube.

Figure 8.13(a) shows the combined effects of oil and augmentation for the low-fin tube. As seen earlier with evaporation, there is a trend toward decreasing $\epsilon_{a/s'}$ as mass flux increases, regardless of the oil concentration. Going from the lowest to the highest mass flux causes $\epsilon_{a/s'}$ to decrease by 25% to 30%. The oil is seen to have a weak effect on $\epsilon_{a/s'}$ in contrast with the evaporation results shown in Figure 8.9, where $\epsilon_{a/s'}$ shows a somewhat greater variation with oil concentration. The maximum increase in $\epsilon_{a/s'}$ with increasing oil concentration is between 5% and 10%. As discussed earlier, this trend should not be interpreted to mean that heat transfer is increasing with increasing oil concentration in the



(a)



(b)

Figure 8.13. Evaporation enhancement factor showing the combined effects of oil and augmentation (ϵ_a/s) in a micro-fin tube and a low-fin tube

low-fin tube, but rather that oil diminishes heat transfer performance less in the low-fin tube than in the smooth tube.

Figure 8.13(b) repeats two of the curves from Figure 8.13(a) and adds micro-fin tube results for comparison. The micro-fin tube performance is consistently better than that of the low-fin tube at all oil concentrations and mass fluxes. Both tubes show a weak dependence on oil concentration. With pure R-22, $\epsilon_{a/s}$ with the low-fin tube is 10% to 15% lower than that with the micro-fin tube, but because of the lesser heat transfer degradation with increasing oil concentration in the low-fin tube, $\epsilon_{a/s}$ values for the two tubes converge at higher oil concentrations. At 5.0% oil, $\epsilon_{a/s}$ for the low-fin tube is only 5% to 10% lower than $\epsilon_{a/s}$ for the micro-fin tube, versus a 10% to 15% difference with pure refrigerant.

Pressure Drop

As with the other tubes, pressure drop data are fitted with quadratic curves, then pressure drop enhancement factors, Ψ , are calculated from these the curves. Comments regarding uncertainties and data scatter, which were made in Chapter 6 for the smooth tube, are also applicable to low-fin tube results. Standard deviations of pressure drop measurements and confidence intervals on the regression curves are given in Appendix D.

Pure Refrigerant

Pressure drop results for the low-fin tube along with those for the smooth tube are shown in Figure 8.14. For both evaporation and condensation, there is an increase in pressure drop due to the internal fins. In terms of enhancement factors, these data are presented in Figure 8.15, which also includes $\Psi_{a/s}$ for the micro-fin tube. For evaporation, the curve for the low-fin tube is relatively flat, showing only a weak dependence on mass flux. The highest value of $\Psi_{a/s}$ is about 1.9 near 200 kg/m²·s, with the value falling to around 1.5 at 400 kg/m²·s. The condensation plot shows a much greater variance with mass flux, starting around 1.7 at low mass flux, peaking at over 2.6, then falling to 1.6 at the highest mass flux.

Referring to Figure 8.3, which shows heat transfer enhancement factors ($\epsilon_{a/s}$) for the low-fin tube, it can be seen that during evaporation, heat transfer enhancement is

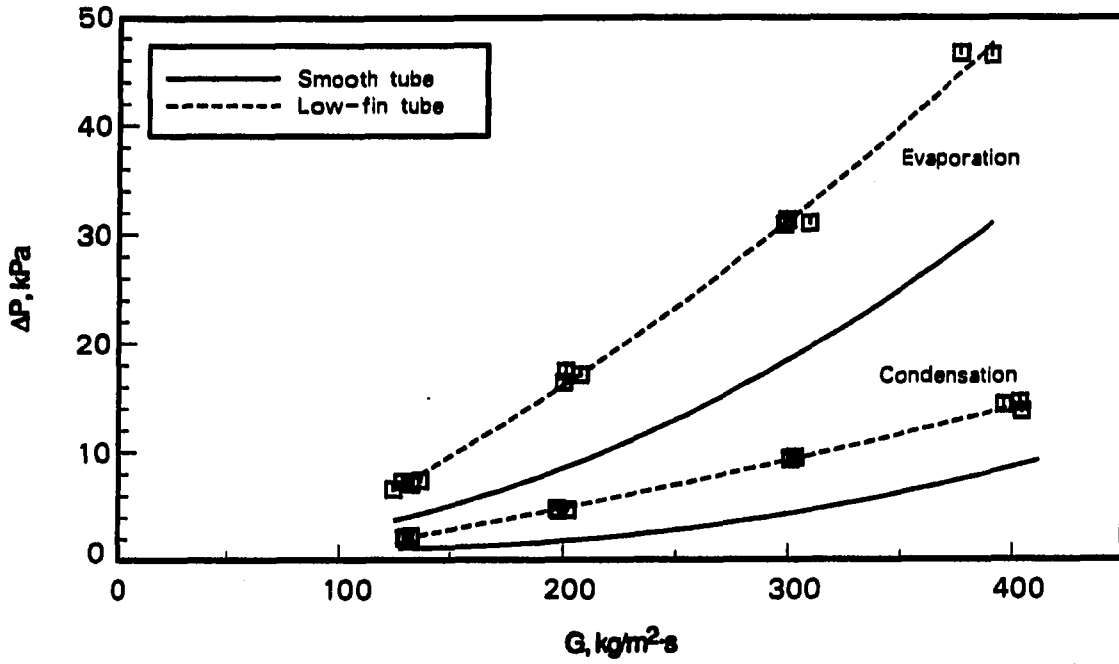


Figure 8.14. Evaporation and condensation pressure drop with pure R-22 in smooth and low-fin tubes

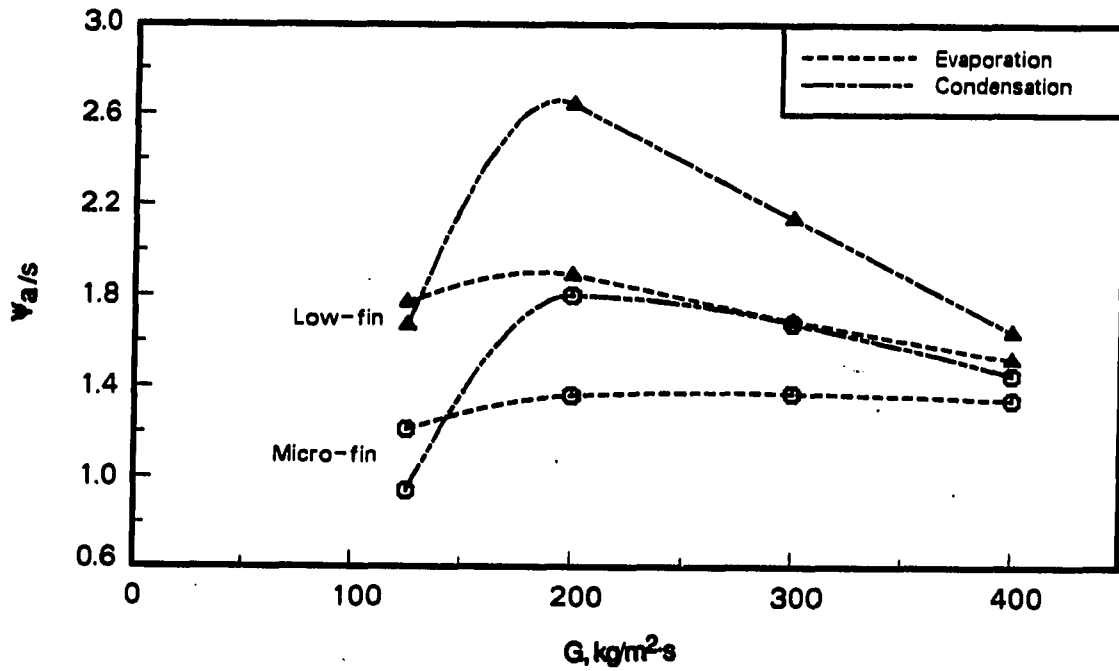


Figure 8.15. Pressure drop enhancement factor ($\Psi_{a/s}$) for evaporation and condensation in a micro-fin tube and low-fin tube

greater than pressure drop enhancement by at least 20% for all conditions. For condensation, however, pressure drop enhancement is generally greater, except at the lowest mass fluxes. The difference is greatest at $200 \text{ kg/m}^2\cdot\text{s}$, where $\Psi_{a/s}$ is 30% higher than $\epsilon_{a/s}$. As mass flux approaches $400 \text{ kg/m}^2\cdot\text{s}$, however, the difference narrows such that $\Psi_{a/s}$ is approximately equal to $\epsilon_{a/s}$.

Figure 8.15 also includes micro-fin tube results, which can be compared with those of the low-fin tube. The shapes of the curves for both tubes display the same trends, indicating that mass flux effects are similar. The magnitude of $\Psi_{a/s}$, however, differs between the tubes. Considering only mass fluxes greater than $200 \text{ kg/m}^2\cdot\text{s}$, the pressure drop penalty in the low-fin tube is 15% to 45% higher than that in the micro-fin tube for both evaporation and condensation, depending on mass flux. Higher pressure drop with higher fins is consistent with previously published results.

Refrigerant-Oil Mixtures

Evaporation Evaporation pressure drop with refrigerant-oil mixtures is shown in Figure 8.16. Oil increases the pressure drop in general, but at lower mass fluxes, the curves of several concentrations converge, making trends difficult to assess. At high mass flux, the pressure drop is seen to increase with each incremental increase in oil concentration.

Pressure drop enhancement factors due to oil, $\Psi_{a/a}$, are plotted in Figure 8.17: as a function of mass flux in part (a) and as a function of oil concentration in part (b). At low mass flux, $\Psi_{a/s}$ ranges from less than 1.0 to about 1.6 depending on oil concentration, but at higher mass fluxes, curves become flatter and values for all concentrations converge, falling between 1.1 and 1.25. Figure 8.17(b) shows curves for all of the different mass fluxes with the exception of $125 \text{ kg/m}^2\cdot\text{s}$. This is markedly different from the others, and it is not included due to the previously discussed uncertainty associated with this condition. An upward trend in $\Psi_{a/a}$ with increasing oil concentration can also be observed.

To compare the overall pressure drop performance of the two augmented tubes, $\Psi_{a/s}$ is plotted for the low-fin tube and micro-fin tube in Figure 8.18. Figure 8.18(a) is plotted versus mass flux and shows that for mass fluxes greater than $200 \text{ kg/m}^2\cdot\text{s}$, pressure

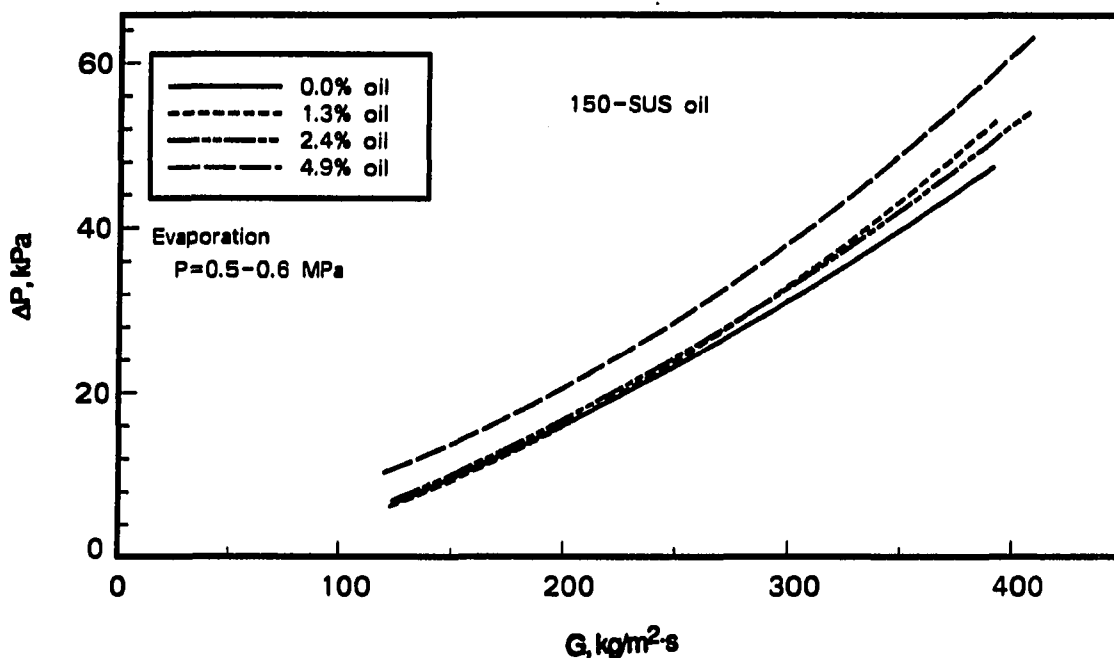
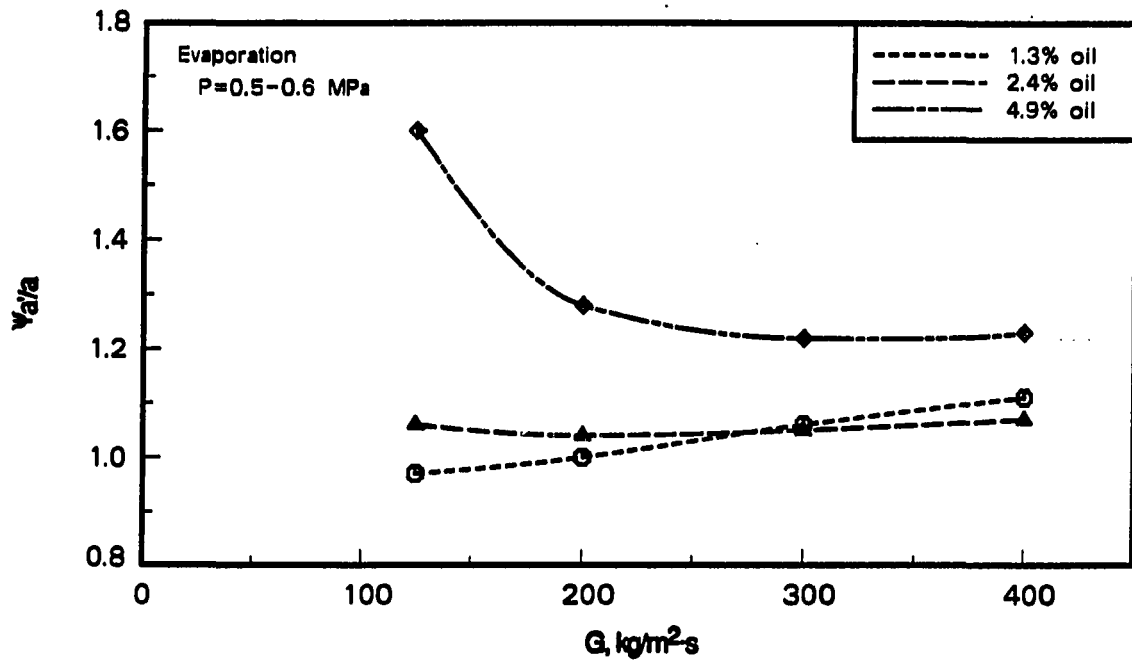


Figure 8.16. Evaporation pressure drop in a low-fin tube with mixtures of R-22 and oil

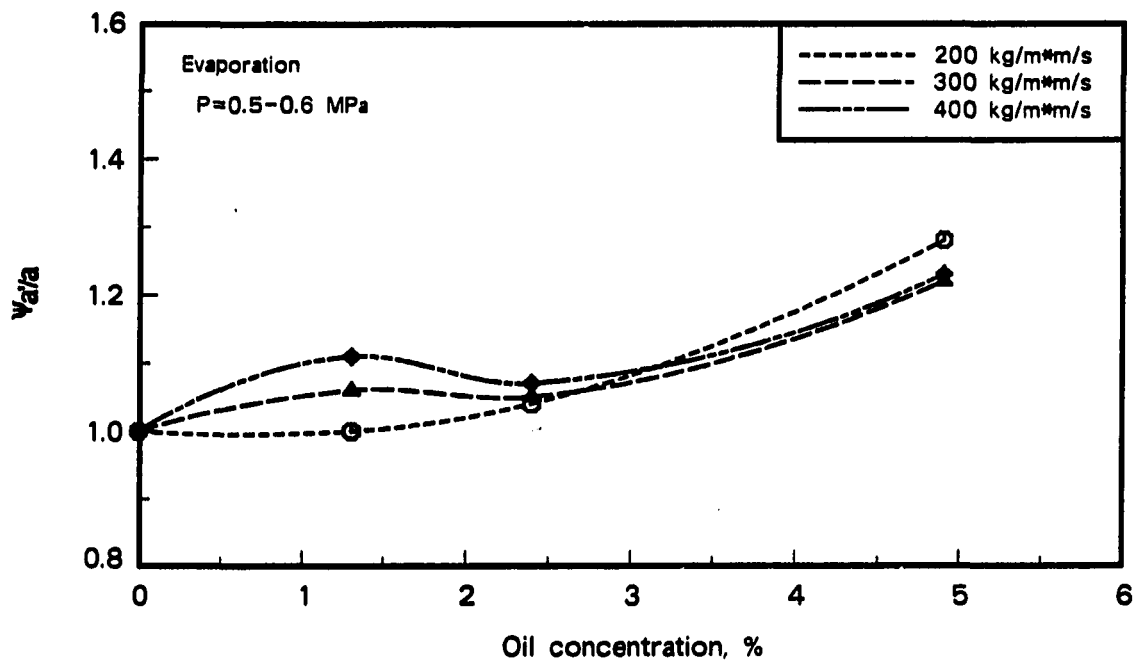
drop in the low-fin tube is on average about 20% higher than that in the micro-fin tube. Curves for both tubes are relatively flat, indicating no great influence of mass flux on $\Psi_{a/s}$. Part (b) of Figure 8.18 shows $\Psi_{a/s}$ plotted versus oil concentration. Again, curves tend to be grouped by tube type, with those for the low-fin tube lying above those for the micro-fin tube. As in Figure 8.18(a), curves are relatively flat, so $\Psi_{a/s}$ is not a strong function of oil concentration. In plots having $\Psi_{a/s}$ as the ordinate, curves with a slope near zero indicate that the effect of oil in the augmented tube is similar to its effect in the smooth tube.

Condensation Results during condensation are presented in Figure 8.19. As during evaporation, there is an increase in pressure drop with the addition of oil, but the condensation curves are more closely grouped. Once again, curves at low mass flux converge, making assessment of trends difficult.

The effect of oil addition is shown in Figure 8.20. Figure 8.20(a) plots $\Psi_{a/a}$ versus mass flux and indicates that there is little mass flux influence above 200 kg/m²·s. The spread in values of $\Psi_{a/a}$ with changing oil concentrations is small: 1.05 to 1.15.

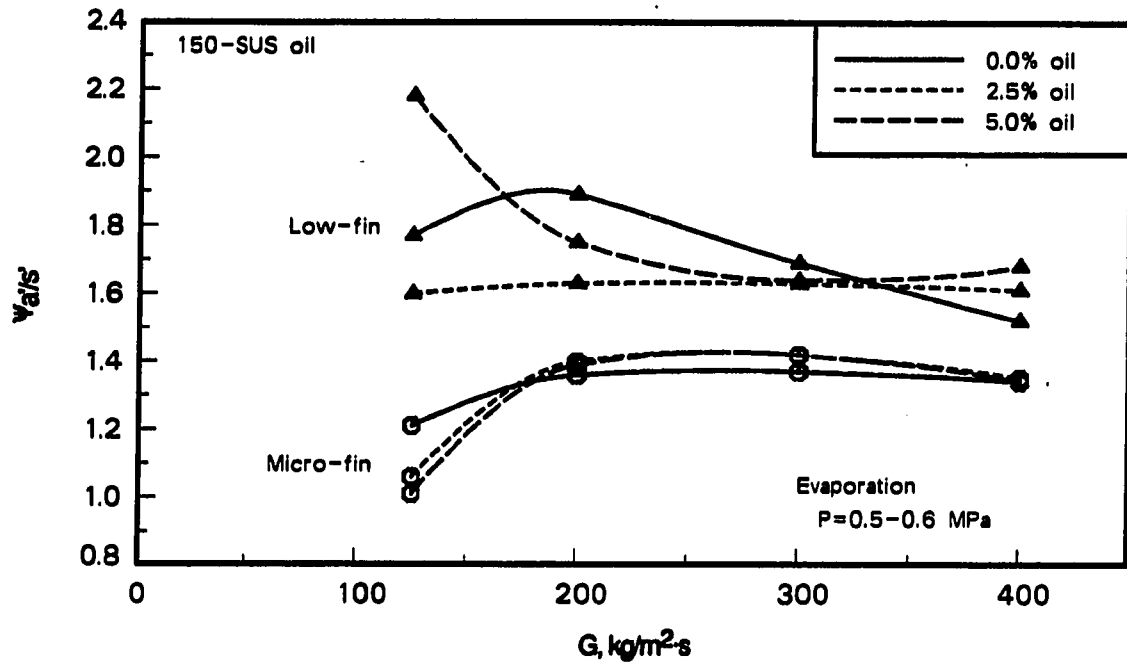


(a)

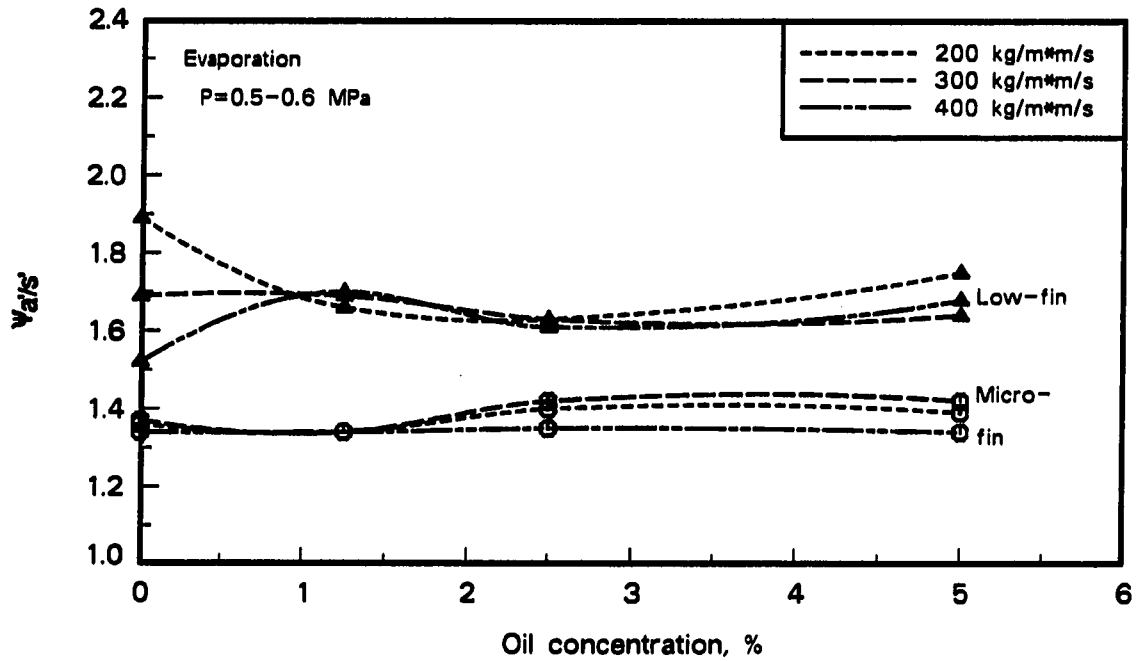


(b)

Figure 8.17. Pressure drop enhancement factor due to the effects of oil ($\Psi_{a/a}$) for evaporation in a low-fin tube



(a)



(b)

Figure 8.18. Pressure drop enhancement factor showing the combined effects of oil and augmentation ($\Psi_{a/s}$) for evaporation in a micro-fin tube and a low-fin tube

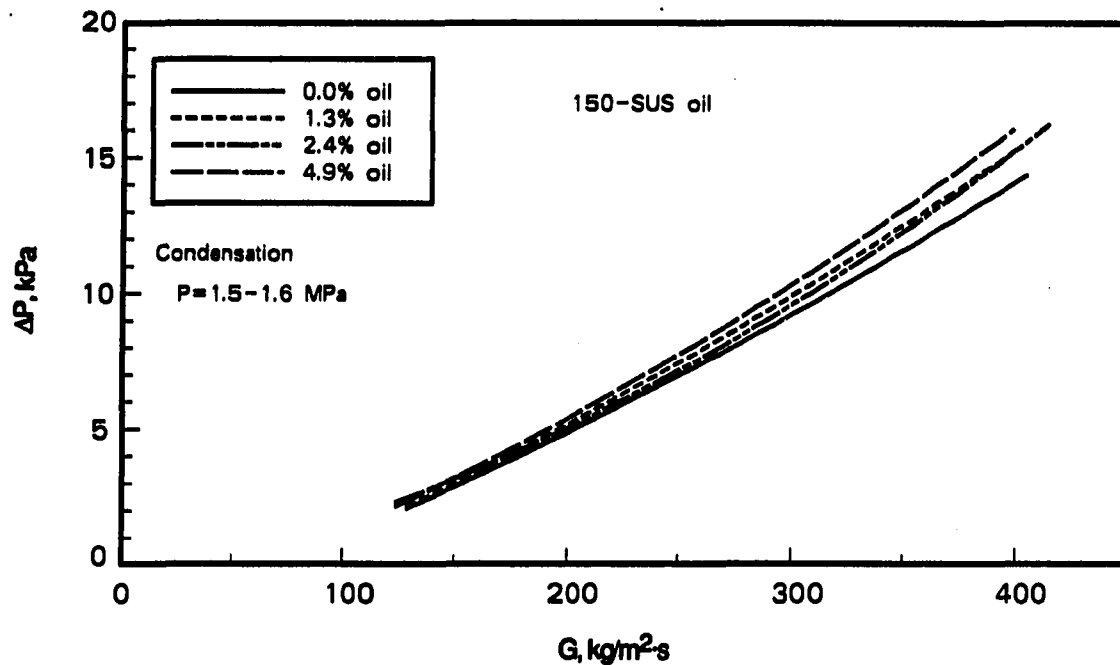


Figure 8.19. Condensation pressure drop in a low-fin tube with mixtures of R-22 and oil

Figure 8.20(b) shows the same data plotted as a function of oil concentration. The curves are tightly grouped and show a general upward trend with increasing oil concentration.

The combined effects of oil and augmentation are shown in Figure 8.21, which plots $\Psi_{a'/s'}$ versus mass flux in part (a) and versus oil concentration in part (b). Also included for comparison are micro-fin tube results reported earlier. Pressure drop in the low-fin tube is almost a factor of 5.0 greater than that in the smooth tube at the worst conditions, while micro-fin pressure drop is up to a factor of 3.5 greater than smooth tube pressure drop. As noted in the micro-fin discussion in Chapter 7, these values are quite high compared to other enhancement factors obtained in this test program.

For evaporation (Figure 8.18), curves are grouped by tube type, but the grouping is somewhat more complex for condensation (Figure 8.21). For both tubes, pure refrigerant condensation results are well below the those with refrigerant-oil mixtures. Curves for refrigerant-oil mixture results, however, are grouped by tube type, as for evaporation in Figure 8.18. The separation of curves depicting pure refrigerant results from those showing

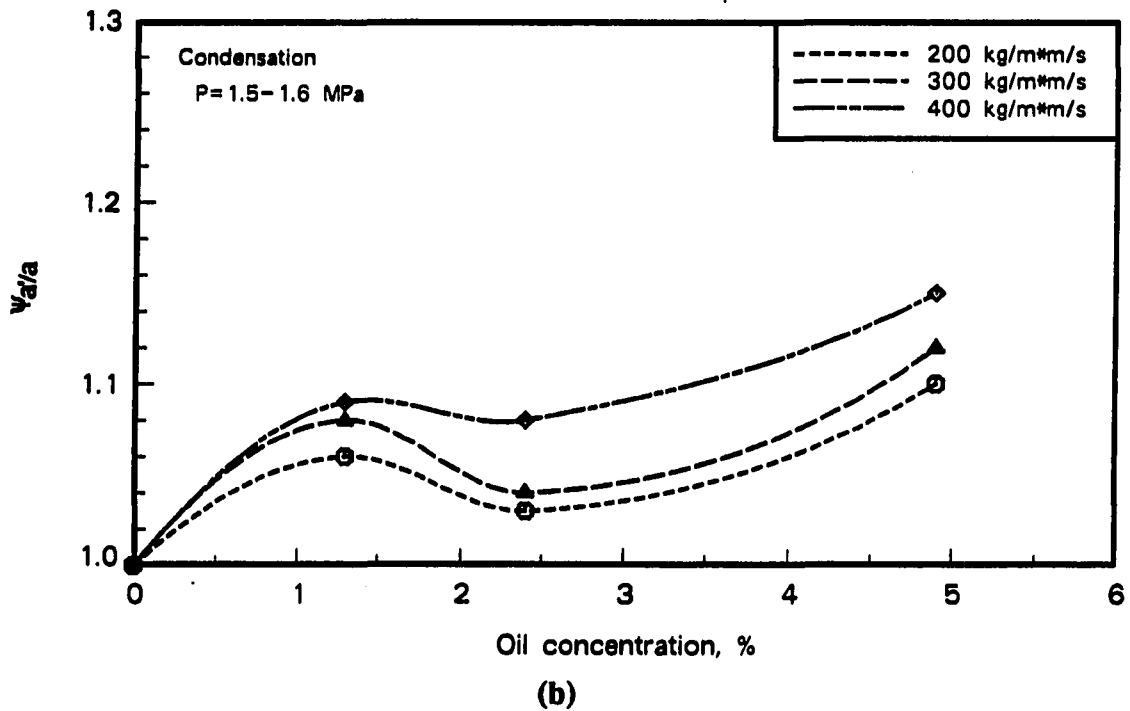
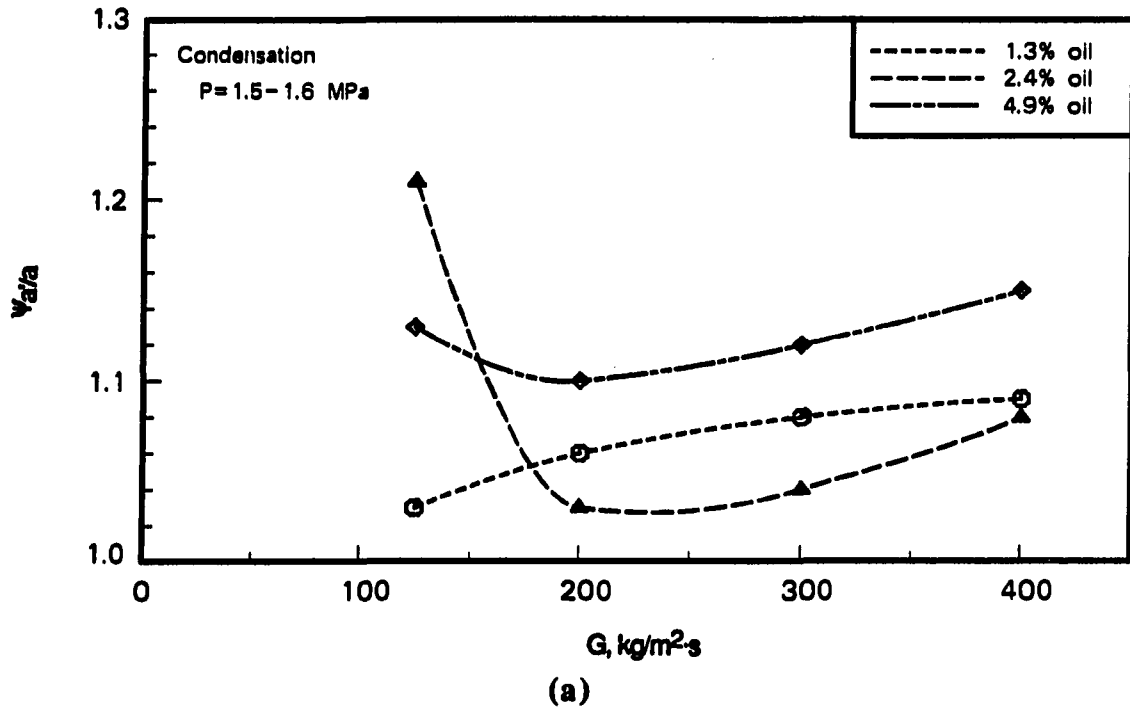
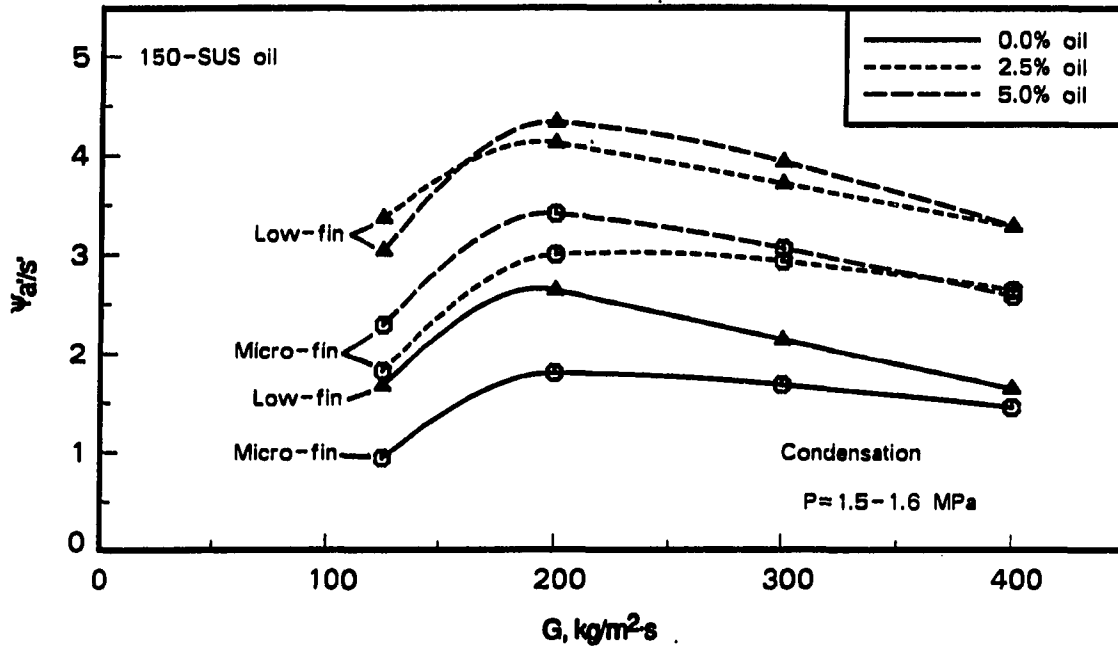
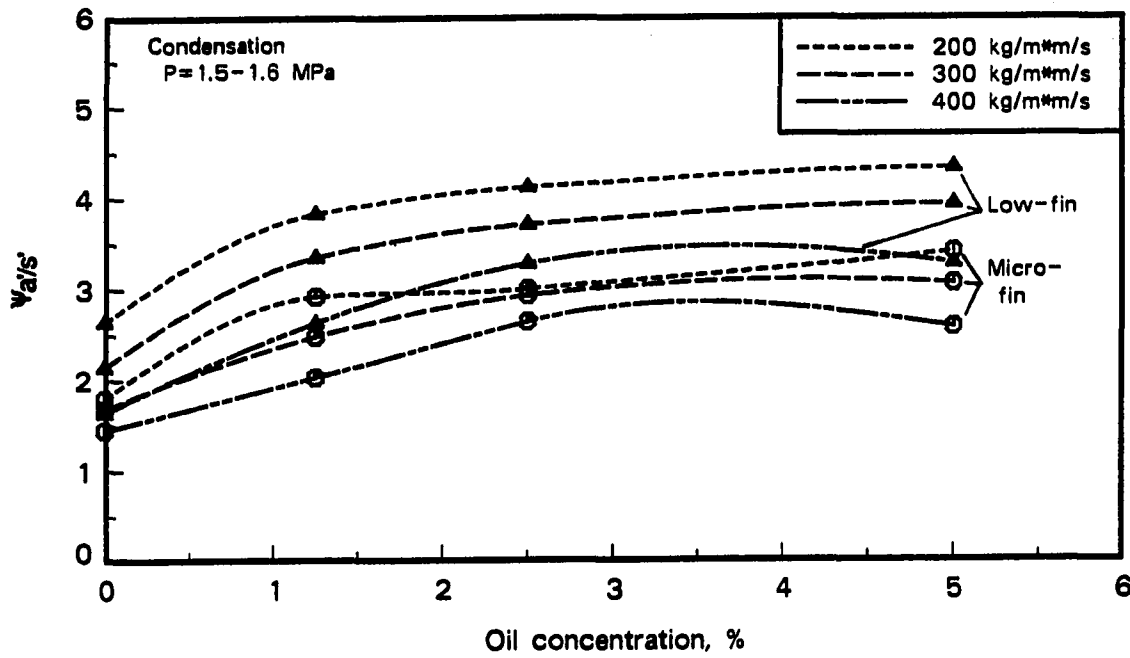


Figure 8.20. Pressure drop enhancement factor due to the effects of oil ($\psi_{a/a}$) for condensation in a low-fin tube



(a)



(b)

Figure 8.21. Pressure drop enhancement factor showing the combined effects of oil and augmentation ($\Psi_{a/s'}$) for condensation in a micro-fin tube and a low-fin tube

refrigerant-oil mixture results is due to the decreasing pressure drop with increasing oil concentration observed in the smooth tube. As mentioned during the micro-fin tube discussion, it is uncertain how universally applicable comparisons with smooth tube results might be, because the anomalous behavior may have been caused by a unique combination of test conditions and rig geometry. It is observed that pressure drop results in the low-fin tube are consistently higher by about 20% to 50% than the corresponding micro-fin tube results over most of the mass flux range.

Figure 8.21(b) plots $\Psi_{a/s}$ versus oil concentration. As in part (a), low-fin results are above the corresponding micro-fin results. After an initial increasing trend of $\Psi_{a/s}$ with increasing oil concentration, the curves flatten somewhat at concentrations above 2.5%. The sharp increase at low concentrations is due once again to the anomalous behavior in the smooth tube. The levelling at higher concentrations indicates that the effect of oil on smooth tube pressure drop becomes similar to its effect on pressure drop in the augmented tube.

Summary

Experimental results using a low-fin tube with pure refrigerant and refrigerant-oil mixtures were presented in this chapter. Only 150-SUS oil was tested in the low-fin tube, so comparisons with the other tubes are limited to this oil. There have been no previous publications reporting on the performance of refrigerant-oil mixtures in this type of tube. A summary of major conclusions is presented below along with numerical examples at a representative mass flux of $300 \text{ kg/m}^2\text{-s}$ unless stated otherwise.

Evaporation

1. Pure refrigerant heat transfer performance in the low-fin tube is comparable to that in the micro-fin tube. The enhancement factor, $\epsilon_{a/s}$, decreases from 2.4 at $200 \text{ kg/m}^2\text{-s}$ to 1.8 at $400 \text{ kg/m}^2\text{-s}$. This compares to an area increase due to fins of 1.8.
2. Only minimal heat transfer enhancement is observed with oil, and only at a concentration of 1.25%. At higher concentrations, heat transfer is degraded. This contrasts with the smooth tube and micro-fin tube, which exhibit enhancement factors of 1.3 and 1.1, respectively.

3. The heat transfer enhancement due to oil is not a strong function of mass flux in the low-fin tube. This is similar to the micro-fin tube, but contrasts somewhat with the smooth tube, whose performance shows a greater dependence on mass flux.
4. The heat transfer performance of the low-fin tube relative to the smooth tube diminishes as oil is introduced. The value of $\epsilon_{a'/s'}$ falls to about 1.5 versus a pure refrigerant value ($\epsilon_{a/s}$) of slightly more than 2.0. This performance is slightly poorer than the micro-fin tube, but heat transfer nonetheless continues to be enhanced significantly even with oil present.
5. The pure refrigerant pressure drop enhancement factor, $\Psi_{a/s}$, is around 1.8, considerably higher than that for the micro-fin tube (1.4). Heat transfer enhancement is greater than the pressure drop increase.
6. Pressure drop increases with increasing oil concentration, but shows little mass flux influence. With 5% oil, $\Psi_{a'/a}$ is between 1.2 and 1.3. These results are similar to those in both the smooth and micro-fin tubes.

Condensation

1. The pure refrigerant heat transfer enhancement factor, $\epsilon_{a/s}$, is just under 2.0 at 200 kg/m²·s and falls to 1.6 at 400 kg/m²·s. This is about 10% lower than the micro-fin tube.
2. Condensation heat transfer in the low-fin tube tends to decrease with oil. The magnitude of the degradation, however, is only about one-half as large as in the smooth tube and micro-fin tube. The value of $\epsilon_{a'/a}$ is about 0.95 for a 5% oil concentration in the low-fin tube, compared to a value of just under 0.9 in the smooth tube and micro-fin tube.
3. Mass flux does not have a large influence on the effect of oil.
4. The condensation heat transfer performance of the low-fin tube relative to the smooth tube increases slightly when oil is added to refrigerant, even though absolute performance declines. The value of $\epsilon_{a'/s'}$ rises to a value of just over 2.1 with 5% oil, compared to a pure refrigerant value ($\epsilon_{a/s}$) of slightly under 2.0.

5. Pure refrigerant pressure drop is significantly higher in the low-fin than in either of the other tubes. The value of $\Psi_{a/s}$ is almost 2.2, compared to 1.7 in the micro-fin tube. The pressure drop increase is greater than the heat transfer enhancement at most conditions.
6. Pressure drop increases with increasing oil concentration, with $\Psi_{a/a}$ reaching a value of about 1.1 with 5% oil. There is little influence of mass flux on the value of $\Psi_{a/a}$. Because of the decrease in pressure drop with the smooth tube when oil is added, the pressure drop performance of the low-fin tube relative to the smooth tube worsens with oil. The value of $\Psi_{a'/s'}$ reaches nearly 4.0 at a 5% oil concentration.

CHAPTER 9

COMPARISON AND PERFORMANCE EVALUATION OF THE THREE TUBES

The previous two chapters have made comparisons among the three tubes in this investigation using enhancement factors, but comparisons have been limited to heat transfer or pressure drop alone. This chapter first reviews performance criteria suggested in the past, including those for heat transfer or pressure drop alone, for overall tube performance, and for heat exchanger design. The final part of this chapter adopts one of the overall performance criteria and compares the performance of the three tubes tested.

Previous Performance Evaluation Criteria

Heat Transfer Performance with Single Tubes

The heat transfer enhancement factor, ϵ , which is a simple ratio of heat transfer coefficients, has been defined earlier in Chapter 5. This is probably the most common heat transfer performance parameter reported in the literature. In other publications, the enhancement factor has generally been used to evaluate only the effects of augmentation techniques ($\epsilon_{a/s}$), but in the current work, the definition is extended to include the effects of oil as well.

Luu [134] used a size reduction index, keeping mass flux, heat duty, diameter and temperature difference fixed, to evaluate heat transfer performance. This index is given by

$$R_h = \frac{A_a}{A_s} = \frac{\bar{h}_s}{\bar{h}_a} \quad (9.1)$$

It is indicative of potential heat exchanger size reductions and is simply the reciprocal of the heat transfer enhancement factor, ϵ .

Pressure Drop Performance with Single Tubes

An enhancement factor for pressure drop (Ψ), analogous to that for heat transfer, was defined in Chapter 5 and has been used in past publications. Like the heat transfer enhancement factor, the pressure drop enhancement factor has been defined in this research program to account for the effects of oil, as well as augmentation.

Some researchers, looking at local pressure drop effects, adopted the pressure gradient ratio (for example, [111]). The pressure gradient ratio uses pressure drop per unit length, rather than total pressure drop, which is more desirable when local heat transfer data are obtained. When calculating this ratio over the entire tube length, it is identical to the pressure drop enhancement factor used in the present study.

Overall Performance with Single Tubes

It is desirable to define tube performance with a single comparative parameter that takes into account both heat transfer and pressure drop. Several such parameters have been suggested in past studies, but all can be reduced to approximately the same formulation. For these parameters to indicate major improvement in heat exchanger performance, as opposed to single tube performance, the two-phase heat transfer coefficient should be the controlling, or at least a significant, thermal resistance.

Luu [134] defined a pressure drop index, $R_{\Delta P}$, which has a form that looks similar to the pressure drop enhancement factor:

$$R_{\Delta P} = \frac{\Delta P_a'}{\Delta P_s} \quad (9.2)$$

The numerator, however, is not simply the measured pressure drop in the augmented tube. Rather, this term is obtained by subtracting the momentum component of the measured pressure drop, multiplying the frictional component by the size reduction index ($R_h = 1/\epsilon$, a measure of heat transfer performance), and then adding back the momentum contribution. The expression for $R_{\Delta P}$ becomes

$$\begin{aligned} R_{\Delta P} &= \frac{R_h \cdot (\Delta P - \Delta P_m)_a + \Delta P_{a,m}}{\Delta P_s} = \frac{R_h \cdot \Delta P_a}{\Delta P_s} + \frac{(1 - R_h) \cdot \Delta P_{a,m}}{\Delta P_s} \\ &= \frac{\Psi}{\epsilon} + \frac{[1 - (1/\epsilon)] \cdot \Delta P_{a,m}}{\Delta P_s} \approx \frac{\Psi}{\epsilon} \end{aligned} \quad (9.3)$$

where

$$(\Delta P - \Delta P_m)_a = \Delta P_{a,f} \quad (9.4)$$

Because the momentum component of pressure drop, ΔP_{am} , is much smaller than the frictional component, the pressure drop index is approximately the ratio of the pressure drop enhancement factor to the heat transfer enhancement factor.

Azer et al. [125] defined two parameters combining heat transfer and pressure drop effects. The first of these is the pumping power per unit heat transfer rate, P/Q , evaluated with fixed geometry and fixed inlet temperature and pressure. The pumping power, P , and the heat transfer rate, Q , are

$$P = \frac{\dot{m}}{\rho} \cdot \Delta P \quad (9.5)$$

$$Q = h \cdot A \cdot \Delta T \quad (9.6)$$

Although Azer et al. reported this quantity separately for smooth and augmented tubes, a ratio can be formed comparing the parameter P/Q in augmented tubes to that in smooth tubes:

$$\frac{(P/Q)_a}{(P/Q)_s} = \frac{\left[\frac{\dot{m} \cdot \Delta P}{\rho \cdot h \cdot A \cdot \Delta T} \right]_a}{\left[\frac{\dot{m} \cdot \Delta P}{\rho \cdot h \cdot A \cdot \Delta T} \right]_s} \quad (9.7)$$

With the assumptions of constant length and nominal diameter, constant flow rate, constant pressure, and constant temperature difference, this reduces to the following expression:

$$\frac{(P/Q)_a}{(P/Q)_s} = \frac{(\Delta P/h)_a}{(\Delta P/h)_s} = \frac{(\Delta P_a/\Delta P_s)}{(h_a/h_s)} = \frac{\psi}{\epsilon} \quad (9.8)$$

Note that in an actual heat exchanger, all of these quantities would not remain fixed because the higher heat transfer coefficient in the augmented tube would lead to different exit conditions (higher quality or superheat) and/or to a portion of the heat exchanger with very little heat transfer (h and ΔT much smaller). In real situations, some other parameter(s) (such as length, temperature difference, etc.) would be changed to obtain fixed exit conditions. For a comparison of performance, however, it is useful to use a hypothetical case with fixed tube length and to assume that h remains constant for the entire length.

The second factor defined by Azer et al. was the ratio of heat flux per unit pressure drop with augmentation to that without augmentation. With the same assumptions as above,

$$\frac{\left[\frac{Q/A}{\Delta P}\right]_a}{\left[\frac{Q/A}{\Delta P}\right]_s} = \frac{\left[\frac{h \cdot \Delta T}{\Delta P}\right]_a}{\left[\frac{h \cdot \Delta T}{\Delta P}\right]_s} = \frac{(h_a/h_s)}{(\Delta P_a/\Delta P_s)} = \frac{\epsilon}{\psi} \quad (9.9)$$

Reid et al. [111] compared different tubes using an enhancement performance ratio, defined as the ratio of heat transfer enhancement to pressure drop enhancement

$$\text{enhancement performance ratio} = \frac{\epsilon}{\psi} \quad (9.10)$$

Thus, with some appropriate assumptions, all of these parameters combining heat transfer and pressure drop performance can be put in terms of a ratio of the two enhancement factors defined in Chapter 5, although an approximation must be introduced to reduce Luu's ratio to these terms.

For the parameters having Ψ in the numerator, values less than one indicate improvements when compared to smooth tube performance. For the other parameters, values greater than one indicate improved relative performance. Although these overall performance ratios are useful for comparison purposes, design priorities may cause tubes with an overall performance less than a smooth tube to be desirable nonetheless. An example would be a design in which heat exchanger size reduction is more important than pumping power requirements. In such a case, the heat transfer enhancement factor, ϵ , would become the most important performance parameter.

Heat Exchanger Design

Several publications during the past fifteen years have discussed presentation of performance data and rational procedures to evaluate enhanced tube performance (for example, [167–172]). Most of the discussions have concerned single-phase heat transfer, but Jensen [171] and Webb [172] concentrated on evaporation and condensation. Jensen discussed the data requirements to evaluate enhanced evaporation and condensation in tubes. Webb emphasized performance evaluation criteria as part of the heat exchanger design

process. The application of these evaluation criteria to a heat exchanger requires decisions regarding design constraints, such as fixed versus variable area, fixed versus variable temperature difference, etc.

In refrigeration systems, size is often important and the possibility of smaller heat exchangers is a distinct advantage. In space-constrained applications (such as appliances and transportation refrigeration), the advantage is evident, but size reduction is a benefit in most applications. Other benefits include: (1) lower fan power requirements in air-to-refrigerant heat exchangers leads to lower noise levels), (2) smaller heat exchangers translate into lower costs for many of the parts (however, augmented tubes themselves are more costly), and (3) a smaller compressor is required if heat transfer increases by more than pressure drop. In each case listed, cost is an important factor and a trade-off between capital cost and operating cost is usually required to determine the optimal system design.

Performance Evaluation of the Tubes Tested

The use of evaluation criteria based on heat exchanger design requires assumptions about the geometric configuration and the parameter(s) to optimize. Because this study used single, straight tubes and did not attempt to incorporate any of the enhanced tubes into a practical heat exchanger, a simpler parameter using a combination of ϵ and Ψ is used to evaluate tube performance.

The enhancement performance ratio defined in Equation 9.10 has been chosen for performance comparisons in this study (the approach of Reid and Azer). This ratio, ϵ/Ψ , is indicated by the symbol θ . The heat transfer term in the numerator is inversely proportional to heat exchanger size (capital cost) while the pressure drop term in the denominator is directly proportional to increased pumping power (operating cost). (Note that other costs are involved, which are not included in this ratio, such as tube costs.) The enhancement performance ratio, therefore, is inversely proportional to a portion of the costs, indicating that values of θ greater than unity are advantageous. As discussed earlier, the overall advantage of an augmented tube in a heat exchanger is dependent on other factors as well, such as the relative importance of the internal and external thermal resistances, so the magnitude of θ may not reflect the performance gain obtained in a heat exchanger.

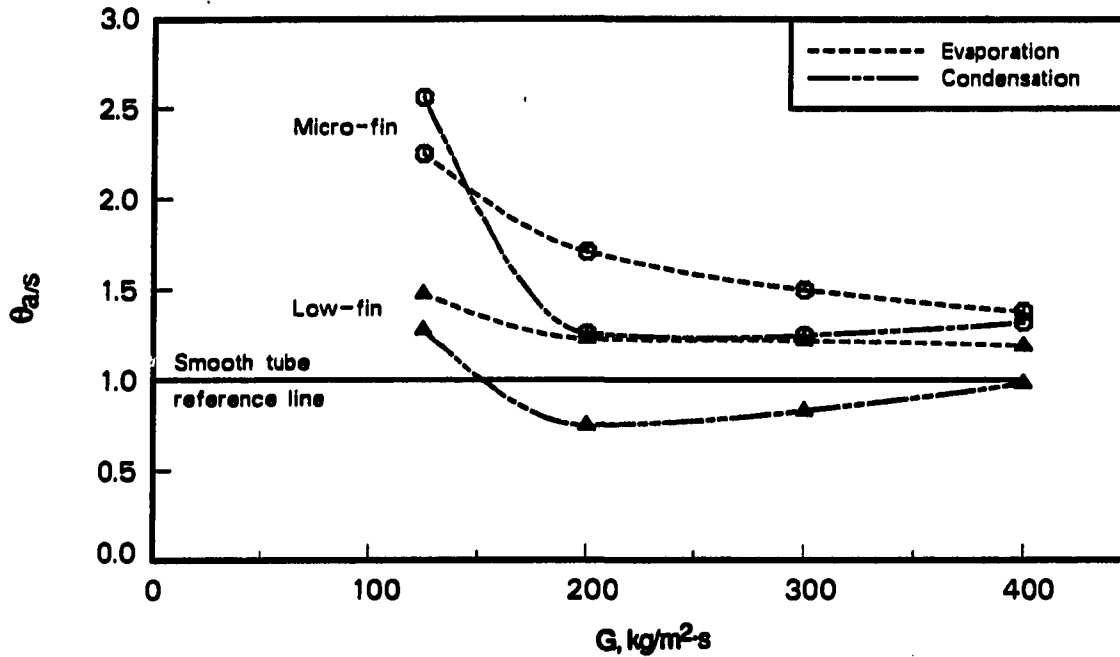


Figure 9.1. Enhancement performance ratio ($\theta_{a/s}$) for evaporation and condensation of pure R-22 in micro-fin and low-fin tubes

Overall performance comparisons will be similar in scope to those discussed earlier for heat transfer or pressure drop alone: comparisons of the enhanced tubes to the smooth tube with pure refrigerant, comparisons of each tube with refrigerant-oil mixtures to its performance with pure refrigerant, and comparisons of the enhanced tubes with refrigerant-oil mixtures to the smooth tube with similar refrigerant-oil mixtures. Subscript nomenclature is identical to that used with ϵ and Ψ in previous chapters.

Pure Refrigerant

Enhancement performance ratios with pure refrigerant are shown in Figure 9.1. Points above the smooth tube reference line ($\theta = 1$) indicate improved overall performance relative to the smooth tube. The micro-fin tube exhibits improved performance relative to the smooth tube for both evaporation and condensation, but $\theta_{a/s}$ for the low-fin tube drops below 1.0 during condensation. As discussed earlier, there are large relative uncertainties in the pressure drop, particularly at low mass fluxes. The abrupt changes in slope and

magnitude of the $\theta_{a/s}$ curves below $200 \text{ kg/m}^2\cdot\text{s}$, especially during condensation, can be attributed to this.

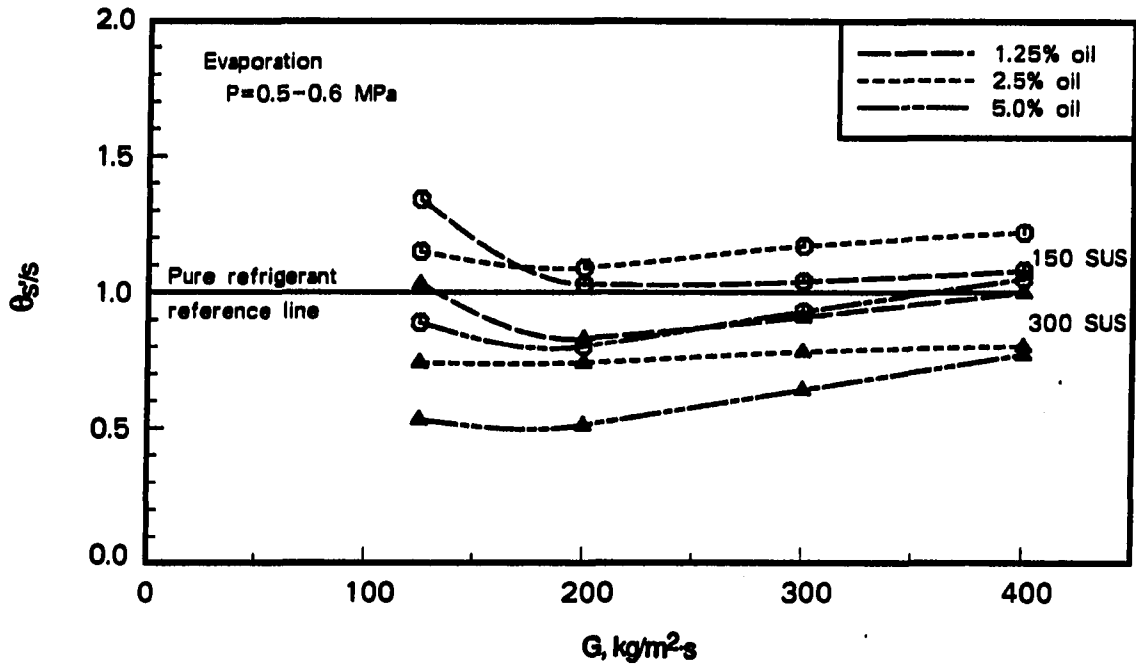
Comparing Figure 9.1 (θ versus G) with Figure 8.5 (ϵ versus G), it is observed that all curves shift downward, that is $\theta < \epsilon$. This behavior is consistent with a general pressure drop increase in augmented tubes relative to smooth tubes. With evaporation, the micro-fin and low-fin tubes show quite similar heat transfer performance, but the overall performance of the micro-fin tube is superior due to its lower pressure drop. With condensation, the micro-fin tube shows superior heat transfer performance, as well as overall performance. The relative advantage of the micro-fin tube over the low-fin tube increases when using θ , rather than ϵ , as the basis of comparison.

Refrigerant-Oil Mixtures

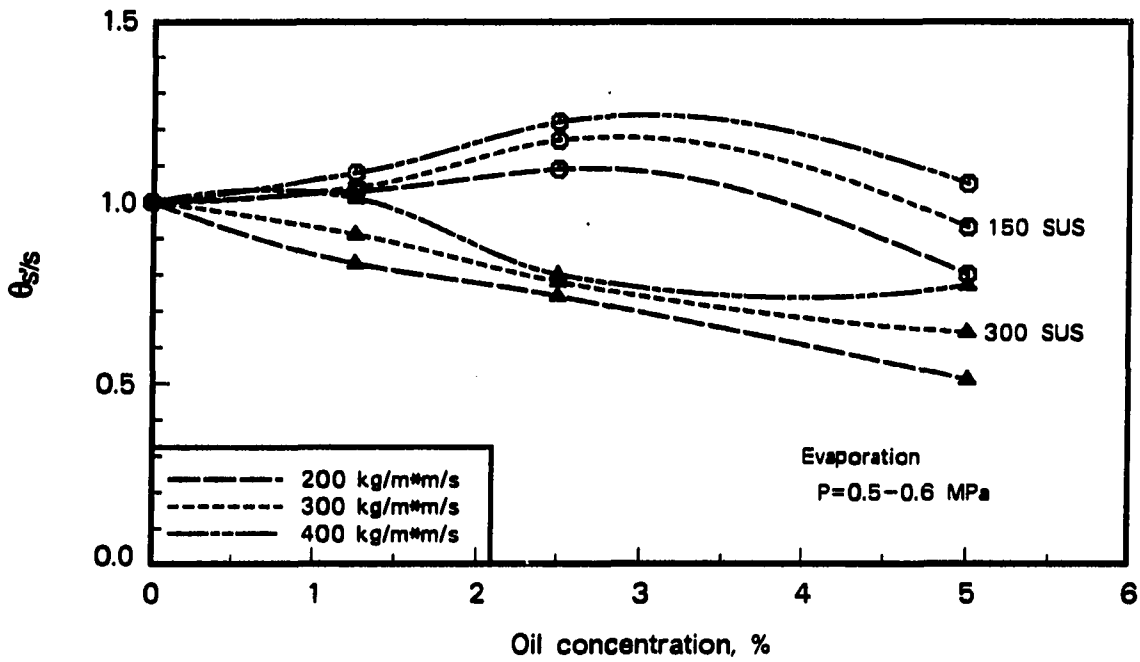
The next three sections describe the performance of each tube with refrigerant-oil mixtures compared to the same tube with pure refrigerant. This indicates the effect of oil alone on the performance of a given tube. The final section compares the enhanced tubes with refrigerant-oil mixtures to the smooth tube with similar mixtures, indicating the in-tube performance change obtained when replacing a smooth tube with an enhanced tube in a system containing oil.

Each figure that follows has two parts: θ is plotted versus mass flux in part (a) and versus oil concentration in part (b). Because of high uncertainties, particularly in the pressure drop component of θ , at mass fluxes under $200 \text{ kg/m}^2\cdot\text{s}$ (see Table D.7), curves for $125 \text{ kg/m}^2\cdot\text{s}$ are not included in part (b) of any figure and comments in the text generally disregard this mass flux when discussing performance trends.

Smooth tube compared to itself Evaporation results are shown as $\theta_{s'/s}$ versus mass flux in Figure 9.2(a). The $\theta_{s'/s}$ curves are relatively flat, with a slight increasing tendency as mass flux increases. Only at lower oil concentrations with 150-SUS oil is the overall performance improved. This improvement is due to the large heat transfer enhancement with 150-SUS oil in the smooth tube (see Figures 6.4 and 6.6). With 150-SUS oil, $\theta_{s'/s}$ ranges from about 0.8 to 1.2, depending on concentration and mass flux; with 300-SUS oil, $\theta_{s'/s}$ remains below 1.0, lying between 0.5 and 1.0.



(a)



(b)

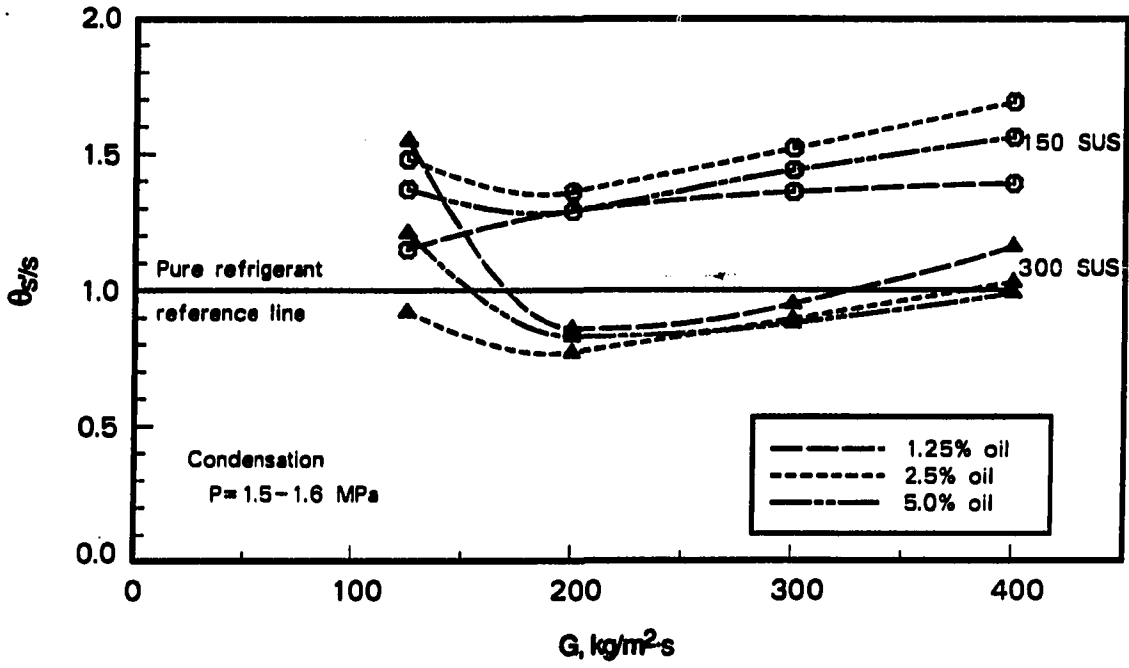
Figure 9.2. Evaporation enhancement performance ratio showing the effects of oil alone (θ_s'/s) in a smooth tube

Part (b) of Figure 9.2 replots the same data versus oil concentration, leaving out the curve for $200 \text{ kg/m}^2\cdot\text{s}$. Except for an initial increase in $\theta_{a'/a}$ at low concentrations of 150-SUS oil, there is a general trend of decreasing $\theta_{s'/s}$ with increasing oil concentration. Curves for different mass fluxes are grouped together for a given oil type, indicating a weak dependence on mass flux, but the higher mass fluxes generally have slightly higher values of $\theta_{s'/s}$.

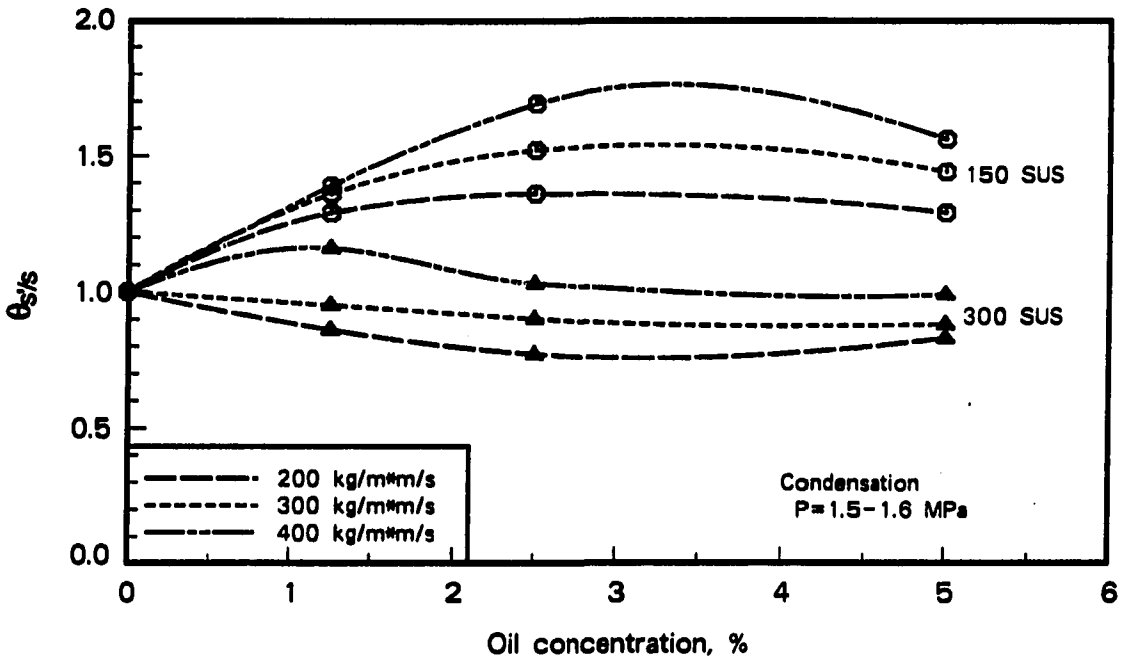
Figure 9.3 includes condensation results for both oils. In part (a), $\theta_{s'/s}$ is shown versus mass flux. As with evaporation, there is a slight upward trend with increasing mass flux (disregarding mass fluxes below $200 \text{ kg/m}^2\cdot\text{s}$), and 150-SUS oil results are generally above those with 300-SUS oil. Values of $\theta_{s'/s}$ vary from 1.3 to 1.7 for 150-SUS oil and from 0.7 to 1.1 for the more viscous oil. The enhancement performance ratio for condensation is considerably higher than that for evaporation, in spite of heat transfer enhancement during evaporation and heat transfer degradation during condensation. This behavior is due to the significant decrease in condensation pressure drop observed with the addition of oil. As discussed earlier, these results may have been caused by the particular geometry and flow conditions of this test program.

Figure 9.3(b) shows the same data as in part (a), but plotted so that trends with variations in oil concentration can be observed. The shapes of the curves are similar to the evaporation curves shown in Figure 9.2(b), but the values of $\theta_{s'/s}$ are somewhat higher. As during evaporation, performance with 150-SUS oil is higher than that with 300-SUS oil, and overall performance appears to improve slightly with increasing mass flux.

Micro-fin tube compared to itself Enhancement performance ratios ($\theta_{a'/a}$) for the micro-fin tube during evaporation of refrigerant-oil mixtures are depicted in Figure 9.4. Oil generally causes a decrease, or at best a very minimal increase, in the overall performance, as seen by the position of the curves below the pure refrigerant reference line in Figure 9.4(a). The curve shape is similar to that of the smooth tube, namely a slight increase in performance with increasing mass flux above $200 \text{ kg/m}^2\cdot\text{s}$. Results for the micro-fin tube are somewhat lower than for the smooth tube, with $\theta_{a'/a}$ ranging from about 0.7 to 1.05 with 150-SUS oil and from 0.5 to 0.8 with 300-SUS oil. These values indicate that performance is generally better at a given oil concentration with the lower viscosity, 150-SUS oil.



(a)



(b)

Figure 9.3. Condensation enhancement performance ratio showing the effects of oil alone (θ_s/s) in a smooth tube

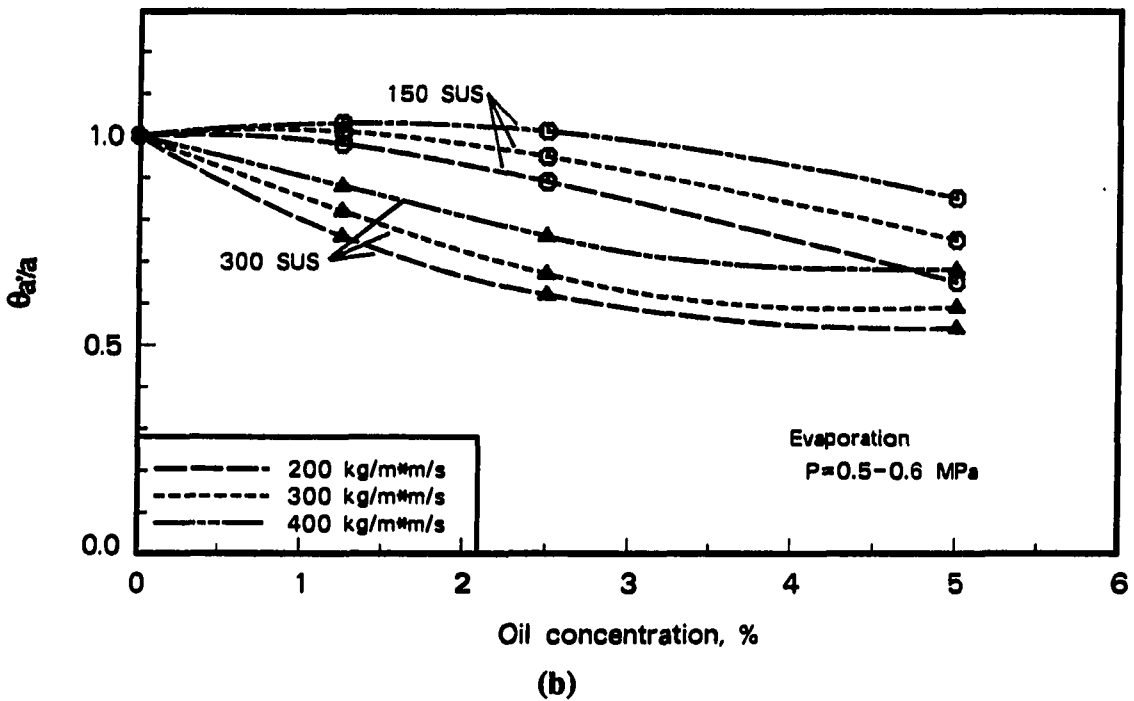
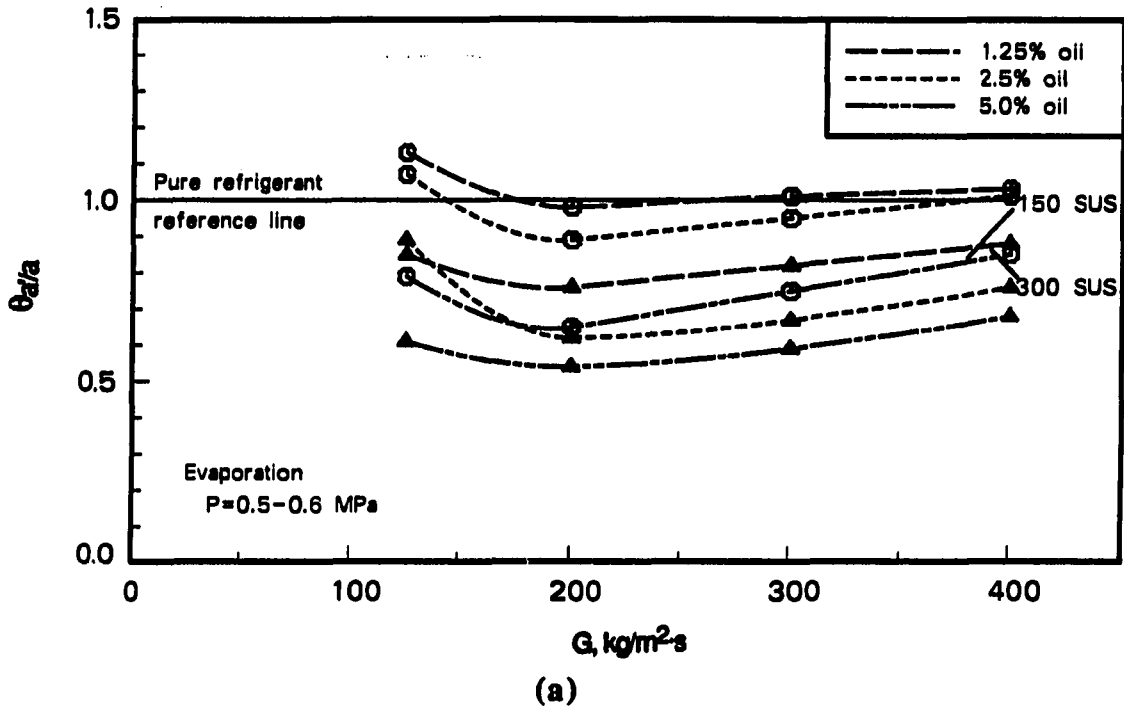


Figure 9.4. Evaporation enhancement performance ratio showing the effects of oil alone (θ_a/a) in a micro-fin tube

Figure 9.4(b) shows the trends with changing oil concentrations. There is essentially no peak seen with refrigerant-oil mixtures in the micro-fin tube, but a steady, orderly decrease in $\theta_{a/a}$ with increasing oil concentration. At 5.0% oil concentration, $\theta_{a/a}$ falls to between 0.55 and 0.7 with 300-SUS oil and to between 0.7 and 0.85 with 150-SUS oil. Overall performance, therefore, decreased by 15% to 45% when compared to pure refrigerant.

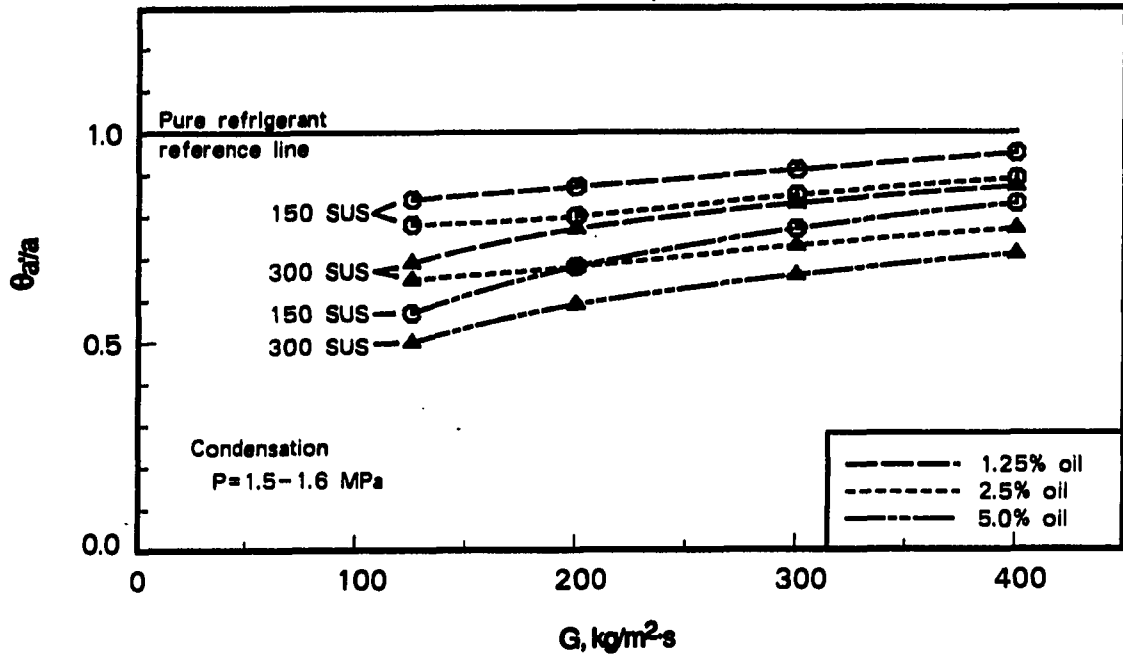
Condensation enhancement performance ratios are presented in Figure 9.5. In part (a), all curves fall below the pure refrigerant reference, with no enhancement observed. As in all previous cases, there is a slight trend of increasing θ with increasing mass flux. Curves for both oils are interspersed in this figure, but in all cases, the curve for 150-SUS oil is above that for the corresponding concentration of 300-SUS oil. For mass fluxes above $200 \text{ kg/m}^2\cdot\text{s}$, $\theta_{a/a}$ ranges from 0.6 to 0.95, indicating a slightly better relative performance with oil for condensation than for evaporation.

Figure 9.5(b), with oil concentration as the abscissa, shows more clearly the better performance of 150-SUS oil relative to 300-SUS oil. As with evaporation, there is a steady, but not abrupt, decrease in $\theta_{a/a}$ as the oil concentration increases.

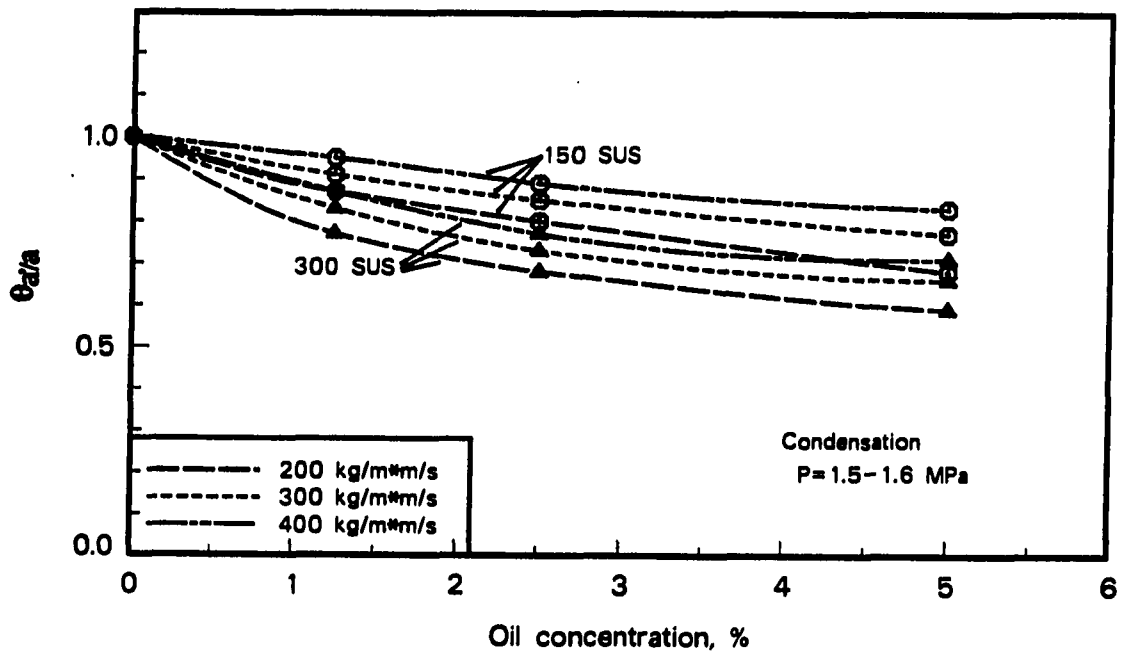
Low-fin tube compared to itself The low-fin tube was tested with 150-SUS oil only. Enhancement performance ratios during evaporation are shown in Figure 9.6. The plot in part (a) is similar to micro-fin tube results shown in Figure 9.4(a) with only minimal enhancement at the lowest oil concentration. Curves for the low-fin tube are somewhat flatter and have a downward, rather than upward, slope. Values of $\theta_{a/a}$ are somewhat lower with the low-fin tube than at corresponding conditions with the micro-fin tube and range from 0.65 to slightly greater than one.

Figure 9.6(b) plots $\theta_{a/a}$ versus oil concentration. The general trend with increasing oil concentration is downward, but with slight enhancement at the lowest oil concentration. The flatness of the curves in part (a) is reflected in the grouping of curves in part (b).

Condensation enhancement performance ratios are presented as a function of mass flux in Figure 9.7(a). Performance is degraded at all oil concentrations and mass fluxes, but the degradation is less severe than during evaporation: a minimum $\theta_{a/a}$ of 0.8 during condensation versus 0.65 during evaporation. There is a very slight decreasing trend in

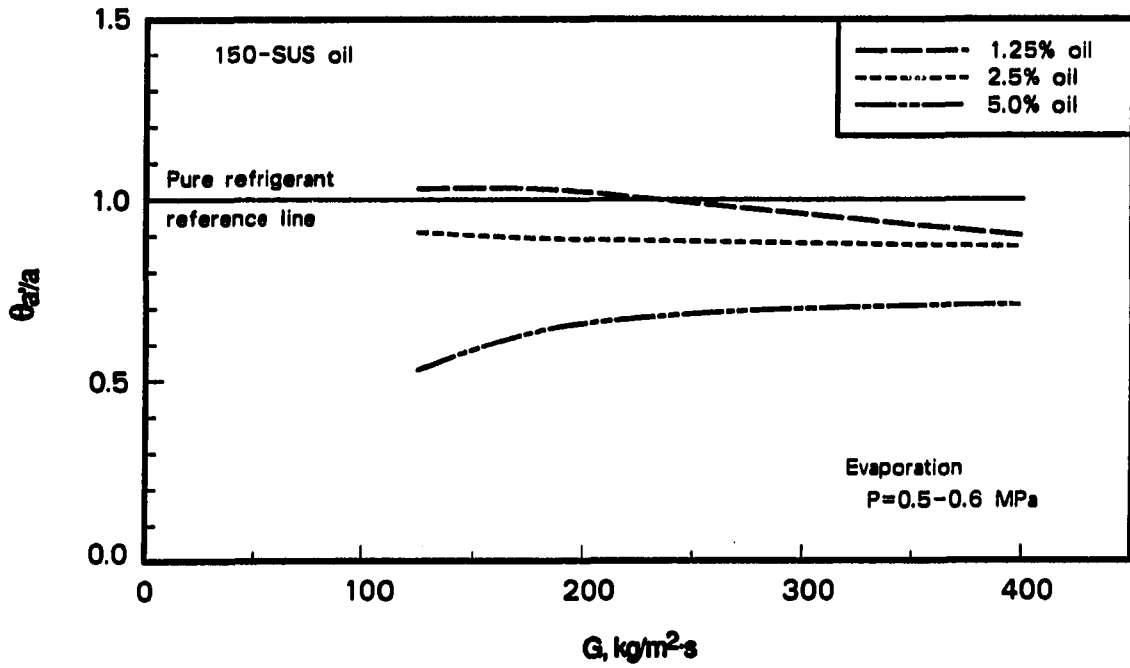


(a)

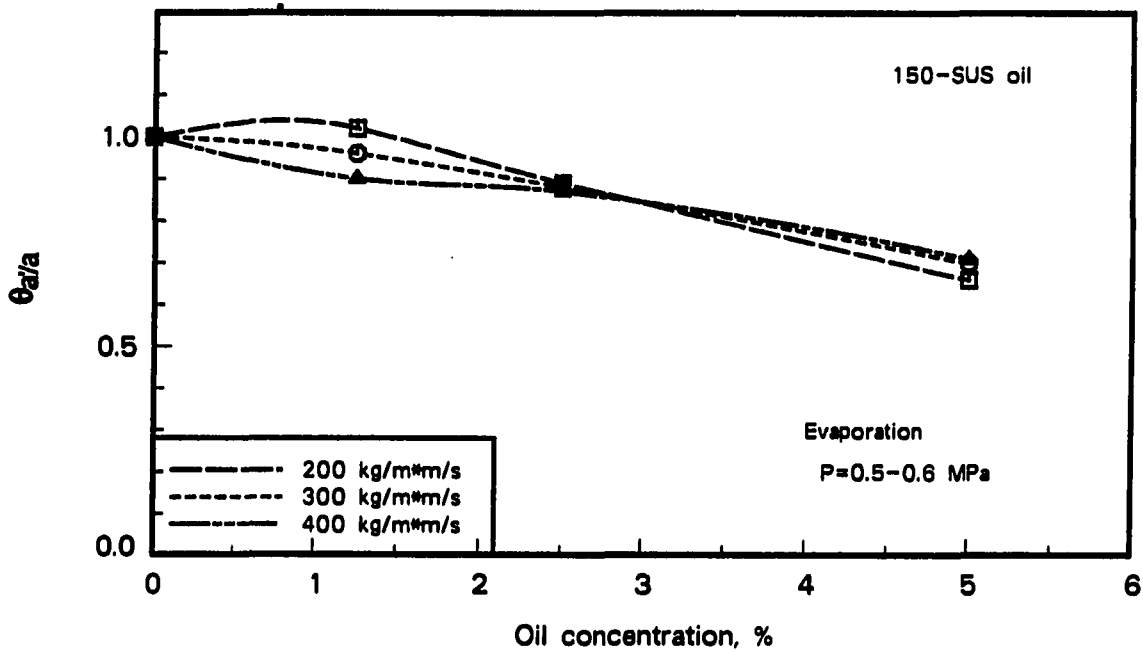


(b)

Figure 9.5. Condensation enhancement performance ratio showing the effects of oil alone (θ_a/a) in a micro-fin tube

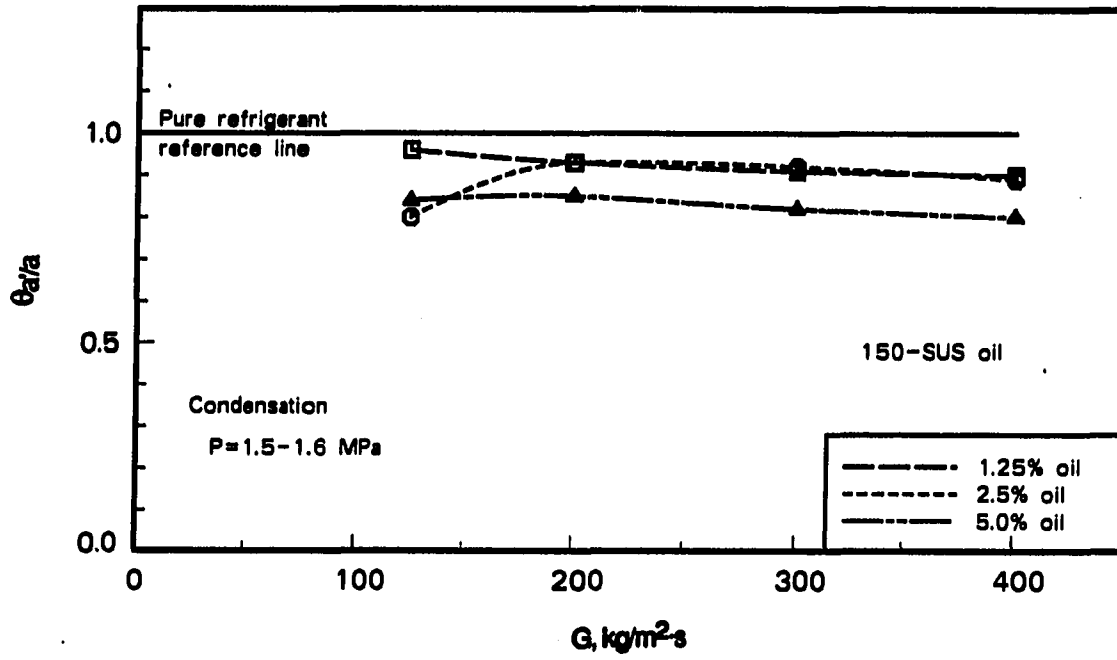


(a)

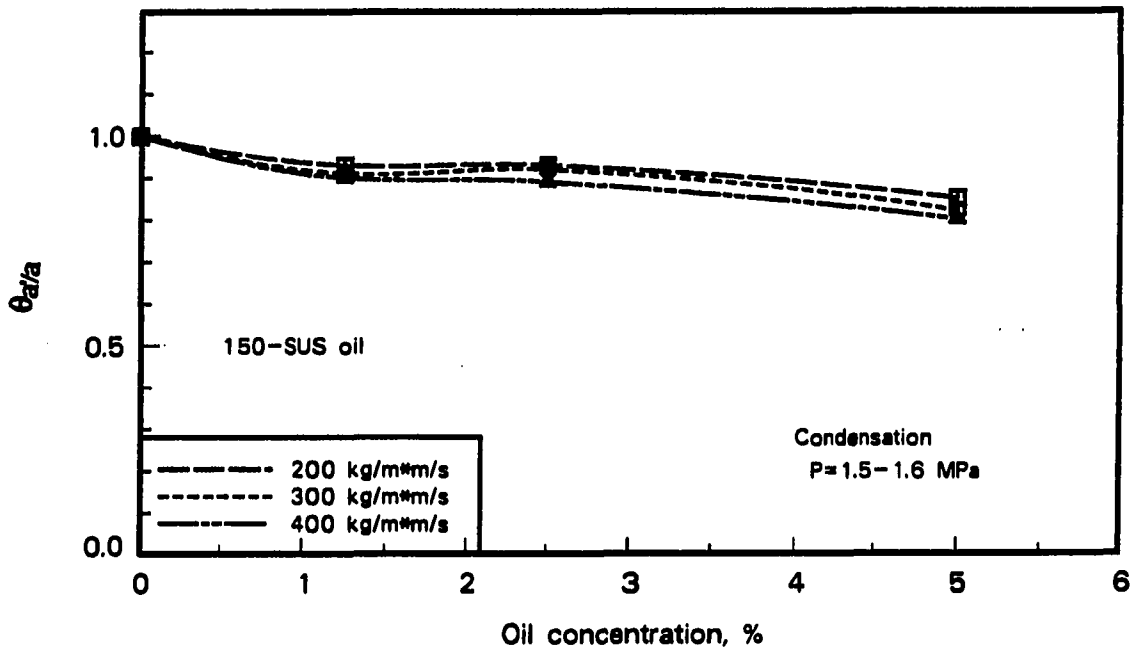


(b)

Figure 9.6. Evaporation enhancement performance ratio showing the effects of oil alone (θ_a/a) in a low-fin tube



(a)



(b)

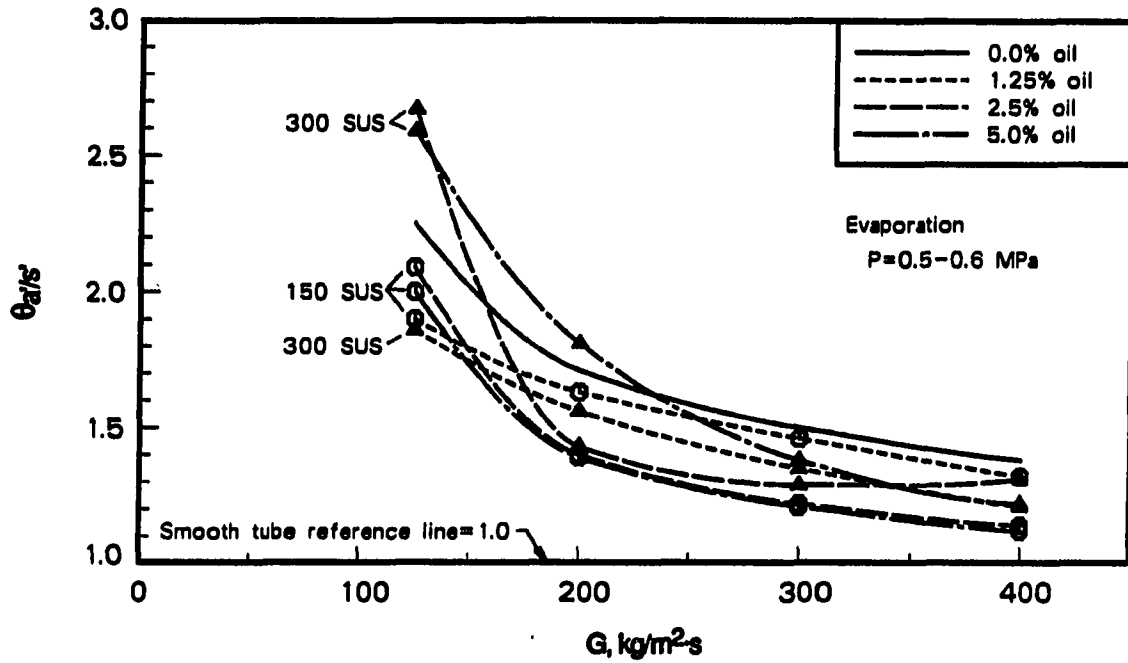
Figure 9.7. Condensation enhancement performance ratio showing the effects of oil alone (θ_a/a) in a low-fin tube

$\theta_{a/a}$ with increasing mass flux, but all curves are relatively flat, with $\theta_{a/a}$ between 0.8 and 0.95 for all test conditions. Figure 9.7(b) shows all curves tightly grouped and a steady, gentle downward trend in $\theta_{a/a}$ with increasing oil concentration.

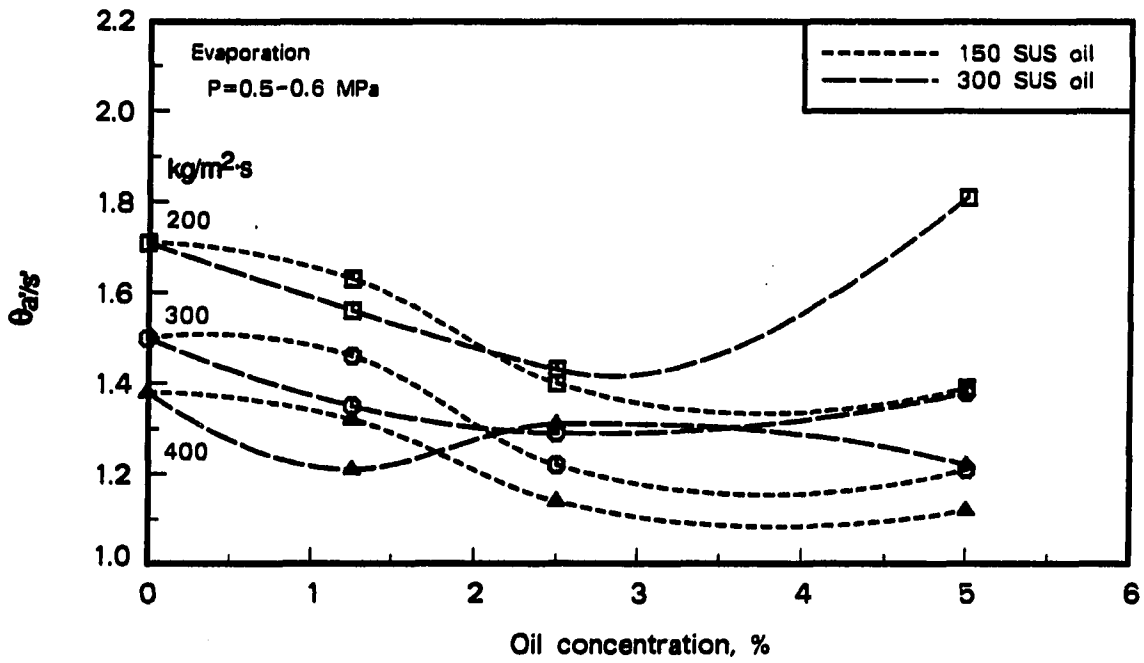
Augmented tubes compared to the smooth tube Enhancement performance ratios for the augmented tubes relative to the smooth tube are presented in this section. Figures 9.8 and 9.9 present $\theta_{a/s'}$ for the micro-fin tube during evaporation and condensation with two different oil types. Figures 9.10 and 9.11 show low-fin tube results and repeat the micro-fin results with 150-SUS oil for comparison.

Figure 9.8(a) plots $\theta_{a/s'}$ versus mass flux with mixtures of both oils in the micro-fin tube. The pure refrigerant enhancement performance ratio ($\theta_{a/s}$) is also included. At mass fluxes above $200 \text{ kg/m}^2\text{-s}$, values of $\theta_{a/s'}$ with oil are generally less than $\theta_{a/s}$, indicating that overall performance is degraded with the addition of oil. The trend in $\theta_{a/s'}$ is downward with increasing mass flux. Also significant, however, is the maintenance of $\theta_{a/s'}$ above 1.0, indicating that the micro-fin tube has a performance advantage relative to the smooth tube at all conditions. Values of $\theta_{a/s'}$ range from 1.15 to 1.30 at high mass flux and from 1.4 to 1.8 at $200 \text{ kg/m}^2\text{-s}$. Trends with oil type or concentration are difficult to see with many of the curves intersecting, probably due to uncertainties and curve fitting. Figure 9.8(b) shows $\theta_{a/s'}$ versus oil concentration. Curves showing results with 150-SUS oil are rather orderly, and approximately parallel, but results with 300-SUS oil appear more random, making trends difficult to discern. If the curve for 300-SUS oil at $200 \text{ kg/m}^2\text{-s}$ is neglected, the remaining curves show a general, though not universal, trend of decreasing $\theta_{a/s'}$ with increasing oil concentration.

Condensation results are shown in Figure 9.9. Part (a) plots $\theta_{a/s'}$ versus mass flux for both oils and includes $\theta_{a/s}$ for pure refrigerant. As during evaporation, performance with oil is less than that with pure R-22. However, unlike evaporation, performance does not remain higher than that of the smooth tube at all conditions and is as much as 30% lower. Curves of $\theta_{a/s'}$ are flatter during condensation, showing less influence of mass flux. The value of $\theta_{a/s'}$ is generally higher with 300-SUS oil than with 150-SUS oil. This trend can be traced to the decrease in condensation pressure drop with the addition of 150-SUS oil, while with 300-SUS oil there is no significant change in pressure drop. Figure 9.9(b)

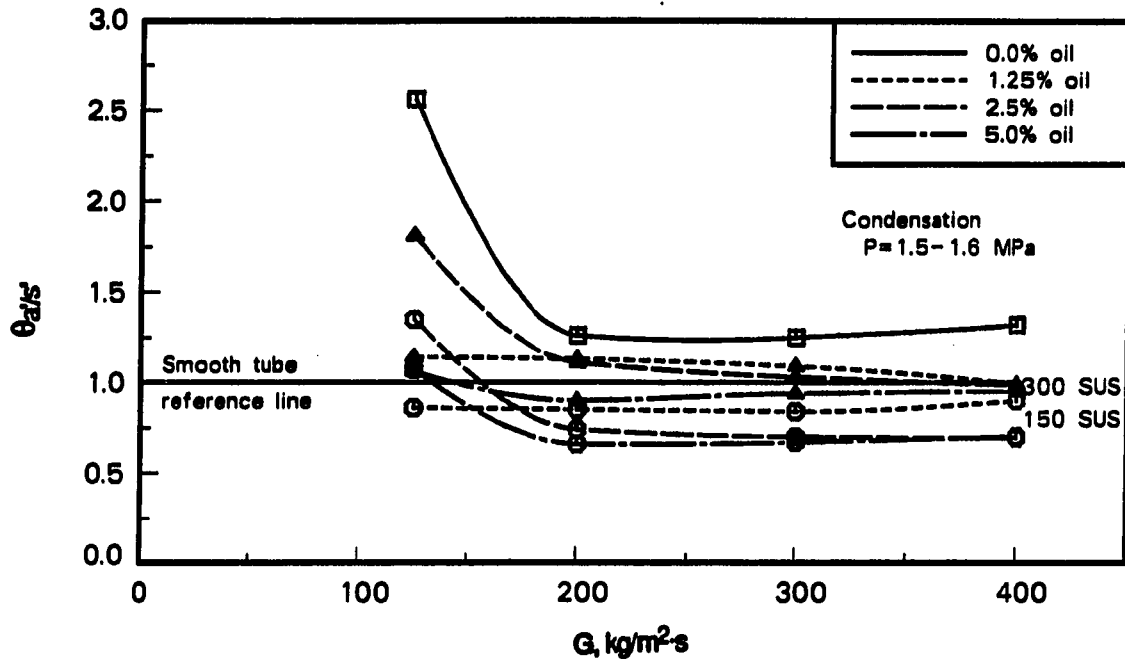


(a)

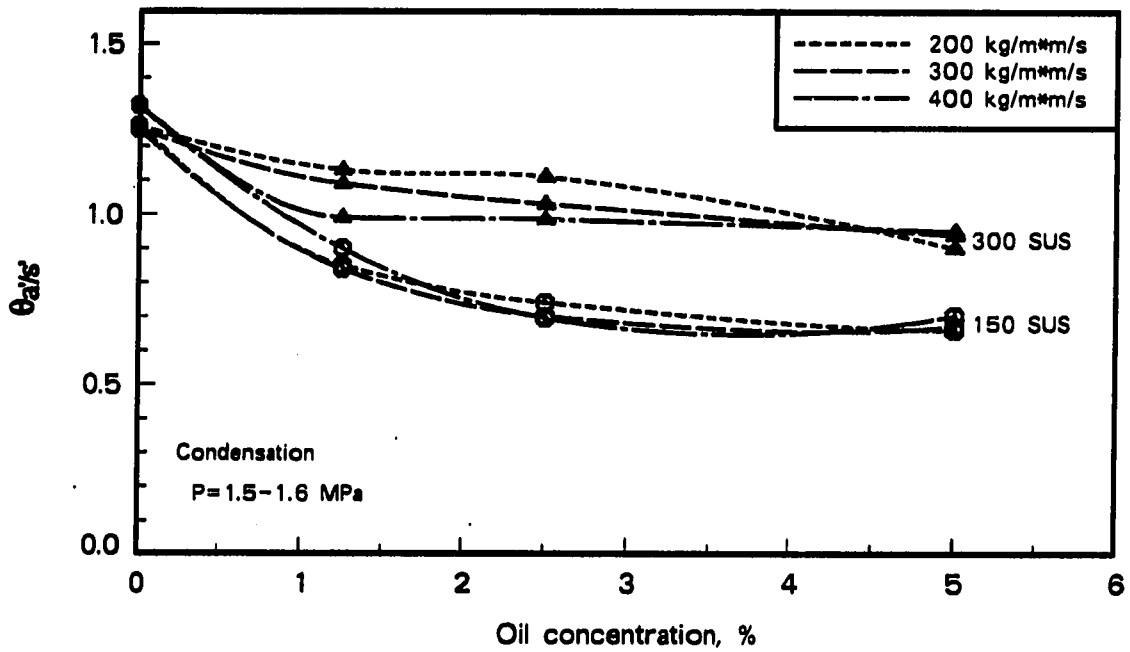


(b)

Figure 9.8. Evaporation enhancement performance ratio showing the combined effects of oil and augmentation ($\theta_{a/s}$) in a micro-fin tube



(a)



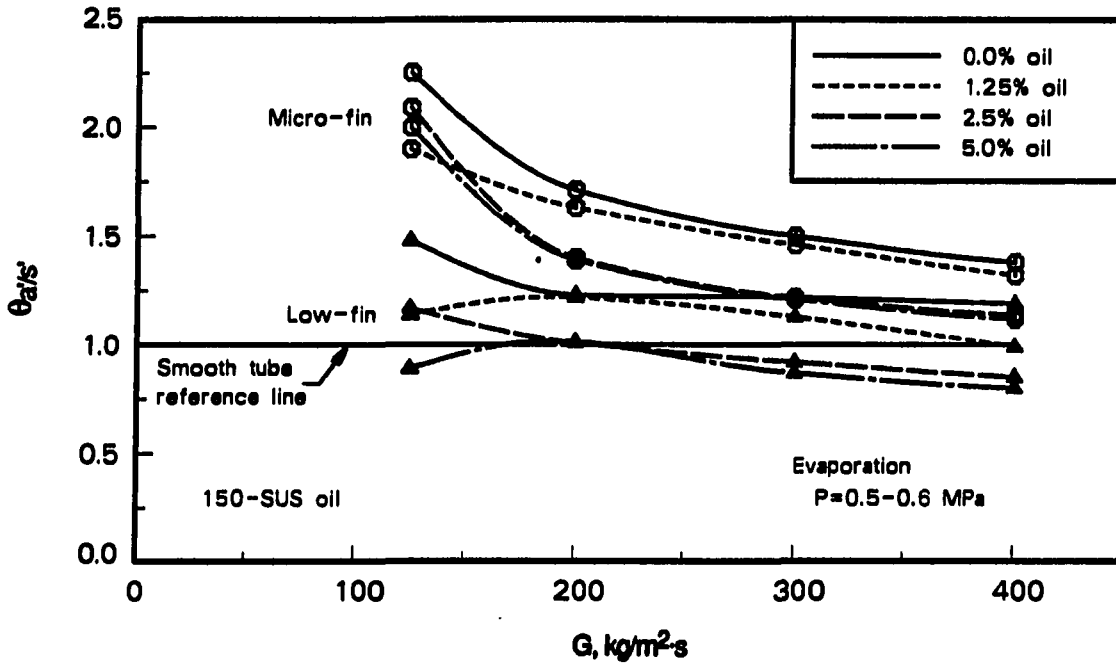
(b)

Figure 9.9. Condensation enhancement performance ratio showing the combined effects of oil and augmentation ($\theta_{a/s}$) in a micro-fin tube

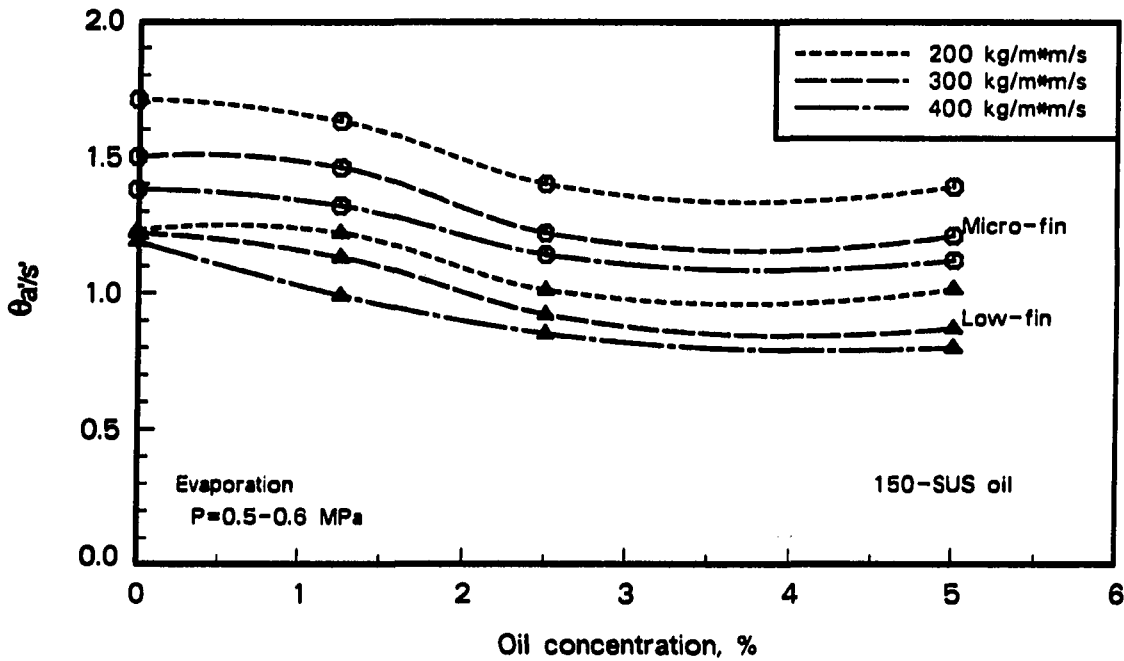
replots data from Figure 9.9(a) as a function of oil concentration. For both oils, there is a downward performance trend with increasing oil concentration. The performance ratio with 300-SUS oil remains near 1.0 or higher for most conditions, whereas performance with 150-SUS oil again shows a greater degradation with increasing oil concentration.

A comparison of enhancement performance ratios during evaporation in low-fin and micro-fin tubes is shown in Figure 9.10. All data shown are for mixtures of 150-SUS oil only. As previously, part (a) plots results versus mass flux; also included are curves using pure refrigerant ($\theta_{a/s}$) for both tubes. Limiting observations to mass fluxes of 200 kg/m²·s or greater, $\theta_{a/s}$ tends to fall slightly with increasing mass flux. For both tubes, results with oil are poorer than those with pure refrigerant. Performance with enhanced tubes is better than that with a smooth tube, except for the low-fin tube at higher oil concentrations, for which $\theta_{a/s}$ drops below 1.0. The micro-fin tube maintains a 20% to 40% performance advantage over the low-fin tube for most conditions. A plot of these data versus oil concentration is presented in Figure 9.10(b). There is a tendency for $\theta_{a/s}$ to fall with increasing oil concentration, but all curves are relatively flat at oil concentrations of 2.5% to 5.0%. At these concentrations, $\theta_{a/s}$ for the micro-fin tube is between 1.1 and 1.4 and for the low-fin tube between 0.8 and 1.0.

Condensation results for micro-fin and low-fin tubes are given in Figure 9.11. Part (a) shows that curves for both tubes with oil, as well as for the low-fin tube with pure refrigerant, lie below the smooth tube reference line. The minimum value of $\theta_{a/s}$ is around 0.5 for the low-fin tube with 5.0% oil concentration. As mentioned several times, the low values of $\theta_{a/s}$ for condensation are due to the unusual observation of decreasing pressure drop with the addition of oil in the smooth tube. In spite of these low values for $\theta_{a/s}$, comparisons can still be made between the two augmented tubes. As with evaporation, micro-fin tube overall performance is superior to that in the low-fin tube, generally by about 30%. It can also be seen that there is very little influence of mass flux above 200 kg/m²·s. Figure 9.11(b) shows a rather steep decline in $\theta_{a/s}$ with the initial addition of oil, but little effect of increasing oil concentration as the concentration became greater than 1% or 2%. The advantage of the micro-fin tube is perhaps more clearly seen in part (b) and the observation of weak mass flux influence is supported by the tightly grouped curves.

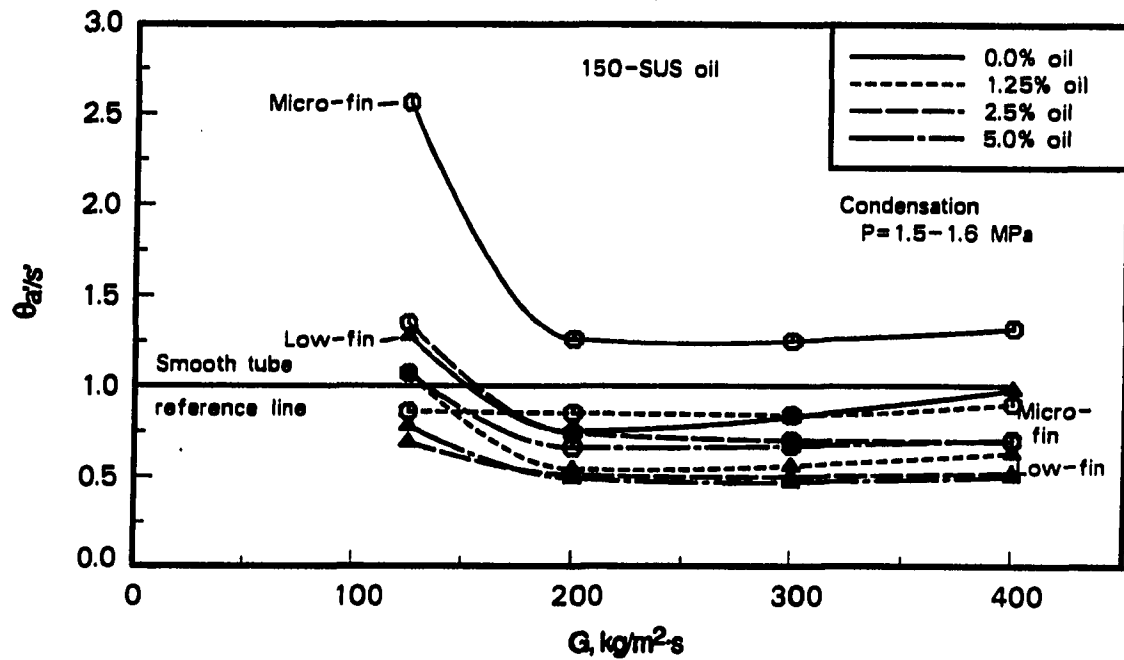


(a)

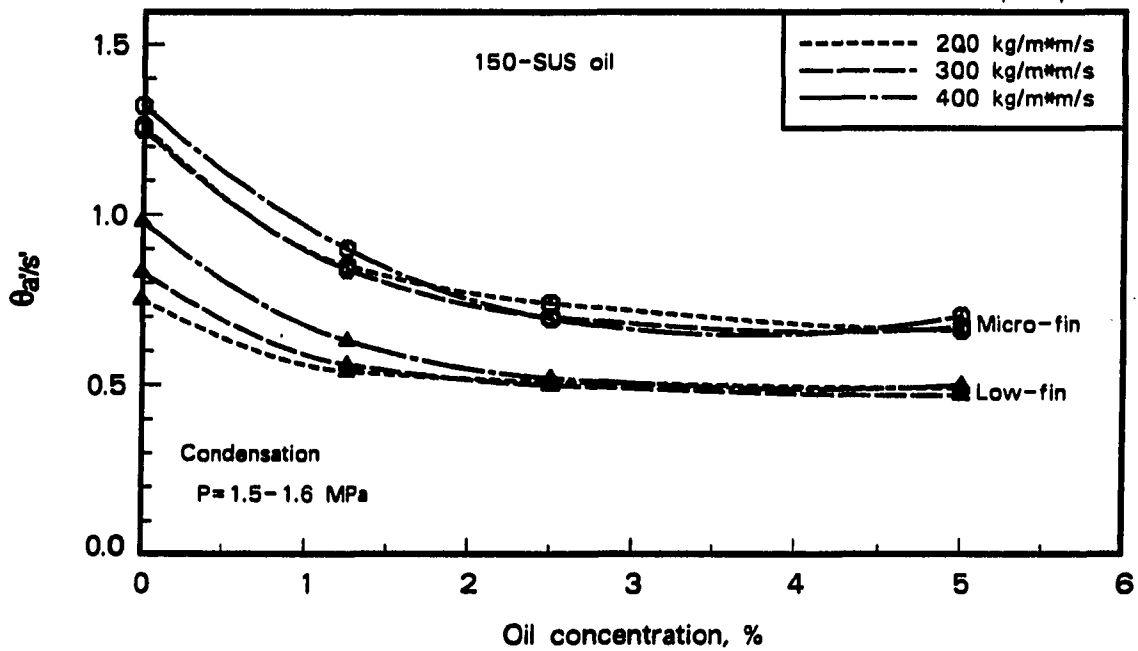


(b)

Figure 9.10. Evaporation enhancement performance ratio showing the combined effects of oil and augmentation ($\theta_{a/s}$) in a micro-fin tube and a low-fin tube



(a)



(b)

Figure 9.11. Condensation enhancement performance ratio showing the combined effects of oil and augmentation ($\theta_{a/s}$) in a micro-fin tube and a low-fin tube

Summary

This chapter has compared the overall performance of the three tubes tested, beginning with a brief review of performance factors used by earlier investigators. These factors, which combine heat transfer and pressure performance, can generally be reduced to a ratio of the heat transfer enhancement factor (ϵ) to the pressure drop enhancement factor (Ψ), or the reciprocal of this ratio.

For the current investigation, the ratio ϵ/Ψ is defined as the enhancement performance ratio and designated by the symbol θ . Table 9.1 is a summary of the effects of oil alone in each of the three tubes tested. Table 9.2 summarizes the overall performance of the augmented tubes with refrigerant-oil mixtures compared to the smooth tube with the same mixture. Values of θ greater than unity generally point to improved performance relative to a smooth tube; larger values of θ indicate better performance.

When the overall performance of a tube with refrigerant-oil mixture is compared to the performance of that same tube with pure refrigerant ($\theta_{s'/s}$ or $\theta_{a'/a}$), general trends are:

1. Performance tends to degrade when oil is added to the refrigerant. The exception to this is the smooth tube with 150-SUS oil, which exhibits an increase in $\theta_{s'/s}$.
2. With each increasing oil concentration, performance tends to decrease further.
3. Performance with 300-SUS oil is from 10% to 50% below that with 150-SUS oil.

From the enhancement performance ratios comparing augmented tube performance to smooth tube performance with a similar oil concentration ($\theta_{a/s}$ or $\theta_{a'/s'}$), the following observations hold:

4. The micro-fin tube shows better overall performance than the low-fin tube at all oil concentrations (comparison with 150-SUS oil only).
5. Performance of the micro-fin tube with 300-SUS oil tends to be higher than with 150-SUS oil. This is due to a decrease in smooth tube performance with 300-SUS oil, rather than to an improvement in micro-fin tube performance. However, the absolute performance of the micro-fin tube is worse with 300-SUS oil (see item 3 above).
6. The enhancement performance ratio to decreases with each increase in oil concentration.

Table 9.1. Enhancement performance ratios of each tube with refrigerant-oil mixtures compared to the same tube with pure refrigerant ($\theta_{s'/s}$ and $\theta_{a'/a}$) at 300 kg/m².s

Oil %	Evaporation					Condensation				
	Tube type and oil SUS					Tube type and oil SUS				
	Smooth ^a		Micro-fin		Low-fin	Smooth		Micro-fin		Low-fin
	150	300	150	300	150	150	300	150	300	150
1.25	1.05	0.90	1.00	0.85	1.00	1.35	0.95	0.90	0.85	0.90
2.5	1.15	0.80	0.95	0.70	0.90	1.50	0.90	0.85	0.75	0.90
5.0	0.95	0.65	0.75	0.60	0.70	1.45	0.90	0.75	0.65	0.80

^aColumns for smooth tube show $\theta_{s'/s}$; other columns show $\theta_{a'/a}$.

Table 9.2. Enhancement performance ratios of the augmented tubes compared to the smooth tube with pure refrigerant ($\theta_{a/s}$) and refrigerant-oil mixtures ($\theta_{a/s'}$) at 300 kg/m².s

Oil Concentration (%)	Evaporation			Condensation		
	Tube and oil type			Tube and oil type		
	Micro-fin		Low-fin	Micro-fin		Low-fin
	150 SUS	300 SUS	150 SUS	150 SUS	300 SUS	150 SUS
0.0 ^a	1.50	1.50	1.20	1.25	1.25	0.85
1.25	1.45	1.35	1.10	0.85	1.10	0.55
2.5	1.20	1.30	0.90	0.70	1.00	0.50
5.0	1.20	1.35	0.85	0.65	0.95	0.45

^aRow with 0.0% oil concentration shows $\theta_{a/s}$; other rows show $\theta_{a/s'}$.

CHAPTER 10

CORRELATIONS FOR DESIGN WITH REFRIGERANT-OIL MIXTURES

The designer of refrigeration equipment needs to reliably estimate heat transfer and pressure drop performance of heat exchangers when oil is present in the refrigerant. Correlations are the tool generally available to the designer to estimate component performance. Correlations range from models based on first principles, which may be applicable to a wide range of conditions, to purely empirical curve fitting techniques, whose applicability is limited to the conditions of the particular data base used. Between these two extremes are semi-empirical expressions that combine fundamental principles with experimental data. Theoretical models are often useful in understanding physical phenomena, but they usually require modifications with empirical data to be of practical use. The first part of this chapter gives a brief review of correlations proposed by other researchers for pure refrigerant in smooth and finned tubes and for refrigerant-oil mixtures in smooth tubes. The review is intended to be representative, but not exhaustive. Several of these earlier correlations for pure refrigerant in smooth tubes were used in Chapter 6 for comparison with experimental results. The second part of the chapter describes the development during this research program of predictive equations for refrigerant-oil mixtures in enhanced tubes.

Review of Correlations from the Literature

This section reviews past work on correlation development, emphasizing those that have been applied to refrigerants. The discussion of augmented tube correlations is limited to internally finned tubes because these are most relevant to the tubes used in this study.

Many of the correlations that are discussed use subscripts on various quantities to indicate whether liquid or vapor properties are used to determine that particular quantity. The subscript *l* refers to liquid, while *v* refers to vapor. For parameters such as Reynolds number, which include flow or velocity terms in addition to property terms, the subscripts *l* and *v* imply further that the parameter is based on liquid flow alone or vapor flow alone, respectively. Additionally, the subscript *lo* is introduced to indicate that all of the flow is

assumed liquid and fluid properties are those of the liquid. For the Reynolds number, the definitions of these subscripts are illustrated below:

$$Re_l = \frac{G \cdot (1-X) \cdot d}{\mu_l} \quad (10.1a)$$

$$Re_{lo} = \frac{G \cdot d}{\mu_l} \quad (10.1b)$$

$$Re_v = \frac{G \cdot X \cdot d}{\mu_v} \quad (10.1c)$$

Pure Refrigerant Heat Transfer in Smooth tubes

Many correlations have been proposed over the years to predict heat transfer performance in plain tubes. Some of these have been general, applying to a variety of fluids and flow conditions, while others have been restricted to a particular flow regime or class of fluids. The discussion below reviews earlier correlations that have been used successfully with refrigerants or that have been used as the basis of correlations for augmented tubes or refrigerant-oil mixtures. Additional reviews of correlations are available in the literature [119,134,158,173,174].

Evaporation Pierre [175] published a correlation for average heat transfer during evaporation of R-12 in a horizontal tube. He found a relatively simple functional relationship between Nusselt number and two other parameters. These parameters are the Reynolds number based on total flow with liquid properties (Re_{lo}) and a parameter that Pierre called a boiling number (K). Pierre's boiling number is not the number generally defined in the literature, but is defined as

$$K = \frac{\Delta X \cdot i_{fg}}{l \cdot g} \quad (10.2)$$

The correlation for complete evaporation is

$$Nu_l = 0.00028 \cdot (Re_{lo} \cdot K)^{0.8} \quad (10.3)$$

and for incomplete evaporation, it is

$$Nu_l = 0.00097 \cdot Re_{lo} \cdot K^{0.5} \quad (10.4)$$

This correlation was used as the basis for several proposed correlations, discussed below, that include augmentation or oil effects.

The correlation of Sani [176] was developed using data from vertically downward flow of water. The correlation equation is based on the quality-dependent Lockhart–Martinelli parameter [75]:

$$\frac{Nu}{Re_l^{0.8} Pr^{0.33}} = 340 \left[Bo + 0.00015 \cdot \left(\frac{1}{\chi_{tt}} \right)^{0.67} \right] \quad (10.5)$$

where the Lockhart–Martinelli parameter is defined by

$$\chi_{tt} = \left[\frac{1-X}{X} \right]^{0.9} \left[\frac{\rho_v}{\rho_l} \right]^{0.5} \left[\frac{\mu_l}{\mu_v} \right]^{0.1} \quad (10.6)$$

Chaddock and Brunemann [177] proposed a correlation of similar form based on refrigerant data in horizontal tubes. Their correlation is

$$\frac{h_{TP}}{h_{l0}} = 1.91 \left[Bo \times 10^4 + 1.5 \cdot \left(\frac{1}{\chi_{tt}} \right)^{0.67} \right]^{0.6} \quad (10.7)$$

Shah [178] developed correlation equations from an earlier chart-based correlation. His correlation is a function of boiling number, Froude number, and convection number. At low qualities, nucleate boiling dominates; while at high qualities, convection dominates. For horizontal flow, Shah's correlation is

$$\frac{h_{TP}}{h_l} \equiv \Psi \quad (10.8)$$

where Ψ is evaluated by the following procedure:

$$N \equiv 0.38 \cdot Fr^{0.3} \cdot Co \quad (10.9)$$

$$\Psi_{cb} = \frac{1.8}{N^{0.8}} \quad (10.10)$$

For $N > 1$

$$\Psi_{nb} = 230 \cdot Bo^{0.5}, \quad Bo > 3.0 \times 10^{-5} \quad (10.11a)$$

$$\Psi_{nb} = 1 + 46 \cdot Bo^{0.5}, \quad Bo < 3.0 \times 10^{-5} \quad (10.11b)$$

For $0.1 < N \leq 1.0$

$$\Psi_{bs} = E \cdot Bo^{0.5} \cdot e^{2.74 \cdot N \cdot 0.1} \quad (10.12)$$

For $N \leq 0.1$

$$\Psi_{bs} = E \cdot Bo^{0.5} \cdot e^{2.74 \cdot N^{-0.15}} \quad (10.13)$$

The value of Ψ is the larger of Ψ_{cb} and Ψ_{nb} or Ψ_{bs} .

The constant E in the expressions above depends on Bo :

$$E = 14.7, \quad Bo \geq 11 \times 10^{-4} \quad (10.14a)$$

$$E = 15.43, \quad Bo < 11 \times 10^{-4} \quad (10.14b)$$

Gungor and Winterton [157] used data for seven fluids to develop a generalized evaporation correlation. Their correlation adds a pool boiling term to a convective term. These terms come from correlations developed by other investigators and are each multiplied by a correction factor. The general form of the correlation is

$$h_{TP} = E \cdot h_l + S \cdot h_{nb} \quad (10.15)$$

where the convective term is based on the Dittus-Boelter/McAdams equation [154]:

$$h_l = 0.023 \cdot Re_1^{0.8} \cdot Pr_1^{0.4} \cdot k_l / d \quad (10.16)$$

The nucleate boiling term is

$$h_{nb} = 55 \cdot (P^*)^{0.12} \cdot (-\log_{10} P^*)^{-0.55} \cdot M^{-0.5} \cdot q^{0.67} \quad (10.17)$$

The correction terms are defined by the following expressions:

$$E = 1 + 24000 \cdot Bo^{1.16} + 1.37 \cdot \chi_{tt}^{-0.86} \quad (10.18a)$$

$$S = \frac{1}{1 + 1.15 \times 10^{-6} \cdot E^2 \cdot Re_1^{1.17}} \quad (10.18b)$$

For horizontal tubes with Froude number less than 0.05, E and S are multiplied by correction factors. For E , the correction is

$$Fr^{(0.1-2 \cdot Fr)} \quad (10.19a)$$

and for S ,

$$\sqrt{Fr} \quad (10.19b)$$

Kandlikar [158] has recently revised an earlier correlation based on the superposition of a nucleate boiling term and a convective term. Like Gungor and Winterton, Kandlikar used a large data bank with several different fluids. His correlation equation is

$$\frac{h_{TP}}{h_l} = C_1 \cdot C_o^{C_2} \cdot (25 \cdot Fr)^{C_5} + C_3 \cdot Bo^{C_4} \cdot F_{fl} \quad (10.20)$$

The constants C_1 – C_5 are tabulated in the paper. They are applicable to all fluids, but depend on the convection number. The term F_{fl} is fluid-specific, with a value of 2.2 for R-22. Values for ten fluids are given in the paper.

Condensation The correlation of Akers et al. [179] predicts average heat transfer coefficient using a single-phase similarity expression. The correlation is

$$\bar{h}_{TP} = E \cdot \frac{k_l}{d} \cdot Re_e^e \cdot Pr_l^{1/3} \quad (10.21)$$

where the equivalent Reynolds number is the Reynolds number calculated as if the entire flow were liquid multiplied by the following correction term:

$$(1-X) + X \cdot \sqrt{\frac{\rho_l}{\rho_v}} \quad (10.22)$$

The constants E and e , dependent on the equivalent Reynolds number, are

$$E = 0.0265 \quad e = 0.8 \quad \text{for } Re_e > 5 \times 10^4 \quad (10.23a)$$

$$E = 5.03 \quad e = 1/3 \quad \text{for } Re_e \leq 5 \times 10^4 \quad (10.23b)$$

Another single-phase similarity correlation with a simple form is that of Boyko and Kruzhilin [180]. This correlation predicts average heat transfer coefficients and is

$$\bar{h}_{TP} = 0.024 \cdot \frac{k_l}{d} \cdot Re_{lo}^{0.8} \cdot Pr_l^{0.43} \frac{\left(\frac{\rho}{\rho_m}\right)_{in}^{0.5} + \left(\frac{\rho}{\rho_m}\right)_{out}^{0.5}}{2} \quad (10.24)$$

where

$$\frac{\rho}{\rho_m} = 1 + \left[\frac{\rho_l - \rho_v}{\rho_v} \right] \cdot X \quad (10.25)$$

Chato [181] developed a momentum-energy integral method based on Nusselt's analysis [182] for predicting condensation heat transfer in horizontal and inclined tubes. For horizontal tubes, the correlation is

$$\bar{h}_{TP} = 0.468 \left[\frac{g \cdot \rho_l \cdot (\rho_l - \rho_v) \cdot i_{fg} \cdot (1 + 0.68 \cdot Ja) \cdot k_l^3}{\mu \cdot r \cdot \Delta T} \right]^{0.25} \quad (10.26)$$

where ΔT is the wall superheat.

Azer et al. [183,184] developed a correlation using an annular flow analysis with a von Karman velocity distribution in the condensate film. The final form of the correlation is

$$h_{TP} = 0.153 \cdot \frac{k_l}{d} \cdot Pr_l \cdot Re_v^{0.9} \cdot \left(\frac{\mu_v}{\mu_l} \right) \left(\frac{\rho_l}{\rho_v} \right)^{0.5} \cdot X^{0.9} \cdot \frac{\phi}{t^+} \quad (10.27)$$

where

$$\phi = 1 + 1.0986 \cdot \chi_{tt}^{0.039} \quad (10.28)$$

$$t^+ = 3.88 \cdot Pr_l^{0.663} \cdot (4.67 - X) \quad \text{for } X > 0.18 \quad (10.29)$$

The Reynolds number is based on total mass flow and the viscosity of saturated vapor.

Like Azer et al., Traviss et al. [161] assumed annular flow with the von Karman velocity distribution through the film. The correlation is

$$h_{TP} = \frac{k_l}{d} \cdot \frac{Pr_l \cdot Re_l^{0.9}}{F2} \cdot F1 \quad (10.30)$$

where

$$F1 = 0.15 \cdot \frac{1}{\chi_{tt}} + 2.85 \cdot \chi_{tt}^{-0.476} \quad (10.31)$$

$$F2 = 0.707 \cdot Pr_l \cdot Re_l^{0.5} \quad \text{for } Re_l \leq 50 \quad (10.32a)$$

$$F2 = 5 \cdot Pr_l + 5 \cdot \ln[1 + Pr_l \cdot (0.09636 \cdot Re_l^{0.585} - 1)] \quad \text{for } 50 < Re_l \leq 1125 \quad (10.32b)$$

$$F2 = 5 \cdot Pr_l + 5 \cdot \ln(1 + 5 \cdot Pr_l) + 2.5 \cdot \ln(0.00313 \cdot Re_l^{0.812}) \quad \text{for } Re_l > 1125 \quad (10.32c)$$

Cavallini and Zecchin [162] proposed a correlation that is simple in form and based on refrigerant condensation in a horizontal tube. An analytical study was also performed to support the correlation. The equation in dimensionless form is

$$Nu_{TP} = 0.05 \cdot Re_e^{0.8} \cdot Pr_1^{0.33} \quad (10.33)$$

The equivalent Reynolds number is defined by

$$Re_e = Re_v \left(\frac{\mu_v}{\mu_l} \right) \left(\frac{\rho_l}{\rho_v} \right)^{0.5} + Re_l \quad (10.34)$$

Shah [160] developed a broad-based correlation using data with ten fluids. Of the ten fluids, four were refrigerants. The equation of Shah is

$$h_{TP} = 0.023 \frac{k_l}{d} \cdot Re_{l0}^{0.9} \cdot Pr_1^{0.4} \cdot \left[(1-X)^{0.8} + \frac{3.8 \cdot X^{0.76} \cdot (1-X)^{0.04}}{(P^*)^{0.38}} \right] \quad (10.35)$$

Pure Refrigerant Heat Transfer in Finned Tubes

Earlier attempts to correlate the performance of finned tubes have usually involved the modification of an established smooth tube correlation: a correction term (or terms), new values for constants in the correlation, or redefining some parameter(s) such as the characteristic dimension. Correlations in the literature are generally tailored to a specific tube geometry and there is as yet no generally applicable correlation that can be applied to a finned tube having arbitrary fin shape, fin height, spiral angle, etc. Several earlier correlations are described below. None of the correlations found were developed using micro-fin tubes.

Evaporation Lavin and Young [103] used different equations for nucleate boiling and annular flow regimes and determined one constant in each. The equations are from earlier investigators. For nucleate boiling,

$$Nu_{TP} = E \cdot \left[\frac{q \cdot d_e}{\mu \cdot i_{fg}} \cdot Pr \right]^{0.69} \cdot \left[\frac{\rho_l}{\rho_v} - 1 \right]^{0.31} \cdot \left[\frac{p \cdot d_e}{\sigma} \right] \quad (10.36)$$

and for the annular regime,

$$\frac{h_{TP}}{h_l} \cdot \left[\frac{G \cdot i_{fg}}{q} \right]^{0.1} = E \cdot \left[\frac{1+X}{1-X} \right]^{1.16} \quad (10.37)$$

Azer and Sivakumar [109] chose the correlation of Sani [176] for smooth tube heat transfer and applied a correction factor:

$$\frac{h_{TPa}}{h_{TPs}} = 1 + 0.00137 \cdot (F_1)^{4.635} \cdot (F_2)^{-9.863} \quad (10.38)$$

where F_1 and F_2 are geometric factors first proposed by Carnavos [185]. The term F_1 is the ratio of actual free flow area in the tube to the open core flow area while F_2 is the ratio of the internal area of a smooth tube having the same maximum inside diameter as the finned tube to the actual inside surface area of the finned tube. They also applied the same correction technique to the correlation of Pierre [175] and found the final correlation of finned tube data to be somewhat better.

Several papers were found that discussed correlations in corrugated tubes. Although these tubes are not finned, they have enough in common geometrically with finned tubes to warrant mention. Withers and Habdas [95], Kawai and Machiyama [96], and Kawai and Yamada [97] all used the basic form of Pierre's correlation and modified the constants. Withers and Habdas defined a parameter called severity, and found the constants in the correlation to change with severity. There was no attempt, however, to develop a functional relationship between severity and the constants. The severity is

$$\Phi = \frac{f^2}{p \cdot d_i} \quad (10.39)$$

where f was the ridge height, rather than fin height.

Condensation Vrabie et al. [138] successfully used the Cavallini and Zecchin [162] correlation in finned tubes by defining the characteristic dimension as the hydraulic diameter. They modified the correlation by adding a pressure term, but this term was added for both smooth and finned tubes and is not a correction for augmentation.

For finned tubes, Luu [134] modified the correlation of Boyko and Kruzhilin [180] with a geometric correction factor suggested by Royal [174]. The correlation is

$$h_{TPa} = h_{TPs} \left[\frac{f^2}{w \cdot d_i} \right]^{-0.22} \quad (10.40)$$

The correction factor is quite similar to the severity, Φ , of Withers and Habdas.

Using the correlation of Akers et al. [179] as a starting point, Azer and Said [143] developed a correlation that generally predicted heat transfer in finned tubes within $\pm 30\%$ of experimental data. The earlier correlation is multiplied by a correction factor:

$$\bar{h}_{TPa} = \bar{h}_{TPs} \cdot [1 + 0.93 \cdot (F_1)^{0.23} \cdot (F_2)^{0.58} \cdot (F_3)^{4.17} \cdot Re_1^{0.054}] \quad (10.41)$$

where F_1 , F_2 , and F_3 are geometric parameters proposed by Carnavos [185]. The definitions of F_1 and F_2 were given earlier and

$$F_3 = \sec \beta \quad (10.42)$$

Recently, Kaushik and Azer [186] made an attempt to correlate data from several investigators using different tubes and fluids. Like Azer and Said [143], they used the correlation of Akers et al. [179] as the starting point and added three types of modifiers: (1) a term based on the critical pressure, P_{crit} , (2) a term reflecting the cooling rate, and (3) the geometric parameters F_1 , F_2 , and F_3 defined earlier. The correlation for $F_1 < 1.4$ is

$$\frac{Nu}{Pr^{0.333}} = 2.078 \cdot Re_e^{0.507} \cdot \left[\frac{\Delta X \cdot d_i}{l} \right]^{0.198} \cdot \left[\frac{P_i}{P_{crit}} \right]^{-0.14} \cdot F_1^{0.874} \cdot F_2^{-0.814} \quad (10.43a)$$

and for $F_1 > 1.4$, the correlation is

$$\frac{Nu}{Pr^{0.333}} = 0.391 \cdot Re_e^{0.507} \cdot \left[\frac{\Delta X \cdot d_i}{l} \right]^{0.198} \cdot \left[\frac{P_i}{P_{crit}} \right]^{-0.14} \cdot F_1^{4.742} \quad (10.43b)$$

The correlation predicts the majority of data points used in its formulation within $\pm 30\%$.

As with evaporation, results of studies in corrugated tubes are also mentioned briefly. Kawai and Machiyama [96] found that condensation correlated with an equation of the form proposed by Chato [181]:

$$h_{TPa} = E \cdot \left[\frac{\rho^2 \cdot k^3 \cdot i_{fg}}{d_i \cdot \mu \cdot \Delta T} \right]^e \quad (10.44)$$

where ΔT is the saturation temperature less the wall temperature. The constants E and e varied with tube geometry.

Refrigerant-Oil Mixture Heat Transfer in Smooth Tubes

As with augmented tube correlations, those for refrigerant-oil mixtures are generally modifications of existing pure refrigerant correlations. These correlations tend to be condition-specific and often require different constants for different oil concentrations, even though the oil type remains unchanged.

Evaporation Chaddock and Mathur [34] correlated refrigerant-oil data as a relatively simple function of χ_{tt} alone. Their correlation, which correctly predicted about 90% of the data within $\pm 35\%$, is

$$\frac{h_{TP}}{h_l} = E \cdot \left[\frac{1}{\chi_{tt}} \right]^e \quad (10.45)$$

The constants E and e vary with oil concentration, and h_l is based on properties of refrigerant-oil mixture at the global average oil concentration.

Tichy et al. [41] developed a complex expression with three adjustable constants for the correlation of evaporation heat transfer with refrigerant-oil mixtures. Their expression is

$$Nu_{TP} = Nu_{SP} \cdot 10^{k_1 / (\log_{10} \chi_{tt} - k_2)} \quad (10.46)$$

where

$$k_1 = k_{1a}(\omega_o) + k_{1b}(\omega_o) \cdot \log_{10} Ja \quad (10.47a)$$

$$k_2 = k_{2a}(\omega_o) - 2 \cdot \log_{10} Ja \quad (10.47b)$$

and k_{1a} , k_{1b} , and k_{2a} are empirically determined constants that vary with oil concentration. The single-phase Nusselt number is calculated from the Dittus-Boelter/McAdams equation [154]. The correlation represents approximately 85% of the data within $\pm 35\%$.

Condensation The only correlation found was that of Tichy et al. [47]. They applied a correction factor to the pure refrigerant correlation of Shah [160]:

$$Nu = Nu_{Shah} \cdot \left[0.88 + \left(\frac{Re_{ref}}{Re_{lo}} \right)^{1.99} \right] \cdot e^{-5.0 \omega_o} \quad (10.48)$$

The term in brackets [] is a correction at low mass flux and is unrelated to the presence of oil; the oil correction is the exponential term. Properties used in Shah's correlation are those of pure refrigerant. About 82% of the data fall within $\pm 20\%$ of the correlation.

Refrigerant-Oil Mixture Heat Transfer in Finned Tubes

There have been no previous studies proposing correlation expressions for refrigerant-oil mixtures inside augmented tubes.

Pure Refrigerant Pressure Drop in Smooth Tubes

As with heat transfer, many correlations have been proposed to predict pressure drop during two-phase flow. The discussion below presents several correlation expressions that have been successfully used by earlier investigators. Unlike many of the heat transfer correlations discussed above, most of the pressure drop correlations were not developed from refrigerant data, but rather from steam-water data. These correlations, therefore, might be expected to show more deviation from experimental results.

In horizontal tubes, the pressure gradient is the sum of contributions caused by friction and momentum. The pressure gradient is

$$\left(\frac{dP}{dz}\right) = \left(\frac{dP}{dz}\right)_f + \left(\frac{dP}{dz}\right)_m \quad (10.49)$$

In evaporators or condensers such as were used in this study, the momentum pressure drop is usually small in comparison with the frictional pressure drop, so emphasis is usually placed on the prediction of frictional pressure gradient. It is common in many two-phase pressure drop correlations to determine pressure drop by multiplying a single-phase pressure drop by a two-phase friction multiplier, ϕ^2 . Depending on the basis of the single-phase friction factor, equivalent expressions for the frictional pressure gradient are derived:

$$-\left(\frac{dP}{dz}\right)_f = -\left(\frac{dP}{dz}\right)_{f_1} \cdot \phi_1^2 = \frac{2 \cdot f_1 \cdot G^2 \cdot (1-X)^2 \cdot v_1}{d} \cdot \phi_1^2 \quad (10.50a)$$

$$-\left(\frac{dP}{dz}\right)_f = -\left(\frac{dP}{dz}\right)_{f_{10}} \cdot \phi_{10}^2 = \frac{2 \cdot f_{10} \cdot G^2 \cdot v_1}{d} \cdot \phi_{10}^2 \quad (10.50b)$$

$$-\left(\frac{dP}{dz}\right)_f = -\left(\frac{dP}{dz}\right)_{f_v} \cdot \phi_v^2 = \frac{2 \cdot f_v \cdot G^2 \cdot X^2 \cdot v_v}{d} \cdot \phi_v^2 \quad (10.50c)$$

where the friction factor, f , is determined by expressions such as

$$f = \frac{0.079}{\text{Re}^{0.25}} \quad (10.51a)$$

or

$$f = \frac{0.046}{\text{Re}^{0.2}} \quad (10.51b)$$

The Reynolds number used in Equation 10.51 depends on the subscript of the friction factor (see Equation 10.1).

Practical pressure drop correlations can be divided into two broad classifications, based on the underlying assumptions of the flow model: homogeneous flow and separated flow. The homogeneous model assumes that vapor and liquid flow at the same velocity in thermodynamic equilibrium. In spite of the weakness of these assumptions for many situations, this model has often been successful in predicting two-phase pressure drop. The homogeneous model considers the liquid and vapor to flow as a single-phase having suitable mean values for properties. It is assumed that a suitably defined single-phase friction factor can be used for two-phase flow. The pressure gradient with this model is

$$-\left(\frac{dP}{dz}\right) = \frac{2 \cdot f_{TP} \cdot l \cdot G^2 \cdot \bar{v}}{d} + G^2 \cdot \frac{d\bar{v}}{dz} \quad (10.52)$$

The first term on the right is the frictional term, while the second is the momentum term. The two-phase friction factor is defined as in Equations 10.51, with an appropriate average viscosity in the Reynolds number. If one chooses the friction factor from Equation 10.51a and defines average viscosity by

$$\frac{1}{\bar{\mu}} = \frac{X}{\mu_v} + \frac{(1-X)}{\mu_l} \quad (10.53)$$

then the two-phase friction multiplier for homogeneous flow becomes

$$\phi_{10}^2 = \left[1 + X \cdot \left(\frac{v_v - v_l}{v_l}\right)\right] \cdot \left[1 + X \cdot \left(\frac{\mu_l - \mu_v}{\mu_v}\right)\right]^{-0.25} \quad (10.54)$$

Pierre [44] used the homogeneous model as a basis for correlating frictional pressure drop in horizontal tubes during the evaporation of refrigerant. Pierre found a simple functional relationship between the friction factor and the nondimensional grouping $Re_{l0} \cdot K^{-1}$, where K is called the boiling number by Pierre and is defined in Equation 10.2. The friction factor is

$$f = 0.0185 \cdot (Re_{l0} \cdot K^{-1})^{-1/4} \quad (10.55)$$

and pressure drop is calculated by

$$\frac{\Delta P}{L} = \left[f + \frac{(X_2 - X_1) \cdot d}{\bar{X} \cdot l} \right] \cdot G^2 \cdot \frac{\bar{v}}{d} \quad (10.56)$$

where

$$\bar{v} = \frac{\bar{X}}{\bar{\rho}_v} + \frac{(1 - \bar{X})}{\rho_l} \approx \bar{X} \cdot \bar{v}_v \quad (10.57)$$

The second type of correlation is based on the separated flow model. This model makes the more realistic assumption that vapor and liquid flow at different velocities and uses empirical correlations to relate the void fraction and two-phase friction factor to the independent flow variables.

Lockhart and Martinelli [75] developed a generalized parameter χ , defined as

$$\chi^2 = \frac{\left(\frac{dP}{dz}\right)_l}{\left(\frac{dP}{dz}\right)_v} = \frac{Re_v^m}{Re_l^n} \cdot \frac{C_l}{C_v} \cdot \frac{\mu_l}{\mu_v} \cdot \frac{\rho_v}{\rho_l} \quad (10.58)$$

The four constants take on different values, depending on the type of flow in each phase. For evaporation and condensation, flow is generally assumed turbulent in both phases and the subscript *tt* is added to denote turbulent-turbulent. Using appropriate values for the constants, χ_{tt} reduces to the expression shown earlier in Equation 10.6. Lockhart and Martinelli correlated two-phase friction multipliers as functions of χ using charts, but several investigators have proposed equations to approximate the graphically derived values.

Although they found the Lockhart-Martinelli correlation reasonably accurate, Dukler et al. [187] tried to develop a more physically grounded approach. They have two cases of

practical interest. Case I (called Dukler I) is the homogeneous model with a new equation to determine the appropriate average viscosity:

$$\mu = \bar{\rho} \cdot [X \cdot v_v \cdot \mu_v + (1-X) \cdot v_l \cdot \mu_l] \quad (10.59)$$

The second case (called Dukler II) is based on the separated flow model. The frictional pressure gradient according to the Dukler II correlation is

$$\left(\frac{dP}{dz}\right)_f = \frac{2 \cdot G^2 \cdot f_o}{d \cdot \rho_l} \cdot \frac{\rho_l}{\bar{\rho}} \cdot \eta \cdot \delta \quad (10.60)$$

where

$$\eta = 1.0 + \frac{1.0}{1.281 - 0.478 \cdot \lambda + 0.444 \cdot \lambda^2 - 0.094 \cdot \lambda^3 + 0.00843 \cdot \lambda^4} \quad (10.61)$$

$$\lambda = -\ln(1-\alpha_h) \quad (10.62)$$

$$\delta = \frac{\rho_l}{\rho} \cdot \frac{(1-\alpha_h)^2}{1-\alpha} + \frac{\rho_v}{\rho} \cdot \frac{\alpha_h^2}{\alpha} \quad (10.63)$$

$$f_o = 0.0014 + 0.125 \cdot \text{Re}^{-0.32} \quad (10.64)$$

$$\text{Re} = \frac{G \cdot d}{\mu} \cdot \epsilon \quad (10.65)$$

$$\mu = (1-\alpha_h) \cdot \mu_l + \alpha_h \cdot \mu_v \quad (10.66)$$

The application of this correlation requires the introduction of a separate void fraction correlation. Dukler chose the void fraction model of Hughmark and Pressburg [188].

The Lockhart-Martinelli correlation corresponds to a mass flux of 500 to 1000 kg/m²·s and includes no provision for variations of the two-phase friction multiplier with changing mass flux. Attempts have been made to modify existing models to account for the influence of mass flux. Two such correlations are those of Baroczy [163] and Chisholm [164]. Baroczy's method also applies to different fluids through use of a property index defined as

$$\frac{\left[\frac{\mu_l}{\mu_v}\right]^{0.2}}{\left[\frac{\rho_l}{\rho_v}\right]} \quad (10.67)$$

Values for ϕ_{10}^2 are read from a chart as a function of the property index. Mass flux effects are then accounted for through a correction factor, also from a chart, that is a function of the property index.

Chisholm used the following relationship between ϕ_1^2 and χ

$$\phi_1^2 = 1 + \frac{C}{\chi} + \frac{1}{\chi^2} \quad (10.68)$$

Instead of choosing C as a constant, Chisholm introduced a mass flux dependence. For smooth tubes at mass fluxes less than 2000 kg/m²·s, the expression for C is

$$C = \left[0.75 + \left(\frac{2000}{G} - 0.75 \right) \left(\frac{v_v - v_l}{v_l} \right)^{0.5} \right] \cdot \left[\left(\frac{v_v}{v_l} \right)^{0.5} + \left(\frac{v_l}{v_v} \right)^{0.5} \right] \quad (10.69)$$

Reddy et al. [165] presented a correlation that predicts pressure drop of a particular data set better than seven other correlations. The equation that determines the two-phase friction multiplier for water is

$$\phi_{10}^2 = 1 + C \cdot \left[\frac{\rho_l}{\rho_v} - 1 \right] \cdot \left[\frac{735.8 \cdot G}{1. \times 10^6} \right]^{-0.45} \cdot \left[\frac{X_{out}^{1.825} - X_{in}^{1.825}}{1.825} \right] \cdot \frac{1}{\Delta X} \quad (10.70)$$

where

$$C = 1.02 \quad \text{for } P \geq 4 \text{ MPa} \quad (10.71a)$$

$$C = 0.357 \cdot (1 + 10 \cdot P^*) \quad \text{for } 2 \text{ MPa} < P < 4 \text{ MPa} \quad (10.71b)$$

Void Fraction

For the calculation of momentum pressure drop with the separated flow model, it is necessary to have an estimate of the void fraction. Rice [189] evaluated ten void fraction correlations and compared with data from refrigeration systems. He classified the correlations as (1) homogeneous, (2) slip ratio correlated, (3) χ_{tt} correlated, and (4) mass flux dependent. The correlations that agreed best with experimental mass inventory data were in the latter two categories, χ_{tt} correlated and mass flux dependent.

Butterworth [190] reduced six void fraction models into a single equation in which the quantities $A_1, p, q,$ and r are specific to the particular void fraction correlation.

$$\alpha = \frac{1}{1 + A_1 \cdot \left[\frac{1-X}{X} \right]^p \cdot \left[\frac{\rho_v}{\rho_l} \right]^q \cdot \left[\frac{\mu_l}{\mu_v} \right]^r} \quad (10.72)$$

Values for four of these correlations are shown in Table 10.1.

Table 10.1. Constants for void fraction correlation equations

Correlation	Type ^a	A_1	p	q	r
Homogeneous	1	1	1	1	0
Thom [191]	2	1	1	0.89	0.18
Lockhart-Martinelli [75]	3	0.28	0.64	0.36	0.07
Baroczy [192]	3	1	0.74	0.65	0.13

^a1 = Homogeneous, 2 = Slip ratio correlated, 3 = χ_{tt} correlated.

The Hughmark and Pressburg correlation, mentioned earlier, is a mass-flux-dependent correlation based on the following equation:

$$\frac{1}{X} = 1 - \frac{\rho_l}{\rho_v} \cdot \left[1 - \frac{K_2}{\alpha} \right] \quad (10.73)$$

where K_2 is a function of Reynolds number, Froude number, and the no-slip void fraction. Because K_2 is a function of void fraction, an iterative procedure is required. Tabulated values of K_2 are given in [188].

A more easily applied mass-flux-dependent correlation is that of Tandon et al. [193]. For low Reynolds numbers ($50 < Re < 1125$), the correlation is

$$\alpha = \left[1 - 1.928 \cdot \frac{Re_l^{-0.315}}{F(\chi_{tt})} + 0.9293 \cdot \frac{Re_l^{-0.63}}{F(\chi_{tt})^2} \right] \quad (10.74a)$$

and for $Re \geq 1125$,

$$\alpha = \left[1 - 0.38 \cdot \frac{Re_1^{-0.088}}{F(\chi_{tt})} + 0.0361 \cdot \frac{Re_1^{-0.176}}{F(\chi_{tt})^2} \right] \quad (10.74b)$$

where

$$F(\chi_{tt}) = 0.15 \cdot \left[\frac{1}{\chi_{tt}} + \frac{2.85}{\chi_{tt}^{0.476}} \right] \quad (10.75)$$

Pure Refrigerant Pressure Drop in Finned Tubes

Azer and Sivakumar [109] correlated finned tube pressure drop during evaporation by applying a correction to the equation of Pierre [44]. The correlation expression is:

$$\Delta P_{TPa} = (0.628 \cdot F_3^{4.89} \cdot F_4^{-12.29}) \cdot \left[f_{TPa} + \frac{d_j \cdot \Delta X}{X_{avg} \cdot l} \right] \cdot \left[\frac{G^2 \cdot v_{avg} \cdot l}{d_i} \right] \quad (10.76)$$

where F_3 is $\cos \beta$ and F_4 is the ratio of the actual free flow area to the flow area of a smooth tube having an inside diameter equal to the maximum inside diameter of the finned tube [185]. The two-phase friction factor is

$$f_{TPa} = 0.0011 \cdot (Re_{10} \cdot K^{-1})^{-0.112} \quad (10.77)$$

and the Reynolds number is based on the nominal inside diameter, not an equivalent diameter.

Luu [134] found that the Dukler II correlation with homogeneous void fractions gave the best correlation of finned tube condensation results. The only correction required for finned tubes was the use of the hydraulic diameter as the characteristic dimension.

Withers and Habdas [95], using corrugated tubes, correlated pressure drop with Pierre's earlier expression [44]. They, however, changed only the constants in the original expression, rather than adding correction terms like Azer and Sivakumar, and found that the constants varied with the severity parameter, Φ .

Refrigerant-Oil Mixture Pressure Drop in Smooth Tubes

Pierre [44] also correlated the pressure drop of refrigerant-oil mixtures in his study. The form of the correlation is identical to that of pure refrigerant, but the leading constant has more than doubled. The correlation for the friction factor is

$$f = 0.053 \cdot (Re_{10} \cdot K^{-1})^{1/4} \quad (10.78)$$

Oil concentration was in the range of 6% to 12% by volume.

Tichy et al. [47] multiplied a smooth tube, pure refrigerant pressure drop correlation by a polynomial function of oil concentration to estimate both evaporation and condensation pressure drop. For evaporation, they used a quadratic function of oil concentration and the Dukler II/Hughmark correlation. The homogeneous void fraction model was used for the momentum pressure drop. For condensation, the correction factor required only a linear equation in oil concentration and used the Lockhart-Martinelli correlation with homogeneous void fraction. For evaporation, the expression is

$$\Delta P = \Delta P_{\text{corr}} \cdot (1 + 41.3 \cdot \omega_o - 479 \cdot \omega_o^2) \quad (10.79a)$$

and for condensation

$$\Delta P = \Delta P_{\text{corr}} \cdot (0.828 + \omega_o) \quad (10.79b)$$

The sign in front of the factor 479 in Equation 10.79a was positive in the original publication, but it was determined that the term must be negative to be consistent with the author's figures and conclusions.

Correlation of Experimental Heat Transfer Results

Design equations are presented to represent the experimental data obtained during this test program. In some cases, it is possible to substitute mixture properties into an established correlation and predict the effects of oil. In other cases, however, the effect of oil is not so simply described, so the equations proposed are statistically determined. True, generalized correlations of the effect of oil, in particular for evaporation heat transfer, require a more fundamental understanding of the mechanisms by which oil affects performance.

Finned tube performance correlations with pure refrigerant were also investigated, but no new correlations are proposed. However, an expression to estimate the effects of mass flux on enhancement factors is presented in a later section. Correlations with finned tubes, as discussed earlier, have used various geometric parameters and determined the required constants statistically. These correlations have not generally been successful extended to tubes having a different geometry without determining new constants.

None of the earlier finned tube correlations used micro-fin tubes, so there is no existing basis on which to build general correlations. The work of Khanpara [119] has shown that there are at least eight geometric parameters that can affect micro-fin tube performance. Examples are spiral angle, fin height, fin tip shape, etc. Because the work reported here used only one micro-fin and one low-fin tube, little could be done in the way of a geometry-based correlation. Furthermore, it is doubtful that there is a simple geometric parameter that can be used to correlate micro-fin data [122]. Given the current status of finned tube correlations, it is recommended that experimental data, rather than correlation expressions, be used as the basis for enhanced tube performance whenever possible.

Form of Correlations

There are two cases of primary interest to the designer:

1. The effect of oil in a given tube relative to pure refrigerant in the same tube—This case is useful when pure refrigerant data for a given tube is available, either through experimental data or through correlations in which the designer already has confidence.
2. The performance of an augmented tube relative to a smooth tube with pure refrigerant—This case is the one that has been investigated in past studies and a few correlation proposals were discussed earlier in this chapter, however, none of these earlier correlations apply to micro-fin tubes and none are recommended for an arbitrary new geometry without experimental work.

The case of augmented tube performance with refrigerant-oil mixtures to smooth tube performance with similar mixtures is not included above. A combination of cases 1 and 2, however, can be used to estimate the combined effects of oil and augmentation: the pure refrigerant enhancement factor ($\epsilon_{a/s}$) can be multiplied by the oil-enhancement factor for the

augmented tube (ϵ_a/a) and divided by the smooth tube oil-enhancement factor (ϵ_s/s) to yield the enhancement factor combining the effects of oil and augmentation (ϵ_a/s').

Correlations developed during this research predict enhancement factors, rather than absolute performance. This is analogous to many two-phase correlations, which are in the form of $h_{TP}/h_1 = f(Z_1, Z_2, \dots)$. Correlations predicting enhancement factors allow the designer flexibility to use already proven correlations or experimental data as a performance baseline. Additionally, enhancement factors can be readily integrated into existing computer codes, using heat transfer correlations already programmed.

Method

Three major elements are involved in the development of prediction equations to account for refrigerant-oil mixtures and augmentation: (1) trying previously developed correlations for the case of interest, (2) introducing the properties of refrigerant-oil mixtures into existing pure refrigerant correlations, and (3) applying statistical curve fitting techniques.

Statistical constants were determined with the help of the RS/1 statistical software package [194]. This package can fit data to polynomial or other specified functions, and has the capability of multilinear regression analysis. For multiple non-linear regression expressions, the data were first linearized as described by Baustian [4]. The initial regression used five variables, representing a quadratic expression in oil concentration and a linear expression in mass flux. Variables were then selectively eliminated and the multiple regression coefficient (R^2) compared to the previous regression expression. The equation with the fewest variables (the fewest statistical constants) and a sufficiently high value of R^2 (generally ≥ 0.9) was chosen.

Limitations

There are limits to the applicability of the proposed expressions. Already mentioned is the lack of generality with most of the expressions. The data base used to develop these correlations is small compared to that used in the formulation of more general correlations and this should be considered when extending these expressions to different oils, oil concentrations, mass fluxes, tube geometries, etc.

A further limitation, also mentioned in an earlier chapter, is that only average heat transfer coefficients and total pressure drops are used to develop these correlations. Many numerical design codes calculate local values as they step through the heat exchanger, but this research did not yield local heat transfer coefficient or pressure gradient information.

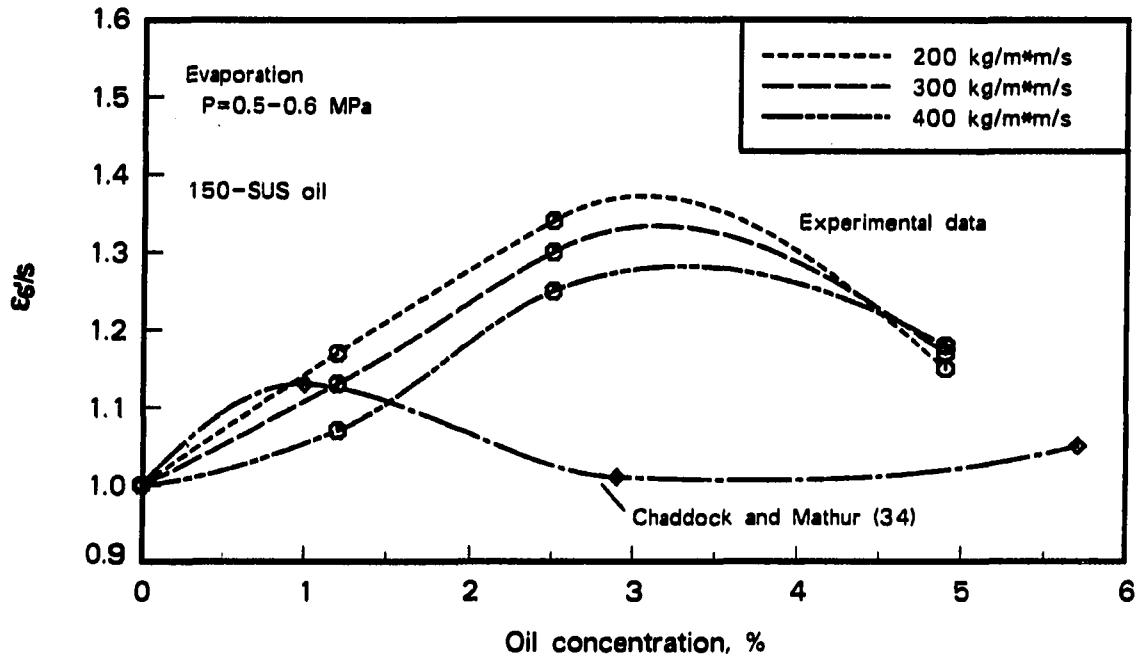
Evaporation: Oil Effects in a Smooth Tube

Previous correlations for refrigerant-oil mixtures Correlations for evaporation of refrigerant-oil mixtures in smooth tubes were formulated by Chaddock and Mathur [34] and Tichy et al. [41]. These were presented in Equations 10.45 and 10.46 and consist of two or three statistically determined constants applied to various functional relationships. Both of these correlations require a numerical integration of local values to obtain average coefficients. Additionally, the Tichy correlation requires the wall superheat as a term in the Jakob number. Wall temperatures were not measured in this test program, so wall superheat must be estimated.

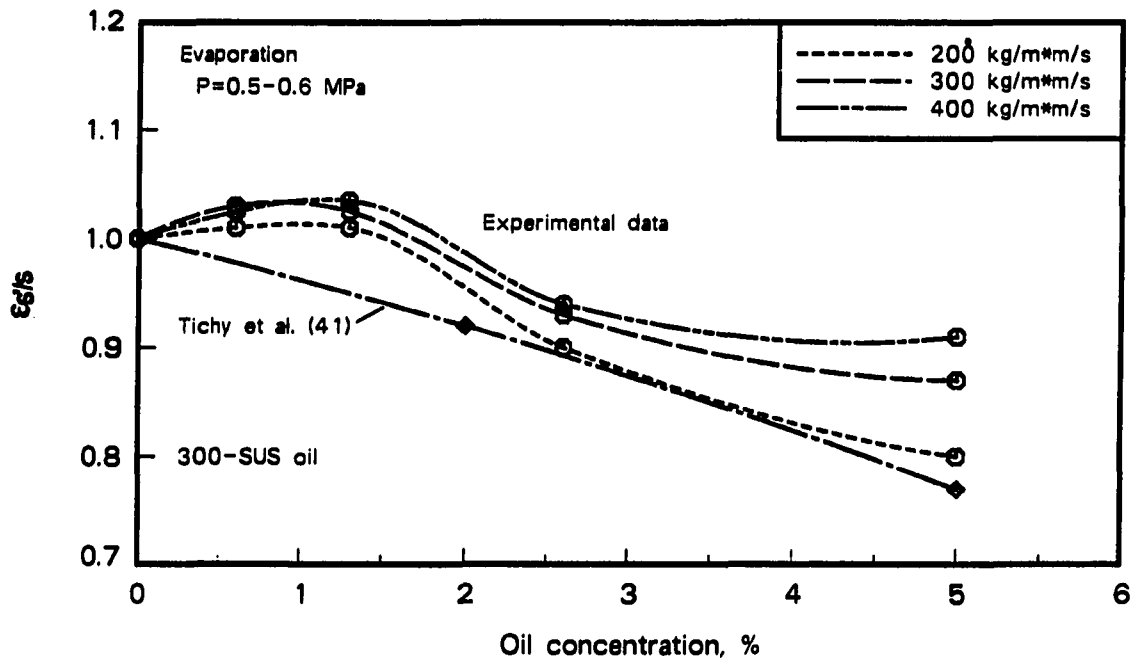
Figure 10.1 plots values of ϵ_s/s based on these correlations along with experimental results at three mass fluxes. Neither of the correlations has a mass flux dependence. Because Chaddock and Mathur used 150-SUS oil and Tichy used 300-SUS oil, each correlation is compared with the corresponding data from this investigation. The correlation of Chaddock and Mathur predicts heat transfer enhancement, but the curve shape is unlike that from the current research, showing a dip, rather than a maximum, at around 2.5% oil. Agreement with current data is within a few percent at high and low concentrations, but at around 2.5% oil, current data are about 35% higher than predicted.

With 300-SUS oil, the correlation of Tichy et al. predicts some enhancement at low qualities, but the integrated average over a quality range of 15% to 85% [as depicted in Figure 10.1(b)] shows a degradation at both of the correlated oil concentrations. The correlation agrees relatively well with the current data at $200 \text{ kg/m}^2\text{s}$ and remains within 15% of experimental values for all conditions shown.

Although both correlations show agreement at some conditions, it was decided to develop equations explicitly dependent on oil concentration, rather than equations that require different constants for each oil concentration. Furthermore, neither of these



(a)



(b)

Figure 10.1. Comparison of refrigerant-oil mixture evaporation heat transfer predictions with experimental data

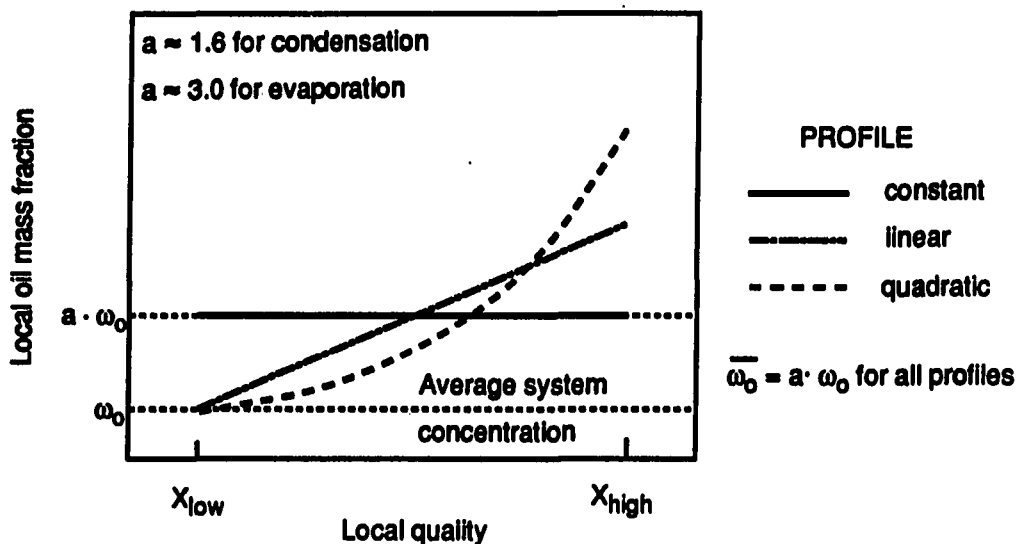


Figure 10.2. Examples of oil concentration profiles used with correlations

correlations has a dependence on mass flux, while the current data show some mass flux dependency. Mass flux, however, has a weaker effect than oil concentration.

General correlations for pure refrigerants Mixture properties were substituted into the three general correlation used for comparison in Chapter 6 [157-159] to calculate predicted enhancement factors, $\epsilon_{S'/S}$. The average oil concentration for these calculations was three times the flowing average, as determined by hold-up tests (see Chapter 6). Three different oil concentration profiles (constant, linear, and quadratic) were tried, with all three yielding similar predictions for $\epsilon_{S'/S}$. Therefore, the simplest profile (constant concentration through the test section) was chosen. These three concentration profiles are illustrated schematically in Figure 10.2.

It should be noted that all of the existing correlations included only pure substances in their data bases, and not mixtures of volatile and nonvolatile liquids. Therefore, predicting refrigerant-oil mixture performance with these correlations extends them beyond their intended range, so discussion of trends based on these correlations may be somewhat speculative.

Figure 10.3 shows the results of using mixture properties in existing correlations and it indicates that agreement with experimental results is not very good. This is not

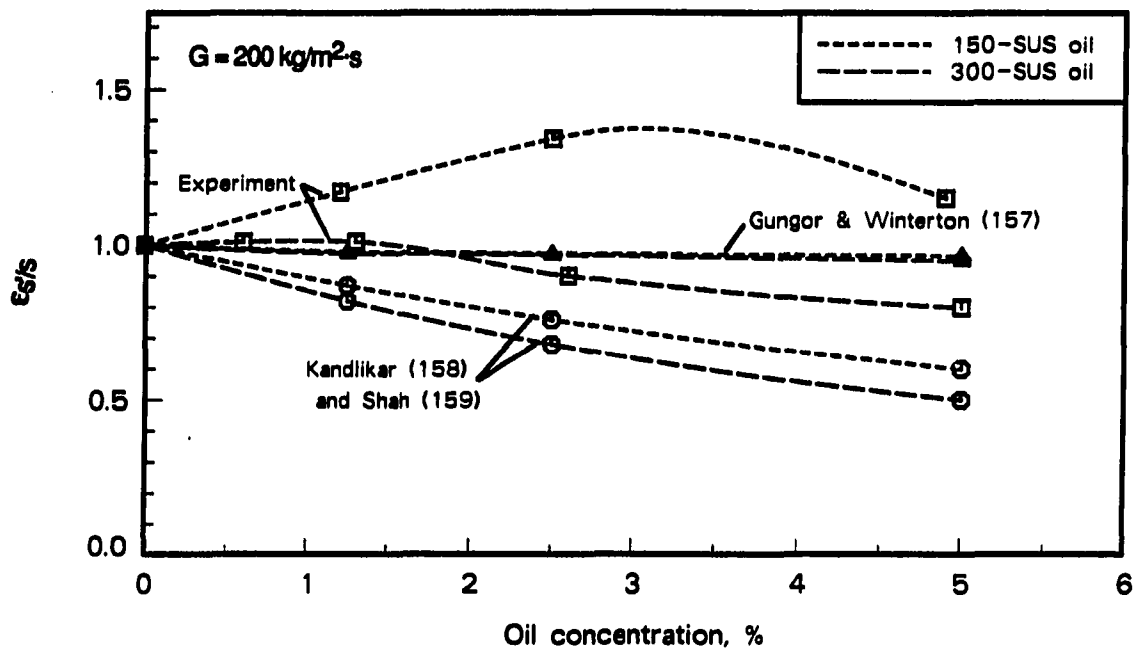


Figure 10.3. Results using refrigerant-oil mixture properties in pure refrigerant evaporation heat transfer correlations

surprising, because properties associated with heat transfer and fluid flow performance (e.g., viscosity, thermal conductivity, etc.) change monotonically with increasing oil concentration, as reflected by the curves in Figure 10.3. (See Chapter 2 for equations that predict refrigerant-oil mixture properties.) Experimental data, however, show that heat transfer increases at low concentrations and then declines as the concentration increases further. This is true for both oils, although the magnitude of the enhancement with 300-SUS oil is minimal. Substitution of refrigerant-oil mixture properties into evaporation correlations leads to a steady decrease of predicted evaporation performance as oil concentration increases. None of the generalized correlations predict enhancement.

None of the enhancement factors predicted by the correlations show a mass flux dependence, since both numerator and denominator are based on the same correlation and are the same function of mass flux. The enhancement factors predicted by Gungor and Winterton are virtually constant over the range of oil concentrations, varying by at most 5% from pure refrigerant values. Kandlikar and Shah, on the other hand, each predict

Table 10.2. Convective and nucleate boiling predictions for pure refrigerant and refrigerant-oil mixtures

Gungor and Winterton [157]						
G	Pure R-22			5% oil		
kg/m².s	Conv.	Nucl.	Total	Conv.	Nucl.	Total
200	2750 ^a	1190	3940	1500	2320	3820
400	4790	1110	5900	2610	2970	5580

Kandlikar [158]						
G	Pure R-22			5% oil		
kg/m².s	Conv.	Nucl.	Total	Conv.	Nucl.	Total
200	1960	1720	3680	1090	1100	2190
400	3410	3000	6410	1900	1910	3810

^aW/m².°C.

significant decreases in heat transfer with increasing oil concentration, and the magnitude of the predicted decrease is almost identical.

The correlations of Gungor and Winterton and Kandlikar are formed from the superposition of nucleate and convective boiling components. To see if any insight into the observed heat transfer results could be gained from looking at these components, correlation predictions with mixture properties were calculated separately for nucleate and convective boiling. Table 10.2 gives the results from these calculations. For Kandlikar, both components of heat transfer decrease with the addition of oil, leading to an overall decrease. Gungor and Winterton, however, predict a sharp increase in the nucleate boiling component, which almost compensates for the decrease in the convective component, leaving the total heat transfer prediction changed relatively little.

Although the actual mechanism of heat transfer enhancement remains a matter of speculation, the nucleate boiling component of the Gungor and Winterton correlation is the only prediction of evaporation enhancement in any of the correlations, indicating that the enhancement could be caused by a nucleate boiling phenomenon. On the other hand, Kandlikar shows a sharp decrease in the nucleate boiling term, so the answer remains unclear. Chapter 3 includes a discussion on pool boiling with refrigerant-oil mixtures, but the literature is contradictory with some workers reporting enhancement and others reporting degradation.

As a sidelight, it is interesting to note in Table 10.2 that even though the two correlations agree quite well when predicting total pure refrigerant heat transfer, the relative importance of convective and nucleate boiling is quite different indicating that the physics of the situation is probably not modeled well by one or both of the correlations.

As mentioned earlier, heat transfer enhancement with the addition of small quantities of oil has been reported in several past studies. None of the researchers who observed this phenomenon were able to offer a certain explanation, however, the promotion of annular flow due to surface tension effects [30], foaming in the evaporator, and delay of dryout [19] have been suggested as possible causes. Promotion of annular flow and delay of dryout would primarily affect the convective region of the evaporator, while foaming would probably have the greatest effect in the nucleate boiling region. Without the observation of flow patterns, it is difficult to clarify the physical grounds for the observed behavior; and without a physical understanding, it is difficult to develop model-based correlations.

Development of statistical prediction equations The failure of the general correlations to predict evaporation performance make it necessary to use statistical procedures to develop design equations. The effects of three parameters appear to be important: oil concentration, oil viscosity, and, to a lesser extent, mass flux. Because there were only two oil viscosities in these tests and the two oils came from different refiners, separate prediction equations for the two oils are presented, rather than incorporating viscosity explicitly. Unlike earlier correlations, which require different constants at different oil concentrations, the prediction equations developed here are explicit functions of oil concentration, as well as mass flux.

Statistical equations are developed in two ways. The first method assumes that the effects of viscosity, thermal conductivity, etc., are predicted by the generalized correlations discussed above. These effects are then superposed on some other unknown phenomenon, causing the distinctive peaking of heat transfer performance. Curve fitting is applied only to the part of the enhancement not predicted by the correlations. The second method is strictly curve fitting, with no attempt to incorporate physical understanding. This method has the advantage of not requiring the use of correlations, numerical integration, or determination of mixture properties, so these equations are easier for the designer to use.

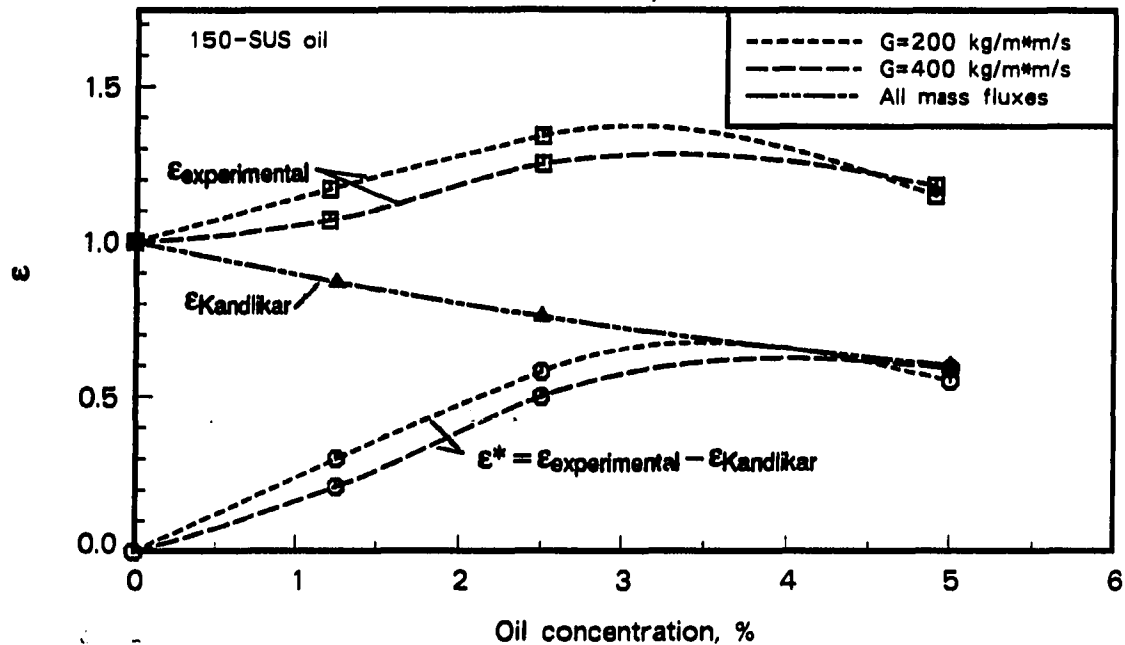


Figure 10.4. Example showing the residual enhancement factor, ϵ^* , relative to enhancement factors from experiments and from a correlation

For the first method above (superposition of correlation and unknown phenomenon to determine total performance), Kandlikar's correlation is used to determine $\epsilon_{s'/s_{corr}}$ and this enhancement factor is subtracted from $\epsilon_{s'/s_{exp}}$ to yield a residual enhancement factor, denoted ϵ^* . As an illustration, Figure 10.4 shows these components separately for 150-SUS oil. The shape of the ϵ^* curve suggests an exponential curve having the form $A \cdot (1 - e^{-B \cdot \omega_0})$. Using the RS/1 statistical package to determine A and B, the following equation is found for 150-SUS oil:

$$\epsilon^* = 0.630 \cdot (1 - e^{-59.9 \cdot \omega_0}) \quad (10.80)$$

and for 300-SUS oil:

$$\epsilon^* = 0.323 \cdot (1 - e^{-66.2 \cdot \omega_0}) \quad (10.81)$$

The values of R^2 are greater than 0.9 for both of these expressions, indicating a good fit with only two statistical constants. The enhancement factor, $\epsilon_{s'/s_{pred}}$, is then calculated by

$$\epsilon_{s'/s_{pred}} = \epsilon_{s'/s_{corr}} + \epsilon^* \quad (10.82)$$

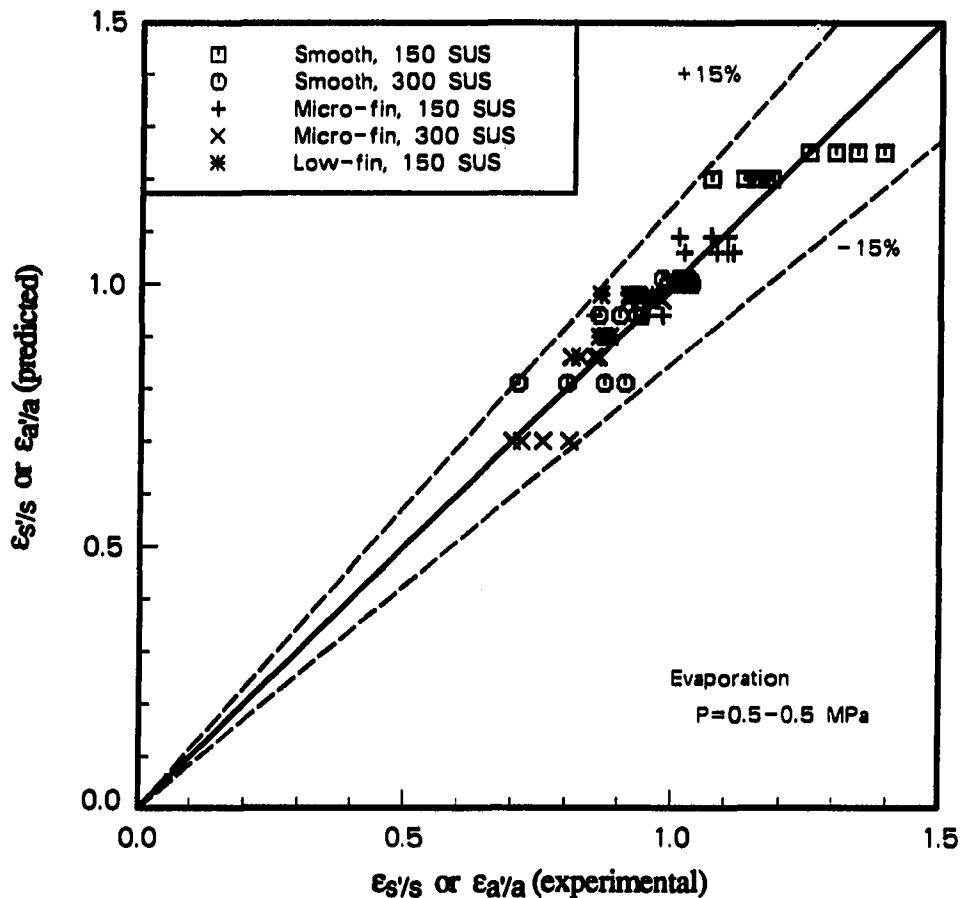


Figure 10.5. Comparison of experimental evaporation heat transfer enhancement factors with predicted values (ϵ_s/s and ϵ_a/a) using correlation-based equations

No mass flux dependence is included in these equations because of (1) the relatively good fit and (2) the already complex calculations required to solve Equation 10.82. Figure 10.5 compares experimental with predicted enhancement factors; experimental values lie within $\pm 15\%$ of predictions. The results shown for finned tubes are discussed later.

For the second method of curve fitting (statistical treatment), several different combinations of parameters were tried, including mass flux terms. It is seen that both exponential and polynomial curves fit the data, but exponential curves have slightly higher values of R^2 . For 150-SUS oil, the equations are

$$\text{exponential: } \epsilon_s/s = 1.03 \cdot e^{(17.7 \cdot \omega_0 - 286 \cdot \omega_0^2 - 0.0496 \cdot G')} \quad (10.83a)$$

$$\text{polynomial: } \epsilon_s/s = 20.4 \cdot \omega_0 - 332 \cdot \omega_0^2 - 0.0610 \cdot G' + 1.03 \quad (10.83b)$$

where G' is a normalized mass flux using $300 \text{ kg/m}^2\cdot\text{s}$ as a reference:

$$G' = G/300$$

For 300-SUS oil, the equations are

$$\text{exponential:} \quad \varepsilon_{s'/s} = 1.03 \cdot e^{\omega_o \cdot (4.98 \cdot G' - 8.77)} \quad (10.84a)$$

$$\text{polynomial:} \quad \varepsilon_{s'/s} = \omega_o \cdot (4.16 \cdot G' - 7.62) + 1.03 \quad (10.84b)$$

Values of R^2 are about 0.9 for Equations 10.83 and 10.84. Note that the parameters used are not the same in Equations 10.83 and 10.84. To maintain R^2 values of 0.9 or higher, more terms are required in the case of 150-SUS oil and this is reflected in the equations.

A comparison of these prediction equations with experimental results is shown in Figure 10.6 and all points lie within a $\pm 10\%$ band. This is somewhat better than using Equations 10.80 and 10.81, but no mass flux terms are included in the earlier equations.

If a phenomenon such as foaming is responsible for evaporation heat transfer enhancement, the validity of the equations presented here may be limited to a specific brand of oil, rather than simply to a specific viscosity. As discussed in Chapter 2, oils have many additives to improve various attributes, including additives to control foaming. Some of these additives may be proprietary or unique to a given brand of oil. This should be kept in mind when using oils other than those used in this investigation or when extending the results to new conditions.

Evaporation: Oil Effects in Finned Tubes

There are no existing correlations of oil effects in finned tubes and, in addition, pure refrigerant correlations for finned tubes are all based on smooth tube correlations such as those discussed above. The development of prediction equations for the finned tubes follows much the same path as for the smooth tube.

Although the magnitude of the enhancement with oil is much smaller in the augmented tubes, and in some cases becomes virtually nonexistent, the pattern of initial enhancement with oil addition, followed by a peak, and then decreasing performance is repeated in these tubes. Once again, none of the existing evaporation correlations predicts these trends correctly. Separate equations are derived for the two different oils and the same two methods described in the previous section are employed. The first method subtracts an

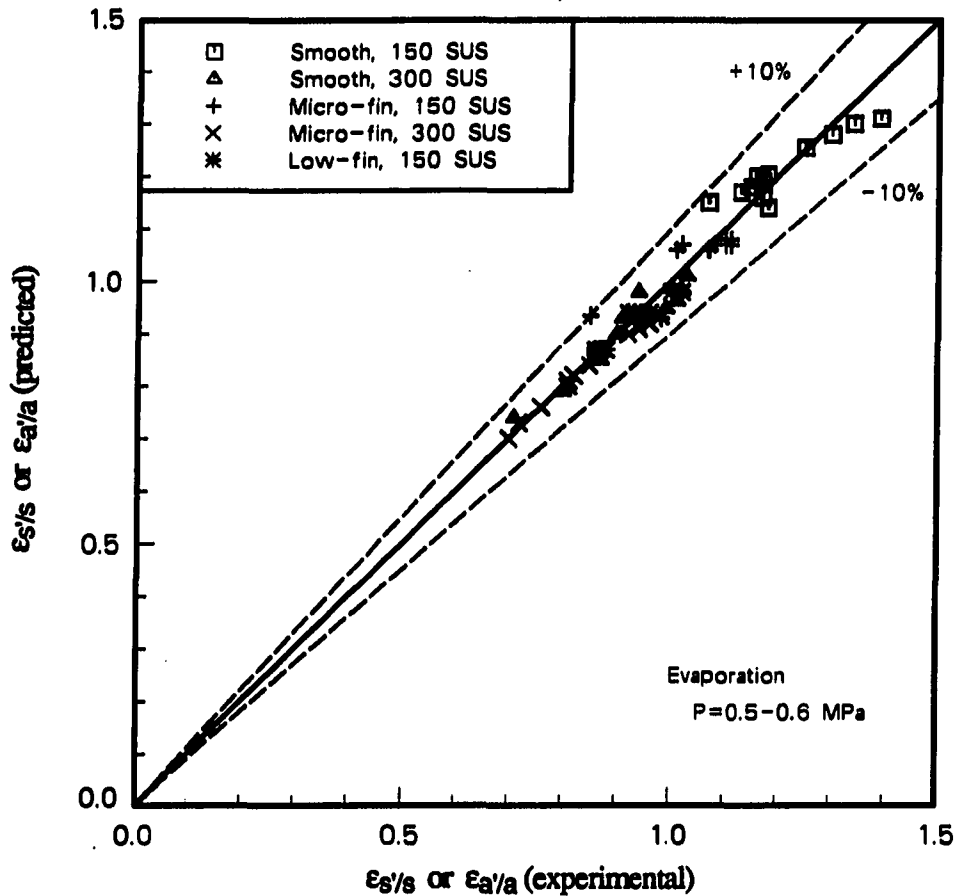


Figure 10.6. Comparison of experimental evaporation heat transfer enhancement factors with predicted values ($\epsilon_{s/s}$ and $\epsilon_{a/a}$) using statistical equations

enhancement factor predicted by an established correlation (Kandlikar in this case) from the experimentally obtained enhancement factor and then correlates only the residual enhancement factor (see Figure 10.4 for an example). The second method is purely statistical and seeks an equation to fit the data with the fewest number of variables.

The residual enhancement factor, ϵ^* , is calculated in the manner described earlier. The shapes of the ϵ^* versus oil concentration plots are similar to those in Figure 10.4 and once again suggest curves of the form $A \cdot (1 - e^{-B \cdot \omega_o})$. The fit is good using this form ($R^2 > 0.8$), even though only two constants are determined. For 150-SUS oil in the micro-fin tube, ϵ^* is calculated by

$$\epsilon^* = 0.349 \cdot (1 - e^{-77.0 \cdot \omega_o}) \quad (10.85)$$

with 300-SUS oil in the micro-fin tube,

$$\epsilon^* = 0.197 \cdot (1 - e^{-110 \cdot \omega_0}) \quad (10.86)$$

and for the low-fin tube (150-SUS oil only),

$$\epsilon^* = 0.349 \cdot (1 - e^{-40.1 \cdot \omega_0}) \quad (10.87)$$

These equations are used in conjunction with Equation 10.82 to determine predicted values of $\epsilon_{a/a}$. Figure 10.5, shown earlier, also depicts data for the finned tubes. Predictions for finned tubes are generally as good as those for the smooth tube.

For the second method, using statistical curve fitting alone, the values of R^2 for the augmented tube equations are somewhat lower than for the smooth tube equations above, given the same number of parameters. However, because the total variation of ϵ is less with the augmented tubes, it is possible to relax the requirement of $R^2 \geq 0.9$ and still keep predicted enhancement factors within $\pm 10\%$ of the experimental values. The micro-fin tube with 150-SUS oil is correlated with the same number of variables as the smooth tube but with $R^2 = 0.75$. With 300-SUS oil, one more parameter is required to give results comparable to the smooth tube and R^2 is above 0.9. The low-fin tube has little dependence on mass flux and can be satisfactorily correlated ($R^2 = 0.87$) with only one oil concentration term. Exponential and polynomial expressions are given below with both forms yielding comparable results.

The following equations predict $\epsilon_{a/a}$ with 150-SUS oil in the micro-fin tube:

$$\text{exponential:} \quad \epsilon_{a/a_{m-f}} = 1.01 \cdot e^{(7.47 \cdot \omega_0 - 178 \cdot \omega_0^2 - 0.0137 \cdot G')} \quad (10.88a)$$

$$\text{polynomial:} \quad \epsilon_{a/a_{m-f}} = 7.69 \cdot \omega_0 - 181 \cdot \omega_0^2 - 0.0193 \cdot G' + 1.01 \quad (10.88b)$$

With 300-SUS oil in the micro-fin tube, the prediction expressions become

$$\text{exponential:} \quad \epsilon_{a/a_{m-f}} = 1.04 \cdot e^{\omega_0 \cdot (89.2 \cdot \omega_0 + 2.87 \cdot G' - 13.5)} \quad (10.89a)$$

$$\text{polynomial:} \quad \epsilon_{a/a_{m-f}} = \omega_0 \cdot (75.9 \cdot \omega_0 + 2.26 \cdot G' - 11.4) + 1.04 \quad (10.89b)$$

For the low-fin tube (150-SUS oil only), enhancement due to oil is predicted by

$$\text{exponential:} \quad \epsilon_{a/a_{l-f}} = 1.02 \cdot e^{-3.19 \cdot \omega_0} \quad (10.90a)$$

$$\text{polynomial:} \quad \epsilon_{a/a_{l-f}} = -2.99 \cdot \omega_0 + 1.02 \quad (10.90b)$$

As before, G' is mass flux normalized to $300 \text{ kg/m}^2\cdot\text{s}$. Figure 10.5, discussed earlier, compares predicted with experimental enhancement factors in the augmented tubes and shows that agreement is within $\pm 10\%$. Once again with the augmented tube equations, equations with mass flux terms show somewhat better agreement with experimental results.

All of the equations given describe the data from the current study within $\pm 15\%$. The method of superposition using Kandlikar's correlation for one of the terms gives reasonably good results with only two statistical constants and no mass flux dependence, but the calculation of ϵ requires numerical integration. The purely statistical equations use more arbitrary constants and require more parameters, but they describe the data somewhat better and can be easily calculated by hand.

Evaporation: Effects of Internal Fins with Pure Refrigerant

No generalized evaporative heat transfer correlation has yet been developed for all types of internally finned tubes or even for a single class, such as micro-fin tubes. The development of micro-fin tube correlations would require the testing of numerous tubes with differing geometric parameters using a variety of fluids. This would be difficult because most of the available micro-fin tubes are similar in geometry. In addition, this greatly expanded test matrix seems unnecessary for the problem at hand because the particular tube geometry used is currently the most popular in refrigeration applications and R-22 is the most applicable refrigerant.

Previous correlations Even though no correlations for micro-fin tube heat transfer were located in the literature, there have been attempts to correlate the performance of tubes having somewhat higher fins. Only the correlation of Azer and Sivakumar [109] is in a form that yields enhancement factor predictions (see Equation 10.38). Using the constants supplied and low-fin tube dimensions to determine F_1 and F_2 , a value of $\epsilon_{a/s} = 1.9$ is obtained. This is equal to the experimental value at about $350 \text{ kg/m}^2\cdot\text{s}$ and within 35% of the maximum observed value, but the correlation has no mass flux dependence.

Development of statistical prediction equations Although no predictive equations for the performance of the enhanced tubes used in this study are developed here, it is observed from the current investigation that heat transfer enhancement factors tend to

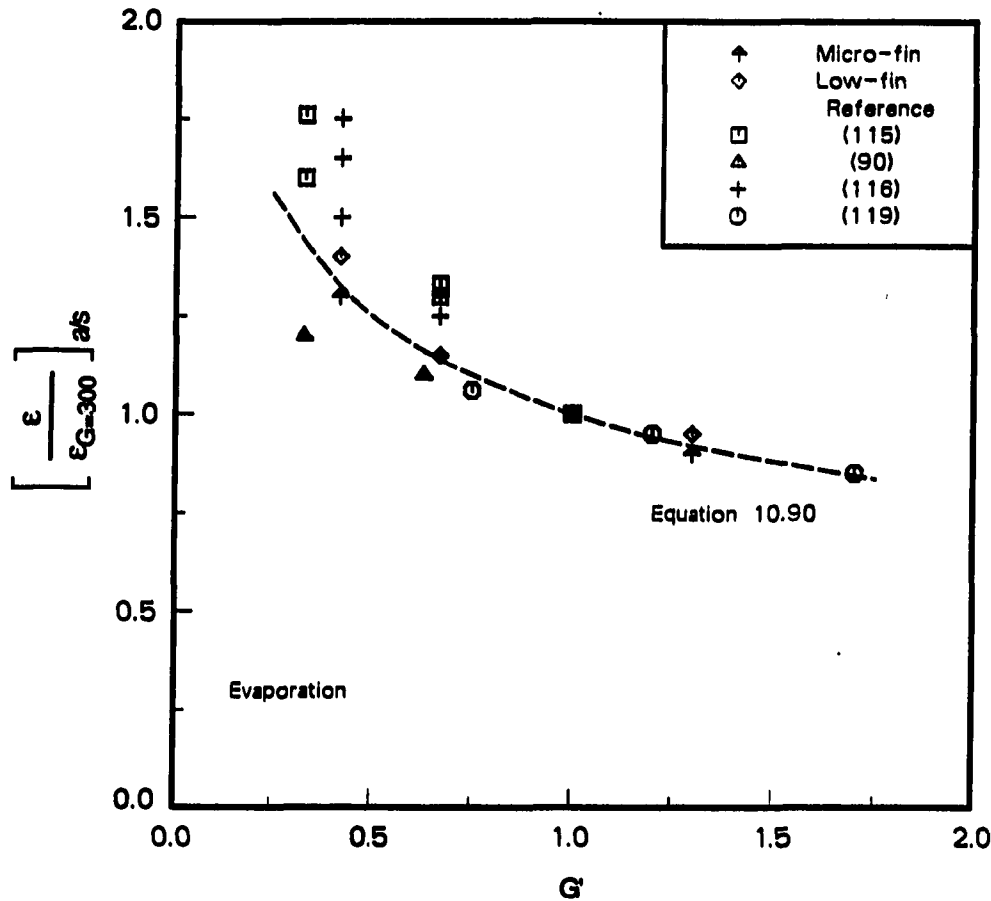


Figure 10.7. Heat transfer enhancement factor ($\epsilon_{a/s}$) versus mass flux, normalized to values at $300 \text{ kg/m}^2\cdot\text{s}$

decrease with increasing mass flux. This trend agrees with data from earlier research with micro-fin tubes [90,115,116,119,122]. These earlier data are pooled with data from the current study to develop an equation for estimating the mass flux effect on heat transfer enhancement. Figure 10.7 plots all of these data, normalized to values of $G = 300 \text{ kg/m}^2\cdot\text{s}$. The current data fall very close to the overall best-fit curve. The following empirical expression represents a best-fit curve ($R^2 = 0.72$) to the data using only one variable and is shown as a dotted line in Figure 10.7:

$$\frac{\epsilon_1}{\epsilon_2} = \left(\frac{G_1}{G_2}\right)^{-0.32} \quad (10.91)$$

The subscripts in Equation 10.91 simply indicate corresponding conditions: ϵ_1 is the heat transfer enhancement factor at a given mass flux, G_1 . Using only data from the current research instead of pooling all of the data, the exponent in Equation 10.91 would be -0.31 , rather than -0.32 .

This equation allows an estimate of heat transfer enhancement at a new mass flux if the enhancement at one mass flux is known. It is recommended that experimental data for the particular tube of interest be used, but if this is not available, data for a similar tube could be found in the literature and a mass flux correction applied to estimate the pure refrigerant performance. There have been insufficient data published to make a similar estimate of the effects of pressure, refrigerant, etc., on the heat transfer enhancement factor.

Condensation: Oil Effects in a Smooth Tube

Previous correlations for refrigerant-oil mixtures The only previous attempt to correlate condensation heat transfer of refrigerant-oil mixtures was that of Tichy et al. [47] (see Equation 10.48), who used 300-SUS oil in R-12. The term that accounts for the effects of oil is a simple decaying exponential

$$\epsilon_s/s = e^{-5.0 \cdot \omega_o} \quad (10.92)$$

A comparison of Equation 10.92 with experimental data is presented in Figure 10.8. The equation underestimates the enhancement factor, but the decreasing trend is modelled. Predictions are within 15% of experimental values over the range of oil concentrations.

General correlations for pure refrigerants Unlike evaporation, the effect of oil on condensation heat transfer is orderly and varies monotonically with oil concentration; oil always degrades heat transfer and the degradation increases as oil concentration increases (see Figures 6.4 and 6.5). A substitution of mixture properties into the condensation correlations [160-162] predicts mixture performance rather well, so it appears that the effect of oil can be described by established principles, as reflected in the correlation expressions. As with evaporation, various oil concentration profiles versus quality are tried to see if agreement improves, but the simplest case of a single, average concentration is satisfactory. (See Figure 10.2 for an illustration of concentration profiles.) The average oil concentration in the condenser, as found during the hold-up tests (see Chapters 6 and 7), is

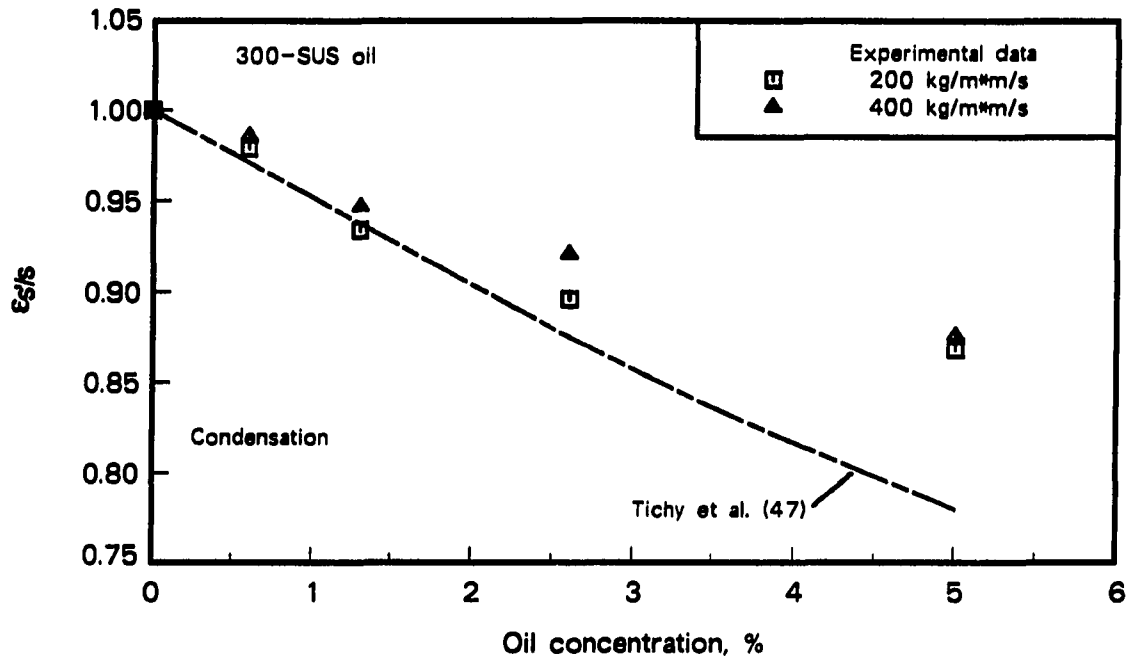


Figure 10.8. Comparison of a refrigerant-oil mixture condensation heat transfer correlation with experimental data

set at 1.6 times the average flowing oil concentration. The effect of mass flux is generally small, and no attempt is made to incorporate a mass flux term in the correlation.

A comparison of predictions of $\epsilon_{s/s}$ derived from each of the three theoretical correlations (see Equations 10.30 through 10.35) with experimental values is presented in Figure 10.9 for both 150- and 300-SUS oil. Agreement is within $\pm 10\%$ for all of the correlations. Even though any of these correlations could be used, those of Cavallini and Zecchin [162] and Shah [160] can be reduced to a simple, easily calculated function of viscosity if it is assumed that specific heat, thermal conductivity, and liquid density remain constant with the addition of oil. This is valid because these properties do, in fact, change much less than viscosity (see Chapter 2). The simplified equation for the enhancement factor based on Cavallini and Zecchin is

$$\epsilon_{s/s} = \left[\frac{\mu_{1r}}{\mu_{1m}} \right]^{0.47} \quad (10.93a)$$

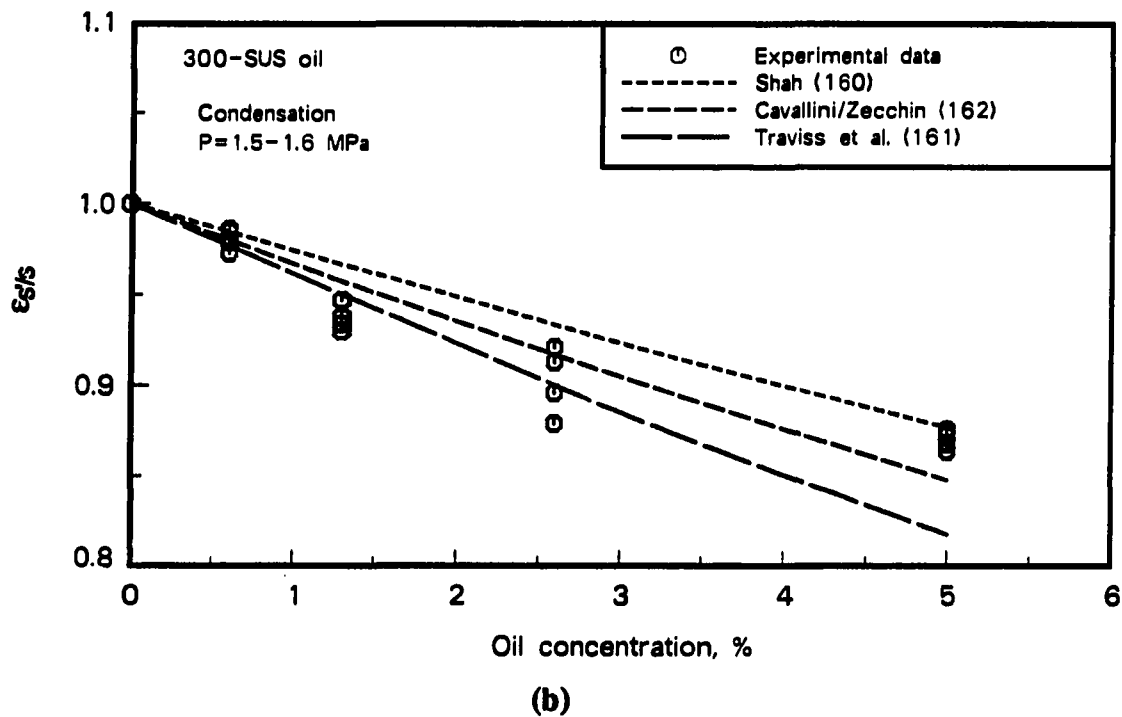
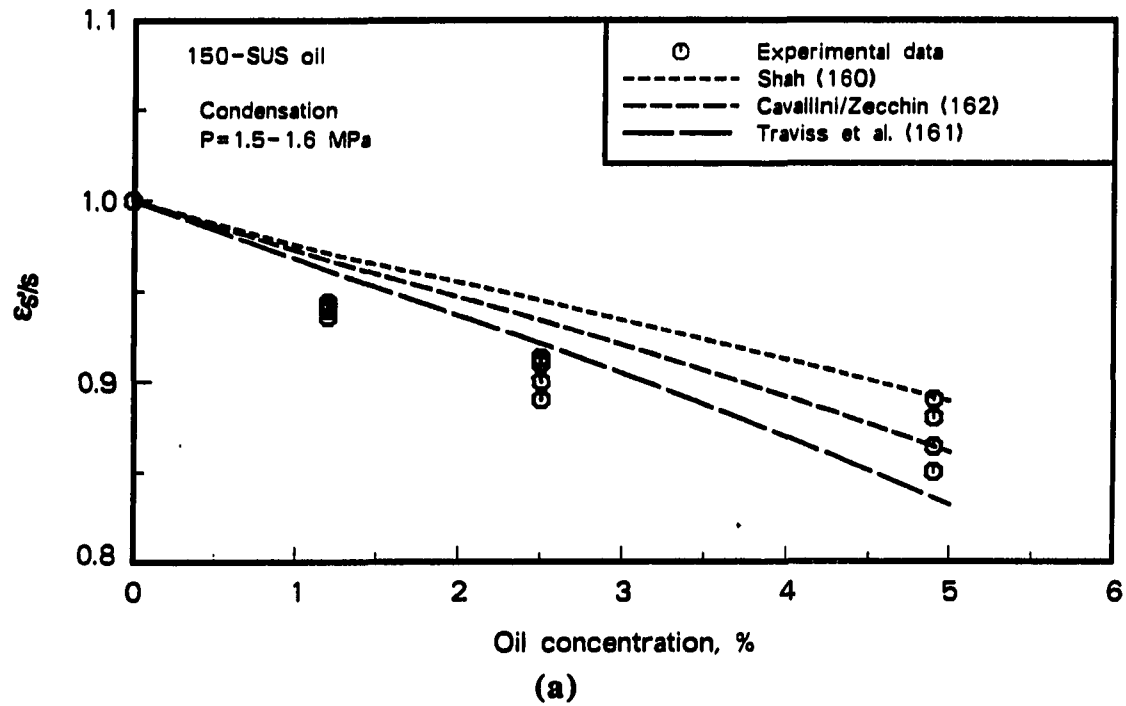


Figure 10.9. Results using refrigerant-oil mixture properties in pure refrigerant condensation heat transfer correlations

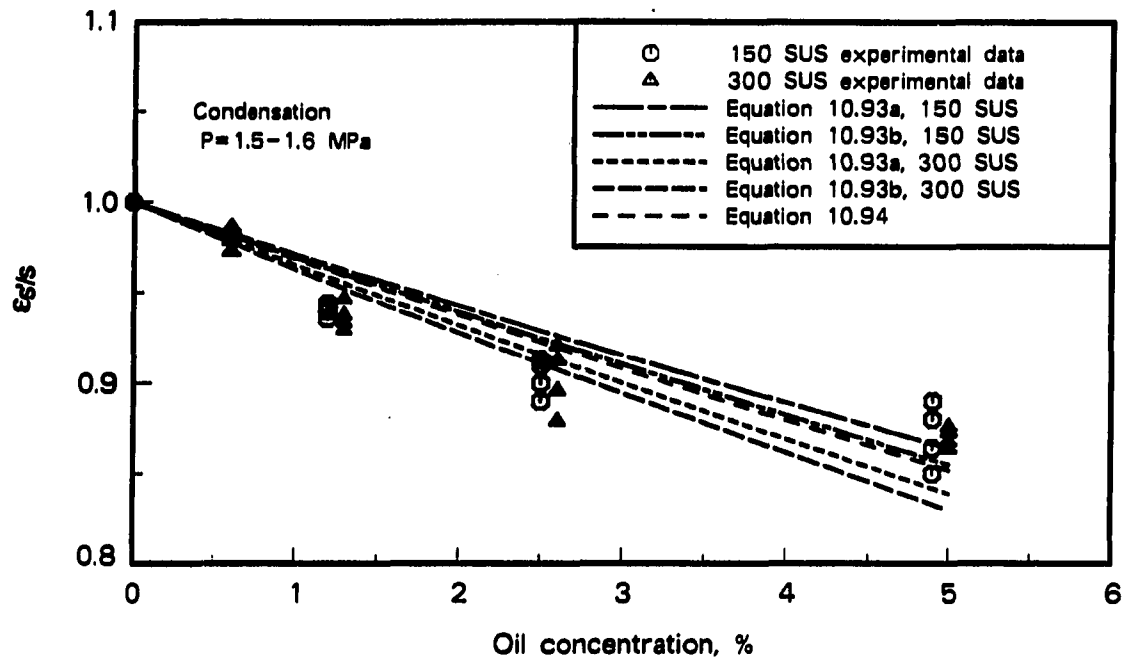


Figure 10.10. Comparison of experimental condensation heat transfer enhancement factors ($\epsilon_{s/s}$) with predictions using statistical and correlation-based equations

From Shah's correlation, it is

$$\epsilon_{s/s} = \left[\frac{\mu_{1r}}{\mu_{1m}} \right]^{0.5} \quad (10.93b)$$

At an oil concentration of 8% in the condenser (the value determined by hold-up tests when the average flowing concentration was 5%), the error introduced by using Equations 10.93 instead of incorporating all of the variable properties in the complete correlations is less than 6% for Shah and less than 3% for Cavallini and Zecchin. Compared to the complete correlations, Equations 10.93 underestimate the heat transfer, with the error becoming smaller as the oil concentration decreases. Figure 10.10 compares experimental heat transfer enhancement factors with those predicted by Equations 10.93. Pooling data for both oil viscosities, a statistical determination of the exponent yields 0.46, indicating that Equation 10.93a is slightly better.

Development of statistical prediction equations Although the three correlations above and Equations 10.93 all predict condensation performance of refrigerant-oil mixtures

well, they require calculation of mixture viscosities. This section presents a simple equation that is of the same form as Tichy's earlier correlation, that fits the current data better. This expression is a simple exponential function of oil mass fraction, thus it does not require the calculation of mixture properties. The equation is

$$\epsilon_{s'/s} = e^{-3.2 \cdot \omega_o} \quad (10.94)$$

The value of R^2 is in excess of 0.9 and all experimental data points are predicted within $\pm 10\%$. A plot of Equation 10.94 is included in Figure 10.10, discussed above.

Condensation: Oil Effects in Finned Tubes

There is no earlier work using refrigerant-oil mixtures in finned tubes with which the current data can be compared. However, the effect of oil in both finned tubes used in this study is similar to that in the smooth tube. For the micro-fin tube, the effect is similar in both tendency and magnitude, while for the low-fin tube, the magnitude of the degradation caused by the oil is somewhat less.

General correlations for pure refrigerants Results with the micro-fin tube are so close to those with the smooth tube that no modifications to the correlations are made. Equations 10.93 and 10.94 apply without modification to the micro-fin tube. With the low-fin tube, heat transfer degradation is only about 40% as large as with the other two tubes and this behavior is reflected in a correction term. Like the smooth tube, the finned tubes did not show a mass flux dependence strong enough to warrant the inclusion of a separate mass flux term. For the micro-fin tube,

$$(\epsilon_{a'/a})_{m-f} = \epsilon_{s'/s} \quad (10.95)$$

For the low-fin tube, the following expression fits the experimental data

$$(\epsilon_{a'/a})_{l-f} = 0.4 \cdot (1.5 + \epsilon_{s'/s}) \quad (10.96)$$

The value of $\epsilon_{s'/s}$ is obtained from Equations 10.93 or 10.94. Figure 10.11 shows a comparison of experimental results with the predictions of Equations 10.95 and 10.96. All data points lie within $\pm 10\%$ of predicted values but the fit is not quite as good as with smooth tube data (see Figure 10.10).

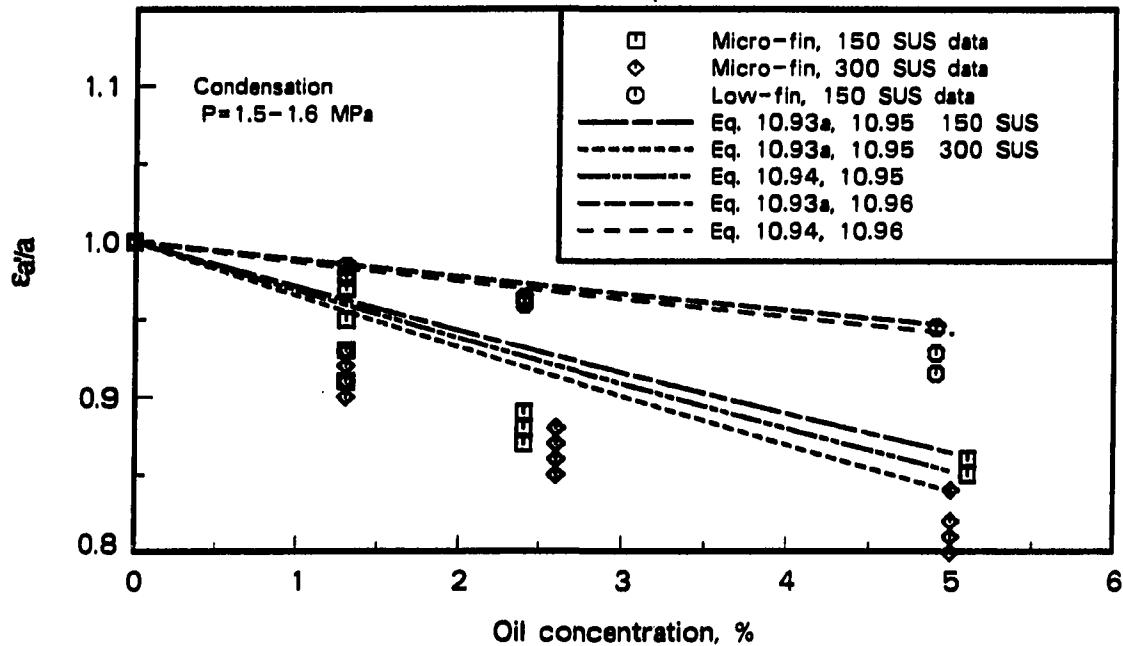


Figure 10.11. Comparison of experimental condensation heat transfer enhancement factors (ϵ_a/a) with predictions using correlation-based equations

Development of statistical prediction equations Equation 10.94, developed for the smooth tube, can be used with reasonable accuracy for the micro-fin tube, but a separate equation of the same form is presented here:

$$(\epsilon_a/a)_{m-f} = e^{-4.0 \cdot \omega_o} \quad (10.97)$$

The constant in the exponent changes from -3.2 in Equation 10.94 to -4.0 in Equation 10.97. Fitting low-fin tube data to the same functional form, the following expression is obtained:

$$(\epsilon_a/a)_{l-f} = e^{-1.7 \cdot \omega_o} \quad (10.98)$$

Plots of these equations with experimental data points are shown in Figure 10.12.

Condensation: Effects of Internal Fins with Pure Refrigerant

Earlier comments regarding evaporation correlations in internally finned tubes generally apply to condensation as well. To date, no correlation has been developed that can a priori predict condensation performance for a variety of tube geometries without empirical,

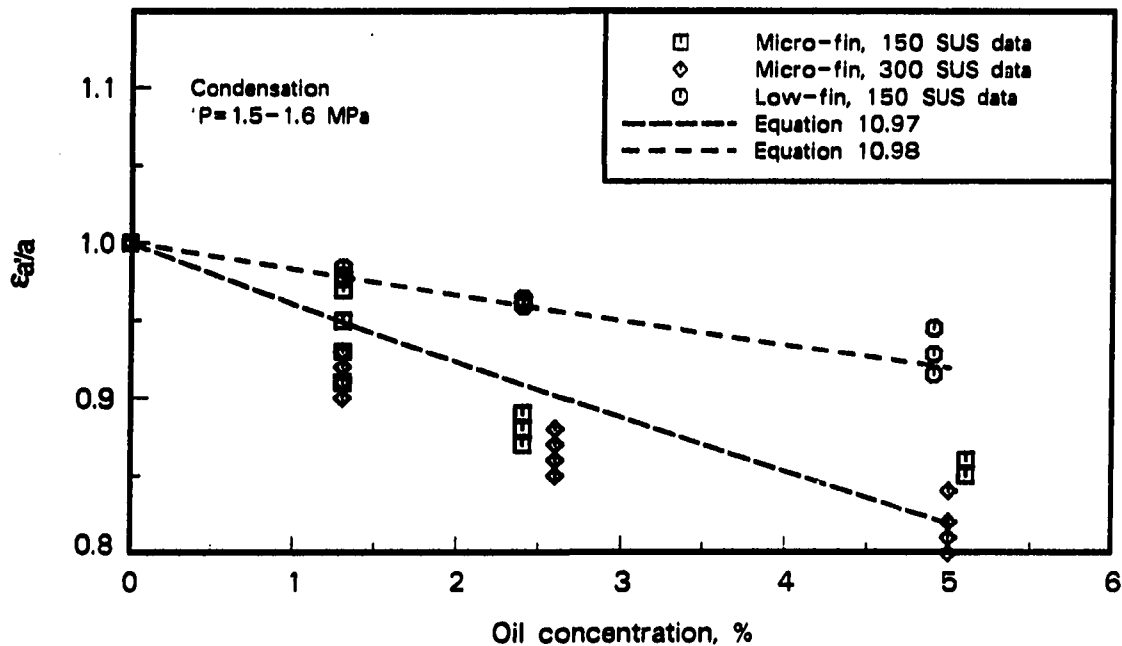


Figure 10.12. Comparison of experimental condensation heat transfer enhancement factors ($\epsilon_{a/a}$) with predictions using statistical equations

geometry-specific constants. The range of tube geometries tested in this study was not sufficient to develop correlations beyond those developed by earlier workers.

Previous correlations No correlations for condensation in micro-fin tubes were found so no comparisons are presented here. Three correlations were found that predicted condensation heat transfer in tubes similar to the low-fin tube used in the current study. Luu [134] used a simple geometric correction factor (see Equation 10.40) and determined an exponent statistically. Substituting appropriate values into Luu's expression and using his exponent, an enhancement factor of 2.3 is predicted for the current low-fin tube, irrespective of mass flux. This is about 10% higher than the experimental value at the lowest mass flux and 30% higher at the highest mass flux.

Azer and Said [143] determined exponents for three geometric parameters as shown in Equation 10.41. At low and high mass fluxes, the predicted values of $\epsilon_{a/s}$ for the low-fin tube used in the current study are 2.8 and 3.0, respectively. These predictions are significantly higher than the experimental values, which are 2.1 and 1.6 at the same mass

fluxes. This correlation has a weak mass flux dependence, but the trend is opposite to that seen in the current data.

Kaushik and Azer [186] used the same basic approach [143], but included a much broader data base. Using this correlation, the enhancement factor does not have a mass flux dependence. Substituting parametric values for the low-fin tube into the correlation, a predicted enhancement factor, $\epsilon_{a/s}$, of 1.9 is obtained. This value agrees with experimental data at a medium mass flux (200 kg/m²·s) and is within $\pm 10\%$ over the entire mass flux range tested.

Development of statistical prediction equations The effect of mass flux was investigated to see if an expression similar to Equation 10.91 could be developed. The trend of decreasing enhancement factor with increasing mass flux, as observed in the current test program, is not consistently supported by the literature. This is in contrast to evaporation, for which most of the literature reported similar trends, particularly for micro-fin tubes.

Already mentioned was the correlation of Azer and Said, which predicts increasing $\epsilon_{a/s}$ with increasing mass flux in low-fin tubes. This increasing trend of $\epsilon_{a/s}$ was also reported by Tatsumi et al. [115]. Several studies [144, 116, 119] found trends that differ depending on the tube; with some tubes, $\epsilon_{a/s}$ increased and with others it decreased. Finally, some studies [90, 134] reported results similar to those reported here.

Since trends from the literature are inconsistent, data from different sources are not pooled as with evaporation, but rather only data from the current study (both micro-fin and low-fin tubes) are used to determine the following equation:

$$\frac{\epsilon_1}{\epsilon_2} = \left(\frac{G_1}{G_2}\right)^{-0.21} \quad (10.99)$$

Again, the subscripts are simply to match corresponding values of ϵ and G . Figure 10.13 plots Equation 10.99 and data from the current investigation on axes normalized with respect to a mass flux of 300 kg/m²·s. Also included in the figure are data from the literature, but these data were not used when determining the exponent in Equation 10.99. The conflicting trends and data scatter are evident in the figure.

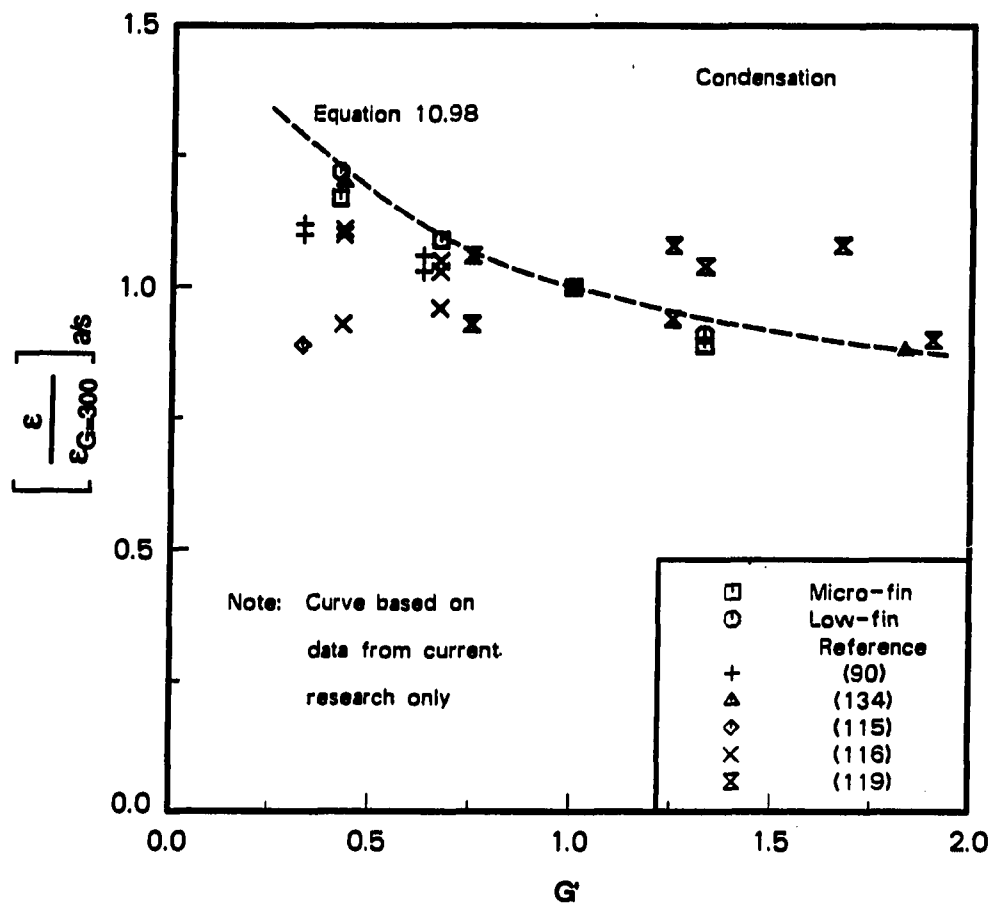


Figure 10.13. Condensation heat transfer enhancement factor ($\epsilon a/s$) versus mass flux, normalized to values at $300 \text{ kg/m}^2 \cdot \text{s}$

Correlation of Experimental Pressure Drop Results

The form, limitations, and development method of the pressure drop prediction equations are quite similar to those for heat transfer. Correlations of past investigators (pure refrigerant, refrigerant-oil mixtures, or finned tubes) are first examined, and then purely statistical equations are also determined.

The development of pressure drop correlations from the current data is complicated somewhat by large relative uncertainties in the experimental data (see Chapters 6 to 8). In addition, correlations that predict pressure drop generally have a higher inherent uncertainty

than those predicting heat transfer. For these reasons, the development of physically-based, generalized correlations is even more difficult for pressure drop than for heat transfer.

Due to higher uncertainties, with both experimental data and the correlations, several simplifications and modifications are made to the procedure used to develop predictive equations. These are (1) criteria for a satisfactory fit are relaxed somewhat, (2) mass flux dependence of the enhancement factor is generally ignored, (3) the momentum component of pressure drop is estimated with the homogeneous model, and (4) no calculations or correlations are attempted at the lowest mass flux due to uncertainties.

Evaporation: Oil Effects in a Smooth Tube

Previous correlations for refrigerant-oil mixtures Only two correlations of refrigerant-oil mixture pressure drop were found in the literature, the first being that of Pierre [44] (see Equation 10.78). This correlation is similar to Pierre's pure refrigerant correlation (Equation 10.55), but includes different values for the constants. The equation is not a function of oil concentration and was developed for 6% to 12% average flowing oil concentration (by volume), somewhat higher than in the results reported here. The oil type was not specified and was mixed with R-12. A calculation of the pressure drop enhancement factor, $\Psi_{s/s}$, based on a ratio of Equations 10.78 and 10.55, yields 2.6. This is almost twice the maximum experimental value using 150-SUS oil. Only the highest concentration from the current data is used for comparison since it approximates the low end of Pierre's data.

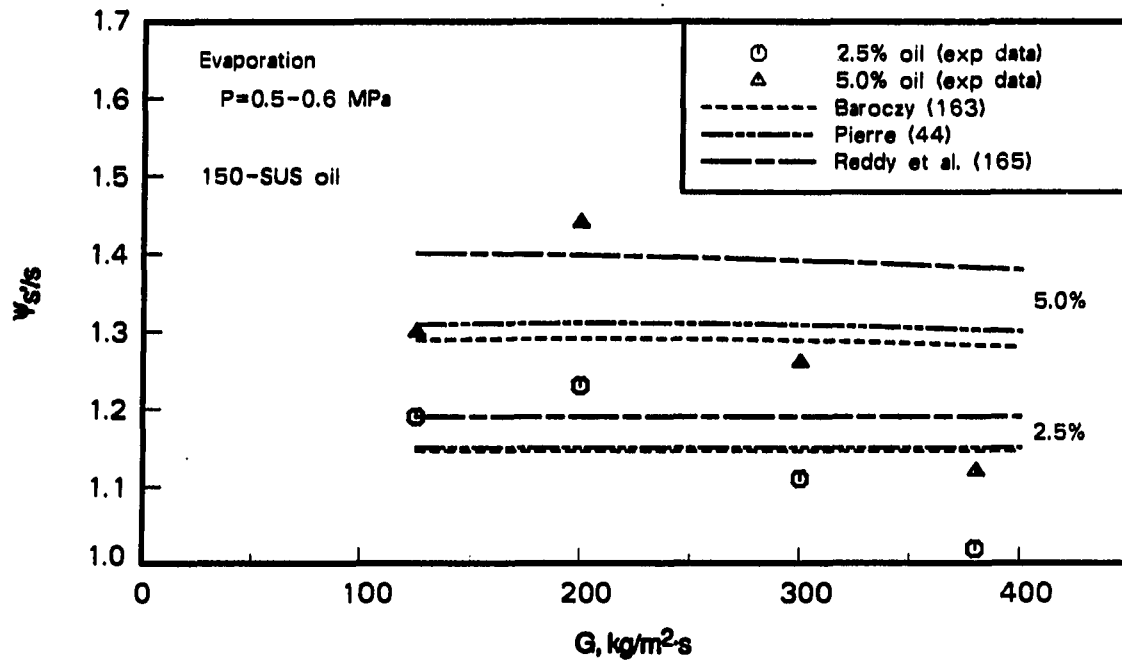
The second published correlation is that of Tichy et al. [41], which uses a simple quadratic function of oil concentration to describe the pressure drop enhancement factor due to 300-SUS oil in R-12 (see Equation 10.79a). This equation yields pressure drop enhancement factors of 1.7 and 1.9 for concentration of 2.5% and 5%, respectively. At these same conditions (300-SUS oil and 200 to 300 kg/m²-s), experimental data from the current investigation are around 1.2 and 1.5. As with the Pierre correlation, data from the current test program are lower than predicted, but agreement with the correlation of Tichy is somewhat better.

Application of general correlations to refrigerant-oil mixtures As was done for heat transfer, property values for refrigerant-oil mixtures are inserted into pure refrigerant correlations [44,75,163-165] to see if properties such as viscosity, density, etc., are sufficient to predict pressure drop performance. For local correlations requiring numerical integration to obtain total pressure drop, local liquid oil concentration is estimated using three concentration profiles: constant, linearly increasing, and quadratically increasing (see Figure 10.2). As with evaporation, the concentration profile has only a minor effect on results, so a constant oil concentration (having a value of three times the flowing average) is used in the evaporator. Because calculations are in terms of enhancement factors, even correlations that show poor agreement with pure refrigerant in the smooth tube (see Chapter 6) are included to see if they might satisfactorily predict relative, rather than absolute, performance with oil.

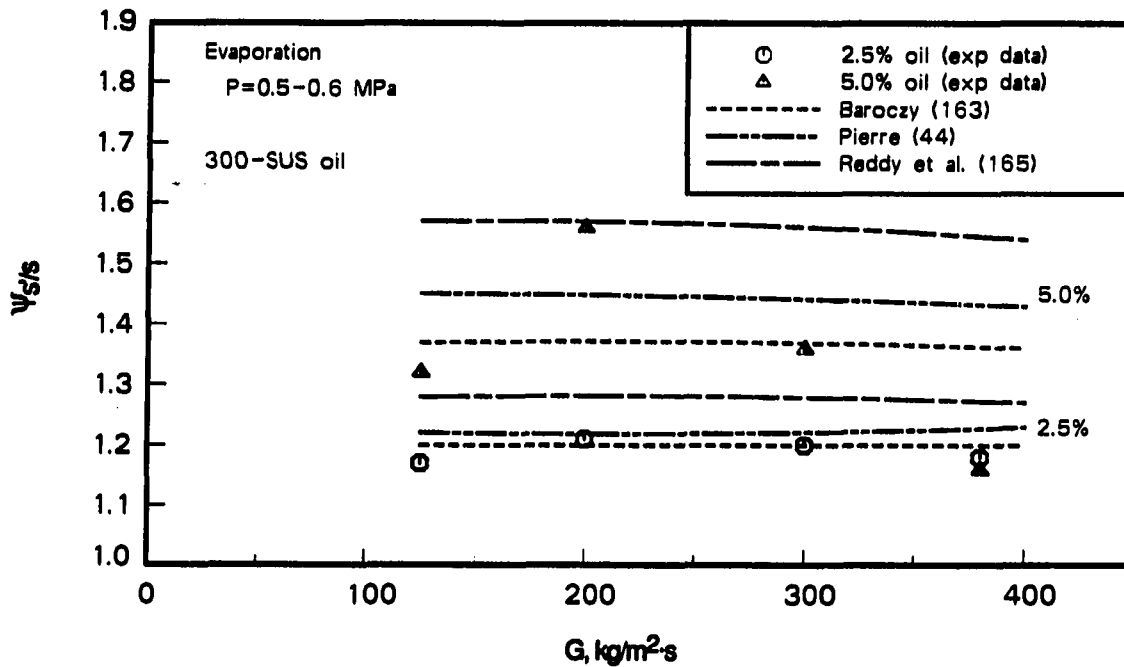
Pressure drop enhancement factors calculated from the previous correlations show virtually no mass flux dependency for any of the correlations. Experimental data show some cases with an apparently large mass flux dependence and others with very little dependence (for an example, see Figure 6.12). However, as discussed earlier, the uncertainties associated with these data are quite large and a mass flux dependence is not included. Of the six pressure drop correlations, all predict an increased pressure drop with the addition of oil, but three greatly underpredict the magnitude of the increase and three are in relatively good agreement. Figure 10.14 includes the three best correlations [44,163,165] and compares these with experimental data as shown earlier in Figure 6.12. Experimental results are generally within $\pm 30\%$ of predictions.

The three correlations not satisfactorily predicting the pressure drop increase are homogeneous, Lockhart and Martinelli [75], and Chisholm [164]. Interestingly, two of these correlations predict the absolute magnitude of pressure drop with pure refrigerant quite well (see Figure 6.9), but nonetheless fail to predict the effect of oil.

Of the three correlations that correctly predict trends with oil, only that of Baroczy [163] is local and thus has to be integrated. This correlation is based on charts and is somewhat cumbersome to implement numerically. The program used to calculate the Baroczy correlation estimates the chart curves in the vicinity of the operating conditions with



(a)



(b)

Figure 10.14. Results using refrigerant-oil mixture properties in pure refrigerant condensation pressure drop correlations

linear approximations. The chart form also prevents the isolation of any particular property effect(s) in order to simplify the relationship between $\Psi_{s/s}$ and oil concentration.

The Pierre pure refrigerant correlation [44] shows reasonably good agreement, however, as discussed in the previous subsection, Pierre actually developed a second correlation with different constants to account for the effects of oil, so this correlation is not intended to be used with oil. The primary factor in this correlation that changes with oil is the liquid viscosity used to determine the Reynolds number. Because of the additive nature of the friction and momentum terms, the ratio of pressure drop predicted with oil to pressure drop predicted with pure refrigerant does not reduce to a simple expression. From Equations 10.55 through 10.57

$$\Psi_{s/s} = \frac{\left[0.0185 \cdot (\text{Re}_{10} \cdot K^{-1})^{-1/4} + \frac{(X_2 - X_1) \cdot d}{X \cdot l} \right]_m}{\left[0.0185 \cdot (\text{Re}_{10} \cdot K^{-1})^{-1/4} + \frac{(X_2 - X_1) \cdot d}{X \cdot l} \right]_r} \quad (10.100)$$

Because the second term (momentum) is small compared to the first term (friction), the enhancement factor based on Pierre's correlation can be approximated by the following expression with errors generally less than 10% for the conditions used in the current research:

$$\Psi_{s/s} \approx \left[\frac{\mu_{1m}}{\mu_{1r}} \right]^{0.25} \quad (10.101)$$

This expression overestimates $\Psi_{s/s}$ by 5% to 10% when compared to Equation 10.100. The mixture viscosity is evaluated at a concentration of three times the flowing average, which accounts for the experimentally determined hold-up in the evaporator (see Chapters 6 and 7).

The Reddy et al. [165] correlation does not predict pure refrigerant pressure drop well, but does predict the effect of oil relatively well. Except for the negligible effect of density with oil, the change in the prediction with oil addition is not due to the two-phase friction multiplier, ϕ_{10}^2 from Equation 10.70, but rather due to the single-phase similarity term (see Equations 10.1, 10.50, and 10.51). This correlation has no additive term for the momentum component, so a ratio of mixture predictions to pure refrigerant predictions can

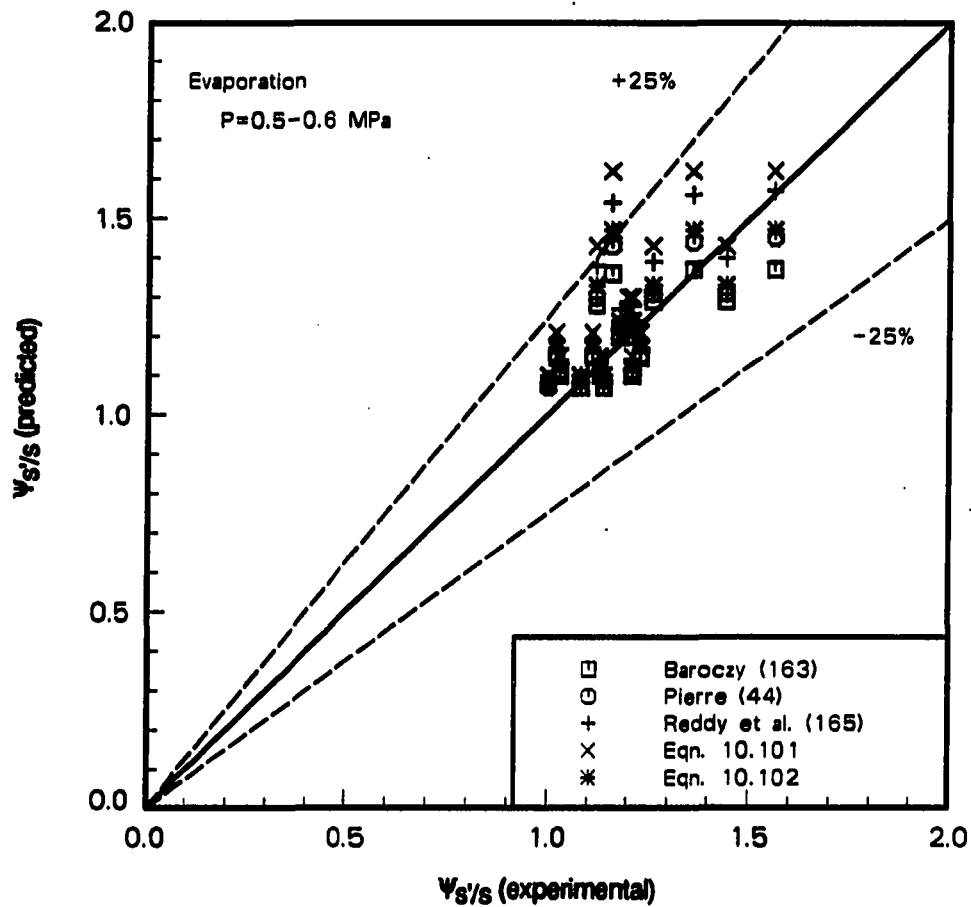


Figure 10.15. Comparison of experimental evaporation pressure drop enhancement factors ($\Psi_{s/s}$) with predictions using correlations and correlation-based equations

be reduced to the following for high Reynolds numbers (as encountered in the current research):

$$\Psi_{s/s} = \left[\frac{\mu_{1m}}{\mu_{1r}} \right]^{0.2} \quad (10.102)$$

This expression is very similar to Equation 10.101 above, and once again the viscosity is evaluated at a concentration of three times the flowing average.

Figure 10.15 plots the predictions of the three best correlations, as well as the simplifications derived from these correlations (Equations 10.101 and 10.102), comparing these with experimental values. Agreement of predictions and experiment is generally within $\pm 25\%$, although the band must be broadened to $\pm 30\%$ to include all of the data.

Development of statistical prediction equations As mentioned in the introduction to the pressure drop section, no mass flux dependency is included in the predictive equations even though there appears to be such a dependency in some cases. The RS/1 [194] statistical package was used as required to determine values of constants in the prediction equations.

Because a ratio of viscosities was previously used successfully in predicting the pressure drop increase due to oil, the first equation presented here shows the best fit exponent on a simple ratio of viscosities. Mixture viscosities are once again evaluated at three times the system average. The equation is determined by pooling all of the data (except that at lowest mass flux).

$$\Psi_{s'/s} = \left[\frac{\mu_{1m}}{\mu_{1r}} \right]^{0.16} \quad (10.103)$$

This equation predicts values of $\Psi_{s'/s}$ slightly lower than the approximations derived from the correlations of Pierre and Reddy et al. (Equations 10.101 and 10.102). Comparing Equation 10.103 to values of $\Psi_{s'/s}$ from the complete correlations above, this equation predicts values within $\pm 2\%$ of those from the Baroczy correlation.

As with heat transfer, predictive equations that are explicit functions of oil concentration and do not require integration or the calculation of properties are presented for pressure drop. The method to determine these equations is similar to that described earlier in the heat transfer discussion, but R^2 is somewhat lower for pressure drop (about 0.7 versus 0.9 for heat transfer). Both polynomial and exponential expressions are presented, with the exponential expressions having a slightly higher value of R^2 . A first-order expression in mass fraction has virtually the same fit as a quadratic, so the simpler expressions are shown.

For 150-SUS oil, the following equations can be used to predict $\Psi_{s'/s}$:

$$\text{polynomial:} \quad \Psi_{s'/s} = 5.43 \cdot \omega_o + 1.01 \quad (10.104a)$$

$$\text{exponential:} \quad \Psi_{s'/s} = 1.01 \cdot e^{4.69 \cdot \omega_o} \quad (10.104b)$$

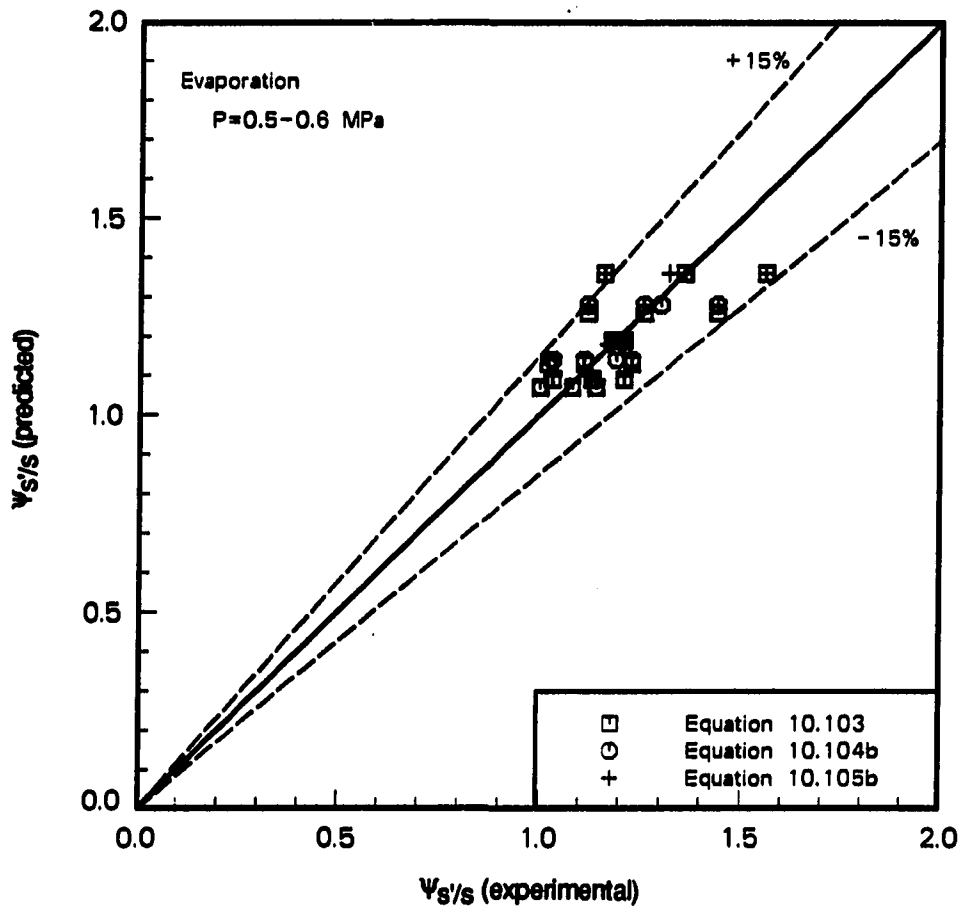


Figure 10.16. Comparison of experimental evaporation pressure drop enhancement factors ($\Psi_{s/s}$) with predictions using statistical equations

and for 300-SUS oil:

polynomial: $\Psi_{s/s} = 6.68 \cdot \omega_0 + 1.02$ (10.105a)

exponential: $\Psi_{s/s} = 1.03 \cdot e^{5.59 \cdot \omega_0}$ (10.105b)

These equations agree quite closely with Equation 10.103 and predictions based on the Baroczy correlation lie closest to these curves. Figure 10.16 plots experimental versus predicted pressure drop enhancement factors for Equations 10.103, 10.104b, and 10.105b. Experimental results lie within $\pm 25\%$ of predictions.

Evaporation: Oil Effects in Finned Tubes

There are no existing correlations of refrigerant-oil pressure drop in finned tubes. The only pure refrigerant correlation for finned tubes (Azer and Sivakumar [109], discussed below) is based on the earlier correlation of Pierre, whose application to refrigerant-oil mixtures has already been discussed.

Application of general correlations to refrigerant-oil mixtures The correlations that show success with refrigerant-oil mixtures in smooth tubes are also applied to the finned tubes, because pressure drop trends with oil are similar. A comparison of predicted and experimental results is presented in Figure 10.17. As with the smooth tube, predictions generally lie within $\pm 25\%$ of experimental values, with only a few points outside of this range. The effect of oil on pressure drop appears to result primarily from viscosity changes in the mixture and remains similar, regardless of surface geometry.

Development of statistical prediction equations The same types of equations that are presented for smooth tubes are also shown for finned tubes: an equation based on a ratio of viscosities and equations that require only oil concentration as an input. Due to uncertainties, mass flux dependent terms as well as results at the lowest mass flux are not included in the statistical procedure.

Fitting an exponent to the ratio of viscosities gives, for the micro-fin tube,

$$(\Psi_{a/a})_{m-f} = \left[\frac{\mu_{1m}}{\mu_{1r}} \right]^{0.16} \quad (10.106a)$$

and for the low-fin tube,

$$(\Psi_{a/a})_{l-f} = \left[\frac{\mu_{1m}}{\mu_{1r}} \right]^{0.14} \quad (10.106b)$$

The exponent for the micro-fin tube is the same as for the smooth tube and for the low-fin tube it is only slightly smaller. At the mixture concentrations used in the current study, the difference between these two equations is less than 3%.

Equations are also given to predict pressure drop performance from the oil concentration, without needing to determine fluid properties. Equivalent polynomial and exponential forms of the equations are presented for each case. As with the smooth tube, a

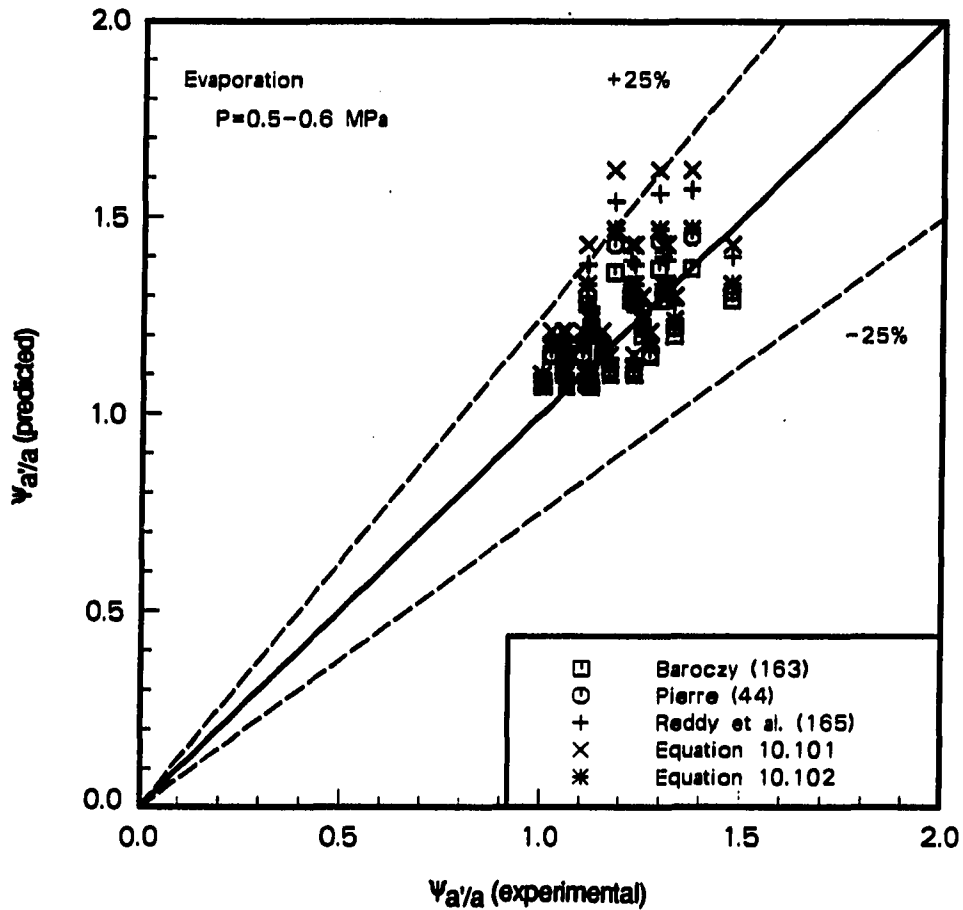


Figure 10.17. Comparison of experimental evaporation pressure drop enhancement factors ($\Psi_{a/a}$) with predictions using correlations and correlation-based equations

first-order expression in oil mass fraction is nearly as good as a second-order expression, so the simpler form is shown below. For mixtures with 150-SUS oil in the micro-fin tube,

$$\text{polynomial:} \quad (\Psi_{a/a})_{m-f} = 6.03 \cdot \omega_o + 0.99 \quad (10.107a)$$

$$\text{exponential:} \quad (\Psi_{a/a})_{m-f} = e^{5.13 \cdot \omega_o} \quad (10.107b)$$

in the low-fin tube

$$\text{polynomial:} \quad (\Psi_{a/a})_{l-f} = 4.92 \cdot \omega_o + 0.99 \quad (10.108a)$$

$$\text{exponential:} \quad (\Psi_{a/a})_{l-f} = 0.99 \cdot e^{4.38 \cdot \omega_o} \quad (10.108b)$$

and for 300-SUS oil in

$$\text{polynomial:} \quad (\Psi_{a/a})_{m-f} = 5.26 \cdot \omega_o + 1.05 \quad (10.109a)$$

$$\text{exponential:} \quad (\Psi_{a/a})_{m-f} = 1.05 \cdot e^{4.58 \cdot \omega_o} \quad (10.109b)$$

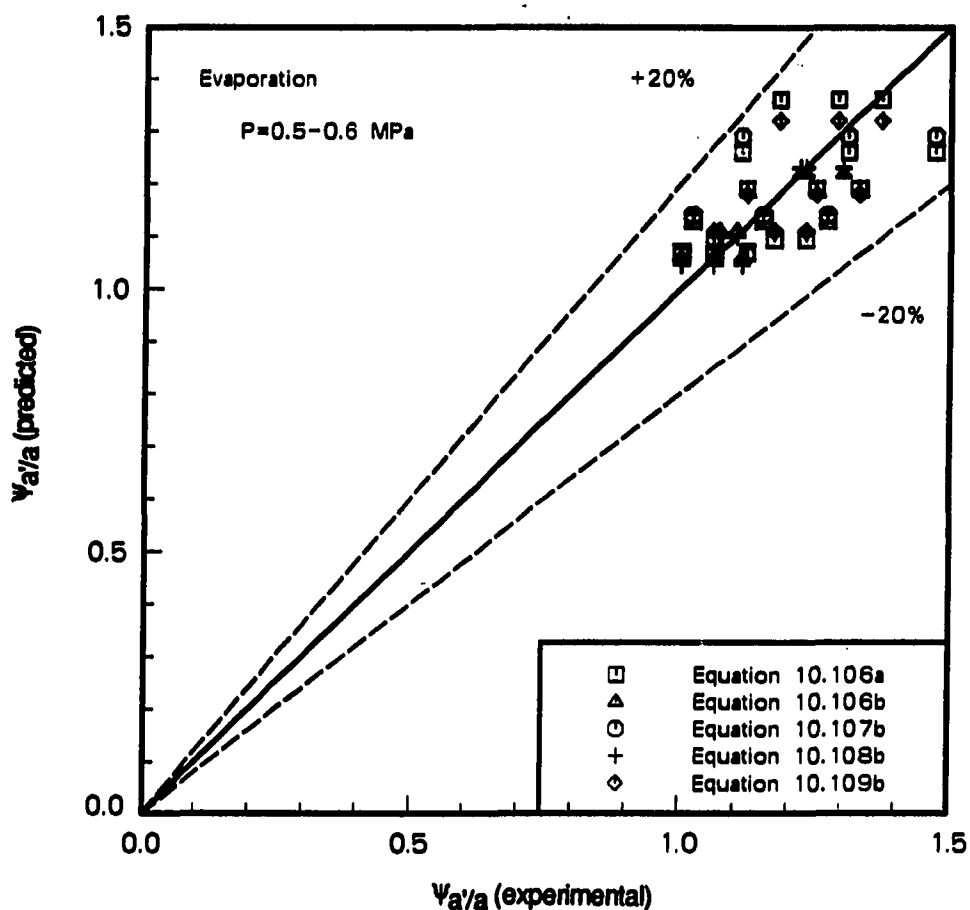


Figure 10.18. Comparison of experimental evaporation pressure drop enhancement factors ($\Psi_{a/a}$) with predictions using statistical equations

For the micro-fin tube, fits are not quite as good as with the smooth tube, with R^2 values of about 0.6 (versus 0.7 in the smooth tube). The low-fin tube, however, has a better correlation coefficient, with R^2 of about 0.8. The better statistical fit with the low-fin tube is due to flatter curves of $\Psi_{a/a}$ versus mass flux (for example, see Figures 7.18 and 8.17).

A comparison of experimental and predicted results for Equations 10.106, 10.107b, 10.108b, and 10.109b is shown in Figure 10.18. Results generally lie within a $\pm 20\%$ band.

Evaporation: Effects of Internal Fins with Pure Refrigerant

Previous correlations No predictive equations for pressure drop in micro-fin tubes were found in the literature, and correlations for tubes similar to the low-fin tube were

limited to one [109] (see Equations 10.76 and 10.77). This correlation, developed with R-113, uses geometric parameters similar to those used in several of the heat transfer correlations for finned tubes, but also uses a modified friction factor expression for finned tubes. There was no correlation for smooth tube pressure drop included in the paper, so no enhancement factors are calculated from the correlation. Using the correlation to estimate total pressure drop in the low-fin tube, a value of 9 kPa is obtained for 200 kg/m²·s, versus around 18 kPa from experimental data. Although the correlation does not predict pressure drop magnitude for the low-fin tube very well, extracting an enhancement factor from one of the figures in the paper yields a value of about 1.8. This agrees well with experimental values, which range from around 1.6 to 1.8.

Development of statistical prediction equations As with heat transfer, it is recommended that experimental data for the tube of interest be used to determine pure refrigerant pressure drop in augmented tubes. This is due to the wide variety of geometries and the lack of any good predictive equations based on geometric parameters.

Because high pressure drop uncertainties prevent the drawing of firm conclusions about secondary effects, the equations proposed to predict pressure drop enhancement factors for the two augmented tubes used in this study are simply constants, with no attempt to include geometric, property, or condition-specific terms. These values are determined at a mass flux of around 300 kg/m²·s, because uncertainties are generally lowest at this mass flux. For the micro-fin tube, the pressure drop enhancement factor is estimated simply as

$$(\Psi_{a/s})_{m-f} = 1.4 \quad (10.110)$$

and for the low-fin tube as

$$(\Psi_{a/s})_{l-f} = 1.7 \quad (10.111)$$

Condensation: Introduction

Condensation pressure drop results display inconsistent trends with the addition of oil. Pressure drop decreases significantly with 150-SUS oil and increases slightly or remains constant with 300-SUS oil at most conditions. As discussed earlier, these results may be due to a particular combination of geometry and flow conditions, causing flow

pattern transitions that do not correspond to those predicted by flow regime maps and, hence, leading to unanticipated pressure drop results. Inconsistent trends, whose physical basis is not understood, along with high experimental uncertainties for condensation pressure drop, combine to make the equations presented here and in the following sections less certain than those presented earlier in this document.

In spite of the difficulties when dealing with condensation pressure drop, it should be noted that pressure drop in the condenser is generally smaller than that in the evaporator. Therefore, in spite of difficulties dealing with condensation pressure drop, precise predictions of condensation pressure drop is not as critical to the accurate prediction of overall system performance as is evaporation pressure drop.

Condensation: Oil Effects in a Smooth Tube

Previous correlations for refrigerant-oil mixtures No experimental results or predictive equations have been published using 150-SUS oil, so the observed decrease of pressure drop with the addition of oil cannot be compared to previous work. The correlation with 300-SUS oil discussed in the following paragraph shows a minor increase in pressure drop with the addition of oil.

Tichy et al. [47] developed the only correlation found in the literature to predict condensation pressure drop of refrigerant-oil mixtures (see Equation 10.79b). As with their evaporation correlation, the effect of oil is represented by a simple polynomial in oil mass fraction multiplied by a pure refrigerant correlation. Using the correlation to predict the pressure drop enhancement factor due to oil ($\Psi_{s/s}$) yields 1.03 and 1.06 for concentrations of 2.5% and 5%, respectively. Experimental results in the mass flux range of 200 to 300 kg/m²·s (300-SUS oil only) are between 1.2 and 1.0 (see Figure 6.14). There is, however, no definite trend in $\Psi_{s/s}$ with increasing oil concentration—in general, 2.5% oil has the highest pressure drop, 5.0% oil has the lowest, and 1.25% oil lies in the middle. Experimental values lie within 20% of those predicted by Tichy, however, this relatively good agreement is principally a result of the close grouping of all the data points. The data do not actually reflect the trend predicted by the correlation, but rather show no definitive trend with either oil concentration or mass flux.

Application of general correlations to refrigerant-oil mixtures As was done with evaporation, the substitution of mixture properties into existing pressure drop correlations is discussed for condensation. The homogeneous model predicts virtually no change with the addition of oil, while the other correlations, with the exception of Baroczy [163], predict modest pressure drop increases with oil. There is almost no distinction between the two oils for any of the correlations, with the predicted increase ranging from 4% to 9% with 5% average oil concentration (corresponding to an experimentally determined concentration of 8% oil in the condenser). For the correlations that reduce to viscosity ratios [44,165], these results are not unexpected. It is interesting to note that the correlation discussed in the preceding paragraph [47] predicts pressure drop increases quite close to those predicted by pure refrigerant correlations with mixture properties inserted.

The Baroczy correlation [163] differs from the others by predicting pressure drop decreases with the addition of oil. Due to the inaccuracy involved with linearizing the curves on Baroczy's charts, this result may, in part, be due to errors in translating the charts to a computer code. However, hand calculations verified the general results. For oil concentrations up to at least 8% in the condenser (5% average flowing concentration), the correlation predicts decreasing pressure drop with increasing oil concentration. Predictions for both oils are similar, but the pressure drop falls slightly more with 300-SUS oil than with 150-SUS oil. At this concentration, the predicted pressure drop decrease is around 12% for 300-SUS oil and 10% for 150-SUS oil. The Baroczy correlation predicts decreasing pressure drop because as viscosity increases, ϕ_{10}^2 decreases faster (from Baroczy's charts) than f_{10} increases (from Equations 10.1 and 10.51).

Although the Baroczy correlation predicts a pressure drop decrease, which agrees with observations from the current test program for 150-SUS oil, the prediction of an even greater pressure drop decrease with a more viscous oil contradicts current results. In addition, the magnitude of the observed pressure drop decrease with 150-SUS oil is significantly greater than that predicted by the correlation.

None of the correlations for pure substances adequately predict the effect of oil during condensation, so the discussion proceeds to the statistical prediction approach.

Development of statistical prediction equations The general approach to developing statistical prediction equations is similar to that described previously: to seek a combination of variables with the RS/1 [194] package to give a satisfactory curve fit with a minimum number of statistically determined constants. As with evaporation, mass flux dependence is neglected and data at $125 \text{ kg/m}^2\cdot\text{s}$ are not included in the curve fits. Unlike evaporation, the viscosity ratio is not used as the basis for a predictive expression because the data do not follow the trend predicted by such a ratio.

Equations similar to those shown earlier are shown below for condensation with mixtures of 150-SUS oil. The equations are functions only of system-average oil concentration and require no calculation of mixture properties. In order for the predicted pressure drop enhancement factor to approximate 1.0 as oil concentration approaches 0%, it is necessary to use second-order terms in the equations, although these terms are not required for an acceptable value of R^2 . Values of R^2 are around 0.9 for both equivalent expressions, one polynomial and one exponential:

$$\text{polynomial:} \quad \Psi_{s'/s} = 361 \cdot \omega_o^2 - 25.4 \cdot \omega_o + 0.99 \quad (10.112a)$$

$$\text{exponential:} \quad \Psi_{s'/s} = e^{(453 \cdot \omega_o^2 - 32.2 \cdot \omega_o)} \quad (10.112b)$$

Experimental and predicted values of $\Psi_{s'/s}$ are compared in Figure 10.19 and agreement is within $\pm 15\%$.

Because of the lack of clear performance trends with increasing concentrations of 300-SUS oil, both polynomial and exponential expressions give curves with poor goodness of fit ($R^2 < 0.1$). However, the range of values for $\Psi_{s'/s}$ is narrow, so a simple constant of 1.0 predicts all experimental values of $\Psi_{s'/s}$ with $\pm 20\%$. No statistical equation is proposed for smooth tube condensation pressure drop with 300-SUS oil. It appears that the assumption of no change in pressure drop with the addition of oil ($\Psi_{s'/s} = 1.0$) produces an adequate fit and that a more complex expression cannot be justified due to uncertainties.

Condensation: Oil Effects in Finned Tubes

No previous work has been reported on refrigerant-oil mixtures in finned tubes. Existing correlations for finned tubes (discussed later) are based on smooth tube correlations

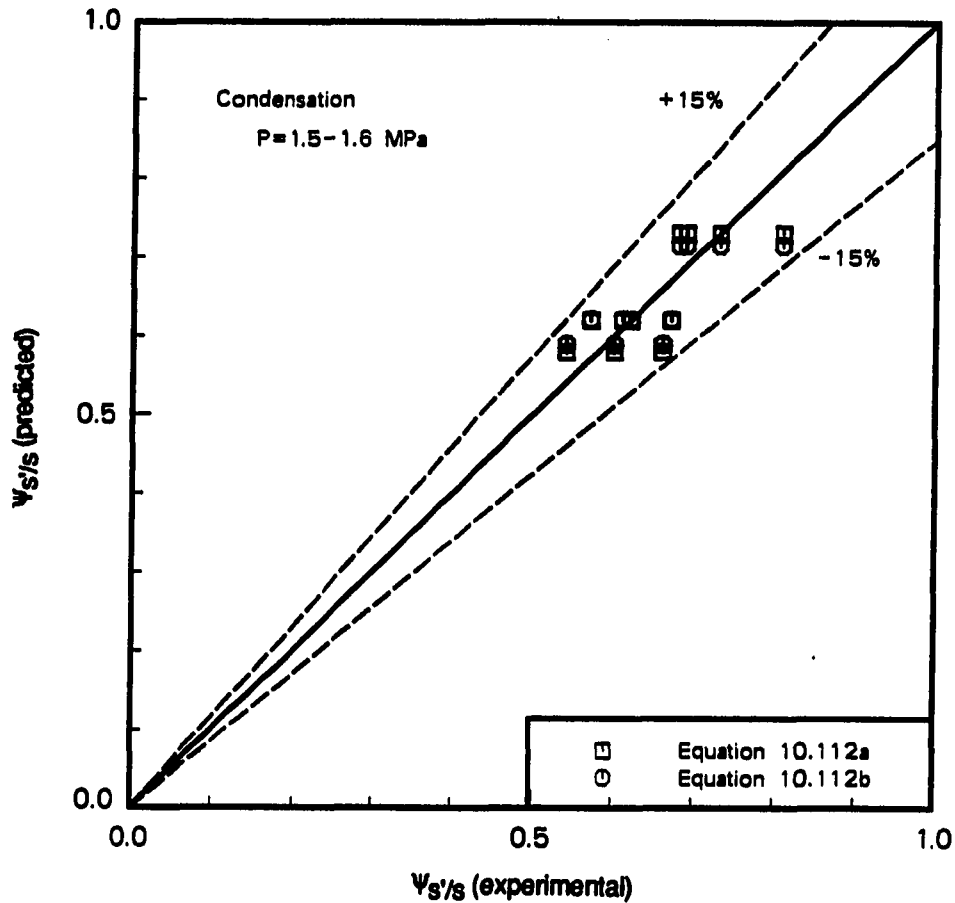


Figure 10.19. Comparison of experimental condensation pressure drop enhancement factors ($\Psi_{s'/s}$) with predictions using statistical equations

like the ones discussed in the preceding section, so these same correlations are now considered as predictors of refrigerant-oil mixture pressure drop in finned tubes.

Application of general correlations to refrigerant-oil mixtures Unlike smooth tube results, pressure drop in finned tubes follows the expected pattern of generally increasing as the concentration of oil (and viscosity) increases (see Figures 7.21 and 8.20). This behavior may be caused by the finned surfaces stabilizing the flow pattern in a particular region, whereas in the smooth tube, the flow is near a predicted flow pattern transition boundary and flow pattern changes may be responsible for the observed pressure drop decrease with increasing oil concentration. There are no flow regime maps for finned tubes, however, so flow pattern observations are needed to clarify the differences between smooth

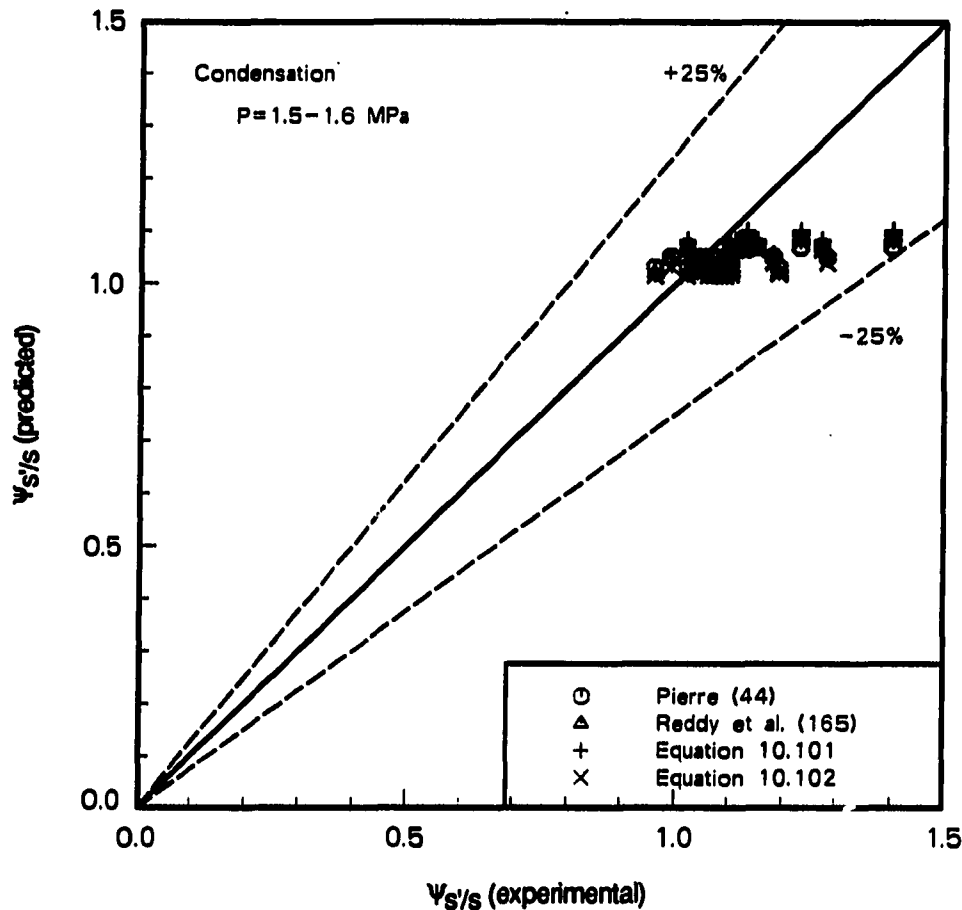


Figure 10.20. Comparison of experimental condensation pressure drop enhancement factors ($\Psi_{a/a}$) with predictions using correlations and correlation-based equations

and finned tube performance. As with evaporation, the two correlations that reduce to a function of viscosity ratio [44,165] also come closest to predicting pressure drop increase in finned tubes, but their predictions are somewhat low. Figure 10.20 compares the predictions of these correlations and their approximations (Equations 10.101 and 10.102) with experimental results. Agreement is within $\pm 25\%$, which is reasonably good. Note, however, that the data points lie approximately along a horizontal line, indicating that agreement is due more to close proximity of the data points, rather than to a prediction of trends. The equations actually predict very little change in pressure drop with the addition of oil.

Development of statistical prediction equations Since viscosity and pressure drop both increase as oil is added with finned tubes, indicating a proportionality, the first predictive equations presented below are based on a ratio of viscosities at the average test section concentration (1.6 times the system-average concentration). For the micro-fin tube,

$$(\Psi_{a/a})_{m-f} = \left[\frac{\mu_{1m}}{\mu_{1r}} \right]^{0.55} \quad (10.113a)$$

and for the low-fin tube,

$$(\Psi_{a/a})_{l-f} = \left[\frac{\mu_{1m}}{\mu_{1r}} \right]^{0.39} \quad (10.113b)$$

The best-fit exponents for condensation are higher than those from the correlation approximations (Equations 10.101 and 10.102), indicating that the pressure drop penalty with the addition of oil is higher on average than that predicted by the correlations. The opposite is seen with evaporation (compare with Equations 10.103 and 10.106). Predictions of Equations 10.113 are compared with experimental data in Figure 10.21. Agreement is generally within $\pm 20\%$, which is about the same as for evaporation.

Equations are presented below that predict pressure drop performance based on oil concentration, without the need to determine fluid properties for a refrigerant-oil mixture. Equivalent polynomial and exponential forms of the equations are shown for each case. A first-order expression is nearly as good as a second-order expression, so the simpler form is used. For mixtures with 150-SUS oil in the micro-fin tube,

$$\text{polynomial:} \quad (\Psi_{a/a})_{m-f} = 2.69 \cdot \omega_o + 0.99 \quad (10.114a)$$

$$\text{exponential:} \quad (\Psi_{a/a})_{m-f} = 0.99 \cdot e^{2.57 \cdot \omega_o} \quad (10.114b)$$

in the low-fin tube,

$$\text{polynomial:} \quad (\Psi_{a/a})_{l-f} = 2.26 \cdot \omega_o + 1.01 \quad (10.115a)$$

$$\text{exponential:} \quad (\Psi_{a/a})_{l-f} = 1.01 \cdot e^{2.11 \cdot \omega_o} \quad (10.115b)$$

and for 300-SUS oil in the micro-fin tube,

$$\text{polynomial:} \quad (\Psi_{a/a})_{m-f} = 5.12 \cdot \omega_o + 1.02 \quad (10.116a)$$

$$\text{exponential:} \quad (\Psi_{a/a})_{m-f} = 1.02 \cdot e^{4.38 \cdot \omega_o} \quad (10.116b)$$

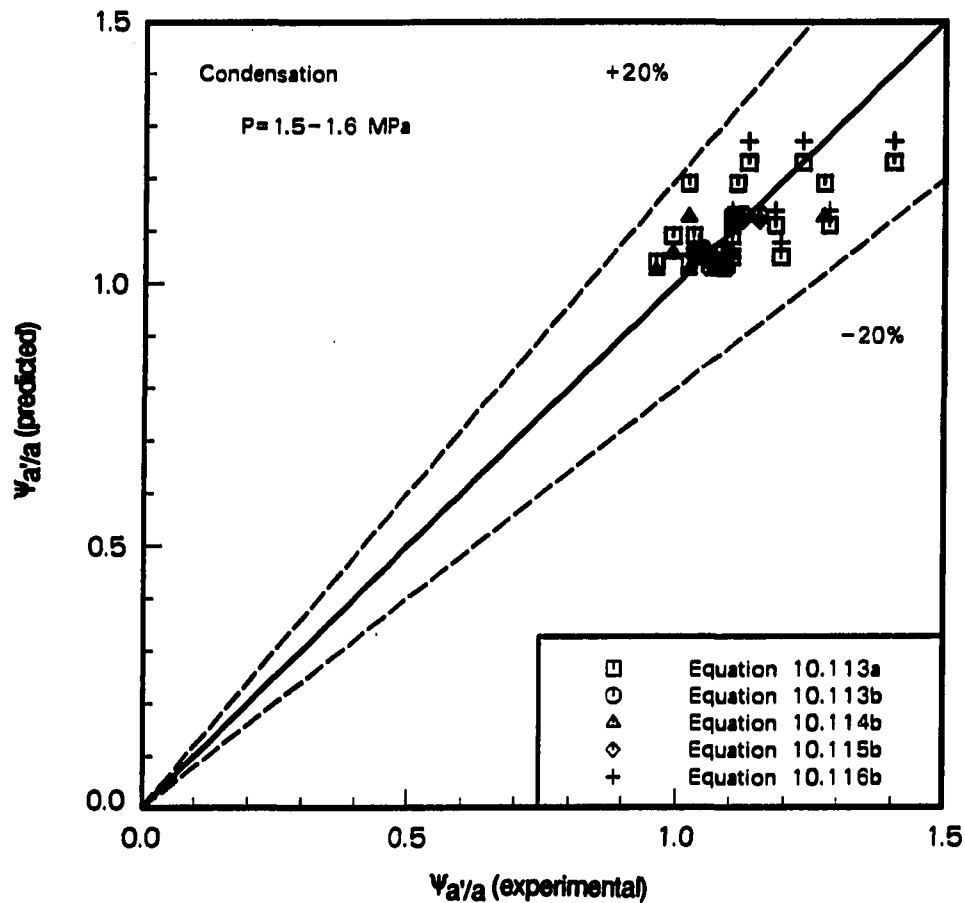


Figure 10.21. Comparison of experimental condensation pressure drop enhancement factors ($\Psi_{a/a}$) with predictions using statistical equations

Values of R^2 range from 0.5 to 0.7, generally lower than for evaporation. Figure 10.21 includes predictions from the exponential forms of Equations 10.114 through 10.116 and compares these with experimental values. Agreement is within 20% for all points, but once again the data are clustered closely so that it is difficult to discern whether the correlating expressions are actually predicting trends.

Condensation: Effects of Internal Fins with Pure Refrigerant

Previous correlations No correlations of micro-fin tube pressure drop have been published. For tubes similar to the low-fin tubes, only Luu [134] has proposed a correlation expression. Luu uses the Dukler II correlation (Equations 10.60 to 10.66) with

homogeneous void fractions. The hydraulic diameter is the characteristic dimension, as used in earlier condensation correlations [138,174]. The pressure drop enhancement factor, therefore, reduces to a ratio which is primarily a function of inside diameter and hydraulic diameter. The enhancement factor is also dependent on void fraction and, through the Reynolds number term in the friction factor, it is a weak function of mass flux. Substituting values for the low-fin tube into Luu's expression yields a value of 2.1 for $\Psi_{a/s}$ at 300 kg/m²·s, almost identical to the experimental value. Neglecting the dependence on void fraction and mass flux, a simple ratio of equivalent smooth tube diameter to hydraulic diameter of the low-fin tube gives a value of 1.9, within 10% of the experimental value.

Development of statistical prediction equations No attempt is made to formulate a correlation based on geometric parameters due to the limited geometries used in this study. It appears, however, that for tubes similar to low-fin tubes, it may be possible to estimate $\Psi_{a/s}$ as a function of inside diameter and hydraulic diameter. Since relative uncertainties are particularly high with condensation pressure drop, the recommended expressions given are constants, without dependence on mass flux, fluid properties, etc. The values are determined at 300 kg/m²·s, the approximate condition of minimum uncertainty for condensation pressure drop. For the micro-fin tube, the pressure drop enhancement factor is

$$(\Psi_{a/s})_{m-f} = 1.7 \quad (10.117a)$$

and for the low-fin tube, the factor is

$$(\Psi_{a/s})_{l-f} = 2.1 \quad (10.117b)$$

Summary

This chapter discussed the development of predictive equations to account for the effects of oil in smooth and augmented tubes. The first part reviewed the literature for previous heat transfer and pressure drop correlations, while the second part presented equations based on data from the current research. The equations developed are in terms of enhancement factors, so they may be easily combined with experimental data or applied to pure refrigerant correlations. Table 10.3 summarizes each of the cases investigated and refers to the appropriate predictive equation(s) presented in this chapter by equation number.

Table 10.3. Summary of predictive equations to account for the effects of oil and augmentation with R-22

Description of case					Basis of predictive equation	
Process	Tube type	Reference tube	Oil (SUS)	Enhancement factor ^a	Simplified correlation ^b	Statistical ^c
Evap. heat transfer	Smooth	Smooth	150	ϵ_s/s	80 with 82 ^d	83
	Smooth	Smooth	300	ϵ_s/s	81 with 82	84
	Micro-fin	Micro-fin	150	ϵ_a/a	85 with 82	88
	Micro-fin	Micro-fin	300	ϵ_a/a	86 with 82	89
	Low-fin	Low-fin	150	ϵ_a/a	87 with 82	90
	Micro-fin	Smooth	None	ϵ_a/s	—	91 ^e
	Low-fin	Smooth	None	ϵ_a/s	—	91 ^e
Cond. heat transfer	Smooth	Smooth	150	ϵ_s/s	93	94
	Smooth	Smooth	300	ϵ_s/s	93	94
	Micro-fin	Micro-fin	150	ϵ_a/a	93	97
	Micro-fin	Micro-fin	300	ϵ_a/a	93	97
	Low-fin	Low-fin	150	ϵ_a/a	93 with 96	98
	Micro-fin	Smooth	None	ϵ_a/s	—	99 ^e
	Low-fin	Smooth	None	ϵ_a/s	—	99 ^e
Evap. pressure drop	Smooth	Smooth	150	ψ_s/s	103	104
	Smooth	Smooth	300	ψ_s/s	103	105
	Micro-fin	Micro-fin	150	ψ_a/a	106a	107
	Micro-fin	Micro-fin	300	ψ_a/a	106a	109
	Low-fin	Low-fin	150	ψ_a/a	106b	108
	Micro-fin	Smooth	None	ψ_a/s	—	110
	Low-fin	Smooth	None	ψ_a/s	—	111
Cond. pressure drop	Smooth	Smooth	150	ψ_s/s	—	112
	Smooth	Smooth	300	ψ_s/s	—	—
	Micro-fin	Micro-fin	150	ψ_a/a	113a	114
	Micro-fin	Micro-fin	300	ψ_a/a	113a	116
	Low-fin	Low-fin	150	ψ_a/a	113b	115
	Micro-fin	Smooth	None	ψ_a/s	—	117a
	Low-fin	Smooth	None	ψ_a/s	—	117b

^aEnhancement factors defined in Chapter 4.

^bGenerally require integration and/or determination of mixture properties; may also include a statistical component.

^cRequire system average oil concentration and mass flux; no integration or properties.

^dNumbers correspond to equation numbers in Chapter 10.

^eOnly partial correlation expression; requires experimental input.

CHAPTER 11 CONCLUSIONS AND RECOMMENDATIONS

Conclusions

With R-22 as the working fluid, the current study has looked at the effects of small quantities ($\leq 5\%$ by weight) of refrigeration oil on heat transfer and pressure drop in a smooth tube and two types of internally finned tubes—a micro-fin tube and a low-fin tube. Naphthenic mineral oils having viscosities of 150 and 300 SUS were used. After a review of the literature, testing was carried out over a range of conditions representative of those found in refrigeration and air conditioning applications. Tests were limited to a single, straight, horizontal tube that was heated or cooled by water circulating in a surrounding annulus. Several tests were carried out to investigate the actual quantity of oil in the test section during evaporation and condensation and compare this quantity to the average system concentration. Upon completion of the experimental phase, a performance comparison of the three tubes was made and predictive equations for heat transfer and pressure drop were developed from the data.

One of the most important general conclusions drawn from this work is that although oil affects the heat transfer and pressure drop performance of condensers and evaporators, with this effect being either negative or positive, tubes having finned inner surfaces maintain a distinct advantage in heat transfer performance when compared with smooth tubes. Heat transfer enhancement observed with pure refrigerants, therefore, is not lost with refrigerant-oil mixtures, though the magnitude of the enhancement may diminish. When the combined effects of heat transfer and pressure drop are considered, the results are less clear. In this case, the augmented tubes may have improved or degraded performance relative to the smooth tube, depending on the particular conditions considered. More specific conclusions are presented below, grouped according to the type of test.

Heat Transfer

The heat transfer coefficient increases with increasing mass flux for all tubes tested; however, the enhancement of the finned tubes relative to the smooth tube tends to decrease

at higher mass flows. A heat transfer enhancement factor, ϵ , is defined as the ratio of heat transfer coefficients at the conditions of interest.

Evaporation The micro-fin and low-fin tube show very similar pure refrigerant heat transfer enhancement, with enhancement factors ($\epsilon_{a/s}$) ranging from approximately 2.7 at 125 kg/m²·s to around 1.9 at 400 kg/m²·s.

Oil with a viscosity of 150 SUS caused some heat transfer enhancement in all three tubes, with peak enhancement factors ($\epsilon_{s/s}$ and $\epsilon_{a/a}$) at 300 kg/m²·s of about 1.3 for the smooth tube, about 1.1 for the micro-fin tube, and slightly above 1.0 for the low-fin tube. There appears to be a tendency of decreasing oil enhancement with increasing fin height and, additionally, the peak occurs at lower oil concentrations as the fin height increases. With 300-SUS oil, peak enhancement factors are slightly more than 1.0 and the performance of the smooth tube and micro-fin tube with oil addition is similar. For both tubes tested with 300-SUS oil (smooth and micro-fin) and the low-fin tube with 150-SUS oil, the effect of oil is generally to degrade performance, except at the lowest oil concentration. The effect of oil appears to be more positive at lower mass fluxes. For example, if enhancement is observed at a particular oil concentration, the enhancement increases at a lower mass flux; if degradation occurs, then the degradation is less severe at lower mass flux.

Comparing finned tube heat transfer performance with refrigerant-oil mixtures to the smooth tube with the same oil concentration, the augmented tubes maintain a significant performance advantage; although, in general, enhancement factors with oil ($\epsilon_{a/s'}$) are smaller than pure refrigerant enhancement factors ($\epsilon_{a/s}$). With the addition of oil, the micro-fin tube shows a performance advantage over the low-fin tube not seen with pure R-22. At 300 kg/m²·s and a concentration of 2.5% 150-SUS oil, $\epsilon_{a/s'}$ for the micro-fin tube is about 1.7 and for the low-fin tube about 1.4. These compare to pure refrigerant enhancement factors ($\epsilon_{a/s}$) of just above 2.0 for both tubes. Although absolute performance with 300-SUS oil is lower, the enhancement factor $\epsilon_{a/s'}$ of the micro-fin tube is higher than with 150-SUS oil. The value of $\epsilon_{a/s'}$ at 300 kg/m²·s falls only to 1.9, versus 1.7 with 150-SUS oil.

Condensation Both augmented tubes show significant heat transfer enhancement with pure refrigerant. The enhancement factor ($\epsilon_{a/s}$) for the micro-fin tube is almost 2.3 at 200 kg/m²·s, falling to 1.9 at 400 kg/m²·s. Low-fin performance is about 10% lower.

No heat transfer enhancement is seen during condensation with refrigerant-oil mixtures. Each incremental increase in oil concentration causes a further decrease in heat transfer. Heat transfer performance is similar with the both 150- and 300-SUS oils, as well as with the smooth and micro-fin tubes. Low-fin tube performance tends to degrade somewhat less with the addition of oil. At a mass flux of 300 kg/m²·s and an oil concentration of 5%, the enhancement factor due to oil ($\epsilon_{s'/s}$ or $\epsilon_{a'/a}$) falls to around 0.9 in the smooth tube and micro-fin tube, but falls only to 0.95 in the low-fin tube. The effect of oil is not generally influenced by the mass flux.

Because the oil affects smooth and augmented tubes in much the same way, the heat transfer performance of the augmented tubes relative to the smooth tube ($\epsilon_{a/s}$ or $\epsilon_{a'/s'}$) remains relatively constant as the oil concentration increases, varying by less than 10% over the range of 0% to 5% oil concentration.

Pressure Drop

Analogous to the heat transfer enhancement factor, a pressure drop enhancement factor, Ψ , is also defined as the ratio of pressure drops at given conditions.

Evaporation Both augmented tubes have a higher pressure drop than the smooth tube. At 300 kg/m²·s, the pressure drop enhancement factor ($\Psi_{a/s}$) is 1.4 for the micro-fin tube and 1.8 for the low-fin tube. These factors are lower than the corresponding heat transfer enhancement factors.

The effect of oil is to increase pressure drop in all three tubes when compared to the pressure drop in the same tube with pure refrigerant. Pressure drop performance is similar with all three tubes and shows little effect of viscosity. The pressure drop increases with each incremental increase in oil concentration. At a concentration of 5% oil, the pressure drop enhancement factor due to oil ($\Psi_{s'/s}$ or $\Psi_{a'/a}$) is around 1.2 to 1.3 for all tubes and with both oils.

Because the effect of oil on pressure drop is similar in all tubes tested, the enhancement factor based on the augmented tube pressure drop with oil to that in the smooth tube with the same oil concentration is approximately constant ($\Psi_{a/s}$ or $\Psi_{a'/s}$). The value of $\Psi_{a'/s}$ varies by 10% or less from the pure refrigerant value ($\Psi_{a/s}$) over the range of oil concentrations tested.

Condensation The increase in pure refrigerant condensation pressure drop in the augmented tubes, relative to the smooth tube, is greater than for evaporation. At a mass flux of 300 kg/m²-s, the enhancement factor for condensation ($\Psi_{a/s}$) is 1.7 in the micro-fin tube and 2.1 in the low-fin tube.

For the augmented tubes, the addition of oil causes the pressure drop to increase. At a concentration of 5% and a mass flux of 300 kg/m²-s, the value of the enhancement factor ($\Psi_{a'/a}$) ranges from about 1.1 to 1.2. Results are similar with both 150- and 300-SUS oil. In the smooth tube, the addition of 300-SUS oil has no pronounced effect either up or down, with $\Psi_{s'/s}$ having a value of approximately 1.0. With 150-SUS oil in the smooth tube, pressure drop decreases by up to 40% ($\Psi_{s'/s} \approx 0.6$). It is hypothesized that this behavior may be due to a flow-regime transition.

The enhancement factor comparing refrigerant-oil mixture pressure drop in the augmented tubes with that in the smooth tube ($\Psi_{a'/s}$) generally increases as oil is added. This is particularly true for 150-SUS oil because of the pressure decrease seen in the smooth tube. The value of $\Psi_{a'/s}$ at a concentration of 5% and a mass flux of 300 kg/m²-s is about 3.0 in the micro-fin tube and 4.0 in the low-fin tube. At similar conditions, but with 300-SUS oil (micro-fin tube only), the value of $\Psi_{a'/s}$ is about 2.0.

Overall Performance

The ratio of heat transfer enhancement factor to the pressure drop enhancement factor is designated as the enhancement performance ratio, θ . This ratio gives an indication of the combined heat transfer and pressure drop performance of a single tube.

The overall performance of each tube compared with itself generally diminishes as oil is added to the refrigerant. This is true for the smooth tube, as well as for the augmented tubes, and the decrease ranges from 10% to 30%. With pure refrigerant, both augmented

tubes have a value of $\theta_{a/s}$ greater than 1.0 for evaporation, while only the micro-fin tube has a value greater than 1.0 for condensation.

Comparing the augmented tubes to the smooth tube with similar oil concentrations ($\theta_{a/s}'$), the micro-fin tube is generally superior to the low-fin tube for both evaporation and condensation. There is a tendency for $\theta_{a/s}'$ to decrease with the addition of oil. This decrease ranges from about 10% to almost 50%. For evaporation, the values of $\theta_{a/s}'$ remain greater than 1.0 for all oil concentrations with the micro-fin tube, but they fall to less than 1.0 at higher concentrations with the low-fin tube. For condensation with 150-SUS oil, the value of $\theta_{a/s}'$ is always less than unity. With 300-SUS oil, $\theta_{a/s}'$ remains greater than or equal to 1.0, except at the highest oil concentration.

Recommendations for Further Research

During the course of this research, several areas suggested themselves as topics of future research. These topics are discussed below.

1. The process of evaporation and condensation with refrigerant-oil mixtures differs from that with pure refrigerant. Several items related to two-phase heat transfer need to be addressed. First, because some refrigerant always remains in solution with the oil, 100% quality is approached asymptotically with refrigerant-oil mixtures. A method of accounting for this phenomenon should be developed, particularly in high quality and superheated regions. Second, due to the nonvolatile nature of oil, the saturation temperature of a refrigerant oil mixture increases as local vapor quality increases and it is a function of local oil concentration, as well as of pressure. Because the heat transfer coefficient is defined based on the fluid temperature, an unambiguous procedure for reporting heat transfer coefficients in refrigerant-oil mixtures should be developed. Finally, the enthalpy of vaporization of an incremental quantity of refrigerant-oil mixtures needs to be determined at varying values of liquid oil concentration. This value is required to accurately determine the vapor quality.
2. In addition to testing with common refrigeration oils, which are generally comprised of several different components, testing with a single-component oil is recommended to obtain a more fundamental understanding of some of the processes involved with two-

phase heat transfer. With a single-component oil, better estimates of local properties could be obtained.

2. Flow visualization studies are needed to help explain some of the apparently anomalous behavior observed during the testing. The mechanism leading to heat transfer enhancement during evaporation of refrigerant-oil mixtures is one area of special interest, and the other is pressure drop behavior during condensation.
3. An obvious extension of the work would be to use different oils and refrigerants (including partly miscible mixtures), a wider range of mass fluxes, different evaporation and condensation pressures, etc. Perhaps the most important extension would be to higher quality regions and the superheated region.
4. Heat and mass flux were linked in this investigation, due to a fixed tube length and fixed inlet and outlet conditions. Work that independently varies mass and heat flux would be useful to isolate the effects of these two parameters.
5. Since many design codes are based on a finite element or finite difference approach, local heat transfer coefficients are sometimes more useful to the designer, so the determination of local or quasi-local coefficients is desirable.
6. Although this study concentrated more on the effects of oil and less on pure refrigerant heat transfer augmentation, the development of generalized predictive correlations for enhanced tubes remains an area of great interest.
7. More complete hold-up measurements are needed, including local, rather than average, oil concentration results. These data would help with the determination of local heat transfer coefficients.

REFERENCES

1. ASHRAE. "Work statement 469 TRP: Effect of oil on heat transfer and pressure drop inside augmented tubes during condensation and evaporation of refrigerants." Atlanta, GA: American Society of Heating, Refrigerating and Air Conditioning Engineers, Inc., 1984.
2. Green, G. H. "Influence of oil on boiling heat transfer and pressure drop in refrigerants 12 and 22." ASHRAE Journal (December 1965): 57-61.
3. Baustian, J. J.; Pate, M. B.; and Bergles, A. E. "Properties of oil-refrigerant liquid mixtures with applications to oil concentration measurement: Part I—Thermophysical and transport properties." ASHRAE Transactions 92 (1985): 55-73.
4. Baustian, J. J. "Development of a sensor for the continuous measurement of oil concentration in a refrigeration system." Ph.D. dissertation, Iowa State University, 1988.
5. ASHRAE. "Refrigerants." In ASHRAE Handbook—1985 Fundamentals. Atlanta, GA: American Association of Heating, Refrigerating and Air-Conditioning Engineers, Inc., 1985.
6. ASHRAE. "Refrigerant tables and charts." In ASHRAE Handbook—1985 Fundamentals. Atlanta, GA: American Association of Heating, Refrigerating and Air-Conditioning Engineers, Inc., 1985.
7. ASHRAE. "Lubricants in refrigerants." In ASHRAE Handbook—1984 Systems. Atlanta, GA: American Association of Heating, Refrigerating and Air-Conditioning Engineers, Inc., 1984.
8. Kendall, J.; and Monroe, K. P. "The viscosity of liquids. II. The viscosity-composition curve for ideal liquid mixtures." Journal of the American Chemical Society 39 (1917): 1787-802.
9. Rohsenow, W. M. "A method of correlating heat transfer for surface boiling of liquids." Transactions of the ASME 74 (1952): 969-76.
10. Sauer, H. J., Jr.; Gibson, R. K.; and Chongrungreong, S. "Influence of oil on the nucleate boiling of refrigerants." In Vol. 1, Heat Transfer 1978: Proceedings of the Sixth International Heat Transfer Conference Held in Toronto 7-11 August 1978, 181-86. Washington, DC: Hemisphere, 1978.
11. Jensen, M. K.; and Jackman, D. L. "Predictions of nucleate pool boiling heat transfer coefficients of refrigerant-oil mixtures." Journal of Heat Transfer 106 (1984): 184-90.
12. McMullan, J. T.; Hughes, D. W.; and Morgan, R. "A suite of computer programs for calculating the thermodynamic properties of refrigerant-oil mixtures." Heat Recovery Systems 5 (1985): 181-94.

13. Hughes, D. W.; McMullan, J. T.; Mawhinney, K. A.; and Morgan, R. "Pressure-enthalpy charts for mixtures of oil and refrigerant R 12." International Journal of Refrigeration 5 (1982): 199-202.
14. "SUNISO Refrigeration Oils from Sonneborn." New York: Witco Chemical Co., ca. 1986.
15. Zimmermann, F. "Influence of oil in refrigerant on evaporation in tubes" (in German). In Bericht über die Jahrestagung 1985 des Deutschen Kälte- und Klimatechnischen Vereins Held in Aachen 20-22 November 1985, 155-69. Stuttgart: Kessler Schnelldruck, 1985.
16. Zimmermann, F. "Influence of oil content in refrigerants on the evaporation in tubes" (in German). Klima Kälte Heizung 14 (1986): 52-56.
17. Jaeger, H. P. "Empirical methods for calculating thermodynamic properties of oil-refrigerant mixtures" (in German). Kältetechnik-Klimatisierung 24 (1973): 35-52.
18. Menze, K., Wieland-Werke AG Metallwerke; Ulm, W. Germany; private communication, 1987.
19. Chaddock, J. B. "Influence of oil on refrigerant evaporator performance." ASHRAE Transactions 82 (1976): 474-86.
20. Shah, M. M. "Heat transfer during film condensation in tubes and annuli: a review of the literature." ASHRAE Transactions 87 (1981): 1086-1105.
21. Bergles, A. E. Heat transfer characteristics of Turbotec tubing. ISU Engineering Research Institute (Ames, IA) ISU-ERI-Ames-81018, 1980.
22. Lazarek, G. M. "Augmentation of two-phase heat transfer and pressure drop of refrigerants in horizontal tubes." International Journal of Refrigeration 3 (1980): 261-72.
23. Bergles, A. E.; Nirmalan, V.; Junkhan, G. H.; and Webb, R. L. Bibliography on augmentation of convective heat and mass transfer — II. ISU Engineering Research Institute (Ames, IA) ISU-ERI-Ames-84221, 1983.
24. Yoshida, S.; and Fujita, Y. "Boiling heat transfer to halogenated hydrocarbon refrigerants" (in Japanese). Transactions of the JAR 1, No. 2 (1984): 1-19.
25. Turaga, M.; and Guy, R. W. "Refrigerant side heat transfer and pressure drop estimates for direct expansion coils. A review of works in North American use." International Journal of Refrigeration 8 (1985): 134-42.
26. Witzig, W. F.; Penney, G. W.; and Cyphers, J. A. "Heat transfer rates of Freon-12 evaporating in a horizontal tube." Refrigerating Engineering 56 (1948): 153-57.

27. Seigel, L. G.; Bryan, W. L.; and Huppert, M. C. "Heat transfer rates for refrigerant boiling in horizontal tube evaporators." Heating, Piping, and Air Conditioning 21 (1949): 159-62.
28. Yoder, R. J.; and Dodge, B. F. "Heat transfer coefficients for boiling Freon-12." Refrigerating Engineering 60 (1952): 156-59.
29. Pierre, B. "The coefficient of heat transfer for boiling Freon-12 in horizontal tubes." Heating and Air Treatment Engineer 19 (1956): 302-10.
30. Worsøe-Schmidt, P. "Some characteristics of flow pattern and heat transfer of Freon-12 evaporating in horizontal tubes." Journal of Refrigeration 3 (1960): 40-44.
31. Green, G. H.; and Furse, F. G. "Effect of oil on heat transfer from a horizontal tube to boiling R-12 mixtures." ASHRAE Journal (October 1963): 63-68.
32. Deane, C. W. "Effect of oil on boiling heat transfer to refrigerant-11." In Appendix E, Report of Advanced Energy Programs Laboratory, General Electric Co., Cincinnati, OH, 1975.
33. Mathur, A. P. "Heat transfer to oil-refrigerant mixtures evaporating in tubes." Ph.D. dissertation, Duke University, 1976.
34. Chaddock, J. B.; and Mathur, A. P. "Heat transfer to oil-refrigerant mixtures evaporating in tubes." In Vol. 2, Multiphase Transport: Fundamentals, Reactor Safety, Applications – Proceedings of the Multi-Phase Flow and Heat Transfer Symposium-Workshop Held in Miami Beach 16-18 April 1979, edited by T. N. Veziroglu, 861-84. Washington, DC: Hemisphere, 1980.
35. Tichy, J. A.; Macken, N. A.; and Duval, W. "An analytical model for condensing and evaporating two-component two-phase annular flow." In Vol. 5, Heat Transfer 1982: Proceedings of the Seventh International Heat Transfer Conference Held in Munich 6-10 September 1982, edited by U. Grigull, E. Hahne, K. Stephan, and J. Straub, 161-66. Washington, DC: Hemisphere, 1982.
36. Malek, A. "Effect of oil contaminant on heat transfer coefficients in refrigerant evaporators" (in French). In Vol. II, Progress in Refrigeration Science and Technology: XVIth International Congress of Refrigeration Proceedings Held in Paris 31 August-7 September 1983, 203-6. Paris: Association pour le Congrès International du Froid de Paris, 1983.
37. Hughes, D. W.; McMullan, J. T.; Mawhinney, K. A.; and Morgan, R. "Influence of oil on evaporator heat transfer (results for R-12 and Shell Clavus oil)." International Journal of Refrigeration 7 (1984): 150-58.
38. Chaddock, J. B.; and Buzzard, G. H. "Effect of oil on heat transfer and pressure drop in refrigerant evaporators — Phase I: R-502." Duke University Department

- of Mechanical Engineering and Materials Science (Durham, NC) ASHRAE RP 224-1, 1980.
39. Chaddock, J. B.; and Buzzard, G. H. "Effect of oil on heat transfer and pressure drop in refrigerant evaporators — Phase II: R-717." Duke University Department of Mechanical Engineering and Materials Science (Durham, NC) ASHRAE RP 224-2, 1983.
 40. Chaddock, J. B.; and Buzzard, G. H. "Film coefficients for in-tube evaporation of ammonia and R-502 with and without small percentages of mineral oil." ASHRAE Transactions 92 (1986): 22-40.
 41. Tichy, J. A.; Duval, W. M. B.; and Macken, N. A. "An experimental investigation of heat transfer in forced-convection evaporation of oil-refrigerant mixtures." ASHRAE Transactions 92 (1986): 450-60.
 42. Shah, M. M. "Visual observations in an ammonia evaporator." ASHRAE Transactions 81 (1975): 295-306.
 43. Chawla, J. M.; and Gauler, K. "Influence of oil content on the pressure drop in evaporator tubes" (in German). Kälte-Rundschau 4 (1968): 65-71.
 44. Pierre, B. "Flow resistance with boiling refrigerants — Part I." ASHRAE Journal (September 1964): 58-65.
 45. Hatada, T.; Senshu, T.; and Koso, T. "Influence of oil on pressure drop of R-22 boiling in horizontal tubes" (in Japanese). Reito 55 (1980): 383-92.
 46. Tichy, J. A.; Duque-Rivera, J.; Macken, N. A.; and Duval, W. M. B. "An experimental investigation of pressure drop in forced-convection condensation and evaporation of oil-refrigerant mixtures." ASHRAE Transactions 92 (1986): 461-72.
 47. Tichy, J. A.; Macken, N. A.; and Duval, W. M. B. "An experimental investigation of heat transfer in forced-convection condensation of oil-refrigerant mixtures." ASHRAE Transactions 91 (1985): 297-308.
 48. Stephan, K.; and Mitrovic, J. "Heat transfer in natural convective boiling of refrigerants and refrigerant-oil mixtures in bundles of T-shaped finned tubes." In Advances in Enhanced Heat Transfer—1981, edited by R. L. Webb, T. C. Carnavos, E. L. Park, Jr., and E. L. Hostetler, 131-46. New York: American Society of Mechanical Engineers, 1981.
 49. Chemobylski, I.; and Ratiani, G. "Heat transfer coefficients of boiling Freon-12" (in Russian). Kholodil'naya Tekhnika 32 (1955): 48-51.
 50. Stephan, K. "The effect of oil on heat transfer of boiling refrigerant 12 and refrigerant 22" (in German). Kältetechnik 16 (1964): 162-66.

51. Dougherty, R. L.; and Sauer, H. J., Jr. "Nucleate pool boiling of refrigerant-oil mixtures from tubes." ASHRAE Transactions 80 (1974): 175-93.
52. Sakaguchi, S.; and Yamazaki, H. "Effect of fluorocarbon concentration on boiling heat transfer of oil-fluorocarbon mixture" (in Japanese). Reito 58 (1983): 913-31.
53. Burkhardt, J.; and Hahne, E. "Influence of oil on the nucleate boiling of refrigerant 11." In Vol. II, Progress in Refrigeration Science and Technology: Proceedings of the XVth International Congress of Refrigeration Held in Venice 23-29 September 1979, 537-44. Padova, Italy: Istituto per la Tecnica del Freddo del C.N.R., 1979.
54. Chongrungreong, S.; and Sauer, H. J., Jr. "Nucleate boiling performance of refrigerants and refrigerant-oil mixtures." Journal of Heat Transfer 102 (1980): 701-5.
55. Hahne, E.; and Noworyta, A. "Calculation of the heat transfer coefficients for nucleate boiling in binary mixtures of refrigerant-oil." International Communications in Heat and Mass Transfer 11 (1984): 417-27.
56. Anikin, A. I.; Danilova, G. N.; and Mirmov, N. I. "Generalized correlation for coefficients of boiling heat transfer of oil-refrigerant mixtures in tubes." Heat Transfer—Soviet Research 16 (1984): 42-52.
57. Jensen, M. K. "Enhancement of the critical heat flux in pool boiling refrigerant-oil mixtures." Journal of Heat Transfer 106 (1984): 477-79.
58. Yamazaki, H.; and Sakaguchi, S. "Heat transfer in nucleate boiling of oil-freon R113 mixtures." Bulletin of JSME 29 (1986): 129-35.
59. Monde, M.; and Hahne, E. "Boiling heat transfer on a fine horizontal wire in a refrigerant-oil mixture." Heat Transfer—Japanese Research 16 (1987): 48-60.
60. Kawahira, H.; Kubo, Y.; and Yokoyama, T. "The effect of an electric field on boiling heat transfer of refrigerant-11." In Conference Record of the 1987 IEEE Industry Applications Society Annual Meeting Held in Atlanta 18-23 October 1987, 1449-54. New York: Institute of Electrical and Electronics Engineers, 1987.
61. Bell, K. I.; Hewitt, G. F.; and Morris, S. D. "Nucleate pool boiling of refrigerant/oil mixtures." Experimental Heat Transfer 1 (1987): 71-86.
62. Sauer, H. J., Jr.; Davidson, G. W.; and Chongrungreong, S. "Nucleate boiling of refrigerant-oil mixtures from finned tubing." American Society of Mechanical Engineers (New York) Paper No. 80-HT-111, 1980.
63. Stephan, K.; and Mitrovic, J. "Heat transfer in natural convective boiling of refrigerant-oil mixtures." In Vol. 5, Heat Transfer 1982: Proceedings of the Seventh International Heat Transfer Conference Held in Munich 6-10 September

- 1982, edited by U. Grigull, E. Hahne, K. Stephan, and J. Straub, 73-87. Washington, DC: Hemisphere, 1982.
64. Arai, N.; Fukushima, R.; Arai, A.; Nakajima, T; Fujie, K; and Nakayama, Y. "Heat transfer tubes enhancing boiling and condensation in heat exchanger of a refrigerating machine." ASHRAE Transactions 83 (1977): 58-70.
 65. Czikk, A. M.; Gottzmann, C. F.; Ragi, E. G.; Withers, J. G.; and Habdas, E. P. "Performance of advanced heat transfer tubes in refrigerant-flooded liquid coolers." ASHRAE Transactions 76 (1970): 96-109.
 66. Reilly, J. T. "Influence of oil contamination on the nucleate pool-boiling behavior of R-114 from a structured surface." M.S. thesis, Naval Postgraduate School, Monterey, CA, 1985.
 67. Wanniarachchi, A. S.; Marto, P. J.; and Reilly, J. T. "The effect of oil contamination on the nucleate pool-boiling performance of R-114 from a porous-coated surface." ASHRAE Transactions 92 (1986): 525-38.
 68. Williams, P. E.; and Sauer, H. J., Jr. "Condensation of refrigerant-oil mixtures on horizontal tubes." ASHRAE Transactions 87 (1987): 52-69.
 69. Wang, J. C. Y.; Al-Kalamchi, A.; and Fazio, P. "Experimental study on condensation of refrigerant-oil mixtures: Part I — Design of the test approach." ASHRAE Transactions 91 (1985): 216-28.
 70. Wang, J. C. Y.; Al-Kalamchi, A.; and Fazio, P. "Experimental study on condensation of refrigerant-oil mixtures: Part II — Results of R-12 and R-22 on the external surface of single and multiple horizontal tubes." ASHRAE Transactions 91 (1985): 229-37.
 71. Abdulmanov, K. A.; and Mirmov, N. I. "Experimental study of heat transfer from oil-contaminated ammonia vapor condensing on horizontal tubes." Heat Transfer—Soviet Research 3 (1971): 176-80.
 72. Sauer, H. J., Jr.; and Williams, P. E. "Condensation of refrigerant-oil mixtures on low-profile finned tubing." In Vol. 5, Heat Transfer 1982: Proceedings of the Seventh International Heat Transfer Conference Held in Munich 6-10 September 1982, edited by U. Grigull, E. Hahne, K. Stephan, and J. Straub, 147-52. Washington, DC: Hemisphere, 1982.
 73. Riedle, K. J.; Macken, N. A.; and Gouse, S. W., Jr. "Oil transport by refrigerant vapor: A literature survey and proposed analytical model." ASHRAE Transactions 78 (1972): 124-34.
 74. Scheideman, F. C.; and Macken, N. A. "Pressure loss of refrigerant-oil mixtures in horizontal pipes." ASHRAE Transactions 81 (1975): 235-49.

75. Lockhart, R. W.; and Martinelli, R. C. "Proposed correlation of data for isothermal, two-phase, two-component flow in pipes." Chemical Engineering Progress 45 (1949): 39-48.
76. Scheideman, F. C.; Jacobs, M. L.; Kazem, S. M.; and Macken, N. A. "Pressure loss of oil-refrigerant mixtures in suction and discharge lines." ASHRAE Transactions 83 (1977): 203-20.
77. Macken, N. A.; Scheideman, F. C.; and Jacobs, M. L. "Pressure loss and liquid transport of oil-refrigerant mixtures in suction and discharge lines." ASHRAE Transactions 85 (1979): 77-92.
78. Yanagisawa, T.; and Shimizu, T. "A study on the flow characteristics of refrigerating oil dissolved in refrigerant" (abstract only). ISME International Journal 30 (1987): 531-32.
79. Downing, R. C. Oil in Refrigeration Systems. Des Plaines, IL: Refrigeration Service Engineers Society, 1967.
80. McMullan, J. T. "Implications of oil-refrigerant interactions for heat pump performance." In Energy Developments: New Forms, Renewables, Conservation—Proceedings of ENERGEX '84 Held in Regina, SK, 14-19 May 1984, edited by F. A. Curtis, 337-42. Toronto: Pergamon, 1984.
81. Hughes, D. W.; McMullan, J. T.; Mawhinney, K. A.; and Morgan, R. "Experimental investigation of the influence of lubricating oil on heat pump performance." International Journal of Energy Research 8 (1984): 213-22.
82. McMullan, J. T.; Murphy, N.; and Hughes, D. W. "The effect of oil on the performance of heat pumps and refrigerators—Part one. Experimental test facility." Heat Recovery Systems and CHP 8 (1988): 53-68.
83. McMullan, J. T.; Murphy, N.; and Hughes, D. W. "The effect of oil on the performance of heat pumps and refrigerators—II. Experimental results." Heat Recovery Systems and CHP 8 (1988): 95-124.
84. Koster, G. J. "Energy savings in ammonia refrigeration plant by using oil scrubbers." Australian Refrigeration, Air Conditioning and Heating 40 (October 1986): 28-30, 32.
85. Reisbig, R. L. "Condensing heat transfer augmentation inside splined tubes." American Society of Mechanical Engineers (New York) Paper No. 74-HT-7, 1974.
86. Kubanek, G. R.; and Miletto, D. L. Evaporative heat transfer and pressure drop performance of Forge-Fin tubes with refrigerant-22. Pointe Claire, PQ: Noranda Research Centre, Noranda Metal Industries, 1976.

87. Kubanek, G. R.; and Miletti, D. L. "Evaporative heat transfer and pressure drop performance of internally finned tubes with refrigerant 22." Journal of Heat Transfer 101 (1979): 447-52.
88. Boling, C.; Donovan, W. J.; and Decker, A. S. "Heat transfer of evaporating Freon with inner fin tubing." Refrigerating Engineering 61 (1953): 1338-40, 1384.
89. Blatt, T. A.; and Adt, R. R., Jr. "The effects of twisted tape swirl generators on the heat transfer rate and pressure drop of boiling Freon 11 and water." American Society of Mechanical Engineers (New York) Paper No. 63-WA-42, 1963.
90. Tojo, S.; Hosokawa, K.; Arimoto, T.; Yamada, H.; and Ohta, Y. "Performance characteristics of multigrooved tubes for air conditioners." Australian Refrigeration Air-Conditioning and Heating 38 (August 1984): 45, 48, 51, 61.
91. Ikeuchi, M.; Yumikura, T.; Fujii, M.; and Yamanaka, G. "Heat-transfer characteristics of an internal microporous tube with refrigerant 22 under evaporating conditions." ASHRAE Transactions 90 (1984): 196-211.
92. Larson, R. L.; Quaint, G. W.; and Bryan, W. L. "Effects of turbulence promoters in refrigerant evaporation coils." Refrigerating Engineering 57 (1949): 1193-95.
93. Bryan, W. L.; and Quaint, G. W. "Heat transfer coefficients in horizontal tube evaporators." Refrigerating Engineering 59 (1951): 67-72.
94. Bryan, W. L.; and Seigel, L. G. "Heat transfer coefficients in horizontal tube evaporators." Refrigerating Engineering 63 (1955): 36-45, 120.
95. Withers, J. G.; and Habdas, E. P. "Heat transfer characteristics of helical corrugated tubes for in-tube boiling of refrigerant R-12." AIChE Symposium Series 70, No. 138 (1974): 98-106.
96. Kawai, S.; and Machiyama, T. "Experimental investigations on heat transfer characteristics of corrugated tubes (on tube side boiling and condensing heat transfer coefficients for refrigerant use)" (in Japanese). Bulletin of the Science and Engineering Research Laboratories No. 71, 1-9. Waseda University, Tokyo, 1975.
97. Kawai, S.; and Yamada, H. "Experimental investigation of the heat transfer characteristics of corrugated tubes for tube side boiling of refrigerants" (in Japanese). Reito 52 (1977): 449-56.
98. Danilova, G. N.; Guygo, E. I.; Borishanskaya, A. V.; Bukin, V. G.; Dyundin, V. A.; Kozyrev, A. A.; Malkov, L. S.; and Malyugin, G. I. "Enhancement of heat transfer during boiling of liquid refrigerants at low heat fluxes." Heat Transfer — Soviet Research 8 (1976): 1-8.
99. Dembi, N. J.; Dhar, P. L.; and Arora, C. P. "An investigation into the use of wire screens in DX-evaporators." In Vol. II, Progress in Refrigeration Science and Technology: Proceedings of the XVth International Congress of Refrigeration

Held in Venice 23-29 September 1979, 485-88. Padova, Italy: Istituto per la Tecnica del Freddo del C.N.R., 1979.

100. Mendes, A.; Yildirim, O. T.; Fu, L. Q.; Kakaç, S.; and Veziroglu, T. N. "Experimental investigation of boiling flow instabilities with heat transfer enhancement." In Proceedings of Condensed Papers of the Third Multi-Phase Flow and Heat Transfer Symposium-Workshop Held in Miami Beach 18-20 April 1983, edited by T. N. Veziroglu, 156. Amsterdam: Elsevier, 1983.
101. Mendes, A.; Yildirim, O. T.; Gürgenci, H.; Kakaç, S.; and Veziroglu, T. N. "Effect of heat transfer augmentation on two-phase flow instabilities in a vertical boiling channel." Wärme- und Stoffübertragung 17 (1983): 161-69.
102. Ditzler, J. W. "Forced convection boiling of refrigerants in an internal-finned horizontal tube." M.S. thesis, Purdue University, 1963.
103. Lavin, J. G.; and Young, E. H. "Heat transfer to evaporating refrigerants in two-phase flow." AIChE Journal 11 (1965): 1124-32.
104. Schlünder, E. U.; and Chawla, J. M. "Local heat transfer and pressure drop with evaporating refrigerant in horizontal inner-fin tubes" (in German). Kältetechnik-Klimatisierung 21 (1969): 136-39.
105. D'Yachkov, F. N. "Investigation of heat transfer and hydraulics for boiling Freon-22 in internally finned tubes." Heat Transfer—Soviet Research 10 (1978): 10-19.
106. Kikkawa, K.; Kawai, S.; and Machiyama, T. "Experimental notes on in-tube boiling and condensing heat transfer coefficient of low-finned tubes with inner-fins for refrigerant use" (in Japanese). Bulletin of the Science and Engineering Research Laboratories No. 77, 45-49. Waseda University, Tokyo, 1977.
107. Malek, A.; and Colin, R. "Evaporators with internal turbulators" (in French). In Vol. II, Progress in Refrigeration Science and Technology: XVIth International Congress of Refrigeration Proceedings Held in Paris 31 August-7 September 1983, 179-82. Paris: Association pour le Congrès International du Froid de Paris, 1983.
108. Sivakumar, V. "Augmentation of boiling heat transfer by internally finned tubes." M.S. thesis, Kansas State University, 1982.
109. Azer, N. Z.; and Sivakumar, V. "Enhancement of saturated boiling heat transfer by internally finned tubes." ASHRAE Transactions 90 (1984): 58-73.
110. Panchal, C. B.; Buyco, E. H.; Yampolsky, J.; and Bell, K. J. "A spirally fluted tube heat exchanger as a condenser and evaporator." In Vol. 6, Heat Transfer 1986: Proceedings of the Eighth International Heat Transfer Conference Held in San Francisco 17- 22 August 1986, edited by C. L. Tien, V. P. Carey, and J. K. Ferrell, 2787-92. Washington, DC: Hemisphere, 1986.

111. Reid, R. W.; Pate, M. B.; and Bergles, A. E. "A comparison of augmentation techniques during in-tube evaporation of R-113." In Boiling and Condensation in Heat Transfer Equipment, edited by E. G. Ragi, T. M. Rudy, T. J. Rabas, and J. M. Robertson, 21-30. New York: American Society of Mechanical Engineers, 1987.
112. Ito, M.; Kimura, H.; and Senshu, T. "Development of high efficiency air-cooled heat exchangers." Hitachi Review 26 (1977): 213-22.
113. Ito, M; and Kimura, H. Boiling heat transfer and pressure drop in internal spiral-grooved tubes." Bulletin of JSME 22 (1979): 1251-57.
114. Kimura, H; and Ito, M. "Evaporating heat transfer in horizontal internal spiral-grooved tubes in the region of low flow rates." Bulletin of JSME 24 (1981): 1602-7.
115. Tatsumi, A.; Oizumi, K.; Hayashi, M.; and Ito, M. "Application of inner groove tubes to air conditioners." Hitachi Review 32 (1982): 55-60.
116. Shinohara, Y.; and Tobe, M. Development of an improved thermo-fin tube." Hitachi Cable Review 4 (1985): 47-50.
117. Uekusa, T.; Tojo, S.; and Kawai, S. "Experimental studies on local evaporating heat transfer of internal spiral-grooved tube. (in Japanese)" Nippon Kikai Gakkai Ronbunshu B Hen 51 (1985): 1042-46.
118. Aoki, Y.; Watanabe, Y.; and Yoshikoshi, A. "Study on improvement of performance of heat exchangers for air conditioners." Technical Review—Mitsubishi Heavy Industries 23 (1986): 252-56.
119. Khanpara, J. C. "Augmentation of in-tube evaporation and condensation of refrigerants 113 and 22 with micro-fin tubes." Ph.D. dissertation, Iowa State University, 1986.
120. Khanpara, J. C.; Bergles, A. E.; and Pate, M. B. "Augmentation of R-113 in-tube evaporation with micro-fin tubes." ASHRAE Transactions 92 (1986): 506-24.
121. Khanpara, J. C.; Bergles, A. E.; and Pate, M. B. "A comparison of in-tube evaporation of refrigerant 113 in electrically heated and fluid heated smooth and inner fin tubes." In Advances in Enhanced Heat Transfer—1987, edited by M. K. Jensen and V. P. Carey, 35-46. New York: American Society of Mechanical Engineers, 1987.
122. Khanpara, J. C.; Pate, M. B.; and Bergles, A. E. "Local evaporation heat transfer in a smooth tube and a micro-fin tube using Refrigerants 22 and 113." In Boiling and Condensation in Heat Transfer Equipment, edited by E. G. Ragi, T. M. Rudy, T. J. Rabas, and J. M. Robertson, 31-39. New York: American Society of Mechanical Engineers, 1987.

123. Fan, L. T.; Lin, S. T.; and Azer, N. Z. "Augmentation of the rate of forced flow boiling heat transfer by means of in-line static mixers." Letters in Heat and Mass Transfer 21 (1977): 849-54.
124. Lin, S. T. "Augmentation of two-phase heat transfer with in-line static mixers." M.S. thesis, Kansas State University, 1979.
125. Azer, N. Z.; Lin, S. T.; and Fan, L. T. "Augmentation of forced flow boiling heat transfer with Kenics motionless mixers." Industrial and Engineering Chemistry Process Design and Development 19 (1980): 246-50.
126. Agrawal, K. N.; Varma, H. K.; and Lal, S. "Boiling of R-12 under swirl flow." In Proceedings of the 5th National Heat and Mass Transfer Conference Held in Hyderabad, India, February 1980, 101-6. n.p.: 1980.
127. Agrawal, K. N.; Varma, H. K.; and Lal, S. "Pressure drop during forced convection boiling of R-12 under swirl flow." Journal of Heat Transfer 104 (1982): 758-62.
128. Agrawal, K. N.; Varma, H. K.; and Lal, S. "A new generalized correlation for predicting swirl flow pressure drops in a horizontal refrigerant 12 evaporator." International Communications in Heat and Mass Transfer 13 (1986): 701-6.
129. Agrawal, K. N.; Varma, H. K.; and Lal, S. "Heat transfer during forced convection boiling of R-12 under swirl flow." Journal of Heat Transfer 108 (1986): 567-73.
130. Agrawal, K. N.; Varma, H. K.; and Lal, S. "An experimental study of the temperature distribution in a horizontal refrigerant 12 evaporator fitted with twisted tapes." In Progress in the Design and Construction of Refrigeration Systems: Proceedings of meetings of B1, B2, E1, E2 of the International Institute of Refrigeration Held at Purdue University 5-8 August 1986, 343-50. Paris: International Institute of Refrigeration, 1986.
131. Bensler, H.P. "Saturated forced-convective boiling heat transfer with twisted-tape inserts." M.S. thesis, University of Wisconsin-Milwaukee, 1984.
132. Jensen, M. K.; Pourdashti, M.; and Bensler, H. P. "Two-phase pressure drop with twisted-tape swirl generators." International Journal of Multiphase Flow 11 (1985): 201-11.
133. Jensen, M. K.; and Bensler, H. P. "Saturated forced-convective boiling heat transfer with twisted-tape inserts." Journal of Heat Transfer 108 (1986): 93-99.
134. Luu, M. "Augmentation of in-tube condensation of R-113." Ph.D. dissertation, Iowa State University, 1979.
135. Luu, M.; and Bergles, A. E. "Augmentation of in-tube condensation of R-113." ISU Engineering Research Institute (Ames, IA) ISU-ERI-Ames-80175, 1980.

136. Luu, M.; and Bergles, A. E. "Augmentation of in-tube condensation of R-113 by means of surface roughness" ASHRAE Transactions 87 (1981): 33-50.
137. Vrable, D. L. "Condensation heat transfer inside horizontal tubes with internal axial fins." Ph.D. dissertation, University of Michigan, 1974.
138. Vrable, D. L.; Yang, W. J.; and Clark, A. "Condensation of refrigerant-12 inside horizontal tubes with internal axial fins." In Vol. III, Heat Transfer 1974: Proceedings of the Fifth International Heat Transfer Conference Held in Tokyo 3-7 September 1974, 250-54. Tokyo: Japan Society of Mechanical Engineers, 1974.
139. Kröger, D. G. "Development of high performance air-cooled refrigerant condensers." Presented to International Institute of Refrigeration Commissions B1, B2, E1 meeting in Belgrade, Yugoslavia, 1977.
140. Luu, M.; and Bergles, A. E. "Enhancement of in-tube condensation of R-113." ASHRAE Transactions 85 (1979): 132-45.
141. Luu, M.; and Bergles, A. E. "Enhancement of horizontal in-tube condensation of refrigerant 113." ASHRAE Transactions 86 (1980): 293-312.
142. Azer, N. Z.; and Said, S. A. Augmentation of condensation heat transfer by internally finned tubes and twisted-tape inserts. Kansas State University Department of Mechanical Engineering (Manhattan) Final Technical Report, 1981.
143. Azer, N. Z.; and Said, S. A. "Augmentation of condensation heat transfer by internally finned tubes and twisted-tape inserts." In Vol. 5, Heat Transfer 1982: Proceedings of the Seventh International Heat Transfer Conference Held in Munich 6-10 September 1982, edited by U. Grigull, E. Hahne, K. Stephan, and J. Straub, 33-38. Washington, DC: Hemisphere, 1982.
144. Said, S. A. "Augmentation of condensation heat transfer of R-113 by internally finned tubes and twisted-tape inserts." Ph.D. dissertation, Kansas State University, 1982.
145. Venkatesh, S. K. "Augmentation of condensation heat transfer of R-11 by internally finned tubes." M.S. thesis. Kansas State University, 1984.
146. Venkatesh, S. K.; and Azer, N. Z. "Enhancement of condensation heat transfer of R-11 by internally finned tubes." ASHRAE Transactions 91 (1985): 128-43.
147. Azer, N. Z.; and Kaushik, N. "Condensation heat transfer enhancement by doubly augmented tubes." ASHRAE Transactions 94 (1988): 000-00.
148. Mori, Y.; and Nakayama, W. "High-performance mist cooled condensers for geothermal binary cycle plants." In Heat Transfer in Energy Problems, edited by T. Mizushima and W.-J. Yang, 211-8. Washington, DC: Hemisphere, 1983.
149. Khanpara, J. C.; Bergles, A. E.; and Pate, M. B. "Augmentation of R-113 in-tube condensation with micro-fin tubes." In Heat Transfer in Air Conditioning and

Refrigeration Equipment, edited by J. A. Kohler and J. W. B. Lu, 35-46. New York: American Society of Mechanical Engineers, 1986.

150. Azer, N. Z.; Fan, L. T.; and Lin, S. T. "Augmentation of condensation heat transfer with in-line static mixers." In Proceedings of the 1976 Heat Transfer and Fluid Mechanics Institute Held in Davis, CA, 21-23 June 1976, edited by A. A. McKillop, J. W. Baughn, and H. A. Dwyer, 512-26. Stanford, CA: Stanford University Press, 1976.
151. Lin, S. T.; Azer, N. Z.; and Fan, L. T. "Heat transfer and pressure drop during condensation inside horizontal tubes with static mixer inserts." ASHRAE Transactions 86 (1980): 649-61.
152. Azer, N. Z.; and Said, S. A. "Heat transfer analysis of annular flow condensation inside circular and semi-circular horizontal tubes." ASHRAE Transactions 92 (1986): 41-54.
153. Said, S. A.; and Azer, N. Z. "Heat transfer and pressure drop during condensation inside horizontal tubes with twisted-tape inserts." ASHRAE Transactions 89 (1983): 114-34.
154. McAdams, W. H. Heat Transmission. 2nd ed. New York: McGraw-Hill, 1942.
155. ASHRAE. "ANSI/ASHRAE Standard 41.4-1984: Standard method for measurement of proportion of oil in liquid refrigerant." Atlanta, GA: American Society of Heating, Refrigerating and Air-Conditioning Engineers, Inc., 1984.
156. Petukhov, B. S. "Heat transfer and friction in turbulent pipe flow with variable physical properties." In Vol. 6, Advances in Heat Transfer, edited by J. P. Hartnett and T. F. Irvine, Jr., 503-64. New York: Academic Press, 1970.
157. Gungor, K. E.; and Winterton, R. H. S. "A general correlation for flow boiling in tubes and annuli." International Journal of Heat and Mass Transfer 29 (1986): 351-58.
158. Kandlikar, S. S. "An improved correlation for predicting two-phase flow boiling heat transfer coefficient in horizontal and vertical tubes." In Heat Exchangers for Two-Phase Flow Applications, edited by J. B. Kitto, Jr. and J. M. Robertson, 3-10. New York: American Society of Mechanical Engineers, 1983.
159. Shah, M. M. "Chart correlation for saturated boiling heat transfer: Equations and further study." ASHRAE Transactions 88 (1982): 185-96.
160. Shah, M. M. "A general correlation for heat transfer during film condensation inside pipes." International Journal of Heat and Mass Transfer 22 (1979): 547-56.
161. Traviss, D. P.; Rohsenow, W. M.; and Baron, A. B. "Forced convection condensation inside tubes: A heat transfer equation for condenser design." ASHRAE Transactions 79 (1972): 157-65.

162. Cavallini, A.; and Zecchin, R. "A dimensionless correlation for the heat transfer in forced convection condensation." In Vol. III, Heat Transfer 1974: Proceedings of the Fifth International Heat Transfer Conference Held in Tokyo 3-7 September 1974, 309-13. Tokyo: Japan Society of Mechanical Engineers, 1974.
163. Baroczy, C. J. "A systematic correlation for two-phase pressure drop." Chemical Engineering Progress Symposium Series 62, No. 64 (1966): 232-49.
164. Chisholm, D. "The influence of mass velocity on friction pressure gradients during steam-water flow." Presented at 1968 Thermodynamics and Fluid Mechanics Convention of the Institute of Mechanical Engineers held in Bristol, UK, March, 1968.
165. Reddy, D. G.; Fighetti, C. F.; and Merilo, M. "Evaluation of two-phase pressure drop correlations for high pressure steam-water systems." In Vol. 1, ASME-ISME Thermal Engineering Joint Conference Proceedings Held in Honolulu 20-24 March 1983, edited by Y. Mori and W.-J. Yang, 251-59. New York: American Society of Mechanical Engineers, 1983.
166. Baker, O. "Simultaneous flow of oil and gas." Oil and Gas Journal 53 (1954): 185-95.
167. Bergles, A. E.; Blumenkrantz, A. R.; and Taborak, J. "Performance evaluation criteria for enhanced heat transfer surfaces." In Heat Transfer 1974: Proceedings of the Fifth International Heat Transfer Conference Held in Tokyo 3-7 September 1974, 234-38. Tokyo: Japan Society of Mechanical Engineers, 1974.
168. Bergles, A. E.; Bunn, R. L.; and Junkhan, G. H. "Extended performance evaluation criteria for enhanced heat transfer surfaces." Letters in Heat and Mass Transfer 1 (1974): 113-20.
169. Webb, R. L. "Performance evaluation criteria for use of enhanced surfaces in heat exchanger design." International Journal of Heat and Mass Transfer 24 (1981): 715-26.
170. Marner, W. J.; Bergles, A. E.; and Chenoweth, J. M. "On the presentation of performance data for enhanced tubes used in shell-and-tube heat exchangers." Journal of Heat Transfer 105 (1983): 358-65.
171. Jensen, M. K. "Enhanced forced convection vaporization and condensation inside tubes." In Heat Transfer Equipment Design, edited by R. K. Shah, E. C. Subbarao, and R. A. Mashelkar, 681-95. New York: Hemisphere, 1988.
172. Webb, R. L. "Performance evaluation criteria for enhanced tube geometries used in two-phase heat exchangers." In Heat Transfer Equipment Design, edited by R. K. Shah, E. C. Subbarao, and R. A. Mashelkar, 697-704. New York: Hemisphere, 1988.

173. Pujol, L; and Stenning, A. H. "Effect of flow direction on the boiling heat transfer coefficient in vertical tubes." In Cocurrent Gas-Liquid Flow, edited by E. R. Rhodes and D. S. Scott, 401-53. New York: Plenum Press, 1969.
174. Royal, J. "Augmentation of horizontal in-tube condensation of steam." Ph.D. dissertation, Iowa State University, 1975.
175. Pierre, B. "Coefficient of heat transfer for boiling Freon-12 in horizontal tubes." Heating and Air Treatment Engineer 19 (1956): 302-10.
176. Sani, R. L. "Downflow boiling and non-boiling heat transfer in a uniformly heated tube." Report UCRL-9023, University of California, Berkeley, 1960.
177. Chaddock, J. B.; and Brunemann, H. "Forced convection boiling of refrigerants in horizontal tubes—Phase 3." Duke University School of Engineering (Durham, NC) Report HL-113, 1967.
178. Shah, M. M. "Chart correlations for saturated boiling heat transfer: Equations and further study." ASHRAE Transactions 88 (1982): 66-86.
179. Akers, W. W.; Deans, H. A.; and Crosser, O. K. "Condensing heat transfer within horizontal tubes." Chemical Engineering Progress Symposium Series 55, No. 29 (1959): 171-76.
180. Boyko, L. D.; and Kruzhilin, G. N. "Heat transfer and hydraulic resistance during condensation of steam in a horizontal tube and in a bundle of tubes." International Journal of Heat and Mass Transfer 10 (1967): 361-73.
181. Chato, J. C. "Laminar condensation inside horizontal and inclined tubes." ASHRAE Journal 4, No. 2 (1962): 52-60.
182. Nusselt, W. "The surface condensation of steam" (in German). Zeitschrift des VDI 60 (1916): 541-69.
183. Azer, N. Z.; Abis, L. V.; and Swearingen, T. B. "Local heat transfer coefficients during forced convection condensation inside horizontal tubes." ASHRAE Transactions 77 (1971): 182-201.
184. Azer, N. Z.; Abis, L. V.; and Soliman, H. M. "Local heat transfer coefficients during annular flow condensation." ASHRAE Transactions 78 (1972): 135-43.
185. Carnavos, T. C. "Heat transfer performance of internally finned tubes in turbulent flow." Heat Transfer Engineering 1, No. 4 (1980): 32-37.
186. Kaushik, N.; and Azer, N. Z. "A general heat transfer correlation for condensation inside internally finned tubes." ASHRAE Transactions 94 (1988): 000-00.
187. Dukler, A. E.; Wicks, M. III; and Cleveland, R. G. "Frictional pressure drop in two-phase flow: B. An approach through similarity analysis." AIChE Journal 10 (1964): 44-51.

188. Hughmark, G. A.; and Pressburg, B. S. "Holdup and pressure drop with gas-liquid flow in a vertical pipe." AICHE Journal 7 (1961): 677-82.
189. Rice, C. K. "The effect of void fraction correlation and heat flux assumption on refrigerant charge inventory prediction." ASHRAE Transaction 93 (1987): 341-67.
190. Butterworth, D. "A comparison of some void-fraction relationships for co-current gas-liquid flow." International Journal of Multiphase Flow 1 (1975): 845-50.
191. Thom, J. R. S. "Prediction of pressure drop during forced circulation boiling of water." International Journal of Heat and Mass Transfer 7 (1964): 709-24.
192. Baroczy, C. J. "Correlation of liquid fraction in two-phase flow with applications to liquid metals." Chemical Engineering Progress Symposium Series 61, No. 57 (1965): 179-91.
193. Tandon, T. N.; Varma, H. K.; and Gupta, C. P. "A void fraction model for annular two-phase flow." International Journal of Heat and Mass Transfer 28 (1985): 191-98.
194. "RS/1 user's guide." Cambridge, MA: BBN Research Systems, 1984.
195. Kline, S. J.; and McClintock, F. A. "Describing uncertainties in single sample experiments." Mechanical Engineering 75 (1953): 3-8.
196. Sieder, E. N.; and Tate, G. E. "Heat transfer and pressure drop of liquids in tubes." Industrial and Engineering Chemistry 28 (1936): 1429-35.

APPENDIX A
EQUIPMENT AND MATERIAL SPECIFICATIONS

Flow Loops

The manufacturer and model number of each component in the test apparatus are shown in Table A.1. Electronic flow meters are shown with the instrumentation in Table A.2.

Table A.1. Components in the flow rig

Loop	Component	Manufacturer	Description or type	Model
R-22	Pump ^a	Wanner Engineering	Positive displacement diaphragm	D-10
R-22	AC superheater	March Beaded Heaters	Nicrome wire	MBH-1500
R-22	After-condenser	American Standard	Shell-and-tube	HCF 02036
R-22	Accumulator ^a	Oil-Air Industries	Bladder	1-1002
R-22	Sight glasses	Allin	1/2 inch, solder fit.	SG-208
R-22	Insulation	Halstead Industrial	Flexible foam	—
R-22	Current source	American Rectifier	1200-amp rectifier	SIMSAF 611225E
Water	Pump	March	Centrifugal	TE-5.5CMD
Water	Heater	Watlow	2000-Watt immersion	BCC 11G3
Glycol	Pump	March	Centrifugal	TE-5.5CMD
Glycol	Cooling unit	Snyder General	R-12, 5 ton	BW-0500 E5
Glycol	Flow meter	Brooks Instrument	Rotameter	1110- 10H3B1A

^a Elastomeric components were either butyl or neoprene, as available from vendors. The bladder and pump diaphragms were replaced during the period of testing due to the limited life of elastomers in contact with refrigerant and oil.

Instrumentation

The instrumentation is specified by manufacturer and model number in Table A.2. Panel meters, pressure gages, etc., which were used only to monitor conditions and not for the acquisition of data, are not included.

Table A.2. Data acquisition and instrumentation components

Component	Manufacturer	Description	Model
Controller	Digital Equipment	Digital computer	Pro 380
Multimeter	Hewlett-Packard	Digital multimeter	3457A
Scanner	Hewlett-Packard	Switch control unit	3488A
Scanner board (3)	Hewlett-Packard	Multiplexer board	44470A
Scanner board (1)	Hewlett-Packard	Matrix switch board	44473A
Thermocouples (20)	Omega	Bare bead or SS sheathed	Type-T
Cold junction	Omega	Electronic ice point	MCJ-T
R-22 flowmeter	Connometer	Positive displacement ($\pm 1\%$)	B13-AAS
Water flowmeter	Water-Mag	Magnetic ($\pm 2\%$)	7485- W1A6AA
System pressure	Sensotec	Strain gage transducer; 0-500 psig ($\pm 0.25\%$)	Z708-18
Power supply	Omega	For pressure transducer	PST-10
Pressure drop	Celesco	Variable reluctance, 10 psid ($\pm 0.25\%$)	P7D -
Power supply/ electronics board	Celesco	For ΔP transducer	03156
Current transducer	Ohio Semitronics	0-20 amp AC to 0-10 VDC ($\pm 0.25\%$)	CT20 TRV

Expendable Materials

The major expendable materials used during this investigation were refrigerant and oil. Throughout the testing, the working fluid was R-22 (chlorodifluoromethane, CHClF_2) manufactured by DuPont or Racon. The 150-SUS oil was refined by Calumet Refining and was designated RO-15. The 300-SUS oil was Suniso 4GS, refined by Witco Chemical.

To clean the oil out of the system and to flush the oil out of the test section during hold-up testing, DuPont R-11 (trichlorofluoromethane, CCl_3F) was used. The oils were fully miscible in R-11. This refrigerant was convenient because it is a liquid near ambient conditions; yet it has a low vapor pressure, allowing easy removal from the system with a vacuum pump.

APPENDIX B EXPERIMENTAL PROCEDURES

This appendix describes the experimental procedures used in this test program. It includes sections on heat transfer and pressure drop testing, oil injection and sampling procedures, as well as the investigation of oil hold-up in the test section.

Heat Transfer and Pressure Drop Testing

The commercial refrigeration unit was allowed to run for several hours prior to testing so the water and glycol mixture would be -25°C or colder at the beginning of testing. Evaporation testing required this low temperature, but condensation testing could begin with a higher temperature. While the refrigeration unit was running, the pump to circulate the cold mixture through the after-condenser was also operating. For condensation tests, the mixture was circulated only through the after-condenser, but for evaporation, it was also circulated around the bladder accumulator.

When a suitable temperature had been achieved, the positive displacement pump was turned on to circulate refrigerant. The entire rig was cooled to its equilibrium temperature before testing began.

While the rig was cooling, other components were prepared:

1. The water in the annulus was circulated and the temperature adjusted to the approximate level desired for testing. For evaporation, the water was cooled to between 5 and 10°C , while for condensation, it was heated to about 30 to 35°C . The water flow rate was adjusted to the desired value by means of a throttle valve on the discharge side of the pump.
2. The boiler power source was prepared for operation by starting the flow of cooling water through the power leads and then the unit was turned on.
3. The pressure level was set by adjusting the air in the bladder accumulator. The pressure could only be approximately set, because pressure depended on the actual test conditions achieved, such as quality range, after-condenser outlet temperature, etc.

After all the above was completed, the refrigerant flow rate was set by adjusting two valves. One valve was in the main flow line to the test section and the other was in the refrigerant by-pass line. These were adjusted so that the desired flow was obtained with a small pressure drop between the pump and test section. By maintaining this pressure drop, the flow rate remained steadier.

With flow rates, temperatures, and pressures set to approximately the desired values, the heaters were turned on and adjusted to give the desired inlet vapor quality. At this point, it was necessary to wait for steady-state conditions before taking data. To determine when steady state had been reached, the data acquisition program had a subroutine to check flow rates, temperatures, pressures, qualities, and heat flows. If the system was approaching an undesired steady-state condition, power levels, flow rates, pressures, etc., were adjusted to drive the system toward desired conditions. Once a desired steady state was achieved, the data acquisition routine was activated.

The data acquisition routine required manual input of ambient temperature, atmospheric pressure, oil concentration, and type of test (that is, evaporation or condensation). After these manual inputs were completed, data acquisition was automatic. When data acquisition was completed, an indication of the deviation for each channel was displayed. If conditions were not sufficiently steady, as indicated by large deviations, the run could be aborted. If all conditions appeared satisfactory, the analysis program was called and the reduced data were printed and stored on a disk.

Due to some problems with zero drift on the differential pressure transducer, the zero point was checked and adjusted as necessary before and after each test run. If it was found that the zero had shifted, corrections were noted on the printouts.

Oil Injection and Sampling

Both oil injection and sampling were accomplished with a modified, double-acting air cylinder as was shown in Figure 4.3. The methods for oil injection, sample removal, and the calculation of the oil concentration are presented below.

Oil Injection

With the piston pushed completely into the cylinder, the small tube attached to the end of the cylinder was placed in a container of oil. The piston was then retracted to draw oil into the cavity in much the same manner that a hypodermic needle is filled. When the cylinder was filled with oil, it was allowed to sit in an upright position (valve end up) so air bubbles would separate to the top. Still held in this position, the piston was pushed in slightly to remove all air. The valve in the end of the cylinder was then closed.

The air side of the cylinder was connected to a nitrogen bottle with a flexible hose and the oil side was connected to the flow loop with small diameter tubing and compression fittings. Prior to tightening the fittings, oil was forced through the small tube and into the dead space of the valve on the flow rig to prevent the injection of air. After tightening the fittings, the valves on the rig and on the cylinder were both opened. A valve on the nitrogen cylinder was then opened slightly so that oil would be injected slowly into the rig.

When the piston was at the limit of its travel and all the oil had been injected, the valves were closed and the cylinder was removed. This process was repeated until the desired amount of oil had been injected. Refrigerant was circulating during the injection process to speed the uniform dispersal of oil throughout the rig.

Oil Sampling

After oil injection, refrigerant was allowed to circulate for several hours, varying the proportion of flow through the pump bypass line and the main flow loop. This enhanced mixing, allowing the mixture to reach a concentration equilibrium.

Sampling was accomplished in much the same manner as injection, but by reversing the steps. The air hose was attached to the air side and the oil side was attached to the rig through the small tubing. The air side was then pressurized to a level higher than the refrigerant. The valves between the cylinder and the rig were opened; the air was bled off gently so the sample could be withdrawn slowly from the flow stream. Refrigerant was circulating during the sampling process.

When a sufficient sample was in the cylinder, both valves were again closed, the cylinder was removed from the rig, and the remaining air pressure released.

Determination of Oil Concentration

Procedure Before a sample was taken, the cylinder was cleaned with R-11 and thoroughly dried. The empty cylinder and filter attachment were weighed (W1) on a balance having an accuracy of ± 0.02 g. After a sample was obtained, the filled cylinder and filter attachment were again weighed (W2). The cylinder was then placed in a vertical position (sample side up) and the valve on the cylinder opened slightly. The refrigerant in the cylinder flashed slowly and the vapor was released through the filter. Any entrained oil in the exiting vapor was thus trapped in the filter. The cylinder was never completely filled with the liquid sample. Thus, when the valve was opened, there was vapor near the exit, which prevented the escape of liquid.

When the pressure of the sample had been reduced to ambient, the temperature was quite low and there was still some refrigerant dissolved in the oil. To remove this dissolved refrigerant, the cylinder was heated with a hot air gun until the temperature was 40 to 45°C. A vacuum pump was then attached to the sample side and a vacuum applied for several minutes. The cylinder and filter attachment were again weighed (W3).

Calculation method The mass fraction of oil in the refrigerant is determined by the following equation:

$$\omega_o = \frac{W3 - W1}{W2 - W1} \quad (\text{B.1})$$

The final value for the oil concentration is the arithmetic mean of three independent tests. The standard deviation of the mean is defined as

$$\sigma = \frac{\sqrt{(\omega_{o1} - \bar{\omega}_o)^2 + (\omega_{o2} - \bar{\omega}_o)^2 + (\omega_{o3} - \bar{\omega}_o)^2}}{\sqrt{3^2 - 3}} \quad (\text{B.2})$$

where $\bar{\omega}_o$ is the arithmetic mean of the independent observations of the oil concentration.

The procedure outlined above and the calculation method are based on ANSI/ASHRAE Standard 41.4-1984 [155], although some variations were made due to constraints of the system. The most significant deviation from the standard is the use of a

smaller sample size so that sample withdrawal would not significantly alter the composition of the system.

Oil Hold-Up

This section outlines the method that was used to measure the amount of oil in the test section during evaporation and condensation tests. Hold-up tests required considerable time, making replication impractical. The time associated with these tests also prevented the determination of the true mass fraction of oil in the test section for all but four of the test runs. For the remainder of the test runs, only the quantity of oil in the test sections was measured, giving information on the relative, rather than absolute, hold-up at various conditions. Even for the cases in which the actual mass fraction of oil was measured, the mass fraction was not local, but rather an averaged over the entire test section.

Isolation of the Test Section

Air actuated ball valves at each end of the test section were latched open with the actuators pre-charged to about 0.2 MPa (30 psig). When desired conditions in the refrigerant flow loop were achieved, a switch was closed to energize a solenoid at each valve. The solenoids unlatched the valves, allowing them to close within 30 to 50 milliseconds, trapping the refrigerant and oil in the test section. Simultaneously, power to the boiler was cut off to avoid overheating and the valve in the pump by-pass line was opened to prevent overpressure. After these critical items were accomplished, the rest of the rig was shut down in a more deliberate fashion.

Measuring only Oil in the Test Section

A bleed valve was opened to allow the R-22 vapor in the test section to slowly escape. When atmospheric pressure was reached, a drain plug on the end of the test tube opposite the bleed valve was opened. An R-11 supply was connected to the bleed valve opening with a flexible hose and R-11 was fed into the test section. A hose led from the drain plug to a 1000-mL filter flask, which collected the R-11 and oil. Four or five rinses with a combined volume of 600 to 700 mL were used to ensure removal of all oil. Additional rinses were found to collect less than 0.1 g of additional residual oil.

The fluid in the collecting vessel was a mixture of primarily R-11 and refrigeration oil, but with a small amount of R-22. To remove the refrigerant, the collecting vessel was placed on a heating element and simultaneously evacuated. When only oil remained, the vessel was weighed and the quantity of oil calculated by subtracting the weight of the clean, empty vessel.

Measuring Refrigerant in the Test Section

For four of the hold-up tests, the amount of R-22 in the test section was measured in addition to the amount of oil. This allowed the calculation of the true mass fraction of oil in the test section. Collecting refrigerant was a slow process; hence, it was only done for a limited number of test runs.

After the test section was isolated with the ball valves as described above, instead of bleeding the refrigerant to the atmosphere, the sampling cylinder (Figure 4.3) was attached to the bleed valve. The valve was opened and refrigerant allowed to flow into the cylinder. To remove as much R-22 as possible, hot (50°C) water was circulated through the annulus and the sample cylinder was cooled with ice. When the pressure in the test section stabilized, the valves were closed and the filled sample cylinder was weighed. This was repeated until the pressure in the test section was less than 0.5 MPa. The mass of refrigerant remaining in the test section was estimated using the volume of the test section and the density of the vapor. Total refrigerant mass was the sum of the samples withdrawn in the cylinder plus the estimate of refrigerant vapor remaining in the test section. The remaining refrigerant vapor was then bled off and the amount of oil was determined as described earlier.

APPENDIX C
DATA ACQUISITION AND ANALYSIS PROGRAM

```

C*****
C   PROGRAM "DARAS.FTN"
C   MAIN DRIVER PROGRAM TO ACQUIRE DATA, ANALYZE DATA, PRINT RESULTS
C   TO BOTH DISC AND PRINTER. MUST BE LINKED TO "IEEE488", "ANALYSIS",
C   AND "OUTPUT". DATA ARE GATHERED VIA AN IEEE-488 BUS AND COMPATIBLE
C   DEVICES. BUS ACCESS ACHIEVED THROUGH A GROUP OF SUBROUTINES FROM
C   THE PRO REAL TIME INTERFACE LIBRARY (PRTL). THE PROGRAM CONSISTS
C   PRIMARILY OF CALLS TO SUBROUTINES WHICH DO ACTUAL DATA MANIPULA-
C   TIONS. A LIST OF THE SUBROUTINES CALLED APPEARS BELOW. (THERE ARE
C   OTHER SUBROUTINES CALLED FROM THE VARIOUS SUBROUTINES LISTED BELOW,
C   BUT THESE ARE LISTED IN THE CALLING SUBROUTINE.)
C
C       INIT    INITIALIZES THE IEEE-488 BUS AND DEVICES
C       TRIAL   CHECKS ON TEST CONDITIONS AND IF STEADY STATE
C       ACQDTA  ACQUIRES DATA VIA THE BUS AND CONVERTS IT TO
C               PHYSICAL DIMENSIONS; ALSO CHECKS DATA DEVIATION
C       ANAL    TAKES THE DATA FROM ACQDTA AND ANALYZES IT TO
C               OBTAIN CALCULATED QUANTITIES
C       SIPRNT  PRINTS THE DATA TO PRINTER AND/OR DISC IN SI UNITS
C       ENPRNT  PRINTS THE DATA TO PRINTER IN ENGLISH UNITS (OPT)
C*****
C   INITIALIZE IEEE-488 BUS AND DEVICES
C
C   N=0 !COUNTER TO PREVENT MULTIPLE CALLS TO CERTAIN PRTL ROUTINES
10  CALL INIT(N)
C
C   DETERMINE THE TEST CONDITIONS AND IF RIG IS APPROX. STEADY STATE
C
C   CALL TRIAL
C   PRINT *, 'ENTER 0 IF ANOTHER TRIAL IS NOT DESIRED--'
C   ACCEPT *, IQ
C   IF(IQ.NE.0) GO TO 10
C
C   DATA ACQUISITION
C
C   CALL INIT(N)
C   CALL ACQDTA
C
C   DATA ANALYSIS
C
C   CALL ANAL
C
C   PRINT RESULTS IN SI AND INQUIRE IF ENGLISH PRINTOUT DESIRED
C
C   CALL SIPRNT(0)
C   PRINT *, 'ENTER 1 IF ENGLISH UNITS PRINTOUT IS DESIRED--'
C   ACCEPT *, IQ1
C   IF(IQ1.EQ.1) CALL ENPRNT
C   PRINT *
C   PRINT *, '***** PROGRAM COMPLETION *****'
C   STOP
C   END

```

```

C*****
C*****
C      MODULE "IEEE488"
C      THIS MODULE CONSISTS OF FOUR SUBROUTINES, PRIMARILY TO COMMUNICATE
C      WITH VARIOUS DATA ACQUISITION DEVICES VIA THE IEEE-488 BUS. THESE
C      ROUTINES RELY ON THE PRO REAL-TIME INTERFACE LIBRARY FOR BUS
C      COMMUNICATIONS. THE SUBROUTINES INCLUDED ARE:
C          INIT      INITIALIZES THE IEEE-488 BUS AND DEVICES
C          TRIAL     GATHERS SOME DATA AND ANALYZES THEM TO DETERMINE
C                   RIG CONDITIONS AND WHETHER STEADY STATE
C          ACQDTA   MAIN DATA ACQUISITION ROUTINE; ALSO INCLUDES THE
C                   CONVERSION OF UNITS TO PHYSICAL DIMENSIONS
C          STRTRL   FUNCTION CONVERTS STRING VARIABLE TO REAL
C*****
C      ++++++
C-----
C      SUBROUTINE INIT(IC)
C-----
C      SUBROUTINE TO INITIALIZE THE IEEE-488 BUS AND ALL DEVICES ON IT.
C      THE DMM IS SET TO REAR TERMINALS AND FOR T/C LEVEL VOLTAGE.
C      THE SUBROUTINES CALLED ARE FROM THE PRTIL.
C
C      INTEGER*2 ISTAT(2)
C      CHARACTER*60 DMMSET
C      DMMSET='TERM REAR;TARM SYN;TRIG SYN;NRDGS 1,SYN;DCV .030'
C      IC=IC+1
C      IF(IC.GT.1) GO TO 10
C      CALL IBINIT(ISTAT,,,2,1)
10    CALL IBREN(ISTAT,2,1)
C      CALL IBLLO(ISTAT,2,1)
C      CALL IBDCL(ISTAT,2,1)
C      CALL IBSEND(ISTAT,'CLOSE 400',9,2,1+2+8,,9) ! SET SCANNER
C      CALL IBSEND(ISTAT,DMMSET,48,2,1+2+8,,22) !SET MULTIMETER
C      RETURN
C      END
C
C      ++++++
C-----
C      SUBROUTINE TRIAL
C-----
C      SUBROUTINE WHICH CHECKS ON SEVERAL KEY PARAMETERS TO ASSURE STEADY
C      STATE OPERATION AT THE DESIRED CONDITIONS PRIOR TO COMMENCING DATA
C      ACQUISITION AND PRINTS RESULTS TO SCREEN. PARAMETERS CHECKED ARE:
C
C          TUBE SIDE INLET TEMP AND PRESSURE
C          TUBE SIDE OUTLET TEMP
C          ANNULUS SIDE INLET AND OUTLET TEMP
C          AFT CONDENSER OUTLET TEMP
C          BOILER INLET TEMP
C          WATER/GLYCOL RESEVOIR TEMP
C          BOILER WALL TEMP
C          TEST SECTION INLET AND OUTLET QUALITY
C
C      SUBROUTINES CALLED ARE:
C
C          IBSEND  PRTIL ROUTINE TO SEND INFO TO IEEE-488 DEVICE

```

```

C          IBRECV  PRTIL ROUTINE TO RECEIVE DATA FROM IEEE-488 DEVICE
C          WAIT    CAUSES EXECUTION TO PAUSE FOR SPECIFIED TIME
C          TCCT    PRTIL ROUTINE TO CONVERT TYPE T T/C VOLTS TO OC
C          STRTRL  FUNCTION TO CONVERT STRING DATA TO REAL NUMBERS
C
C          DIMENSION V(16),T(16)
C          INTEGER*2 ISTAT(2)
C          CHARACTER*66 TSCAN
C          CHARACTER*16 STRDAT
C
C          SET PARAMETERS FOR IEEE-488 CALLS
C
C          TSCAN='SLIST 100-107,100-107,301-307;CMON -1'
C          DATA IPAUSE, IDELAY/8000,150/
C
C          SET SCANNER FOR DESIRED T/C CHANNELS; DMM ALREADY SET IN "INIT"
C
C          CALL IBSEND(ISTAT,TSCAN,37,2,1+2+8,,9)
C
C          SCAN THROUGH T/C CHANNELS TWICE; WAIT 10 SEC BETWEEN SCANS
C
C          DO 10 I=1,16
C          CALL IBSEND(ISTAT,'STEP',4,2,1+2+8,,9)
C          CALL WAIT(IDELAY,1)
C          CALL IBRECV(ISTAT,STRDAT,16,5,1+2,,22)
C          V(I)=STRTRL(STRDAT)
C          IF (I.EQ.8) CALL WAIT(IPAUSE,1)
10         CONTINUE
C
C          SCAN OTHER NECESSARY CHANNELS
C          CHANNEL 301, PRESSURE
C          CALL IBSEND(ISTAT,'STEP',4,2,1+2+8,,9)
C          CALL WAIT(IDELAY,1)
C          CALL IBRECV(ISTAT,STRDAT,16,5,1+2,,22)
C          P=STRTRL(STRDAT)
C          CHANNEL 302, BOILER VOLTAGE
C          CALL IBSEND(ISTAT,'DCV 20.',7,2,1+2+8,,22)
C          CALL IBSEND(ISTAT,'STEP',4,2,1+2+8,,9)
C          CALL WAIT(IDELAY,1)
C          CALL IBRECV(ISTAT,STRDAT,16,5,1+2,,22)
C          BOILV=STRTRL(STRDAT)
C          CHANNEL 303, SHUNT VOLTAGE (BOILER CURRENT)
C          CALL IBSEND(ISTAT,'DCV .03',7,2,1+2+8,,22)
C          CALL IBSEND(ISTAT,'STEP',4,2,1+2+8,,9)
C          CALL WAIT(IDELAY,1)
C          CALL IBRECV(ISTAT,STRDAT,16,5,1+2,,22)
C          BOILI=STRTRL(STRDAT)
C          CHANNEL 304, SUPER HEATER CURRENT
C          CALL IBSEND(ISTAT,'DCV 10.',6,2,1+2+8,,22)
C          CALL IBSEND(ISTAT,'STEP',4,2,1+2+8,,9)
C          CALL WAIT(IDELAY,1)
C          CALL IBRECV(ISTAT,STRDAT,16,5,1+2,,22)
C          SUPI=STRTRL(STRDAT)
C          CHANNEL 305, SUPER HEATER VOLTAGE
C          CALL IBSEND(ISTAT,'ACV 220.',8,2,1+2+8,,22)
C          CALL IBSEND(ISTAT,'STEP',4,2,1+2+8,,9)
C          CALL WAIT(IDELAY,1)
C          CALL IBRECV(ISTAT,STRDAT,16,5,1+2,,22)

```

```

C      SUPV=STRTRL(STRDAT)
      CHANNEL 306, REFRIGERANT FLOW
      CALL IBSEND(ISTAT,'DCV .5',6,2,1+2+8,,22)
      CALL WAIT(IDELAY,1)
      CALL IBSEND(ISTAT,'STEP',4,2,1+2+8,,9)
      CALL WAIT(IDELAY,1)
      CALL IBRECV(ISTAT,STRDAT,16,5,1+2,,22)
      REFFLO=STRTRL(STRDAT)
C      CALL IBSEND(ISTAT,'OPEN 306',8,2,1+2+8,,9)
      CHANNEL 401, WATER FLOW
      CALL IBSEND(ISTAT,'DCI .02',7,2,1+2+8,,22)
      CALL IBSEND(ISTAT,'CLOSE 401',9,2,1+2+8,,9)
      CALL WAIT(IDELAY,1)
      CALL IBSEND(ISTAT,'OPEN 400',8,2,1+2+8,,9)
      CALL WAIT(IDELAY,1)
      CALL IBRECV(ISTAT,STRDAT,16,5,1+2,,22)
      CALL IBSEND(ISTAT,'CLOSE 400',9,2,1+2+8,,9)
      CALL WAIT(IDELAY,1)
      CALL IBSEND(ISTAT,'OPEN 401',8,2,1+2+8,,9)
      WATFLO=STRTRL(STRDAT)

C
C      CONVERT VOLTAGES TO TEMPERATURES IN DEG C USING PRTL SUBROUTINE
C
      CALL TCCT(V,T,16)

C
C      CONVERT OTHER VOTAGES AND CURRENTS TO PHYSICAL DIMENSIONS
C
      BOILI=30000.*BOILI !BOILER CURRENT
      QBOIL=1.27*BOILV*BOILI !BQILER POWER
      SUPI=2.0*SUPI !SUPERHEATER CURRENT
      QSUPH=SUPV*SUPI !SUPERHEATER POWER
      QTOT=QBOIL+QSUPH
      P=P*1000.
      P=(-2.65+16.6*P-.00258*P*P)*6894.4)+.1E6
      WDOTW=(562.5*WATFLO-2.25)*.06313
      WDOTR=1.263E-4*REFFLO*(1285.-3.5*T(14))

C
C      CALCULATE INLET AND OUTLET QUALITY OF REFRIGERANT IN TEST SECTION
C      APPROXIMATIONS ARE USED FOR PROPERTIES
C
      CP=1190.
      TSATR=TSAT(P)
      DELT1=((T(9)+T(10))/2.)-T(11)
      DELT2=((T(9)+T(10))/2.)-T(12)
      TLM=(DELT1-DELT2)/ALOG(DELT1/DELT2)
      DTSENS=TSATR-T(14)-273.2
      QSENS=CP*DTSENS*WDOTR
      HFG=205.E3-0.9E3*(TSATR-273.2)
      XIN=(QTOT-QSENS)/(WDOTR*HFG)

C
      QTEST=WDOTW*4190.*(T(11)-T(12))
      DX=QTEST/(WDOTR*HFG)
      XOUT=XIN+DX
      CALL IBRDA(ISTAT,2,1)

C
C      PRINT RESULTS TO THE CRT
C

```

```

PRINT *
PRINT 99
PRINT 100
PRINT *
PRINT 110, T(1),T(9)
PRINT 120, T(2),T(10)
PRINT 130, T(3),T(11)
PRINT 140, T(4),T(12)
PRINT 150, T(5),T(13)
PRINT 160, T(6),T(14)
PRINT 170, T(7),T(15)
PRINT 180, T(8),T(16)
PRINT *
PRINT 185, TLM
PRINT 190, P/1.E6
PRINT 200, XIN
PRINT 210, XOUT
PRINT 220, WDOTR
PRINT 230, WDOTW
PRINT 240, QTOT
PRINT 250, QTEST
PRINT 99
PRINT *
99  FORMAT(' ', '*****')
100  FORMAT(' ', 'TEMPERATURE IN DEG C', T26, 'TIME 0', T40, ' 0 + 10')
110  FORMAT(' ', 'TEST SECTION INLET', T24, F8.3, T39, F8.3)
120  FORMAT(' ', 'TEST SECTION OUTLET', T24, F8.3, T39, F8.3)
130  FORMAT(' ', 'ANNULUS INLET', T24, F8.3, T39, F8.3)
140  FORMAT(' ', 'ANNULUS OUTLET', T24, F8.3, T39, F8.3)
150  FORMAT(' ', 'AFT CONDENSER OUTLET', T24, F8.3, T39, F8.3)
160  FORMAT(' ', 'BOILER INLET', T24, F8.3, T39, F8.3)
170  FORMAT(' ', 'WATER/GLYCOL RESEVOIR', T24, F8.3, T39, F8.3)
180  FORMAT(' ', 'BOILER WALL', T24, F8.3, T39, F8.3)
185  FORMAT(' ', 'LOG MEAN TEMP DIFFERENCE (OC)', T40, F8.3)
190  FORMAT(' ', 'TEST SECTION INLET PRESSURE (MPa)', T40, F8.5)
200  FORMAT(' ', 'TEST SECTION INLET QUALITY', T40, F6.3)
210  FORMAT(' ', 'TEST SECTION OUTLET QUALITY', T40, F6.3)
220  FORMAT(' ', 'REFRIGERANT FLOW (kg/s)', T40, F8.5)
230  FORMAT(' ', 'ANNULUS WATER FLOW (kg/s)', T40, F7.4)
240  FORMAT(' ', 'BOILER + SUPERHEATER Q (W)', T40, F8.0)
250  FORMAT(' ', 'TEST SECTION Q (W)', T40, F8.0)
RETURN
END

C
C-----
C-----
SUBROUTINE ACQDTA
C-----
C  SUBROUTINE TO ACQUIRE DATA VIA IEEE-488 BUS.  EACH DATA POINT IS
C  SCANNED A TOTAL OF 5 TIMES (DELTA P 35 TIMES), CONVERTED FROM A
C  STRING TO REAL NUMBER, THEN AVERAGED BEFORE CONVERSION TO PHYSICAL
C  DIMENSIONS, WHERE APPLICABLE.  ATM. PRESSURE AND TEMPERATURE ARE
C  REQUESTED AS MANUAL INPUTS.  DATA ARE RETURNED TO THE MAIN PROGRAM
C  VIA A COMMON BLOCK TO BE PASSED TO A DATA ANALYSIS SUBROUTINE.
C  PASSED VALUES ARE:
C
C  PATM=ATMOSPHERIC PRESSURE
C  DATAF(1)=TUBE INLET T
C  DATAF(16)=ANNULUS OUTLET T

```

```

C      (2)=-TUBE OUTLET T      (17)=BOILER OUTLET T
C      (3)=-ANNULUS INLET T   (18)=R-22 FLOW METER T
C      (4)=-ANNULUS OUTLET T  (19)=ANNULUS HEAT EX OUT T
C      (5)=-AFT COND OUTLET T (20)=AMBIENT REFERENCE T
C      (6)=-BOILER INLET T    (21)=TUBE PRESSURE DROP
C      (7)=-WAT/GLYCOL RES T  (22)=TUBE INLET P
C      (8)=-BOILER WALL T     (23)=BOILER V
C      (9)=-      "          (24)=BOILER I
C      (10)=-      "         (25)=SUPER HEATER I
C      (11)=-      "         (26)=SUPER HEATER V
C      (12)=-WAT/GLYCOL RES T (27)=R-22 MDOT (V ONLY)
C      (13)=-TUBE INLET T     (28)=OIL PERCENTAGE
C      (14)=-TUBE OUTLET T    (29)= --OPEN--
C      (15)=-ANNULUS INLET T  (30)=ANNULUS MDOT (mA ONLY)

```

```

EPS(1-30)=PERCENT DEVIATION FROM HIGH TO LOW READINGS FOR EACH OF
THE RESPECTIVE CHANNELS ABOVE.

```

```

DIMENSION REDATA(5,30),DATAF(30),TF(30),EPS(30),DELP(30)
CHARACTER*66 SCAN,S1
CHARACTER*16 RAWDTA
CHARACTER*9 DT
CHARACTER*8 TM
CHARACTER*25 OILTYP,TUBTYP
CHARACTER*12 TYPE
INTEGER*2 ISTAT(2)
COMMON /DTPS/ PATM,DATAF,EPS
COMMON /CHAR/ TYPE, TM,DT,OILTYP,TUBTYP
COMMON /GEOM/ TL,TIDMAX,TOD,AID,HYD,TIDNOM,A1,A2,A3,A4
COMMON /FLAG/ IQ1,IQ2

```

```

C
DATA DATAF,EPS,EPSMAX,PI,TOL/61*0.0,3.14159,.1/
SCAN='SLIST 100-109,200-209,300-307;CMON -1'
S1='STEP'

```

```

C
C
C
DETERMINE CURRENT DATE AND TIME

```

```

CALL DATE(DT)
CALL TIME(TM)

```

```

C
PRINT *, 'MANUAL INPUT OF DATA:'
PRINT *, 'MAKE THE FOLLOWING CHOICES FOR THIS TEST RUN:'
PRINT *, '      SINGLE PHASE = 1      OIL      = 1'
PRINT *, '      EVAPORATION   = 2      NO OIL   = 2'
PRINT *, '      CONDENSATION   = 3'
PRINT *
PRINT *, 'ENTER TWO NUMBERS IN ORDER, SEPARATED BY A COMMA--'
PRINT *
ACCEPT *, IQ1, IQ2
IF (IQ1.EQ.1) THEN
      TYPE='SINGLE PHASE'
ELSE IF (IQ1.EQ.2) THEN
      TYPE='EVAPORATION'
ELSE
      TYPE='CONDENSATION'
END IF
IF (IQ2.EQ.1) THEN

```

```

C

```

```

C      OIL TYPE MUST BE EDITED IF DIFFERENT OIL IS USED
C
          OILTYP='NAPHTHENIC, 150 SUS'
          PRINT *, 'ENTER MASS FRACTION OF OIL--'
          PRINT *
          ACCEPT *, DATAF(28)
      ELSE
          OILTYP='      N/A'
      END IF
      PRINT *, 'ENTER AMBIENT PRESSURE (in Hg) AND TEMPERATURE (F) --'
      PRINT *
      ACCEPT *, PATM, TAMB
      TAMB=(TAMB-32.)*5./9.
      PATM=(PATM/29.92)*.101325E6
C
C      DETERMINE GEOMETRIC PARAMETERS OF TEST SECTION (STORED IN FILE)
C
      OPEN(UNIT=4, FILE='TUBEGEOM.DAT', STATUS='OLD', READONLY)
      READ(4, 600) TL, TIDMAX, TIDNOM, TOD, AID, TUBTYP
      CLOSE(4)
      A1=(TIDNOM**2)*PI/4.
      A2=(AID**2-TOD**2)*PI/4.
      A3=PI*TIDMAX*TL
      A4=PI*TOD*TL
      HYD=AID-TOD
C
C      LOOP 1-5 TO SCAN ALL CHANNELS 5 TIMES; LOOP 1-20 FOR THERMOCOUPLES
C      SEPARATE LOOPS TOTALING 30 SAMPLES FOR PRESSURE DROP
C
      CALL IBSEND(ISTAT, 'DCV 10.', 7, 2, 1+2+8, ,, 22)
      CALL IBSEND(ISTAT, 'CLOSE 300', 9, 2, 1+2+8, ,, 9)
C
C      SCAN PRESSURE DROP 15 TIMES
C
      DO 1 K=1, 15
          CALL IBRCV(ISTAT, RAWDTA, 16, 5, 1+2, ,, 22)
          DELP(K)=STRTRL(RAWDTA)
1      CONTINUE
      CALL IBSEND(ISTAT, 'OPEN 300', 8, 2, 1+2+8, ,, 9)
C
C      SCAN ALL CHANNELS 5 TIMES
C
      PRINT *, 'CURRENTLY ON SCAN NUMBER (OUT OF 5):'
      DO 10 I=1, 5
          PRINT *, I
          IDELAY=150
          CALL IBSEND(ISTAT, 'DCV .03', 7, 2, 1+2+8, ,, 22)
          CALL IBSEND(ISTAT, SCAN, 37, 2, 1+2+8, ,, 9)
C      THERMOCOUPLE LOOP
          DO 20 J=1, 20
              CALL IBSEND(ISTAT, S1, 4, 2, 1+2+8, ,, 9)
              CALL WAIT(IDELAY, 1)
              CALL IBRCV(ISTAT, RAWDTA, 16, 5, 1+2, ,, 22)
              REDATA(I, J)=STRTRL(RAWDTA)
20          CONTINUE
C      CHAN 300, PRESSURE DROP
          CALL IBSEND(ISTAT, 'DCV 10.', 7, 2, 1+2+8, ,, 22)
          CALL IBSEND(ISTAT, S1, 4, 2, 1+2+8, ,, 9)

```

```

      CALL WAIT(IDELAY,1)
      CALL IBRCV(ISTAT,RAWDTA,16,5,1+2,,,22)
      REDATA(I,21)=STRTRL(RAWDTA)
C   CHAN 301, TUBE PRESSURE
      CALL IBSEND(ISTAT,'DCV .03',7,2,1+2+8,,,22)
      CALL IBSEND(ISTAT,S1,4,2,1+2+8,,,9)
      CALL WAIT(IDELAY,1)
      CALL IBRCV(ISTAT,RAWDTA,16,5,1+2,,,22)
      REDATA(I,22)=STRTRL(RAWDTA)
C   CHAN 302, BOILER VOLTAGE
      CALL IBSEND(ISTAT,'DCV 20.',7,2,1+2+8,,,22)
      CALL IBSEND(ISTAT,S1,4,2,1+2+8,,,9)
      CALL WAIT(IDELAY,1)
      CALL IBRCV(ISTAT,RAWDTA,16,5,1+2,,,22)
      REDATA(I,23)=STRTRL(RAWDTA)
C   CHAN 303, BOILER CURRENT (SHUNT VOLTAGE)
      CALL IBSEND(ISTAT,'DCV .03',7,2,1+2+8,,,22)
      CALL IBSEND(ISTAT,S1,4,2,1+2+8,,,9)
      CALL WAIT(IDELAY,1)
      CALL IBRCV(ISTAT,RAWDTA,16,5,1+2,,,22)
      REDATA(I,24)=STRTRL(RAWDTA)
C   CHAN 304, SUPERHEATER CURRENT
      CALL IBSEND(ISTAT,'DCV 10.',7,2,1+2+8,,,22)
      CALL IBSEND(ISTAT,S1,4,2,1+2+8,,,9)
      CALL WAIT(IDELAY,1)
      CALL IBRCV(ISTAT,RAWDTA,16,5,1+2,,,22)
      REDATA(I,25)=STRTRL(RAWDTA)
C   CHAN 305, SUPER HEATER VOLTAGE
      CALL IBSEND(ISTAT,'ACV 220.',8,2,1+2+8,,,22)
      CALL IBSEND(ISTAT,S1,4,2,1+2+8,,,9)
      CALL WAIT(IDELAY,1)
      CALL IBRCV(ISTAT,RAWDTA,16,5,1+2,,,22)
      REDATA(I,26)=STRTRL(RAWDTA)
      IF(REDATA(I,26).LT.5.) REDATA(I,26)=0.
C   CHAN 306, REFRIGERANT FLOW
      CALL IBSEND(ISTAT,'DCV .5',6,2,1+2+8,,,22)
      CALL WAIT(IDELAY,1)
      CALL IBSEND(ISTAT,S1,4,2,1+2+8,,,9)
      CALL WAIT(IDELAY,1)
      CALL IBRCV(ISTAT,RAWDTA,16,5,1+2,,,22)
      REDATA(I,27)=STRTRL(RAWDTA)
C   CHAN 307, OIL FRACTION
C
C   NO DEVICE INSTALLED TO MEASURE OIL FRACTION ON-LINE
C
      REDATA(I,28)=0.0
C   CHAN 401, WATER FLOW
      CALL IBSEND(ISTAT,'DCI .02',7,2,1+2+8,,,22)
      CALL IBSEND(ISTAT,'CLOSE 401',9,2,1+2+8,,,9)
      CALL WAIT(IDELAY,1)
      CALL IBSEND(ISTAT,'OPEN 400',8,2,1+2+8,,,9)
      CALL WAIT(IDELAY,1)
      CALL IBRCV(ISTAT,RAWDTA,16,5,1+2,,,22)
      REDATA(I,30)=STRTRL(RAWDTA)
      CALL IBSEND(ISTAT,'CLOSE 400',9,2,1+2+8,,,9)
      CALL WAIT(IDELAY,1)
      CALL IBSEND(ISTAT,'OPEN 401',8,2,1+2+8,,,9)
10  CONTINUE

```

```

CALL IBSEND(ISTAT,'OPEN 306',8,2,1+2+8,,,9)
CALL IBSEND(ISTAT,'DCV 10.',7,2,1+2+8,,,22)
CALL IBSEND(ISTAT,'CLOSE 300',9,2,1+2+8,,,9)
CALL WAIT(IDELAY,1)
C
C
C
SCAN PRESSURE DROP 15 MORE TIMES
DO 2 K=16,30
    CALL IBRECV(ISTAT,RAWDTA,16,5,1+2,,,22)
    DELP(K)=STRTRL(RAWDTA)
2
CONTINUE
CALL IBSEND(ISTAT,'OPEN 300',8,2,1+2+8,,,9)
C
C
C
NESTED LOOPS TO SUM AND AVERAGE DATA; DETERMINE DEVIATION (NOT STD)
DO 30 J=1,30
    DO 40 I=1,5
        DATAF(J)=DATAF(J)+REDATA(I,J)/5.
40
    CONTINUE
    SUM=0.
    DO 60 I=1,5
        SUM=SUM+(DATAF(J)-REDATA(I,J))**2
60
    CONTINUE
    EPS(J)=SQRT(SUM*.25)
30
CONTINUE
C
C
C
STANDARD DEVIATION OF PRESSURE DROP
SUM=0.
DO 70 I=1,30
    SUM=SUM+DELP(I)
70
CONTINUE
DATAF(21)=(DATAF(21)*5.+SUM)/35.
SUM=0.
DO 80 I=1,30
    SUM=SUM+(DATAF(21)-DELP(I))**2
80
CONTINUE
DO 90 I=1,5
    SUM=SUM+(DATAF(21)-REDATA(I,21))**2
90
CONTINUE
EPS(21)=SQRT(SUM/34.)
C
C
C
PRINT WARNING IF ANY DEVIATION GREATER THAN 10% OF MEASURED VALUE
DO 95 I=1,30
    IF(ABS(DATAF(I)).LT.1E-6) THEN
        EPS(I)=0.
    ELSE
        EPS(I)=EPS(I)/ABS(DATAF(I))
    END IF
    IF(EPS(I).GT.TOL) THEN
        PRINT *,I,DATAF(I),EPS(I),'**'
    ELSE
        PRINT *,I,DATAF(I),EPS(I)
    END IF
95
CONTINUE
PRINT *,'ENTER 0 IF ANALYSIS SHOULD STOP--'
ACCEPT *,IQ

```

```

IF(IQ.EQ.0) STOP
C
C CONVERT T/C VOLTAGES TO DEG C USING PRTIL SUBROUTINE THEN TO KELVIN
C
CALL TCCT(DATAF,TF,20)
C
C TEMPERATURES ARE CORRECTED FOR ANY OFFSET IN THE ICE POINT OR
C ELECTRONICS BY COMPARING THERMOCOUPLE CHANNEL 20 WITH THE MANUALLY
C INPUT TEMPERATURE
C
TCORR=TAMB-TF(20)
DO 50 I=1,19
    DATAF(I)=TF(I)+273.2+TCORR
50 CONTINUE
C
C CONVERT OTHER QUANTITIES TO PHYSICAL DIMENSIONS
C
C PRESSURE CALCULATED FROM CALIBRATION EQUATIONS
C
VM=DATAF(21)
DATAF(21)=(.102+1.02*VM-.00534*VM*VM)*6894.4 !PRESSURE DROP
VM=1000.*DATAF(22)
DATAF(22)=(-2.65+16.6*VM-.00258*VM*VM)*6894.4 !INLET PRESSURE
DATAF(24)=30000.*DATAF(24) !BOILER CURRENT
C DATAF(23 & 26) ARE ALREADY VOLTAGES SO NO CONVERSION IS NEEDED
DATAF(25)=2.0*DATAF(25) !SUPERHEATER CURRENT
600 CALL IBRDA(ISTAT,2,1)
    FORMAT(' ',T2,F6.3,T10,F8.5,T19,F8.5,T28,F8.5,T37,F8.5,T46,A25)
    RETURN
    END
C
C ++++++
C-----
FUNCTION STRTRL(STRING)
C-----
C FUNCTION TO CONVERT STRING VARIABLE AS OUTPUT FROM IEEE-488 DEVICE
C TO REAL NUMBER. STRING IS IN THE FORM: sDDD.DDDDeSDD (s = SIGN)
C
CHARACTER*14 STRING
READ(STRING,10) REALNM
STRTRL=REALNM
10 FORMAT(E14.7)
RETURN
END

C*****
C*****
C MODULE "ANALYSIS.FTN"
C GROUP OF THREE ANALYSIS SUBROUTINES WHICH TAKE THE ACQUIRED DATA,
C ALREADY CONVERTED TO PHYSICAL DIMENSIONS, AND EXTRACT PERFORMANCE
C PARAMETERS. SUBROUTINES ARE:
C ANAL ANALYSIS COMMON TO BOTH ONE- AND TWO PHASE
C PHASE1 ANALYSIS PARTICULARLY FOR SINGLE PHASE FLOW
C PHASE2 ANALYSIS PARTICULARLY FOR CONDENSATION OR
C EVAPORATION
C ALSO INCLUDED ARE TWO GROUPS OF FUNCTION SUBROUTINES, ONE WHICH

```

```

C      CALCULATES THE PROPERTIES OF WATER AND ONE WHICH CALCULATES THE
C      PROPERTIES OF R-22.  THESE ROUTINES ARE LISTED UNDER "ANAL".
C*****
C
C      +-----+
C-----
C      SUBROUTINE ANAL
C
C      SUBROUTINE WHICH TAKES DATA WHICH HAVE ALREADY BEEN CONVERTED TO
C      PHYSICAL DIMENSIONS AND CALCULATES OTHER DERIVED QUANTITIES, e.g.,
C      NUSSELT NUMBER, REYNOLDS NUMBER, HEAT TRANSFER COEFFICIENT, ETC.
C      THE DATA ARE PASSED VIA COMMON BLOCKS.  SUBROUTINES CALLED ARE:
C
C          RHOWAT  WATER DENSITY
C          AMUWAT  WATER VISCOSITY
C          AKWAT   WATER THERMAL CONDUCTIVITY
C          PRWAT   WATER PRANDTL NUMBER
C          MWAT    WATER MASS FLOW RATE
C          RHOLIQ  REFRIG LIQUID DENSITY
C          RHOVAP  REFRIG VAPOR DENSITY
C          AMULIQ  REFRIG LIQUID VISCOSITY
C          AKLIQ   REFRIG LIQUID THERMAL CONDUCTIVITY
C          CPLIQ   REFRIG LIQUID SPECIFIC HEAT
C          TSAT    REFRIG STAURATION TEMPERATURE
C          HFG     REFRIG ENTHALPY OF VAPORIZATION
C          MREF    REFRIG MASS FLOW RATE
C          PHASE1  SINGLE PHASE HEAT TRANSFER ANALYSIS
C          PHASE2  TWO-PHASE HEAT TRANSFER ANALYSIS
C
C      REAL NU
C
C      COMMON BLOCKS IN WHICH DATA ARE RECEIVED
C
C      COMMON /FLAG/ IFLAG1,IFLAG2
C      COMMON /GEOM/ TL,D(5),A(4)
C      COMMON /DTPS/ PATM,DATAF(30),EPS(30)
C
C      COMMON BLOCKS IN WHICH RESULTS ARE RETURNED
C
C      COMMON /PRES/ P(3)
C      COMMON /FLOW/ W(3),OIL
C      COMMON /WATP/ WAT(6)
C      COMMON /HEAT/ Q(3),H(2),UTOT,NU
C
C      C
C      C
C      C      FILL PRESSURE BLOCK
C
C      P(1)=PATM
C      P(2)=PATM+DATAF(22)-.5*DATAF(21)
C      P(3)=DATAF(21)
C
C      C
C      C      FILL FLOW BLOCK
C
C      CALL MWAT(DATAF(3),DATAF(30),TEMP)
C      DATAF(30)=TEMP
C      CALL MREF(DATAF(18),DATAF(27),TEMP)
C      DATAF(27)=TEMP
C      W(1)=DATAF(30)
C      W(2)=DATAF(27)

```

```

W(3)=DATAF(27)/A(1)
OIL=DATAF(28)
C
C
C
FILL WATER PROPERTIES BLOCK

TBAR=(DATAF(3)+DATAF(4)+DATAF(15)+DATAF(16))*0.25
WAT(1)=RHOWAT(TBAR)
WAT(2)=AMUWAT(TBAR)
WAT(3)=AKWAT(TBAR)
WAT(4)=PRWAT(TBAR)
WAT(5)=W(1)/(WAT(1)*A(2))
WAT(6)=WAT(5)*D(4)*WAT(1)/WAT(2)
C
C
C
PARTIALLY FILL HEAT TRANSFER PARAMETER BLOCK

IF(WAT(6).GT.12000.) THEN
  EXP=.806
ELSE
  EXP=.752+7.98E-6*WAT(6)-2.92E-10*WAT(6)*WAT(6)
END IF
NU=.027*((WAT(6)**(EXP))*(WAT(4)**(.33)))
H(1)=NU*WAT(3)/D(4)
C
IF(IFLAG1.EQ.1) THEN
  CALL PHASE1
ELSE
  CALL PHASE2
END IF
RETURN
END
C
C
C-----
SUBROUTINE PHASE1
C-----
C
C
C
SUBROUTINE TO CALCULATE HEAT TRANSFER RESULTS FOR ONE-PHASE TESTS
C
C
C
REAL NU
C
C
COMMON BLOCKS IN WHICH DATA ARE RECEIVED
C
COMMON /FLAG/ IFLAG1,IFLAG2
COMMON /GEOM/ TL,D(5),A(4)
COMMON /DTPS/ PATM,DATAF(30),EPS(30)
COMMON /PRES/ P(3)
COMMON /FLOW/ W(3),OIL
COMMON /WATP/ WAT(6)
C
C
C
COMMON BLOCKS IN WHICH DATA ARE RETURNED
C
COMMON /TEMP/ T(6)
COMMON /HEAT/ Q(3),H(2),UTOT,NU
COMMON /SING/ BAL,XNU(3),REREF,PRREF
COMMON /REFP/ REF(6)
COR=1.28
C
C
FILL TEMPERATURE BLOCK

```

```

C
T(1)=-.5*(DATAF(1)+DATAF(13))
T(2)=-.5*(DATAF(2)+DATAF(14))
T(3)=-.5*(DATAF(3)+DATAF(15))
T(4)=-.5*(DATAF(4)+DATAF(16))
T(6)=-.5*(T(1)+T(2))
DELT1=T(2)-T(3)
DELT2=T(1)-T(4)
DIF=ABS(DELT1-DELT2)
IF (DIF.LT..01) THEN
    T(5)=-.5*(DELT1+DELT2)
ELSE
    T(5)=ABS((DELT1-DELT2)/ALOG(DELT1/DELT2))
END IF

C
C
C
FILL REFRIGERANT PROPERTIES BLOCK

TK=T(6)
REF(1)=RHOLIQ(TK)
REF(2)=0.
REF(3)=0.
REF(4)=AMULIQ(TK)
REF(5)=AKLIQ(TK)
REF(6)=CPLIQ(TK)

C
C
C
FILL HEAT TRANSFER PARAMETER BLOCK

TSATR=TSAT(P(2))
TBAR=(TSATR+DATAF(6))*0.5
CPBAR=CPLIQ(TBAR)
QSENS=W(2)*CPBAR*(TSATR-DATAF(6))
Q(1)=W(2)*REF(6)*(T(2)-T(1))
Q(2)=0.
Q(3)=W(1)*4190.*(T(3)-T(4))
QAVE=(Q(1)+Q(3))*0.5

QELEC=.98*(COR*DATAF(23)*DATAF(24)+DATAF(25)*DATAF(26))
QTOT=Q(3)+QELEC
UTOT=ABS(QAVE/(A(4)*T(5)))
H(2)=(1./UTOT-1./H(1))*(D(1)/D(2))
H(2)=1./H(2)
REFNU=H(2)*D(1)/REF(5)

C
C
C
FILL SINGLE PHASE SPECIFIC BLOCK

BAL=(Q(1)-Q(3))*200./(Q(1)+Q(3))
PRREF=REF(6)*REF(4)/REF(5)
VREF=W(2)/(REF(1)*A(1))
REREF=REF(1)*VREF*D(1)/REF(4)
XNU(1)=REFNU

C
C
C
DITTUS-BOELTER/McADAMS

IF (Q(1).GT.0.) THEN
    XNU(2)=.023*(REREF**.8)*PRREF**.4
ELSE
    XNU(2)=.023*(REREF**.8)*PRREF**.3
END IF

```

```

C
C   PETHUKOV-POPOV
C
C   F=((1.82*ALOG10(REREF)-1.64)**-2)/8.
C   XNU(3)=(F*REREF*PRREF)/(1.+12.7*(PRREF**.667-1.)*F**.5)
C   RETURN
C   END
C
C   ++++++
C-----
C   SUBROUTINE PHASE2
C-----
C   SUBROUTINE TO CALCULATE HEAT TRANSFER RESULTS FOR TWO-PHASE TESTS
C
C   REAL NU,MCP
C
C   COMMON BLOCKS IN WHICH DATA ARE RECEIVED
C
C   COMMON /FLAG/ IFLAG1,IFLAG2
C   COMMON /GEOM/ TL,D(5),A(4)
C   COMMON /DTPS/ PATM,DATAF(30),EPS(30)
C   COMMON /PRES/ P(3)
C   COMMON /FLOW/ W(3),OIL
C   COMMON /WATP/ WAT(6)
C
C   COMMON BLOCKS IN WHICH DATA ARE RETURNED
C
C   COMMON /TEMP/ T(6)
C   COMMON /HEAT/ Q(3),H(2),UTOT,NU
C   COMMON /QUAL/ X(4)
C   COMMON /REFP/ REF(6)
C   COR=1.28
C
C   FILL TEMPERATURE BLOCK
C
C   T(1)=.5*(DATAF(1)+DATAF(13))
C   T(2)=.5*(DATAF(2)+DATAF(14))
C   T(3)=.5*(DATAF(3)+DATAF(15))
C   T(4)=.5*(DATAF(4)+DATAF(16))
C   T(6)=TSAT(P(2))
C   DELT1=T(6)-T(3)
C   DELT2=T(6)-T(4)
C   T(5)=(DELT1-DELT2)/ALOG(DELT2/DELT1)
C
C   FILL REFRIGERANT PROPERTIES BLOCK
C
C   TK=T(6)
C   REF(1)=RHOLIQ(TK)
C   REF(2)=RHOVAP(TK)
C   REF(3)=HFG(TK)
C   REF(4)=AMULIQ(TK)
C   REF(5)=AKLIQ(TK)
C   REF(6)=CPLIQ(TK)
C
C   FILL QUALITY BLOCK

```

```

TBAR=(T(6)+DATAF(6))*0.5
CPBAR=CPLIQ(TBAR)
MCP=W(2)*CPBAR
QBOIL=COR*DATAF(23)*DATAF(24)
QSUPER=DATAF(25)*DATAF(26)
IF(IFLAG1.EQ.2) THEN
    QTOT=QBOIL+QSUPER+80.
ELSE IF(IFLAG1.EQ.3) THEN
    QTOT=.98*(QBOIL+QSUPER)
END IF
QSENS=MCP*(T(6)-DATAF(6))
IF (QSENS.LT.QBOIL) THEN
    QLAT=QBOIL-QSENS
    X(4)=QLAT/(W(2)*REF(3))
    X(1)=(QSUPER+QLAT)/(W(2)*REF(3))
END IF
QTEST=W(1)*4190.*(T(3)-T(4))
C      QTEST IS HEAT TRANS TO REFRIG
X(3)=QTEST/(W(2)*REF(3))
X(2)=X(1)+X(3)
IF(((IFLAG1.EQ.2).AND.(X(3).LT.0.)).OR.((IFLAG1.EQ.3).AND.(X(3).GT.
0.1))) THEN
    PRINT *, 'QUALITY CHANGE IS THE WRONG SIGN FOR TEST TYPE'
    PRINT *, 'ENTER 1 IF ANALYSIS SHOULD CONTINUE--'
    ACCEPT *, IQ
    IF (IQ.NE.1) STOP
END IF
C
C      FILL HEAT TRANSFER PARAMETER BLOCK
C
Q(1)=QBOIL
Q(2)=QSUPER
Q(3)=QTEST
UTOT=Q(3)/(A(4)*T(5))
H(2)=(1./UTOT-1./H(1))*(D(1)/D(2))
H(2)=1./H(2)
RETURN
END
C*****
C*****
C      GROUP OF FUCTION SUBROUTINES TO CALCULATE THE PROPERTIES OF WATER
C      RHOWAT--DENSITY
C      AMUWAT--VISCOSITY
C      AKWAT  --THERMAL CONDUCTIVITY
C      PRWAT  --PRANDTL NUMBER
C      VALIDITY IS 273-320 K.
C      *****
C
C      +-----+
C-----
FUNCTION RHOWAT(TK)
C-----
C      FUNCTION RETURNS THE DENSITY OF WATER IN Kg/m**3 AS A FUNCTION OF
C      TEMPERATURE IN KELVIN. EQUATION IS A 2nd ORDER CURVE FIT FOR
C      TABULATED DATA.
C
T=TK-273.2
RHOWAT=999.93-.034016*T-4.02469E-3*T**2

```

```

RETURN
END
C
C-----
C-----
FUNCTION AMUWAT(TK)
C-----
C     FUNCTION RETURNS THE VISCOSITY OF WATER IN Pa sec AS A FUNCTION OF
C     TEMPERATURE IN KELVIN.  EQUATIONS ARE PIECEWISE 2nd ORDER CURVE
C     FITS FOR TABULATED DATA.
C
T=TK-273.2
IF (T.LT.15.) THEN
      AMU=1.7890-.057413*T+9.29388E-4*T*T
ELSE IF (T.LT.30.) THEN
      AMU=1.6352-.038771*T+3.64901E-4*T*T
ELSE
      AMU=1.4883-.02921*T+2.100E-4*T*T
END IF
AMUWAT=AMU*.001
RETURN
END
C
C-----
C-----
FUNCTION AKWAT(TK)
C-----
C     FUNCTION RETURNS THE CONDUCTIVITY OF WATER IN W/m K AS FUNCTION OF
C     TEMPERATURE IN KELVIN.  EQN. IS A 2nd ORDER FIT TO TABULATED DATA.
C
T=TK-273.2
AKWAT=.5659+2.0235E-3*T-8.6650E-6*T*T
RETURN
END
C
C-----
C-----
FUNCTION PRWAT(TK)
C-----
C     FUNCTION RETURNS THE PRANDTL NUMBER OF WATER AS A FUNCTION OF
C     TEMPERATURE IN KELVIN.  EQNS. ARE PIECEWISE 2nd ORDER CURVE FITS
C     TO TABULATED DATA.
C
T=TK-273.2
IF (T.LT.15.56) THEN
      PRWAT=13.2474-.45818*T+7.2848E-3*T*T
ELSE IF (T.LT.32.22) THEN
      PRWAT=11.9658-.30918*T+3.0003E-3*T*T
ELSE
      PRWAT=10.40116-.213474*T+1.53792E-3*T*T
END IF
RETURN
END
C*****
C*****
C     GROUP OF FUNCTION SUBROUTINES TO CALCULATE THE PROPERTIES OF R-22
C     RHOLIQ--LIQUID DENSITY
C     RHOVAP--VAPOR DENSITY (PURE R-22)

```

```

C          AMULIQ--LIQUID VISCOSITY
C          AKLIQ  --LIQUID THERMAL CONDUCTIVITY
C          CPLIQ  --LIQUID SPECIFIC HEAT
C          TSAT   --SATURATION TEMPERATURE (PURE R-22)
C          HFG    --ENTHALPY OF VAPORIZATION (PURE R-22)
C OIL, WHEN INCLUDED, IS NAPHTHENIC, 150 SUS MINERAL OIL
C *****
C          +-----+
C          |
C          |
C-----|
C          FUNCTION RHOLIQ(TK)
C-----|
C          FUNCTION RETURNS THE DENSITY OF LIQUID R-22 IN Kg/m**3 AS FUNCTION
C          OF TEMPERATURE IN KELVIN. EQUATION IS FROM DOWNING, 1974.
C
C          COMMON /FLAG/ IF1,IF2
C          COMMON /FLOW/ OIL(4)
C
C          ASSIGN CONSTANT VALUES
C
C          TCRIT=664.5
C          AL=32.76
C          BL=54.63441
C          CL=36.74892
C          DL=-22.292566
C          EL=20.4732886
C
C          T=TK*1.8
C          F=1.-(T/TCRIT)
C          RHO=AL+BL*F**.3333+CL*F**.6667+DL*F+EL*F**1.3333
C          RHOLIQ=RHO*16.018
C
C          OIL DENSITY EQN FROM BAUSTIAN ET AL. PHASE I REPORT, EQN. (5)
C          NO CORRECTION FACTOR INCLUDED.
C
C          IF (IF2.EQ.1) THEN
C              T=TK-273.2
C              G=1.-RHOLIQ/(927.-.6*T)
C              RHOLIQ=RHOLIQ/(1.-OIL(4)*G)
C          END IF
C          RETURN
C          END
C
C          +-----+
C          |
C          |
C-----|
C          FUNCTION RHOVAP(TK)
C-----|
C          FUNCTION RETURNS THE DENSITY OF SATURATED VAPOR R-22 IN Kg/m**3 AS
C          A FUNCTION OF TEMPERATURE IN KELVIN. EQUATIONS ARE PIECEWISE 2nd
C          ORDER CURVE FITS OF TABULATED DATA. VALIDITY IS 260-325 K.
C
C          T=TK-273.2
C          IF (T.LT.2.) THEN
C              V=4.6978E-2-1.47054E-3*T+3.41964E-5*T*T
C          ELSE IF (T.LT.14.) THEN
C              V=4.6916E-2-1.42958E-3*T+1.98512E-5*T*T
C          ELSE IF (T.LT.26.) THEN
C              V=4.5461E-2-1.21804E-3*T+1.20536E-5*T*T

```

```

ELSE IF (T.LT.38.) THEN
    V=4.2487E-2-9.87381E-4*T+7.55952E-6*T*T
ELSE
    V=3.8576E-2-7.8003E-4*T+4.80655E-6*T*T
END IF
RHOVAP=1./V
RETURN
END
C
C-----
C-----
FUNCTION AMULIQ(TK)
C-----
C-----
FUNCTION RETURNS THE VISCOSITY OF LIQUID R-22 IN Pa SEC AS FUNCTION
OF TEMPERATURE IN KELVIN. EQUATIONS ARE PIECEWISE 2nd ORDER CURVE
FITS TO TABULATED DATA. VALIDITY IS 260-325 K.
C-----
REAL MOLTOT,MOLOIL,MOLREF
COMMON /FLAG/ IF1,IF2
COMMON /FLOW/ OIL(4)
C
T=TK-273.2
IF (T.LT.16.8) THEN
    AMU=235.723-1.6973*T+.01175*T*T
ELSE
    AMU=234.423-1.5383*T+6.75E-3*T*T
END IF
AMULIQ=AMU*(1.E-6)
IF (IF2.EQ.1) THEN
C
C-----
OIL VISCOSITY FROM SUNISO 3GS DATA WITH CURVE FIT LOG(mu) VS. T
C-----
AMUOIL=10.**((1.9E-4*T*T-4.1E-2*T-.2)
C-----
MIXTURE VISC EQN FROM KENDALL & MONROE, BASED ON MOLE FRACTIONS
C-----
MOLOIL=OIL(4)/318.           ! 318.= MW OF OIL
MOLREF=(1.-OIL(4))/86.5     ! 86.5= MW OF R-22
MOLTOT=MOLOIL+MOLREF
YO=MOLOIL/MOLTOT           ! MOLE FRACTION OIL
YR=MOLREF/MOLTOT           ! MOLE FRACTION R-22
AMUMIX=YR*AMULIQ**.33333+YO*AMUOIL**.33333
AMULIQ=AMUMIX**3
END IF
RETURN
END
C
C-----
C-----
FUNCTION AKLIQ(TK)
C-----
C-----
FUNCTION RETURNS THE CONDUCTIVITY OF LIQUID R-22 IN W/m/K AS A
FUNCTION OF TEMPERATURE IN KELVIN. EQUATION IS A LINEAR FIT TO
TABULATED DATA. VALIDITY IS 260-325 K.
C-----
COMMON /FLAG/ IF1,IF2
COMMON /FLOW/ OIL(4)
C

```

```

T=TK-273.2
AKLIQ=-5.E-4*T+.1002
IF (IF2.EQ.1) THEN
    OILK=.12 ! K NOT STRONG f(T), SO USE CONSTANT VALUE
C
C
EQN (1) FROM BAUSTIAN ET AL. PHASE I REPORT
    F=AKLIQ*(1.-OIL(4))+OILK*OIL(4)
    AKLIQ=F-.72*(OILK-AKLIQ)*(1.-OIL(4))*OIL(4)
END IF
RETURN
END
C
C
+++++
C-----
FUNCTION CPLIQ(TK)
C-----
C
FUNCTION RETURNS THE SPECIFIC HEAT OF LIQUID R-22 IN J/Kg/K AS A
C
FUNCTION OF TEMPERATURE IN KELVIN. EQN. IS A 2nd ORDER CURVE FIT
C
TO TABULATED DATA. VALIDITY 260-325 K.
C
COMMON /FLAG/ IF1,IF2
COMMON /FLOW/ OIL(4)
C
T=TK-273.2
CP=1.1676+2.5057E-3*T+3.8095E-5*T*T
CPLIQ=CP*1000.
IF (IF2.EQ.1) THEN
C
EQN (2) FROM BAUSTIAN ET AL. PHASE I REPORT. Cp VALUE FOR OIL FROM
C
BAUSTIAN TABLE 3; TEMPERATURE DEPENDENCE FROM HOLMAN APPENDIX FOR
C
PROPERTIES OF OIL AS A FUNCTION OF T.
C
    CPLIQ=CPLIQ*(1.-OIL(4))+(1600.+4.2*T)*OIL(4)
END IF
RETURN
END
C
C
+++++
C-----
FUNCTION TSAT(PSAT)
C-----
C
FUNCTION RETURNS THE SATURATION TEMPERATURE OF R-22 IN KELVIN AS A
C
FUNCTION OF THE SATURATION PRESSURE IN Pa. EQUATIONS ARE PIECEWISE
C
2nd ORDER CURVE FITS TO TABULATED DATA. VALIDITY ~.35-2.05 MPa.
C
COMMON /FLAG/ IF1,IF2
COMMON /FLOW/ OIL(4)
C
P=PSAT/1000000.
IF (P.LT..53113) THEN
    T=-45.1146+119.8162*P-58.6123*P*P
    ELSE IF (P.LT..76668) THEN
    T=-37.0614+89.2917*P-29.6119*P*P
    ELSE IF (P.LT.1.0725) THEN
    T=-29.1162+68.4489*P-15.9124*P*P

```

```

ELSE IF (P.LT.1.4605) THEN
    T=-21.2919+53.8*P-9.0422*P*P
ELSE
    T=-12.995+42.4931*P-5.1829*P*P
END IF
TSAT=T+273.2
IF (IF2.EQ.1) THEN

END IF
RETURN
END

C
C
C-----
FUNCTION HFG(TSAT)
C-----
C
C    FUNCTION RETURNS THE ENTHALPY OF VAPORIZATION OF R-22 IN J/Kg AS A
C    FUNCTION OF SATURATION TEMPERATURE (K). EQUATION IS A SECOND ORDER
C    CURVE FIT TO TABULATED DATA. VALIDITY IS 270-310 K.
C
    T=TSAT-273.2
    HFG=204.58-.78515*T-.004225*T*T
    HFG=HFG*1000.
    RETURN
    END

C
C
C-----
SUBROUTINE MWAT(T,I,WDOT)
C-----
C
C    SUBROUTINE TO CALCULATE THE MASS FLOW OF THE WATER IN THE ANNULUS
C    GIVEN WATER TEMPERATURE AND FLOWMETER CURRENT READING ( K AND A ).
C    THE MASS FLOW IS RETURNED IN Kg/s.
C
    REAL I
    WDOT=(562.5*I-2.25)*.06313
    RETURN
    END

C
C
C-----
SUBROUTINE MREF(T,V,WDOT)
C-----
C
C    SUBROUTINE TO CALCULATE THE MASS FLOW OF R-22 IN THE TEST SECTION
C    GIVEN R-22 TEMPERATURE AND FLOWMETER VOLTAGE READING ( K AND V ).
C    THE MASS FLOW IS RETURNED IN Kg/s.
C
    RHOREF=RHOLIQ(T)
    WDOT=1.2628E-4*V*RHOREF
    RETURN
    END
C*****
C*****
C    MODULE "OUTPUT.FTN"
C    GROUP OF TWO SUBROUTINES TO OUTPUT THE DATA TO A PRINTER AND/OR
C    A DISC FILE. THE SUBROUTINES ARE:
C    SIPRNT PRINT OUT RESULTS IN SI UNITS (PRINTER & DISC)

```

```

C          ENPRNT PRINT OUT RESULTS IN ENGLISH UNITS (PRINTER ONLY)
C*****
C
C          +-----+
C-----
C          SUBROUTINE SIPRNT(N)
C-----
C          SUBROUTINE TO PRINT OUT RESULTS IN SI UNITS. DATA PASSED THROUGH
C          COMMON BLOCKS AND FORMATTED FOR OUTPUT.
C
C          REAL L,NU
C          CHARACTER*25 OILTYP,TUBTYP
C          CHARACTER*12 TYPE
C          CHARACTER*9 DT
C          CHARACTER*8 TM
C          COMMON /DTPS/ PATM,DATAF(30),EPS(30)
C          COMMON /CHAR/ TYPE, TM,DT,OILTYP,TUBTYP
C          COMMON /TEMP/ T(6)
C          COMMON /PRES/ P(3)
C          COMMON /FLOW/ W(3),OIL
C          COMMON /HEAT/ Q(3),H(2),UTOT,NU
C          COMMON /QUAL/ X(4)
C          COMMON /GEOM/ L,D(5),A(4)
C          COMMON /REFP/ REF(6)
C          COMMON /WATP/ WAT(6)
C          COMMON /FLAG/ IFLAG1,IFLAG2
C          COMMON /SING/ BAL,PRNU(3),REREF,PRREF
C
C          IF(N.EQ.1) GO TO 777
C
C          OPEN(UNIT=8,FILE='LP:',STATUS='OLD')
C
C          WRITE(8,10)
C          WRITE(8,30)
C          WRITE(8,40) DT, TM
C          WRITE(8,50) TUBTYP
C          WRITE(8,60) TYPE
C          WRITE(8,70) OILTYP
C          WRITE(8,100)
C          WRITE(8,110) P(1)/1.E6
C          WRITE(8,120) P(2)/1.E6
C          WRITE(8,130) P(3)/1.E3,ABS(P(3)*EPS(21)/1.E3)
C          WRITE(8,200)
C          WRITE(8,210) T(1)-273.2
C          WRITE(8,220) T(2)-273.2
C          WRITE(8,230) T(3)-273.2
C          WRITE(8,240) T(4)-273.2
C          WRITE(8,250) T(5)
C          IF (IFLAG1.EQ.1) GO TO 2
C          WRITE(8,260) T(6)-273.2
C          WRITE(8,300)
C          WRITE(8,310) W(2)*(1.-OIL)
C          WRITE(8,350) W(2)*OIL
C          WRITE(8,320) W(1)
C          WRITE(8,330) W(3)
C          WRITE(8,340) OIL
C          WRITE(8,500)
C          WRITE(8,510) D(1)*1000.

```

```

WRITE(8,520) D(2)*1000.
WRITE(8,530) D(3)*1000.
WRITE(8,550) A(1)*1.E6
WRITE(8,560) A(2)*1.E6
WRITE(8,570) L
WRITE(8,590) A(4)
WRITE(8,600)
WRITE(8,610) REF(1)
IF (IFLAG1.EQ.1) GO TO 4
WRITE(8,620) REF(2)
WRITE(8,630) REF(3)/1000.
4 WRITE(8,640) REF(4)*1.E6
WRITE(8,650) REF(5)*1000.
WRITE(8,660) REF(6)/1000.
IF (IFLAG1.EQ.1) THEN
    WRITE(8,670) PRREF
    WRITE(8,680) REREF
END IF
WRITE(8,700)
WRITE(8,710) WAT(1)
WRITE(8,720) WAT(2)*1.E6
WRITE(8,730) WAT(3)*1000.
WRITE(8,740) WAT(4)
WRITE(8,760) WAT(6)
WRITE(8,800)
IF (IFLAG1.EQ.1) GO TO 5
5 WRITE(8,805) Q(1)+Q(2)
WRITE(8,810) Q(3)
WRITE(8,820) NU
WRITE(8,830) UTOT
WRITE(8,840) H(1)
WRITE(8,850) H(2)
IF (IFLAG1.EQ.1) THEN
    WRITE(8,1100)
    WRITE(8,1110) BAL
    WRITE(8,1200)
    WRITE(8,1210) PRNU(1)
    WRITE(8,1220) PRNU(2)
    WRITE(8,1230) PRNU(3)
END IF
WRITE(8,900)
IF (IFLAG1.EQ.1) GO TO 6
6 WRITE(8,920) P(2)/1.E6
WRITE(8,930) W(3)
IF (IFLAG1.EQ.1) GO TO 3
WRITE(8,940) X(1)
WRITE(8,950) X(2)
3 WRITE(8,960) H(2)
C
C
CLOSE(8)
PRINT *, 'ENTER 0 IF DATA SHOULD NOT BE STORED ON A DISC--'
ACCEPT *, IQQ
IF (IQQ.NE.0) THEN
777 OPEN(UNIT=4, FILE='DATA.DAT', STATUS='NEW', CARRIAGECONTROL='FORTRAN')
C
    DO 111 I=1,30
        WRITE(4,1010) I,DATAF(I),EPS(I)

```

111

```

CONTINUE
WRITE(4,1020) PATM
WRITE(4,1030) L,D(1),D(2),D(3)
WRITE(4,1040) TYPE,TM,DT
WRITE(4,1050) OILTYP,TUBTYP
WRITE(4,1000)
WRITE(4,10)
WRITE(4,30)
WRITE(4,40) DT,TM
WRITE(4,50) TUBTYP
WRITE(4,60) TYPE
WRITE(4,70) OILTYP
WRITE(4,100)
WRITE(4,110) P(1)/1.E6
WRITE(4,120) P(2)/1.E6
WRITE(4,130) P(3)/1.E3,ABS(P(3)*EPS(21)/1.E3)
WRITE(4,200)
WRITE(4,210) T(1)-273.2
WRITE(4,220) T(2)-273.2
WRITE(4,230) T(3)-273.2
WRITE(4,240) T(4)-273.2
WRITE(4,250) T(5)
IF (IFLAG1.EQ.1) GO TO 222
WRITE(4,260) T(6)-273.2
222 WRITE(4,300)
WRITE(4,310) W(2)*(1.-OIL)
WRITE(4,350) W(2)*OIL
WRITE(4,320) W(1)
WRITE(4,330) W(3)
WRITE(4,340) OIL
WRITE(4,500)
WRITE(4,510) D(1)*1000.
WRITE(4,520) D(2)*1000.
WRITE(4,530) D(3)*1000.
WRITE(4,550) A(1)*1.E6
WRITE(4,560) A(2)*1.E6
WRITE(4,570) L
WRITE(4,590) A(4)
WRITE(4,600)
WRITE(4,610) REF(1)
IF (IFLAG1.EQ.1) GO TO 444
WRITE(4,620) REF(2)
WRITE(4,630) REF(3)/1000.
444 WRITE(4,640) REF(4)*1.E6
WRITE(4,650) REF(5)*1000.
WRITE(4,660) REF(6)/1000.
IF (IFLAG1.EQ.1) THEN
WRITE(4,670) PRREF
WRITE(4,680) REREF
END IF
WRITE(4,700)
WRITE(4,710) WAT(1)
WRITE(4,720) WAT(2)*1.E6
WRITE(4,730) WAT(3)*1000.
WRITE(4,740) WAT(4)
WRITE(4,760) WAT(6)
WRITE(4,800)
IF (IFLAG1.EQ.1) GO TO 555

```

```

555      WRITE(4,805) Q(1)+Q(2)
        WRITE(4,810) Q(3)
        WRITE(4,820) NU
        WRITE(4,830) UTOT
        WRITE(4,840) H(1)
        WRITE(4,850) H(2)
        IF (IFLAG1.EQ.1) THEN
            WRITE(4,1100)
            WRITE(4,1110) BAL
            WRITE(4,1200)
            WRITE(4,1210) PRNU(1)
            WRITE(4,1220) PRNU(2)
            WRITE(4,1230) PRNU(3)
        END IF
        WRITE(4,900)
        IF (IFLAG1.EQ.1) GO TO 666
666      WRITE(4,920) P(2)/1.E6
        WRITE(4,930) W(3)
        IF (IFLAG1.EQ.1) GO TO 333
        WRITE(4,940) X(1)
        WRITE(4,950) X(2)
333      WRITE(4,960) H(2)
C
        CLOSE(4)
        END IF
C
10      FORMAT(' ',T5,'***** RESULTS OF TEST RUN--SI UNITS ****
1*****')
30      FORMAT(' ',T5,'TEST INFORMATION:')
40      FORMAT(' ',T10,'Date and time--',T50,A9,2X,A8)
50      FORMAT(' ',T10,'Type of tube--',T50,A25)
60      FORMAT(' ',T10,'Type of test--',T50,A12)
70      FORMAT(' ',T10,'Type of oil in mixture--',T50,A25)
100     FORMAT(' ',T5,'PRESSURES:')
110     FORMAT(' ',T10,'Atmospheric pressure(MPa)--',T55,F7.4)
120     FORMAT(' ',T10,'Average tube pressure(MPa)--',T55,F7.4)
130     FORMAT(' ',T10,'Pressure drop in tube(kPa)--',T53,F7.2,1X,'1',F7.2)
200     FORMAT(' ',T5,'TEMPERATURES (OC):')
210     FORMAT(' ',T10,'Tube inlet--',T54,F7.3)
220     FORMAT(' ',T10,'Tube outlet--',T54,F7.3)
230     FORMAT(' ',T10,'Annulus inlet--',T54,F7.3)
240     FORMAT(' ',T10,'Annulus outlet--',t54,F7.3)
250     FORMAT(' ',T10,'Log mean temp difference--',T54,F7.3)
260     FORMAT(' ',T10,'Saturation temp @ avg tube pressure--',T54,F7.3)
300     FORMAT(' ',T5,'FLOW PARAMETERS:')
310     FORMAT(' ',T10,'R-22 mass flow (kg/s)--',t55,F8.5)
320     FORMAT(' ',T10,'Water mass flow (kg/s)--',T55,F7.4)
330     FORMAT(' ',T10,'R-22 mass velocity (kg/m27s)--',T52,F7.1)
340     FORMAT(' ',T10,'Mass fraction oil in mixture--',T55,F7.4)
350     FORMAT(' ',T10,'Oil mass flow (kg/s)--',T55,F10.7)
500     FORMAT(' ',T5,'TEST SECTION GEOMETRY:')
510     FORMAT(' ',T10,'Max tube i.d. (mm)--',T54,F6.2)
520     FORMAT(' ',T10,'Tube o.d. (mm)--',T54,F6.2)
530     FORMAT(' ',T10,'Annulus i.d. (mm)--',T54,F6.2)
550     FORMAT(' ',T10,'Tube cross section area (mm2)--',T53,F6.1)
560     FORMAT(' ',T10,'Annulus cross section area (mm2)--',T53,F6.1)
570     FORMAT(' ',T10,'Test section length (m)--',T55,F6.3)
590     FORMAT(' ',T10,'Tube outside surface area (m2)--',T55,F7.4)

```

```

600  FORMAT( ' ', T5, 'R-22 PROPERTIES IN TEST SECTION (incl. oil):' )
610  FORMAT( ' ', T10, 'Liquid density (kg/m3)--', T52, F7.1 )
620  FORMAT( ' ', T10, 'Vapor density (kg/m3)--', T53, F7.2 )
630  FORMAT( ' ', T10, 'Enthalpy of vaporization (kJ/kg)--', T53, F7.2 )
640  FORMAT( ' ', T10, 'Liquid viscosity (5Pa7s)--', t52, F7.1 )
650  FORMAT( ' ', T10, 'Liquid thermal conductivity (mW/m70C)--', T52, F7.1 )
660  FORMAT( ' ', T10, 'Liquid specific heat (kJ/kg70C)--', t54, F7.3 )
670  FORMAT( ' ', T10, 'Prandtl number--', T54, F7.3 )
680  FORMAT( ' ', T10, 'Reynolds number--', t50, F8.0 )
700  FORMAT( ' ', T5, 'WATER PROPERTIES IN THE ANNULUS:' )
710  FORMAT( ' ', T10, 'Density (kg/m3)--', T52, F7.1 )
720  FORMAT( ' ', T10, 'Viscosity (5Pa7s)--', T52, F7.1 )
730  FORMAT( ' ', T10, 'Thermal conductivity (mW/m70C)--', T52, F7.1 )
740  FORMAT( ' ', T10, 'Prandtl number--', T54, F7.3 )
760  FORMAT( ' ', T10, 'Reynolds number--', T50, F8.0 )
800  FORMAT( ' ', T5, 'HEAT TRANSFER RESULTS:' )
805  FORMAT( ' ', T10, 'Boiler + superheater heat trans. (W)--', T51, F8.1 )
810  FORMAT( ' ', T10, 'Test section heat transfer (W)--', T51, F8.1 )
820  FORMAT( ' ', T10, 'Annulus side Nusselt number--', T52, F8.2 )
830  FORMAT( ' ', T10, 'Overall heat trans. coeff. (W/m270C)--', t51, F8.1 )
840  FORMAT( ' ', T10, 'Shell heat trans. coeff. (W/m270C)--', t51, F8.1 )
850  FORMAT( ' ', T10, 'Tube heat trans. coeff. (W/m270C)--', t51, F8.1 )
900  FORMAT( ' ', T5, '***** SUMMARY OF TEST RESULTS *****
1*****' )
920  FORMAT( ' ', T10, 'Average tube pressure (MPa)--', T55, F7.4 )
930  FORMAT( ' ', T10, 'Refrigerant mass velocity (kg/m27s)--', T52, F7.1 )
940  FORMAT( ' ', T10, 'Vapor quality @ tube inlet--', T54, F7.3 )
950  FORMAT( ' ', T10, 'Vapor quality @ tube outlet--', T54, F7.3 )
960  FORMAT( ' ', T10, 'In-tube heat trans. coeff. (W/m270C)--', t51, F8.1 )
1000 FORMAT( ' ' )
1010 FORMAT( ' ', 'CHAN', T8, I2, T20, G12.5, T44, G11.4 )
1020 FORMAT( ' ', 'PATM=', T10, G12.5 )
1030 FORMAT( ' ', T5, G12.5, T25, G12.5, T45, G12.5, T65, G12.5 )
1040 FORMAT( ' ', T5, A12, T18, A8, T27, A9 )
1050 FORMAT( ' ', T5, A25, T31, A25 )
1100 FORMAT( ' ', T5, 'TUBE SIDE vs. ANNULUS SIDE ENERGY BALANCE:' )
1110 FORMAT( ' ', T10, 'Deviation (%)--', T53, F7.2 )
1200 FORMAT( ' ', T5, 'NUSSULT NUMBER:' )
1210 FORMAT( ' ', T10, 'Nu from testing--', T52, F7.1 )
1220 FORMAT( ' ', T10, 'Nu from Dittus-Boelter--', T52, F7.1 )
1230 FORMAT( ' ', T10, 'Nu from Pethukov-Popov--', T52, F7.1 )
RETURN
END

```

```

C
C
C-----

```

SUBROUTINE ENPRNT

```

C-----
C
C SUBROUTINE TO PRINT RESULTS IN ENGLISH UNITS. DATA PASSED THROUGH
C COMMON BLOCKS AND FORMATTED FOR OUTPUT. ALL VALUES ARE SIMPLY
C CONVERTED WITH CONVERSION FACTORS.
C

```

```

REAL L, NU
CHARACTER*25 OILTYP, TUBTYP
CHARACTER*12 TYPE
CHARACTER*9 DT
CHARACTER*8 TM
COMMON /CHAR/ TYPE, TM, DT, OILTYP, TUBTYP

```

```

COMMON /TEMP/ T(6)
COMMON /PRES/ P(3)
COMMON /FLOW/ W(3),OIL
COMMON /HEAT/ Q(3),H(2),UTOT,NU
COMMON /QUAL/ X(4)
COMMON /GEOM/ L,D(5),A(4)
COMMON /REFP/ REF(6)
COMMON /WATP/ WAT(6)
COMMON /FLAG/ IFLAG1,IFLAG2
COMMON /SING/ BAL,PRNU(3),REREF,PRREF

```

C

```
OPEN(UNIT=8,FILE='LP:',STATUS='OLD')
```

C

```

WRITE(8,10)
WRITE(8,30)
WRITE(8,40) DT, TM
WRITE(8,50) TUBTYP
WRITE(8,60) TYPE
WRITE(8,70) OILTYP
WRITE(8,100)
WRITE(8,110) P(1)/6.8944E3
WRITE(8,120) P(2)/6.8944E3
WRITE(8,130) P(3)/6.8944E3
WRITE(8,200)
WRITE(8,210) T(1)*1.8-459.7
WRITE(8,220) T(2)*1.8-459.7
WRITE(8,230) T(3)*1.8-459.7
WRITE(8,240) T(4)*1.8-459.7
WRITE(8,250) T(5)*1.8
IF (IFLAG1.EQ.1) GO TO 2
WRITE(8,260) T(6)*1.8-459.7
WRITE(8,300)
WRITE(8,310) W(2)*7936.6*(1.-OIL)
WRITE(8,350) W(2)*7936.6*OIL
WRITE(8,320) W(1)*7936.6
WRITE(8,330) W(3)*735.84
WRITE(8,340) OIL
WRITE(8,500)
WRITE(8,510) D(1)*39.37
WRITE(8,520) D(2)*39.37
WRITE(8,530) D(3)*39.37
WRITE(8,550) A(1)*1550.
WRITE(8,560) A(2)*1550.
WRITE(8,570) L*3.281
WRITE(8,590) A(4)*10.76
WRITE(8,600)
WRITE(8,610) REF(1)*.06243
IF (IFLAG1.EQ.1) GO TO 4
WRITE(8,620) REF(2)*.06243
WRITE(8,630) REF(3)*4.3008E-4
WRITE(8,640) REF(4)*2.0887E4
WRITE(8,650) REF(5)*.5778
WRITE(8,660) REF(6)*2.3884E-4
IF (IFLAG1.EQ.1) THEN
    WRITE(8,670) PRREF
    WRITE(8,680) REREF
END IF
WRITE(8,700)

```

2

4

```

WRITE(8,710) WAT(1)*.06243
WRITE(8,720) WAT(2)*2.0887E4
WRITE(8,730) WAT(3)*.5778
WRITE(8,740) WAT(4)
WRITE(8,760) WAT(6)
WRITE(8,800)
IF (IFLAG1.EQ.1) GO TO 5
WRITE(8,805) (Q(1)+Q(2))*3.4121
5 WRITE(8,810) Q(3)*3.4121
WRITE(8,820) NU
WRITE(8,830) UTOT*.1761
WRITE(8,840) H(1)*.1761
WRITE(8,850) H(2)*.1761
IF (IFLAG1.EQ.1) THEN
WRITE(8,1100)
WRITE(8,1110) BAL
WRITE(8,1200)
WRITE(8,1210) PRNU(1)
WRITE(8,1220) PRNU(2)
WRITE(8,1230) PRNU(3)
END IF
WRITE(8,900)
IF (IFLAG1.EQ.1) GO TO 6
6 WRITE(8,920) P(2)/6.8944E3
WRITE(8,930) W(3)*735.84
IF (IFLAG1.EQ.1) GO TO 3
WRITE(8,940) X(1)
WRITE(8,950) X(2)
3 WRITE(8,960) H(2)*.1761
C
C
C
10 FORMAT(' ',T5,'***** RESULTS OF TEST RUN--ENGLISH *****
1*****')
30 FORMAT(' ',T5,'TEST INFORMATION:')
40 FORMAT(' ',T10,'Date and time--',T50,A9,2X,A8)
50 FORMAT(' ',T10,'Type of tube--',T50,A25)
60 FORMAT(' ',T10,'Type of test--',T50,A12)
70 FORMAT(' ',T10,'Type of oil in mixture--',T50,A25)
100 FORMAT(' ',T5,'PRESSURES (psia):')
110 FORMAT(' ',T10,'Atmospheric pressure--',T53,F7.2)
120 FORMAT(' ',T10,'Average tube pressure--',T53,F7.2)
130 FORMAT(' ',T10,'Pressure drop in tube--',T53,F7.2)
200 FORMAT(' ',T5,'TEMPERATURES (OF):')
210 FORMAT(' ',T10,'Tube inlet--',T53,F7.2)
220 FORMAT(' ',T10,'Tube outlet--',T53,F7.2)
230 FORMAT(' ',T10,'Annulus inlet--',T53,F7.2)
240 FORMAT(' ',T10,'Annulus outlet--',t53,F7.2)
250 FORMAT(' ',T10,'Log mean temp difference--',T53,F7.2)
260 FORMAT(' ',T10,'Saturation temp @ avg tube pressure--',T53,F7.2)
300 FORMAT(' ',T5,'FLOW PARAMETERS:')
310 FORMAT(' ',T10,'R-22 mass flow (lbm/hr)--',t52,F8.2)
320 FORMAT(' ',T10,'Water mass flow (lbm/hr)--',T52,F8.2)
330 FORMAT(' ',T10,'R-22 mass velocity (lbm/hr7ft2)--',T50,F8.0)
340 FORMAT(' ',T10,'Mass fraction oil in mixture--',T55,F7.4)
350 FORMAT(' ',T10,'Oil mass flow (lbm/hr)--',T52,F10.4)
500 FORMAT(' ',T5,'TEST SECTION GEOMETRY:')
510 FORMAT(' ',T10,'Max tube i.d. (in)--',T55,F6.3)

```

```

520 FORMAT(' ',T10,'Tube o.d. (in)--',T55,F6.3)
530 FORMAT(' ',T10,'Annulus i.d. (in)--',T55,F6.3)
550 FORMAT(' ',T10,'Tube cross section area (in2)--',T55,F7.4)
560 FORMAT(' ',T10,'Annulus cross section area (in2)--',T55,F7.4)
570 FORMAT(' ',T10,'Test section length (ft)--',T54,F6.2)
590 FORMAT(' ',T10,'Tube outside surface area (ft2)--',T55,F7.4)
600 FORMAT(' ',T5,'R-22 PROPERTIES IN TEST SECTION (incl. oil):')
610 FORMAT(' ',T10,'Liquid density (lbm/ft3)--',T53,F7.2)
620 FORMAT(' ',T10,'Vapor density (lbm/ft3)--',T54,F7.3)
630 FORMAT(' ',T10,'Enthalpy of vaporization (BTU/lbm)--',T53,F7.2)
640 FORMAT(' ',T10,'Liquid viscosity (lbf7s/ft2x(103)2)--',t53,F7.2)
650 FORMAT(' ',T10,'Liquid therm cond (BTU/hr7ft70F)--',T55,F7.4)
660 FORMAT(' ',T10,'Liquid specific heat (BTU/lbm70F)--',t54,F7.3)
670 FORMAT(' ',T10,'Prandtl number--',T54,F7.3)
680 FORMAT(' ',T10,'Reynolds number--',t50,F8.0)
700 FORMAT(' ',T5,'WATER PROPERTIES IN THE ANNULUS:')
710 FORMAT(' ',T10,'Density (lbm/ft3)--',T53,F7.2)
720 FORMAT(' ',T10,'Viscosity (lbf7s/ft2x(103)2)--',T53,F7.2)
730 FORMAT(' ',T10,'Thermal cond. (BTU/hr7ft70F)--',T55,F7.4)
740 FORMAT(' ',T10,'Prandtl number--',T54,F7.3)
760 FORMAT(' ',T10,'Reynolds number--',T50,F8.0)
800 FORMAT(' ',T5,'HEAT TRANSFER RESULTS:')
805 FORMAT(' ',T10,'Boiler+superheater heat trans (BTU/h)--',T51,F8.1)
810 FORMAT(' ',T10,'Test section heat transfer (BTU/h)--',T51,F8.1)
820 FORMAT(' ',T10,'Annulus side Nusselt number--',T52,F8.2)
830 FORMAT(' ',T10,'Overall heat trans coef (BTU/h7ft270F)--',t51,F9.2)
840 FORMAT(' ',T10,'Shell heat trans coef (BTU/h7ft270F)--',t51,F9.2)
850 FORMAT(' ',T10,'Tube heat trans coef (BTU/h7ft270F)--',t51,F9.2)
900 FORMAT(' ',T5,'***** SUMMARY OF TEST RESULTS *****
1*****')
920 FORMAT(' ',T10,'Average tube pressure (psia)--',T53,F7.2)
930 FORMAT(' ',T10,'Refrigerant mass velocity (lbm/h7ft2)--',T50,F8.0)
940 FORMAT(' ',T10,'Vapor quality @ tube inlet--',T54,F7.3)
950 FORMAT(' ',T10,'Vapor quality @ tube outlet--',T54,F7.3)
960 FORMAT(' ',T10,'In-tube heat trans coef (BTU/h7ft270F)--',t51,F9.2)
1100 FORMAT(' ',T5,'TUBE SIDE vs. ANNULUS SIDE ENERGY BALANCE:')
1110 FORMAT(' ',T10,'Deviation (%)--',T53,F7.2)
1200 FORMAT(' ',T5,'NUSELT NUMBER:')
1210 FORMAT(' ',T10,'Nu from testing--',T52,F7.1)
1220 FORMAT(' ',T10,'Nu from Dittus-Boelter--',T52,F7.1)
1230 FORMAT(' ',T10,'Nu from Pethukov-Popov--',T52,F7.1)
RETURN
END

```

APPENDIX D ERROR ANALYSIS

This appendix discusses the experimental uncertainty of the test program. The propagation-of-error method of Kline and McClintock [195] has been used to determine the uncertainties of the inside convective coefficient, mass flux, and vapor quality. The example shown is for a typical, condensation test run (C0X300). All derivatives are evaluated at the conditions of the test run, which are summarized in Table D.1. The values for precision indices (W) come from manufacturer's specifications, information from calibration runs, or estimates based on judgement. The final value of the error represents the absolute value of the maximum expected deviation and is, therefore, a conservative estimate of the expected error. Subscripts used with the precision indices represent the quantity to which the uncertainty applies. (These are not listed separately in the subscripts section of the nomenclature, but can be found in the main body.)

Table D.1. Conditions from condensation test run C0X300

Parameter	Value	Parameter	Value
T_{sat}	39.83 °C	G	299.7 kg/m ² ·s
T_{Win}	29.79 °C	h_j	2834. W/m ² ·°C
T_{Wout}	31.37 °C	\dot{m}_r	0.01469 kg/s
LMID	9.23 °C	\dot{m}_{w}	0.2899 kg/s
P_{tin}	1.531 MPa	C_{PW}	4180. J/kg·°C
ΔP	4.5 kPa	d_j	0.008 m
Q_t	-1920. W	d_o	0.00952 m
Q_{boil}	2941. W/m ² ·°C	l	3.66 m
$Q_{\text{s-h}}$	0. W/m ² ·°C	A_j	0.09199 m ²
U_o	1901. W/m ² ·°C	A_o	0.1095 m ²
h_o	9921. W/m ² ·°C	A_x	5.027 x 10 ⁻⁵ m ²

The uncertainties of regression lines, enhancement factors, oil concentration, and pressure drop are determined statistically at a 95% confidence level. The methods for determining these uncertainties are discussed in separate sections.

Uncertainty of the Inside Convective Coefficient

The determination of the inside convective heat transfer coefficient requires a series of calculations. This section estimates the error of h_i by working through the data reduction equations as outlined in Chapter 5.

Uncertainty of the Heat Transfer in the Test Section

From Equation 5.1, the heat transfer in the test section is

$$Q_{w_r} = \dot{m}w \cdot c_{p_w} (T_{w_{out}} - T_{w_{in}}) \quad (5.1)$$

Substituting the expression ΔT for $(T_{in} - T_{out})$, the uncertainty of Q_t is

$$W_{Q_t} = \left[\left(\frac{\partial Q_t}{\partial \dot{m}} W_{\dot{m}} \right)^2 + \left(\frac{\partial Q_t}{\partial C_p} W_{C_p} \right)^2 + \left(\frac{\partial Q_t}{\partial \Delta T} W_{\Delta T} \right)^2 \right]^{\frac{1}{2}} + \text{uncertainty in loss / gain} \quad (D.1)$$

where

$$\frac{\partial Q_t}{\partial \dot{m}} = C_p \cdot \Delta T \quad (D.2)$$

$$\frac{\partial Q_t}{\partial C_p} = \dot{m} \cdot \Delta T \quad (D.3)$$

$$\frac{\partial Q_t}{\partial \Delta T} = \dot{m} \cdot C_p \quad (D.4)$$

Using the values from Table D.1 to evaluate the derivatives gives

$$\frac{\partial Q_t}{\partial \dot{m}} = -6604. \quad \text{J/kg}$$

$$\frac{\partial Q_t}{\partial C_p} = -0.4580 \quad \text{kg} \cdot \text{C/s}$$

$$\frac{\partial Q_t}{\partial \Delta T} = 1212. \quad \text{J/s} \cdot \text{C}$$

The manufacturer's specified uncertainty for the magnetic flow meter is $\pm 2\%$, yielding

$$W_{\dot{m}} = 5.798 \times 10^{-3} \text{ kg/s}$$

The uncertainty of C_p is estimated to be

$$W_{C_p} = 20.0 \text{ J/kg}\cdot^\circ\text{C}$$

From calibration of the annulus inlet and outlet thermocouples, the uncertainty in the measurement of ΔT is estimated to be

$$W_{\Delta T} = 0.050 \text{ }^\circ\text{C}$$

Finally, the heat loss from the test section is estimated as 1% because the annulus was well insulated and the temperature difference between the water and the ambient air was never greater than 13°C . Substituting all of these values into Equation D.1 gives an estimate for W_{Q_t} :

$$W_{Q_t} = [(-6604 \times 5.798 \times 10^{-3})^2 + (-0.458 \times 20)^2 + (1212 \times 0.05)^2]^{1/2} + 1920 \times 0.01 = \boxed{91.5 \text{ W} = W_{Q_t}}$$

Uncertainty of the Overall Heat Transfer Coefficient

The overall heat transfer coefficient, U_o , is determined from Equation 5.3:

$$U_o = \frac{Q_t}{(A_o \cdot \text{LMTD})} \quad (5.3)$$

where

$$\text{LMTD} = \frac{\Delta T_1 - \Delta T_2}{\ln(\Delta T_1/\Delta T_2)} \quad (5.4)$$

$$\Delta T_1 = T_{r_{\text{sat}}} - T_{W_{\text{in}}} \quad (5.7)$$

$$\Delta T_2 = T_{r_{\text{sat}}} - T_{W_{\text{out}}} \quad (5.8)$$

The uncertainty of U_o is estimated by the following equation:

$$W_{U_o} = \left[\left(\frac{\partial U_o}{\partial Q_t} W_{Q_t} \right)^2 + \left(\frac{\partial U_o}{\partial A_o} W_{A_o} \right)^2 + \left(\frac{\partial U_o}{\partial LMTD} W_{LMTD} \right)^2 \right]^{\frac{1}{2}} \quad (D.5)$$

where

$$\frac{\partial U_o}{\partial Q_t} = \frac{1}{(A_o \cdot LMTD)} \quad (D.6)$$

$$\frac{\partial U_o}{\partial A_o} = -\frac{Q_t}{LMTD} \cdot \frac{1}{A_o^2} \quad (D.7)$$

$$\frac{\partial U_o}{\partial LMTD} = -\frac{Q_t}{A_o} \cdot \frac{1}{(LMTD)^2} \quad (D.8)$$

Evaluating the derivatives yields

$$\frac{\partial U_o}{\partial Q_t} = -0.9900 \text{ m}^{-2} \cdot \text{C}^{-1}$$

$$\frac{\partial U_o}{\partial A_o} = -17,360 \text{ W} / \text{C} \cdot \text{m}^4$$

$$\frac{\partial U_o}{\partial LMTD} = 206.0 \text{ W} / \text{m}^2 \cdot \text{C}^2$$

The value for W_{Q_t} has already been established above, however W_{A_o} and W_{LMTD} must be calculated from the defining equations for A_o and LMTD. Equation 5.4 defines LMTD and A_o is defined by

$$A_o = \pi \cdot d_o \cdot l \quad (D.9)$$

It follows that

$$W_{A_o} = \left[\left(\frac{\partial A_o}{\partial d_o} W_{d_o} \right)^2 + \left(\frac{\partial A_o}{\partial l} W_l \right)^2 \right]^{\frac{1}{2}} \quad (D.10)$$

where

$$\frac{\partial A_o}{\partial d_o} = \pi \cdot l \quad (D.11)$$

$$\frac{\partial A_o}{\partial l} = \pi \cdot d_o \quad (D.12)$$

The derivatives are

$$\frac{\partial A_o}{\partial d_o} = 11.50 \text{ m}$$

$$\frac{\partial A_o}{\partial l} = 0.02991 \text{ m}$$

The uncertainties in the dimensions are estimated as

$$W_{d_o} = 3.0 \times 10^{-5} \text{ m}$$

$$W_l = 5.0 \times 10^{-3} \text{ m}$$

The uncertainty for A_o can now be estimated:

$$W_{A_o} = [(11.50 \times 3.0 \times 10^{-5})^2 + (0.02991 \times 5.0 \times 10^{-3})^2]^{1/2} = 3.76 \times 10^{-4} \text{ m}^2$$

Because the tube wall is thin, the uncertainty for A_i (which is used later in Equation D.20) is approximately equal to that for A_o :

$$W_{A_i} \approx W_{A_o} = 3.76 \times 10^{-4} \text{ m}^2$$

An estimate of the uncertainty of LMTD is given by

$$W_{\text{LMTD}} = \left[\left(\frac{\partial \text{LMTD}}{\partial \Delta T_1} W_{\Delta T_1} \right)^2 + \left(\frac{\partial \text{LMTD}}{\partial \Delta T_2} W_{\Delta T_2} \right)^2 \right]^{1/2} \quad (\text{D.13})$$

where

$$\frac{\partial \text{LMTD}}{\partial \Delta T_1} = \frac{1}{\ln(\Delta T_1/\Delta T_2)} - \frac{\Delta T_1 - \Delta T_2}{[\ln(\Delta T_1/\Delta T_2)]^2} \cdot \frac{1}{\Delta T_1} \quad (\text{D.14})$$

$$\frac{\partial \text{LMTD}}{\partial \Delta T_2} = \frac{-1}{\ln(\Delta T_1/\Delta T_2)} + \frac{\Delta T_1 - \Delta T_2}{[\ln(\Delta T_1/\Delta T_2)]^2} \cdot \frac{1}{\Delta T_2} \quad (\text{D.15})$$

Substituting numerical values and evaluating the derivatives,

$$\frac{\partial \text{LMTD}}{\partial \Delta T_1} = 0.4726$$

$$\frac{\partial \text{LMTD}}{\partial \Delta T_2} = 0.5298$$

The uncertainties of ΔT_1 and ΔT_2 must now be evaluated:

$$W_{\Delta T_1} = \left[\left(\frac{\partial \Delta T_1}{\partial T_{rsat}} W_{T_{rsat}} \right)^2 + \left(\frac{\partial \Delta T_1}{\partial T_{win}} W_{T_{win}} \right)^2 \right]^{\frac{1}{2}} \quad (D.16)$$

where

$$\frac{\partial \Delta T_1}{\partial T_{rsat}} = 1.$$

$$\frac{\partial \Delta T_1}{\partial T_{win}} = -1.$$

Because T_{rsat} is based on the average pressure in the test section, the uncertainty of T_{rsat} is due to errors in the measurement of P_{avg} and in the conversion of a pressure to a temperature. The uncertainty is

$$W_{T_{rsat}} = \left[\left(\frac{\partial T_{rsat}}{\partial P_{avg}} W_{P_{avg}} \right)^2 \right]^{\frac{1}{2}} + \text{P-to-T conversion error} \quad (D.17)$$

where

$$P_{avg} = P_{in} - 0.5 \cdot (\Delta P) \quad (D.18)$$

The following equation estimates $W_{P_{avg}}$:

$$W_{P_{avg}} = \left[\left(\frac{\partial P_{avg}}{\partial P_{in}} W_{P_{in}} \right)^2 + \left(\frac{\partial P_{avg}}{\partial \Delta P} W_{\Delta P} \right)^2 \right]^{\frac{1}{2}} \quad (D.19)$$

The derivatives are evaluated as

$$\frac{\partial P_{avg}}{\partial P_{in}} = 1.0$$

$$\frac{\partial P_{avg}}{\partial \Delta P} = -0.5$$

Based on the maximum deviation of calibration data from the calibration equation, $W_{P_{in}}$ is estimated as 0.003 MPa. The error for ΔP is estimated as two standard deviations of the mean for ΔP . For condensation runs at 300 kg/m²·s, this error is typically 0.005 MPa. Substituting these values yields the solution to Equation D.19:

$$W_{P_{avg}} = [(0.003)^2 + 0.25(0.005)^2]^{1/2} = 0.003905 \text{ MPa}$$

Pressure to temperature conversion is accomplished with a piecewise, second-order curve fit of tabulated data [6]. Comparing saturation temperatures generated by the equations with those in the original table, the maximum deviation is about 0.02 °C.

Equation D.17 can now be solved if the derivative is estimated from tabulated data:

$$\frac{\partial T_{\text{rsat}}}{\partial P_{\text{avg}}} = 27.21 \text{ } ^\circ\text{C/MPa}$$

Thus,

$$W_{T_{\text{rsat}}} = (27.21 \times 0.003905) + 0.02 = 0.126 \text{ } ^\circ\text{C}$$

An estimate for W_{T_w} is

$$\text{Uncertainty due to thermocouple wire} = 0.3 \text{ } ^\circ\text{C}$$

$$\text{Uncertainty due to temperature offset} = 0.05 \text{ } ^\circ\text{C}$$

$$\text{Uncertainty due to fin effect, incomplete mixing, etc.} = 0.05 \text{ } ^\circ\text{C}$$

Assuming the partial derivative of each factor above with respect to T_w is unity, then

$$W_{T_w} = [(0.3)^2 + 2 \cdot (0.05)^2]^{1/2} = 0.308 \text{ } ^\circ\text{C}$$

All of the quantities in Equation D.16 are now known, so it can be solved:

$$W_{\Delta T_1} = [(0.126)^2 + (-0.308)^2]^{1/2} = 0.33 \text{ } ^\circ\text{C}$$

Calculating $W_{\Delta T_2}$ yields the same result:

$$W_{\Delta T_2} = W_{\Delta T_1} = 0.33 \text{ } ^\circ\text{C}$$

Equation D.13 may now be solved for W_{LMTD} :

$$W_{\text{LMTD}} = [(0.4726 \times 0.33)^2 + (0.5298 \times 0.33)^2]^{1/2} = 0.24 \text{ } ^\circ\text{C}$$

All quantities on the right hand side of Equation D.5 are now determined:

$$W_{U_o} = [(-0.99 \times 91.5)^2 + (-17360 \times 3.76 \times 10^{-4})^2 + (206 \times 0.24)^2]^{1/2} =$$

$$\boxed{103 \text{ W/m}^2 \cdot ^\circ\text{C} = W_{U_o}}$$

Uncertainty of the Annulus-Side Convective Coefficient

The outside (or annulus-side) convective heat transfer coefficient is obtained from a calibration equation (Equation 5.11). The general form of the equation is that used in several single-phase heat transfer correlations, e.g., Dittus-Boelter/McAdams (McAdams [154]) and Sieder-Tate [196]. Because parts of these earlier correlations are used without alteration (such as the Prandtl number exponent) and other parts are changed to fit the annulus calibration data (such as the Reynolds number exponent), it is difficult to precisely determine the uncertainty of h_o .

For purposes of this analysis, it is estimated that W_{h_o} is $\pm 5\%$. Single-phase correlations generally agree with experimental data within $\pm 10\%$; but because the equation is customized by the calibration procedure, the uncertainty should be somewhat lower.

Uncertainty of the inside Convective Coefficient

The inside convective heat transfer coefficient is calculated using Equation 5.10:

$$h_i = \frac{1}{\left[\frac{1}{U_o} - \frac{1}{h_o} \right] \frac{A_i}{A_o}} \quad (5.10)$$

Applying the same propagation-of-error procedure used above:

$$W_{h_i} = \left[\left(\frac{\partial h_i}{\partial U_o} W_{U_o} \right)^2 + \left(\frac{\partial h_i}{\partial h_o} W_{h_o} \right)^2 + \left(\frac{\partial h_i}{\partial A_i} W_{A_i} \right)^2 + \left(\frac{\partial h_i}{\partial A_o} W_{A_o} \right)^2 \right]^{\frac{1}{2}} \quad (D.20)$$

where

$$\frac{\partial h_i}{\partial U_o} = \left[\frac{1}{h_o - U_o} + \frac{U_o}{(h_o - U_o)^2} \right] \frac{A_o \cdot h_o}{A_i} \quad (D.21)$$

$$\frac{\partial h_i}{\partial h_o} = \left[\frac{1}{h_o - U_o} - \frac{h_o}{(h_o - U_o)^2} \right] \frac{A_o \cdot U_o}{A_i} \quad (D.22)$$

$$\frac{\partial h_i}{\partial A_i} = - \frac{A_o \cdot h_o \cdot U_o}{h_o - U_o} \cdot \frac{1}{A_i^2} \quad (D.23)$$

$$\frac{\partial h_i}{\partial A_o} = \frac{1}{A_i} \cdot \left[\frac{1}{U_o} - \frac{1}{h_o} \right] \quad (D.24)$$

Substituting appropriate values from Table D.1 yields

$$\frac{\partial h_i}{\partial U_o} = 1.822$$

$$\frac{\partial h_i}{\partial h_o} = -0.06688$$

$$\frac{\partial h_i}{\partial A_i} = -30,430 \text{ W/m}^4 \cdot \text{°C}$$

$$\frac{\partial h_i}{\partial A_o} = 25,560 \text{ W/m}^4 \cdot \text{°C}$$

Equation D.20 can now be solved:

$$W_{hi} = [(1.822 \times 103)^2 + (-0.06688 \times 496)^2 + (-30430 \times 3.76 \times 10^{-4})^2 + (25560 \times 3.76 \times 10^{-4})^2]^{1/2} = \boxed{191. \text{ W/m}^2 \cdot \text{°C} = W_{hi}}$$

The uncertainty of the inside convective heat transfer coefficient is just under 7% for this condensation example. Evaporation tests tend to have a higher uncertainty. Using the procedure outlined for a typical evaporation test (E0X300), the uncertainty is about 10%.

In general, uncertainty with enhanced tubes is slightly greater than that with a smooth tube. To minimize uncertainty, it is desirable to have both the maximum possible LMTD and $h_o \gg h_i$, but because h_i is large for augmented tubes, it is necessary to reduce LMTD and/or h_o to maintain the same quality change through the test section. The test conditions, therefore, are a trade-off between a large LMTD and a large h_o . For typical augmented tube runs, the uncertainties for a single test are about three percentage points higher than comparable smooth tube runs.

Uncertainty of the Mass Flux

The mass flux is calculated by

$$G = \frac{\dot{m}_f}{A_x} \quad (\text{D.25})$$

where A_x is the cross-sectional flow area of the tube. As above,

$$W_G = \left[\left(\frac{\partial G}{\partial \dot{m}_r} W_{\dot{m}_r} \right)^2 + \left(\frac{\partial G}{\partial A_x} W_{A_x} \right)^2 \right]^{\frac{1}{2}} \quad (D.26)$$

where

$$\frac{\partial G}{\partial \dot{m}_r} = \frac{1}{A_x} = 19,890 \text{ m}^{-2} \quad (D.27)$$

$$\frac{\partial G}{\partial A_x} = -\frac{\dot{m}_r}{A_x^2} = -5.814 \times 10^6 \text{ kg/m}^4 \cdot \text{s} \quad (D.28)$$

The refrigerant flow meter has a specified accuracy of better than $\pm 1\%$, so, using 1% as an estimate,

$$W_{\dot{m}_r} = 1.469 \times 10^{-4} \text{ kg/s}$$

The cross sectional area is calculated from

$$A_x = \pi \cdot d_i^2 / 4 \quad (D.29)$$

The uncertainty is

$$W_{A_x} = \left[\left(\frac{\partial A_x}{\partial d_i} W_{d_i} \right)^2 \right]^{\frac{1}{2}} \quad (D.30)$$

where

$$\frac{\partial A_x}{\partial d_i} = \pi \cdot d_i / 2 = 0.01257 \text{ m} \quad (D.31)$$

From an earlier estimate of W_{d_i} ,

$$W_{d_i} = 0.00003 \text{ m}$$

Therefore,

$$W_{A_x} = [(0.01257 \times 0.00003)^2]^{1/2} = 3.771 \times 10^{-7} \text{ m}^2$$

Solving Equation D.26,

$$W_G = [(19890 \times 1.469 \times 10^{-4})^2 + (-5.814 \times 10^6 \times 3.771 \times 10^{-7})^2]^{1/2} =$$

$$\boxed{3.65 \text{ kg/m}^2 \cdot \text{s} = W_G}$$

This represents an uncertainty in the mass flux of slightly over 1.2%.

Uncertainty of the Vapor Quality

Uncertainties for both inlet quality, X_{in} , and quality change through the test section, ΔX_t , are calculated in this section, once again using test run COX300 as an example.

Inlet Quality

Combining Equations 5.12 and 5.14 – 5.16, a single expression for X_{in} is derived:

$$X_{in} = \frac{1}{i_{fg}} \left[\frac{0.98 \cdot (V \cdot I)_h}{\dot{m}_r} - C_{pr} \cdot (T_{sat} - T_{hin}) \right] \quad (D.32)$$

For simplification, let NP be the net power from the heaters to the refrigerant $[0.98 \cdot (V \cdot I)_h]$ and let ΔT be the temperature difference $[T_{sat} - T_{hin}]$. The propagation-of-error expression for X_{in} is then

$$W_{X_{in}} = \left[\left(\frac{\partial X_{in}}{\partial i_{fg}} W_{i_{fg}} \right)^2 + \left(\frac{\partial X_{in}}{\partial NP} W_{NP} \right)^2 + \left(\frac{\partial X_{in}}{\partial \dot{m}} W_{\dot{m}} \right)^2 + \left(\frac{\partial X_{in}}{\partial C_{pr}} W_{C_{pr}} \right)^2 + \left(\frac{\partial X_{in}}{\partial \Delta T} W_{\Delta T} \right)^2 \right]^{\frac{1}{2}} \quad (D.33)$$

where

$$\frac{\partial X_{in}}{\partial i_{fg}} = -\frac{1}{i_{fg}^2} \left[\frac{NP}{\dot{m}_r} - C_{pr} \cdot (\Delta T) \right] \quad (D.34)$$

$$\frac{\partial X_{in}}{\partial NP} = \frac{1}{i_{fg} \cdot \dot{m}_r} \quad (D.35)$$

$$\frac{\partial X_{in}}{\partial \dot{m}} = -\frac{NP}{i_{fg} \cdot \dot{m}_r^2} \quad (D.36)$$

$$\frac{\partial X_{in}}{\partial C_{pr}} = -\frac{\Delta T}{i_{fg}} \quad (D.37)$$

$$\frac{\partial X_{in}}{\partial \Delta T} = -\frac{C_{pr}}{i_{fg}} \quad (D.38)$$

Substituting values from Table D.1:

$$\frac{\partial X_{in}}{\partial i_{fg}} = -5.233 \times 10^{-6} \text{ kg/J}$$

$$\frac{\partial X_{in}}{\partial NP} = 4.086 \times 10^{-4} \text{ W}^{-1}$$

$$\frac{\partial X_{in}}{\partial \dot{m}} = -80.16 \text{ s/kg}$$

$$\frac{\partial X_{in}}{\partial C_{pr}} = -2.485 \times 10^{-4} \text{ kg} \cdot \text{C}/\text{J}$$

$$\frac{\partial X_{in}}{\partial \Delta T} = -7.383 \times 10^{-3} \text{ } ^\circ\text{C}^{-1}$$

The uncertainty of the enthalpy of vaporization is estimated as

$$W_{i_{fg}} = 1000 \text{ J/kg}$$

For the net power, the uncertainty of the gross power measurement is estimated as $\pm 2\%$.

The uncertainty due to losses through the insulation is estimated at $\pm 2\%$ of the reading. The total uncertainty for the net power is, therefore, $\pm 2.8\%$:

$$W_{NP} = 82.35 \text{ W}$$

The uncertainty of the refrigerant mass flow was calculated earlier as

$$W_{\dot{m}_r} = 1.469 \times 10^{-4} \text{ kg/s}$$

The specific heat uncertainty is estimated as

$$W_{C_{pr}} = 30.0 \text{ J/kg} \cdot \text{C}$$

Finally, the uncertainty of the temperature difference is the same as the uncertainty for ΔT_1 and ΔT_2 calculated earlier, even though the temperatures here are not the same. The uncertainties of each term in the expression for ΔT , however, are the same, so the overall uncertainty is equal:

$$W_{\Delta T} = 0.33 \text{ } ^\circ\text{C}$$

Equation D.33 can now be solved for $W_{X_{in}}$:

$$W_{X_{in}} = [(-5.233 \times 10^{-6} \cdot 1000)^2 + (4.086 \times 10^{-4} \cdot 82.35)^2 + (-80.16 \cdot 1.469 \times 10^{-4})^2 + (-2.485 \times 10^{-4} \cdot 30)^2 + (-7.383 \times 10^{-3} \cdot 0.33)^2]^{1/2} = \boxed{0.037 = W_{X_{in}}}$$

The uncertainty of the inlet quality is about $\pm 4\%$ quality.

Quality Change

From Equation 5.17, the expression for quality change through the test section is

$$\Delta X = \frac{Q_t}{\dot{m}_r \cdot i_{fg}} \quad (5.17)$$

Applying the propagation-of-error method,

$$W_{\Delta X} = \left[\left(\frac{\partial \Delta X}{\partial Q_t} W_{Q_t} \right)^2 + \left(\frac{\partial \Delta X}{\partial i_{fg}} W_{i_{fg}} \right)^2 + \left(\frac{\partial \Delta X}{\partial \dot{m}} W_{\dot{m}} \right)^2 \right]^{1/2} \quad (D.39)$$

where

$$\frac{\partial \Delta X}{\partial Q_t} = \frac{1}{\dot{m}_r \cdot i_{fg}} \quad (D.40)$$

$$\frac{\partial \Delta X}{\partial i_{fg}} = -\frac{Q_t}{\dot{m}_r} \cdot \frac{1}{i_{fg}^2} \quad (D.41)$$

$$\frac{\partial \Delta X}{\partial \dot{m}} = -\frac{Q_t}{i_{fg}} \cdot \frac{1}{\dot{m}_r^2} \quad (D.42)$$

Solving these partial derivatives yields

$$\frac{\partial \Delta X}{\partial Q_t} = 4.086 \times 10^{-4} \text{ 1/W}$$

$$\frac{\partial \Delta X}{\partial i_{fg}} = 4.708 \times 10^{-6} \text{ kg/J}$$

$$\frac{\partial \Delta X}{\partial \dot{m}} = 53.40 \text{ s/kg}$$

All of the uncertainties in Equation D.39 have already been determined, so the equation can be solved for $W_{\Delta X}$:

$$W_{\Delta X} = [(4.086 \times 10^{-4} \cdot 91.5)^2 + (4.708 \times 10^{-6} \cdot 1000)^2 + (53.4 \cdot 1.469 \times 10^{-4})^2]^{1/2} = \boxed{0.039 = W_{\Delta X}}$$

Like the inlet quality, the quality change has an uncertainty of about $\pm 4\%$ quality.

Uncertainty of the Oil Concentration

The uncertainty in the oil concentration measurement was determined by the standard deviation of three independent observations, per ANSI/ASHRAE Standard 41.4-1984 [155]. The uncertainty is about ± 0.1 weight percent for all cases.

Uncertainty of the Pressure Drop

A statistical uncertainty is determined for the pressure drop measurements. Because the fluctuations in pressure drop are large relative to the reading, instrumentation uncertainties are negligible in comparison. Table D.2 lists the pressure drop uncertainties in terms of the average standard deviation for each tube at various mass fluxes and oil concentrations. Table D.3 summarizes the uncertainty by showing the highest, lowest, and mean standard deviation for each tube. There is no discernible pattern in the standard deviation variations; differences are probably due to the particular conditions of a given test and not to the tube type, oil type, etc.

Uncertainty of the Regression Lines

The correlation coefficients for the curves (h_i and ΔP versus G) are in the range of 0.86 to 0.99 and are above 0.9 in most cases. To estimate the uncertainty of the regression lines, confidence intervals about the mean predicted value (either h_i or ΔP) are presented at the 95% confidence level. The confidence interval is defined by

Table D.2. Average standard deviations of the pressure drop measurements ^a

Test type ^b	G kg/m ² ·s	Oil %						
		150 SUS				300 SUS		
		0.0	1.3	2.5	5.0	1.3	2.5	5.0
1	125	0.7	2.0	0.4	1.3	3.2	3.2	8.1
1	200	1.7	0.6	0.8	2.2	2.5	2.3	4.4
1	300	0.7	0.6	0.5	1.7	2.4	2.3	3.3
1	400	0.4	1.4	0.5	1.5	2.2	2.3	3.7
2	125	1.3	1.4	3.9	2.4	1.4	2.6	2.7
2	200	1.9	3.2	3.4	4.0	2.5	2.1	3.7
2	300	1.8	3.4	2.6	3.8	1.8	1.7	1.2
2	400	2.0	1.6	3.8	2.1	1.0	2.1	1.4
3	125	0.9	—	1.0	2.1	3.1	1.2	2.7
3	200	1.9	—	1.8	2.4	2.6	1.8	2.2
3	300	2.0	2.8	1.8	2.3	2.7	2.0	2.0
3	400	2.0	1.8	1.6	3.0	2.5	1.6	2.0
4	125	1.0	1.1	1.2	1.5	2.2	1.8	3.0
4	200	2.1	1.6	1.5	1.6	2.6	3.3	2.9
4	300	2.4	2.4	1.6	2.0	2.5	1.4	1.1
4	400	2.4	2.5	2.8	1.6	2.0	1.6	1.6
5	125	1.7	0.7	0.7	0.8	—	—	—
5	200	1.8	1.1	1.8	1.0	—	—	—
5	300	1.2	1.5	0.7	2.7	—	—	—
5	400	1.4	2.8	1.1	2.9	—	—	—
6	125	1.4	2.5	2.6	3.5	—	—	—
6	200	2.0	2.8	3.5	4.4	—	—	—
6	300	2.0	3.0	1.8	2.2	—	—	—
6	400	2.1	2.0	1.9	1.5	—	—	—

^aTabulated values in kPa.

^b1 = Smooth tube condensation
 2 = Smooth tube evaporation
 3 = Micro-fin tube condensation

4 = Micro-fin tube evaporation
 5 = Low-fin tube condensation
 6 = Low-fin tube evaporation

Table D.3. Summary of pressure drop standard deviations

Test type ^a	High (kPa)	Low (kPa)	Average (kPa)
1	8.1	0.4	2.1
2	4.0	1.0	2.4
3	3.0	0.9	2.1
4	3.3	1.0	2.0
5	2.9	0.7	1.5
6	4.4	1.4	2.4

^aSame as Table D.2 above.

$$CI = t(v,\gamma) \cdot \delta \cdot \sqrt{\frac{1}{n} + \frac{(G - \bar{G})^2}{(n-1) \cdot s_G^2}} \quad (D.43)$$

where

$t(v,\gamma)$ = t-statistic

v = degrees of freedom

γ = confidence level

δ = standard error of the estimate

s_G^2 = variance of G for the data set

The calculation is carried out with four representative cases for both h_i and ΔP . (See Tables E.1, E.4, E.7, and E.10 for heat transfer data and Tables E.7, E.10, E.17, and E.19 for pressure drop data.) The t-statistic is obtained from statistical tables and the other terms in Equation D.43 are calculated using the RS/1 statistical package [194]. Tables D.4 and D.5 give the confidence intervals in absolute terms, as well as in percentages of the prediction, at low, medium, and high mass fluxes. Figures D.1 and D.2 are plots of the regression equations along with confidence intervals for the sample cases. The uncertainty of the heat transfer coefficient from the regression equation ranges from about 2% to 10% of the predicted value. The pressure drop uncertainty in absolute terms is on the order of 1 kPa or less, which is generally less than 25% in percentage terms. However, for some condensation cases at low mass flux, the uncertainty is over 60% of the predicted value.

Table D.4. Calculated confidence intervals for heat transfer coefficient regression equations at 95% confidence level

Test description	Uncertainty estimate (W/m ² ·°C)			Uncertainty estimate (%)		
	Low G ^a	Med. G	High G	Low G	Med. G	High G
Smooth, evap.	256	161	305	9.6	3.8	5.5
Smooth, cond.	76	51	96	3.5	2.0	3.0
Micro-fin, evap.	452	288	493	6.1	3.2	4.7
Micro-fin, cond.	155	91	177	2.9	1.6	2.8

^aLow G=125 kg/m²·s, Med. G=250 kg/m²·s, High G=400 kg/m²·s.

Table D.5. Calculated confidence intervals for pressure drop regression equations at 95% confidence level

Test description	Uncertainty estimate (kPa)			Uncertainty estimate (%)		
	Low G ^a	Med. G	High G	Low G	Med. G	High G
Smooth, evap.	0.72	0.47	0.91	19.	4.0	3.1
Smooth, cond.	0.72	0.42	0.66	62.	15.	7.5
Micro-fin, evap.	0.99	0.62	1.07	21.	3.5	2.4
Micro-fin, cond.	0.20	0.12	0.26	19.	2.3	2.0

^aLow G=125 kg/m²·s, Med. G=250 kg/m²·s, High G=400 kg/m²·s.

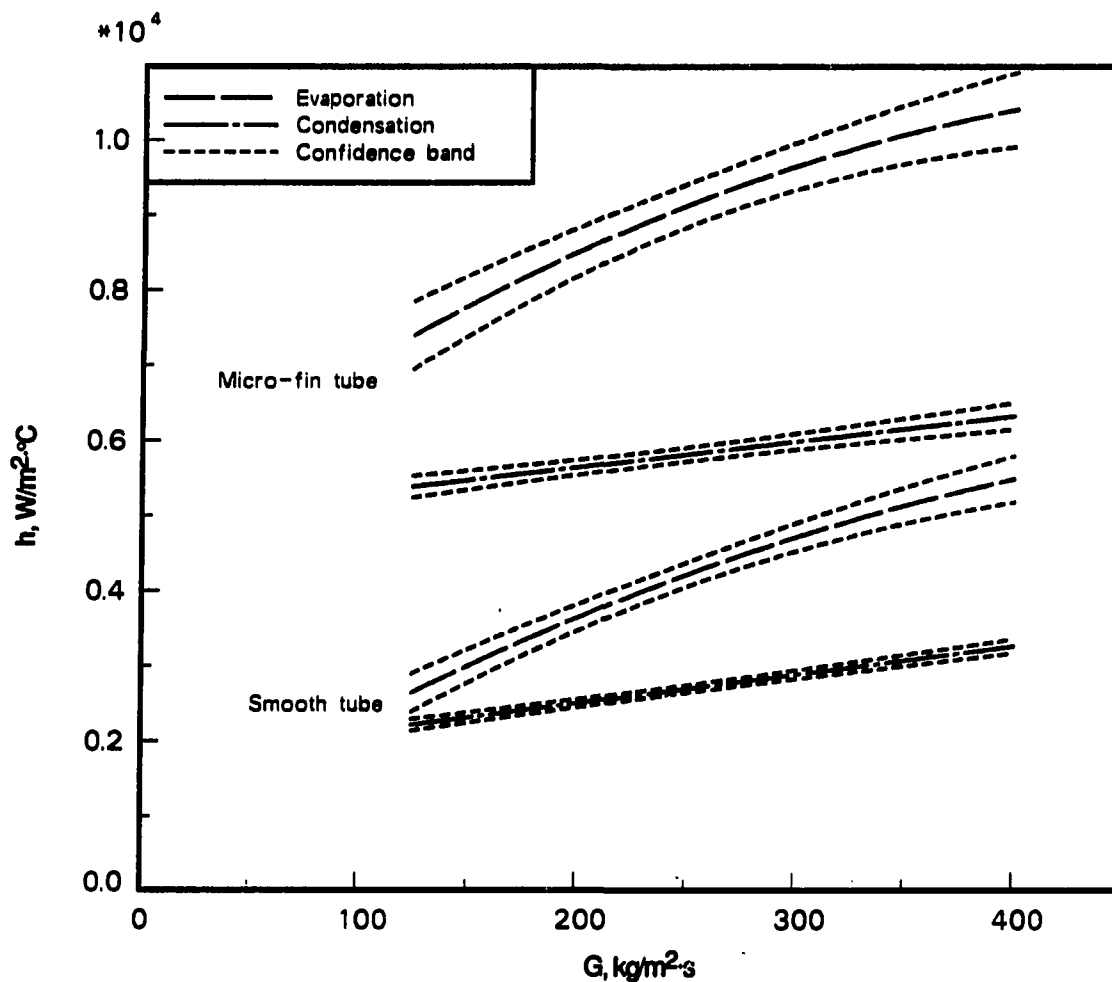


Figure D.1. Regression lines and confidence intervals (95%) for typical evaporation and condensation heat transfer cases

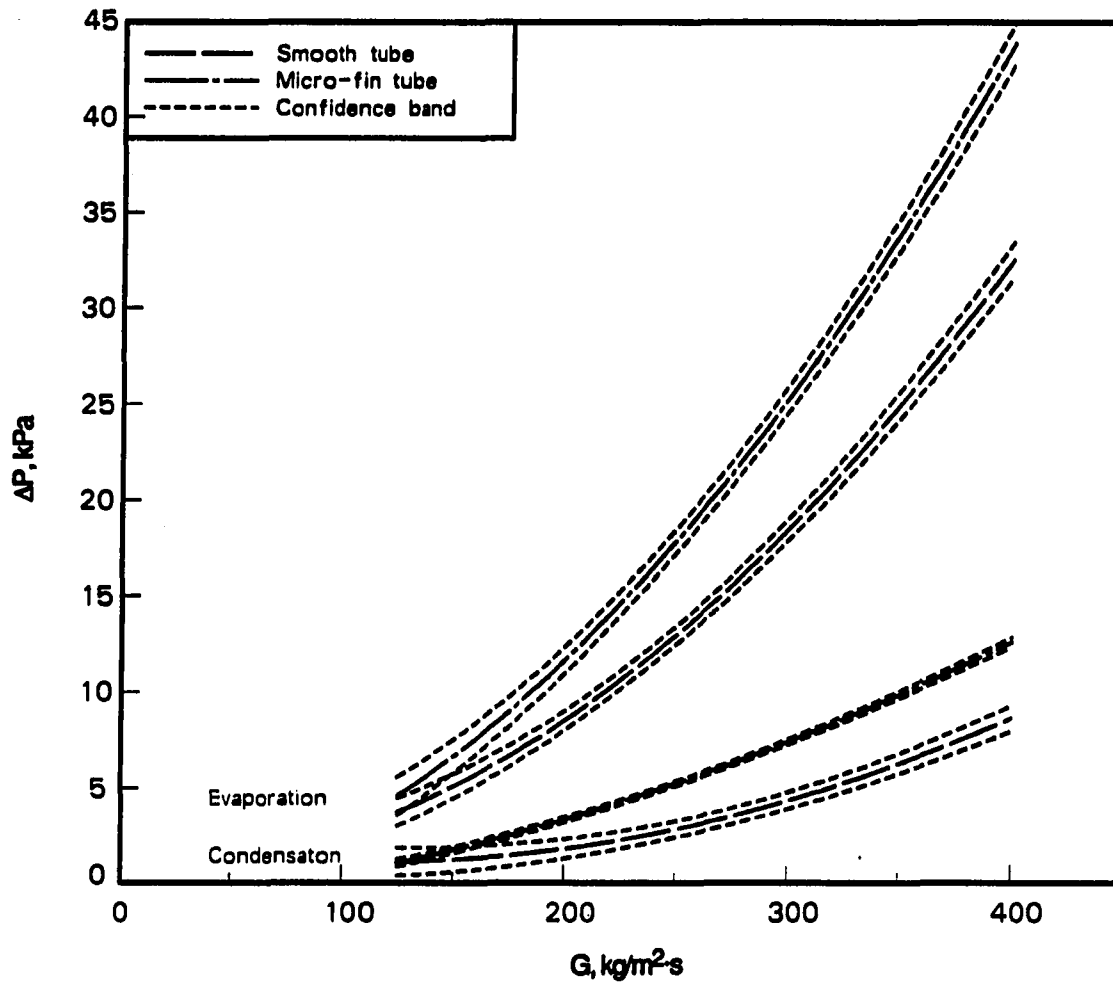


Figure D.2. Regression lines and confidence intervals (95%) for typical evaporation and condensation pressure drop cases

Uncertainty of the Enhancement Factors, ϵ and Ψ

The same cases discussed in the previous section are used as examples, with the uncertainty at a particular condition estimated from the confidence interval calculations.

From the definition of enhancement factors:

$$EF = \frac{Z_1}{Z_2} \quad (D.44)$$

where

EF = either ϵ or Ψ

Z = either h or ΔP

The propagation-of-error method is used to calculate the uncertainty of the enhancement factor, but the precision indices are estimated from the uncertainties of the regression lines. The propagation-of-error equation is

$$W_{EF} = \left[\left(\frac{\partial EF}{\partial Z_1} \cdot W_{Z_1} \right)^2 + \left(\frac{\partial EF}{\partial Z_2} \cdot W_{Z_2} \right)^2 \right]^{1/2} \quad (D.45)$$

where

$$\frac{\partial EF}{\partial Z_1} = \frac{1}{Z_2} \quad (D.46)$$

$$\frac{\partial EF}{\partial Z_2} = -\frac{Z_1}{Z_2^2} \quad (D.47)$$

Substituting numerical values from the sample cases, Table D.6 is obtained.

Table D.6. Estimated uncertainty of enhancement factors ($\epsilon_{a/s}$ and $\Psi_{a/s}$) as a percentage of the calculated values

	Low G ^a	Med. G	High G
$\epsilon_{a/s}$ (evap.)	11.	5.0	7.3
$\epsilon_{a/s}$ (cond.)	4.7	2.7	4.3
$\Psi_{a/s}$ (evap.)	29.	5.0	3.9
$\Psi_{a/s}$ (cond.)	64.	15.	8.0

^aLow G \approx 125, Med.G \approx 250, High G \approx 400 kg/m²·s.

Uncertainty of the Enhancement Performance Ratio, θ

The enhancement performance ratio (θ), like the enhancement factors, is formed from a ratio. Therefore, Equations D.45 through D.47 also describe the uncertainty of θ if ϵ and ψ are substituted for Z_1 and Z_2 , respectively. Using the values from Table D.6, the uncertainty of the performance enhancement ratio, $\theta_{a/s}$, is shown below in Table D.7.

These uncertainties are generally higher than any of the others discussed previously, and they are particularly high at the lowest mass flux. The uncertainty for condensation is about double that for evaporation, due primarily to the higher relative pressure drop uncertainty for condensation.

Table D.7. Uncertainty estimate for the enhancement performance ratio (θ) as a percentage of calculated values

	Low G ^a	Med. G	High G
$\theta_{a/s}$ (evap.)	31.	7.2	11.
$\theta_{a/s}$ (cond.)	64.	15.	9.0

^aLow G=125, Med. G=250, High G=400 kg/m²·s.

**APPENDIX E
TABULATED DATA**

Table E.1. Smooth tube evaporation with pure refrigerant

Test Run	Oil %	G kg/m ² ·s	h W/m ² ·°C	X _{in} %	X _{out} %	P MPa	T _{sat} °C	ΔP ^a kPa
E0X123	—	123	2740	21	92	0.48	-1.1	—
E0X127	—	127	2810	20	82	0.50	0.1	—
E0X130	—	130	2350	21	82	0.47	-1.7	—
E0X196	—	196	3840	20	91	0.48	-1.1	—
E0X200	—	200	3640	19	78	0.49	-0.5	—
E0X219	—	219	3790	18	87	0.47	-1.7	—
E0X298	—	298	4340	16	70	0.51	0.7	—
E0X300	—	300	4800	20	82	0.53	1.9	—
E0X301	—	301	4870	19	78	0.52	1.3	—
E0X396	—	396	5310	17	87	0.46	-2.4	—
E0X399	—	399	5650	18	84	0.48	-1.1	—

^aFor pressure drop data, see Table E.17.

Table E.2. Smooth tube evaporation with refrigerant plus 150-SUS oil

Test Run	Oil %	G kg/m ² ·s	h W/m ² ·°C	X _{in} %	X _{out} %	P MPa	T _{sat} °C	ΔP ^a kPa
E1X121	1.2	121	3280	15	77	0.50	0.1	—
E1X123		123	2890	10	69	0.51	0.7	—
E1X126		126	2880	10	68	0.51	0.7	—
E1X150		150	3680	9	81	0.53	1.9	—
E1X181		181	4030	19	86	0.48	-1.1	—
E1X204		204	4390	20	82	0.53	1.9	—
E1X215		215	4540	19	83	0.53	1.9	—
E1X302		302	5240	18	78	0.57	4.2	—
E1X303		303	5210	17	78	0.56	3.7	—
E1X399		399	5830	16	79	0.52	1.3	—
E1X403	1.2	403	5840	15	78	0.51	0.7	—
E2X122	2.5	122	3470	17	84	0.49	-0.5	—
E2X125		125	3540	17	83	0.49	-0.5	—
E2X126		126	3650	13	77	0.55	3.1	—
E2X201		201	5080	15	77	0.55	3.1	—
E2X208		208	5180	14	75	0.55	3.1	—
E2X299		299	6050	13	79	0.56	3.7	—
E2X305		305	6020	13	76	0.57	4.2	—
E2X384		384	6900	13	80	0.58	4.8	—
E2X393	2.5	393	6870	12	76	0.58	4.8	—

^aFor pressure drop data, see Table E.18.

Table E.2. (continued)

Test Run	Oil %	G kg/m ² ·s	h W/m ² ·°C	X _{in} %	X _{out} %	P MPa	T _{sat} °C	ΔP ^a kPa
E5X125	4.9	125	2930	17	84	0.52	1.3	—
E5X130		130	3150	17	80	0.53	1.9	—
E5X195		195	4060	20	90	0.50	0.1	—
E5X197		198	3940	16	75	0.51	0.7	—
E5X198		198	4590	19	81	0.52	1.3	—
E5X204		204	4540	18	78	0.52	1.3	—
E5X296		296	5140	20	86	0.56	3.7	—
E5X303		303	5500	19	79	0.56	3.7	—
E5X393		393	6400	23	71	0.53	1.9	—
E5X394		394	6600	21	80	0.58	4.8	—
E5X402	4.9	402	6610	21	81	0.58	4.8	—

Table E.3. Smooth tube evaporation with refrigerant plus 300-SUS oil

Test Run	Oil %	G kg/m ² ·s	h W/m ² ·°C	X _{in} %	X _{out} %	P MPa	T _{sat} °C	ΔP kPa
E0C126	0.6	126	2650	15	92	0.47	-1.7	—
E0C132		132	2510	16	93	0.43	-4.4	—
E0C133		133	2670	15	84	0.45	-3.1	3.6
E0C197		197	3750	15	80	0.50	0.1	8.7
E0C199		199	3650	14	74	0.48	-1.1	8.4
E0C201		201	3690	15	82	0.48	-1.1	9.9
E0C289		289	4720	16	82	0.49	-0.5	19.2
E0C301		301	4800	15	80	0.49	-0.5	20.4
E0C305		305	4850	15	81	0.48	-1.1	21.7
E0C387		387	5550	17	81	0.50	0.1	38.0
E0C390		390	5610	18	81	0.51	0.7	37.1
E0C397		397	5750	20	84	0.55	3.1	36.9
E0C401	0.6	401	5470	17	75	0.53	1.9	36.6
E1C126	1.3	126	2600	17	85	0.50	0.1	3.8
E1C127		127	2660	17	84	0.50	0.1	4.2
E1C130		130	2670	17	80	0.49	-0.5	4.2
E1C195		195	3660	14	83	0.50	0.1	8.7
E1C196		196	3670	13	77	0.49	-0.5	9.1
E1C201		201	3550	14	79	0.50	0.1	10.4
E1C268		268	4500	19	80	0.55	3.1	18.0
E1C276		276	4630	18	78	0.55	3.1	18.7
E1C279		279	4560	18	74	0.54	2.5	18.7
E1C386		386	5780	18	78	0.58	4.8	31.3
E1C387		388	5510	18	76	0.58	4.8	30.7
E1C388	1.3	388	5470	18	79	0.56	3.7	33.0

Table E.3. (continued)

Test Run	Oil %	G kg/m ² ·s	h W/m ² ·°C	X _{in} %	X _{out} %	P MPa	T _{sat} °C	ΔP kPa
E2C122	2.6	122	2320	15	78	0.47	-1.7	5.1
E2C124		124	2200	15	78	0.49	-0.5	4.0
E2C137		137	2290	14	71	0.49	-0.5	4.4
E2C194		194	3310	16	77	0.54	2.5	10.2
E2C197		197	3230	15	75	0.53	1.9	8.9
E2C198		198	3100	17	76	0.50	0.1	10.9
E2C203		203	3450	16	82	0.51	0.7	10.9
E2C296		296	4260	18	81	0.55	3.1	21.1
E2C297		297	4330	18	81	0.56	3.7	21.7
E2C389		389	5040	17	81	0.53	1.9	36.9
E2C390		390	5300	22	84	0.56	3.7	38.1
E2C396		396	4980	19	80	0.54	2.5	37.4
E2C398	2.6	398	5090	16	78	0.52	1.3	35.8
E5C126	5.0	126	1930	16	76	0.53	1.9	5.3
E5C130		130	2110	15	71	0.52	1.3	4.7
E5C136		136	2050	15	84	0.51	0.7	6.2
E5C144		144	2170	11	84	0.47	-1.7	6.3
E5C211		211	2880	10	80	0.53	1.9	14.1
E5C217		217	3020	14	84	0.53	1.9	16.2
E5C218		218	2970	13	82	0.52	1.3	16.4
E5C277		278	3960	20	83	0.56	3.7	23.1
E5C278		278	4120	19	81	0.53	1.9	23.7
E5C287		287	4140	19	77	0.55	3.1	22.3
E5C302		302	4070	17	76	0.52	1.3	25.2
E5C360		360	4730	21	81	0.57	4.2	33.9
E5C372		372	4690	19	75	0.56	3.7	32.8
E5C378	5.0	378	4790	18	71	0.54	2.5	34.8

Table E.4. Smooth tube condensation with pure refrigerant

Test Run	Oil %	G kg/m ² ·s	h W/m ² ·°C	X _{in} %	X _{out} %	P MPa	T _{sat} °C	ΔP ^a kPa
C0X125	—	125	2290	90	14	1.55	40.4	—
C0X126	—	126	2290	90	14	1.54	40.2	—
C0X129	—	129	2200	84	3	1.51	39.4	—
C0X200	—	200	2440	91	7	1.53	39.9	—
C0X201	—	201	2490	90	5	1.51	39.4	—
C0X299	—	299	2800	90	10	1.53	39.9	—
C0X300	—	300	2830	89	11	1.53	39.9	—
C0X395	—	395	3320	92	10	1.54	40.2	—
C0X400	—	400	3300	90	8	1.54	40.2	—

^aFor pressure drop data, see Table E.19.

Table E.5. Smooth tube condensation with refrigerant plus 150-SUS oil

Test Run	Oil %	G kg/m ² ·s	h W/m ² ·°C	X _{in} %	X _{out} %	P MPa	T _{sat} °C	ΔP ^a kPa
C1X127	1.2	127	2100	89	4	1.51	39.4	—
C1X128		128	2130	93	7	1.52	39.6	—
C1X131		131	2170	85	7	1.50	39.1	—
C1X202		202	2320	84	8	1.53	39.9	—
C1X204		204	2320	84	9	1.54	40.2	—
C1X205		205	2310	83	10	1.53	39.9	—
C1X302		302	2670	83	10	1.56	40.7	—
C1X304		304	2660	81	9	1.55	40.4	—
C1X395		395	3110	85	9	1.55	40.4	—
C1X403	1.2	403	3130	81	8	1.55	40.4	—
C2X125	2.5	125	2080	86	4	1.54	40.2	—
C2X130		130	2050	85	3	1.51	39.4	—
C2X202		202	2190	85	8	1.55	40.4	—
C2X203		203	2210	83	6	1.55	40.4	—
C2X301		301	2530	85	5	1.53	39.9	—
C2X302		301	2570	83	8	1.54	40.2	—
C2X396		396	3040	88	11	1.54	40.2	—
C2X398		398	3010	84	9	1.53	39.9	—
C2X405	2.5	405	3020	85	8	1.53	39.9	—
C5X128	4.9	128	1880	88	3	1.55	40.4	—
C5X129		129	1880	85	1	1.53	39.9	—
C5X197		198	2170	86	5	1.54	40.2	—
C5X198		198	2240	89	6	1.54	40.2	—
C5X296		296	2460	79	0	1.52	39.6	—
C5X300		300	2470	79	3	1.52	39.6	—
C5X404		404	3010	85	4	1.51	39.4	—
C5X405		405	2960	85	3	1.51	39.4	—
C5X411	4.9	411	2930	78	3	1.51	39.4	—

^aFor pressure drop data, see Table E.20.

Table E.6. Smooth tube condensation with refrigerant plus 300-SUS oil

Test Run	Oil %	G kg/m ² ·s	h W/m ² ·°C	X _{in} %	X _{out} %	P MPa	T _{sat} °C	ΔP kPa
C0C127	0.6	127	2250	90	14	1.65	43.0	1.0
C0C131		131	2190	80	5	1.62	42.2	0.8
C0C132		132	2180	92	27	1.55	40.4	1.1
C0C200		201	2400	87	16	1.55	40.4	2.8
C0C201		201	2380	87	16	1.55	40.4	2.3
C0C202		201	2390	87	17	1.55	40.4	2.3
C0C294		294	2820	86	17	1.56	40.7	4.9
C0C295		295	2780	85	15	1.56	40.7	4.4
C0C297		297	2790	86	18	1.55	40.4	4.8
C0C396		396	3310	85	15	1.59	41.5	7.8
C0C397		397	3210	85	15	1.59	41.5	7.7
C0C399	0.6	399	3310	84	14	1.59	41.5	7.8

Table E.6. (continued)

Test Run	Oil %	G kg/m ² ·s	h W/m ² ·°C	X _{in} %	X _{out} %	P MPa	T _{sat} °C	ΔP kPa
C1C126	1.3	126	2060	84	10	1.51	39.4	0.8
C1C127		127	2100	84	13	1.50	39.1	0.8
C1C128		127	2090	84	13	1.50	39.1	0.8
C1C201		202	2240	84	10	1.55	40.4	1.9
C1C202		202	2280	84	9	1.55	40.4	1.8
C1C205		205	2250	82	11	1.55	40.4	1.7
C1C296		296	2610	89	13	1.54	40.2	4.6
C1C298		298	2660	83	12	1.52	39.6	4.2
C1C299		299	2630	84	11	1.52	39.6	4.4
C1C397		397	3140	86	13	1.56	40.7	7.1
C1C399		399	3080	86	12	1.57	40.9	6.6
C1C402	1.3	402	3130	84	11	1.57	40.9	7.0
C2C124	2.6	124	1970	85	14	1.52	39.6	1.2
C2C125		125	1980	84	15	1.52	39.6	1.0
C2C127		127	1910	82	10	1.51	39.4	1.2
C2C200		200	2190	86	16	1.50	39.1	2.2
C2C202		202	2170	84	16	1.50	39.1	1.9
C2C204		204	2180	84	14	1.50	39.1	2.4
C2C295		295	2530	85	13	1.51	39.4	4.2
C2C300		300	2570	83	12	1.51	39.4	4.6
C2C301		301	2580	86	15	1.52	39.6	4.3
C2C392		392	3060	84	11	1.50	39.1	7.3
C2C396		396	3040	86	12	1.51	39.4	7.5
C2C398		398	3080	86	13	1.50	39.1	7.4
C2C400	2.6	400	3050	86	12	1.51	39.4	—
C5C127	5.0	127	1920	85	14	1.57	40.9	0.7
C5C130		130	1960	83	10	1.55	40.4	0.8
C5C131		130	1930	82	13	1.56	40.7	1.0
C5C200		201	2140	85	9	1.57	40.9	2.0
C5C201		201	2100	86	8	1.57	40.9	2.0
C5C203		203	2090	80	6	1.56	40.7	1.8
C5C293		293	2410	88	13	1.56	40.7	4.1
C5C296		296	2430	87	12	1.57	40.9	3.9
C5C301		301	2490	82	12	1.55	40.4	4.5
C5C398		398	2910	88	12	1.58	41.2	7.2
C5C401		401	2970	85	13	1.55	40.4	—
C5C402		403	2930	87	13	1.57	40.9	8.0
C5C403	5.0	403	2880	86	12	1.58	41.2	7.6

Table E.7. Micro-fin tube evaporation with pure refrigerant

Test Run	Oil %	G kg/m ² .s	h W/m ² .°C	X _{in} %	X _{out} %	P MPa	T _{sat} °C	ΔP kPa
E0A118	—	118	7460	22	86	0.50	0.1	4.2
E0A119	—	119	7280	21	82	0.51	0.7	4.4
E0A123	—	123	7720	21	81	0.51	0.7	4.2
E0A125	—	125	6510	20	80	0.51	0.7	4.0
E0A203	—	203	8760	19	90	0.47	-1.7	13.1
E0A204	—	204	9290	15	82	0.50	0.1	12.0
E0A301	—	301	9160	16	86	0.55	3.1	26.2
E0A305	—	306	9890	17	85	0.55	3.1	26.4
E0A306	—	306	9620	16	83	0.54	2.5	25.4
E0A316	—	316	9290	16	80	0.55	3.1	26.2
E0A381	—	381	10660	18	78	0.55	3.1	41.7
E0A394	—	394	10420	18	81	0.55	3.1	42.5
E0A396	—	396	10360	17	76	0.54	2.5	41.9

Table E.8. Micro-fin tube evaporation with refrigerant plus 150-SUS oil

Test Run	Oil %	G kg/m ² .s	h W/m ² .°C	X _{in} %	X _{out} %	P MPa	T _{sat} °C	ΔP kPa
E1A121	1.3	122	7430	16	81	0.56	3.7	4.3
E1A122		122	8380	16	82	0.56	3.7	4.4
E1A123		123	8400	18	85	0.56	3.7	4.0
E1A126		126	8150	16	79	0.56	3.7	4.3
E1A202		202	10400	19	85	0.49	-0.5	14.4
E1A204		204	9780	17	79	0.50	0.1	12.8
E1A210		210	9270	15	75	0.52	1.3	12.8
E1A213		213	9410	16	83	0.48	-1.1	16.6
E1A297		297	9750	15	87	0.54	2.5	27.0
E1A303		303	10270	14	84	0.55	3.1	27.6
E1A304		304	10190	12	74	0.55	3.1	25.5
E1A391		391	10600	15	71	0.55	3.1	—
E1A392		392	10600	18	78	0.55	3.1	42.1
E1A393	1.3	392	10620	18	77	0.56	3.7	41.6
E2A123	2.4	124	7910	19	84	0.48	-1.1	5.2
E2A124		124	7800	19	82	0.48	-1.1	5.0
E2A127		127	7760	19	83	0.48	-1.1	5.2
E2A128		128	8980	18	79	0.48	-1.1	5.1
E2A199		199	9110	20	83	0.50	0.1	15.0
E2A202		203	9420	17	70	0.49	-0.5	13.8
E2A203		203	9880	19	82	0.49	-0.5	15.5
E2A207		207	9790	16	68	0.49	-0.5	13.7
E2A296		296	10380	16	84	0.50	0.1	29.5
E2A303		303	10310	15	80	0.50	0.1	29.9
E2A304		304	10460	15	80	0.50	0.1	30.0

Table E.8. (continued)

Test Run	Oil %	G kg/m ² ·s	h W/m ² ·°C	X _{in} %	X _{out} %	P MPa	T _{sat} °C	ΔP kPa
E2A376		376	10890	22	90	0.59	5.3	45.6
E2A394		394	10600	19	79	0.59	5.3	42.1
E2A396		396	10870	20	86	0.58	4.8	47.1
E2A399		399	10430	17	76	0.58	4.8	42.9
E2A405	2.4	405	10530	19	77	0.60	5.9	42.6
E5A123	5.1	123	6070	20	80	0.51	0.7	5.1
E5A125		125	5760	19	81	0.51	0.7	4.9
E5A127		126	6430	19	77	0.51	0.7	5.3
E5A128		128	6500	18	78	0.51	0.7	5.3
E5A194		194	8060	18	84	0.52	1.3	15.7
E5A198		198	8320	17	83	0.52	1.3	15.9
E5A200		200	8560	17	83	0.52	1.3	16.8
E5A294		294	8980	17	85	0.51	0.7	33.1
E5A300		300	9400	16	84	0.50	0.1	33.4
E5A303		303	9230	17	85	0.49	-0.5	34.7
E5A306		306	9400	16	81	0.52	1.3	33.4
E5A384		384	10070	19	78	0.58	4.8	45.5
E5A388		388	10030	19	78	0.57	4.2	46.7
E5A391		391	10090	18	76	0.56	3.7	47.0
E5A392	5.1	392	9810	18	77	0.55	3.1	46.6

Table E.9. Micro-fin tube evaporation with refrigerant plus 300-SUS oil

Test Run	Oil %	G kg/m ² ·s	h W/m ² ·°C	X _{in} %	X _{out} %	P MPa	T _{sat} °C	ΔP kPa
E0D119	0.6	119	7430	11	93	0.47	-1.7	6.2
E0D124		124	8120	10	81	0.48	-1.1	5.1
E0D129		129	7230	11	79	0.46	-2.4	5.0
E0D203		203	9130	17	86	0.52	1.3	14.9
E0D204		204	8980	17	81	0.52	1.3	14.6
E0D205		205	8850	16	85	0.52	1.3	14.6
E0D292		292	9750	17	78	0.52	1.3	27.6
E0D294		294	9360	13	79	0.50	0.1	28.2
E0D300		300	9600	13	77	0.50	0.1	28.7
E0D304		304	9860	15	82	0.48	-1.1	30.3
E0D352		353	10340	14	89	0.51	0.7	44.5
E0D385		385	10610	18	83	0.54	2.5	46.0
E0D391		391	10460	19	78	0.56	3.7	44.6
E0D396	0.6	396	10500	18	79	0.55	3.1	46.4

Table E.9. (continued)

Test Run	Oil %	G kg/m ² .s	h W/m ² .°C	X _{in} %	X _{out} %	P MPa	T _{sat} °C	ΔP kPa
E1D125	1.3	125	6570	8	77	0.45	-3.1	6.1
E1D126		126	7010	10	77	0.49	-0.5	5.6
E1D130		130	7050	7	78	0.47	-1.7	5.9
E1D131		131	6810	6	75	0.45	-3.1	5.1
E1D195		195	7580	13	82	0.51	0.7	13.5
E1D198		199	7970	13	80	0.50	0.1	13.7
E1D199		199	8330	12	81	0.49	-0.5	12.3
E1D204		204	8050	11	76	0.49	-0.5	13.5
E1D295		295	8900	15	84	0.49	-0.5	30.9
E1D296		296	9070	12	78	0.51	0.7	28.4
E1D301		301	9280	15	80	0.50	0.1	30.7
E1D303		303	9330	12	78	0.50	0.1	31.1
E1D391		391	10190	17	85	0.57	4.2	47.2
E1D405		406	10110	16	83	0.56	3.7	48.5
E1D406	1.3	406	10160	16	85	0.55	3.1	49.2
E2D118	2.6	118	5910	14	80	0.51	0.7	4.4
E2D124		125	5960	13	77	0.52	1.3	4.7
E2D127		127	6020	12	75	0.51	0.7	—
E2D187		187	6920	13	82	0.53	1.9	13.2
E2D189		189	7190	13	82	0.56	3.7	12.9
E2D200		200	7090	11	76	0.55	3.1	12.6
E2D205		205	7290	11	77	0.54	2.5	13.5
E2D270		270	7790	19	78	0.56	3.7	27.8
E2D271		271	7990	18	80	0.58	4.8	28.9
E2D279		279	8040	18	74	0.55	3.1	29.3
E2D283		283	7900	17	79	0.61	6.4	30.1
E2D373		373	8740	22	70	0.60	5.9	45.2
E2D382		382	8660	22	62	0.62	6.9	41.9
E2D383	2.6	383	8860	21	65	0.58	4.8	46.5
E5D125	5.0	125	5090	11	83	0.51	0.7	7.0
E5D132		132	5490	10	83	0.51	0.7	7.1
E5D184		184	6180	10	81	0.59	5.3	12.8
E5D200		200	6010	9	78	0.58	4.8	13.7
E5D201		201	6120	9	77	0.56	3.7	13.7
E5D228		228	6300	11	79	0.63	7.4	17.2
E5D270		270	7210	20	82	0.60	5.9	30.3
E5D273		273	7200	19	76	0.60	5.9	29.8
E5D278		278	7140	18	70	0.60	5.9	29.3
E5D283		283	7330	18	72	0.59	5.3	26.7
E5D367		367	7990	27	77	0.63	7.4	46.5
E5D372		372	8090	15	69	0.58	4.8	46.3
E5D384	5.0	384	8330	15	66	0.61	6.4	44.7

Table E.10. Micro-fin tube condensation with pure refrigerant

Test Run	Oil %	G kg/m ² ·s	h W/m ² ·°C	X _{in} %	X _{out} %	P MPa	T _{sat} °C	ΔP kPa
C0A126	—	121	5370	90	5	1.56	40.7	1.1
C0A127	—	122	5440	90	6	1.56	40.7	1.2
C0A131	—	126	5230	87	5	1.55	40.4	1.1
C0A197	—	190	5560	90	9	1.55	40.4	2.6
C0A198	—	190	5660	89	10	1.55	40.4	2.9
C0A200	—	193	5870	92	6	1.53	39.9	3.0
C0A201	—	193	5420	90	7	1.55	40.4	3.0
C0A295	—	284	6080	90	15	1.56	40.7	6.7
C0A304	—	292	5840	93	9	1.52	39.6	7.1
C0A305	—	293	6130	90	15	1.56	40.7	7.4
C0A395	—	380	6180	89	13	1.52	39.6	11.5
C0A398	—	382	6190	88	13	1.53	39.9	11.5
C0A399	—	383	6300	89	13	1.52	39.6	11.4

Table E.11. Micro-fin tube condensation with refrigerant plus 150-SUS oil

Test Run	Oil %	G kg/m ² ·s	h W/m ² ·°C	X _{in} %	X _{out} %	P MPa	T _{sat} °C	ΔP kPa
C1A124	1.3	124	5200	88	5	1.55	40.4	—
C1A127		127	5360	85	5	1.54	40.2	—
C1A129		129	5180	80	3	1.53	39.9	—
C1A202		202	5460	85	10	1.50	39.1	—
C1A205		205	5260	83	10	1.50	39.1	—
C1A216		216	5390	77	11	1.50	39.1	—
C1A296		296	5730	88	19	1.55	40.4	—
C1A297		296	5520	89	16	1.57	40.9	8.4
C1A301		301	5400	86	7	1.59	41.5	7.2
C1A306		306	5320	83	8	1.55	40.4	7.0
C1A395		395	5830	85	12	1.52	39.6	12.0
C1A399		398	5870	84	11	1.53	39.9	11.7
C1A400	1.3	400	5550	84	12	1.52	39.6	11.8
C2A122	2.4	122	4940	83	10	1.54	40.2	1.5
C2A124		124	4450	82	8	1.53	39.9	1.4
C2A127		127	4600	81	9	1.53	39.9	1.3
C2A199		199	5280	86	16	1.56	40.7	3.4
C2A201		201	5150	84	14	1.56	40.7	3.6
C2A202		202	5020	81	9	1.57	40.9	3.3
C2A203		203	4920	81	9	1.56	40.7	3.4
C2A298		298	5180	85	14	1.56	40.7	7.9
C2A299		299	5440	84	14	1.56	40.7	8.3
C2A398		399	5530	85	13	1.59	41.5	12.2
C2A399		399	5450	85	12	1.61	42.0	12.1
C2A401	2.4	401	5450	84	12	1.60	41.7	12.3

Table E.11. (continued)

Test Run	Oil %	G kg/m ² ·s	h W/m ² ·°C	X _{in} %	X _{out} %	P MPa	T _{sat} °C	ΔP kPa
C5A122	5.1	122	4400	82	14	1.54	40.2	1.7
C5A124		124	4680	88	12	1.57	40.9	1.6
C5A126		126	4370	81	9	1.56	40.7	1.7
C5A200		200	4980	80	8	1.58	41.2	4.2
C5A201		201	4940	81	9	1.59	41.5	4.3
C5A202		202	5000	85	11	1.60	41.7	4.0
C5A295		295	5330	83	11	1.52	39.6	7.8
C5A298		298	5100	82	9	1.51	39.4	8.6
C5A301		301	5160	90	14	1.53	39.9	8.1
C5A304		304	5070	84	10	1.52	39.6	7.9
C5A403		403	5390	86	11	1.52	39.6	13.5
C5A405		405	5300	86	9	1.56	40.7	12.6
C5A413	5.1	413	5310	84	10	1.56	40.7	13.1

Table E.12. Micro-fin tube condensation with refrigerant plus 300-SUS oil

Test Run	Oil %	G kg/m ² ·s	h W/m ² ·°C	X _{in} %	X _{out} %	P MPa	T _{sat} °C	ΔP kPa
C0D118	0.6	119	5160	88	4	1.59	41.5	—
C0D119		120	5080	88	5	1.59	41.5	1.4
C0D120		120	5310	87	6	1.65	43.0	1.3
C0D125		125	5270	84	4	1.63	42.5	1.2
C0D193		193	5180	86	12	1.54	40.2	3.6
C0D194		194	5440	86	9	1.54	40.2	3.4
C0D198		198	5390	88	10	1.55	40.4	3.6
C0D296		297	5510	87	14	1.60	41.7	8.0
C0D297		298	5500	87	14	1.60	41.7	7.9
C0D298		298	5480	87	13	1.61	42.0	7.7
C0D399		399	5850	88	13	1.61	42.0	11.8
C0D400		400	5850	88	14	1.60	41.7	12.4
C0D403	0.6	403	5790	87	15	1.59	41.5	11.5
C1D123	1.3	123	5050	87	4	1.57	40.9	1.6
C1D128		128	4950	87	6	1.63	42.5	1.7
C1D129		128	4960	87	4	1.60	41.7	1.6
C1D131		131	5040	85	4	1.59	41.5	1.7
C1D200		200	5150	91	16	1.59	41.5	3.9
C1D203		203	5210	89	17	1.58	41.2	3.9
C1D204		204	5170	89	18	1.56	40.7	3.7
C1D296		296	5390	91	16	1.55	40.4	8.3
C1D299		300	5390	89	15	1.55	40.4	8.1
C1D300		300	5480	90	14	1.55	40.4	8.2
C1D398		398	5770	85	15	1.52	39.6	13.2
C1D399		399	5590	85	14	1.53	39.9	12.8
C1D404	1.3	404	5770	83	14	1.52	39.6	13.1

Table E.12. (continued)

Test Run	Oil %	G kg/m ² .s	h W/m ² .°C	X _{in} %	X _{out} %	P MPa	T _{sat} °C	ΔP kPa
C2D128	2.6	128	4830	84	7	1.59	41.5	1.6
C2D129		129	4790	88	17	1.54	40.2	1.8
C2D198		198	4710	89	13	1.50	39.1	4.2
C2D199		199	4890	90	13	1.50	39.1	3.9
C2D203		203	4860	89	15	1.51	39.4	4.3
C2D293		293	5240	86	11	1.54	40.2	8.6
C2D294		294	5140	87	12	1.54	40.2	8.3
C2D297		297	5190	88	10	1.54	40.2	8.7
C2D395		395	5400	85	13	1.55	40.4	13.7
C2D399		399	5370	86	12	1.58	41.2	13.5
C2D400	2.6	400	5420	86	13	1.57	40.9	13.9
C5D120	5.0	120	4400	85	12	1.53	39.9	1.8
C5D122		122	4580	83	12	1.54	40.2	—
C5D124		124	4580	82	10	1.55	40.4	2.0
C5D207		208	4690	84	9	1.58	41.2	4.5
C5D208		208	4590	84	9	1.56	40.7	4.2
C5D211		211	4680	83	11	1.56	40.7	4.7
C5D294		294	4850	84	17	1.50	39.1	9.7
C5D297		297	4690	88	15	1.52	39.6	9.3
C5D301		301	4800	85	13	1.52	39.6	9.6
C5D394		394	5100	83	6	1.55	40.4	13.5
C5D398		398	4990	85	6	1.57	40.9	13.7
C5D401	5.0	401	5120	85	10	1.57	40.9	14.5

Table E.13. Low-fin tube evaporation with pure refrigerant

Test Run	Oil %	G kg/m ² .s	h W/m ² .°C	X _{in} %	X _{out} %	P MPa	T _{sat} °C	ΔP kPa
E0B124	—	124	6990	16	87	0.48	-1.1	6.6
E0B128	—	128	7270	16	86	0.47	-1.7	7.3
E0B132	—	132	7010	15	81	0.48	-1.1	7.1
E0B136	—	136	6970	15	77	0.48	-1.1	7.4
E0B200	—	200	8980	18	82	0.48	-1.1	16.4
E0B201	—	201	8940	18	81	0.47	-1.7	17.4
E0B207	—	207	9070	18	77	0.48	-1.1	17.1
E0B298	—	298	9450	18	87	0.58	4.8	30.9
E0B299	—	299	9490	18	87	0.58	4.8	31.3
E0B309	—	309	9310	17	84	0.57	4.2	31.0
E0B376	—	376	10010	22	80	0.56	3.7	46.6
E0B390	—	390	10310	21	77	0.54	2.5	46.4

Table E.14. Low-fin tube evaporation with refrigerant plus 150-SUS oil

Test Run	Oil %	G kg/m ² .s	h W/m ² .°C	X _{in} %	X _{out} %	P MPa	T _{sat} °C	ΔP kPa
E1B123	1.3	123	6760	14	82	0.51	0.7	6.8
E1B125		125	6970	14	81	0.50	0.1	6.7
E1B129		129	7060	10	80	0.49	-0.5	6.6
E1B195		195	8590	15	73	0.48	-1.1	14.9
E1B199		199	9200	15	69	0.47	-1.7	15.5
E1B203		203	9370	15	71	0.47	-1.7	16.2
E1B302		302	9770	18	77	0.55	3.1	32.6
E1B307		307	9530	15	83	0.52	1.3	34.5
E1B309		309	9560	14	84	0.52	1.3	37.0
E1B389		389	10260	21	74	0.52	1.3	50.0
E1B390		390	10230	21	72	0.50	0.1	54.4
E1B391	1.3	391	9930	20	73	0.51	0.7	53.0
E2B124	2.4	124	6560	19	82	0.53	1.9	7.3
E2B128		129	6790	14	80	0.52	1.3	6.9
E2B129		129	6520	18	81	0.52	1.3	7.7
E2B130		130	6980	18	76	0.52	1.3	7.6
E2B201		201	8380	18	88	0.53	1.9	17.1
E2B202		202	7880	17	81	0.54	2.5	17.1
E2B203		203	8220	18	78	0.51	0.7	17.6
E2B204		203	8330	17	82	0.53	1.9	16.5
E2B292		292	8560	12	72	0.58	4.8	31.3
E2B295		295	8740	24	73	0.62	6.9	32.7
E2B297		297	8890	14	70	0.59	5.3	30.5
E2B383		383	9120	19	74	0.55	3.1	52.2
E2B405		405	9260	17	70	0.58	4.8	52.0
E2B406	2.4	406	9290	16	70	0.60	5.9	53.5
E5B120	4.9	120	6010	9	91	0.45	-3.1	10.9
E5B126		126	6230	10	87	0.45	-3.1	11.9
E5B129		129	5600	9	83	0.45	-3.1	12.0
E5B136		136	6150	14	84	0.47	-1.7	12.1
E5B198		198	7520	13	81	0.52	1.3	19.4
E5B202		202	7240	12	79	0.52	1.3	17.3
E5B203		203	7360	12	78	0.52	1.3	20.2
E5B286		286	8460	17	83	0.52	1.3	38.5
E5B292		293	8110	16	74	0.52	1.3	37.1
E5B293		293	8370	16	79	0.52	1.3	37.7
E5B390		390	8460	20	80	0.54	2.5	59.7
E5B397		397	8810	20	86	0.56	3.7	60.6
E5B409	4.9	409	8940	18	83	0.57	4.2	61.5

Table E.15. Low-fin tube condensation with pure refrigerant

Test Run	Oil %	G kg/m ² ·s	h W/m ² ·°C	X _{in} %	X _{out} %	P MPa	T _{sat} °C	ΔP kPa
COB129	—	129	4760	88	9	1.60	41.7	2.1
COB132	—	132	4700	85	13	1.66	43.3	2.3
COB197	—	197	4790	86	10	1.58	41.2	4.8
COB198	—	198	4900	85	8	1.57	40.9	4.6
COB202	—	202	5030	82	4	1.56	40.7	4.7
COB205	—	205	5060	80	5	1.54	40.2	4.7
COB300	—	301	5090	89	9	1.52	39.6	9.4
COB301	—	301	5100	91	11	1.51	39.4	9.3
COB303	—	303	4950	84	9	1.50	39.1	9.5
COB308	—	308	5040	85	8	1.50	39.1	9.5
COB396	—	396	5310	93	14	1.56	40.7	14.3
COB401	—	401	5320	91	10	1.57	40.9	15.0
COB403	—	403	5260	87	10	1.60	41.7	14.5
COB404	—	404	5340	91	9	1.59	41.5	13.7

Table E.16. Low-fin tube condensation with refrigerant plus 150-SUS oil

Test Run	Oil %	G kg/m ² ·s	h W/m ² ·°C	X _{in} %	X _{out} %	P MPa	T _{sat} °C	ΔP kPa
C1B128	1.3	129	4740	85	11	1.55	40.4	2.2
C1B129		129	4730	84	8	1.55	40.4	2.4
C1B130		129	4690	84	8	1.56	40.7	2.3
C1B197		199	4810	86	14	1.59	41.5	4.6
C1B198		198	4710	86	14	1.60	41.7	4.8
C1B199		199	4830	86	12	1.59	41.5	5.0
C1B298		299	4890	87	22	1.54	40.2	9.8
C1B299		299	4910	87	21	1.53	39.9	10.3
C1B302		302	5000	88	21	1.54	40.2	10.4
C1B392		392	5190	90	18	1.54	40.2	15.1
C1B394		394	5220	90	28	1.55	40.4	14.7
C1B401	1.3	401	5170	88	17	1.55	40.4	15.2
C2B124	2.4	124	4530	89	13	1.62	42.2	2.2
C2B126		126	4570	87	14	1.61	42.0	2.3
C2B127		127	4610	81	11	1.61	42.0	2.4
C2B200		201	4730	85	24	1.55	40.4	5.5
C2B201		201	4780	86	17	1.54	40.2	5.2
C2B202		202	4740	86	15	1.51	39.4	—
C2B300		300	4890	89	11	1.55	40.4	9.8
C2B301		301	4850	87	11	1.56	40.7	9.2
C2B302		301	4800	86	11	1.56	40.7	9.9
C2B306		306	5020	83	9	1.57	40.9	9.3
C2B399		399	5120	84	11	1.53	39.9	16.0
C2B409		409	5100	84	17	1.58	41.2	15.9
C2B414	2.4	414	5100	79	12	1.55	40.4	15.7

Table E.16. (continued)

Test Run	Oil %	G kg/m ² .s	h W/m ² .°C	X _{in} %	X _{out} %	P MPa	T _{sat} °C	ΔP kPa
C5B124	4.9	124	4670	88	14	1.54	40.2	2.0
C5B125		125	4510	88	13	1.53	39.9	2.1
C5B126		125	4420	88	14	1.53	39.9	2.3
C5B127		126	4430	88	17	1.55	40.4	1.9
C5B201		201	4600	91	17	1.61	42.0	5.5
C5B203		203	4520	90	14	1.60	41.7	4.9
C5B296		296	4600	89	19	1.59	41.5	10.1
C5B297		297	4630	88	20	1.59	41.5	10.0
C5B393		393	4760	88	19	1.53	39.9	16.3
C5B396		396	4850	88	17	1.53	39.9	16.2
C5B398	4.9	398	4840	90	12	1.55	40.4	15.2

Due to problems with the pressure drop transducer during the initial smooth tube testing with pure refrigerant and refrigerant plus 150-SUS oil, the smooth tube tests had to be repeated to obtain pressure drop data. The data from these repeated tests are presented in the tables that follow. They were not stored in disk files, so have no test run designation code.

Table E.17. Smooth tube evaporative pressure drop with pure refrigerant

Oil %	G kg/m ² .s	X _{in} %	X _{out} %	P MPa	T _{sat} °C	ΔP kPa
—	125	20	88	0.45	-3.1	3.5
—	128	20	92	0.44	-3.7	4.4
—	131	20	91	0.45	-3.1	3.8
—	202	18	75	0.47	-1.7	8.4
—	203	18	80	0.48	-1.1	9.3
—	208	18	76	0.46	-2.4	9.0
—	302	17	74	0.48	-1.1	19.4
—	303	15	72	0.49	-0.5	18.0
—	387	23	77	0.48	-1.1	31.2
—	390	22	73	0.50	0.1	30.7

Table E.18. Smooth tube evaporative pressure drop with refrigerant plus 150-SUS oil

Oil %	G kg/m ² ·s	X _{in} %	X _{out} %	P MPa	T _{sat} °C	ΔP kPa
1.3	125	13	81	0.49	-0.5	3.7
	125	11	74	0.52	1.3	3.3
	127	11	73	0.51	0.7	3.7
	205	12	78	0.49	-0.5	9.9
	206	12	77	0.50	0.1	9.4
	208	12	78	0.50	0.1	9.7
	283	16	75	0.48	-1.1	19.4
	287	16	74	0.48	-1.1	19.5
	388	15	69	0.50	0.1	30.0
	393	15	69	0.49	-0.5	30.8
1.3	397	15	64	0.48	-1.1	30.8
2.4	117	18	79	0.48	-1.1	3.7
	118	17	81	0.48	-1.1	4.6
	119	18	75	0.47	-1.7	4.1
	186	14	76	0.48	-1.1	8.7
	193	16	72	0.49	-0.5	8.6
	194	16	72	0.49	-0.5	9.3
	198	16	75	0.49	-0.5	9.8
	200	15	73	0.49	-0.5	10.5
	292	15	78	0.53	1.9	20.0
	293	15	74	0.52	1.3	20.0
	294	14	81	0.52	1.3	24.5
	298	13	78	0.52	1.3	21.0
	300	13	75	0.52	1.3	19.8
	388	12	81	0.56	3.7	32.5
2.4	398	11	75	0.56	3.7	30.2
4.9	119	23	78	0.55	3.1	4.2
	122	21	78	0.56	3.7	4.3
	130	19	76	0.55	3.1	4.4
	197	16	85	0.52	1.3	14.0
	198	16	88	0.52	1.3	14.4
	200	15	81	0.54	2.5	11.9
	281	15	85	0.52	1.3	21.4
	288	15	81	0.53	1.9	20.8
	298	15	74	0.55	3.1	20.4
	388	20	84	0.58	4.8	35.9
4.9	389	21	79	0.55	3.1	34.2

Table E.19. Smooth tube condensing pressure drop with pure refrigerant

Oil %	G kg/m ² .s	X _{in} %	X _{out} %	P MPa	T _{sat} °C	ΔP kPa
—	127	88	4	1.60	41.7	1.0
—	130	86	5	1.60	41.7	1.0
—	198	91	14	1.57	40.9	2.1
—	201	90	15	1.57	40.9	2.0
—	201	90	15	1.57	40.9	2.2
—	302	93	9	1.69	44.0	3.8
—	303	91	17	1.51	39.4	4.7
—	303	91	11	1.56	40.7	4.1
—	409	93	23	1.46	38.0	9.7
—	410	92	19	1.61	42.0	8.0
—	411	94	23	1.47	38.3	9.9

Table E.20. Smooth tube condensing pressure drop with refrigerant plus 150-SUS oil

Oil %	G kg/m ² .s	X _{in} %	X _{out} %	P MPa	T _{sat} °C	ΔP kPa
1.3	127	94	11	1.54	40.2	0.9
	127	87	11	1.53	39.9	0.8
	128	92	10	1.55	40.4	0.7
	131	89	10	1.59	41.5	1.0
	198	90	14	1.59	41.5	1.7
	202	88	13	1.58	41.2	1.6
	300	85	11	1.60	41.7	2.9
	303	82	9	1.59	41.5	2.8
	303	86	9	1.59	41.5	2.8
	400	95	18	1.61	42.0	5.8
	401	91	17	1.58	41.2	6.0
	402	95	19	1.62	42.2	6.0
	409	87	14	1.49	38.8	5.8
1.3	409	87	15	1.49	38.8	6.6
2.4	122	83	17	1.53	39.9	0.7
	122	83	17	1.52	39.6	0.6
	122	83	17	1.53	39.9	0.6
	191	84	12	1.54	40.2	1.3
	192	83	13	1.54	40.2	1.2
	192	83	12	1.55	40.4	1.1
	292	84	10	1.55	40.4	2.4
	297	87	11	1.57	40.9	2.5
	303	83	10	1.57	40.9	2.5
	400	87	13	1.55	40.4	4.8
	400	87	13	1.55	40.4	4.7
2.4	407	86	12	1.55	40.4	4.7

Table E.20. (continued)

Oil %	G kg/m ² .s	X _{in} %	X _{out} %	P MPa	T _{sat} °C	ΔP kPa
4.9	128	93	10	1.53	39.9	0.8
	131	80	11	1.55	40.4	0.6
	131	80	14	1.58	41.2	0.9
	194	80	17	1.63	42.5	1.1
	196	86	19	1.68	43.8	1.2
	201	83	20	1.69	44.0	1.1
	294	93	24	1.55	40.4	2.8
	300	90	22	1.54	40.2	2.4
	302	89	21	1.55	40.4	2.8
	382	86	18	1.57	40.9	4.2
	391	87	21	1.61	42.0	4.7
	393	86	20	1.60	41.7	4.7
4.9	394	86	20	1.59	41.5	4.6

Table E.21. Smooth tube evaporation oil hold-up with 150-SUS oil

Oil %	G kg/m ² .s	X _{in} %	X _{out} %	P MPa	T _{sat} °C	M _{oil} g	M _{R-22} g
1.3	203	15	85	0.52	1.3	1.6	—
2.5	209	15	90	0.53	1.9	2.6	—
5.0	202	15	90	0.49	-0.5	5.3	28.
5.0	110	20	90	0.51	0.7	4.8	—
5.0	301	15	85	0.53	1.9	5.0	—
5.0	199	15	90	0.79	15.0	5.3	—
5.0	146	20	10°C ^a	0.48	-1.1	7.7	—
5.0	148	15	15°C ^a	0.50	0.1	9.5	—

^aSuperheated exit conditions.

Table E.22. Smooth tube condensation oil hold-up with 150-SUS oil

Oil %	G kg/m ² .s	X _{in} %	X _{out} %	P MPa	T _{sat} °C	M _{oil} g	M _{R-22} g
1.3	201	80	10	1.52	39.6	1.4	—
2.5	202	80	5	1.51	39.4	2.6	—
5.0	200	80	5	1.49	38.8	5.0	58.
5.0	103	75	5	1.55	40.4	5.2	—
5.0	297	80	10	1.51	39.4	4.8	—

Table E.23. Micro-fin tube evaporation oil hold-up with 150-SUS oil

Oil %	G kg/m ² ·s	X _{in} %	X _{out} %	P MPa	T _{sat} °C	M _{oil} g	M _{R-22} g
1.3	201	15	85	0.52	1.3	1.9	—
2.5	203	15	85	0.52	1.3	2.9	—
5.0	202	15	85	0.49	-0.5	5.8	33.
5.0	202	15	85	0.51	0.7	5.9	—
5.0	118	15	90	0.50	0.1	6.2	—
5.0	299	15	85	0.54	2.5	5.7	—
5.0	197	15	85	0.79	15.0	5.6	—
5.0	165	20	15°C ^a	0.46	-2.4	19.	—

^aSuperheated exit conditions.

Table E.24. Micro-fin tube condensation oil hold-up with 150-SUS oil

Oil %	G kg/m ² ·s	X _{in} %	X _{out} %	P MPa	T _{sat} °C	M _{oil} g	M _{R-22} g
1.3	202	80	10	1.52	39.6	1.9	—
2.5	200	80	10	1.54	40.2	3.2	—
5.0	200	80	5	1.51	39.4	6.3	67.
5.0	201	80	10	1.52	39.6	6.6	—
5.0	102	75	5	1.50	39.1	6.2	—
5.0	304	80	10	1.52	39.6	6.7	—

Table E.25. Smooth tube oil hold-up with 300-SUS oil

Test type ^a	Oil %	G kg/m ² ·s	X _{in} %	X _{out} %	P MPa	T _{sat} °C	M _{oil} g
E	1.3	204	15	85	0.51	0.7	1.8
E	2.6	196	15	90	0.58	4.8	3.2
E	5.0	194	15	95	0.54	2.5	5.3
C	1.3	202	80	10	1.49	38.8	1.4
C	2.6	204	80	5	1.47	38.3	2.3
C	5.0	209	80	5	1.53	39.9	5.2

^aE = evaporation; C = condensation.

Table E.26. Micro-fin tube oil hold-up with 300-SUS oil

Test type ^a	Oil %	G kg/m ² ·s	X _{in} %	X _{out} %	P MPa	T _{sat} °C	M _{oil} g
E	1.3	199	15	85	0.51	0.7	2.0
E	2.6	196	15	80	0.58	4.8	3.6
E	5.0	198	15	85	0.53	1.9	4.0
C	1.3	194	80	10	1.48	38.5	1.8
C	2.6	191	80	10	1.52	39.6	3.2
C	5.0	192	85	5	1.47	38.3	6.3

^aE = evaporation; C = condensation.